How fungal pathogens communicate with plant cells and cause disease

Submitted by

Laura Elisabeth Baggaley

to the University of Exeter as a thesis for the degree of Doctor of Philosophy in Biological Sciences, March 2021

I certify that all material in this thesis which is not my own work has been identified and that any material that has previously been submitted and approved for the award of a degree by this or any other University has been acknowledged.

Signature: L. Baggaley

ABSTRACT

Warmer atmospheric conditions are creating a climate increasingly suitable for the spread of crop pathogens and pests, significantly reducing crop yields. Fungal pathogens are responsible for approximately 15% of crop losses; therefore, an enhanced understanding of how fungal plant pathogens communicate with plant cells and cause disease is necessary to improve global food security. *Zymoseptoria tritici*, the main causal agent of Septoria tritici blotch in wheat, and *Fusarium graminearum*, the main causal agent of Fusarium Head Blight in small-grain cereals, are fungal pathogens of global importance based on both scientific and economic impact. The interactions of these pathogens and their hosts is relatively understudied. Therefore, the aim of this project was to develop novel approaches to understand the relationship of *Z. tritici* and *F. graminearum* with wheat during infection.

The processes which determine whether successful infection is established within the host (compatible interaction) or not, whereby host defence is successful and no infection is established (incompatible interaction), are still not fully understood. Consequently, the present study aimed to produce *Z. tritici* metabolic biosensors to determine the fungal response to the host in both compatible and incompatible interactions. However, the results demonstrated that higher expression of the biosensor construct, mitroGFP2-Orp1, is needed for this tool to be of future use.

Unlike *Z. tritici*, *F. graminearum* can travel intracellularly in the host once successful infection has been established. This is facilitated by pit-fields (PFs) which are abundant in plasmodesmata (PD). Thus, a series of approaches were developed to investigate the *F. graminearum*-PD interaction at both the cellular

and molecular levels. A high-throughput wheat coleoptile infection assay was adapted to image PD when infected with the wildtype PH-1, and mutant GT2 and MAP1 strains. Particle bombardment was used to generate stable wheat plasma membrane (PM) reporter lines, utilising the genes *At*LTI6b and *Zm*ROP7, for live-cell imaging of PFs during infection. However, no or low expression of the PM constructs resulted in this experiment being unsuccessful. Finally, bioinformatics analyses were used to identify wheat proteins involved in PD-permeability control, *At*BG_PPAP and *At*PDLP orthologs, for use in virus-induced gene silencing experiments to assess how *F. graminearum* hyphal progression is regulated within the host.

The present study has provided novel datasets, approaches and tools, which have the potential to improve not only *Z. tritici* and *F. graminearum* research, but that of a multitude of fungal-host interactions as well as crop protection strategies.

ACKNOWLEDGEMENTS

Firstly, I would like to express gratitude for my main PhD supervisors, Kim Hammond-Kosack and Mike Deeks, for their continuous guidance, perseverance and advice, and for giving me this opportunity. I would also like to thank Christine Faulkner, Martin Urban and Nick Talbot, other members of my PhD committee, who were always there to provide training and guidance when needed. I am extremely grateful to the Rothamsted Bioimaging department, Smita Kurup, Kirstie Halsey and Hannah Walpole, for taking the time to train and advise me. Thank you to the Rothamsted Specialist Cereal Transformation team, especially, Caroline Sparks, and Alison Huttly for helping me design wheat transformation experiments and taking the time to listen and be patient. Many thanks to Suzanne Clark of the Rothamsted Statistics department for help with data analysis. I would also like to thank the past and present members of the Rothamsted Wheat Pathogenomics team, in particular Kostya Kanyuka for bioinformatics assistance and Ana Machado and Mike Grimwade-Mann for help with the coleoptile assay. I am grateful to Mike Deeks' group at the University of Exeter, for their constant support and friendship, as well as Nic Helmstetter for help with fungal transformations and Francesco Valente for carrying on the work I left behind. Thank you to all the support staff for maintaining the controlled environment facilities and laboratory equipment, and to Donna Fellowes for always helping students to get the best out of their time at Rothamsted.

I would also like to thank the British Society of Plant Pathology (BSPP) for providing a grant to travel to an international conference. This project was funded funded by the UK BBSRC-funded South West Biosciences Doctoral Training Partnership (BBSRC SWBio DTP) (BB/M009122/1).

To my friends, at Rothamsted, Exeter and on my DTP, especially Laura, Caitlin, Tom and Siobhan, I could not have done this without your constant support and belief. To my family, I thank you for always being there, checking in on me and believing in me. Finally, to Alex, for all the care, love and understanding you have shown me along the way, making it all a little bit easier.

TABLE OF CONTENTS

LIST OF FIGURES AND TABLES

LIST OF APPENDICES

LIST OF ABBREVIATIONS

ADON	Acetyl-deoxynivalenol
ADP	Adenosine diphosphate
ALSV	Apple latent spherical virus
ANOVA	Analysis of variance
ATMT	Agrobacteria tumefaciens mediated transformation
ATP	Adenosine triphosphate
Avr	Avirulence
BCA	Biological control agent
BF	Brightfield
BLAST	Basic local alignment search tool
BM	Basal media
BSMV	Barley stripe mosaic virus
BW	Bobwhite
CalS	Callose synthase
cDNA	Complementary deoxyribonucleic acid
CFD	Cut flower dye assay
CIMMYT	International Maize and wheat Improvement Centre
CLSM	Confocal laser scanning microscopy
CMV	Cucumber mosaic virus
COX4	Cytochrome c oxidase subunit 4
cpGFP	Circularly permuted green fluorescent protein

CRISPR-Cas	Clustered regularly interspaced short palindromic repeats and CRISPR-associated protein
cv	cultivar
DEG	Differentially expressed gene
DMI	Demethylation inhibitors
DNA	Deoxyribonucleic acid
DON	Deoxynivalenol
DPDA	Detached petal disc assay
dSTORM	Direct stochastic optical reconstruction microscopy
DTT	Dithiothreitol
DUF	Domain of unknown function
EDTA	Ethylenediamine tetra-acetic acid
eGFP	Enhanced green fluorescent protein
EHM	Extrahaustorial membrane
EMBL	European molecular biology laboratory
EMS	Ethyl methanesulfonate
EPT	12,13-epoxytrichothec-9-ene
ER	Endoplasmic reticulum
ETI	Effector triggered immunity
ETS	Effector triggered susceptibility
FACS	Fluorescent-activated cell sorting
FAO	Food and Agriculture Organisation
ff.spp.	Formae speciales

FHB	Fusarium head blight
FoMV	Foxtail mosaic virus
FP	Fluorescent protein
FRET	FÖrster resonance energy transfer
G418	Geneticin
GFP	Green fluorescent protein
GH	Glycosyl hydrolase
GLLM	Generalised linear mixed model
GM	Genetic modification
gRNA	Guide ribonucleic acid
GSL	Glucan synthase-like
GTPase	Guanosine triphosphatase
He	Helium
HIGS	Host induced gene silencing
HR	Hypersensitive response
HVR	Hypervariable region
Hyg	Hygromycin
IDT	Integrated DNA technologies
IM	Induction media
kan	Kanamycin
KO	Knock out
LMM	Linear mixed model
LS	Longitudinal (section)
MAMP	Microbe associated molecular pattern
MAPK	Mitogen activated protein kinase
Mg	Magnesium

MoT	*Magnaporthe oryzae* pathotype *Triticum* (*MoT*)
MP	Movement protein
N-STORM	Nikon stochastic optical reconstruction microscopy
NCBI	National Centre for Biotechnology Information
NEB	New England Biosciences
NHR	Non-host resistance
NIV	Nivalenol
NRRL	Northern regional research laboratory
ORF	Open reading frame
PA	Phosphatidic acid
PAM	Periarbuscular membrane
PAMP	Pathogen associated molecular pattern
PBM	Peribacteroid membrane
PCR	Polymerase chain reaction
PD	Plasmodesmata
PDCB	Callose-binding protein
PDLP	Plasmodesmata-located prorin
PDS	Particle delivery system
PF	Pit-field
PFD	Post-bloom fruit drop
PI	Propidium iodide
PM	Plasma membrane

PMA	Propidium monoazide
PRR	Pathogen recognition receptor
PTGS	Post-transcriptional gene silencing
PTI	Pathogen triggered immunity
qPCR	Quantitative polymerase chain reaction
QTL	Quantitative trait loci
R	Resistance gene
REML	Residual maximum likelihood analysis
RFP	Red fluorescent protein
rif	Rifampicin
RNA	Ribonucleic acid
RNAi	Ribonucleic acid interference
roGFP	Reduction-oxidation sensitive green fluorescent protein
ROS	Reactive oxygen species
RT	Room temperature
SA	Salicylic acid
SAR	Systemic acquired resistance
SC	Species complex
SCF	European Commission Scientific Committee on Food
SE	Standard error
SEL	Size exclusion limit
SMC	Secondary metabolite cluster
sRNA	Small ribonucleic acid

ssRNA	Single-stranded ribonucleic acid
STB	Septoria tritici blotch
sur	Sulfonylurea
T3SS	Type 3 secretion system
TDI	Tolerable daily intake
TE	Tris-EDTA
TMD	Transmembrane domain
TMV	Tobacco mosaic virus
TRV	Tobacco rattle virus
TS	Transverse (section)
UN	United Nations
USA	United States of America
UTR	Untranslated region
UV	Ultraviolet
VIF	Virus-induced flowering
VIGS	Virus induced gene silencing
VOX	Virus mediated overexpression
WGA	Wheat germ agglutinin
WHO	World Health Organisation
WT	Wild-type
YPD	Yeast peptone dextrose
ZEA	Zearalenone
ZtGFP	Zymoseptoria tritici optimised green fluorescent protein

LIST OF UNITS

$	American dollar
bp	Base pairs
cm	Centimetre
dpi	Days post inoculation
°C	Degrees Celsius
€	Euro
g	Gram
h	Hour
hpi	Hours post inoculation
kb	Kilobase
kDa	KiloDalton
kg	Kilogram
T_m	Melting temperature
µg	Microgram
µl	Microlitre
µm	Micrometres
µM	Micromole
ml	Millilitre
mm	Millimetres
mM	Millimole
min	Minutes
M	Mole
nm	Nanometres
nt	Nucleotides
%	Percent

s	Seconds
Tpm	Transcripts per million
V	Volts

CHAPTER 1: Introduction

1.1 The current pressures on global agriculture

The United Nations (UN) has stated that by 2050 70% more food must be produced than at present in order to feed an estimated 9.6 billion people[1]. Over the past two decades, global, regional and local efforts have led to significant increases in agricultural production (crops, livestock, fisheries and forestry); however, according to the Food and Agriculture Organisation of the UN (FAO) and World Health Organization (WHO), 842 million people continue to suffer from chronic hunger[2,3]. Limited agricultural land availability means we must maximise crop yields on the arable land already in use. If this approach to increase the production of healthy and nutritious food and feed products was made possible, and specifically in combination with reduced food waste through the entire supply chain, we would have a better chance to feed the current global population as well as the population of future generations; this is a problem which can only be solved my multinational cooperation efforts.

Current opinion favours the theory that we are undergoing a fourth agricultural revolution, evolving from the previous “green revolution” and consequential integration of man-made pesticides and fertilisers in the last century[4,5]. Agriculture is currently relying more and more upon information and communication technology (ICT) with a movement towards the Internet of Things, robotics, and Artificial Intelligence (AI)[5,6]. The Internet of Things is defined as a communication network of internet-connected computing devices that can send and receive data[7]. The development of agricultural sensors alongside machine learning has allowed farmers and scientists to monitor growing conditions,

including soil health, infection, temperature and rainfall, through the use of artificial technologies[7].

With the need to increase food production the introduction of such technologies is necessary and is possibly the only way we can achieve food security. Unfortunately, modern agro-ecosystems have resulted in biodiversity losses with many crops being grown in monocultures[8]. Our reliance on single resistant cultivars and single-target antifungals provides ideal conditions for the emergence of pre-existing or new pathogenic strains[8]. Traded goods also add another dimension of agricultural threat allowing diseases to spread globally[8]. Therefore, a move towards monitoring and modelling crop yields artificially may be the next step in improving modern agro-ecosystems.

Current evidence has determined that there is a need for these new systems: programmes to aid fertiliser and pesticide application precision, robots to milk cows and the use of drones and geospatial imaging to identify problems in a unit or area, such as the detection of drought or the presence of a pathogenic threat[5,9-11]. However even with these advancements, research is still needed to understand how we as scientists can increase crop yield and quality, by studying in the field as well as in the laboratory at a molecular, cellular and genetic level.

Crop yields are threatened by a variety of biotic and abiotic factors. Cereals can be grown across temperate and sub-tropical regions and are therefore exposed to a range of different soil types and climatic conditions. Many smallholder farms are based in underdeveloped areas with little access to help following natural disasters, as well as no access to expensive fertilisers, high quality seed to

provide vigorous high yielding plants, or expensive preventative measures which will ensure crop protection against pests and disease. These communities also rely upon rainfed agriculture[12]. Water storage can be used for supplemental irrigation but many are dependent on rainfall alone, and in regions where rainfall is unpredictable high levels of food insecurity, poverty and malnutrition are observed[12]. Between 2005 and 2015, $96 billion was lost in crops and livestock as a result of natural disasters, which include: diseases, pests, forest fires, floods and storms[13]. However, drought was the most destructive solo threat causing losses of $29 billion[13].

Cereal crops are essential for the survival of the human population[14]. Making up more than 50% of the world's caloric intake, cereal grains are grown in greater quantities and provide more energy than any other type of crop, and are therefore termed 'staple crops'[14]. In order to keep up with demand, as of 2015 cereal production needed to increase by 40% overall to reach demand in 2050[15]. All cereals are members of the grass family (Poaceae) and include wheat, barley, maize, rice, rye, sorghum and millet. Cereal production has continued to increase since the green revolution. Production in 2021 is predicted to be 1.7% higher than in 2020 at 2,817 million tonnes[16]. Furthermore, cereal yield has increased from 1431kg per hectare in 1961 to 4074kg per hectare in 2017[17] . However, this year-to-year expansion in cereal yields is not always as large as predicted. For example, in 2019 excessively wet conditions in the US led to delays in sowing maize plantations resulting in an estimated loss of 45 million tonnes[18]. Current projections suggest climate change will have a devasting effect on wheat and maize yields, two of the most essential crops in the human diet[19]. In Africa alone reductions of up to 20% are expected[19]. The 'business as usual' attitude cannot

be our future approach to agriculture if we are to save small-holder farms which are crucial in developing regions globally[19].

There has therefore been a move to sustainable intensive agriculture, which is particularly important where the use of other technologies is not viable. The main practices that can help us achieve this are as follows: conservation agriculture, efficient water management, healthy soil, integrated pest management, improved crops and varieties, and fertiliser efficiency[19,20]. A declining birth rate and a stabilising human population gives us the opportunity to protect the natural resources already available[20]. However, at the centre of providing agricultural sustainability is the need for cooperation at the international, national and local levels, to ensure policies and strategies are drawn up fairly to have the smallest impact possible with the greatest gains in terms of crop yields and productivity[21]. The concept of sustainable agriculture has been discussed extensively over the last few decades and we are yet to see the results of this.

As climatic conditions change around the globe, one of the biggest challenges will be tackling the pests and pathogens that migrate as a result of global warming[22]. The extra stress these climatic changes will put on host plants will also alter pathogen-host interactions[23]. Plants are constantly under attack from a range of pests, including insects, bacteria, viruses, fungi, protists and nematodes, as well as larger organisms including mammals and birds. Commonly, pesticides and partially resistant cultivars are used to control these diseases, however neither method is efficient enough to significantly reduce crop losses[24]. It is also now well established that after the use of chemicals for a long or short period of time, dependent upon the pest/pathogen, host and pesticide used, the

pest/pathogen will develop resistance/insensitivity or overcome the host's defences[24,25]. Research into the most prevalent pests and plant pathogens is therefore ongoing. With resulting crop losses of between 20-40% occurring annually, it is critical that we understand the lifecycles of these organisms if we are going to be able to prevent large crop losses, and ensure local, regional and global food security for future generations[26-28].

1.2 Literature review – The biology of floral pathogens

1.2.1 A threat to food security – why do microbes colonise flowers?

Amongst all living land plants, 90% are angiosperms (flowering plants), which are responsible for the survival of most terrestrial life on earth[29]. In comparison to the evolution of all extant seed plants (angiosperms and gymnosperms), which occurred 310-350 million years ago, the evolution of the flower is relatively recent at 140-250 million years ago and begins to show great diversification 40-150 million years later[30-34]. The arrival of the flower and its role as a reproductive organ created an ideal environment for both pathogenic and symbiotic microbes to survive and complete their life cycles. Flowers are nutrient-rich environments, which have multiple niches suited to different microbial needs, differing in chemical composition, longevity and morphology – all of which change as the plant develops and matures; flowers also present pathogens with a newly emerged clean niche[35-38]. However, using flowers as a host tissue also has risks in that spore release needs to be timed well, even more so where transmission relies upon pollinators.

The number of floral-infecting plant microbes reaches into the hundreds, all varying in host specificity, including specialists or generalists, and with narrow to

wide geographical distributions. Even though many of these diseases have been investigated since the 1800's, progress in the field has not been collectively assessed, with many new research fields appearing over the last decade. In this section of my introduction, I will focus on fungi, bacteria and viruses, all of which show variations in their modes of floral infection and subsequent disease outcomes. Oomycetes were also investigated but at the time of writing only one floral tissue-infecting oomycete had been reported. *Sclerospora graminicola*, a pathogen of maize and pearl millet, infects the panicle and converts floral tissue into leaf-like structures[39,40]. Please note, in this review floral microbes are considered to be microbes which interact with or infect floral tissue but may not exclusively colonise flowers. Table 1.1 details floral microbes of high global importance. It should be noted that this table does not include numerous floral microbes many of which may be globally important, but rather focuses on individual species or genera that have been relatively extensively researched and published on.

Floral infecting fungi are the most prevalent and well characterised. In the 2006 review 'Biology of Flower-Infecting Fungi', by Ngugi and Sherm, 104 fungal species within 29 genera were listed[41,13]. Flower-fungal interactions can be divided into four main categories: pathogenic, by mimicry, mutualism, or a combination of these. Many pathogenic fungi and oomycetes are well studied as a result of their agricultural and economic impact. For example, for the smut fungus, *Ustilago maydis,* which typically infects maize, even though losses are small they are still extremely expensive because of high crop prices[42].

On the other hand, bacterial and viral floral infections tend to have a lower occurrence or are harder to detect, and are therefore sparsely documented. However, this does not mean they are not as economically damaging. A fire blight outbreak, *Erwinia amylovora*, in 2000 in Michigan, resulted in apple losses of up to $42 million[43]. It is likely that there are hundreds of undiscovered floral fungal, oomycete, bacterial and viral pathogens that are not economically relevant.

Table 1.1 Floral microbes of high global importance.

Type of microbe	Latin/genus/group name	Common name	Host(s)	Tissue(s) infected	Mode of infection	Mode of transmission
Fungus	*Botrytis cinerea* (A)	Gray mold	Over 200 dicots (and some monocots) incl. grapes	All aerial parts of the host	Necrotroph	Wind and rain
	Claviceps purpurea (A)	Ergot	Range of grasses incl. cereals	Ovaries	Biotroph	Insects and rain
	Epichlöe (A)	e.g. Grass choke disease	Grasses – Pooideae	All aerial parts of the plant	Biotroph (endophytic)	Seed
	Fusarium graminearum (A)	Fusarium head blight	Small grain cereals – wheat, barley etc.	Floral tissues around anthesis	Hemi-biotroph	Insect, rain and wind dispersed
	Microbotryum violaceum (B)	Anther smut	*Silene latifolia*	Flowers	Biotroph	Insect (fungus sterilizes host replacing pollen with spores)
	Monilinia vaccini-corymbosi (A)	Mummy berry disease	Blueberries	Flowers	Hemi-biotroph	Insects (pseudoflowers)
	Tilletia indica (B)	Karnal bunt	Wheat	Infects grains at flowering	Facultative biotroph	Wind, seed and soil
	Ustilago maydis (B)	Corn smut	Maize	All aerial parts of the plant	Biotroph	Wind, rain and other vectors
Bacteria	*Erwinia amylovora*	Fire blight	Apple, pears and other Rosaceae	Flowers	Semi-necrotroph/ necrotroph	Insects, rain and wind
	Pseudomonas syringae pv. actinidiae (50 pathovars)	Kiwi bacterial canker	Kiwifruit	Flowers	Biotroph	Pollen, wind and rain
	Phytoplasma	e.g. Witches' broom	Over 100 species – monocots and dicots	Phloem (causes phyllody – floral tissue to leafy tissue)	Biotroph	Insects (e.g. leafhoppers)
Virus*	Cucumber mosaic virus	-	1200 species (monocots and dicots)	Systemic infection	Biotroph	Insects (aphids)
	Apple latent spherical virus	-	Apple trees	Systemic infection	Biotroph	Nematodes

NB: This table is not inclusive of all important floral microbes but focuses on those which have been thoroughly researched/published.
* Most viruses infect all tissues

As the climate changes, new disease associations are likely to emerge as pathogens move to fill new ecological niches, or alternatively may be more suited to infect new hosts and/or new niches in different climatic conditions. The rice blast fungus, *Magnaporthe oryzae*, is one such example, with it typically causing losses in rice yields. In 2016 Bangladesh first spotted outbreaks of this disease in wheat fields (the wheat infected strain is named *Pyricularia oryzae* pathotype *Triticum*) and could not immediately identify the causal organism, losses of up to 100% were observed [44]. Additionally, as a result of improved DNA extraction, sequencing techniques and ongoing research, previously undiscovered floral disease associations are being determined. Dead flower buds on pear trees were previously a mystery with no known causal agent identified; however, a significant number of affected flower buds are now known to be infected with *Alternaria*[45]. Furthermore, cashew powdery mildew has recently been attributed to two different pathogens, *Erysiphe quercicola* and *Erysiphe necator*[46].

1.2.2 Pathogen molecular, transcriptomic and gene function analysis in compatible floral interactions

A compatible interaction can be defined as one in which successful infection has been established, whereas an incompatible interaction is where infection is unsuccessful and plant defence has the upper hand. For floral pathogenic or mutualistic interactions to be compatible, a series of changes must occur at the molecular, transcriptomic and gene function levels; in this section I will solely focus on the pathogen. Comparative transcriptomic studies, involving *Fusarium graminearum* and its host wheat, have reported that *F. graminearum* is able to activate substrate-responsive and defence-responsive genes[47]. Microsatellite fragment analysis has been performed to indicate a high level of genotypic

variation in *Botrytis* spp. within a single strawberry blossom, demonstrating its ability to survive and adapt[48]. Moreover, a specific transcriptomic signature in bacterial witch's broom disease in soybean, leads to morphological and metabolic changes attracting insects to further disease transmission[49]. The use of transcriptomics in defining the biology of floral pathogens therefore has an extremely broad applicability.

When considering floral microbes at the molecular level, the role of effectors and effector-triggered susceptibility (ETS) is a well explored area of investigation. Interestingly, a topic which has been explored in multiple systems over the last few years is how effectors are able to extend their functions beyond the host, to either directly or indirectly interact with their corresponding insect vectors. The bacterial genus *Phytoplasma* produces effectors that are able to moderate host development and defence to attract insects. In one specific case, the effector SAP54 was shown to be required to attract leafhopper vectors independently of any developmental changes, with *Phytoplasma* being responsible for engineering leaf-like flowers[50,51]. At the gene level, transcriptomic studies carried out on thrips, which have been shown to transmit tospoviruses, have identified virus-responsive thrip genes which are most likely crucial for viral replication within the insect[52]. It is not only proteinaceous effectors that serve a crucial role in infection, with RNAs being shown to serve a role in bacterial movement inside the host. *E. amylovora* relies upon three Hfq-dependent (RNA chaperone) small RNAs (sRNAs) – ArcZ, OmrAB and RmaA – to regulate swimming motility in the host[53]. sRNAs have also been shown to aid the transmission of viruses by inducing early flowering, for example, potato spindle tuber viroid in tomato plants[54].

Crosstalk between the host and pathogen adds another level of complexity to these compatible interactions. Even though infection is allowed to occur, a large proportion of the time the pathogen does not remain undetected. A recent study analysed pathogen and host gene expression side-by-side – *Claviceps purpurea*, an ergot fungus which targets the ovaries, and *Secale cereale*[55]. This study demonstrated plant recognition of the fungus due to the upregulation of defence genes, but also a pathogen response via the detection of highly expressed redundant genes likely to be putative effectors[55]. Pathogens can also mimic host mechanisms and therefore remain undetected. The false rice smut fungus, *Villosiclava virens*, mimics ovary fertilisation upon infection and therefore encourages the plant to provide nutrients for false smut ball development[56].

Plant volatiles play a large role in plant defence and pathogen transmission, performing a role in pollinator attraction, and therefore to some extent the geographical location of the host. The ability of a pathogen to control the transmission part of its life cycle, whether by attracting more insects or by attracting more of a specific insect vector, gives a fitness advantage. For example, cucumber mosaic virus (CMV)-infected tomato plants (*Solanum lycopersicum*) and *Arabidopsis thaliana* emit volatiles which alter the behaviour of bumblebees (*Bombus terrestris*), making them more attractive to the hosts[57]. However, this is now thought to be mutually beneficial for both the pathogen and the host. Bumblebee sonication enhances pollen export, self-fertilisation and seed yield, without which the increased viral load would result in a decreased seed yield[57]. In turn this could outweigh the need for pathogen resistance and therefore susceptible individuals will remain in the population aiding viral transmission[57]. Although not strictly floral infection, many fungal pathogens rely

upon floral mimicry, producing pseudoflowers to spread infection via insect vectors relying upon visual or olfactory cues. *Monilinia vaccinii-corymbosi* (Mvc), which causes mummy berry disease in blueberries, produces pseudoflowers/infected leaves that produce the two floral volatiles cinnamyl alcohol and cinnamic aldehyde, attracting pollinators and favouring bees which are thought to be the most effective spore carriers for this disease[58].

1.2.3 Plant defence strategies against floral pathogens

Coevolving alongside their corresponding pathogens, plants themselves have developed defences to prevent or alter these interactions to their own advantage. Anti-microbial resistance is not discussed within this review due to the extensive amount of published research in this field, and because numerous reports have determined antimicrobials to not be floral-pathogen specific.

The reproductive success of a plant largely relies on flower development and high seed yields, consequently, stresses during this time can affect seed production. Evolutionarily, plants have adapted to coping with much higher levels of stress during this time, including pathogen attack, which can alter the flowering time of the host[59]. Age-related resistance is known to be a phenomenon whereby host resistance occurs as a plant develops and is sometimes triggered by the transition to flowering[59]. However, the molecular relationship between flowering time and disease resistance is remains unclear[59].

Changes in volatile composition as a tool to aid pathogen transmission has been discussed above, however plant volatiles are produced by all parts of the plant and are primarily used to attract pollinators and defend against herbivores and

pathogens. These volatiles can also be in the form of plant hormones. Many defence volatiles produced by the host also have antimicrobial properties, with many pathogens having evolved mechanisms to neutralise them, volatiles as antimicrobial compounds will be briefly addressed. Many volatile compounds are not floral microbe specific but are produced in response to a broad range of pathogens, enabling systemic signalling within a plant as well as between plants, avoiding vascular modes of communication which would likely take longer to establish and be manipulated by pathogenic mechanisms[60]. *A. thaliana* infected with *Pseudomonas syringae* pv. *tomato* DC3000, has been shown to have less bacterial growth than mutant plant lines lacking (*E*)-β-caryophyllene, a major volatile emitted by *A. thaliana* stigmas as well as the flower; cell damage was reduced and seed production was higher when the volatile was expressed suggesting a role in plant defence[61]. Volatiles with antimicrobial properties can be produced throughout the flower. Linalool is produced in plant nectar. In *Penstemon digitalis*, bacteria isolated from the floral tissue grew more slowly in response to linalool production in the phyllosphere[62]. Plant defence volatiles can also be both tissue-origin and substance specific[62]. Floral volatiles can be responsible for the bacterial composition of host tissues. Two floral volatiles, 2-phenylethyl alcohol and phenylacetonitrile, lower the diversity of bacteria on *Saponaria officinalis* flowers, making the bacterial communities of the hosts flowers and leaves fundamentally different[63].

Aside from flowering time and duration, which can be considered pre-formed plant defences, other floral responses to pathogens are induced upon infection. Many but not all these induced mechanisms alter hormonal pathways to bring about a response. An example of this was revealed by using virus-induced gene

silencing (VIGS) to silence the expression of a jasmonic acid biosynthesis pathway protein and an ethylene regulatory protein, demonstrating the need for these hormones in the defence of roses against gray mold disease caused by *Botrytis cinerea*[64]. Comparatively, RNA-seq analysis of this same interaction also revealed the need for brassinosteroids in petal defence against *B. cinerea*[65]. Furthermore, a transcriptional study in *A. thaliana* focused on flower-specific changes in response to fungal pathogen inoculation – changes were evident across different floral organs[66] . In the sepals, expression of genes for chemical stimuli and metabolic processes were upregulated with salicylic acid in both the petals and the sepals being higher than in the leaves, protecting the hosts reproductive organs[66]. When these hormonal pathways are manipulated by the pathogen plant defences are not only lowered, but viral insect vectors are also affected – a common theme seen throughout this review. Orthotospoviruses (some of which infect tomatoes) produce non-structural protein (NSs) which directly interacts with MYC signaling pathways, to regulate jasmonate[67] . This results in MYC pathway suppression and consequently the suppression of volatile monoterpenes, which would usually repel western flower thrips; this mechanism therefore allows the virus to increase vector attraction and enhance vector performance[67].

Detection of a pathogen by the host also leads to the activation of resistance genes (R genes), many of which are associated with quantitative trait loci (QTL). These traits can be determined by both genetic and transcriptional studies. *Claviceps purpurea*, the ergot fungus, prompted the discovery of four QTL's in the durum wheat cultivar, Greenshank, associated with ergot resistance, three of which had a disproportionate number of differentially expressed genes (DEGs)[68].

Alternatively, phenotypic attributes can be used as a starting point for mapping QTLs. Maize husks, layers of leaves which protect the ear from pathogenic attack, can vary in length, width and the number of layers between different inbred lines. Using linkage mapping and genome wide association studies, these three husk traits were found to be controlled by five genes situated within three QTL loci[69]. As previously discussed, many floral pathogens infect other plant tissues, including the Fire blight bacteria, *E. amylovora*. Studies mapping resistance to QTL's between this pathogen and one of its hosts, apple trees, have primarily focused on shoot infection rather than the more common floral infection; evidence now suggests that resistance in this case is independent of the targeted tissue, with both shoot and floral infection being controlled by a single major QTL[70].

On the other hand, defensive mutualism has been identified as a mechanism whereby a floral endophyte is able to protect its host from further pathogenic attack. Infections of grasses by *Epichloe* spp., seed transmissible ascomycete endophytic fungi which compete for photosynthates and flowers, have been shown to alleviate the symptoms of grass head smut, caused by *Ustilago bullata*[71].

1.2.4 Discoveries in the floral microbiome

Flowers are rarely, if ever, sterile, even when newly opened some microbial interactions are taking place. However, the variation in microbial composition between flowers of the same and different species, and within different floral tissues of the same flower, demonstrates the abundance and diversity of the floral microbiome[72]. The composition of the phyllosphere can be dramatically changed when a pathogenic microbe is present. However, where attempts have been

made to change the phyllosphere artificially, clearing the floral microbial niche, reducing native yeast, fungal and bacterial populations substantially, these niches were shown to recover within 24 hours[73].

Nectar is a well-studied example of how tissue-independent microbial colonisation can occur within the plant, in this case it is a result of visiting pollinators and nectar robbers. However, nectar robbers (carpenter bees) have been shown to increase microbial abundance by 10 times the amount than that following pollination (hummingbirds)[72]. Flowers that had experienced nectar loss were abundant in bacterial specialists that could cope with osmotic stress; Acetobacteraceae and Metschnikowiaceae[72]. This study therefore demonstrated the complexity between the visitor's flowers receive[72].

A pathogenic microbe's interaction, with other floral microbes, can influence the onset of disease and alter the microbial diversity within the flower. *Pseudomonas syringae* pv. *actinidiae* (*Psa*), the main causal agent of bacterial canker in kiwi fruit vines, interacts with epiphytic microbes on the leaves and flowers, altering the kiwifruit phyllosphere; this interaction also differed between highly cultivated kiwifruit species. For example, where *Actinidia deliciosa* was present large decreases in phyllosphere microbial diversity were seen (these tests were done on leaf tissue, but similar results are likely to also be seen in the floral tissue)[74]. A syndemic relationship between *Psa, Pseudomonas syringae* pv. *synringae* and *Pseudomonas viridiflava,* was also discovered leading to higher pathogenic capabilities[74].

1.2.5 What are the latest methodologies for studying floral microbes?

Many of the methodologies that were developed decades ago still come into play today and are used to generate new tools for studying floral microbes. Floral dipping as a plant transformation tool has been successfully used for decades, but the technique has recently been adapted for use in non-flowering organisms, such as the fungus *Epichloë*, to produce reporter strains using the fluorescent proteins GFP and DsRed in an attempt to understand the host-endophyte interaction, as well as interactions between different *Epichloë* species[75,76]. However here focus will be given to the many new and/or adapted methodologies that have been used over the last decade to gain a better understanding of phyllosphere composition and function. These include, the use of model floral systems, virus induced gene silencing (VIGS)/virus mediated overexpression (VOX), artificial inoculation techniques and new bioimaging procedures.

Twenty-five years ago, *A. thaliana* was established as a model plant, and has now been used to represent floral pathogen interactions for which *Arabidopsis* is not normally the host. In 2002 this was shown to be the case for *F. graminearum* and *Fusarium culmorum*, both of which can cause Fusarium head blight (FHB) in cereal crops by infection of the floral tissue[77]. Subsequent studies have used this pathosystem to determine variation in resistance as well as cellular, molecular and genetic mechanisms[77-79]. Plum Pox virus, a disease which causes fruit deformation, also has an *Arabidopsis*-based pathosystem established, allowing for research into resistant and susceptible traits[80,81]. More recently *A. thaliana* has been used as a model host for the false smut fungus, *Villosiclava virens*[82,83]. In this unlikely host, *V. virens* was shown to use an alternative defence gene repertoire (than in its main host rice) through the activation of certain pathogenesis-related genes[82]. This newly established pathosystem will therefore

now allow for molecular and genetic studies in an easier, more high-throughput manner[82].

VIGS can be used to study the molecular and genetic aspects of floral infection via gene silencing; utilising viruses which typically cause systemic infections, including in the floral tissues. *Microbotryum lychnidis-dioicae*, a smut fungus of *Silene latifolia*, causes masculinisation of female flowers. With the aim of determining how this fungal masculinisation is induced, and how sex is determined in the host, in future work, the apple latent spherical virus (ALSV) was used to produce a successful VIGS vector and was shown to migrate into the floral meristem[84]. ALSV has also been used for virus induced flowering (VIF), a method of inducing early flowering, whereby strawberry plants flowered approximately two months after inoculation, producing a useful tool for plant breeding[85]. VIGS can also be used in conjunction with other assays to identify new genetic traits. A tobacco rattle virus (TRV)-VIGS system, previously established in roses, has been used simultaneously with a detached petal disc assay (DPDA) to identify genes responsible for disease resistance against the fungus, *Botrytis cinerea*; RhLOX5 and EIN3, for jasmonic acid and ethylene mediated resistance respectively[64]. This assay not only works for functional analysis but can be adapted for high throughput uses[64].

Many adult plant inoculation assays face problems with large amounts of space in which to grow the host plants and conduct the assays, as well as the time and other resources needed. As mentioned above DPDA can solve some of these issues. *Colletotrichum abscissium*, a fungus which causes post-bloom fruit drop (PFD) in citrus can be inoculated onto citrus flowers *in vitro,* producing the typical

PFD symptoms, forming a high-throughput screen which does not have to be performed in the field[86].

Detecting individual infection phases is critical to understanding how to prevent plant pathogen attack. Thermal imaging is a relatively old technology that has recently been used to detect infected plants before they reach the symptomatic phase of infection. Rose powdery mildew (*Podosphaera pannosa var. rosae*) and gray mold (*B. cinerea*) can both be detected using thermography. Rose powdery mildew results in the development of small water-soaked areas which decrease the temperature of the leaf[87]. Similarly for gray mold, areas of the leaf where small lesions form exhibit a decrease in temperature[87]. However tissue necrosis leads to a temperature increase[87]. Development of the cut-flower dye (CFD) assay has generated an alternative visualisation methodology for assessing tissue damage. CFD allows cut white flowers to be dyed any colour. Taking into account that damaged tissue will be unable to transport water and dyes can be used to visualise hyphae, this system can help visualise floral tissues that are usually difficult to analyse. The fungus *M. oryzae* causes rice blast which can affect the panicles. The panicles are difficult to section for imaging purposes, and like all rice tissue, tend to wither and lose their colour shortly after being sampled[88]. CFD has therefore helped detect rice blast within the panicles, highlighting lesions and areas where fungal hyphae has blocked the vascular tissue[88]. This methodology also allows for digital image capture and follow up computational-based analyses.

The detection of different infection phases does not only rely on bioimaging. qPCR has been adapted to identify different stages in the life cycle of *Monilinia* spp. – fungal pathogens that cause disease in the blossoms and fruits of stone

fruits. For *Monilinia fructicola,* qPCR combined with propidium monoazide (PMA) (a photoreactive DNA-binding dye used to detect viable cells), referred to as PMA-qPCR, has been used to distinguish between dead and viable conidia; few studies have used this technique to quantify viable fungal bacteria[89]. To control the spread of *Monilinia* spp. the latent phase of infection has also been successfully identified in asymptomatic fruit and flowers using qPCR[90].

1.2.6 Applied uses of floral microbe research

As described above, VIF has been developed as a useful tool for plant breeding, allowing for induced flowering in not only strawberries but also apples and pears[91]. This is now a developed technique that can be applied in the field. As this has already been discussed briefly in this review, it shall not be explored further here.

The vast array of floral microbe antagonistic interactions has led to the development of many novel biocontrol strategies. Distributing biocontrol agents (BCA) by using natural vectors would allow for increased efficacy of BCAs through targeted floral-specific delivery systems. *E. amylovora* is detrimental in apple and pear orchards. Using the Japanese orchard bee, *Osmia cornifrons*, a *Bacillus subtilis* control agent was shown to be efficiently dispersed to apple blossoms, effectively combatting *E. amylovora*[92]. Secondary inoculation, of newly opened flowers has also been achieved using vector delivery[92]. This technique can now be considered for other top fruit orchard or glasshouse-based horticultural or flower production pathosystems. In an earlier study, *E. amylovora* was mutated to investigate the primary metabolites needed for full virulence. Pre-treatment of apple flowers with an arginine-auxotroph suggested that this non-

pathogenic strain could be used to treat wild-type *E. amylovora* as a result of nutritional competition[93].

Nanoparticles have antimicrobial properties. There are many reasons for this including: enzyme inhibition and disruption of membrane and cell wall biosynthesis[94]. Whilst these have been tested extensively in medicine, their applications in plant research have only just begun to surface. Nanoparticle compounds (metallic and non-metallic) have been shown to have antifungal properties on *B. cinerea* inoculated rose petals and silver nanoparticles have been applied to paper packaging used to transport orchid flowers, reducing *Colletotrichum gloeosporioides* infection[95,96].

Protocols for detecting early infection in plants have already been mentioned in this review, however, this has relied upon the development of already existing methodologies such as PCR and thermal imaging, which rely on taking samples and therefore are limited by the small scale of work possible. The honeybee, *Apis mellifera,* can be used to detect early viral infection. By visiting a large cohort of flowering plants, collecting pollen and nectar, honeybees were able to provide a sample for high-throughput sequencing, allowing for the early detection of viruses within specific geographical regions[97].

1.2.7 Newly recognised floral pathogen problems

Climate change and habitat loss are two factors responsible for altering species distributions. Species that are not native to a geographical area bring with them pathogens that currently do not exist within that region, resulting in species that were currently sheltered from these pathogens suddenly being exposed.

Pollinator decline can partially be attributed to a phenomenon known as pathogen spillover. The honeybee, *A. mellifera*, is usually managed and therefore can be introduced into an area where their range overlaps with native bees. However they can carry the parasite, *Nosema ceranae,* the causal agent of nosemosis which shortens the lifespan of the infected bee[98]. In laboratory conditions where both *A. mellifera* and the Australian stingless bee, *Tetragonula hockingsi,* were present, the parasite was shown to be transmitted via flowers and was able to establish in the *T. hockingsi* population[99]. On the other hand, a simple solution to help stabilise pollinator populations may be to meet certain dietary requirements – in bees this stimulates a stronger immune response[100]. Sunflower (*Helianthus annuus*) pollen has been shown to reduce *Crithidea bombi* (protozoa) infection in bumble bees (*Bombus impatiens*) and *N. ceranae* infection in the European honeybee (*A. mellifera*)[100].

Interestingly, a similar concept has been explored in mosquitos, whereby sugar meal (nectar and fruit) intake affects the transmission of parasites carried by the insects. *Anopheles coluzzii* is a vector for the *Plasmodium falciparum* parasite which typically causes malaria in humans. Different plant sugar sources were able to either positively or negatively affect parasite development and transmission intensity[101]. Therefore, a move to plant species, whose flowers and fruit negatively impact these traits could help control these non-plant diseases[101]. Diseases could also be passed through mosquito populations, with nectar being a potential pathogenic source. *Francisella tularensis*, a bacterial pathogen which causes disease in humans, can be distributed this way, having been shown to survive in nectar, with mosquitoes that feed from infected sources becoming colonised by the pathogen[102].

1.2.8 Concluding remarks

Floral microbes are at the centre of the food security crisis we face today. Pathogenic fungi, oomycetes, bacteria and viruses, as well as their insect vectors, are given the most attention and focus in our attempt to prevent and control devastating global plant diseases. However, those microbes that work mutualistically with their hosts and thrive alongside one another are just as important. Phyllosphere research over the last decade has shown the extent of these relationships, demonstrating new methodologies in which we can begin to understand these interactions and new problems we may face in the future. Further translation of the findings described in this review is needed if we are to develop disease control strategies and utilise beneficial microbes. With a constantly changing climate, new microbial interactions will develop, and further discoveries will come to light.

This review section of the introduction will be converted in due course to a standalone review and the appropriate journal for publication will be sought, for example, Annual Review Phytopathology, Trends in Plant Sciences, PloS Pathogens.

1.3 Fusarium head blight (FHB) and its impact in cereal agriculture

The genus, *Fusarium*, is now the third largest group of filamentous fungi. Some have a sexual phase whereas others do not. Many cause plant infections in a range of hosts in mainly sub-tropical and tropical conditions whilst others are major pathogens in regions with a moderate temperate climate. A survey of the most critical plant-pathogenic fungi identified both *Fusarium graminearum*, the

main causal agent of Fusarium Head Blight (FHB) in all small grain cereals, and *Fusarium oxysporum,* which causes wilt and stem rot in a range of hosts, in the top 10 fungal pathogens – these were ranked in order of their scientific and economic importance[103,104]. An assessment undertaken by the American horticultural society demonstrated that of 108 plant species of agricultural and horticultural significance, 83 have their production affected by one or more *Fusarium* species[103]. Many of these pathogens are of no threat to humans or animals, however the production of mycotoxins by some can make infected crops unsuitable for human and animal consumption. Additionally, some species can cause diseases in immunocompromised humans[105-108]. However, it should also be noted that not all *Fusarium* species are harmful, for example *Fusarium venenatum* is a popular meat substitute (Quorn™)[109].

1.3.1 FHB and its economic impact

As previously mentioned, 20-40% of crop yields are lost annually as a result of pests and plant pathogens[26]. However, up to 20% of crop losses can be accounted for by fungal plant pathogens[110]. Between 1993 and 2001 FHB has accounted for losses of approximately $2.492 billion (hard red spring wheat, soft red winter wheat, durum wheat and barley)[111]. With both direct and indirect losses this is thought to have reached an estimated $7.7 billion – more recent statistics are unavailable[111]. Crucially, China, Russia, India, France and the USA account for up to 50% of the world's wheat production, with all five countries reporting regular FHB epidemics[112,113]. These losses are not just restricted to the farmers; economic impacts are felt by those in regional economies, including those in the retail trade and insurance[114]. Economic losses are largely accounted for by reductions in grain quality, but also grain yield and ecosystem health. FHB is a

disease of all small-grain cereals including wheat and barley. *F. graminearum* (teleomorph *Gibberella zeae*) is now the main causal agent of FHB. However, several other *Fusarium* spp. also cause FHB, as a part of the *F. graminearum* species complex (FGSC), including *F. acaciae-mearnsii*, *F. aethiopicum*, *F. asiaticum*, *F. austroamericanum*, *F. boothii*, *F. brasilicum*, *F. cortaderiae*, *F. gerlachii*, *F. louisianense*, *F. meridionale*, *F. mesoamericanum*, *F. nepalense*, *F. ussurianum*, and *F. vorosii.* *F. culmorum* is also a well-known causal agent of FHB but is not included in the FGSC. *Microdochium* spp. are also known to cause this disease[114,115].

Population shifts in FHB pathogens have been reported by various different surveys which have been associated with larger yield losses as a result of increased pathogen toxicity, aggressiveness and mycotoxin changes[114,116]. A main influential factor to these population variations is climate change. For example, it is well known that *F. graminearum* related FHB epidemics tend to occur when there is an optimal combination of environmental conditions. Europe has seen a shift from FHB being mainly caused by *F. culmorum,* to *F. graminearum* becoming the main causal agent [114]. Various reasons have been theorised about this species shift but none have significant evidentiary backing. Currently these consist of, a) importation with another industry such as maize production, b) higher temperatures and more humid conditions favouring *F. graminearum,* and c) certain aspects of the *F. graminearum* lifestyle, including ability to sexually reproduce and production of ascospores and aggressiveness. These phenotypes would all give *F. graminearum* an advantage over *F. culmorum*[114,117-119]. This trend remains for the majority of European countries, however Italy has seen a shift away from *F. graminearum* as the main cause of FHB, to *F. poae*.

Figure 1.1 – *Fusarium graminearum*-induced Fusarium head blight epidemic distribution. Recorded distribution (black dots) of *F. graminearum* and the modelled predicted distribution (grey) with continued climate change – based on meteorological data taken from 1950-2000. Taken from Backhouse (2014).

The distribution of FHB epidemics because of *F. graminearum* has the potential to spread, and this has successfully been modelled, taking into account nine different parameters describing the full annual climate (BIOCLIM)[120]. The predicted distribution for *F. graminearum* was seen to be much more extensive than its current distribution, with epidemics extending into most major areas of rain-fed wheat production (Fig.1.1)[120]. Many pathogens have a high potential for genetic adaptation allowing them to spread to areas they have previously not been recorded, which brings additional problems. Knowing the species and mycotoxin profile is critical to detect toxins in the food supply chain as well as to evaluate the risk of contaminated grain[114]. Knowing the *Fusarium* species responsible can also help monitor the spread of the disease as well as inform and optimise management strategies.

1.3.2 Mycotoxins

Mycotoxins can be defined as toxic secondary metabolites secreted by a fungus. Several have been associated with the *Fusarium* genus. Whereas *Microdochium* spp. responsible for FHB disease do not produce these toxins. Mycotoxins typically contaminate cereal grains but have also been shown to contaminate other food crops, especially nut bearing species[121]. Contamination makes the grain unsuitable for human and animal consumption and can lead to mycotoxicosis, if consumed either directly or as part of a food chain [79,106-108,122,123]. Mycotoxicosis can either be an acute or chronic condition depending upon the duration of exposure and the dose, with chronic exposure usually being defined by low dose exposure over an extended period of time, leading to cancers (if the mycotoxin is carcinogenic) and other irreversible conditions[124-126]. Mycotoxicosis can also lead to societal problems when contaminated grain is consumed locally.

Mycotoxins are produced upon induction of secondary metabolite clusters or biosynthetic gene clusters (BGC). These usually consist of two or more genes situated together in the genome[127]. BGC's for mycotoxins include genes with a range of functions, including enzymes for alteration of the parent structure, genes that assist in metabolite transportation and expression regulation, as well as those that encode for other proteins such as polyketide synthases (PKS) and non-ribosomal peptide synthases (NRPS), amongst others[128,129]. There are still some uncertainties as to how and why mycotoxins are produced by *Fusarium*, but research in this area will be critical in controlling the disease and preventing grain contamination[128].

Fusarium fungi produce a range of different toxins including the fumonisins, zearalenones and the trichothecenes. The economically important maize pathogen, *Fusarium verticillioides*, produces Fumonisins, although non-producing isolates remain fully virulent[126,130,131]. Adverse health effects are inconclusive but there is evidence to suggest Fumonisins can contribute to cancers and birth defects[132]. Fumonisin B_1 is the major form found in food and has been shown to be highest in maize/maize-based products[132]. In some parts of the world contamination levels in maize can reach as high as 100 mg/kg[133]. Regulatory standards for Fumonisins in the European Union (EU), state limits of 4mg/kg (4ppm) and 1mg/kg (1ppm) for foods requiring further processing and unprocessed foods respectively. Fumonisins are synthesised by condensation of alanine into an acetate-derived precursor[126,134]. Fumonisins are structurally similar to sphingoid bases and are therefore thought to operate via disruption of sphingolipid metabolism (Fig.1.2)[135].

Zearalenones (ZEA), non-steroidal estrogenic metabolites, are another group of mycotoxins produced by several *Fusarium* spp. including *F. graminearum*[126]. High levels of these toxins are usually detected in animal feed as a result of improper storage – these toxins are therefore particularly important with respect to livestock[136,137]. ZEA's are naturally produced by some crops, such as maize, but can contaminate other's including wheat, barley and rice[136]. Their heat stability means ZEA's are unlikely to be successfully eradicated from the food chain and are responsible for reproductive problems in domestic animals and hyperestrogenic syndromes in humans[136,138]. ZEA's have a chemical formula of $C_{18}H_{22}O_5$ and in *F. graminearum* are synthesised via the polyketide pathway (Fig. 1.2)[126,136].

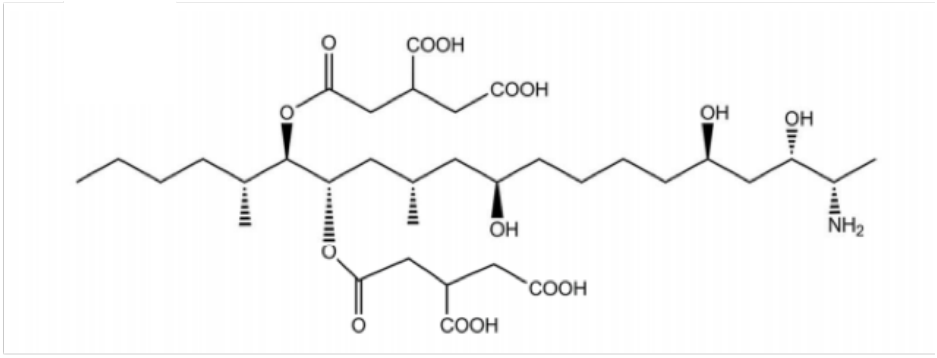

Fumonisin B_1

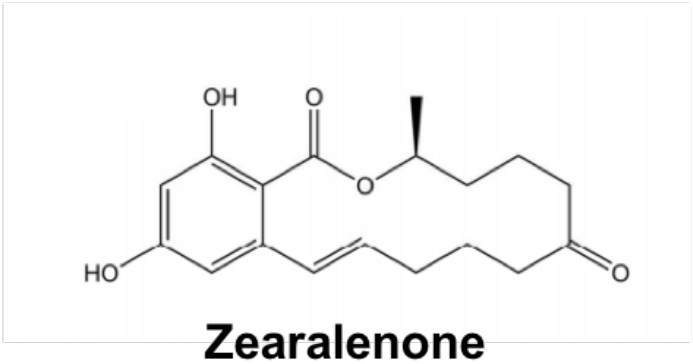

Zearalenone

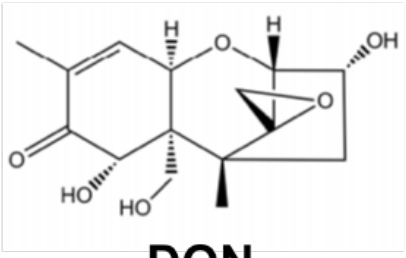

DON

Figure 1.2 – Chemical structures of Fusarium mycotoxins. Only the main toxins mentioned in the main text are represented here. Images taken from Huang *et al.* (2018).

Trichothecenes can be considered of great economic importance and have a significant impact in the cereal agriculture industry[104]. Some of the most well studied include: deoxynivalenol (DON), nivalenol (NIV) and T-2 toxin, and can be essential for virulence[79,128]. Trichothecenes are extremely diverse, non-volatile, sesquiterpenoids and are characterised by a C9,10 double bond and a tricyclic 12,13-epoxytrichothec-9-ene (EPT)[128]. Variation in the 15 carbon backbone as well as variation in the functional groups attached to this is what allows the trichothecenes to be categorised into four groups: type B trichothecenes have an additional C8 keto group in comparison to type A and is where DON and NIV fall, types C and D are non-Fusarium mycotoxins and will therefore not be discussed further[106,128]. It was originally thought that trichothecenes worked exclusively through the inhibition of protein synthesis but is now considered more complex, involving a ribotoxic response activating mitogen activated protein kinases (MAPK)[106,139,140]. DON, commonly referred to as vomitoxin, is one of the most common contaminants found in grain and is commonly produced by *Fusarium* spp., including *F. graminearum* and *F. culmorum*, being present in 90% of all samples analysed (Fig.1.2)[141]. DON will be discussed more extensively in 1.3.3.

Similar to a change in FHB species distribution, there has also been a transition in DON mycotoxin chemotype distribution. North America has shown a transition in the mycotoxin chemotype of *F. graminearum*, from 15-acetyl DON (ADON) to 3-ADON, with the distribution of these populations rapidly expanding[114]. The dynamics of this are still unclear with many hypotheses being disproved – such as 3-ADON having increased aggressiveness in comparison to 15-ADON isolates as a result of higher levels of trichothecene production and faster growth; however it is likely a result of combinations of factors already discussed[114,142].

1.3.3 DON and the *F. graminearum* toxisome

The trichothecene mycotoxin, DON, is essential for successful *F. graminearum* infection in wheat. Although not necessary during initial infection, DON is needed to suppress host defences during the colonisation process, such as cell wall thickening at the rachis[143]. Fifteen *TRI* genes are responsible for producing the enzymes needed for trichothecene synthesis, located at three different loci on different chromosomes – with the main cluster consisting of 12 of these genes[144]. Of these, *TRI5* is the most well characterised and is responsible for the first step in the trichothecene biosynthetic pathway, producing the enzyme trichodiene synthase[122]. Expression of TRI5 is highest at the infection front, with strong expression in the rachis tissue[145]. Trichothecenes act as virulence factors in plants. *TRI5* knockout mutants have reduced virulence in comparison to the wild-type strain and strains that do not produce DON cannot spread within the plant tissue successfully[79,143].

To avoid the harmful effects of mycotoxins themselves and make secondary metabolite synthesis more efficient, one mechanism employed by the fungus is to compartmentalise parts of these secondary metabolite biosynthetic pathways into organelles called toxisomes[146-148]. For DON the two enzymes produced by genes *TRI1* and *TRI4*, cytochrome P450 oxygenases, both localise to toxisomes[149]. Toxisomes are thought to form from organised smooth endoplasmic reticulum in response to trichothecene induction[147]. Recently an *F. graminearum* class I myosin has been shown to interact with TRI1 and participate in toxisome formation[149].

As a result of the hazards mycotoxins pose to both humans and animals, regulations have been put in place to ensure damaging levels do not enter the food chain. The farmer, merchant or processor is responsible for these limits, and

they may require lower concentrations on intake so the grain conforms to legal levels at the end of the production process[150]. Often mycotoxin hotspots occur within a harvest and/or shipment and therefore standards have been put in place to enable an accurate mycotoxin concentration calculation, taking into account the entire harvest[151]. For DON and ZEA the tolerable daily intake (TDI) has been set at 1 and 0.2µg/kg bodyweight/day respectively by the European Commission Scientific Committee on Food (SCF)[152]. Legal limits are also in place for other mycotoxins worldwide – Fig. 1.3.

1.3.4 The *F. graminearum* life cycle

F. graminearum infections are most devastating during crop anthesis which causes increased susceptibility[153]. Over-wintering saprophytically on crop debris, sexual ascospores or asexual conidia gradually develop over several months[113]. When moist conditions prevail spores are subsequently dispersed via wind, rain or insect-mediated mechanisms, landing within the wheat floral tissues (Fig.1.4)[113,153,154]. Once the anthers protrude from the wheat ears, they tend to crack open resulting in a natural wound being present to allow hyphal entry and growth along the anther filament before colonisation of the spikelet.

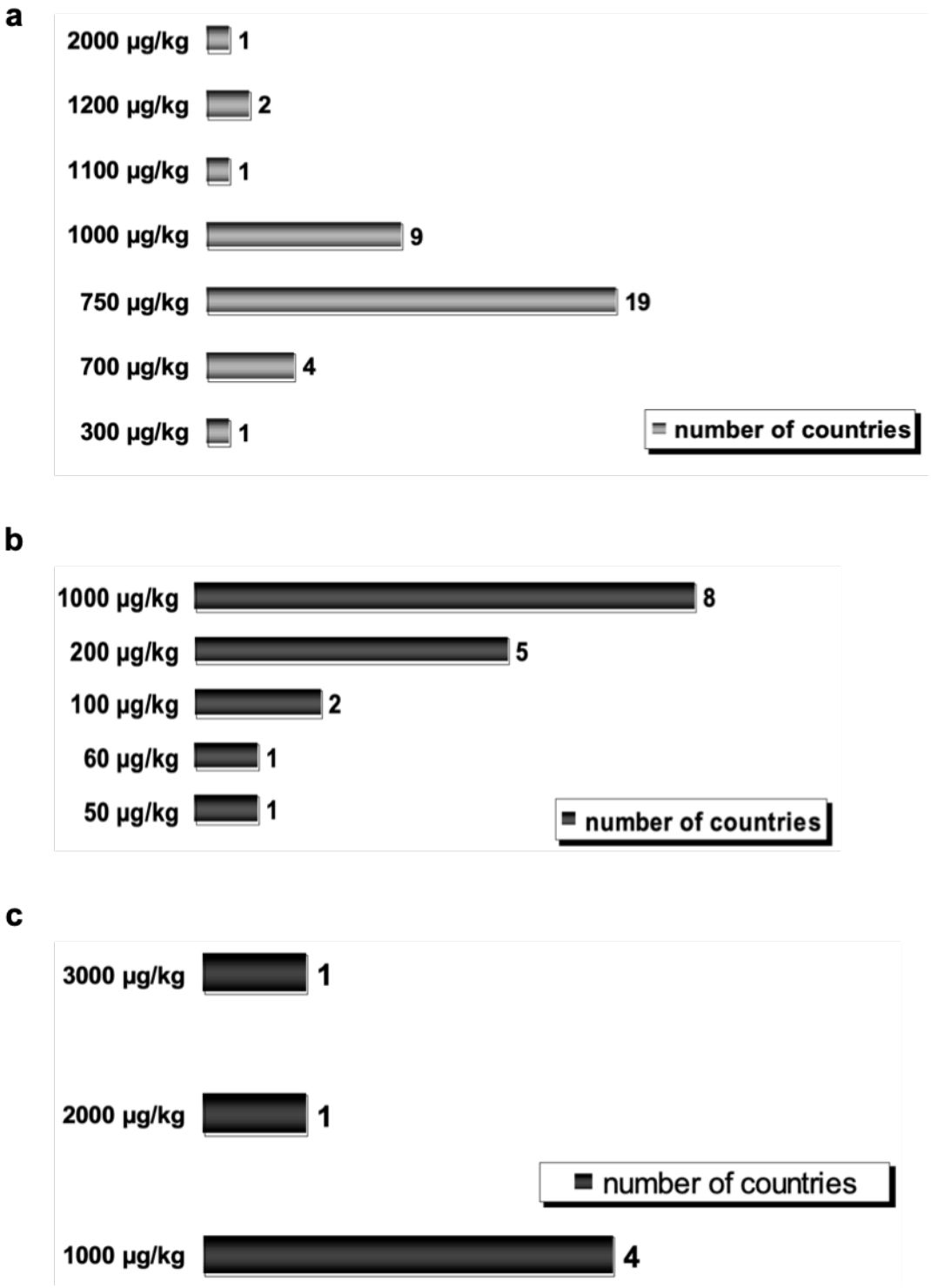

Figure 1.3 – Worldwide mycotoxin limits. (a) Worldwide limits for DON in wheat (flour) and other cereals. (b) Worldwide limits for ZEA in maize and other cereals. (c) Worldwide limits for fumonisins in maize. All figures taken from Mycotoxin regulations in 2003 and current developments http://www.fao.org/3/a-y5499e.pdf

Following spore germination on the abaxial surface of the glumes or in the florets, approximately 6-12 hours post inoculum (hpi), entry into the host can also be gained via the stomata or other wounds as well as via the glumes. The fusaria are non-appressorium producing unlike other filamentous ascomycetes[154,155]. Specialised, unbranched, runner hyphae growing epiphytically on the surface of the plant form infection cushions, an organised hyphal mass from which infection hyphae are produced[156,157]. Infection cushions synthesise a plethora of enzymes such as cutinases, peptidases, lipases and cellulases, which degrade the plant cuticle and cell wall[156,158-161]. There is some evidence to suggest that during anthesis the chemical composition of the glumes is altered making them more susceptible to infection, however this still remains unclear[154]. By 24-36 hpi *F. graminearum* produce infection hyphae which in turn allow the fungus to produce penetration pegs and invade the ovary, lemma and palea (inner side)[155]. It is towards the end of this stage where the unbranched hyphae begin to grow intercellularly, colonising the areas around the cells with some intracellular growth i.e. pericarp parenchyma cells of the ovary, this resembles a biotrophic infection stage[155,162]. Changes in the host cells also occur, with cells in the parenchyma collapsing, cell wall structure and composition changes and the degradation of organelles and cytoplasm[155]. These first few days of infection are asymptomatic, i.e. no macroscopic symptoms can be seen, and minimal plant defence responses are mounted as the fungus colonises the tissue[113]. There is little evidence to suggest the fungus gains nutrients from the plant at this stage, which leads to some controversy as to whether the fungus has an initial biotrophic phase as part of a hemibiotrophic life cycle. *F. graminearum* utilises its own energy stores in the asymptomatic phase of infection.

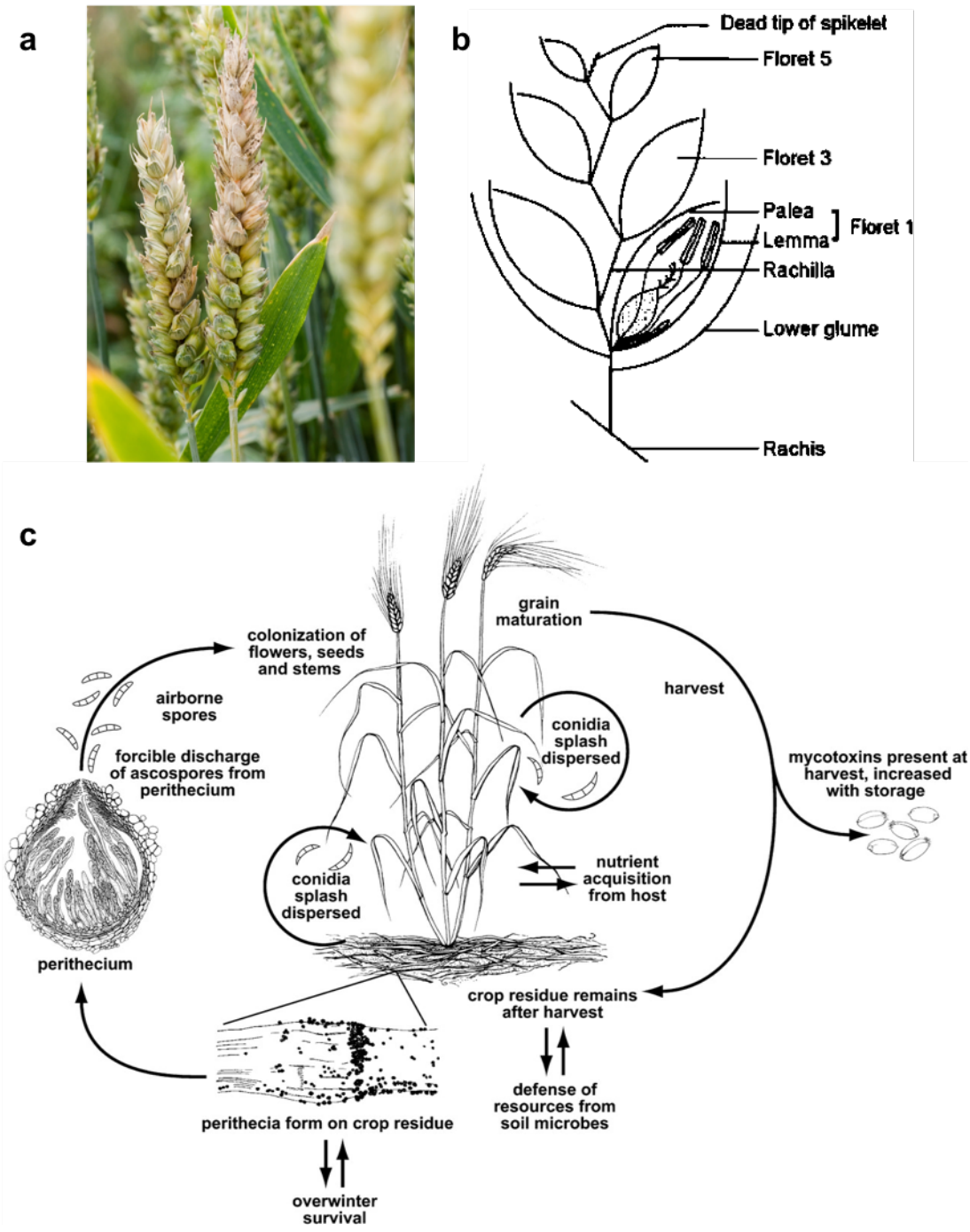

Figure 1.4 – *Fusarium graminearum* infection. (a) Fusarium head blight occurs soon after the wheat spike has flowered causing characteristic tissue bleaching (image provided by the Rothamsted Research Visual Communications Unit). (b) Wheat spikelet diagram to aid understanding of *F. graminearum* infection mechanisms. Taken from Kirby and Appleyard (1987). (c) Sexual life cycle of *F. graminearum* in wheat. Taken from Trail (2009).

At around 5 days post-infection (dpi) the hyphae reach the rachis, colonising the vasculature as well as the cortex[143,155,163]. A switch to the symptomatic phase results in premature floral tissue senescence and partial or entire wheat ear bleaching. The grain itself is colonised by the fungus, becoming shrivelled and undersized as it is contaminated with mycotoxins[164]. Within the wheat tissue cell death occurs, necrotic lesions form and the vascular tissues become occluded[113,165]. The transition between asymptomatic and symptomatic phases corresponds to one of intercellular to intracellular hyphal growth (Fig.1.5)[113,165]. Eventually cells collapse (phloem, chlorenchyma and parenchyma) as a result of hyphal colonisation and mycotoxin induction with the culm and pith cavity being colonised by 12 dpi[166,167]. Multiple mechanisms are utilised by *F. graminearum* hyphae to traverse host cell walls. Intercellular hyphae possess the ability to directly penetrate host cells[113]. Alternatively, intracellular hyphae can produce penetration pegs, as well as utilise pit-fields (PFs) by temporarily restricting their diameter[113]. Sporulation then occurs within the infected florets allowing for the continuation of host infection (Fig.1.4).

The infection process has been spatially, temporally, phenotypically and transcriptionally determined within a single wheat spike, with the hyphal infection front penetrating the tissue at least 1cm ahead of any macroscopic symptoms[113,168]. Once the host cell has been intracellularly colonised, host cell organelles and nuclei are lost[113]. Fungal biomass also decreases due to self-autophagy until asexual sporulation occurs at external surfaces[113].

1.3.5 The *F. graminearum* genome

The fully assembled and annotated *F. graminearum* genome was first published in 2007[160]. The reference genome for the *F. graminearum* isolate PH-1 (NRRL 31084), was nearly completed in 2014, with the remaining two gaps and misassembles in the genome being corrected in 2017[169,170]. PH-1, originally identified in North America, was chosen as the reference genome for a number of reasons: sporulation stability, ease of culturing, high virulence and consequently high DON production. The PH-1 genome is mapped onto four chromosomes and is a total of 38.06 Mb in size[160]. There are a substantial amount of hypervariable regions (HVRs), exhibiting high levels of recombination, within the genome, but no active transposons. Some of these HVRs contain gene clusters responsible for the production of various known and unknown secondary metabolites and toxins, some of which have been discussed above[160,169].

A well annotated genome has resulted in accurate effectome and secretome predictions, approximating 600 effector proteins; effectors are molecules produced by a pathogen to manipulate host metabolic processes[171]. Many of these lack annotations and have no predicted functions, however proteins/enzymes involved in cell wall degradation are abundant in the *F. graminearum* genome, in comparison to many other fungal pathogens, for example the *Zymoseptoria tritici* genome has relatively few[171]. Most of these identified putative *F. graminearum* effectors have unknown functions. Recently three effector genes, highly induced during the first week of infection, *FGSG_01831, FGSG_03599* and *FGSG_12160,* were all shown, when transiently expressed in *Nicotiana benthamiana*, to suppress chitin induced reactive oxygen species (ROS) production and to affect plant immunity[172]. However only *FGSG_01831* had any effect on FHB, reducing DON

contamination and the impact of initial infection[172]. There are more than 70 gene clusters responsible for the production of secondary metabolites and toxins, some of which have been discussed above.

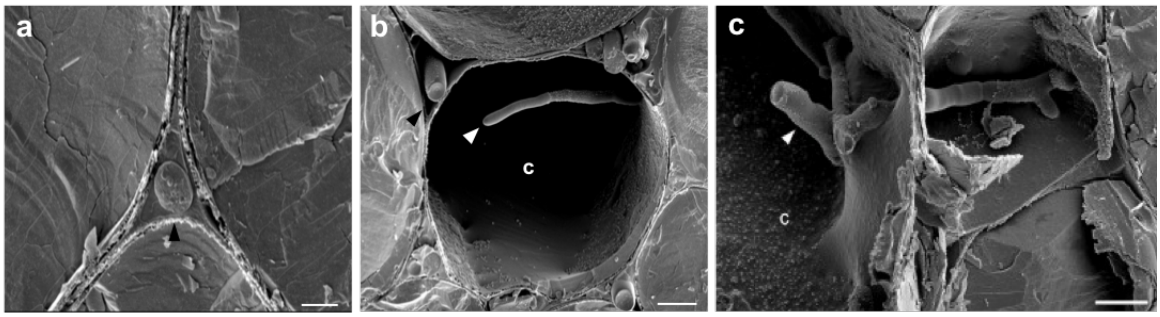

Figure 1.5 – Transition of hyphal growth during *Fusarium graminearum* infection. (a) Hyphal invasion during early infection of wheat tissue. Hypha can be seen growing extracellularly between live plant cells. (b) Hyphal penetration of dead host cells. (c) Hyphal grow between host cells utilising pit-fields. Black arrowheads = intercellular hyphae, white arrowheads = intracellular hyphae, c = cortex. Bar = 10 µm. Taken from Brown, Urban *et al.* 2010.

1.3.6 Current *F. graminearum* infection model

In 2017 a study on the spatial-temporal analysis of the wheat-*F. graminearum* transcriptome during asymptomatic and symptomatic infection, published an infection model of this interaction – see Fig. 1.6[168]. This model allowed for the comparison between this transcriptomic data and the previously characterised histological data providing the field with the first insight into the virulence strategies employed by *F. graminearum* in the rachis tissue during infection[113,165]. In the years since its publication new information has arisen, including the discovery of lipase Fgl1, and effectors FGSSP6/7 and FGSSP32/33 (unpublished), with some information important to the infection process not being included, for example, the use of PFs by the fungus to travel intracellularly[113,159].

New models will therefore need to be produced as more infection mechanism evidence comes to light.

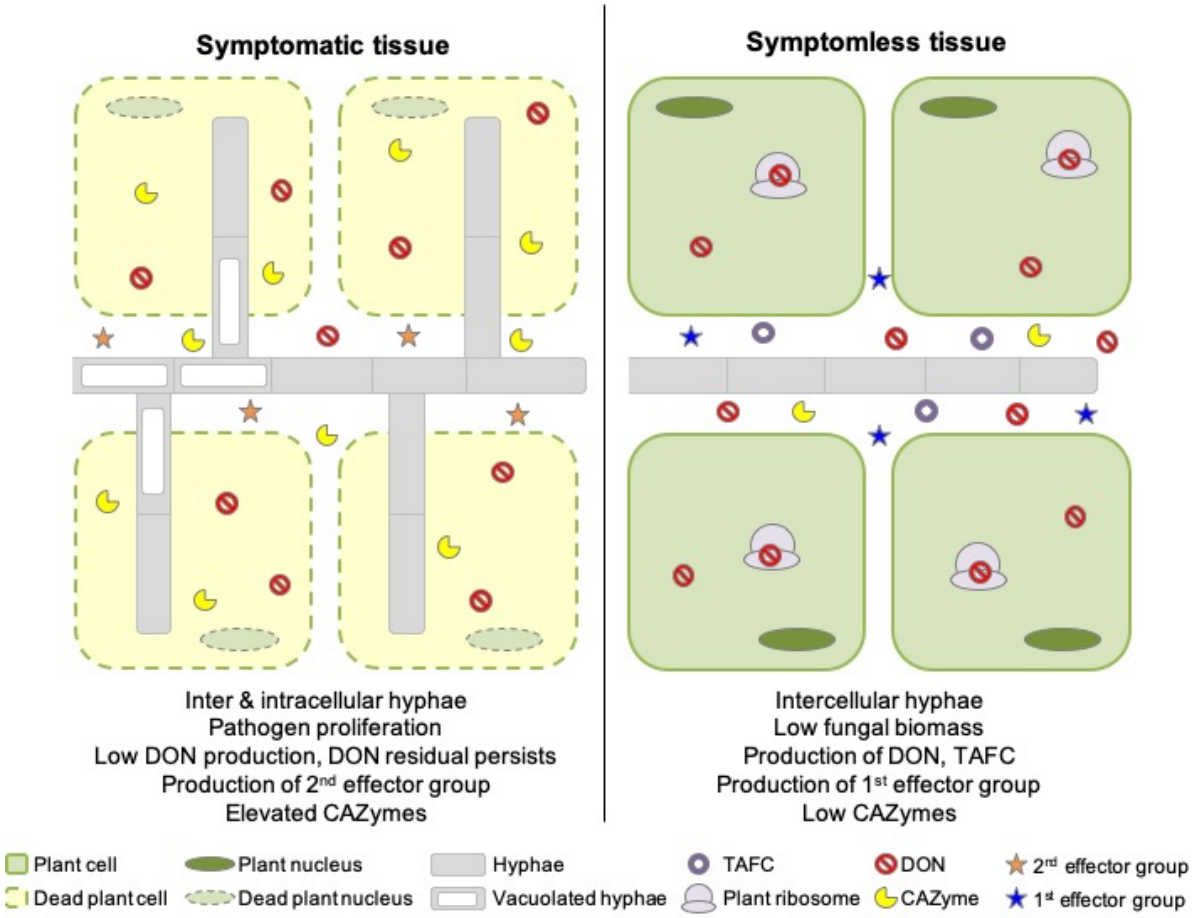

Figure 1.6 – A spatial temporal model for *Fusarium graminearum* infection of wheat floral tissue. A depiction of putative virulence strategies initiated during compatible interactions during the symptomless and asymptomatic phase. CAZyme, carbohydrate-active enzyme; DON, deoxynivalenol; TAFC, triacetyl fusarinine C. Taken from Brown et al. 2017.

1.3.7 Management of *F. graminearum*

F. graminearum is typically managed through the application of fungicides as well as through the use of partially resistant cultivars – however this is insufficient to prevent disease[104]. As FHB epidemics are becoming more frequent and more widely distributed it is important *F. graminearum* control is improved. There are

several approaches to this, from cultural practices to disease forecasting, some of which will be discussed here.

Two common cultural approaches to the control of FHB are crop rotation and tillage. Crop rotation, whereby in between each susceptible crop plantation a non-host crop is sown, has been shown to decrease FHB intensity as well as DON concentration. One study was able to demonstrate that a lower FHB intensity was seen after a wheat-soybean rotation, with DON levels being 25% lower in wheat, with higher inoculum levels being found after a wheat-maize rotation, as a result of corn residue maintaining high inoculum levels over-winter[173,174]. However, taking this approach has little economic benefit to the farmer and therefore may not be a viable option. On the other hand, deep tillage helps to bury infected crop residue and thereby reduce FHB disease intensity. However, this type of intense cultivation can lead to soil erosion which is not beneficial for food production in the long run[174]. Irrigation management is also an approach that can be taken. For successful infection *F. graminearum* needs warm, moist conditions, therefore in areas where rainfall is minimal controlling watering of the crops may be beneficial to the farmer[174].

The most cost-effective approach to FHB control is to find or breed cultivars with genetic resistance – however most cultivars are only partially resistant. In broad terms there are three main forms of resistance: type I – resistance to initial pathogen penetration, type II – resistance to disease spread within the spikelet, and type III – low mycotoxin accumulation[175]. In practice only type II resistance has been successfully deployed by plant breeders and is used in commercial crops[175,176]. Wheat accessions with complete FHB resistance have not been

found[175]. Type II resistance traits are controlled via numerous major and minor quantitative trait loci (QTL). The *Fhb1* QTL from the Sumai-3 cultivar is to date the most successfully deployed but, shows varying levels of resistance across different genetic backgrounds[175]. Even though there have been various attempts to breed this QTL into various wheat cultivars only a few attempts have been successful[175]. Many locally bred cultivars also show varying levels of FHB resistance, however the QTL's responsible for these traits have a considerably smaller effect than *Fhb1*[175]. Many QTL's have an additive effect, meaning a combination of FHB resistant QTL's is usually greater than just using one alone – which is the case when using *Fhb1* with other QTL's[175,177]. In 2008, seven genes within the *Fhb1* QTL interval were cloned and evaluated, but none were found to function in FHB resistance[178]. Recently, the wheat gene *WFhb1-1*, previously shown to reside within the *Fhb1* QTL, has been cloned and shown to be an important FHB resistance gene with potential antifungal properties[179-182]. As a result of these major breakthroughs FHB resistance improvements in wheat and other cereal other crops will be forthcoming[183].

Chemical control via fungicide applications is one of the most common approaches taken and can offer some crop protection but does not come without its own challenges. The fungicides most commonly used against FHB are the demethylation inhibitors (DMI), and include: metconazole, propiconazole, prothioconazole and tebuconazole. Combinations of these are used as a result of *F. graminearum* being intrinsically resistant to azole fungicides[174,184]. These are typically applied at the anthesis stage or shortly after, i.e. the T3 spray, as this is when the crop is most susceptible to FHB. However not all tillers will flower simultaneously meaning a single fungicide application may not protect the crop

sufficiently. The timing of fungicide application is therefore critical; one study demonstrated that application of fungicide 20 days after anthesis reduced mycotoxin accumulation but not FHB disease, to reduce the disease itself fungicide needed to be applied at anthesis[185]. For many farmers using chemical control is not economically viable, especially as the treatment is not always substantially effective and the risk of a disease-outbreak cannot always be determined[174,186]. The emergence of fungicide resistant *F. graminearum* isolates, with examples in both the US and China against different fungicide classes, has shown there is a need for a change in strategy to reduce both disease and mycotoxin load – widespread resistance to multiple fungicides would be catastrophic[187,188].

With no one approach offering complete protection, biological control is a strategy that can be combined with others. However, the use of BCA's faces many similar challenges to fungicide applications[174]. This approach has been tested with both bacterial and fungal control agents. *Lactobacillus plantarum* SLG17 and *Bacillus amyloliquefaciens* FLN13 were tested successfully as BCA's against FHB *Fusarium* spp. in durum wheat[189]. Both bacterial species could be considered as BCA's but for adequate control multiple applications would be needed from the heading period until anthesis[189]. In another study *Trichoderma* spp. were tested as possible BCAs, but even though *Trichoderma gamsii* 6085 was able to control the disease on rice, when tested on wheat the BCA was unable to grow successfully and therefore no disease control occurred [190]. One of the difficulties with this approach is that to find one potentially successful candidate, many must be screened which is extremely time-consuming and expensive. Also, the results produced in the laboratory are not necessarily reproduced in the field when other

biotic and abiotic factors will be interacting with the microbes. Results from US field trials suggest that alone BCA's have little effect on reducing disease or DON levels, but rather work best when used alongside fungicides, enhancing fungicide efficacy[174,184]. However, no BCAs are currently commercially available[174].

The best chance of managing FHB is an integrated control strategy. A study from 2007 focused on mixing crop rotations, fungicides and cultivar resistance in various combinations[191]. In summary, when tested alone crop rotation reduced FHB severity by 50%, addition of a more resistant cultivar to a crop rotation system further reduced FHB severity to 82%[191]. The combination of crop rotation, a more resistant cultivar and application of an effective fungicide applied at anthesis led to a 92% FHB severity decrease, reductions in DON were also seen[191]. This evidence shows how an intensive integrated management system can be significantly more effective. As well as combining completely different modes of FHB control, the application of single or multiple different fungicides works more effectively when used in conjunction with resistant rather than susceptible cultivars[174]. Integrated management is therefore the best approach in regions where FHB epidemics are currently a common occurrence and should be considered for those areas where FHB is expected to be a problem in the future.

1.4 Other important global wheat fungal pathogens

Wheat production is threatened by many other pathogens. The 2012 paper by Dean *et al.* identified the top 10 fungal plant pathogens for all crop species based on scientific and economic importance[104]. Out of the 10 chosen, five were wheat pathogens: *Puccinia* spp., *Blumeria graminis* f. sp. *tritici, Zymoseptoria tritici*, *F.*

graminearum and *Magnaporthe oryzae*[104]. Even though my project primarily focuses on *F. graminearum* and *Z. tritici,* I have included this section to briefly provide some comparative information on these three other globally important pathogens and how they interact with the host intracellularly. With the exceptions of *Z. tritici* and *M. oryzae* pathotype *Triticum*, the life cycles of these other fungal plant pathogens will not be discussed.

1.4.1 *Puccinia* spp.

More commonly known as rust fungi, these narrow host-range basidiomycetes, can cause severe losses worldwide. The most prevalent of these species is *Puccinia triticina* responsible for causing leaf (brown) rust (Fig. 1.7). Other important species include *Puccinia graminis* f. sp. *tritici* – stem (black) rust – and *Puccina striiformis* – stripe (yellow) rust (Fig. 1.7). The arrival, emergence and rapid spread of the formidable Ug99 strain in Uganda in 1998 signified a new vulnerability in wheat crops worldwide, rendering up to 80% susceptible to the fungus[192,193]. The Ug99 strain is still at present causing farmers and scientists great difficulty.

Figure 1.7 – *Puccinia* infected wheat. (A) *Puccinia graminis* f. sp. *tritici* (stem rust) infected wheat stem, exhibiting uredinial and telial spore stages. Image taken from Dean *et al.* 2012. (B) *Puccinia striiformis* f. sp. *tritici* (stripe rust) infected wheat flag leaf. Image taken from Dean *et al.* 2012. (C) *Puccinia triticina* infected wheat leaf. Image taken from an article link via the British Society of Plant Pathology (BSPP) website – Gultyaeva *et al*. 2020.

P. triticina, *P. graminis* f. sp. *tritici* and *P. striiformis* are all obligate, biotrophic and macrocyclic, following heteroecious lifecycles[104]. These pathogens produce specialised infection structures called haustoria, which develop from hyphae (on the surface as well as intercellular) or spores. Haustoria penetrate individual plant cells, invaginating the host membrane, whilst it remains intact. Nutrients can then be transported across the host membrane and haustorial membrane for nutrient uptake by the pathogen – the area between the haustorial membrane and host membrane is the extrahaustorial matrix (EHM) – and vice versa. Refer to Fig. 1.8 for haustoria morphology. The pathogen uses this system to deliver various types of small proteinaceous effectors and other molecules which interact and manipulate host cell structure and function, suppressing plant defence responses. Some of the most well-studied effectors are from *P. striformis* f. sp.

tritici (Pst), for example: PEC6, which suppresses PTI and *Pst*_12806, a haustoria-specific effector, which is translocated into plant chloroplasts to suppress basal immunity[194,195].

To date 80 genes related to leaf rust resistance have been identified, with 44% from wild progenitor and non-progenitor species[196]. However, most of these confer race-related resistance and lose their effectiveness within a few years[197,198]. The availability of *Puccina* spp. genome sequences, elucidation of their life cycles, as well as advances in genetic mapping has allowed researchers to investigate the control of these pathogens in greater detail[104]. Re-emergence of wheat stem rust has shown the importance of forecasting epidemics and how critical early-warning signs of a crop disease are to agricultural and scientific communities.

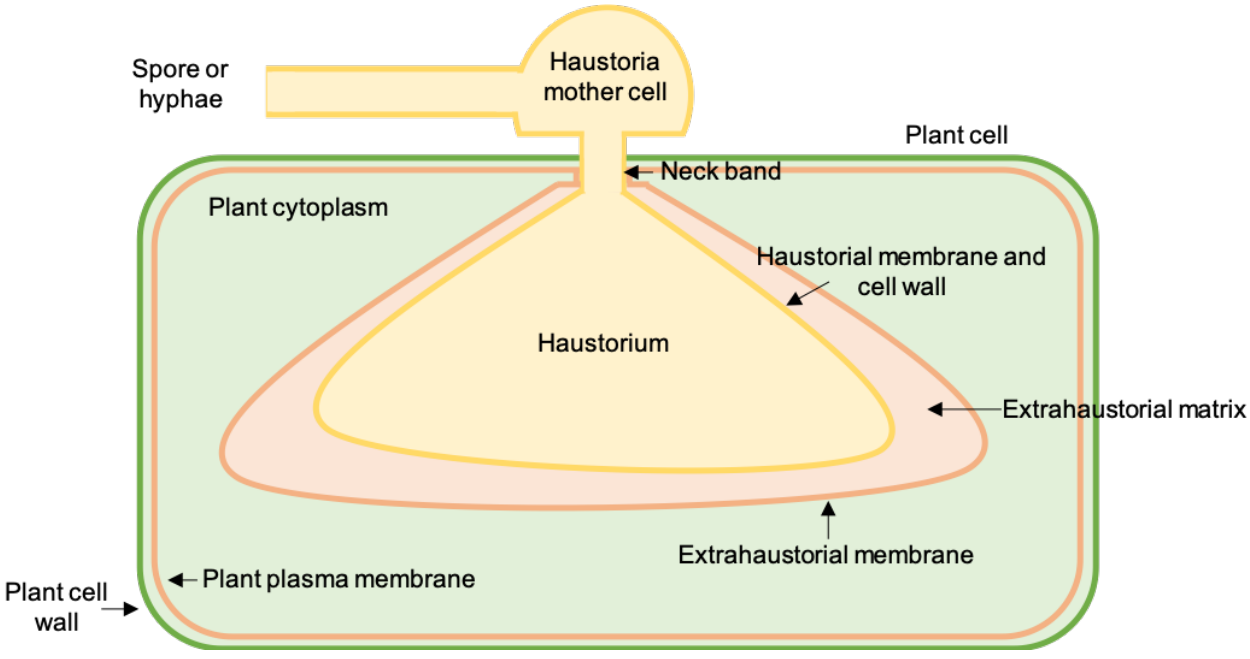

Figure 1.8 – Schematic of fungal haustoria.

1.4.2 *Blumeria graminis*

B. graminis is an ascomycete which causes powdery mildew in grasses, including the cereal crops wheat and barley[104] (Fig. 1.9). It has been classified into eight formae speciales (ff.spp.)[199]. Losses arise as a result of reductions in yields, with infections being monitored to ensure the crop remains economically viable[104]. Disease management is usually a mixture of fungicide application and the use of resistant cultivars[104]. The *Mla* locus in barley has 32 alleles responsible for conferring resistance against powdery mildew (*B. graminis* f. sp. *hordei*), with approximately 60 being described in the literature to date[200,201].

Figure 1.9 – *Blumeria graminis* f. sp. *hordei* infected barley leaves.

Powdery mildew symptoms most commonly occur on leaf tissue, but can also be seen on the stems and ears, forming fluffy, white pustules that produce spores[202]. Black spore cases (cleistothecia) eventually develop[202]. Initially *Blumeria* produces a short primary germ tube, a secondary germ tube is then produced

within a few hours which in turn elongates and differentiates into a hooked appressorium, a penetration peg emerging from this structure is enough to penetrate host tissue, allowing the fungus to enter the host via the epidermal cell wall[104]. Like *Puccina*, *Blumeria* also produces haustoria (Fig. 1.8) to exchange nutrients and for the manipulation of host defences as part of a biotrophic lifecycle. However with *Blumeria* the haustoria are usually multidigitate – a central elliptical body from which a number of finger-like structures emerge[203]. Three days after inoculation conidia are produced[104].

As with most candidate effector genes, those secreted by *B. graminis* are clustered in families within the fungal genome[204]. Similarly, many of these effectors have conserved domains, however in *B. graminis* some possess a novel lipid binding domain[204]. The metalloprotease effector BEC1019, isolated from *B. graminis* f. sp. *hordei*, critical for haustoria formation, has recently been shown to increase host susceptibility to both biotrophic and necrotrophic fungal pathogens i.e. *B. graminis* f. sp. *tritici* (*Bgt*) and *Gaeumannomyces graminis* var. *tritici* (*Ggt*)[205-207].

1.4.3. *Zymoseptoria tritici*

Due to Chapter 3 focusing on *Z. tritici*, this fungus has only been discussed briefly here. The life cycle of the pathogen will be discussed in more detail in Chapter 3, however please refer to Fig. 1.10 for a summary of this.

Z. tritici (formerly *Mycosphaerella graminicola*) is the causative fungal, pathogenic, ascomycete of Septoria tritici blotch (STB), a foliar disease of wheat (*Triticum* species) that occurs in temperate regions globally (Fig. 1.10)[208]. STB is responsible for the largest crop yield reductions during wet conditions (relative to

other crop diseases) in Europe, with losses reaching up to between 30 and 40% annually[209,210]. STB's high economic importance is demonstrated by the annual €400 million cost of attempting to control the disease ($275 million in the US)[211]. However, solid facts concerning the financial, as well as crop yield and implications of the disease are difficult to find – these facts are usually a result of extrapolating data and should not be used in agricultural decision making[212].

The interaction between *Z. tritici* and its host, wheat, is relatively understudied and consequently the success of current control strategies is debateable, with the need for better disease control solutions in the future[212]. STB is largely managed by the extensive application of fungicides, resulting in the expansion of fungicide resistant strains and cause for environmental concern[213]. Other methods under investigation include the use of resistant cultivars and biological control methods – which have not yet been used commercially[214-217]. Globally, wheat germplasm has provided 20 distinct genetic loci, conferring high levels of resistance to STB[218]. The most well studied of these genes is *Stb6*. *Stb6* functions on the basis of the gene-for-gene hypothesis; virulent *Z. tritici* isolates possess the *AvrStb6* gene[219].

Many control problems are caused by the lifestyle of the pathogen; *Z. tritici* exhibits a latent phase, where the fungus has some interaction with the leaf, but no disease symptoms are detected – ranging from 14-28 days[212]. Available fungicides are only effective for 7 days within this latent period and once the onset of symptoms occurs these are ineffective. Infrared thermography has recently been used as a tool for detecting *Z. tritici* infection in winter wheat before disease symptoms can be seen – differences in crop canopy temperatures are able to

indicate biotic stresses within the crop and can therefore be used as a high-throughput, non-invasive, diagnostic method[220].

Although a threat to food security, *Z. tritici* is an effective model organism for studying genetics, population dynamics and evolution[104]. Long-term datasets demonstrate this species' ability to adapt in relation to climate change, which could indicate future changes in its global dispersal[221,222]. Altered climate patterns in addition to intensive farming practices can influence the severity of the disease, and therefore implementing disease management practices in agriculture, such as understanding fungal behaviour as a way to find the optimal fungicide, will be fundamental to controlling the disease[212]. An understanding of the *Z. tritici* infection mechanism is therefore critical if new ways of counteracting wheat crop losses in temperate regions are to be developed.

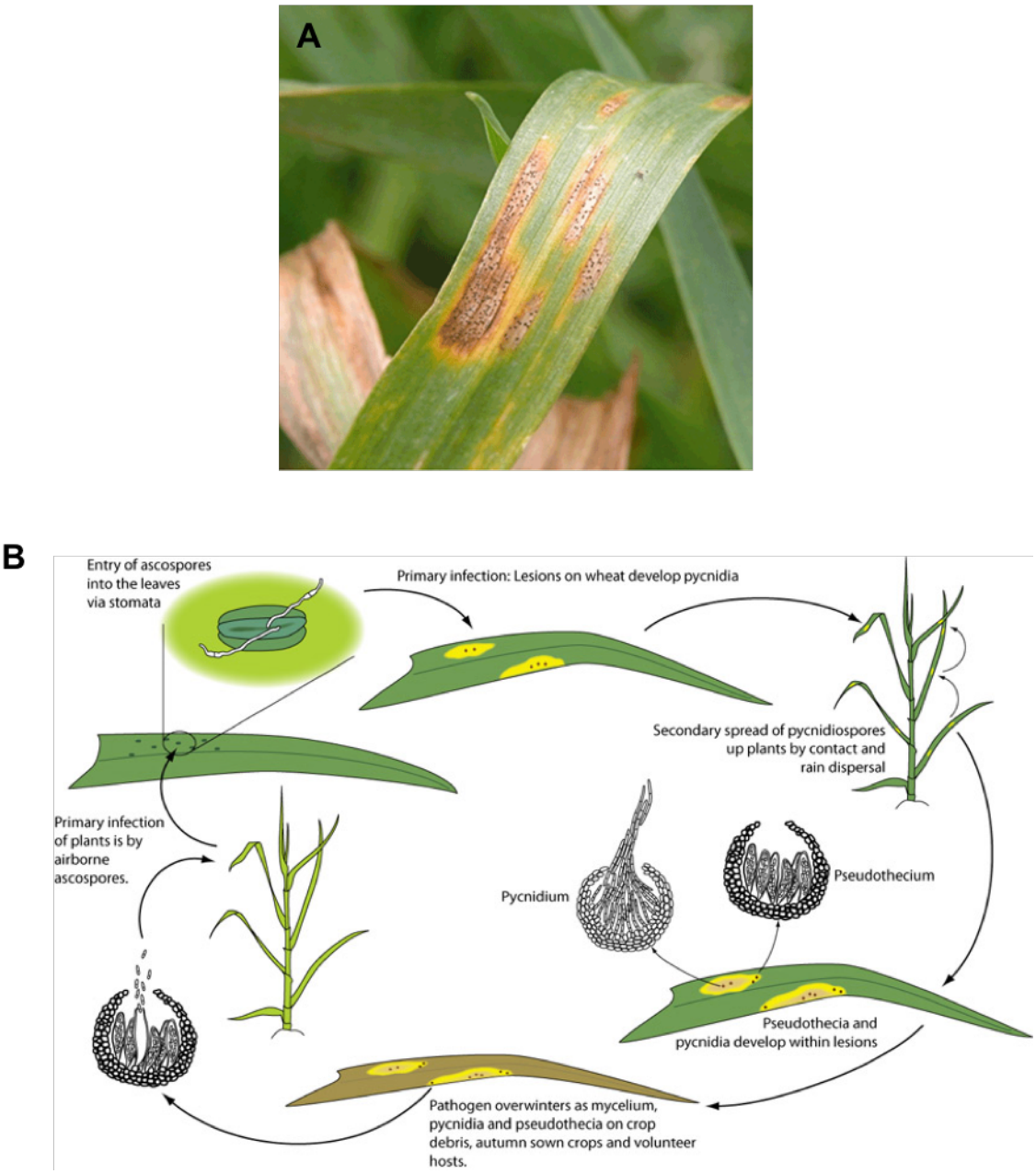

Figure 1.10 – *Zymoseptoria tritici* infection. (A) STB on wheat. Yellow regions indicate chlorotic tissue whereas brown areas show the development of necrotic lesions. Taken from Dean et al. (2010). (B) *Z. tritici* infection cycle. Primary infection is initiated by ascospores whereas pycnidiaspores cause the secondary spread of infection. Taken from Ponomarenko, Goodwin and Kema (2011).

Overall, the wheat-*Z. tritici* interaction falls into three main chronological categories (Fig. 1.10) – the first of which is the fungus's entry into the host. The second stage of infection is tissue colonisation (Fig. 1.11). After gaining entry via the stomata, *Z. tritici* hyphae begin intercellularly colonising the tissue. On average, the first 14-28 dpi – this can vary between 6-36 dpi depending upon the wheat genotype and *Z. tritici* strain – are asymptomatic, whereby the fungus uses a stealth pathogenesis approach[212,223,224]. Subsequently there is a switch to necrotrophy, which has been identified by extensive transcriptomic analyses, in which widespread tissue colonisation and cell death occur as nutrients are drawn from the surrounding host cells[218,225].

As with all other fungal pathogens, *Z. tritici* uses a repertoire of effector proteins to manipulate the host during infection. Several of these ensure successful infection in wheat and maintain pathogenesis; three LysM effectors enable the fungus to infect the host, by remaining undetected during the asymptomatic phase, protecting the fungus, by preventing the plant from recognising chitin in the fungal cell walls[226]. In non-host species, apoplastic effectors have been shown to be recognised by the host inducing chlorosis or cell death[227].

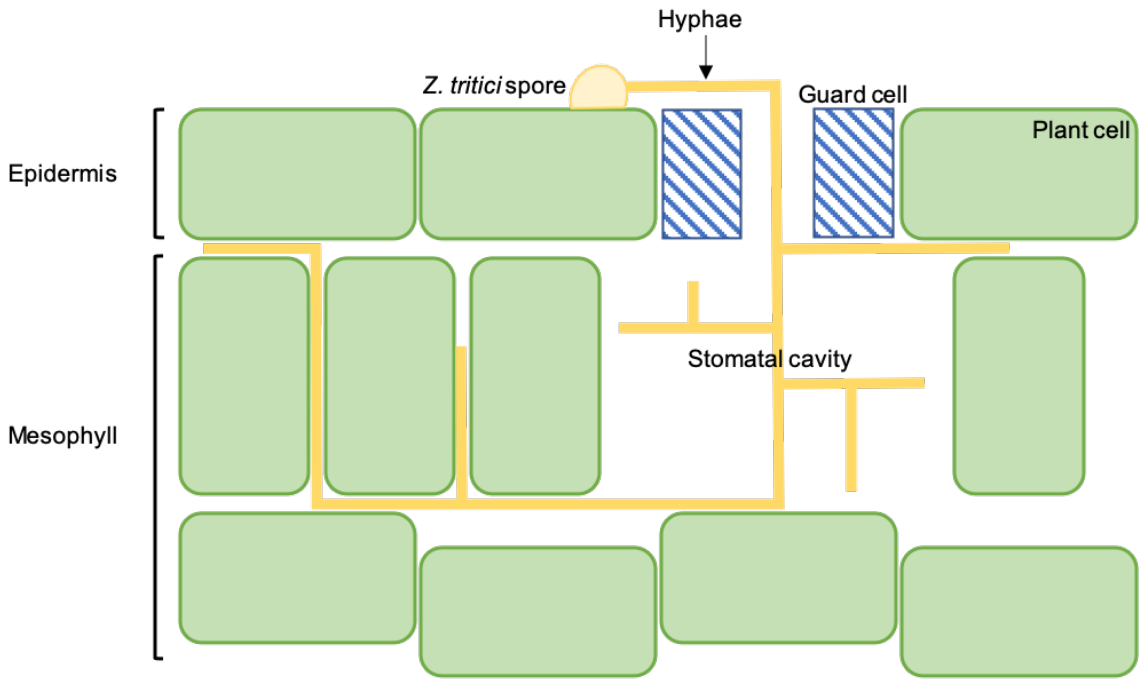

Figure 1.11 – *Zymoseptoria tritici* colonisation of wheat tissue. Following germination hyphae enter via the stomata and colonise the stomatal cavity. Hyphae then begin to colonise the apoplast of the surrounding tissues and begin to branch. Programmed cell death eventually occurs in the plant cells allowing further fungal proliferation.

1.4.4 *Magnaporthe oryzae Triticum* pathotype – wheat blast

In recent decades wheat blast has become a devasting fungal disease that threatens food security and safety in South Asia and South America[228]. Wheat blast is caused by the filamentous ascomycete, *Magnoporthe oryzae* pathotype *Triticum* (*MoT*), which is distinct from rice blast causing pathotypes (Fig. 1.12). It was first identified in Brazil in 1985, affecting 3 million hectares in the 1990s in South America[229]. In 2016, a wheat blast outbreak in Bangladesh affected up to 15,000 hectares, causing losses of up to 51%, the first outbreak seen outside of South America[229]. In some cases, yield losses of 100% have been witnessed[228]. Infection leads to reductions in not only yield but also grain quality, causing the grain to become shrivelled and deformed less than a week after initial infection[229].

Wheat blast requires warm, humid conditions to develop. The spread of the disease can be facilitated by wind-carried spores that land within the spikelet, as well as via crop residues and infected seeds[229], however seed-borne inoculum is thought to be responsible for the disease's spread[230]. The molecular crosstalk between *MoT* and wheat is relatively underexplored with effector biology being limited – much more is known about the rice blast pathotype, *M. oryzae* pathotype *oryzae*[231]. Resistance to *MoT* is thought to resemble that seen in rice blast, working on a gene-for-gene basis, with an interaction between host R genes and pathogen Avr genes[232,233]. Of the few R genes that have been discovered in hexaploid wheat, Rmg8 (Resistance to *Magnaporthe grisea* 8) is the only one that can work above 24°C, conferring resistance at both the seedling and heading stages; most other hexaploid wheat R genes are found to be temperature sensitive[234].

Infection is initiated when conidia land upon the wheat tissue, germinating six hours after contact[231]. The germ tube tip swells upon recognition of the plant surface at 12 hpi, eventually forming a structure called the appressorium; a specialised cell type used to promote fungal infection[231,235]. As the appressorium forms, the turgor pressure created, converts this pressure into a mechanical force, producing a penetration peg allowing *MoT* to infiltrate the hosts tissue via the epidermal cell layer or stalk cuticle[231,236-238]. Once inside the fungus is able to spread both intracellularly and intercellularly, colonising the tissue eventually leading to necrosis and cell death 72-96h later (symptoms are first seen after 48h)[44,235] – see Fig. 1.12. In cases where the wheat spikelet is infected; at 72h the rachis is infected and the fungus begins to spread along the spikelet, resulting in chlorosis[235]. Vascular bundles, parenchyma, cortex, epidermis, the phloem sieves and xylem vessels are all colonised during infection[235].

Similar to *F. graminearum* infection in wheat, *M. oryzae* utilises the PFs to travel intracellularly and colonise the tissue in rice[236]. I will now explore this part of the interaction in further detail.

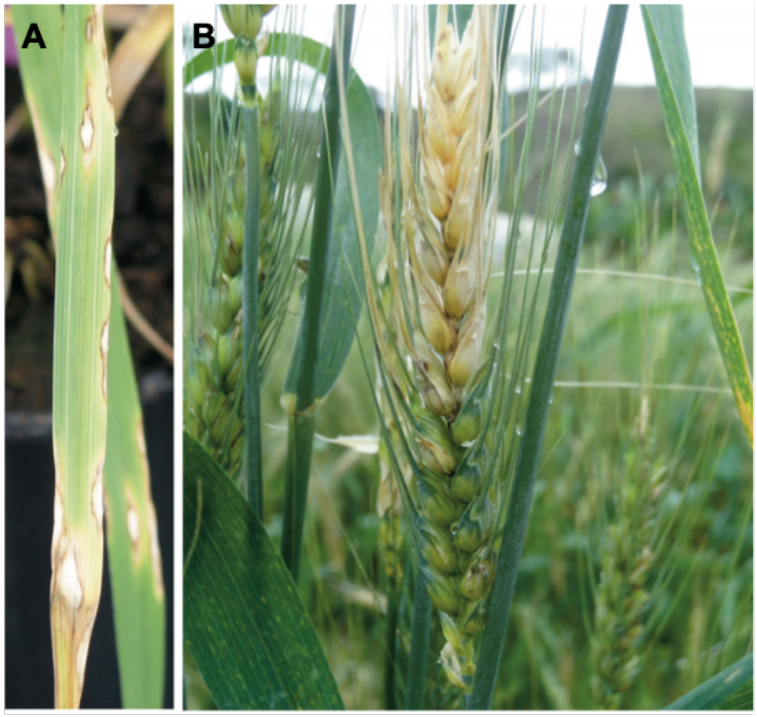
A
B

C

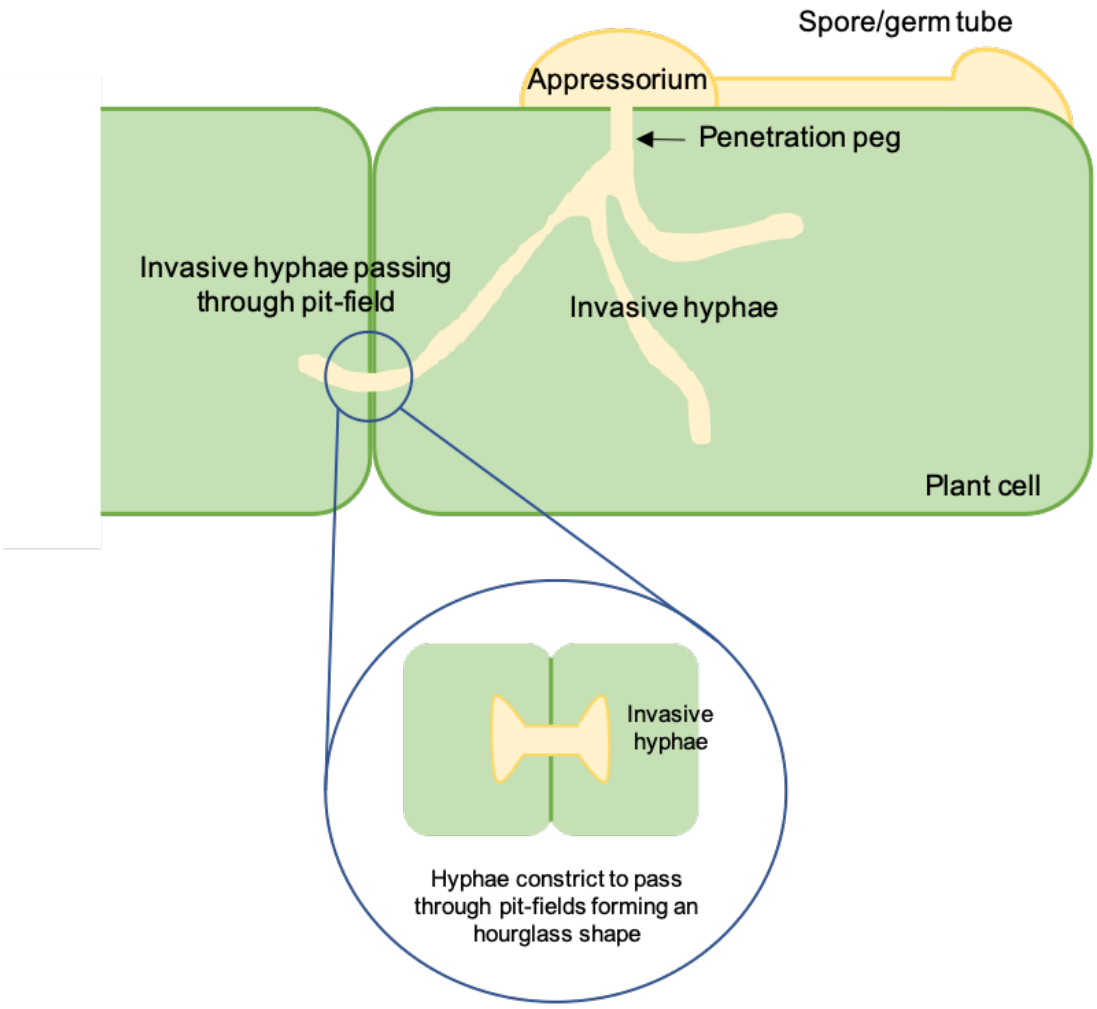
Spore/germ tube
Appressorium
Penetration peg
Invasive hyphae passing through pit-field
Invasive hyphae
Plant cell
Invasive hyphae
Hyphae constrict to pass through pit-fields forming an hourglass shape

Figure 1.12 – *Magnaporthe oryzae* infection and colonisation. (A) Wheat blast symptoms on wheat leaves. (B) Wheat blast symptoms on the wheat spikelet. (A) and (B) taken from *Ceresini* et al. 2019. (C) Infection and colonisation mechanism of rice blast.

1.5 Plasmodesmata

In a plant cell the plasma membrane (PM) sits between the cell wall and the cytoplasm, with its primary functions being to protect the cell from its surroundings, maintaining cellular homeostasis, and allowing for molecular exchange to take place. The PM, similar to other cellular membranes, is composed of proteins and lipids, forming a phospholipid bilayer. Proteins and microdomains give the PM a degree of heterogeneity, allowing for interactions with a broad range of different molecules. Continuity of the PM between cells is achieved via plant-specific structures.

Cell-to-cell communication relies upon plant-specific connections between cells called plasmodesmata (singular: plasmodesma) (PD) (Fig.1.13). Specific areas of the cell wall, namely the PFs, are abundant in 'pits', where the cell wall is thinner than normal, in turn allowing for fluid and molecular exchange via PD. These channels not only allow cytoplasmic continuity between adjacent cells, but also that of the plasma membrane (PM) (as previously mentioned) and endoplasmic reticulum (ER) – via a structure called the desmotubule[239-241]. Small molecules, RNAs and proteins use these structures to travel through tissues[242]. With the possibility of thousands of PD being present at a single cellular interface, the capacity of these small structures to maintain a communication network throughout the plant is huge[242].

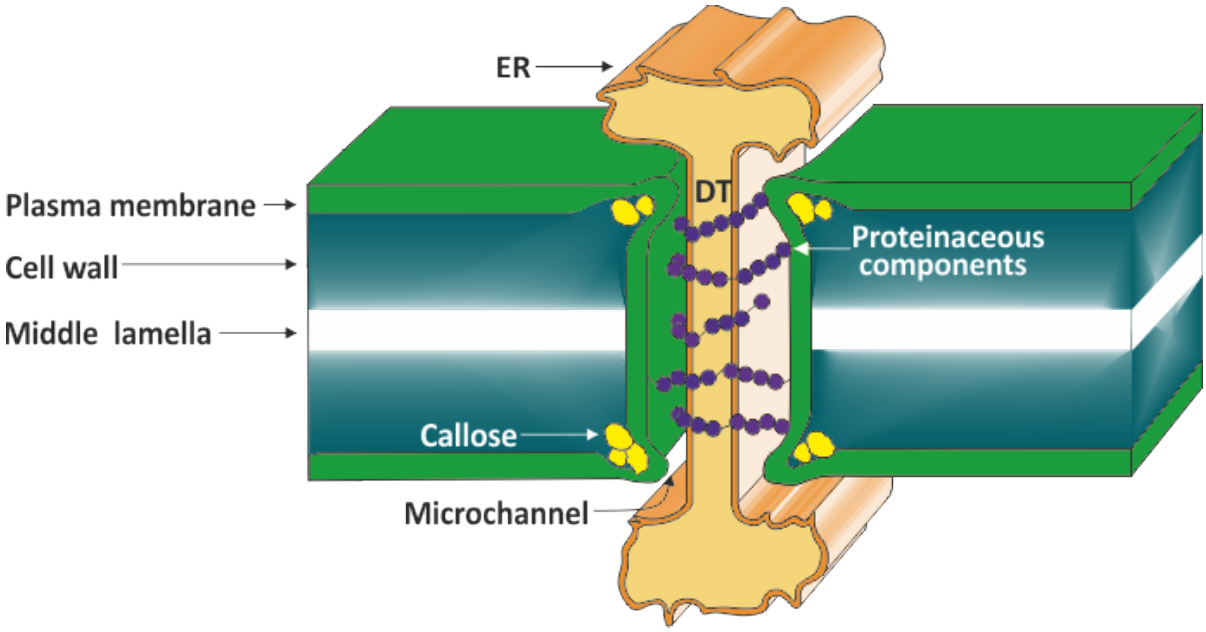

Figure 1.13 – Simple plasmodesmata structure. Schematic diagram of PD detailing main structural components.

1.5.1 PD structure

PD display a range of different architectures; as well as having PD that traverse the cell walls as a straight tubular structure (Fig. 1.13), there are those which branch, forming a more elaborate connection between cells[243]. Independent of whether PD branch or not, all PD tend to range from 10-50nm in width. Whether or not a PD has a primary or secondary structure is determined by a series of developmental processes. Primary PD are formed during cytokinesis[243]. As the cell divides, ER tubules extend across the phragmoplast[243-245]. These tubules are then trapped as a result of fusing Golgi vesicles, delivering material to the growing cell plate[243]. The enclosing cytoplasmic strands around the ER tubules eventually form the PD, with the ER strands becoming the desmotubule connecting the ER of adjacent cells[243]. To begin with primary PD are unbranched, randomly distributed, single connections[243]. Through further growth and cell differentiation these primary PD become modified, developing branches[243].

Comparatively, secondary PD do not form during cell division, developing independently of cytokinesis. It is now known that there are two types of secondary PD – a) those which originate from simple PD to form twinned PD and b) those which form separately without pre-existing PD[246]. There are multiple models eluding as to how these secondary structures form. Two main theories for the formation of twinned PD exist: a) cell wall loosening and expansion, with new cell wall material being inserted in between PD or b) ER strands inserting near a pre-existing PD, followed by the insertion of cell wall materials[246-248]. However, the formation of *de novo* PD, those which do not need a pre-existing PD to form, is less well researched, with little idea as to how their formation initiates[246]. The most likely explanation revolves around thinning of cell walls, but this has not been studied extensively[243,246].

1.5.2 PD permeability

PD play important roles throughout development, being studied extensively in leaf maturation and embryogenesis; in the case of embryogenesis, PD are shown to be both temporally and spatially regulated corresponding to different morphogenetic regions[249,250]. PD also respond to external cues from both biotic and abiotic sources, including: osmotic stress, wounding, the presence of toxic compounds and microbial interactions (both pathogenic and non-pathogenic)[251-253].

Early studies concluded that the maximum molecular weight that could pass through a single PD was 1 kDa, however further research has now shown that depending upon environmental conditions, molecules of up to 50 kDa, and possibly larger, can be transported through PD[249,254-258]. The size exclusion limit

(SEL) is the term used to describe the size of the largest molecule able to diffuse through the PD[259]. Changes in SEL's can account for changes in communication between cells, restricting/permitting the passage of certain molecules.

PD permeability is regulated in one of two ways, by a) callose deposition and degradation and/or b) proteinaceous components. Callose, a ß-1,3-glucan polysaccharide, can be deposited in the neck region of the PD at the cell wall/PM interface, the more that is deposited the smaller the SEL and the smaller the molecules that can diffuse through[260]. This reversible process is a fine balance between two groups of enzymes: the glucan synthase-like enzymes (or callose synthases), responsible for callose deposition and the ß-1,3-glucanases, responsible for degradation[261]. Recruitment of callose to PD is still poorly understood, but it is now recognised that upon pathogen perception, via pathogen-associated molecular patterns (PAMPS)/pattern recognition receptors (PRRs), various molecules, including receptors, are recruited to the PD, starting signalling cascades which result in callose deposition[242,262].

Proteinaceous components can also be recruited to the PD during different environmental conditions, with the PM at the PD consisting of its own unique micro-domains in comparison to the rest of the PM[242]. These proteins can be responsible for triggering callose deposition and interact with diffusing molecules[263,264].

1.5.3 *F. graminearum* and callose deposition

Callose degradation and deposition at PD is crucial in normal conditions and is a mechanism used to regulate cell-to-cell communication, at both a local and systemic level, controlling the size of the molecules that can pass from one cell to the next. Therefore, even though small they are extremely important to plant development and survival, with some PD protein *Arabidopsis* knock-out or suppression mutants displaying dwarf phenotypes[264]. Because of this significance they are ideal targets for pathogens who want to spread successfully through the plant host.

Callose deposition in *F. graminearum* has previously been well characterised, however the network of interactions between genes that trigger or inhibit callose deposition in the host and *F. graminearum* is complex. Partially resistant wheat cultivars, such as Sumai-3, have been shown to have increased callose deposition when inoculated with *F. graminearum*, where the rachilla meets the rachis, eluding to its increased resistance to *F. graminearum* in comparison to more susceptible cultivars[167]. Similarly, another study was able to show this same behaviour was exhibited by a susceptible wheat cultivar (Nandu) upon deletion of the secreted lipase FGL1; overall this resulted in a loss of virulence[265,266]. On the other hand, more recently, the secondary metabolite, Fusaoctaxin A, has been shown to be essential for the inhibition of callose deposition in wheat[267]. Without this metabolite the fungal mutant was unable to travel from cell-to-cell and became encased in the initially infected cell with increased callose deposition seen by the production of papillae as well as thickened cell walls[267].

1.5.4 Pathogens and the PM

The PM contains PRRs which in turn recognise PAMPS, resulting in pathogen triggered immunity (PTI)[268,269]. This innate immune response by the plant prevents many pathogens invading host tissue, however some have developed solutions to overcome this barrier. As a second line of defence some plants have developed R proteins which are able to recognise effectors and defend the plant against them, namely effector-triggered immunity (ETI)[269,270]. Host defences are finally overcome when the pathogen has adapted strategies to either cross or/and manipulate the PM remaining undetected once this process has been completed. Similar barriers need to be overcome by mutualistic microbes to allow a beneficial relationship to be established.

Viruses can successfully infect a plant host by directly being delivered into the plant – either by an insect-vector when tapping into the phloem to feed, or via a wound site on the plant, both of which avoid the PM. In contrast, most pathogenic bacteria use secretion systems to bypass the PM and deliver effectors directly into the cell[271]. However, Rhizobia create a mutualistic relationship with the host plant, creating a structure called an infection thread, which grows into the plant, invaginating the root hair PM. These Rhizobia are eventually released into the plants cytoplasm encased in a peribacteroid membrane (PBM)[269]. Many fungi and oomycetes also cause PM invagination upon infection. In Mycorrhiza this membrane is named the periarbuscular membrane (PAM) and allows for the exchange of nutrients between the fungus and its host[269,272,273]. On the other hand, in the case of pathogenic fungi this PM invagination makes way for the haustoria and is called the EHM.

1.5.5 Pathogens and the PD

PD are essential for cell-to-cell communication in development and plant defence, and therefore represent important targets for manipulation by plant pathogens, allowing for both localised and systemic spread of infection throughout the plant[274,275].

Virus-PD interactions are the most well studied. Once inside the cell many viruses produce specialist movement proteins (MP), non-structural proteinaceous components, some of which interact directly with the PD or through its associated molecules, permitting the transport of entire viral complexes[275,276]. For example, the tobacco mosaic virus (TMV) has been shown to produce MPs which alter PD permeability, through both secretory pathway and cytoskeletal interference[277,278]. On the other hand, bacteria do not interact with the PD so directly. Remaining in intercellular spaces, bacteria use mechanisms, such as the type 3 secretion system (T3SS), to deliver molecules, such as effectors, into the host cell, which in turn manipulate PD to aid infection[275].

Fungal pathogen-PD interactions have only recently been studied in detail. The rice blast fungus, *M. oryzae*, exploits the PD through an alternative means in comparison to viruses and bacteria. Microscopic studies demonstrated the constriction of *M. oryzae* invasive hyphae (IH) to pass through these cytoplasmic junctions and grow intracellularly[236,275]. No indication of permanent physiological PD remodelling or damage is present, with the diameter of the hyphae decreasing to approximately 0.5μm, which is still 10 times larger than the maximum PD size of 50nm[236,275]. Further genetic and biochemical studies of both the host tissue and defence responses, as well as the infection mechanisms of fungal

pathogens, may help to elucidate how fungi can grow intracellularly without damaging PD structure or eliciting an immune response by the plant.

Evidence suggests *F. graminearum* also utilises PD to aid intracellular hyphal spread in wheat tissues once the cell contents has been lost[113]. Detailed microscopic studies have demonstrated *F. graminearum* operates a similar mechanism to that employed by *M. oryzae*, during which the intracellular hyphae constrict to pass through the PD before diameter enlargement in the adjacent cell (Fig.1.14) – however, this has not been explored further via live-cell imaging[113].

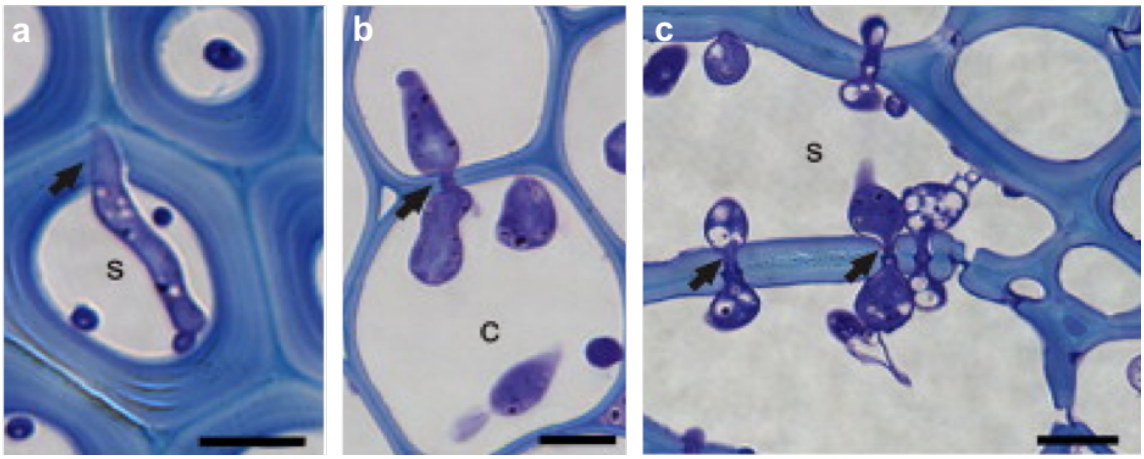

Figure 1.14 – Plasmodesmata-*Fusarium graminearum* interaction. Modes of intracellular hyphal movement. (a) Penetration of thickened cell wall. (b) and (c) Utilisation of a pit-field to pass between dead host cells via hyphal constriction. Transverse 1 µm cross-sections stained with 0.1 % toluidine blue O, pH 9. Black arrows = fungal hyphae traversing host cell walls, c = cortex, s = sclerenchyma. Bar = 10 µm. Taken from Brown *et al.* (2010).

1.6 Investigation of cellular mechanisms using microscopy

1.6.1 Basic microscopy principles

Please note, for the main body of this study I have focused on the use of stereo- and confocal microscopy so these have been discussed in detail here.

Broadly speaking, light microscopy can be split into two techniques, brightfield and fluorescence. The latter of these will be discussed more thoroughly throughout this chapter section. Light microscopes themselves can be split into two categories: the compound microscopes (which will not be discussed in detail here) and stereomicroscopes, these typically have a resolution of between 100-200nm. In brief, compound microscopes are necessary if a sample requires accurate measurements, high magnification, or to view characteristics deep within the sample[279]. On the other hand, stereomicroscopes (also referred to as dissection microscopes) are typically used at lower magnifications, imaging the surface of the sample, and rely upon the light being reflected to successfully image the specimen. Stereomicroscopes permit large sections to be imaged as a result of a greater depth of field and working distance, giving this type of microscopy an advantage in terms of preventing the need for sample manipulation and therefore damage, especially if the tissue is needed for further analysis, allowing real-time imaging to a certain degree. Stereomicroscopes have two spatially-separated optical paths imaging the sample at two different angles (parallax), giving the viewer a three dimensional image in return[280]. Diagrams have been included to help visualise these light paths and features without going into too much detail (Fig.1.15). Addition of fluorescence to samples being analysed via stereomicroscopy is also common, the principles of which are

discussed throughout the remainder of this section. Additionally, axiophot microscopes are upright epifluorescent light microscopes that can be used for phase contrast and differential interference contrast as well as the stated fluorescence microscopy, and are most commonly used for fixed samples. Axiophot microscopes can be used for live-cell imaging but are not ideal for this and produce no quantitative measurements.

Confocal laser scanning microscopy (CLSM) became a mainstream research tool first in the 1980's, specifically for fluorescent samples[281]. These microscopes enable thicker specimens to be imaged with greater resolution – in the focal (horizontal) plane this reaches around 200nm and along the optic axis (vertical plane) around 500nm – contrast and sensitivity[281]. Light from a laser is used to image a singular spot within the sample, where the laser is focused is where the tissue is excited, inducing fluorescence. The emission from the sample is imaged onto a detector which measures the fluorescent intensity of this area, in turn being equivalent to one pixel. The emitted light is essentially filtered through a pinhole to block out other surrounding light. The rest of the image is acquired as the laser scans across the specimen, exciting one point at a time. This is usually done in one focal plane; a three-dimensional image can be built up by combing multiple images into a stack (z-stack). Image acquisition can be achieved by using lasers of different wavelengths to excite the specimen, depending on what you are trying to image within the sample. Complex computational software, alongside various mechanical elements are all needed to produce an image as well as change aspects such as resolution and exposure times. It should also be noted that CLSM allows for multi-spectral imaging, splitting wavelengths up into smaller increments to analyse light emitted in stages. CLSM is considered to be the best

system for a wide-range of both advanced and routine imaging applications but is however, limited by its speed and sensitivity[281].

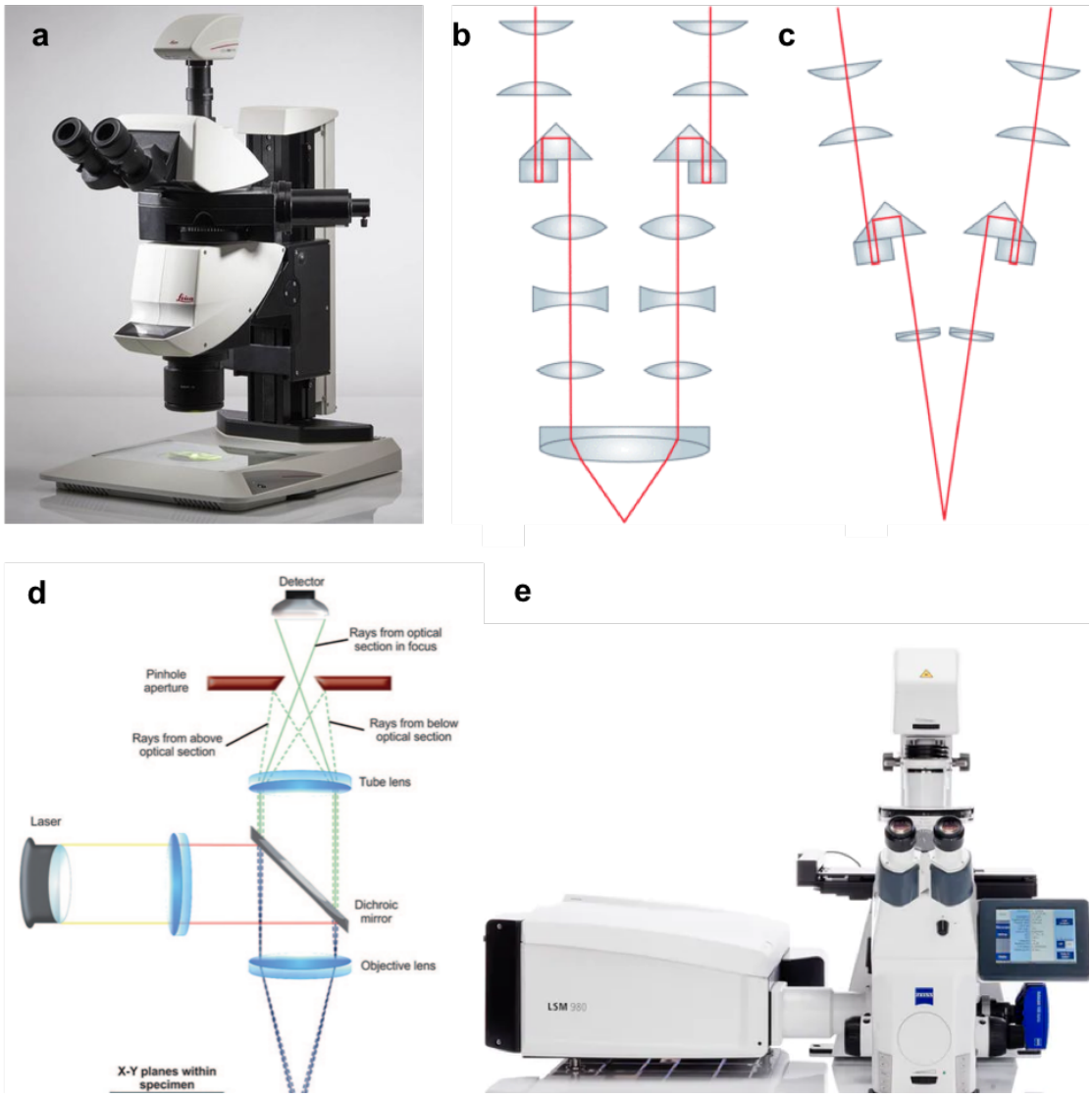

Figure 1.15 – Light microscopes and light paths. (a) Stereomicroscope model Leica M205 FA. (b) and (c) alternate light paths for stereomicroscopy – (b) conventional stereomicroscope with a large working distance, (c) alternative light path with a longer working distance for medical applications. Images taken from Leica Microsystems (www.leica-microsystems.com). (d) CLSM light path. Image taken from Dahms (2015). (e) CLSM model Zeiss LSM780. Image taken from Zeiss (www.zeiss.co.uk).

To gain a clear understanding of the intricate mechanisms involved in a plant's interaction with its environment, tools have been developed which allow researchers to visualise what would otherwise be difficult to see, even with the use of a microscope. The discovery of green fluorescent protein (GFP) in the early 1960's, redefined how we study cells and molecules, providing high spatial and temporal resolution[282,283]. This key event led to the characterisation of further fluorescent proteins (FP) in use today, and to the synthesis of FPs that are not naturally available. These proteins contain a structure called a chromophore. When excited with light of a certain wavelength, the chromophore's structure experiences a conformational change, leading to the emission of light at a longer wavelength. Due to these properties, FPs have been utilised routinely across kingdoms, to help us visualise, locate, quantify and understand the interactions between certain molecules.

Since the development of plant transformation techniques (either transiently or stable via Agrobacterium-mediated, or bombardment methods) scientists have been able to readily generate lines expressing single or multiple FPs[284]. Fluorescence-Activated Cell Sorting (FACS) is one application made possible through FP discovery. One of the first examples was through the production of an *Arabidopsis* root gene expression map[285]. Fluorescing cells were isolated from non-fluorescing neighbouring cells by enzymatic digestion of the cell walls[285-287]. These protoplasts could then be processed using FACS, grouping cells based on their fluorescence[285-287]. This enabled the production of an *Arabidopsis* root map, identifying differences in gene expression across different root zones and developmental stages[287].

However, more frequently, FPs have been used to tag predicted or known proteins helping elucidate their location(s), movement(s) and function(s). Even with the completion of the *Arabidopsis* genome in 2000, 30% of genes had no computationally predicted function in the public domain by 2006[287-289]. For more recently completed and more complicated genomes, e.g. maize and wheat, this figure for predicted proteins of unknown function is even higher[287]. In *Arabidopsis,* high-throughput methods, whereby *Arabidopsis* cDNAs were randomly fused to GFP, determined the location of gene products of unknown function[290]. However, adding fluorescent tags can itself cause problems including protein misfolding, inactivation, aggregation and mislocalisation. Splice variants could also easily be missed.

One of the main problems faced when using microscopy to study plant cellular mechanisms is autofluorescence (defined as natural fluorescence emitted by biological structures/substances following excitation by radiation of a specific wavelength). If a compound shares similar excitation and emission wavelengths to that of the FP, this can interfere with the results obtained; additionally, this can vary throughout different plant tissues and developmental phases as well as during periods of stress[291]. However spectral imaging can alleviate some of this unwanted sample background by separating the wavelengths[284]. When using CLSM, which utilises excitation lasers, cellular damage can occur when the tissue is exposed, this itself can then cause interfering autofluorescence. Weakly expressed fluorescent proteins can also be a problem, this can often occur when the gene of interest is expressed under the native promoter[287].

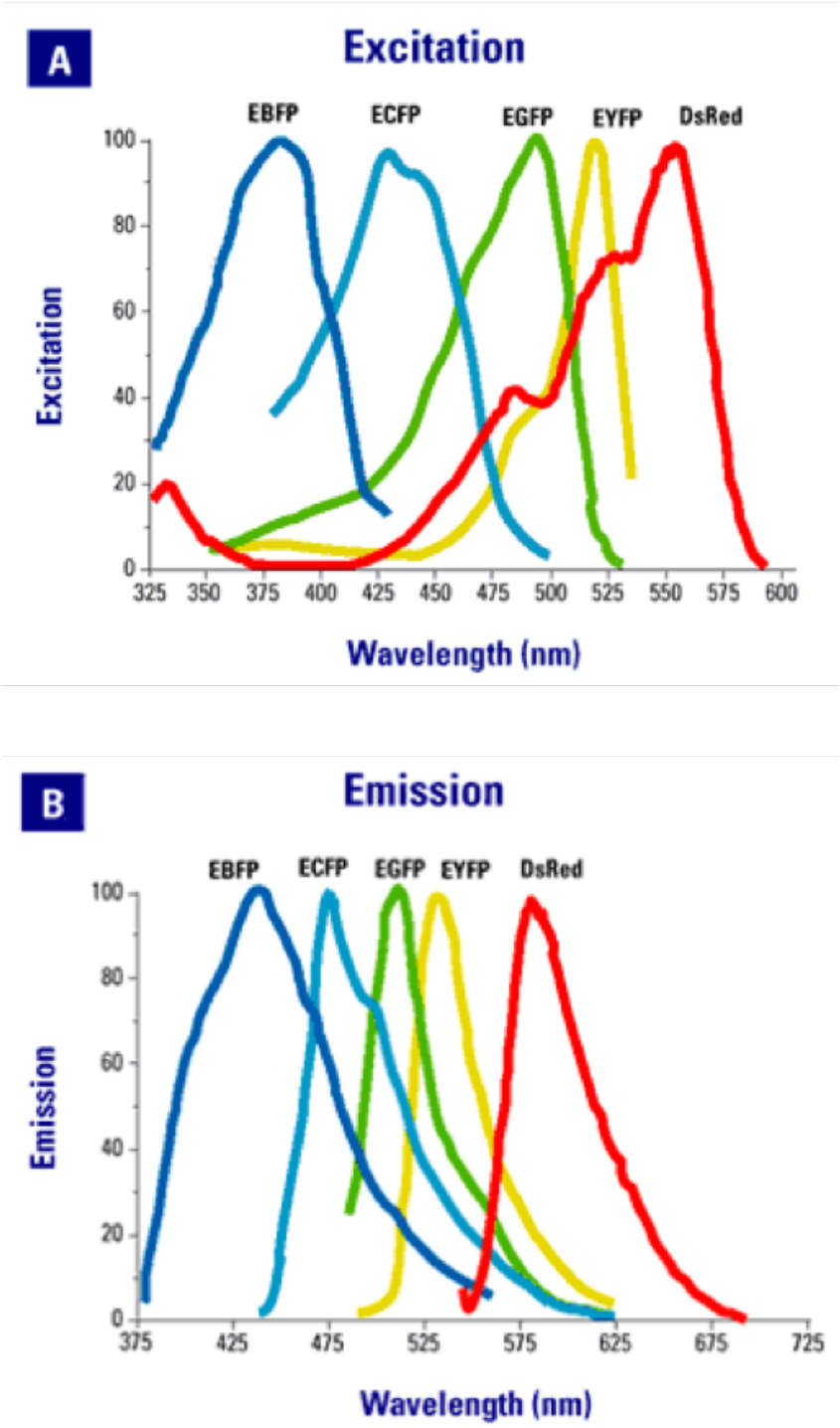

Figure 1.16 – Spectra from common fluorescent proteins. (A) Excitation spectra. (B) Emission spectra. Taken from takarabio.com.

1.6.3 Use of reporter lines in plant pathology

Multiple FPs may be used simultaneously to study the interaction between two organisms, either by: a) tagging two separate molecules within the same organism or b) tagging the organisms separately with different FPs in order to explore the interaction, more specifically at the cellular level. In this instance the wavelengths of each FP reporter need to be distinct, and there is a need to make sure each emission spectra does not overlap and can be distinguished easily from one another. The excitation and emission spectra for common fluorescent proteins are shown in Fig. 1.16.

The interactions between plant pathogens and their hosts, at both the molecular and cellular levels, have been, and continue to be, determined through the production of both plant reporter lines and pathogen reporter strains. Effectors delivered via the T3SS in bacteria, have recently been effectively tagged with GFP to determine their destination within the host[292]. Delivery of tagged effectors into the host was previously hindered by the incompatibility between the T3SS and the GFP construct, preventing effector entry into the host[292]. When exploring the interaction between *Pseudomonas syringae* and *Arabidopsis* or *Nicotiana benthamiana,* a split GFP system was engineered, whereby both the effector of interest and a subcellular location are tagged with part of the GFP protein, emitting fluorescence only once both parts of the GFP protein meet[292].

From a cellular perspective, reporter lines can be used more generally to effectively highlight the organisms of interest. Reporter lines of *Z. tritici* have been optimised to express *Zt*GFP, a codon-optimised version of GFP for better expression cytoplasmically, allowing for better visualisation within its host,

wheat[293]. Subsequently, this initial study led to the production of GFP (eGFP and *Zt*GFP) based vectors which highlighted seven subcellular locations within *Z. tritici,* including the PM, nucleus and ER[294].

Alternatively, both a pathogen reporter strain and a plant reporter line, can be used in unison to reveal communication between and in response to each other. The importance of vacuole maintenance in rice cells during its biotrophic interaction with *M. oryzae* during infection was demonstrated with a series of fluorescent proteins[295]. Various different rice and fungal reporter lines were used together, where the rice lines were GFP-based with the fungal reporter lines being mCherry-based, ensuring excitation and emission wavelengths of each fluorescent protein were in different parts of the spectrum[295]. However, the process of transforming plant pathogens is difficult, and complications in transforming some hosts, for example collateral genetic damage, means it is relatively rare to have a system whereby reporter lines are available for all the required organisms.

1.6.4 Imaging plant PM and PD

Imaging of the PM can be achieved using two different approaches. Reporter lines can be produced for the plant species under study – however depending on the size of the experiment, facilities available, and expense, this may not be possible. This is also dependent on the transformation methodologies available for the species in question and ease of finding proteins that localise to the PM. The main advantage of this option over the alternative, is that any adverse effects are likely to be avoided if the reporter protein localises to the PM successfully, whereby the plant will remain healthy for its entire life cycle. The second option is to stain the PM, this is most frequently done with propidium iodide (PI)[296]. PI is

toxic, as is the case with many other stains, therefore it is not useful for live-cell imaging over long time periods, however it is much quicker and cheaper to use than carrying out a transformation experiment. PI can also be used as a test of viability, if the PM has been damaged the dye can pass through into the cytoplasm, staining the nucleus indicating cellular damage – other dyes are also available such as FM4-64[296,297]. Other problems with these stains occur when trying to image deeper tissues and strong staining of surfaces can interfere when searching for details within a structure[296]. Additionally, plasmolysis can be used to separate the PM from the cell wall for imaging.

In comparison to the PM, which is a large enough structure to be easily seen, PD are approximately 50nm in diameter at their largest and are therefore much more difficult to image. Despite this PD can be imaged using light microscopy, but a fine level of resolution cannot be achieved this way and therefore this requires electron microscopy[298]. Fluorescent tags for PD can be produced by utilising viral MPs and fusing them to a FP[299]. These target different regions of the PD; however what MPs target what PD regions is still unknown[298]. Many other PD associated proteins have now been alluded to and continue to be discovered as imaging and proteomic studies advance; it is likely some of these will be developed as reporter genes[298]. Alternatively stains such as aniline blue which stains callose can be used for labelling PD in acidic conditions, however this stain is toxic to the plant and fades rapidly but, can be used both quantitively and qualitatively[300,301].

1.7 Project aims, objectives and hypotheses to be tested

Technological advancements and the generation of complete genomes in the last couple of decades have now made it possible for researchers to study fungal pathogens in more detail at both the cellular and molecular level. This project focused on producing new tools and methodologies to fill in knowledge gaps that currently have not been addressed. This project began with focus given to *Z. tritici*, a non-floral pathogen of wheat, before switching primarily to the floral invader, *F. graminearum,* and its interaction with PD, which currently remains uncharacterised and needs multiple tools and datasets creating to achieve this aim. I therefore hope to highlight the steps that can be taken in terms of creating individual tools and also show how these can be used to work towards a more collective goal. By having taken this approach I hope to show the flexibility of the tools produced and the use of them when studying a range of pathogens as well as their uses in other fields of research. This project can therefore be split into the two following objectives:

- To identify the cellular and molecular mechanisms needed for successful fungal infection and hyphal growth (*Z. tritici* metabolic biosensors, wheat PM reporter lines and wheat tissue profiles – uninoculated and *F. graminearum* inoculated).

- To explore the functional role(s) of PD-associated wheat proteins (using the material from the first objective and virus-induced gene silencing (VIGS)).

1.7.1 Hypotheses to be tested

1. *Z. tritici* metabolic biosensors can identify key changes at the cellular and molecular levels during compatible and incompatible interactions.

2. Stable wheat PM reporter lines are effective tools in identifying the *F. graminearum*-PD interaction at the cellular level.

3. *F. graminearum* utilises the PD for intracellular hyphal growth, aiding successful colonisation of wheat floral and non-floral tissues.

CHAPTER 2: Experimental procedures

2.1 Plant material and growth conditions

Susceptible hexaploid wheat (*Triticum aestivum*) cultivar Bobwhite (BW) was used for all experiments. This cultivar was bred by the International Maize and Wheat Improvement Centre (CIMMYT, Mexico), and was chosen for these experiments as a result of its susceptibility and its ability to produce three to four tillers which usually flower simultaneously. All plant material unless otherwise stated was grown in a category 3 controlled environment facility in the following conditions: 16h day – 22 °C and 8h night – 18 °C cycles at 65% humidity.

2.2 Fungal strains, cultures and stocks

The wild-type *F. graminearum* strain PH-1 (NRRL 31084), the mating locus mutated PH1:GFP and mutant ΔFgGT2 and ΔFgMAP1 strains, were regularly cultured on plates containing synthetic nutrient poor agar (SNA) comprising: 0.1% KH_2PO_4, 0.1% KNO_3, 0.1% $MgSO_4$ x $7H_2O$, 0.05% KCl, 0.02% glucose, 0.02% sucrose and 2% agar. These cultures were left to grow for 8 days before the addition of 300µl TB3 (0.3% yeast extract, 0.3% Bacto Peptone and 20% sucrose) to induce high levels of fresh conidial growth, conidia were then harvested after two days. Plates were incubated at room temperature in boxes providing constant illumination using both white-light and near-UV light. Spores were harvested using 3ml sterile water, these cultures were filtered using miracloth (Calbiochem) and their concentrations were adjusted, experiment dependent, using sterile water. These cultures were then stored at -80°C as a water solution before use. These methods have been previously published in Urban *et al.* 2002[77].

2.3 Wheat floral inoculations

Please note, wheat floral inoculations were not performed as part of this study. This method has been included to allow the reader to make comparisons between wheat floral inoculations and the coleoptile assay.

For wheat spike inoculations spore suspensions of 4 x 10^4/ml were used. To closely mimic wheat floral infection in the field, inoculations were only carried out when the appearance of anthers was first seen. A 5µl droplet of spore suspension was placed within the two spikelets in the middle of the spike, between the palea and lemma. Control inoculations were carried out using sterile water. Following inoculations, plants were placed in a chamber and sprayed with water to represent humid conditions for 72h, for the first 24h this chamber was placed in darkness. After this time the humidity chamber was removed, and plants were left in the original controlled environment conditions (~65% relative humidity, see above). For each treatment, a minimum of three inoculations per treatment were carried out. These methods have been previously described in Urban *et al.* 2003[302].

2.4 Coleoptile assay

The following coleoptile assay protocol described below is adapted from the one described in Zhang *et al.* 2012[303]. Wheat seeds, *cv*. BW, were sown in perlite, placed within small-covered boxes in controlled conditions: 16h day – 22°C and 8h night –18°C cycles. After 3 days most coleoptiles were ready for inoculation. Pipette tips were cut and lined with filter paper which was subsequently soaked in an *F. graminearum* spore suspension (1 x 10^5 spores/ml). For controls, untreated and water-inoculated coleoptiles were used. To assist infection, 2mm

of the coleoptile tip was removed, and the soaked filter paper was placed over the wounded coleoptile. The box was covered and placed in the dark overnight before being uncovered. Infection could then be monitored for the development of a lesion, typically from 3 dpi where the box would then be left open, to 7 dpi. The design of each coleoptile inoculation experiment is described in more detail in the relevant chapters.

2.5 Gel electrophoresis

For all cloning, DNA fragments/plasmids were separated using gel electrophoresis. To set up the equipment a 1-2% agarose gel was produced by heating agarose gel powder in 1x TBE buffer (1x composition: 89mM Tris, 89mM boric acid, 2mM EDTA, pH of 10x TBE: 8.3) for either a 50ml or 100ml gel, until completely dissolved. Before the gel was poured into a cast with a comb for wells, ethidium bromide was added (5µl per 100ml gel) once the gel had cooled to approximately 50ºC. Once the gel was set, the comb was removed, and the gel was placed in the electrophoresis tank containing 1x TBE buffer in solution with additional ethidium bromide (approximately 5µl). Samples to be loaded into the gel were mixed with a 1x loading dye (Qiagen – bromophenol blue, xylene cyanol and orange G). DNA ladders were loaded into each gel as size references (Lambda_BstEII_DNA ladder, New England Biolabs or 100 base pair (BP) DNA ladder, GeneRuler, Fermentas). DNA samples were run at 80V for 40-80 mins depending upon the required band separation. DNA fragments were then visualised using UV light, in short bursts, and imaged using the Gene Genius imager and GeneSnap software (version 7.1; Syngene).

2.6 Polymerase chain reaction (PCR) and primer design

All primers were produced using the National Centre for Biotechnology Information (NCBI) Primer-BLAST tool (https://www.ncbi.nlm.nih.gov/tools/primer-blast/). Adhering to guidelines produced by Thermo Fischer and European Molecular Biology Laboratory (EMBL), primers were designed based on the following: a length of between 18-30 nucleotides (nt), a melting temperature (T_m) between 55°C and 65°C, a GC content between 40-60% and avoiding runs of 4 or more of the same base and intra-primer homology. Unless stated otherwise primers were purchased from Eurofins. Primers were delivered in a dehydrated format and were resuspended upon delivery with sterile water to 100µM. Primers were aliquoted from these stocks to prevent contamination and diluted to a final concentration of 10µM and stored at -20°C. For each 25µl PCR reaction: 12.5µl Red Taq mix (Sigma-Aldrich – 20mM Tris-HCl, pH 8.3, with 100mM KCl, 3mM MgCl2, 0.002 % gelatin, 0.4mM dNTP mix (dATP, dCTP, dGTP, TTP), stabilisers, and 0.06 unit/ml of Taq DNA Polymerase) 0.5µl forward primer, 0.5µl reverse primer, 20-100ng DNA template (depending upon circularised or linearised plasmid) and sterile water to a final volume of 25µl. Thermal cycling conditions: initial denaturation – 97°C 3 mins, 35 cycles – 97°C 10 s, annealing temperature varied with primer requirements, 72°C 1 min/kb, final extension 72°C 5 min and hold at 4°C. The PCR machines used were T100 Thermal Cycler (Bio-Rad).

2.7 Light microscopy and photography

Sample preparation is described in each chapter as a wide range of tissues have been used and their preparation differs depending upon the experiment. Unless otherwise stated all stereomicroscopy was carried out using the Leica M205 FA

stereomicroscope and all CLSM used the Zeiss LSM780 confocal microscope. Further details are mentioned in individual chapters. All photography was carried out using a Nikon D80 digital camera (17-70mm lens) with all photographs being taken against a black velvet background.

2.8 Data storage

Microscope images were all stored on two bioimaging drives – one shared and the other not. For each image the raw data file was stored and used to produce a tagged image format (TIF) file. For microscope images, photographs and other data files i.e. statistics and spreadsheets, a work drive, shared with other members of the Wheat Pathogenomics, Rothamsted Research team, was used to store the data. All files were backed up using OneDrive and a personal hard drive. All data was separated into folders and sub-sectioned depending on the experiment and type of data – the specifics of this will be described for the different experiments in each individual chapter.

CHAPTER 3: Metabolic biosensors in *Zymoseptoria tritici*

Note this chapter is taken from the following:

SWBio DTP rotation project 1 – Quantifying the metabolic state of the plant pathogenic fungus, *Zymoseptoria tritici* (2017)

All methodologies listed in the 'Experimental procedures' section of this chapter were carried out by me. Where results or methods were carried out by Francesco Valente, University of Exeter (as this was a project I started at the University of Exeter before my move to Rothamsted Research) this will be stated – the methods F. Valente used will be included alongside their results.

F. Valente doctoral thesis – Sub-cellular responses of wheat epidermal cells to *Zymoseptoria tritici.* (2020).

ore.exeter.ac.uk/repository/handle/10871/122567

3.1 Introduction

3.1.1 *Z. tritici* life cycle

Z. tritici is used for genetic studies as a result of its dimorphic growth, growing either in a "yeast-like" form (blastospores) or as filamentous hyphae depending upon the external cues i.e. the media chosen for the culture[304]. Even though both forms are found in nature here I will focus on the filamentous growth form, essential for successful entry and colonisation of the host.

There is some controversy surrounding the nature of the infection mechanisms deployed by *Z. tritici*. During infection, there is a switch from biotrophic to

necrotrophic growth – suggesting this ascomycete is hemibiotrophic. However, some characteristics of infection do not specifically fit into these categorical restraints, leaving this topic under debate[305]. Overall, the wheat-*Z. tritici* interaction falls into three main chronological categories – the first of which is the fungus's entry into the host. Initial infection is a result of ascospores (usually airborne) as well as pycnidiospores (which can lie dormant in soil and plant debris) landing upon the wheat leaves and undergoing germination[306]. *Z. tritici* hyphae then enter the plant directly via stomata[306]. However, studies discussing the mechanisms exhibited by the fungus, allowing entry via stomatal penetration, are inconsistent. Some suggest a chemoattractant ('thigmotropic signal') draws the hyphae towards the stomata, whereas others suggest that this is an entirely stochastic process[306-309].

The second stage of infection is tissue colonisation. After gaining entry via the stomata, *Z. tritici* hyphae begin intercellularly colonising the tissue. On average, the first 14-28 dpi – this can vary between 6-36 dpi depending upon the wheat genotype and *Z. tritici* strain – are asymptomatic, whereby the fungus uses a stealth pathogenesis approach[212,223,224]. During this phase the fungus acts biotrophically, showing little increase in biomass, with evidence of infection only present using microscopy at the intercellular level[310,311]. With almost no cell death occurring during this phase there is some debate as to what the fungus utilises as an energy source during this time[305]. Subsequently there is a switch to necrotrophy, which has been identified by extensive transcriptomic analyses, in which widespread tissue colonisation and cell death occur as nutrients are drawn from the surrounding host cells[218,225]. The formation of chlorotic tissue followed by necrotic lesions is parallel to the main final stage of infection, the formation of

fruiting bodies – a high proportion of which are asexual pycnidia, allowing for the continuation of the *Z. tritici* infection cycle[306,309].

However, what determines whether successful *Z. tritici* infection is established, to some extent, remains unclear, with numerous biological mechanisms contributing towards compatible and non-compatible interactions. Incompatible infection of non-host grasses compared with the susceptible wheat host displays differential gene expression patterns, indicating different genes are needed for successful stomatal penetration[312,313]. The transcription factor, Zt107320, is lowly expressed in incompatible non-host interactions in comparison to successful wheat infection[312]. Furthermore, Zt107320 serves a role in pathogen growth, cell wall composition and the dimorphic switch[312]. Additionally, in susceptible wheat cultivars, *Z. tritici* can target and suppress host immune-related signalling pathways, resulting in a phenomenon termed 'systemic-induced susceptibility'[314]. This response also results in the host becoming more susceptible to secondary bacterial infections and can systemically change the wheat host's microbiome[314].

As with all other fungal pathogens, *Z. tritici* uses a repertoire of effector proteins to manipulate the host during infection. Several of these ensure successful infection in wheat and maintain pathogenesis; three LysM effectors enable the fungus to infect the host, by remaining undetected during the asymptomatic phase, protecting the fungus, preventing the plant from recognising chitin in the fungal cell walls[226]. In non-host species, apoplastic effectors have been shown to be recognised by the host inducing chlorosis or cell death[227].

3.1.2 Detection of *Z. tritici*

Detecting *Z. tritici* in the field requires the use of infrared technologies or hyperspectral remote sensing[220,315]. In the laboratory, novel primer sets can be used to rapidly identify *Z. tritici* on wheat leaf tissue[316]. However, to image the fungus at the cellular and molecular level in real-time requires FPs. Furthermore, to image specific biological mechanisms taking place within *Z. tritici* during infection, FPs need to be localised.

For detection of *Z. tritici* during infection a series of RFP-based vectors have previously been produced[317]. These RFP vectors were shown not to affect pathogen virulence[317]. Imaging of an eGFP-expressing strain and mCherry-expressing *Z. tritici* strain in the wheat host further demonstrated the infection process, determining that pycnidia were formed by a single strain[317]. Organelle-specific FPs have also been developed in *Z. tritici* to understand some of the biological processes and mechanisms that occur during infection[294]. These reporter strains have been used to visualise the PM, ER, peroxisomes, autophagosomes, chromosomes and the actin cytoskeleton[294]. However, even though these reporter systems provide an insight into the *Z. tritici*-wheat infection at the cellular level, what changes occur in the fungus during compatible and incompatible interactions at the metabolic level is still unclear.

3.1.3 Biosensors

Biosensors are tools that can successfully be utilised to provide quantitative measurements of an organisms' metabolic state at both the cellular and subcellular level, indicating changes in a biological process under a range of different conditions or stresses. Within a cell a variety of metabolites are detected by naturally occurring biosensors, for example, enzymes or transcription factors;

it is this knowledge that has allowed researchers to adapt these mechanisms for use in metabolic engineering and the creation of synthetic biosensors[318]. Before the establishment of such biosensors, metabolic state was determined using luciferase. As an ATP-consuming enzyme, luciferase can be expressed within the organism of interest. Upon addition of luciferin (the substrate), fluorescence is produced in an ATP dependent manner, which in turn can be imaged[319-321]. Problems with this methodology consist of weak luminescent signals as well as poor spatial and temporal readings, highlighting the need for a more robust biosensor system[319,322].

In the past decade there has been a noticeable transition towards biosensors which have been designed, synthesised and developed, to improve their function and specificity. As an alternative to using luciferase as an ATP biosensor, the affinity of a bacterial protein for ATP can be exploited, transforming it into a direct, fluorescent reporter of the ATP/ADP ratio – namely Perceval[319]. This biosensor's ability to provide a quantitative measure of adenylate nucleotides stems from the bacterial trimeric, intracellular, GlnK1 protein[319]. As a member of the PII-protein family, Perceval's role resides in nitrogen regulation, specifically ammonium transport involved in glutamine synthesis[323]. Originating from *Methanococcus jannaschii,* GlnK1 must bind with Mg-ATP as well as 2-ketoglutarate to allow for ammonia transportation, due to the presence of both ligands being indicative of a healthy metabolism[319,324,325]. Coupled with circularly permuted GFP (cpGFP) – whereby the N- and C-termini are connected to bring them close to the chromophore for greater fluorescent signal intensity – this conformational change in GlnK1 following the attachment of ATP – and the by-product competition of ADP for these sites, whose successful binding becomes more likely in times of

metabolic stress due to the lack of available ATP – enables this biosensor to become a quantitative fluorescent marker of the ATP/ADP ratio within a cell[319,326].

Calcium is a common biosensor target, due to the fact it is an important signalling molecule involved in developmental and physiological processes, that fluctuates in different subcellular compartments depending upon the environment. Calcium imaging has been achieved at both the cellular and subcellular level in guard cells, roots and pollen tubes[327]. The biosensor GO-ATeam is one such example[327,328]. This is a Förster (or fluorescence) resonance energy transfer (FRET) probe; whereby a donor fluorophore when excited transfers energy to a nearby acceptor fluorophore in the vicinity, the acceptor's emission wavelength is longer and can therefore be specifically detected. GO-ATeam is used to directly measure ATP status via calcium ion (Ca^{2+}) levels in HeLa cells. Binding of ATP results in a conformational change increasing FRET efficiency[328]. This biosensor was later adapted to include a mitochondrial signal allowing it to become a subcellular biosensor[328,329]. More recently, detection of the signalling lipid phosphatidic acid (PA), has been used to create a new biosensor system[330]. Interactions between PA and other molecules are not well understood due to other imaging methods not providing high quality spatio-temporal resolution in plant cells[330]. The FRET biosensor, PAleon, has therefore been developed, which is sensitive enough to image PA dynamics and PA concentration at the plasma membrane (PM), determining PA signalling mediates the salt stress response[330].

Redox states of some metabolites can also be used to create biosensors. Reduction-oxidation sensitive GFP2-Orp1 (roGFP2-Orp1) produces a proximity dependent response to hydrogen peroxide (H_2O_2) levels[331]. H_2O_2 is usually

created during photosynthesis, photorespiration and respiration; it can act as a signalling molecule but is also a reactive oxygen species (ROS), which at high levels can create cellular stress[332]. Orp1 is a peroxidase which acts as part of a redox relay within the cell. Upon contact with H_2O_2, Orp1 oxidizes the transcription factor, Yap1, resulting in the formation of disulfide bonds and consequently a transcriptional response (Fig. 3.1)[331,333,334]. The Ybp1 protein is also involved, acting as a scaffold for the oxidation event[331]. However, Orp1 has also been shown to form an efficient redox relay with roGFP2 in place of Yap1, enabling roGFP2-Orp1 to be a biosensor of H_2O_2 by the production of a quantitative, ratiometric, fluorescent signal, determined by the excitation profile of the GFP protein in relation to its oxidation state (Fig.3.1)[331,335]. For the experiment performed here, Ybp1 is not involved. Orp1 is physically coupled to the roGFP2, ensuring the redox reaction occurs between Orp1 and roGFP2 only.

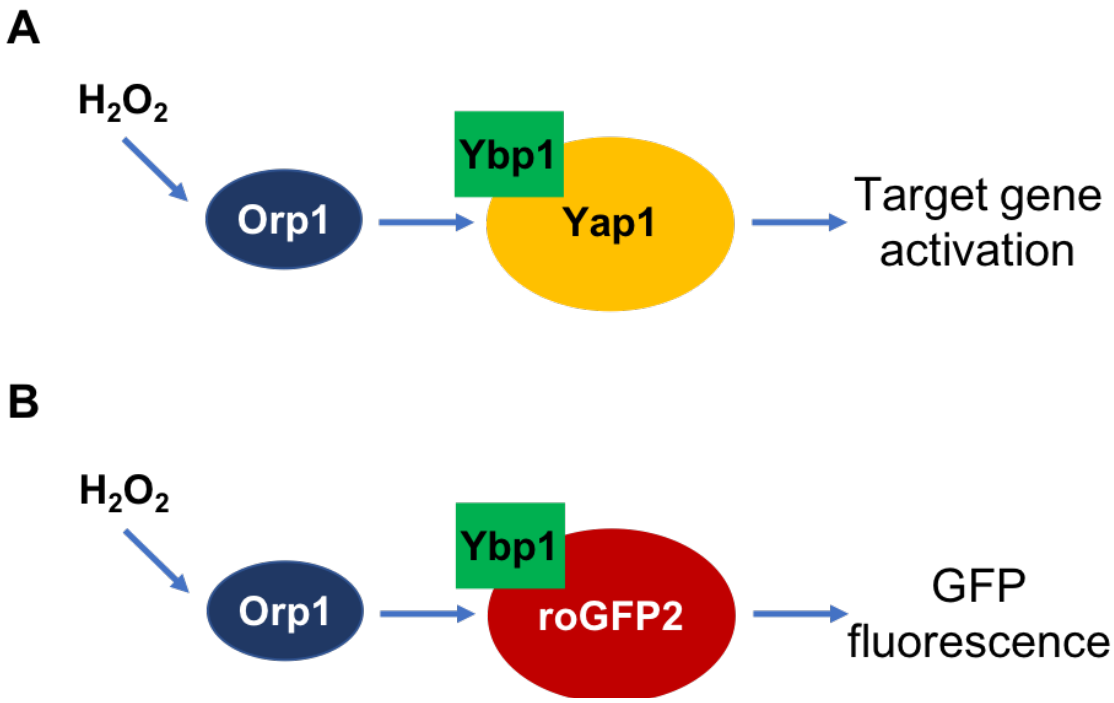

Figure 3.1 – Schematic representation of Yap1/roGFP2 biosensor activation. In both (A) and (B) H_2O_2 is detected by Orp1 which in turn implements the oxidation of either Yap1 (A), resulting in target gene activation following the entry of Yap1 into the nucleus, or roGFP2 (B) in the biosensor pathway, resulting in GFP fluorescence. In both cases this oxidation event is mediated by the protein Ybp1. The roGFP2-Orp1 biosensor produced in this chapter is made as a recombinant protein and therefore does not require Ybp1. Adapted from Rodrigues-Pousada *et al.* 2019.

3.1.4 Chapter aims and hypothesis

This chapter focuses on the design and production of metabolic biosensors in the fungus, *Z. tritici,* as an approach to understand the interaction between the fungus and its host, wheat. Evidence shows some wheat-*Z. tritici* interactions are compatible whereas others are incompatible, whereby the *Z. tritici* infection is successful or unsuccessful, respectively[336]. This seems to be determined at the stomatal interface, where the hyphae either enter to cause infection, enter but are prevented from establishing an infection – shown to be linked to an increase of H_2O_2 production by the host – or do not enter at all[308]. Microscopic studies have partially enabled the visualisation of the *Z. tritici* infection process, however, there is limited literature providing any detailed explanation on what makes an interaction between the two organisms compatible or not[293,317,336,337]. In this study, I have attempted to produce two ratiometric biosensors that localise to the mitochondria, in order to assess the metabolic state of *Z. tritici.* The mitochondria were chosen as they are considered the 'powerhouse' of the cell, producing ATP in optimal conditions and are the main source of ROS production when the cell is stressed. The hypothesis that is therefore being tested is that during incompatible

interactions the *Z. tritici* hyphae are under greater physiological stress at guard cell apertures than in compatible interactions.

3.2 Experimental procedures

Unless stated otherwise all reagents used were purchased from Sigma-Aldrich®.

3.2.1 Biosensor design and cloning

The previously generated biosensors, roGFP2-Orp1 and Perceval had been shown to be used successfully in their respective studies and worked via different mechanisms, these were therefore chosen as the backbones for developing *Z. tritici* mitochondrial biosensors[319,331,335]. Additionally, roGFP2-Orp1 was immediately available to us through the Smirnoff group, University of Exeter. This biosensor had already been modified to contain a mitochondrial signal, the cytochrome C oxidase subunit 4 (COX4, *Saccharomyces cerevisiae*) – forming mitroGFP2-ORP1. The Perceval biosensor was designed and codon optimised, using a repeat smashing algorithm (http://genedesign.jbei.org/RepeatSmashing), with the addition of a duplicated mitochondrial signal, Cytochrome C oxidase subunit 8 (COX8, *S. cerevisiae*) – forming mitoPerceval2. Synthesis of this gene was carried out by Integrated DNA Technologies® (IDT) and was resuspended in TE buffer, pH 8.0 (10mM Tris, 1mM EDTA), according to the IDT recommendations.

Biosensors were introduced into the appropriate overexpression vectors using Gateway® cloning. Gateway® PCR primers were designed and purchased from Eurofins (Appendix 1) and used for biosensor gene amplification in conjunction with Phusion® High-Fidelity DNA Polymerase (New England Biolabs® Inc.). **The mitoPerceval2 biosensor did not progress past this stage; the remaining**

methods are only applicable to mitroGFP2-Orp1. Gateway® BP and LR Clonase kits were purchased from Invitrogen™ and the corresponding Invitrogen™ protocols were followed. For all transformation steps, competent DH5α *Escherichia coli* cells were used. Recovery of plasmid DNA following each cloning step was mediated by the Thermo Scientific™ GeneJET Plasmid Miniprep Kit. Restriction digests were carried out to confirm the resulting vector was correct using FastDigest™ restriction enzymes and FastDigest™ buffer, purchased from Thermo Scientific™, followed by gel electrophoresis. Donor vector, pDONR207 (gen^R) was used for the Gateway® BP reaction (Appendix 2) and was propagated using competent *ccdB E. coli* (gen^R, cam^R) following the Thermo Scientific™ competent *ccdB E. coli* transformation protocol. Recovered plasmids were sent to Source Biosciences for sequencing – primers purchased from Eurofins (Appendix 3). Destination vectors, for the Gateway® LR reaction, were donated by the Haynes group, University of Exeter – pYSKH2 (*LB-Ku70LF-Ku70(Z. tritici)-ptrpC-*$G418^R$*-pZtTEF-ccdB-Ku70RF-RB*) and pYSKH4 (thought to be pYSKH3, see below) (*LBKu70LF- Ku70(Z. tritici)-ptrpC-*Sur^R*-pZtTEF-ccdB-Ku70RF-RB*) (Appendix 4 and 5)[338]. All experiments were carried out with the appropriate controls.

3.2.2 *Z. tritici* transformation

Competent *Agrobacterium tumefaciens* strain EHA105 (rif^R), was transformed with the expression clones produced via Gateway® cloning (rif^R, kan^R)[339]. The transformed EHA105 were used to transfer the expression clones into the *Z. tritici ku70* null strain HLS1000 (Δ*ku70:*$G418^R$) using a standard *A. tumefaciens* mediated transformation (ATMT) protocol[338,340-342]. HLS1000 was grown for 10 days on yeast peptone dextrose agar (YPD agar, per litre: 10g yeast extract, 20g

peptone, 20g dextrose and 20g agar media); incubated at 19˚C for 5 days, before being transferred to a fresh YPD plate and being incubated at 19˚C for a further 5 days[338]. Induction media (IM) and IM agar (10mM K_2HPO_4, 10mM KH_2PO_4, 2.5mM NaCl, 2mM $MgSO_4.7H_2O$, 0.7mM $CaCl_2$, 10um $FeSO_4$, 4mM $(NH_4)_2SO_4$, 10mM glucose, 40mM fresh MES buffer, 0.5% glycerol, ddH_2O added to make final volume, for solid media add 2% agar), supplemented with acetosyrigone (200μM), was used for the ATMT[338,341,342]. Approximately 10 days after the *Z. tritici* transformation, 20 transformants were removed for early sub-selection and the plates were returned to 19˚C for the remainder of the 3 weeks before 20 more were selected. mitroGFP2-Orp1 subcultures were grown on YPD or Basal media (BM) (per litre: 1.7g yeast nitrogen base without amino acids or ammonium sulfate, 2g asparagine, 1g NH_4NO_3, 10g glucose and 20g agar, pH 6.0 with 1M Na_2HPO_4), amended with geneticin (G418) (200μg/ml) or sulfonylurea (sur) (10μg/ml)[340,343].

3.2.3 Microscopy

To identify the transformant colonies that were most likely to contain the mitroGFP2-Orp1 biosensor, the *Z. tritici* sub-culture plates were screened using the Leica MZ16F stereomicroscope (GFP: excitation wavelength: 488nm, emission filter: 505-530nm). Those colonies which expressed abnormally high levels of fluorescence were sampled, and the cells were resuspended in 20μl of sterile water, with 5μl of suspension being pipetted onto a glass slide and analyzed using confocal microscopy[344]. Untransformed HLS1000 cells were used as a control. All confocal microscopy was carried out using the Leica TCS SP8 (excitation wavelength: 405nm and 488nm, emission wavelength: 505-530nm). For GFP spectral analysis, 11 excitation wavelengths (between 491-628nm) were used, and emission signal intensity readings were taken at five sites. These were

than averaged for each excitation wavelength and the standard error (SE) was calculated. For imaging only, 5 biological replicates were examined. For the spectral analysis only one biological replicate was used (line 5) as this was a preliminary experiment. Five technical replicates were carried out on this single sample.

3.3 Results

3.3.1 roGFP2-Orp1 and Perceval are suitable *Z. tritici* metabolic biosensor candidates

From initial knowledge and extensive literature searches two biosensors were highlighted and investigated further as potential metabolic biosensor candidates, namely roGFP2-Orp1 and Perceval[319,331]. mitroGFP2-Orp1 was readily available and had already been shown to work successfully in plant tissue (*Arabidopsis thaliana*) by the donating group (Smirnoff Group, University of Exeter). On the other hand, Perceval measures the ATP/ADP ratio using a completely different cellular mechanism, relying upon nitrogen regulation as opposed to H_2O_2 production for mitroGFP2-Orp1[319,331]. The Perceval biosensor had previously not been designed with a mitochondrial signal peptide, however a previously discussed biosensor, mitGO-ATeam2, had successfully used COX8 (Cytochrome c Oxidase subunit 8) for mitochondrial localisation in *Saccharomyces cerevisiae*[328]; Perceval was therefore designed with a duplicated COX8 mitochondrial signal – as this construct was synthesised, further validation studies for the design of the construct were not carried out.

3.3.2 *mitoPerceval2* could not successfully be amplified for biosensor production

mitoPerceval2 was synthesized by IDT. During the design of the biosensor, it was realised the construct contained a high number of repetitive nucleotide regions, which could interfere with gene synthesis due to interference with the process of combining oligonucleotide stretches; the construct was therefore optimised with alternate redundant codon combinations to reduce the number of repetitive regions. Direct Gateway® BP cloning reactions were unsuccessful. Using pre-designed Gateway® PCR primers (Appendix 1) amplification of the *mitoPerceval2* gene template from the synthesised plasmid was attempted but was also unsuccessful. To ensure the synthesised biosensor gene had the correct sequence and could be reproduced, a series of troubleshooting approaches were taken. Pairwise BLAST (https://blast.ncbi.nlm.nih.gov) results between the quality control data received with the synthesised gene and the nucleotide sequence sent for synthesis, matched with 100% coverage and identity. Second, the Gateway® PCR primers were verified, with both primer sequences being present within the gene. Following on from these initial investigations, restriction digests (Fig. 3.2), indicated DNA of the correct size, 4694 bp (pUCIDT-AMP*:mitoPerceval2*), was present providing evidence the biosensor (and IDT plasmid – pUCIDT-AMP) was present in the DNA resuspension.

Sequencing results (using Source Bioscience M13 primers) also verified the presence of the *mitoPerceval2* gene.

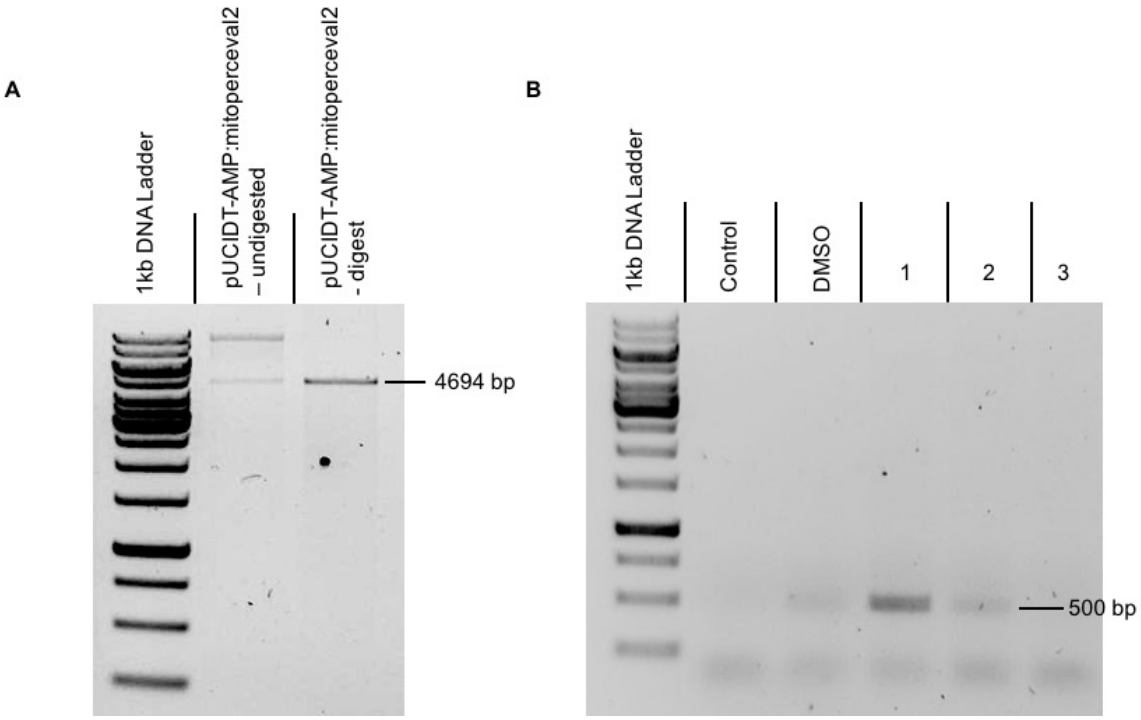

Figure 3.2 – (A) pUCIDT-AMP*:mitoPerceval2* linearisation. The third of 4 troubleshooting approaches. Presence of pUCIDT-AMP*:mitoPerceval2* both undigested and digested: 4694 bp. Two bands are present in the undigested lane due to the single-stranded nicked nature of undigested plasmid. 1 kb DNA ladder purchased from Thermo Scientific™. Restriction enzyme used was *NcoI*. **(B) Evidence of a low stringency PCR reaction.** Fragments can be seen in lanes: DMSO, 1 and 2 at approximately 500 bp. 10x [*pUCIDT-AMP:mitoPerceval2*] was used for reactions 1-3. Control contained no DNA to test for contamination. DMSO reaction contained 1x [*pUCIDT-AMP:mitoPerceval2*] with 1.5 µl DMSO. Reactions 1-3 contained no DMSO and had increasing annealing temperatures: 1 – 50 ˚C, 2 – 54.4 ˚C and 3 – 60 ˚C. 1 kb DNA ladder purchased from Thermo Scientific™.

A second PCR reaction was therefore attempted, in which a 10x concentration of pUCIDT-AMP:*mitoPerceval2* was used, as well as one sample containing the addition of DMSO, to disrupt any secondary structures which could be causing amplification issues and the addition of a temperature gradient (50°C, 54.4°C and 60°C). Gel electrophoresis results, (Fig. 3.2), indicated the presence of a DNA fragment; with the strongest band being present at 50°C (no DMSO). However, the fragment produced was approximately 500bp long, unlike the expected band of 1942bp, if *mitoPerceval2* had been successfully amplified, suggesting this fragment was an artefact of a low stringency reaction. A two-step PCR reaction followed this and was also unsuccessful. As a result of limited time, expense, and a series of unsuccessful results the production of the *mitoPerceval2* overexpression vector did not progress further.

3.3.3. Overexpression vectors, pYSKH2 and pYSKH4, were found to be suitable for *Z. tritici* biosensor transformation

The remaining biosensor gene, *mitroGFP2-Orp1,* was cloned into both the pYSKH2 and pYSKH3 destination vectors (Haynes Group, University of Exeter), with gene presence being confirmed by sequencing[338]. Alongside this, a single restriction enzyme digest of the two destination vectors was carried out to confirm that their characteristics were as listed in the vector suite[338]. The digestion of pYSKH3 with *NcoI*, should have produced five fragments corresponding to the five *NcoI* restriction sites (5'-CCATGG-3'). However, in total seven fragments were present (Fig. 3.3). Following the *A. tumefaciens* transformation with the produced expression clones, a colony PCR was performed (Fig. 3.3 and Appendix 6). The fragment produced, encapsulated the region of the plasmid

containing the selective marker and its corresponding promoter and terminating sequence. A fragment of approximately 1500bp, was correct for pYSKH2 (primer amplified region = 1472bp). However, for pYSKH3 with the *hyg*^{R} gene of 1025bp (primer amplified region = 1441bp) the fragment produced was unexpectedly larger at approximately 3000bp.

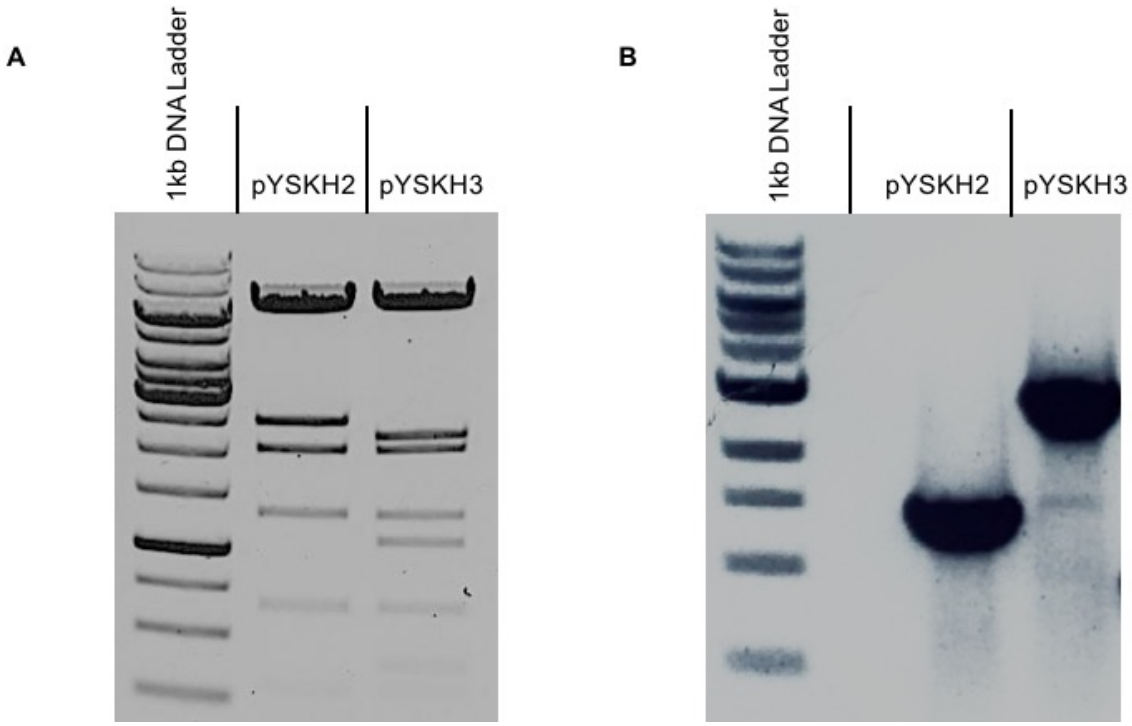

Figure 3.3 – (A) Restriction enzyme digest of overexpression vectors. Both pYSKH2 and pYSKH3 should produce 5 fragments after application of *NcoI*. The band produced at approximately 2000 bp in both overexpression vector lanes is most likely due to the presence of an uncharted *NcoI* site (digest with *HindIII* produced the correct fragment sizes). For pYSKH2 all remaining fragments are correct. pYSKH3 shows 7 other fragments which is not consistent with the presence of the *Hyg*^{R} gene. 1 kb DNA ladder purchased form Thermo Scientific™. **(B) Colony PCR of resistant markers.** Bands produced correspond to fragment sizes of approximately 1500 bp and 3000 bp for pYSKH2 and pYSKH3, respectively. Image produced by the Haynes group. 1 kb DNA ladder purchased from New England BioLabs® Inc.

To provide confirmation and further clarity of the overexpression vectors' characteristics, sequencing of the selective marker was initiated. This identified the resistance marker of pYSKH3 as not *hyg* but rather *sur*; with a primer amplified region of 2891bp, coinciding with the size of the fragment produced during the colony PCR reaction. Further sequencing results indicated that the plasmid still possessed the same characteristics, including the same *pZtTEF* promoter, and only had a different selection marker – this construct was therefore mislabelled and was matched in the overexpression vector inventory to pYSKH4 (Appendix 5). This overexpression vector will now be referred to as pYSKH4.

3.3.4 *Z. tritici* transformation was successful for pYSKH4*:mitroGFP2-Orp1*

Ten days following the *Z. tritici* transformation, plates were removed from the incubator to assess fungal growth and to create sub-cultures. In comparison, the control plate (no antibiotic) and the selection plates (with antibiotic) for pYSKH2*:mitroGFP2-Orp1*, displayed little difference in colony number, (Fig. 3.4), and therefore this biosensor, was not carried forward in this study. On the other hand, a substantial difference in growth could be seen for pYSKH4*:mitroGFP2-Orp1*, with individual colonies developing on the selection plates in comparison to the hyphal lawn that had developed on the control plate; pYSKH4*:mitroGFP2-Orp1* was therefore sub-cultured to remove any background WT *Z. tritici* growth. The purity of the transformants was not assessed in the interest of time but should be evaluated in future/similar experiments.

3.3.5 pYSKH4:*mitroGFP2-Orp1* shows variation in expression between *Z. tritici* cells

From the first set of 20 sub-cultures that had been grown, five lines were identified using the stereomicroscope as producing a stronger than average GFP signal, i.e. not one as a result of natural autofluorescence; these lines were therefore investigated further by confocal microscopy. As these were preliminary biosensor tests, no ratiometric quantitative data was collected. GFP fluorescence was measured at excitation wavelengths of both 405nm and 488nm (wavelengths used to detect the oxidised/reduced biosensor state respectively).

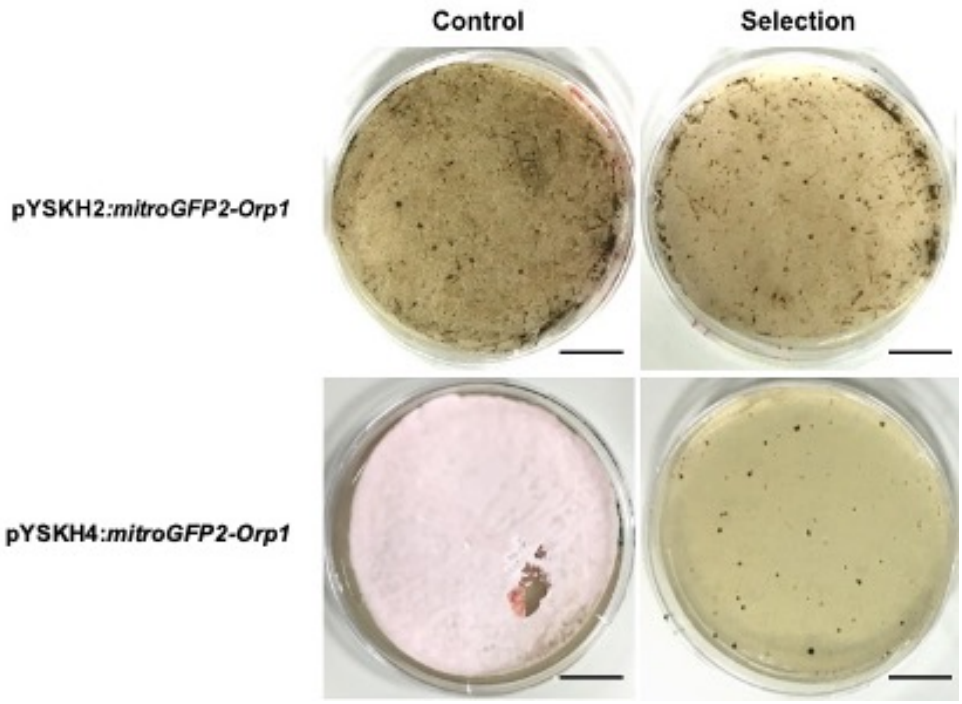

Figure 3.4 – *Zymoseptoria tritici* transformation colonies. (A) pYSKH2*:mitroGFP2-Orp1* – YPD agar selection plates contained G418 (200ug/ml*)* (B) pYSKH4*:mitroGFP2-Orp1* – BM agar selection plates contained sur (10ug/ml). For both constructs the selection plates also contained kanamycin (100ug/ml*).* Controls consisted of the same designated media without antibiotic selection. All colonies grown on cellophane discs. Scale bar = 2cm.

All five lines tested showed a GFP signal, however, the intensity of this varied greatly between lines, (Fig. 3.5) – lines 5 and 7 demonstrate this. Line 5 was brighter than all other lines tested, with line 7 being representative of the others displaying a weaker GFP signal, with less evidence of mitroGFP2-Orp1 biosensor fluorescence being present at an excitation wavelength of 488 nm. In comparison to line 7, line 5 displayed a clear localization of GFP signal in areas of the cells, some of which corresponded to subcellular locations seen in the differential interference contrast (DIC) images.

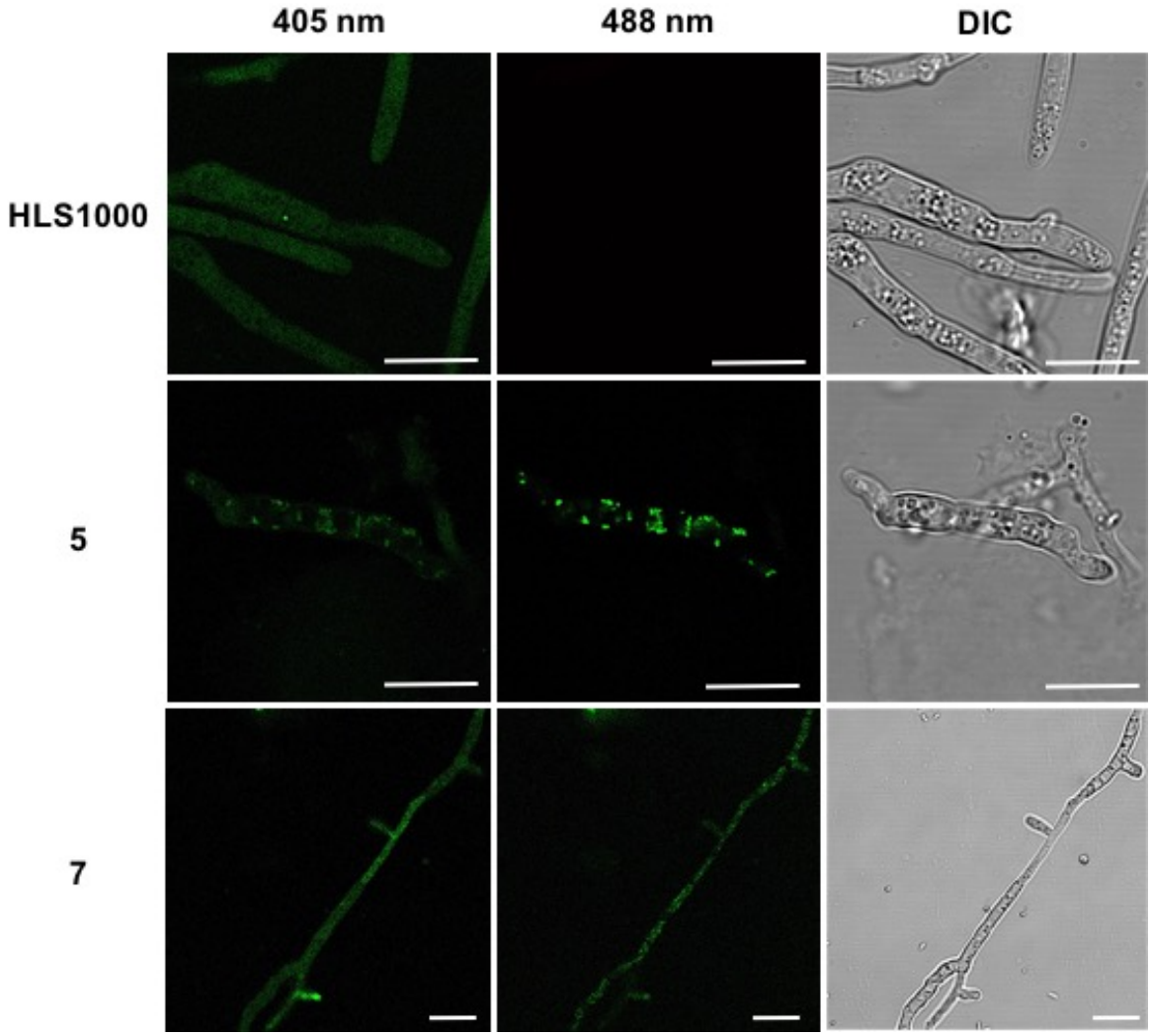

Figure 3.5 – *mitroGFP2-Orp1* expression. HLS1000 cells that had not undergone the transformation process were used as a control. Lines 5 and 7 each show different expression levels of *mitroGFP2-Orp1*. For each sample excitation wavelengths of 405nm and 488nm and a GFP emission filter (585-615nm) were used. DIC images have been added for cellular reference. Scale bars = 10μm.

For all images collected at an excitation wavelength of 405nm, any localisation could not clearly be determined, with the signal being spread throughout the cell and a higher level of auto-fluorescence also being produced. The control sample (HLS1000) displayed high autofluorescence at 405nm with minimal autofluorescence at 488nm. A clear difference can be seen in signal localisation and intensity between lines 5, 7 and the control, with both signals being much weaker in the control sample. Spectral analysis confirmed, for line 5, that the signal produced was emitted by GFP (Fig. 3.6) – the large drop in signal intensity after an emission wavelength of 500nm indicates this. As this was only a preliminary test to assess GFP emission, control measurements were not taken here. These initial investigations into the success of the mitroGFP2-Orp1 biosensor confirm that GFP is being expressed inside the *Z. tritici* cells at differing intensities.

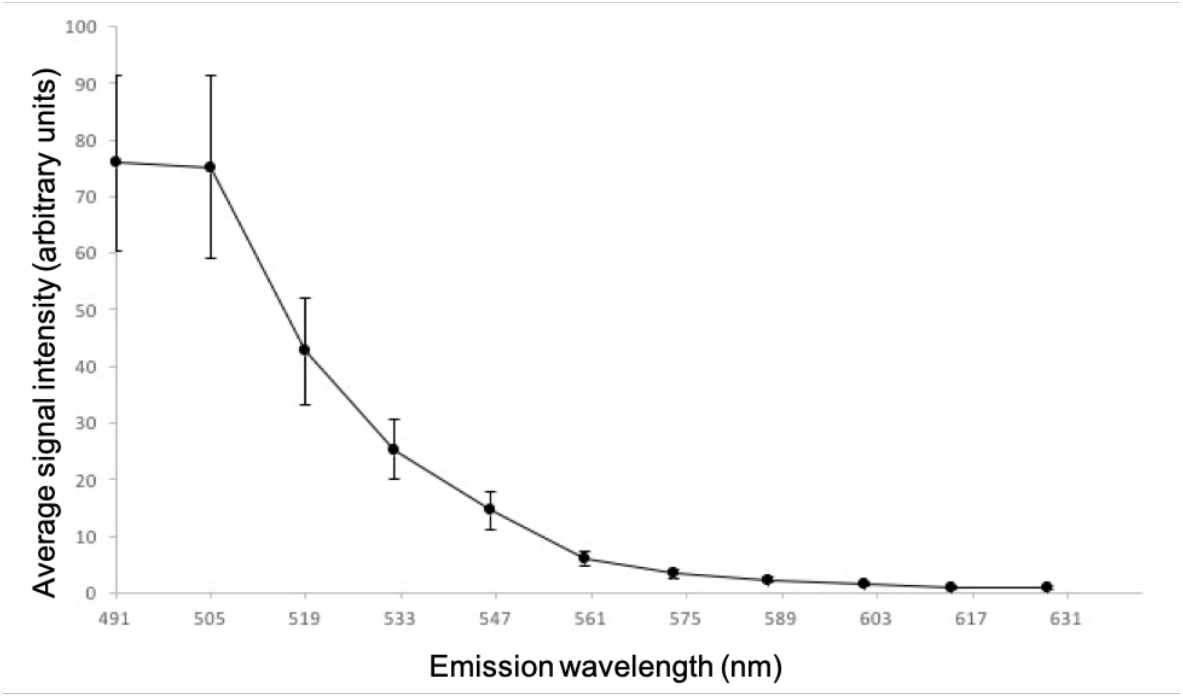

Figure 3.6 – mitroGFP2-Orp1 spectral data. These measurements were taken for line 5 only. Five samples were taken corresponding to five areas of localized high signal intensity and values were averaged at each of the 11 emission wavelengths shown. The emission wavelength, x-axis, displays the beginning of a set of 14nm windows. Errors bars are equal to ± 1 standard error (SE) to indicate the variance between samples. Raw data is shown in Appendix 7.

Please note: All results (and corresponding methodologies) discussed from this point forward are not my own, but a product of follow-up work carried out by Francesco Valente (Thesis submitted February 2020) another PhD student within the Deeks group, University of Exeter. I was unable to carry on this project myself as I was required to transfer to Rothamsted Research to focus on *F. graminearum*.

3.3.6 mitroGFP2-Orp1 line 5 displays sensitivity to other ROS species

The mitroGFP2-Orp1 biosensor was designed to quantitively measure the metabolic state of *Z. tritici* in both compatible and incompatible interactions in wheat – more specifically at the epidermal interface where the interaction between the hyphae and guard cells takes place. I had previously hypothesised that in an incompatible interaction, where the hyphae were unable to successfully infect the host, the hyphae would experience an oxidative stress response induced as a result of plant-defence responses. As mentioned in the previous section, line 5 of the pYSKH4:*mitroGFP2-Orp1* transformants displayed the greatest GFP intensity. This line was therefore taken forward by Francesco Valente for further live-cell imaging, investigating how effective the biosensor was both *in vitro* and *in planta* when stressed.

Hyphae were exposed to dithiothreitol (DTT), a redox reduction reagent, H_2O_2 and sterile Milli-Q H_2O, *in vitro,* and were consequently imaged using the Leica TCS SP8 confocal microscope (Fig. 3.7). Matlab and Fiji were both used to analyse images (Fig. 3.8). The oxidised/reduced biosensor state (405nm/488nm) was used to quantify the effects of the three reagents (added 10 minutes prior to imaging) on the *Z. tritici* hyphae over the course of four biological replicates. The addition of DTT treatment (10mM) lead to a reduction reaction, and therefore an average 405/488nm ratio of 0.695 (if primarily an oxidation event as would be expected in the presence of ROS, we would expect a value over 1). It should be noted that these values are relative, controls are needed with every experiment setup as an exact ratio depends on the relative laser intensities; measuring the extreme oxidation and reduction of the probe and measuring relative to these values will ensure reliability. Upon addition of H_2O_2 (100mM), the hyphae

experienced oxidative stress and therefore the 405/488nm ratio was calculated at 1.031. As a control sterile Milli-Q H_2O was applied to the fungal hyphae, however the 405/488nm ratio produced after subsequent analysis was 1.086. As H_2O is not a redox reagent, a significant oxidation value would not be expected when applied to this ratiometric biosensor. This suggests that the mitroGFP2-Orp1 biosensor may not be H_2O_2-dependent but is rather affected by other ROS species, possibly as a result of having lost the Orp1 protein (Fig.3.9 and Fig.3.10).

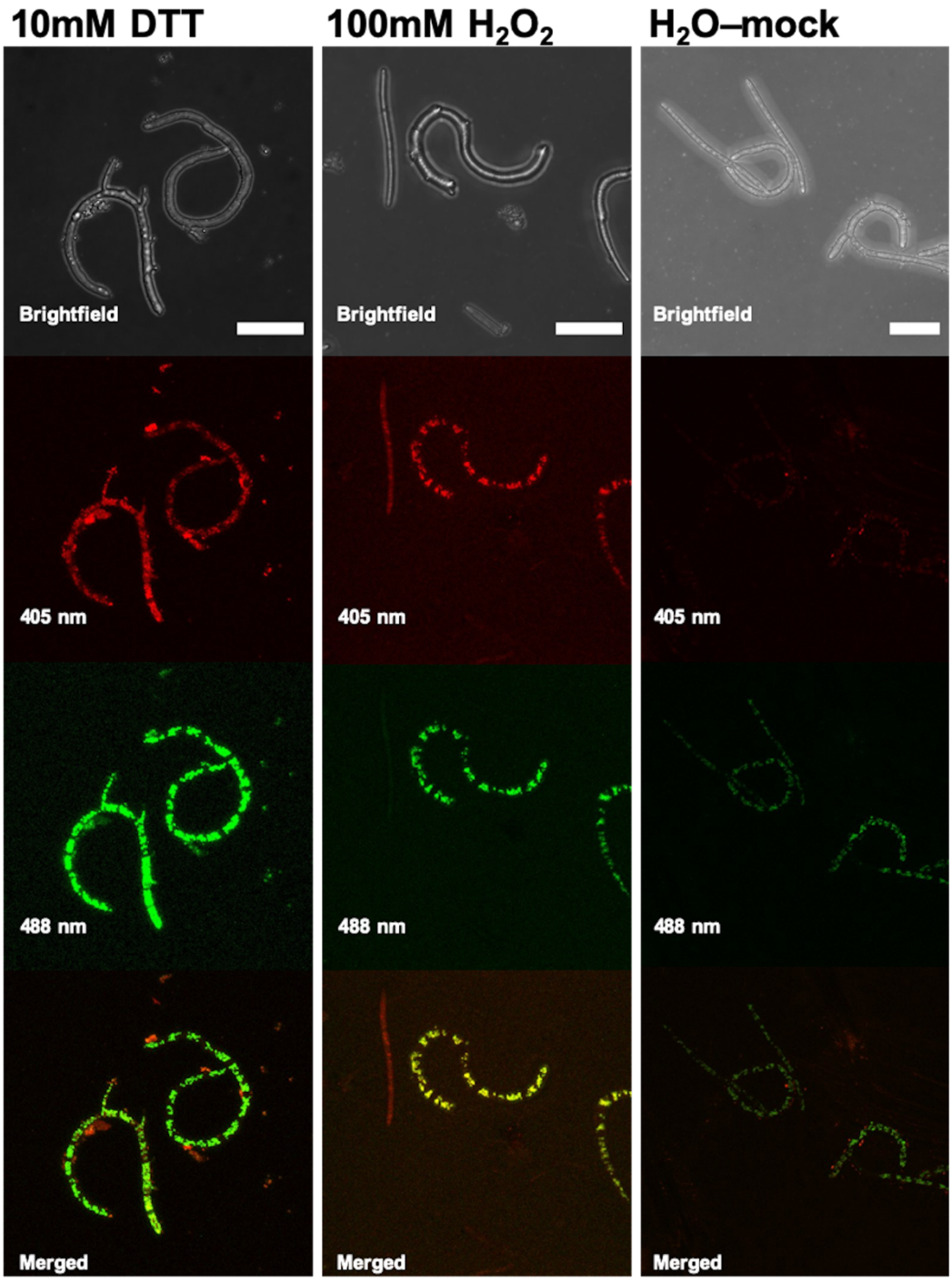

Figure 3.7 – Expression of mitroGFP2-Orp1 in *Zymoseptoria tritici*. *Z. tritici* (HLS10000) transformed with the mitroGFP2-Orp1 biosensor was exposed to 10mM DTT, 100mM H_2O_2 and H_2O. Bars = 20μm. Figure courtesy of Francesco Valente, University of Exeter.

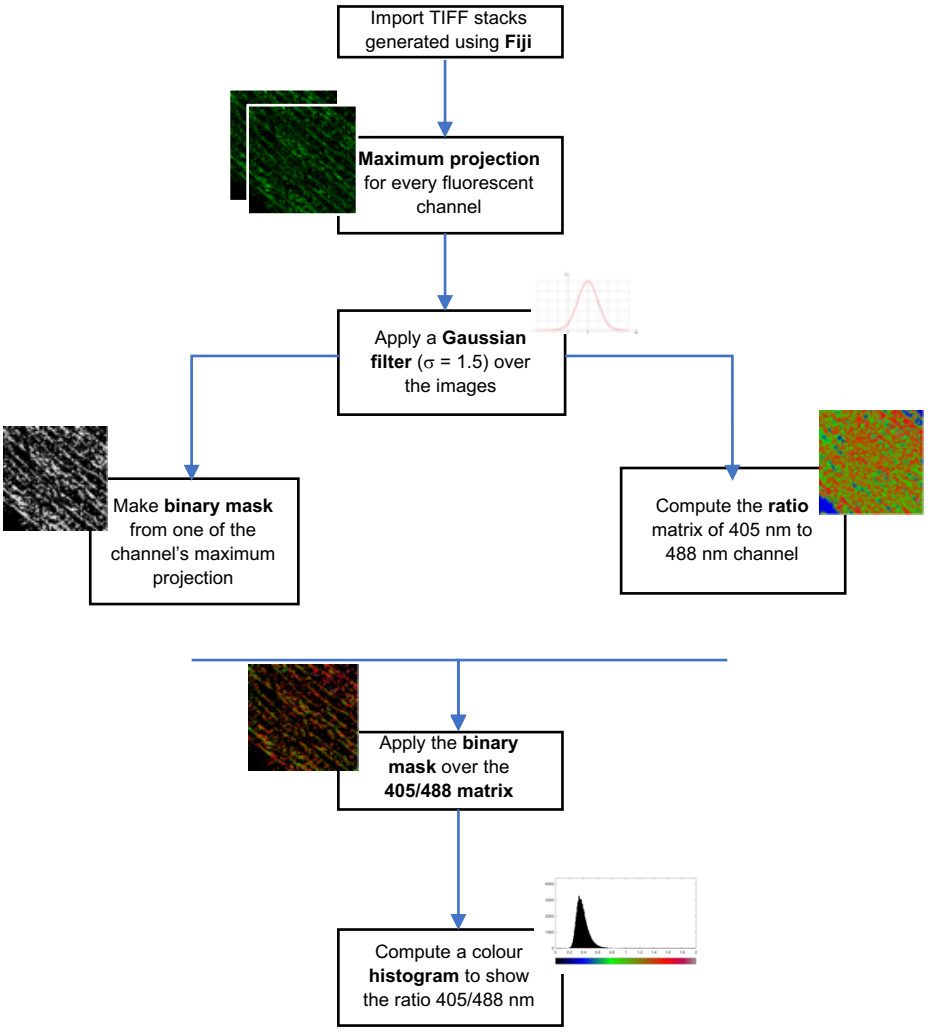

Figure 3.8 – Ratiometric image acquisition and analysis flowchart. Live-cell images were collected and imported as Tiff files into Matlab using Fiji. The script was designed to exclude autofluorescence (exclusion mask) and calculate the ATP/ADP (405nm/488nm) ratio. A histogram was thereby produced to show these results. Figure courtesy of Francesco Valente, University of Exeter.

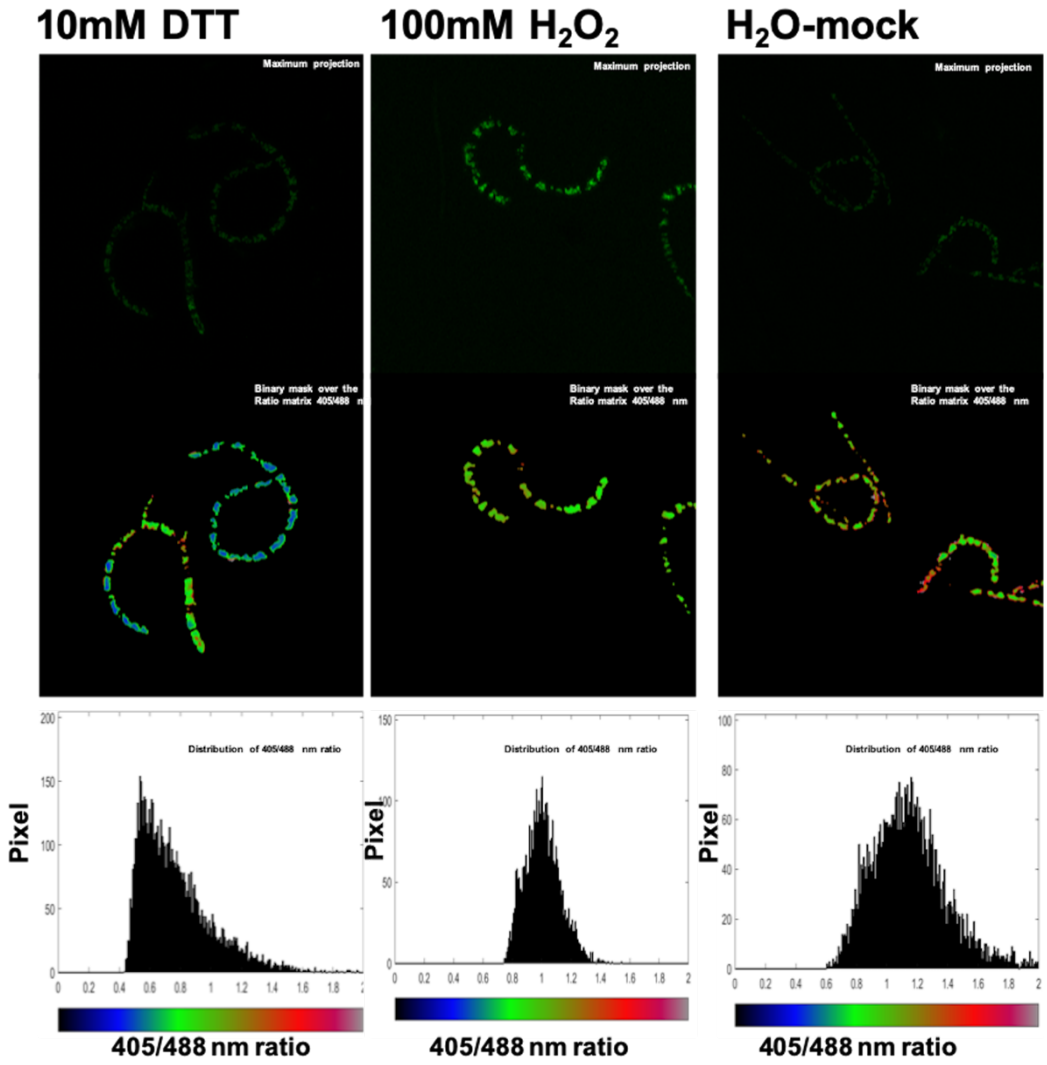

Figure 3.9 – Ratiometric analysis on *Zymoseptoria tritici* mitroGFP2-Orp1 line 5. *Z. tritici* hyphae (HLS10000) were treated with the following for 10 minutes: 10mM DTT, 100mM H_2O_2 and H_2O. Images demonstrate the use of the Matlab-based program shown in Fig. 3.8 for calculating the 405/488nm ratio in the cell from the GFP signal. The distribution of the 405/488 nm ratio values, displayed on the histograms, show values ranging between 0 and 2. Figure courtesy of Francesco Valente, University of Exeter.

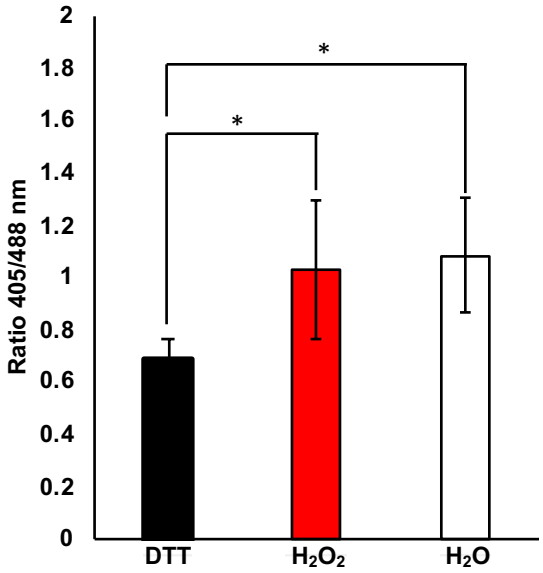

Figure 3.10 – Fluorescence ratio of *Zymoseptoria tritici* mitroGFP2-Orp1. DTT treatment resulted in the reduction of roGFP2; H_2O_2 treatment resulted in the oxidation of roGFP2; the mock control (sterile Milli-Q H_2O) induced greater oxidation of roGFP2 than H_2O_2. There was no statistical significance between H_2O_2-treated samples and the control. Bars show standard deviation. *P<0.05 (two sample t-test). Figure courtesy of Francesco Valente, University of Exeter.

3.3.7 Integration of mitroGFP2-Orp1 into the *Z. tritici* Ku70 locus was unsuccessful

It was hypothesised that the *mitroGFP2-Orp1* transgene in line 5 had been damaged by the integration event and that there could be a mutation in the open reading frame (ORF). Following genomic DNA extraction of transformed *Z. tritici* mycelia, Phusion HR enzyme (NEB) and primers TEF1-FWD and Ku70_EXT-REV were used to perform a diagnostic PCR to determine if the integration site of *mitroGFP2-Orp* was at the *Ku70* locus (correct integration = 3500bp product).

The reliability of the ORF was also investigated (Fig. 3.11). The products of these PCR experiments were analysed by gel electrophoresis and purified PCR products were sequenced by Eurofins (Fig.3.12). Alignment was carried out using SnapGene and BioEdit Sequence Alignment Editor.

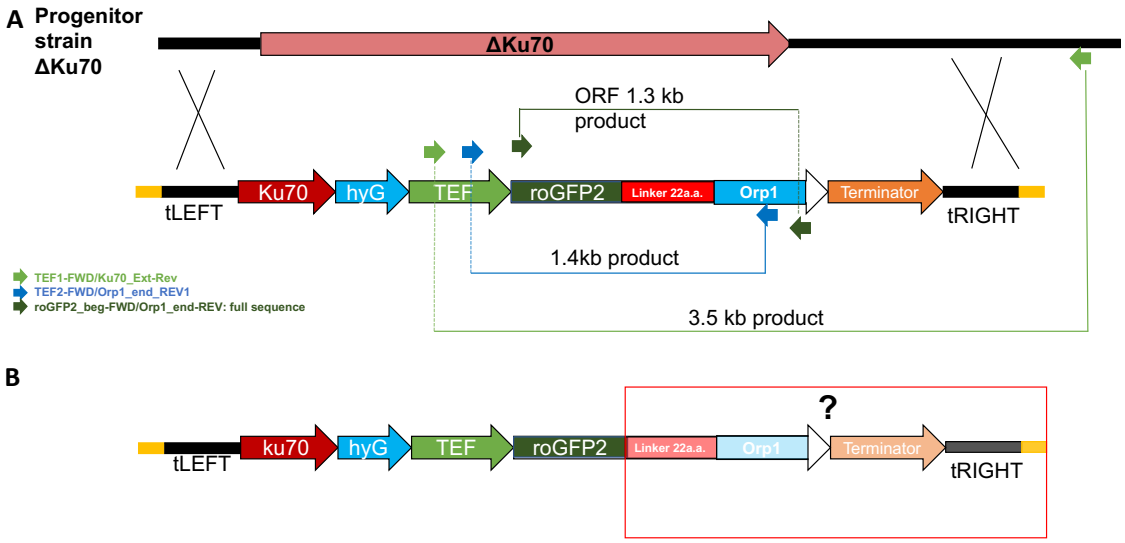

Figure 3.11 – Schematic representation of mitroGFP2-Orp1 integration into the *Zymoseptoria tritici* HLS1000 genome. A) Primers used to test successful biosensor integration in the recipient genome at the Ku70 locus – TEF2-FWD/Orp1_end-REV1 and roGFP2_beg-FWD/Orp1_end-REV. B) Deletion of the linker between the roGFP2 and Orp1 proteins in line 5 was indicated by the results. Reproduced from Cairns (Cairns *et al.*, 2015). Figure courtesy of Francesco Valente, University of Exeter.

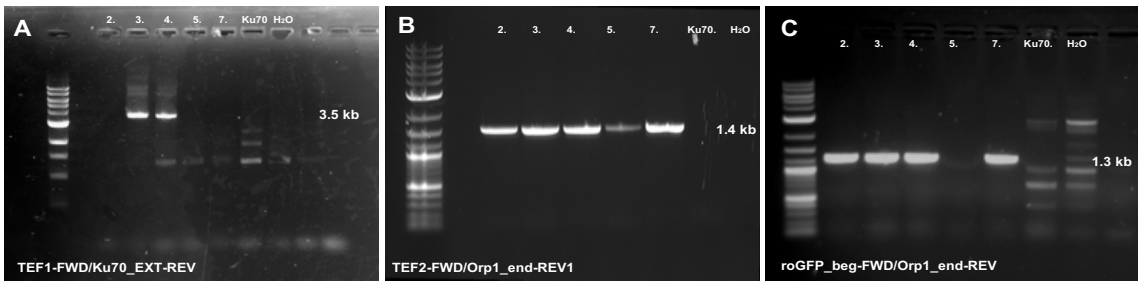

Figure 3.12 – *Zymoseptoria tritici* mitroGFP2-Orp1 integration. (A) PCR carried out on transformed lines 2-7 to amplify the right flank of the pYSKH4 vector/construct (*Ku70* gene), expected fragment size = 3.5kb. (B) PCR for the promoter pZtTEF and ORF of the pYSKH4 expression vector, expected fragment size 1.4kb. (C) PCR of the full ORF with an expected fragment size of 1.3kb. Genomic DNA extracted from the Ku70 *Z. tritici* strains was used as a negative control. (A) 1kb DNA (B) and (C) 1kb Plus ladders. Agarose gel (2% (w/v) in TAE) electrophoresis. Figure courtesy of Francesco Valente, University of Exeter.

The conclusion from line 5 was that the biosensor was damaged and that the dimmer lines represented the intact construct. Therefore, the ability of these intact lines to be used for ratiometric work was investigated. Focus was given to the transformed *Z. tritici* line 5, for the aforementioned reasons, however for this part of the study, other lines that showed reduced fluorescence in comparison to line 5 were used in contrast. Sequencing results suggested lines 3 and 4 had correctly integrated the biosensor into their genomes, however the results for line 5 did not, showing an absence of the *orp1* gene at the Ku70 locus, suggesting its integration elsewhere within the genome – its effectiveness as a H_2O_2 biosensor may therefore be limited. Lines 3, 4 and 5 were all tested *in planta* for analysis of the fungal-host interaction. All images were taken using the Leica TCS SP8 confocal microscope in the wheat cultivar Riband (Fig. 3.13). All three lines tested

displayed varying levels of fluorescence with line 5 being the brightest. However, even though this was the case none were sufficiently bright enough to produce a ratiometric measurement.

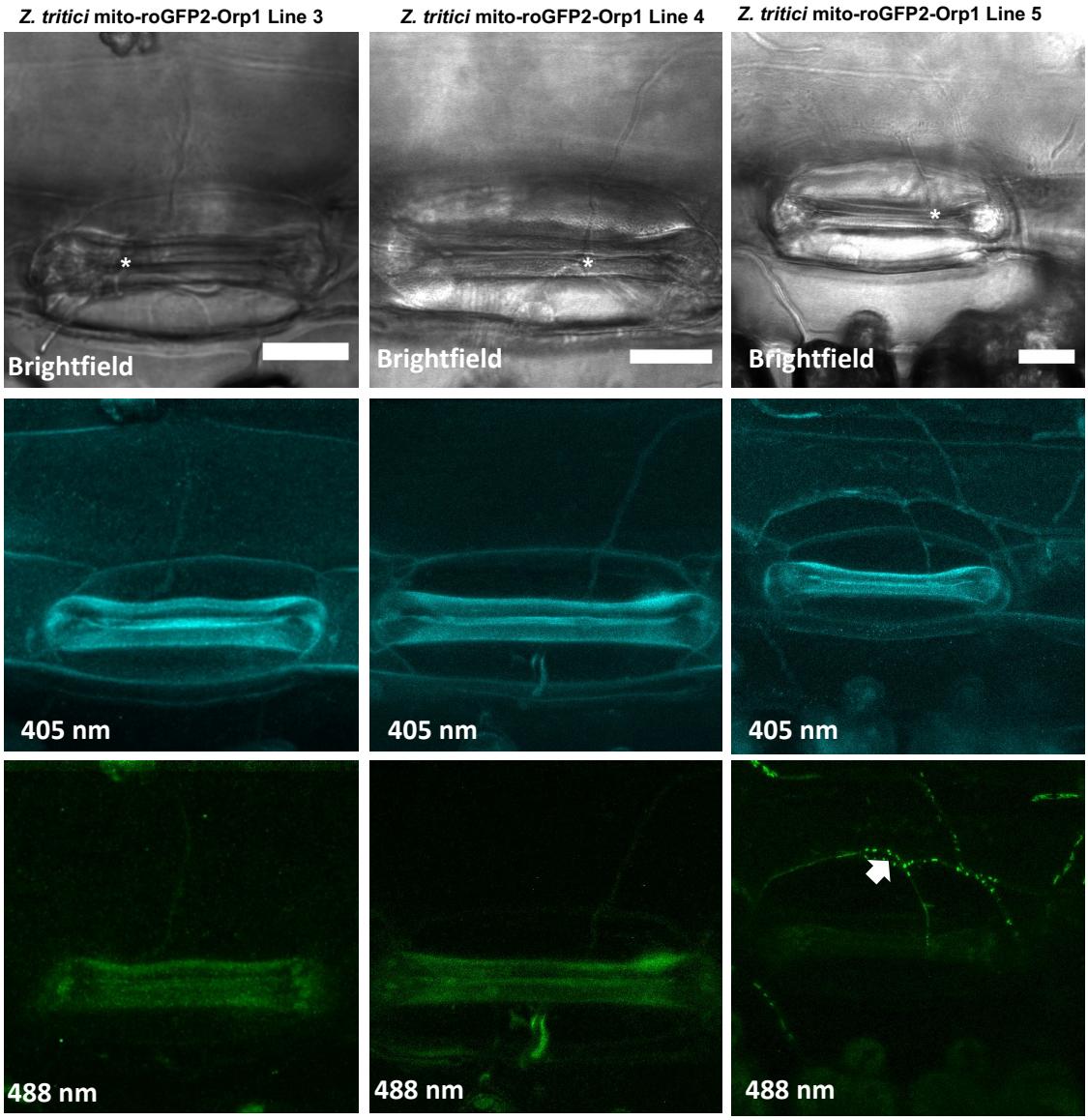

Figure 3.13 – Use of mitroGFP2-Orp1 *Zymoseptoria tritici* during infection. Asterisks showing the *Z. tritici* hyphae position. White arrow = mitochondria GFP fluorescence. Scale bars 20μm. Figure courtesy of Francesco Valente, University of Exeter.

3.4 Discussion

In this study I have attempted to construct two biosensors, mitroGFP2-Orp1 and mitoPerceval2, adapted for localization to the mitochondria, to obtain quantitative measurements in order to determine the metabolic state of *Z. tritici* cells during early infection, and allow for comparisons to be made between compatible and incompatible interactions in the fungus and wheat host. Problems with mitoPerceval2 biosensor production redirected the study to focus on mitroGFP2-Orp1 only. Previous research had successfully demonstrated the uses of similar biosensors in eukaryotic cells, with many focusing on microbial functionality[345]. *mitroGFP2-Orp1* had been donated by the Smirnoff group, University of Exeter, who had previously worked with the biosensor *in planta* using *A. thaliana*. On the other hand, *Perceval* was modified to accommodate a subcellular, in this case mitochondrial, function; both biosensors possessed *Saccharomyces cerevisiae* mitochondria targeting signals. Fig. 3.5 indicates that at an excitation wavelength of 405nm, not all mitroGFP2-Orp1 molecules are localized to the mitochondria and some remain cytosolic following translation most likely as a result of mislocalisation or accumulation within the secretory pathway as a result of construct size/conformation. Other studies which have used a roGFP-based biosensor have used the yeast leader sequence, ATP9, providing an alternative approach to the COX8 signal used here[329]. ATP9 is a component of mitochondrial membrane ATPase (www.uniprot.org/uniprot/P61828) that is 76 aa in length and has two transmembrane domains (TMDs). On the other hand, COX8 is a component of cytochrome c oxidase (www.uniprot.org/uniprot/P04039) that is 78 aa in length and possesses a helical TMD. When aligned using the NCBI BLAST tool no significant similarities are found.

mitoPerceval2 could not be successfully cloned via the direct Gateway® BP reaction or via PCR. Following a series of troubleshooting steps, the conclusion was reached that the production of the short 500bp fragment (Fig. 3.2) created during a PCR reaction, was an artefact of low stringency. Even though many repetitive regions had been replaced within the gene a high number still existed, increasing the likelihood of secondary structure or polymer formation, making *mitoPerceval2* more difficult to manipulate in reactions such as those during PCR. For future studies and biosensor designs it would therefore be recommended to avoid high incidences of repetitive regions. If *mitoPerceval2* is needed for further research, plasmid linearisation would be recommended to make the fragment of interest more accessible to any reactants. Alternatively, using a different polymerase could also solve this problem. The design of the overexpression vectors, pYSKH2 and pYSKH4, makes them specific to Gateway® cloning[338]. The difficulties surrounding the *mitoPerceval2* reaction could otherwise be eliminated by using an alternative cloning approach, such as Golden Gate assembly[346].

Prior to biosensor production it was discussed as to whether the use of a constitutive promoter, such as *pZtTEF*, in conjunction with an overexpressed transgene, could produce atypical *Z. tritici* characteristics, both at the genotypic and phenotypic level[347]. With no reference data to indicate the signal strength of such biosensors in other fungal expression vectors (as opposed to the ones used here), overexpressing the biosensors was the preferred and most well-suited starting approach. As seen in Fig. 3.5 the overexpression of the mitroGFP2-Orp1 biosensor does not always result in strong levels of expression with some lines still only emitting weak GFP signals. It is likely that the constant production of the biosensor, will be energetically costly to the fungus. Any cells that possess a high

level of biosensor expression may be selected against for this reason, explaining why many cells were only seen to express intermediate levels of GFP. Any resulting abnormalities in the transgenic strain, in comparison to the non-transgenic strain, would be seen in older cell cultures but more likely during infection assays, this analysis has not been performed here. Pre-existing evidence also suggests there is a possibility of producing hypervirulent fungal strains as a result of gene overexpression[348].

Creating a hypervirulent strain as a result of mitroGFP2-Orp1 biosensor overexpression is a possibility that should be considered. The presence of high levels of this H_2O_2 detector could increase the quantity of redox relay reactions occurring within a cell. In this scenario, mitroGFP2-Orp1 would act as a sink for H_2O_2 upon binding to one another. Hence, the transformed cells would be able to cope with higher-than-average levels of H_2O_2 when metabolically stressed, creating a more virulent *Z. tritici* strain, however there is no mention of this in the literature. One study focusing on the use of a roGFP2 biosensor in the filamentous fungi *Botrytis cinerea*, has demonstrated the utilisation of redox relays during fungal development and tissue differentiation, introducing the possibility of an altered *Z. tritici* phenotype being produced with an increase in redox relay reactions[349]. Alternatively, the overexpression of *mitoPerceval2* is less likely to result in the production of a hypervirulent strain but would rather affect energetic expense acting as a sink for ATP. If successful biosensor *Z. tritici* strains are produced in the future, their growth on solid media and infection assays *in planta* will be needed to assess virulence and mutant phenotypes. These results can then be compared to those of the wild-type (WT) HLS1000 strain. If the results from such experiments suggest that the overexpression of

these biosensors is causative of an altered phenotype, there are several different approaches that can be taken. As previously discussed, different expression vectors can be used to prevent biosensor overexpression and in turn restore the WT phenotype if a mutant one is created. Alternatively, overexpression vectors with an inducible promoter, *pZtNIA1*, could be utilised, preventing the constant overexpression of the biosensor, reducing energy costs, and minimizing phenotypic changes[338].

The low transformation efficiency of *Z. tritici* resulted in the production of very few successful transgenic colonies being produced[223]. The large difference in growth seen between the selection and control plates (Fig. 3.4) for the transgenic, pYSKH4*:mitroGFP2-Orp1*, strain indicates that the colonies formed on the selective media are likely to be successful transformants. No difference was present, in terms of *Z. tritici* growth, between the selection and control plates for the pYSKH2*:mitroGFP2-Orp1* strain – it is therefore highly-probable that this transformation was unsuccessful. Even though the pYSKH2 overexpression vector was recommended to us for use, the literature states the HLS1000 *Z. tritici* strain used for the transformation process possesses $G418^R$ as does the pYSKH2 vector, making transformant selection near-impossible[338].

Subcultured colonies were grown to allow for microscopic analyses. Microscopic analysis was chosen as an initial test to confirm the presence of the biosensor in the cells by GFP excitation (Fig. 3.5). Spectral analysis (Fig. 3.6) demonstrated the emitted signal was GFP due to the drop-in signal intensity after a wavelength of 505nm – the end of the GFP excitation spectrum. No quantitative measurements were taken from these initial screens as it needed to be

determined what lines possessed the greatest biosensor overexpression beforehand. Localisation of the emitted signal could be seen to occur within rounded structures in the cells analysed. MitoTracker® could be used in the future to determine whether or not this signal originates from the mitochondria as demonstrated in the literature[350]. If this is the case the signal emitted by the MitoTracker® should coincide with that emitted by mitroGFP2-Orp1.

A study into the use of a roGFP2-based biosensor in the rice fungal pathogen, *Magnaporthe oryzae,* demonstrated that signal intensity was highly dependent upon the developmental stage of the cells being tested[351]. Fluctuations of endogenous ROS during development were also discovered and due to the production of ROS by the host plant during a pathogenic attack, this study also demonstrated the ability of *M. oryzae* to withstand high levels of ROS bombardment enabling it to overcome its hosts immune response[351]. The successful production of a mitroGFP2-Orp1 biosensor in *Z. tritici* would therefore allow these areas to be investigated.

Further research of the mitroGFP2-Orp1 biosensor to test its function *in vitro,* by Francesco Valente (Deek's group, University of Exeter), demonstrated that following the application of DTT, H_2O_2 and sterile Milli-Q H_2O (reducing, oxidising and a stable molecule respectively), anomalous results were produced with H_2O eliciting a response typical of an oxidation event (405/488nm ratio = 1.086). This could be explained by the biosensor being sensitive to other ROS besides H_2O_2 but could also have been a result of a fault in the biosensor/its insertion into the genome. Diagnostic PCRs and subsequent sequencing revealed that line 5 (the brightest of the transformed *Z. tritici* lines) suggested successful integration of the

biosensor gene at the *Ku70* locus had not been achieved. The high level of GFP expression seen was therefore most likely a result of the loss of the *Orp1* gene and therefore line 5 is not suitable for use as a biosensor of H_2O_2. On the other hand, lines 3 and 4 did show successful integration into the genome but were too lowly expressed to produce significant measurements as biosensors.

Further approaches to solve the issues discussed above are necessary. These include: the use of the endogenous *Z. tritici* Orp1, codon-optimisation of GFP for *Z. tritici* and western blots to confirm protein expression. A *Z. tritici* codon-optimised *GFP* gene has already been produced and has been shown to be more stable and more highly expressed than eGFP in the cytoplasm[293]. If these properties are maintained in the mitochondria a biosensor with higher expression could be produced. Other *Z. tritici* transformation vector sets also exist, such as those which use the succinate dehydrogenase locus as a 'soft-landing' site for genes[352]. However, these may need to be modified for use as biosensors as they have previously been constructed with a reporter gene[352]. If low expression continues to be a problem with this fungal mitochondrial biosensor, metabolic biosensors for other ROS-producing subcellular compartments could be developed i.e. the peroxisomes.

During incompatible interactions, when the hyphae cannot enter through the stomata successfully or can, in which case the infection process is halted by unknown factors, it is theorised that the host plant can sense the attack by the fungus and therefore produces a chemical signal or repellent, deterring the *Z. tritici* hyphae from entering any further and conferring resistance to the plant. Consequently, if this or something similar is occurring the fungus may become

stressed and in turn produce its own H_2O_2 which may then be detected by the roGFP2-Orp1 biosensor. One study has addressed the production of high levels of H_2O_2 by the plant preventing intercellular hyphal spread but it is likely other mechanisms are involved, especially when there is some hyphal constraint before entry into the host[308,310]. Recent developments have led to the discovery of the *Z. tritici* avirulence gene, *AvrStb6,* responsible for interactions with the resistant *Stb6* gene in wheat, triggering a strong resistant response against *Z. tritici* attack[353]. Incompatible interactions are shown to occur between the Swiss 1E4 *Z. tritici* strain and the wheat cultivars: Chinese spring, Cadenza and Shafir, with compatible interactions occurring with cultivars lacking the *Stb6* gene – Obelisk and Taichung[353]. There is some debate however as to how the host prevents infection progression after fungal entry at the stomata, during incompatible interactions, following the recognition of AvrStb6 by the host. Evidence has shown the presence of increased host levels of H_2O_2 in the first few days of the incompatible interaction with levels being considerably less during compatible ones, suggesting the resistance that occurs is a result of a hypersensitive response which happens following AvrStb6 recognition[308,353]. If this is the case the mitroGFP2-Orp1 biosensor should detect changes in *Z. tritici* H_2O_2 in response to host H_2O_2 levels thus enabling molecular details at the guard cell aperture during such interactions to be determined.

The mitroGFP2-Orp1 biosensor could also be used to learn more concerning non-host resistance (NHR). A recent NHR model system has been established for *Z. tritici* in *Nicotiana benthamiana*[227]. This study determined that as a result of NHR in *N. benthamiana* little successful stomatal penetration could be observed[227]. It was therefore suggested that the recognition of secreted effector

proteins by the host may trigger a resistance response[227]. Furthermore, this model has enabled the identification of effector proteins responsible for successful infection which may possess a similar function during infection of the host[227]. Use of mitroGFP2-Orp1 in non-host environments could therefore also provide us with greater molecular detail about what is happening at the host-*Z. tritici* interface.

Recently, it has been determined that among isolates of *Z. tritici* there is a high degree of infection development differentiation, both spatially and temporally during each infection stage[354]. The mitroGFP2-ORP1 biosensor produced in the present study could therefore help determine the metabolic states of these different isolates during infection, and help link genetic diversity and phenotypic variation between isolates and their interactions with the wheat host[354].

This chapter has laid the foundations for producing a successful mitroGFP2-Orp1 *Z. tritici* biosensor in the future to study the early interaction at the stomatal aperture between this pathogenic fungus and its host, wheat. We aimed to produce a mitochondria-localised biosensor that would allude to the metabolic state at the cellular level in *Z. tritici*. Low expression has meant that currently the transformed lines are of little use as biosensors but, it may be possible to produce a more highly expressed line. Further study could therefore lead to the production of a promising new biosensor for the study of metabolic state in *Z. tritici*, which in turn has the potential to be used in other plant pathosystems.

CHAPTER 4: Cellular characterisation of wheat floral tissue and the adaptation of the coleoptile assay as a high-throughput imaging tool

4.1 Introduction

To use the tools and methodologies devised, generated and refined throughout this thesis an understanding of the host tissue is required – in the case of both *Z. tritici* and *F. graminearum*, this is wheat. Even though studies have explored and presented the *F. graminearum*-wheat interaction at the cellular level, there is still limited information available for the cellular structure of wheat floral tissue prior to inoculation and coleoptile tissue prior to and during infection[113,337]. Characterisation of wheat tissues at the cellular level is therefore crucial if we are to fully understand the infection process elicited by *F. graminearum* as well as numerous other wheat pathogens. Probably, many researchers have characterised these tissues previously but have not published them or made them publicly available – this is therefore one of the main aims of this chapter.

For the present chapter the spring wheat *cv.* Bobwhite was used – a cultivar shown to be fully susceptible to *F. graminearum* and used for *F. graminearum* strain PH-1 *in planta* experimentation at Rothamsted for >20 years[302]. Typically, the *F. graminearum*-wheat interaction is studied using a wheat floral assay, whereby single spikelets are inoculated at anthesis to replicate field entry conditions. The general hexaploid wheat floral anatomy has already been schematically represented within Fig. 1.4 in Chapter 1. Briefly, in the mature plant, the embryo is surrounded by a series of 'boat'-shaped tissues – the palea, lemma and glumes; collectively forming a floret. Four florets make up individual spikelets, which in turn are positioned on either side of the wheat spike stem or rachis[113]. On average a single wheat spike is approximately 10 cm in length, consisting of

13-17 spikelets, with anthesis commencing from the spikelets in the centre of the spike and from the lowest pair of florets in each spikelet[113]. However, as a result of Covid-19 restrictions, the time-consuming wheat floral assay was unsuitable, therefore a high-throughput assay was needed to study the wheat-*F. graminearum* interaction.

4.1.1 Coleoptile assay

In 2012 the wheat coleoptile assay was developed to study the *F. graminearum* transcriptome in a high-throughput *in planta* system[303]. Whether this assay is translatable to all wheat floral tissue infection studies is still out for debate, with transcriptional differences occurring between infection in floral and coleoptile tissues[303]. However, a study from 2019 has shown the coleoptile is effective for studying *F. graminearum* infection at the cellular level via CSLM, and that during this interaction hyphae pass from one cell to the next via PFs as seen in the floral tissue[113,355]. To allow for comparisons to be made between fixed and stained infected wheat floral tissue, a similar histological approach is needed in the coleoptile. A study from 1965 had previously investigated the coleoptile tip in this way but a broader understanding of the coleoptile tissue is needed here[356].

Within the past decade the coleoptile assay has been further developed and refined at Rothamsted Research (Harpenden, UK). A modified bioassay was originally established by Dr Ana Machado following quite closely the original protocol published by Zhang *et al.* 2012. This protocol was then further refined by Mr Mike Grimwade-Mann by introducing the use of the pipette tip to hold the Fusarium spore-soaked filter paper in place over a greater time period; for the majority of wheat cultivars where the coleoptile rapidly grows away from the

emerging 1st true leaf which prevents infection[303]. The new methodology is shown in Fig. 4.1. The wheat coleoptile can be inoculated with WT *F. graminearum*, to produce a reproducible compatible interaction and can therefore be used as a high-throughput experimental system; cutting down a typical wheat floral inoculation assay of three months (seed sown to results obtained), to a 10-day experiment. This was an ideal bioassay to use during the Covid-19 restrictions because regular and consistent plant care over long periods was either very difficult or impossible.

In this chapter, my aim was to characterise the coleoptile tissue in its uninoculated and inoculated states. I attempted this firstly with the PH-1 WT *F. graminearum* strain before using the ΔFgGT2 and ΔFgMAP1 mutants which have previously been shown in the literature to have little if any pathogenicity – refer to Fig. 4.2[79,302,357]. ΔFgGT2, was also selected as a result of the mutation being in a glycosyltransferase gene, critical for cell wall formation, which could therefore possibly affect the infection process at the PD[357]. On the other hand, ΔFgMAP1 was chosen as MAP1 is homologous to PMK1 in *M. oryzae*, which has been shown to be essential for passage through the PD[302,358]. By using mutants that are unable to successfully infect the wheat floral tissue it was hypothesised that these mutants would be arrested early in infection or within the first cell. This would allow for comparisons to be made with WT infection at the cellular level in both the pathogen and the host.

During tissue characterisation I investigated the use of the PD by the *F. graminearum* hyphae in the coleoptile tissue and then compared these cellular studies within the coleoptile to those reported for wheat floral tissues during

infection. Collectively, these studies work towards the objective of investigating hyphal growth at both the intercellular and intracellular levels over the early time-course of the *F. graminearum*-wheat interaction.

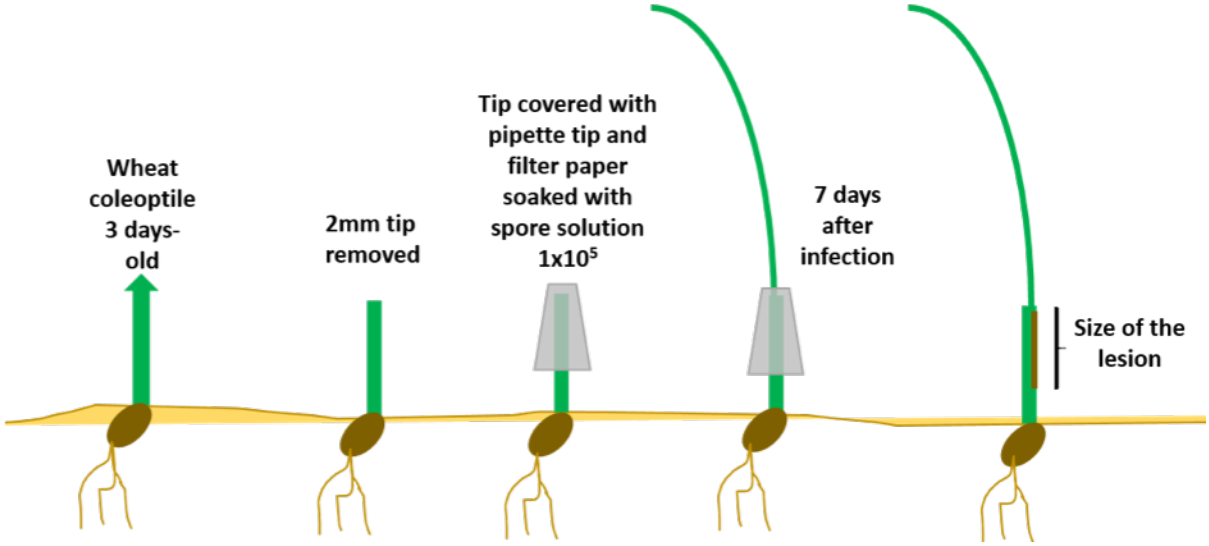

Figure 4.1 – Coleoptile assay. Image developed by Ana Machado, Rothamsted Research.

Figure 4.2 – *Fusarium graminearum* wheat ear infection with PH-1, ΔFgGT2 and ΔFgMAP1. Images taken from Cuzick et al. 2008 and King et al. 2017.

4.2 Experimental procedures

Due to the nature of the experiments no technical replicates were performed.

4.2.1 Preparation of individual tissues prior to sectioning

Wheat floral tissue was taken around the time of anthesis. Immediately prior to sectioning the floral tissues – lemma, palea and rachis – were excised from the uninoculated wheat spikelet. For coleoptile tissue that was to be fixed and resin embedded, the roots were excised, and the coleoptile tissue was removed, intact, from the seedling. This took place for coleoptiles at both 3- and 5-days post-inoculation (dpi). For staining of living/fresh coleoptile tissue, a small section was cut away from the coleoptile using a scalpel and transferred to an Eppendorf tube for staining. For each experiment three biological replicates were used.

4.2.2 Fixation, embedding, sectioning and imaging of wheat floral and coleoptile tissues for compound light microscopy

The following protocol has been provided by the Rothamsted Research bioimaging department and is described in Ruzin 1999[359]. Each sample was rotated for 24h at room temperature (RT) in a capped glass vial containing: 4% paraformaldehyde (Sigma-Aldrich®) and 2.5% glutaraldehyde (Sigma-Aldrich®) in 0.1M Sorenson's phosphate buffer (NaH_2PO_4:Na_2GPO_4, pH 7.2), fixative. Following this the samples were washed three times in 0.05M Sorenson's phosphate buffer for 30 min. Dehydration of the samples was carried out using a graded ethanol series, i.e., 10%-30% ethanol, increased by a 10% increment every 30 min, followed by 40%–100%, increased by 10% every hour with a change of solution every 30 minutes. At 70% the sample was left overnight at 4°C before continuing with the graded ethanol series. Infiltration of the samples was achieved using increasing concentrations of hard grade LR White resin (TAAB) (ratios of dry 100% ethanol:LR white for 1 h each – 1:4, 2:3, 3:2, 4:1, 100% LR white overnight). Samples were than embedded in plastic capsules, in 100% LR white both horizontally and vertically for both transverse (TS) and longitudinal (LS) sectioning – four to five independent samples were embedded per treatment. Due to the experimental design and time required, the experiment was not repeated. However, three (or more) biological replicates were explored per treatment per time point and then sectioned (see Table 4.1). These samples were then polymerised in a nitrogen oven at 60°C for 20h.

Table 4.1 – Fixed samples for each wheat tissue characterisation experiment.

Experiment	Treatment	Number of independent samples	Number of samples for transverse sectioning	Number of samples for longitudinal sectioning
Floral tissue – Palea[1]	Untreated	3	2	1
Floral tissue – Lemma[1]	Untreated	3	2	1
Floral tissue – Rachis	Untreated	3	2	1
Coleoptile (3dpi)	Untreated	3	2	1
Coleoptile (3dpi)	Water	3	2	1
Coleoptile (3dpi)[2]	PH-1	5	3	2
Coleoptile (3dpi)	ΔFgGT2	3	2	1
Coleoptile (3dpi)[3]	ΔFgMAP1	3	3	0

[1] Palea and lemma tissue could not be successfully sectioned longitudinally as a result of tissue structure.

[2] PH-1 inoculated coleoptiles were investigated at 5dpi, but a high extent of tissue damage due to infection meant samples at 5dpi were not considered viable for PD discovery research.

[3] Longitudinal samples produced but tissue damage during the fixing process meant these sections were not reliable.

dpi = days post-inoculation

TS and LS semi-thin 1µm sections of the LR White embedded samples were cut using the Leica Rotary 2255 microtome. Typically, 30 sections were made from each embedded tissue block. Sections were then placed on polysine-coated microscope slides (Thermo Scientific™) before being dried on a hot plate at 50°C. To reveal the overall cellular structure, the location of the *F. graminearum* hyphae and the positions of any host cell responses, samples were stained with 0.1%

toluidine blue O (TBO, aqueous) suspended in 1% sodium tetraborate (w/v) pH 9[113]. Any plasmolysis of cells was identified from CLSM images previously obtained (Chapter 5 Appendix 23) – these samples were placed on a glass slide and soaked in 0.8M mannitol for 30 min at room temperature, using filter paper to draw the solution across the tissue, with a coverslip holding it in place. Sections were orientated by creating a nick in the resin embedded samples, which could be seen during imaging. Where sequential sections were taken, 10 sections were placed in order per slide. Where the next sequential section could not be used, for example, due to damage, the next one was taken. Sections were mounted in Permount™ mounting medium (Fisher Chemical™) and covered with a glass cover slip. Mounted slides were stored in labelled slide boxes, each slide was identified using the treatment, sample number, slide number, the date of sample fixation and the date of sectioning. All sections were imaged and captured using the Zeiss Axioimager Z2 microscope – ZEN image software. Scale bars were automatically calculated by the software. All images (and corresponding raw data files) are stored on Rothamsted Research shared drives, both in the bioimaging department and a shared group folder. Each section image is saved in a file corresponding to the sample it originated from. All data is backed up on OneDrive and personal hard drives.

4.2.3 Measuring coleoptile growth and analysis

Coleoptile growth was measured over the course of 1-10 days, with day 1 being the day after the seeds were sown. All coleoptiles were measured to the nearest 0.5 mm using a tape measure. Any movement of the plants to gain access for measurements was minimal to prevent any unnecessary disturbances. Water-inoculated and PH-1 inoculated coleoptiles were measured in pairs. In each pair,

one coleoptile was left untreated (control) and the other was inoculated. Five pairs were present per box, approximately equally distanced apart; 10 pairs (10 biological replicates) were measured per repeat, with three repeats of the experiment being done for the water-inoculated and PH-1 inoculated coleoptile experiments and corresponding controls. Inoculations were carried out on day 3, as per the coleoptile assay protocol stated in Chapter 2. It should also be noted that to inoculate the coleoptile 1-2 mm are cut off the tip which may be responsible for any variation seen. To prevent any cross-contamination all PH-1 inoculated coleoptile pairs and water-inoculated coleoptile pairs were grown in separate growth boxes. Even though it would have been ideal to move each pair to another space in the box every day to avoid any positional effects, this was not possible because this would have caused too much damage to the plants.

Growth curves were produced for all water inoculated samples and their corresponding controls and all PH-1 inoculated samples and their controls. All other statistics were performed in Genstat® (version 19.1) with the help of Suzanne Clark, Statistics, Rothamsted Research, UK. For days 2-7 of coleoptile growth (as this was the time frame in which growth occurred) analysis of variance (ANOVA) tests were done for each day for the blocking structure: occasion (replicate)/seedling-pair/seedling, determining the p-value statistic for each day, testing the significance of inoculation on coleoptile growth. Permutation tests, whereby the test statistics are calculated for all possible rearrangements of all data points, were also done do remove variance heterogeneity – these results were not used here. The standard error of the means (SEM) for the difference between the two treatments was also calculated. Gompertz curves, a

mathematical model typically used to describe the growth of an organism, were fitted to each coleoptile[360,361].

4.2.4 Quantification hyphal progression

Three independent TS water-inoculated and PH-1-inoculated samples were selected for hyphal quantification (three biological replicates). In total, 30 sequential sections were taken per sample. Due to time constraints measurements were only taken at sections 1, 5, 10, 15, 20, 25 and 30μm. Section 1 was taken from the middle of the lesion, working outwards towards section 30 – Fig. 4. 3. The vascular bundle opposite the PH-1 induced lesion was used as another control due to its low hyphal titre. The number of intercellular hyphae, intracellular hyphae and times hyphae crossed possible PFs were quantified. To count the number of hyphae, images were taken using the 20x objective using the Zeiss Axioimager Z2. The images produced when then used to count the hyphae. The field of view selected was the vasculature and the cells surrounding this (this is where most hyphal colonisation occurred) – an example of this can be seen in Fig. 4.4. Intercellular hyphae were defined as hyphae that colonised the space between cells, intracellular hyphae as those inside the plant cells and PF-associated events where hyphae crossed from one cell to the next. If there was any ambiguity, this area of the image was first expanded, to try and identify the hyphae and furthermore to determine what quantifiable category each hypha belonged to. Where a hypha was growing from an intercellular to intracellular space, these were counted as intracellular hyphae as the fungus had made this transition in colonisation behaviour; wheat rachis colonisation is typically in this direction, from intercellular to intracellular and not vice versa.

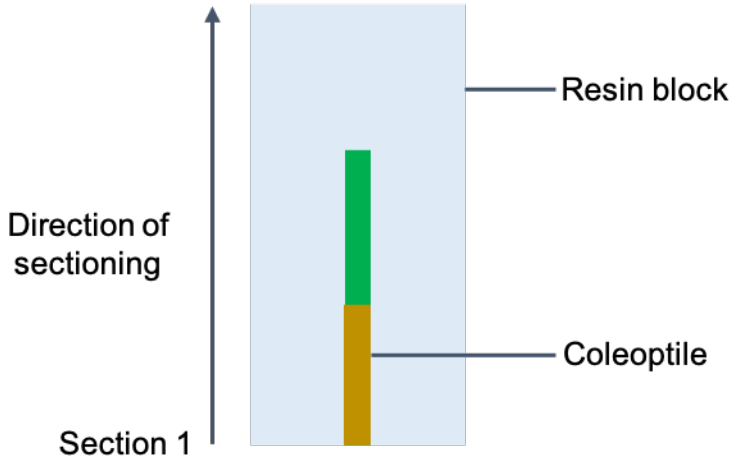

Figure 4.3 – Sequential sectioning of the wheat coleoptile for hyphal quantification. The sample was embedded with the lesion at the cutting edge. Section 1 was therefore taken from the cutting edge/centre of the lesion (brown). Consecutive sections were subsequently taken in the direction of the arrow, working from the lesion outwards. It should be noted coleoptile tissue is almost transparent when fixed and embedded, the colour here is shown for clarity.

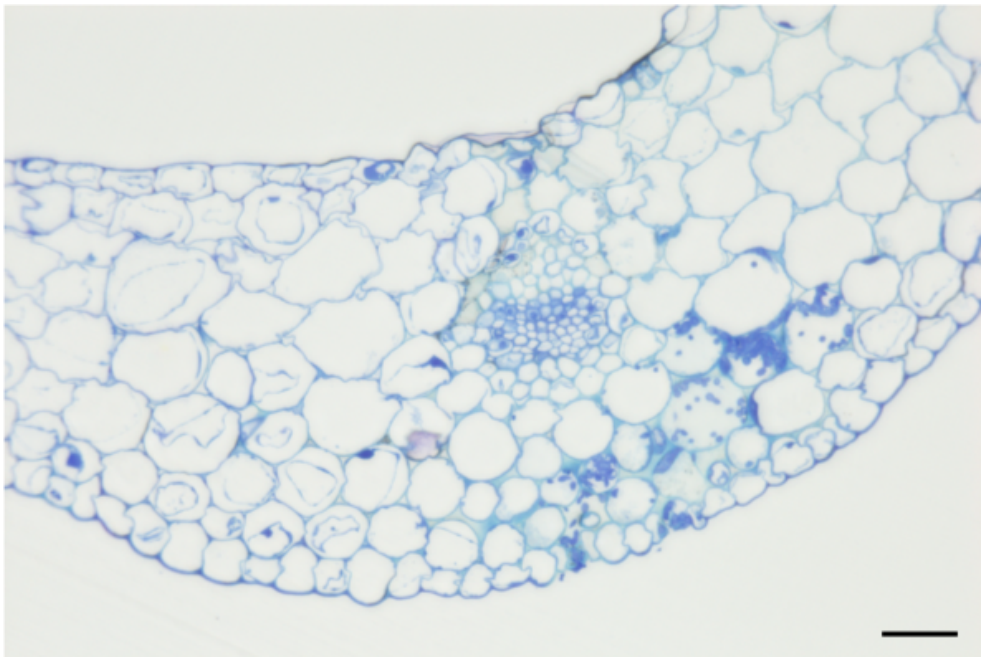

Figure 4.4 – Field of view for hyphal quantification. A 20x objective was chosen for the images to ensure all hyphae were captured. Images were all taken around the vascular bundle as this is where most if not all hyphae grew. In this image, there are 64 intracellular and 14 intercellular hyphae. Bar = 50μm.

Statistical analyses were done in Genstat® (version 19.1) with the help of Suzanne Clark, Statistics, Rothamsted Research, UK. Boxplots of the total number of hyphae were produced before the data was logged and an ANOVA was calculated providing p-values for the total number of hyphae between different treatments and across the sample (sections 1-30). The data was then treated proportionally: the numbers of intracellular and intercellular hyphae. Graphics were produced to represent these findings – this included a residual maximum likelihood analysis (REML), as the data was unbalanced[362]. This analysis was considered to be the most suitable as the data was proportional and binomial and would usually fit a linear mixed model (LMM) but, as the data was at two extremes (unbalanced) and therefore this analysis was not suitable[363]. The low number of hyphae crossing PFs resulted in these not being included in the analysis, a table of these results is still presented.

4.2.5 Coleoptile staining

For each histochemical stain used, three coleoptile samples (three biological replicates), both water-inoculated and PH-1 inoculated were selected. This was a 'proof of concept' experiment and was therefore not repeated. Untreated samples were also imaged to measure background autofluorescence under the microscope conditions used for each stain.

Wheat germ agglutinin (WGA)-Alexa Fluor 488 (Invitrogen™), was used to stain chitin, and therefore fungal hyphae in the coleoptile[364]. Tissue was left in 10% KOH at 70°C for 4 min. The tissue was then washed in 1x phosphate buffered saline (PBS, pH 7.4) 3 times before being stained with WGA, 10 μg/ml for 10 min. Samples were then washed with PBS buffer and mounted on a glass slide in dH_2O. Samples were imaged on the confocal microscope (Zeiss LSM780 – Zen

image software), excitation/emission maxima of WGA-Alexa Fluor 488 ~495/519 nm. Scale bars were automatically calculated by the software.

Coleoptile tissue was stained with propidium iodide (PI) (Invitrogen™), to highlight the cell wall. The sample was placed in 1 μg/ml PI in dH_2O for 5 min and washed with dH_2O. Samples were imaged on the confocal microscope (Zeiss LSM780 – Zen image software), excitation/emission maxima of PI are 493/636 nm. Scale bars were automatically calculated by the software.

Images are stored on Rothamsted Research shared drives and backed up on OneDrive and personal hard drives. Each image is stored in an experiment specific file, with a sample number and name detailing the conditions. Dates for each analysis were also recorded.

4.3 Results

4.3.1 Fixing, sectioning and staining of the wheat palea, lemma and rachis demonstrates the cell layers and detailed features of each tissue

To understand in more detail the results presented in other chapters, I have characterised the wheat floral tissue at the cellular level without infection. Please note – I have not attempted to characterise the floral tissue when inoculated as this has already been shown previously[113] Fixing wheat floral tissue has highlighted anatomical features, both previously described and new, which allude to some of the infection mechanisms employed by *F. graminearum*. Refer to Fig. 4.5 for examples of untreated wheat floral tissue morphology as discussed below.

The palea, the most visually translucent and thinnest of the three tissues studied here, was shown to possess 6/7 cell layers at its thinnest point, consisting of an

upper epidermal layer followed by multiple underlying mesophyll layers (parenchyma). Towards the corner points of the palea are regions of high chloroplast density, which correspond with stomata and vascular bundles, which occur at these thicker, stronger corner points as opposed to the thinner tissue in the centre of the structure. The central palea displays few if any chloroplasts and stomata. Upon initial observation the lemma had a similar structure but immediately appeared thicker in terms of cell layers, approximately 8/9, consisting of upper and lower epidermal layers followed by the parenchyma, similar to the palea. The lemma also possesses a high chloroplast frequency, however, few stomata mean these are more widely dispersed along the breadth of the tissue, with vasculature occurring along the 'corners/edges' of the lemma. The lower epidermis of the lemma consists of 'interlocking' cells which are likely to change throughout development. Even though there is evidence PD occur within the palea and rachis, none could clearly be seen here, it is likely these would become clearer during infection.

Structurally important for the wheat spike, the rachis is much thicker in comparison to the palea and lemma; composed of approximately 17/18 cell layers, with the central vascular bundles located in the cortex, surrounded by the sclerenchyma and epidermis. Regions densely populated with chloroplasts, situated adjacent to stomata and small vascular bundles, were found protruding from the inside of the epidermis, corresponding to the stripy macroscopic phenotype of the rachis in the intact wheat spike. Thick cell walls in the rachis showed the presence of PFs, possible stretching of the cell walls during sectioning may have made these larger than normal (10-50nm) in appearance, however this cannot be confirmed (Fig. 4.6). PFs could be seen in both TS and LS sections. Fig. 4.6 also demonstrates how difficult the PD are to images in

healthy wheat tissues. Cell wall thickness of the rachis parenchyma cells was approximately 5.5µm, in the lemma and palea this was lower at approximately 1.1µm thick.

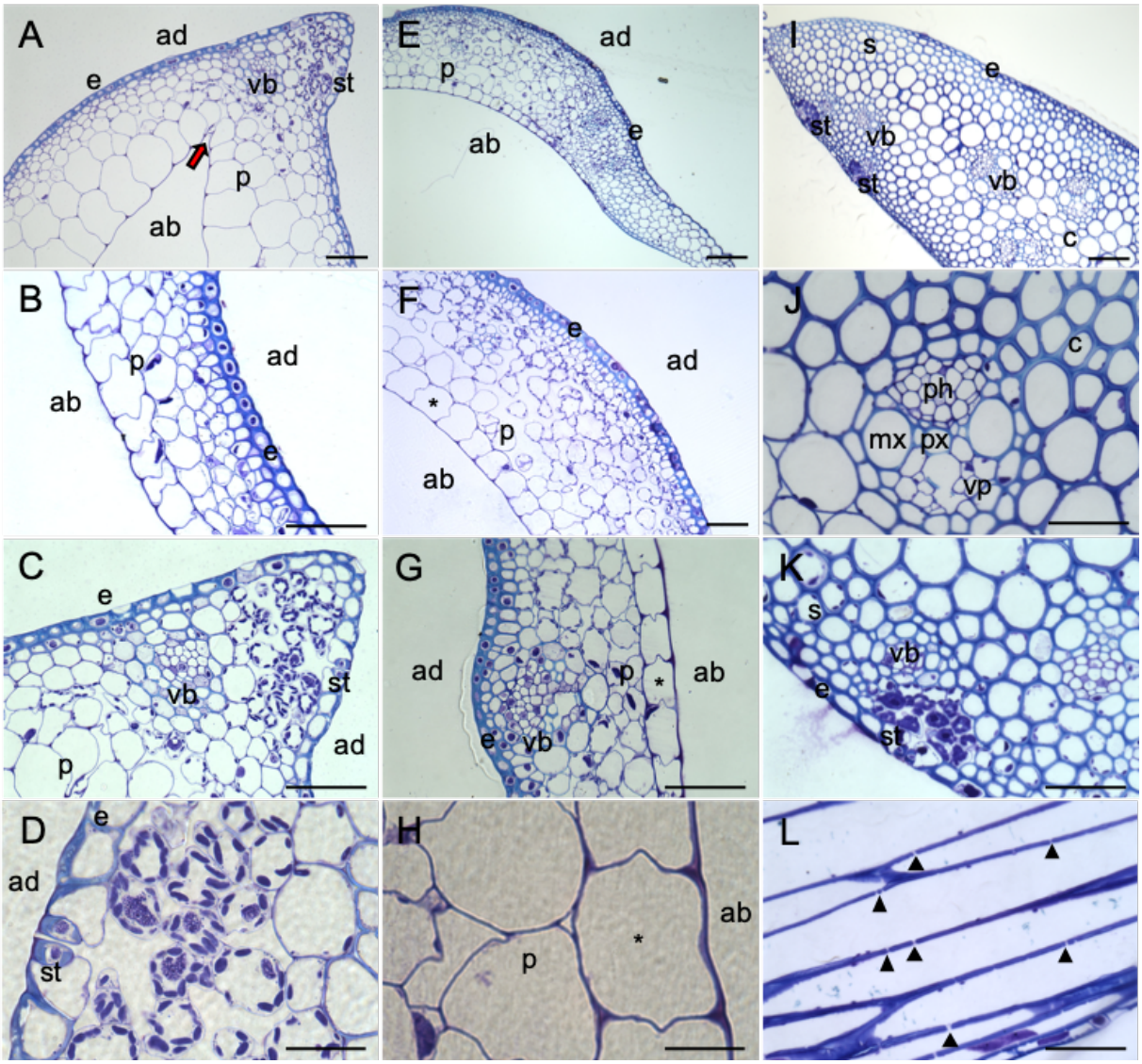

Figure 4.5 – Uninfected wheat floral tissue cellular morphology. All sections were fixed using LR white resin, 1 µm thick and stained with 0.1% toluidine blue O, pH 9. (A-D) Palea (transverse sections) – chloroplasts (dark purple) and associated stomata and vascular bundles can be seen concentrated in the corners of the 'boat'-like tissue structure. At its thickest the centre of the palea is 6-7 cell layers thick (B). Red arrow in (A) indicates the section focused on in (C and D) at a higher magnification. (E-H) Lemma (transverse sections) – chloroplasts are distributed throughout the length of the structure, with vascular bundles (G) towards the edges. The lemma is approximately 9-11 cell layers thick (F) with the abaxial parenchymal cell layer consisting of 'interlocking cells' (G and H). (I-L) Rachis (I-K – transverse, L – longitudinal section) – chloroplasts are situated in small areas along the epidermis (I) with their associated stomata (K). Vascular bundles are adjacent to stomata and in the cortex of the rachis (I and J). Longitudinal sections show small gaps between adjacent cells, possibly pit-fields visible due to tissue damage. (L). s = stomata, vb = vascular bundles, ab = abaxial, ad = adaxial, p = parenchyma, s = schlerenchyma, c = cortex, e = epidermis, mx = metaxylem, px = protoxylem, ph = phloem, vp = vascular parenchyma, * = 'interlocking cells', black arrowheads = plasmodesmata. Bars: A ,E ,I = 100 µm; B, C, F, G, J, K, L = 50 µm; D, H = 20 µm.

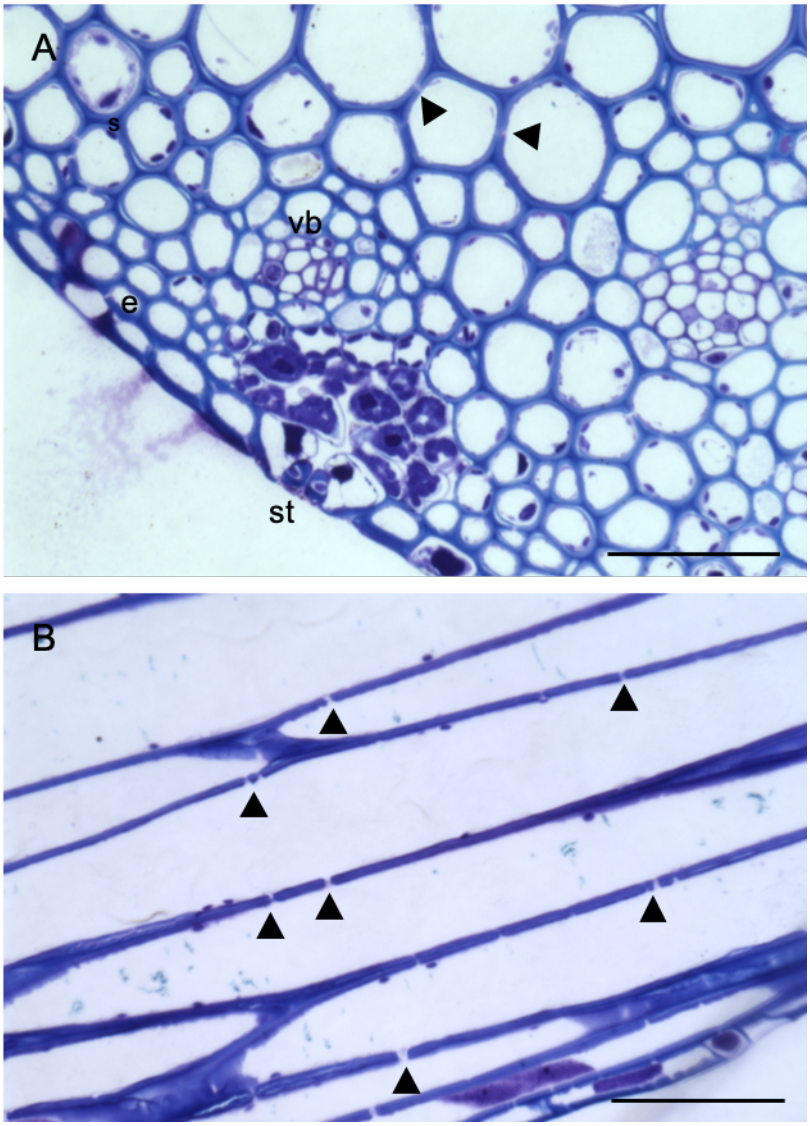

Figure 4.6 – Pit-fields in wheat rachis tissue. (A) Transverse rachis section. (B) Longitudinal rachis section. All sections were fixed using LR white resin, 1µm thick and stained with 1% toluidine suspended in 1% sodium tetraborate, pH 9. e = epidermis; vb = vascular bundle; st = stomata. Black arrowheads show pit-fields in parenchyma cells. Bar = 50 µm.

4.3.2 Investigating the cellular organisation of healthy coleoptile tissue

To characterise the healthy wheat coleoptile tissue a similar imaging approach was taken as for the wheat floral tissue – Fig. 4.7 – allowing for comparisons to be made to inoculated coleoptile tissue. At its thinnest, the coleoptile is approximately five cell layers thick, consisting of inner and outer epidermal cell layers that enclose three inner mesophyll cell layers. At either side of the coleoptile is a vascular bundle (two vasculature bundles in total per coleoptile), whereby chloroplasts are in greater abundance in comparison to the rest of the tissue and are associated with stomata. Upon visual inspection the coleoptile is a relatively translucent tissue in comparison to the lemma and rachis and most likely contains less chloroplasts as it is the short-lived protective organ of the seedling, which then dies back. Chlorophyll content was not quantified in this study. Longitudinal sections were also taken, like the floral tissue the sample was slightly pulled apart by the sectioning process. No evidence of PD in TS or LS could be seen here, however these may be difficult to image without fungal hyphae being present. Cell wall thickness in the coleoptile parenchyma is approximately 1.5 µm.

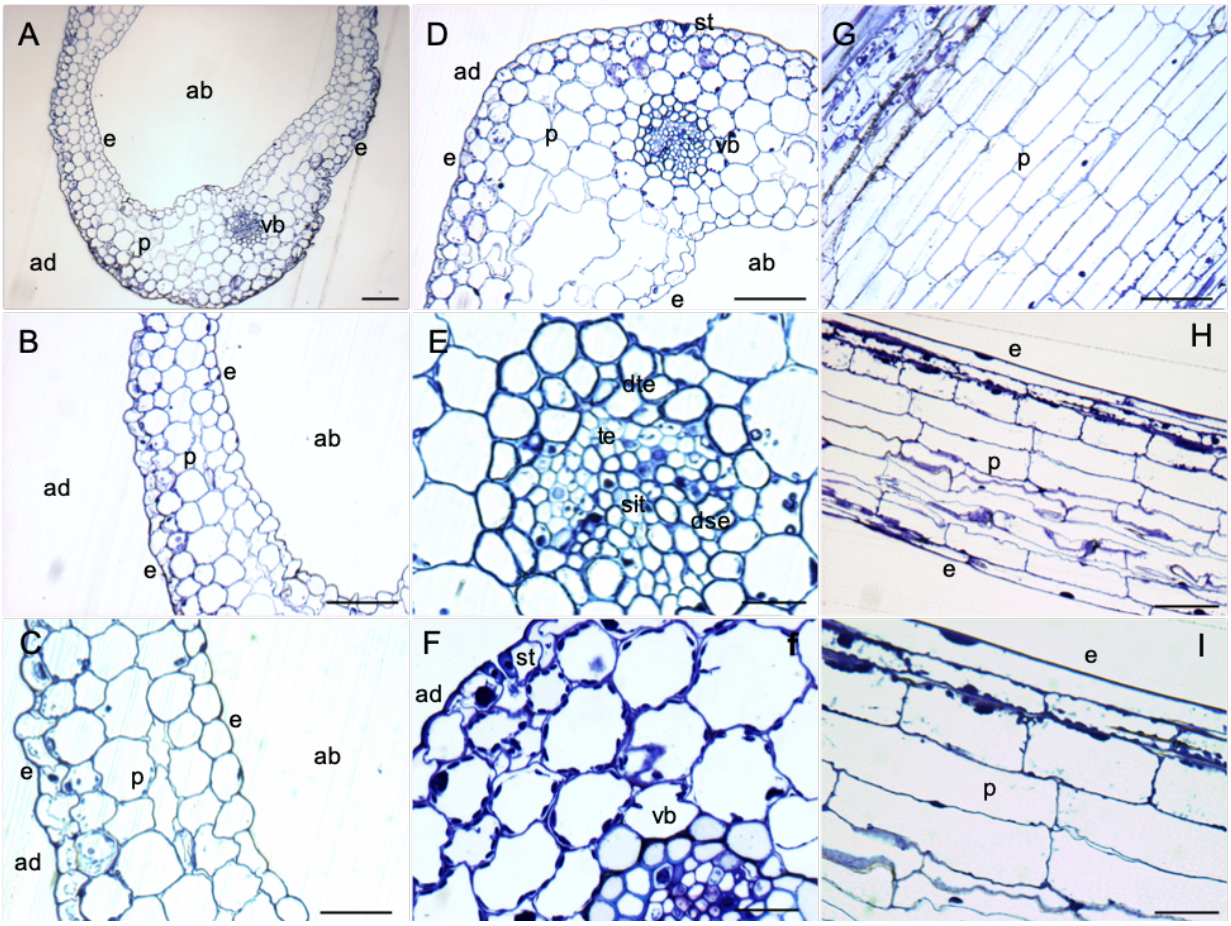

Figure 4.7 – Control wheat coleoptile tissue cellular morphology. This coleoptile tissue is in the equivalent growth phase seen at 3 days post-inoculation. All sections fixed in LR white resin, 1 µm thick and stained with 0.1% toluidine blue O, pH 9. (A-C) Transverse sections showing general coleoptile structure. The two 'corners' of the coleoptile contain vascular bundles with the tissue in between each tissue being void of vasculature and containing few chloroplasts. (D-F) Transverse sections showing vascular bundle structure. Differences between the vasculature in the coleoptile and floral tissues are seen due to age of tissue and therefore developmental stage. (G-I) Longitudinal coleoptile sections demonstrating difficulty in visualising PD. ab = abaxial, ad = adaxial, e = epidermis, p = parenchyma, vb = vascular bundle, st = stomata, sit = sieve tube, te = lignified tracheary element, dse = differentiating sieve element, dte = differentiating tracheary element. Bars: A,B,D,G = 100 µm; C,H = 50; E,F,I = 25 µm.

4.3.3 Wheat coleoptile growth analysis

Understanding the growth rate of the wheat coleoptile, was considered important in the context of hyphal growth and hyphal behaviour *in planta*. How coleoptile growth affects *F. graminearum* infection progression has not been investigated previously. To gain a more detailed understanding of this, coleoptile growth studies were done – the raw data for this can found in Appendix 8 and Appendix 9.

To make this study statistically robust, 10 pairs of coleoptiles were analysed per repeat (three repeats in total), with one coleoptile per pair being inoculated with either PH-1 or water after 3 days. This therefore accounted for any slight variations in growth conditions that could have possibly caused any change in coleoptile length, i.e. position of the coleoptiles in the growth box. Water inoculated controls, also accounted for the 1-2mm of tissue removed from the coleoptile prior to inoculation. For all coleoptiles, both untreated and inoculated, a series of general coleoptile growth characteristics were observed. Most coleoptiles germinated around day 2, growth on days 3 and 4 increased exponentially, with the daily rate of extension being highest on day 4, thereafter diminishing and then halting by day 6/7. The 1st true seedling leaf (i.e. Zadok scale 10) emerged from the coleoptile after the fourth day (with the occasional exception whereby the seedling leaf emerged on day 3). On day 8 the coleoptiles were beginning to show the first visible signs of senescence at the tips. Slight variations in final coleoptile lengths were seen. Possibilities for this include the placement of the coleoptiles in the growth boxes used, however the evidence shown here does not suggest this is the case and is most likely a result of natural

coleoptile variation and/or initial seed size. Quantitative growth curves are given in Fig. 4.8 for all 30 pairs of water-inoculated and PH-1 inoculated coleoptiles.

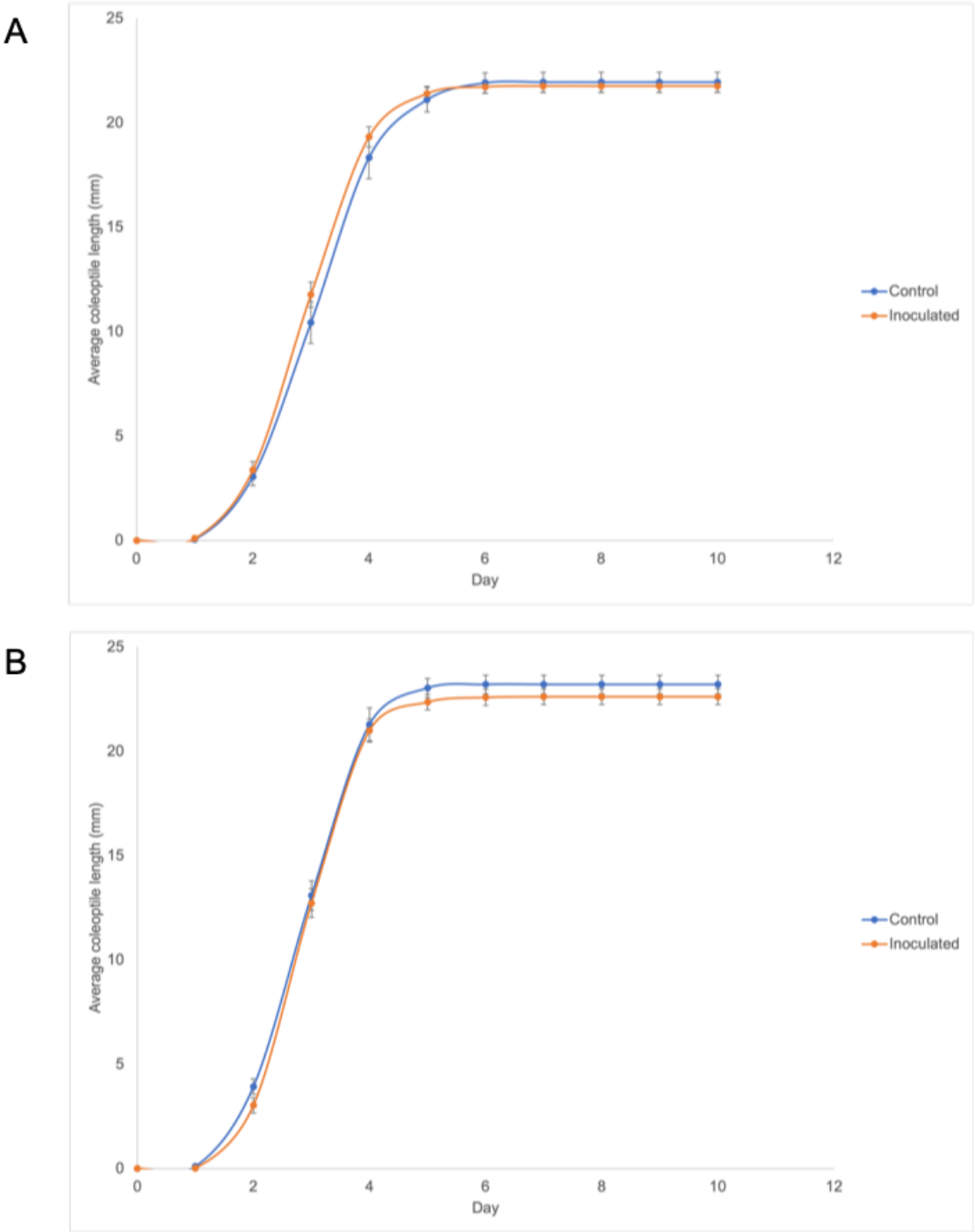

Figure 4.8 – Wheat coleoptile growth curves. (A) Blue represents uninoculated (control) coleoptile growth, whereas orange represents water-inoculated coleoptile growth. Water-inoculated coleoptiles were inoculated with water only containing no spores. Average height of the control = 21.9 mm, average height for water-inoculated coleoptiles = 21.7 mm (B) Blue represents uninoculated (control) coleoptile growth, whereas orange represents *Fusarium graminearum,* PH-1, inoculated coleoptiles. Average height of the control = 23.2 mm, average height for PH-1 inoculated coleoptile = 22.6 mm. Inoculations took place on day 3 of coleoptile growth. Error bars represent the standard error of the mean (SEM).

For the growth curve (Fig. 4.8) and the following statistical analyses six independent coleoptiles have had their data removed (see Appendix 8 and 9) as they did not successfully germinate or grow and were therefore considered unsuitable for successful infection. Analysis of variance (ANOVA) tests were run for days 2 to 6 as this was when most coleoptile growth occurred (separate analyses were necessary due to the large changes in coleoptile growth seen over time). This analysis was used to compare the following interactions: the effect of treatment (water or PH-1) on between pair variation, the effect of inoculation (control or inoculated) on within pair variation and whether or not treatment and inoculation were independent of one another. No significant difference ($p<0.05$) was calculated for any of these tests as seen in Table 4.2. These statistical results therefore demonstrate that there was no significant difference in the growth of the inoculated and non-inoculated coleoptiles indicating infection did not affect coleoptile growth significantly. Gompertz regression models were also fitted to each individual coleoptile, to assess the effect on any treatment on growth, most

coleoptiles were shown to fit this model[360,361]. However, the collection of more data between days 3 and 4 when growth is exponential would improve the fit of the model. These data are not shown here as approximately 120 coleoptiles were analysed in total – the values and summary statistics for this analysis and the analysis above can be found in Appendix 10 and 11.

Table 4.2 – Analysis of variance (ANOVA) p-values for coleoptile growth data.

Day of growth	Effect of treatment* on between pair variation	Effect of inoculation^ on within pair variation	Are treatment* and inoculation^ independent of each other?
2	0.427	0.064	0.933
3	0.775	0.688	0.348
4	0.303	0.681	0.981
5	0.193	0.252	0.610
6	0.495	0.101	0.947

*PH-1 or water; ^control or inoculated
Please note, no results were found to be statisitically significant.

4.3.4 Detailed microscopic and quantitative analysis of water and PH-1 inoculated wheat coleoptiles

Coleoptiles were inoculated with water (as a control) or *F. graminearum* strain PH-1 and were then fixed at both 3 dpi and 5 dpi. The circumference of each coleoptile was kept intact. To make it easier to characterise the *F. graminearum* infection process each coleoptile was sliced transversely in the centre of the lesion before fixation to ensure diseased tissue was analysed; healthy tissue

surrounding the lesion displayed no signs of infection. Brief microscopic analysis of both the 3 dpi and 5 dpi PH-1 coleoptile samples, indicated the 3 dpi samples should be used to image and quantify the hyphal-coleoptile interaction. At 5 dpi, the coleoptile tissue was observed to have lost all structure, large hyphal bodies could be identified, however any information on cellular interactions between *F. graminearum* and the host could not be determined (Appendix 12). All data going forward is therefore related to the analysis of the 3 dpi PH-1 inoculated wheat coleoptile, the water control for 3 dpi is also shown.

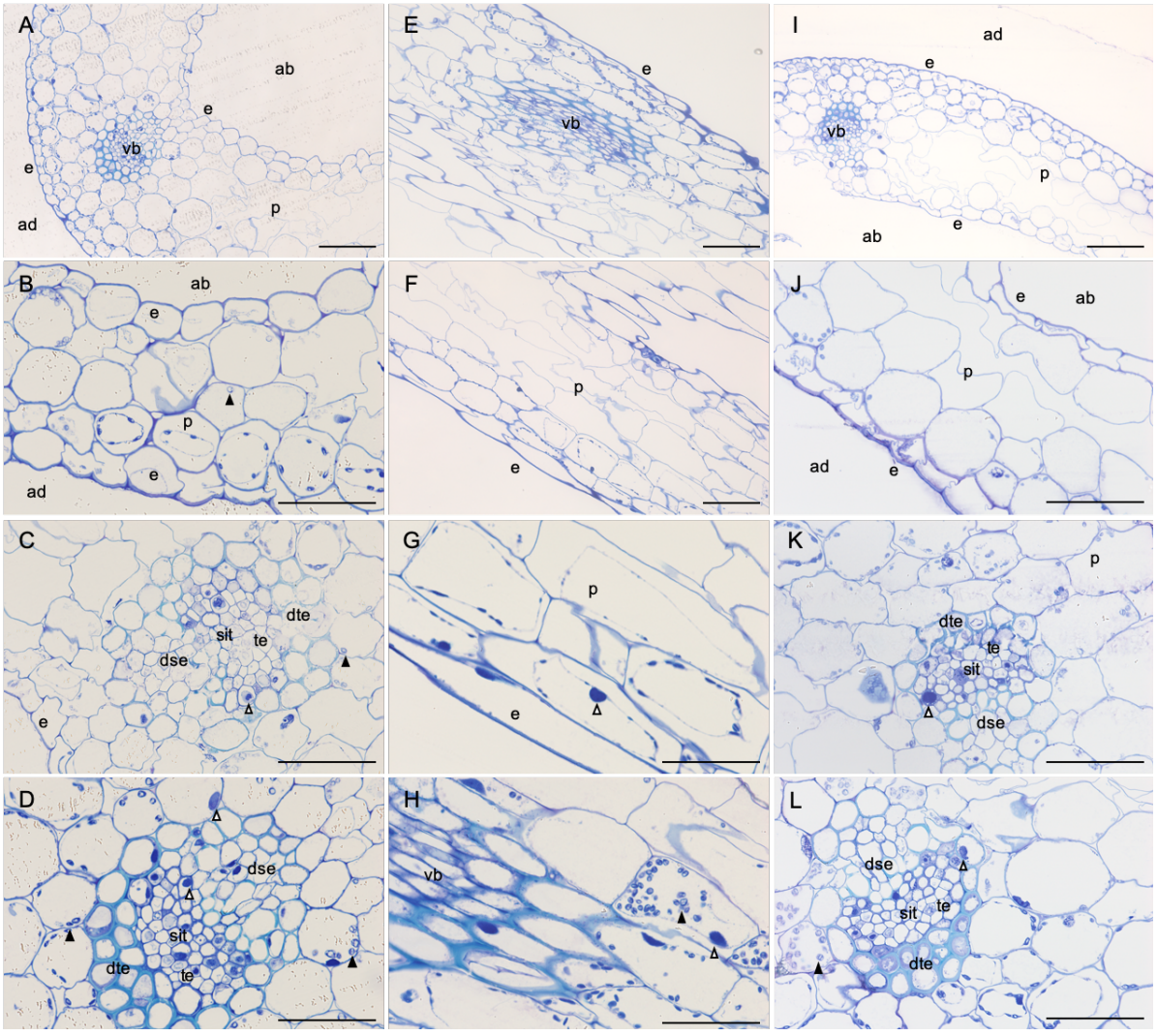

Figure 4.9 – Water-inoculated wheat coleoptile tissue cellular morphology (3 days post-inoculation). All sections fixed in LR white resin, 1µm thick and stained with 0.1% toluidine blue O, pH 9. A-D, E-H and I-L show sections taken from three separate samples showing coleoptile structure. A-D and I-L display transverse sections, whereas E-H longitudinal sections. The two 'corners' of the coleoptile contain vascular bundles with the tissue in between each bundle being void of vasculature and containing few chloroplasts. Pit-fields cannot be visualised. Sections B and D display tissue plasmolysis under controlled conditions. Chloroplasts (or other plastids) can be seen to adhere to the plasma membrane around the vasculature/outer cells of the coleoptile in all samples, these have not been labelled. ab = abaxial, ad = adaxial, e = epidermis, p = parenchyma, vb = vascular bundle, sit = sieve tube, te = lignified tracheary element, dse = differentiating sieve element, dte = differentiating tracheary element. Black arrowheads = starch grain structures, white arrowheads = nuclei (only those that are confirmed are labelled). Bars: A,E,F,I = 100 µm; B,C,D,G,H,J,K,L = 50 µm.

In addition to the untreated coleoptile dataset, a further control was produced by inoculating coleoptiles with water. Representative images for this day 3 control are given in Fig. 4.9 for comparison against the inoculated samples. The results seen here are similar, if not the same, to the untreated coleoptile dataset, demonstrating the methodology does not induce any dramatic tissue changes at the cellular level. It should also be noted that there was no lesion development for either of these controls. Coleoptile inoculation with PH-1 however produced a small lesion 3 dpi – Fig. 4.10. By 5 dpi, the main lesion was well-developed, approximately double in size to that seen at 3 dpi, in some cases tissue death could be observed elsewhere on the coleoptile, however this varied between samples – Fig. 4.11.

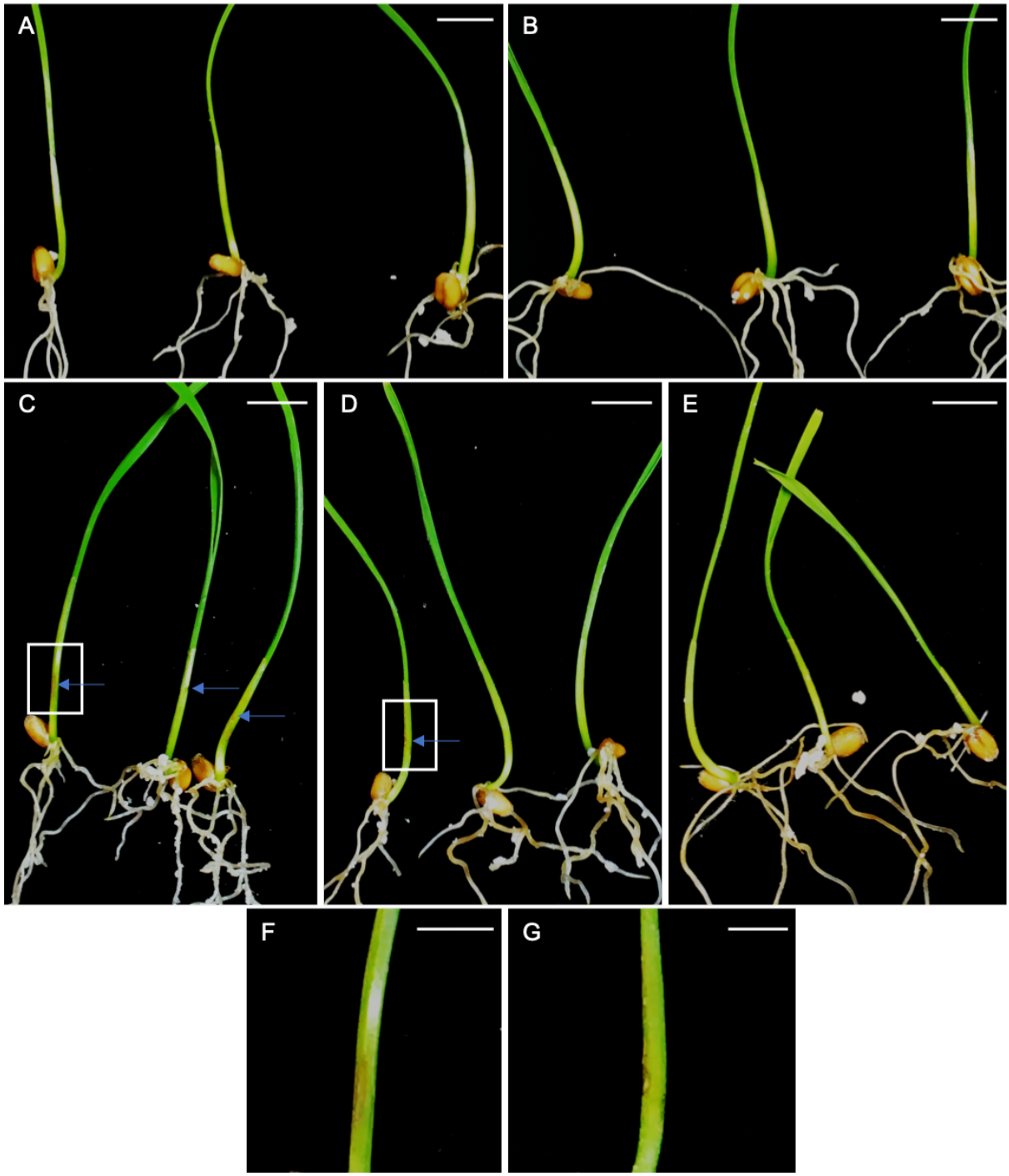
A
B
C
D
E
F
G

Figure 4.10 – Wheat coleoptile lesion development 3 days post-inoculation. (A) Untreated control, (B) Water inoculated control, (C) PH-1 inoculated, (D) ΔFgGT2 mutant inoculated, (E) ΔFgMAP1 mutant inoculated, (F) PH-1 lesion close-up, indicated by white box in (C), (G) ΔFgGT2 mutant lesion close-up, indicated by white box in (D). All images were photographed on a black velvet background. Blue arrows indicate lesions. Bars: A-E = 10 mm, F,G = 5 mm.

Before quantifying *F. graminearum* infection in the wheat coleoptile, microscopic observations were noted. Any artefacts in the tissue i.e., as a result of the fixing process were identified. Lines across the images are a result of the sectioning process, even though the tissue was fixed, due to the delicate nature of the tissues some coleoptiles were slightly damaged during the process (this has not affected the results). Also, the staining of some artefacts can be misleading, therefore only confirmed structures were used in the analysis here. Structures that look similar to stained starch granules in the literature could also be observed in the controls and inoculated coleoptiles. Starch granule structure and approximate size made it possible to distinguish between them and the hyphae when at a high enough resolution. *F. graminearum* hyphae were shown to stain a deep blue/purple with TBO, in comparison to the healthy surrounding tissue which was generally lighter. Hyphae tended to be larger and more circular (when cut transversely) than chloroplasts and smaller than nuclei. Starch granules were observed to stain a similar colour to the hyphae but could be distinguished by their hollow appearance.

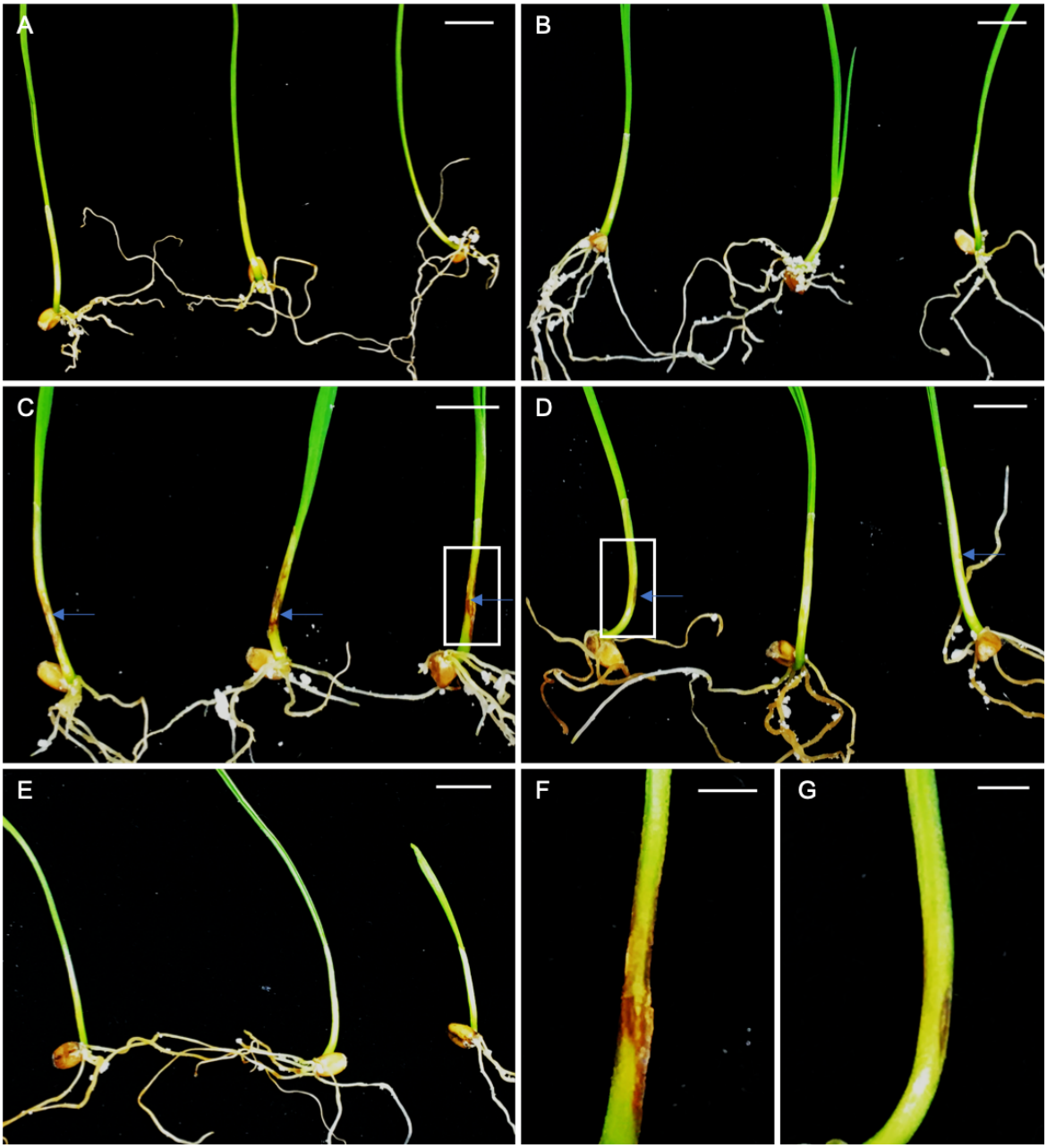

Figure 4.11 – Wheat coleoptile lesion development 5 days post-inoculation. (A) Untreated control, (B) Water inoculated control, (C) PH-1 inoculated, (D) ΔFgGT2 mutant inoculated, (E) ΔFgMAP1 mutant inoculated, (F) PH-1 lesion close-up, indicated by white box in (C), (G) ΔFgGT2 mutant lesion close-up, indicated by white box in (D). All images were photographed on a black velvet background. Blue areas indicate lesions. Bars: A-E = 10 mm, F,G = 2.5 mm.

The importance of using both transverse and longitudinal sections is evident throughout this study. Both are needed to visualise the infection process. TS sections allow for clear visualisation of hyphae which cannot be as clearly seen in LS sections. However, LS sections allow for imaging of other structures such as the nuclei, which are not seen as regularly in the TS sections. A mixture of both TS and LS sections have therefore been used where available (for the ΔFgMAP1 mutant only transverse sections were available). For PH-1 inoculated coleoptiles, as shown in Fig. 4.12, hyphal density was highest near the vasculature, although few hyphae had actually entered the vascular bundle. Also, the tissue connecting the vascular bundles displayed no signs of hyphal colonisation. Hyphae were observed growing both intercellularly and intracellularly by 3 dpi in parenchymal and epidermal cells, the sclerenchyma (thicker walled specialist cells) were not colonised. Both small and large parenchymal/epidermal cells can be seen to be densely packed with hyphae, with this varying in subsequent sections as each sample was investigated. The images obtained also suggest the hyphae do not stay in the same focal plane during growth, instead dipping in and out of an individual section. Many of the sections explored from the inoculated samples examined in detail (including those seen at 5 dpi) displayed nuclei that had strand-like projections, this was noted in at least three independent samples as seen in Fig. 4.13, this phenotype was not evident in the control samples. These nuclei were frequently found in LS sections in the parenchyma cells and just under the epidermis, hyphae were not present in these cells. In TS sections nuclei with strand-like projections were a rarer event but, were not found in areas with high hyphal densities. No hyphae were found in cells where this occurred. The PH-1 inoculated coleoptiles also show evidence of direct hyphal entry into the tissue via the stomata and not only

via the cut surface – this had previously been documented[303]. How frequently stomata occur on the coleoptile surface has not been quantified; from initial observations stomata also seem less common in the coleoptile than in the floral tissue.

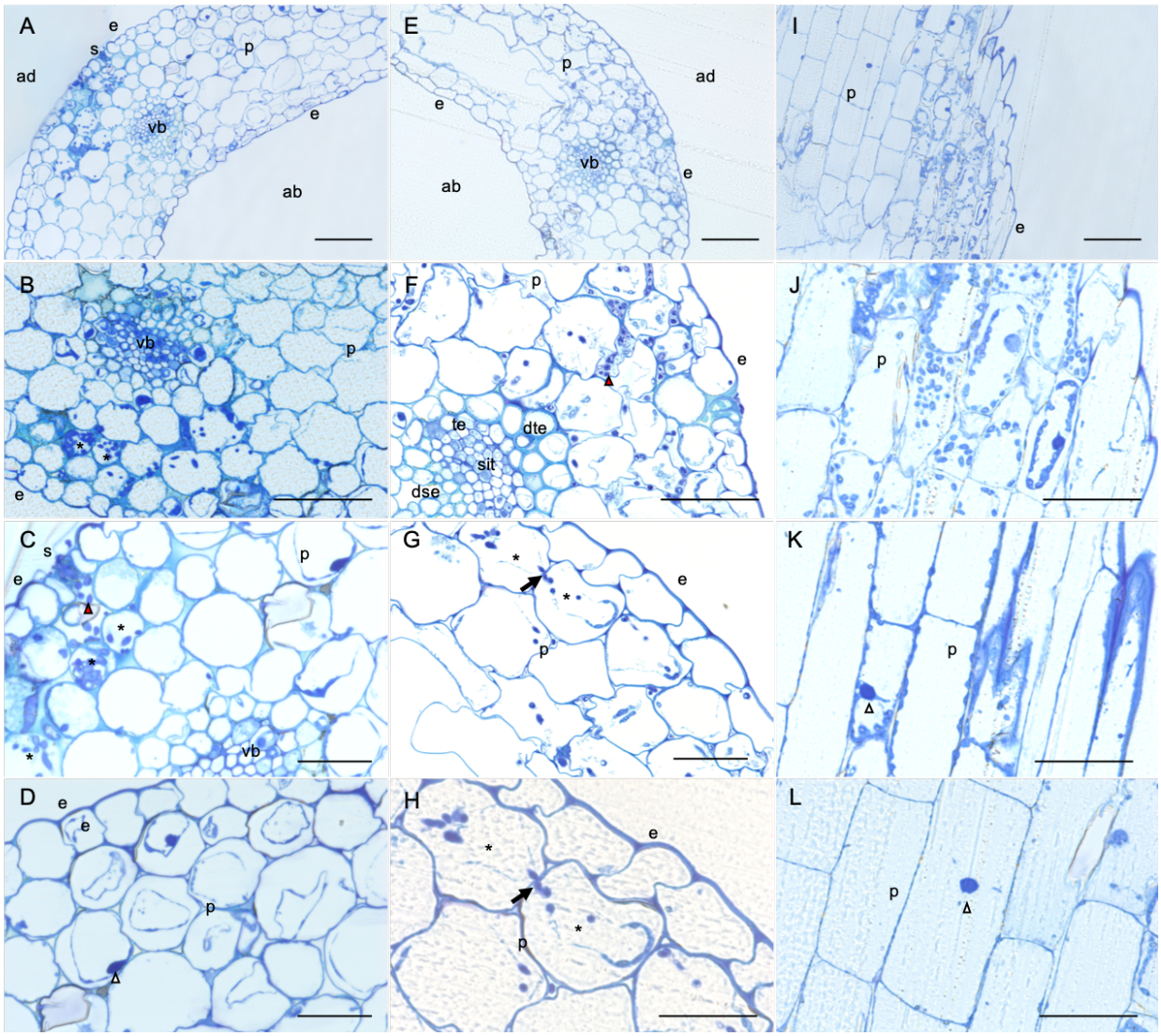

Figure 4.12 – PH-1 inoculated wheat coleoptile tissue cellular morphology (3 days post-inoculation). All sections fixed in LR white resin, 1µm thick and stained with 0.1% toluidine blue O, pH 9. A-D, E-H and I-L show sections taken from three separate samples showing coleoptile structure. A-D and E-H display transverse sections, whereas I-L longitudinal sections. Sections D and G display tissue plasmolysis. Chloroplasts (or other plastids) can be seen to adhere to the plasma membrane around the vasculature/outer cells of the coleoptile in all samples, these have not been labelled. A and C display hyphal entry via the stomata, with sections G and H showing hyphal growth via pit-fields. Hyphae could not be easily identified in the longitudinal sections. Nuclei with stand-like projections are shown in K and L. J displays cells densely populated with starch granules and plastids. ab = abaxial, ad = adaxial, e = epidermis, p = parenchyma, vb = vascular bundle, s = stomata, sit = sieve tube, te = lignified tracheary element, dse = differentiating sieve element, dte = differentiating tracheary element. Black arrowheads = starch grain structures, white arrowheads = nuclei (only those that are confirmed are labelled), red arrowheads = intercellular hyphae, * = cells with intracellular hyphae, black arrow = hyphae passing through pit-fields. Bars: A,E,I = 100 µm; B,C,D,F,G,J,K = 50 µm; H,L = 25 µm.

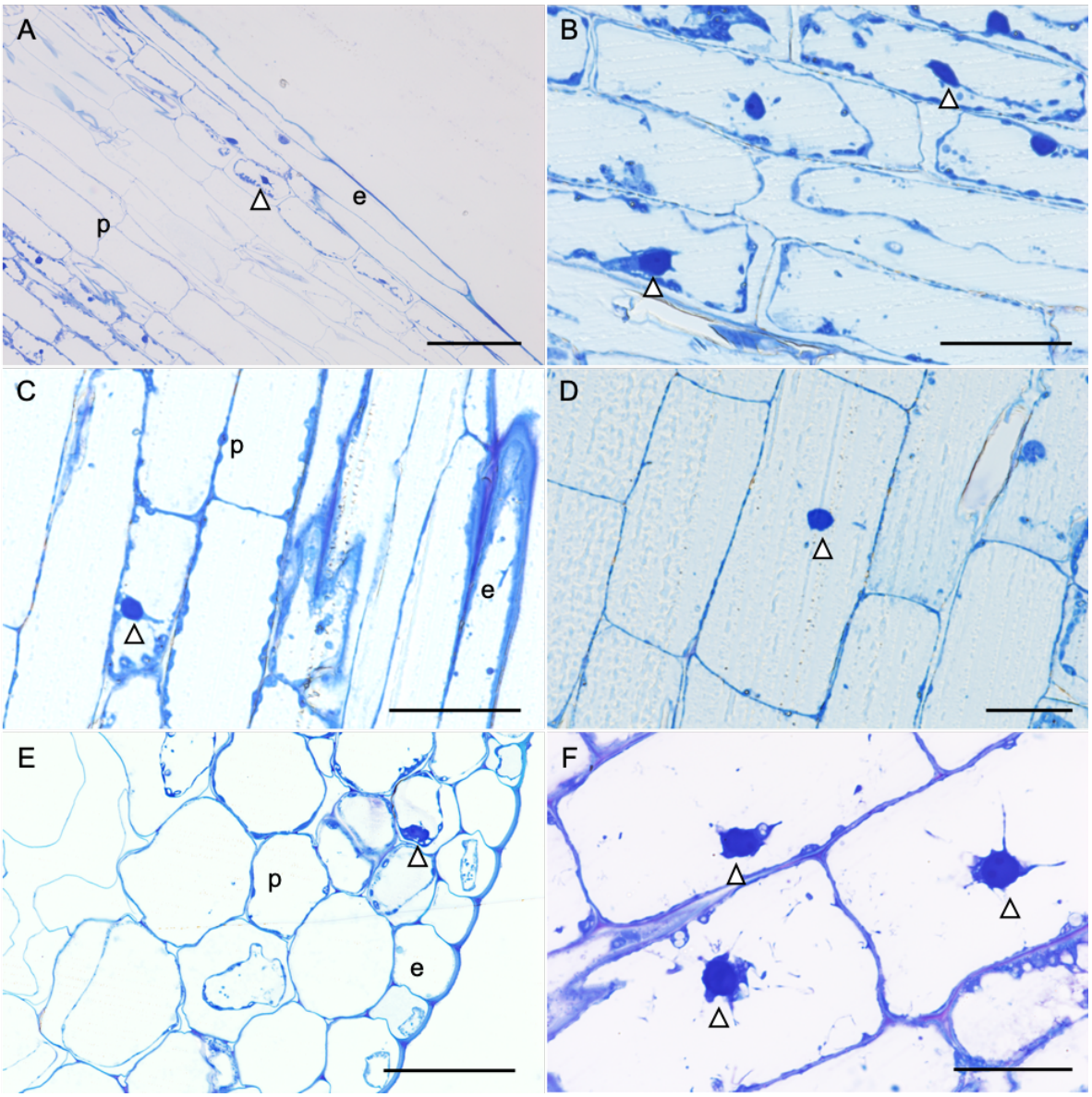

Figure 4.13 – Nuclei with strand-like projections in PH-1 infected wheat coleoptile tissue. All sections fixed in LR white resin, 1 µm thick and stained with 0.1% toluidine blue O, pH 9. (A)-(D) 3 days post inoculation. (E) and (F) 5 days post inoculation. Nuclei with strand-like projections were seen in the parenchyma as well as cells just underneath the epidermis – longitudinal sections were more conducive to displaying nuclei. White arrowheads = nuclei with strand-like projections. Bars: A = 100µm; B, C, E = 50µm; D, F = 25µm.

4.3.5 Detailed microscopic analysis of the *F. graminearum* mutant strains GT2 and MAP1 inoculated wheat coleoptiles

In comparison to the PH-1 inoculated coleoptiles, the macroscopic symptoms presented by the ΔFgGT2 and ΔFgMAP1 inoculated coleoptiles were minimal or non-existent, respectively (Fig. 4.10 and Fig. 4.11). Small lesions could be seen on some ΔFgGT2 infected coleoptiles at 3 dpi; these lesions had not developed any further by 5 dpi, suggesting the infection had not spread into the surrounding tissue. If infection was arrested *in planta,* in all likelihood only a small number of cells would contain hyphae, with some of the visible lesion being a result of localised plant defensive responses to infection – there is therefore no guarantee the few cells with hyphae will be successfully sectioned. Also, not all inoculated samples displayed a lesion (~50%). The ΔFgMAP1 *F. graminearum* mutant infected coleoptiles displayed no macroscopic symptoms, there was no lesion present at 5 dpi, suggesting infection was either not successful or exceptionally restricted. Representative images are given in Fig. 4.10 and Fig. 4.11.

Imaging of fixed sections for both the ΔFgGT2 and ΔFgMAP1 mutant strains, displayed no presence of any hyphae. Following fixation, the small ΔFgGT2 inoculated coleoptile lesions could no longer be identified as a result of clearing the sample, however ΔFgGT2 and ΔFgMAP1 inoculated coleoptile samples were prepared as for PH-1, so that the lesion was present at the cutting surface. No hyphae were seen in sections taken for either mutant – this is shown in Fig. 4.14 and Fig. 4.15. Hyphal quantification of PH-1 inoculated coleoptiles is discussed in the section below, to allow for comparisons to be made between *F. graminearum* strains in the future. Plasmolysis in the coleoptile was observed in all samples – controls, PH-1 inoculated samples, ΔFgGT2 and ΔFgMAP1.

Comparisons in the number of plasmolysed cells between strains has not been done here but may be a useful characteristic to quantify in the future. No nuclear strand-like projections were seen for either of the mutant strains.

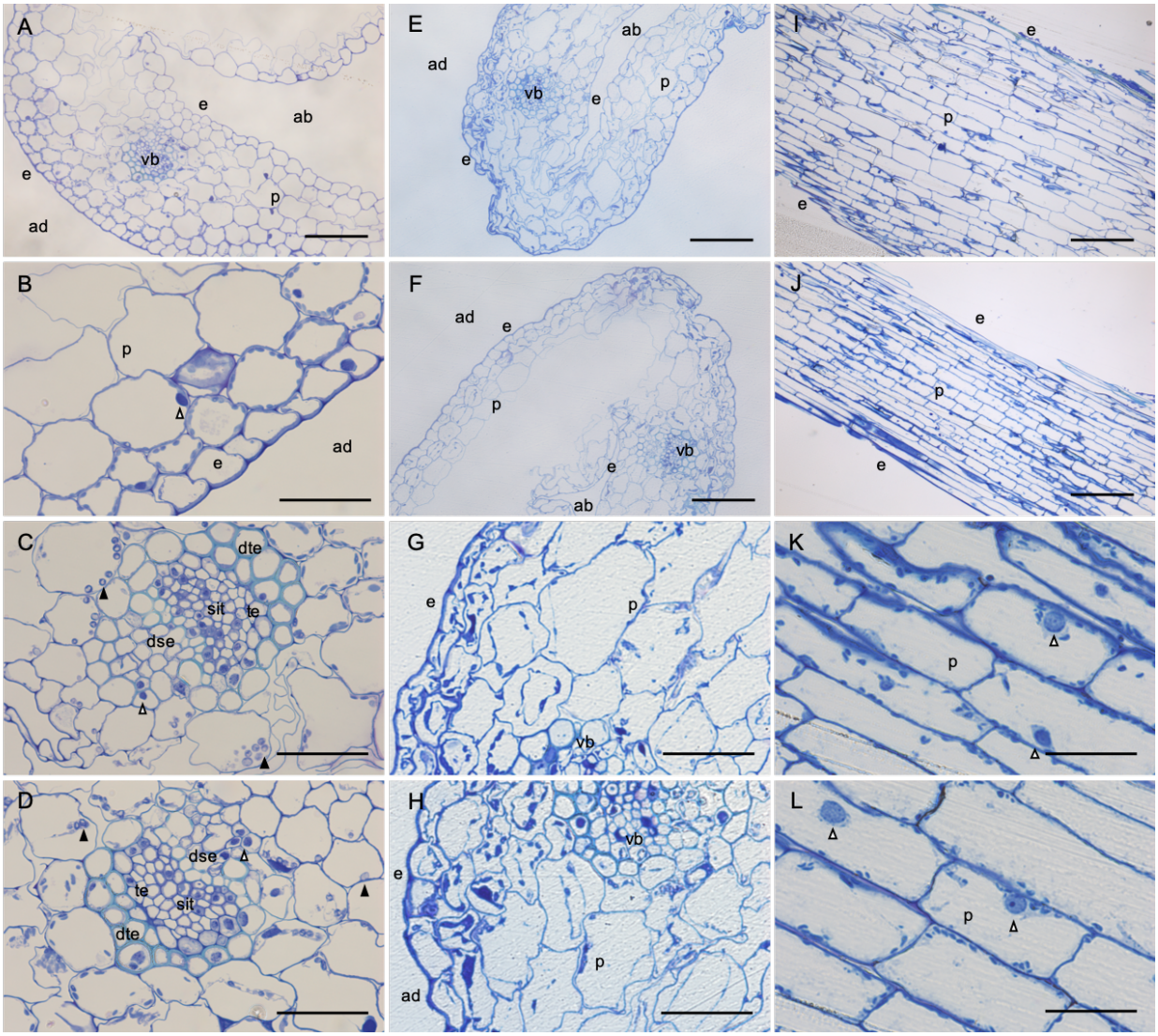

Figure 4.14 – ΔFgGT2 inoculated wheat coleoptile tissue cellular morphology (3 days post-inoculation). All sections fixed in LR white resin, 1µm thick and stained with 0.1% toluidine blue O, pH 9. A-D, E-H and I-L show sections taken from three separate samples showing coleoptile structure. A-D and E-H display transverse sections, whereas I-L longitudinal sections. Sections G and H display tissue plasmolysis. Chloroplasts (or other plastids) can be seen to adhere to the plasma membrane around the vasculature/outer cells of the coleoptile in all samples, these have not been labelled. ab = abaxial, ad = adaxial, e = epidermis, p = parenchyma, vb = vascular bundle, sit = sieve tube, te = lignified tracheary element, dse = differentiating sieve element, dte = differentiating tracheary element. Black arrowheads = starch grain structures, white arrowheads = nuclei (only those that are confirmed are labelled). Bars: A,E,F,I,J = 100 µm; B,C,D,G,H,K,L = 50 µm.

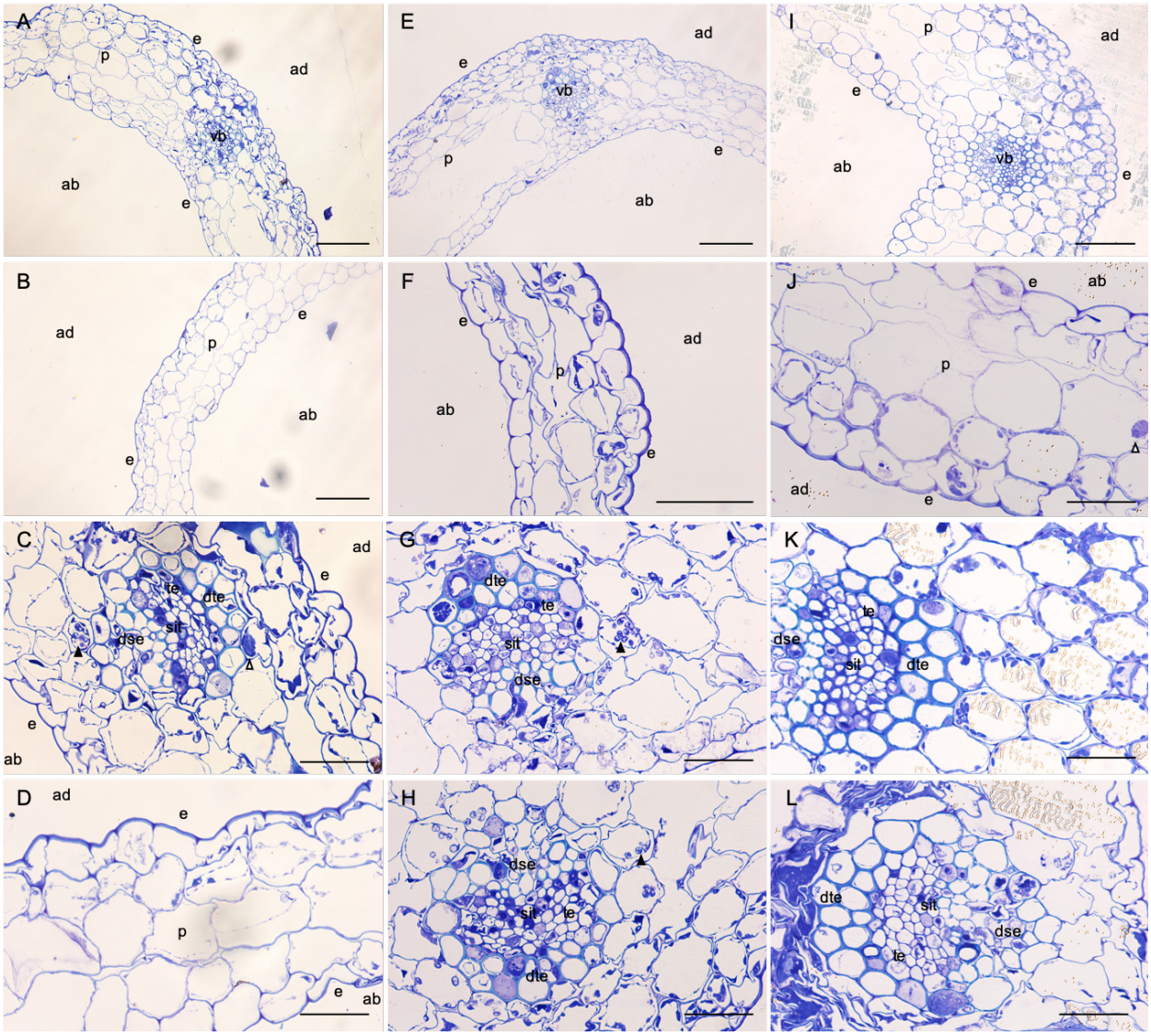
A
e
p
ad
vb
ab
e
E
ad
e
vb
p
e
ab
I
p
ad
e
ab
vb
e
B
ad
e
p
ab
e
F
e
ad
p
ab
e
J
e
ab
p
Δ
ad
e
C
ad
e
te
dte
sit
dse
Δ
e
ab
G
dte
te
sit
dse
K
te
dse
sit
dte
D
ad
e
p
e
ab
H
dse
sit
te
dte
L
dte
sit
dse
te

Figure 4.15 – ΔFgMAP1 inoculated wheat coleoptile tissue cellular morphology (3 days post-inoculation). All sections fixed in LR white resin, 1µm thick and stained with 0.1% toluidine blue O, pH 9. A-D, E-H and I-L show sections taken from three separate samples showing coleoptile structure. All sections shown are transverse, no longitudinal sections were available. Sections F and D display tissue plasmolysis. Chloroplasts (or other plastids) can be seen to adhere to the plasma membrane around the vasculature/outer cells of the coleoptile in all samples, these have not been labelled. ab = abaxial, ad = adaxial, e = epidermis, p = parenchyma, vb = vascular bundle, sit = sieve tube, te = lignified tracheary element, dse = differentiating sieve element, dte = differentiating tracheary element. Black arrowheads = starch grain structures, white arrowheads = nuclei (only those that are confirmed are labelled). Bars: A,B,E,F,I = 100 µm; C,D,G,H,J,K,L = 50 µm.

4.3.6 Hyphal quantification in *F. graminearum* inoculated wheat coleoptiles

Quantifying hyphal characteristics *in planta*, will provide a comparative dataset for comparing infection of different *F. graminearum* strains and /or different tissue types. These data sets will in the future help build a model of the infection process. As I only have a small dataset here, this statistical analysis will act as a preliminary investigation for future experiments. The water-inoculated control sections were shown to have no hyphae and were therefore not directly included in the analysis – this control has served its purpose as a standard for infection. The parameters: number of intracellular hyphae, number of intercellular hyphae and number of hyphae crossing PFs, were used. The statistics described compare the PH-1 coleoptile lesion against the opposite side of the coleoptile, which has few if any hyphae and can therefore be used as an in-sample control. Distance along the sample transect has also been factored into the analysis. As

30 sequential sections were taken per sample, this quantification explores 30μm of the sample. As a result of the approach adopted all sections are likely to have either remained within a single cell in some cases or passed to adjacent cells in others. Larger sample transects may therefore be needed in the future as cells can be in the range of 10-100μm[365].

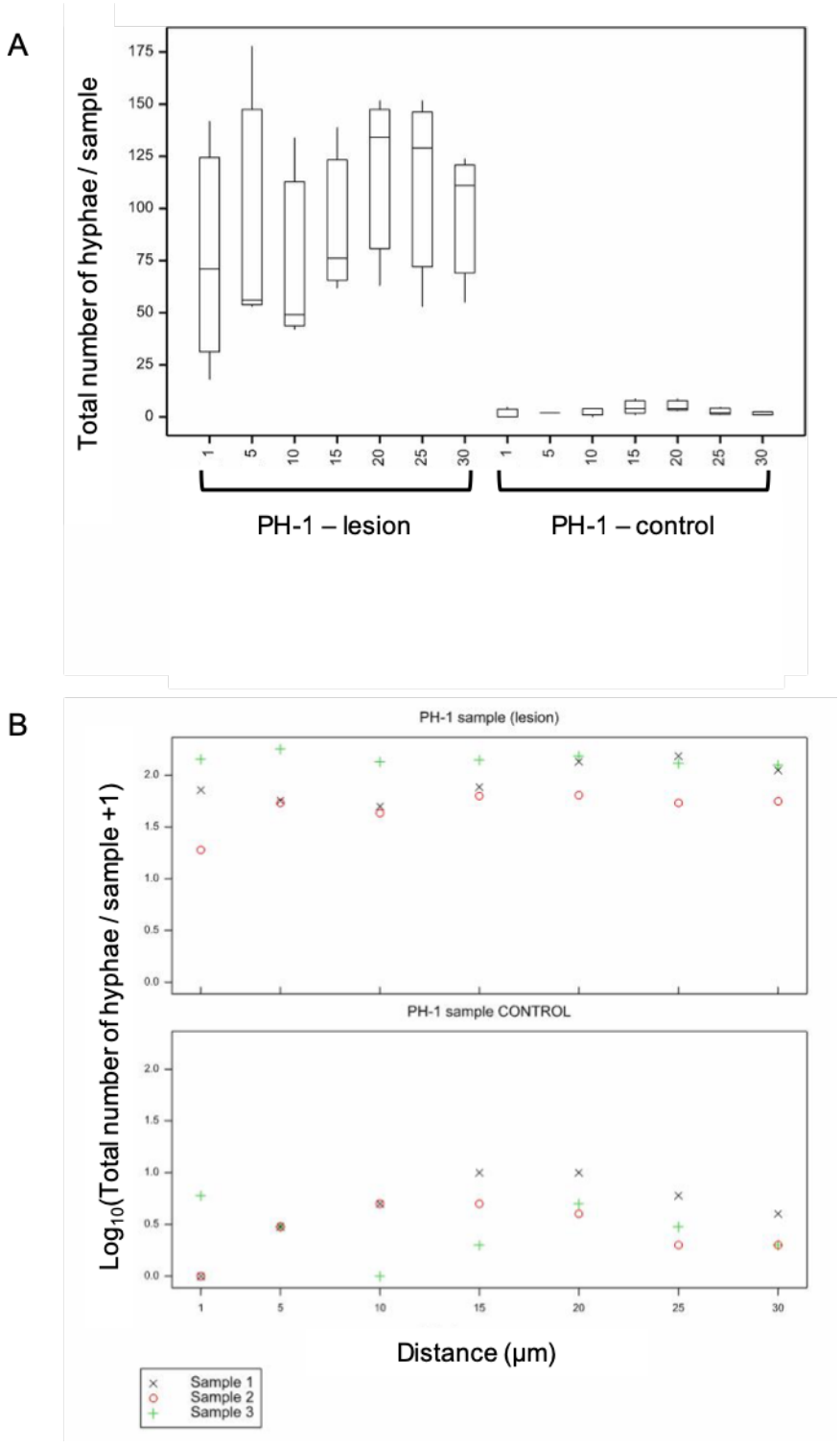

Figure 4.16 – Statistical analysis for total number of *Fusarium graminearum* hyphae in coleoptile tissue. (A) Boxplot of total number of hyphae by distance and treatment. (B) Scatterplot of logged total number of hyphae by distance and treatment. PH-1 sample (lesion) = the side of the coleoptile with infection, PH-1 sample CONTROL = the side of the infected sample without a lesion. Distance is measured from the middle of the coleoptile lesion outwards (i.e. 1 to 30).

The number of total hyphae (intracellular and intercellular) was first investigated. (The raw data and analysis/summary statistics for this can be found in the Appendix 13 and Appendix 14). A boxplot of the total number of hyphae over distance for both the PH-1 lesion and control side of the sample, visually demonstrated a clear split between the number of hyphae found in the lesion and those found on the opposite side of the coleoptile (Fig. 4.16). However, this data was skewed, and was consequently logged for further analysis (Fig 4.16). The transformed data clearly displayed a significantly greater number of hyphae in the lesion than in the control. This was reiterated by the ANOVA results, whereby treatment effect, i.e. the lesion or control side of the inoculated coleoptile, on the results had a p-value of 0.012. On the other hand, distance across a sample did not play a significant part with a p-value of 0.283. Finally, the relationship between treatment and distance showed they acted independently ($p = 0.803$). A residual maximum likelihood (REML) analysis determined the means for distance at different levels of treatment[362]. This reiterated the fact that the two datasets that are being compared here are at two extremes, the lesion side has many hyphae whereas the opposite side of the coleoptile does not (Fig. 4.17).

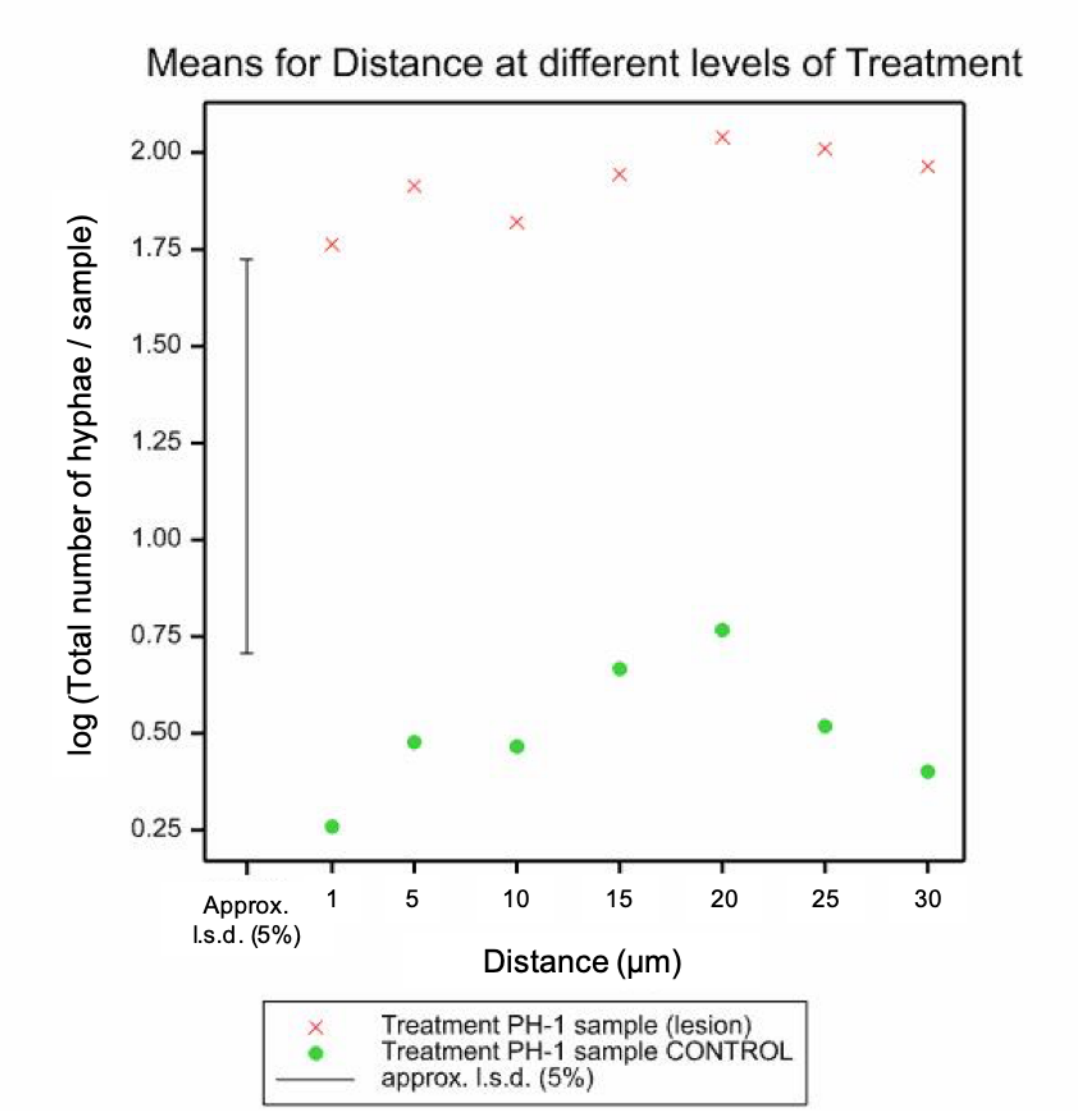

Figure 4.17 – Residual maximum likelihood (REML) analysis predicting means by distance and treatment. PH-1 sample (lesion) = the side of the coleoptile with infection, PH-1 sample CONTROL = the side of the infected sample without a lesion. Distance is measured from the middle of the coleoptile lesion outwards (i.e. 1 to 30). l.s.d = least significant difference.

A second approach was to then treat intracellular and intercellular hyphae as proportions of the total number of hyphae. Attempts to fit a generalised linear mixed model (GLMM) to the data was unsuccessful as the datasets were considered to be at two extremes as mentioned above[366]. This as well as the structure of the data has meant in this case the best output is purely graphical. The proportion of intracellular hyphae/total hyphae, displayed in Fig. 4.18, shows that in two of three samples on the control side all hyphae present are intracellular, the third has more intercellular hyphae. On the lesion side, a greater proportion of hyphae are intracellular than intercellular. Fig. 4.16 and Fig. 4.18 indicate that the total number of hyphae in sample 2 is lower than in samples 1 and 3. Similarly, sample 1 in Fig. 4.18 is the only sample with intercellular hyphae present on the non-inoculated side of the coleoptile. This suggests there is some variation in the infection process, with infection proceeding quicker in sample 1 and slower in sample 2.

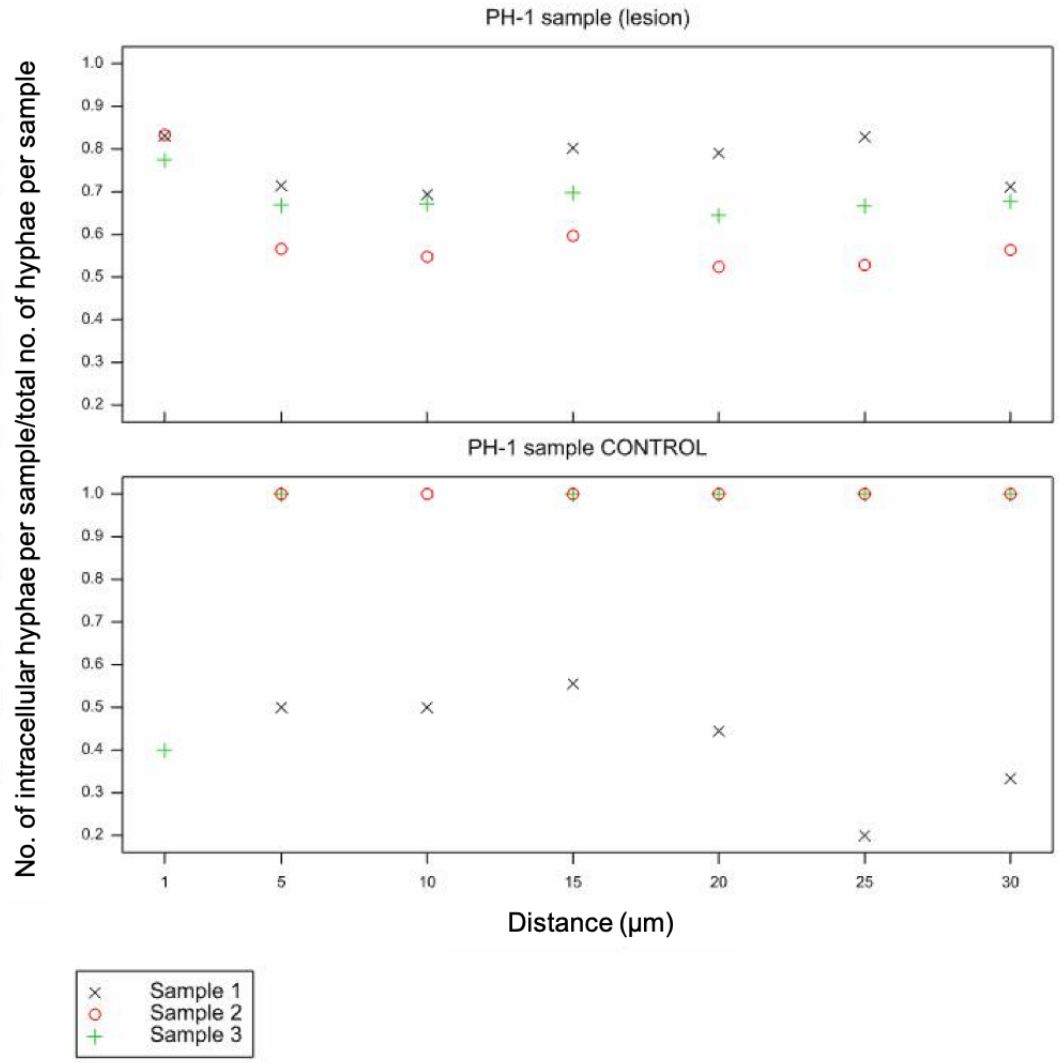

Figure 4.18 – Proportion of intracellular *Fusarium graminearum* hyphae. Where there are no data points, values were 0. PH-1 sample (lesion) = the side of the coleoptile with infection, PH-1 sample CONTROL = the side of the infected sample without a lesion. Distance is measured from the middle of the coleoptile lesion outwards (i.e. 1 to 30).

The number of hyphae crossing PFs per section was small and therefore wasn't statistically analysed, these results are shown in Table 4.3. A maximum of two hyphae passing through what are hypothesised to be PFs, are seen at any one time point. Sample 2 had no hyphae crossing through PFs, whereas sample 3

had the most. Once again indicating infection was moving at different paces in each sample.

Table 4.3 – Number of *Fusarium graminearum* hyphae crossing pit-fields in the wheat coleoptile.

	Number of *F. graminearum* hyphae crossing pit-fields[1]								
	Water-inoculated coleoptiles			PH-1 inoculated coleoptiles – in-sample control			PH-1 inoculated coleoptiles – lesion		
Distance across sample[2] (µm)	S1	S2	S3	S1	S2	S3	S1	S2[3]	S3
1	0	0	0	0	0	0	0	0	0
5	0	0	0	0	0	0	0	0	2
10	0	0	0	0	0	0	0	0	2
15	0	0	0	0	0	0	0	0	1
20	0	0	0	0	0	0	1	0	1
25	0	0	0	0	0	0	1	0	0
30	0	0	0	0	0	0	0	0	1

S = sample

[1] – There is no evidence these crossing points are pit-fields, this is the current hypothesis.

[2] – Distance across sample is relative to the visible lesion, sectioning outwards from the lesion centre.

[3] – The data in Figure 4.18 indicates that the *F. graminearum* infection in sample 2 was progressing more slowly than in samples 1 and 3.

4.3.7 Identifying the *F. graminearum*-plasmodesmata interaction in wheat coleoptiles

Sectioning of PH-1 inoculated coleoptiles revealed hyphae were able to utilise possible PFs to grow intracellularly (it should be noted that they have not been confirmed as PFs). From the fixed samples investigated, the hyphae were localised around the vasculature and therefore the PD-*F. graminearum* coleoptile interaction could only be viewed successfully in transverse sections. Examples of PF-PD colonisation can be seen in Fig. 4.19 both in the general parenchyma tissue (A), and in the cortical cells adjacent to vascular bundles (B). Panel (C) demonstrates a section in which a hypha is branching and attempting to cross cell walls at multiple points. Hyphae constrict to pass from one cell to the next before increasing their size in the adjacent cell, as observed previously in wheat floral tissue[113]. Most hyphae, in transverse profile, are displayed width ways, with only the hyphal circumference on display. However, Fig. 4.19, also displays hyphae being imaged lengthways, growing across the cell before passing through a PF and invading the adjacent cell.

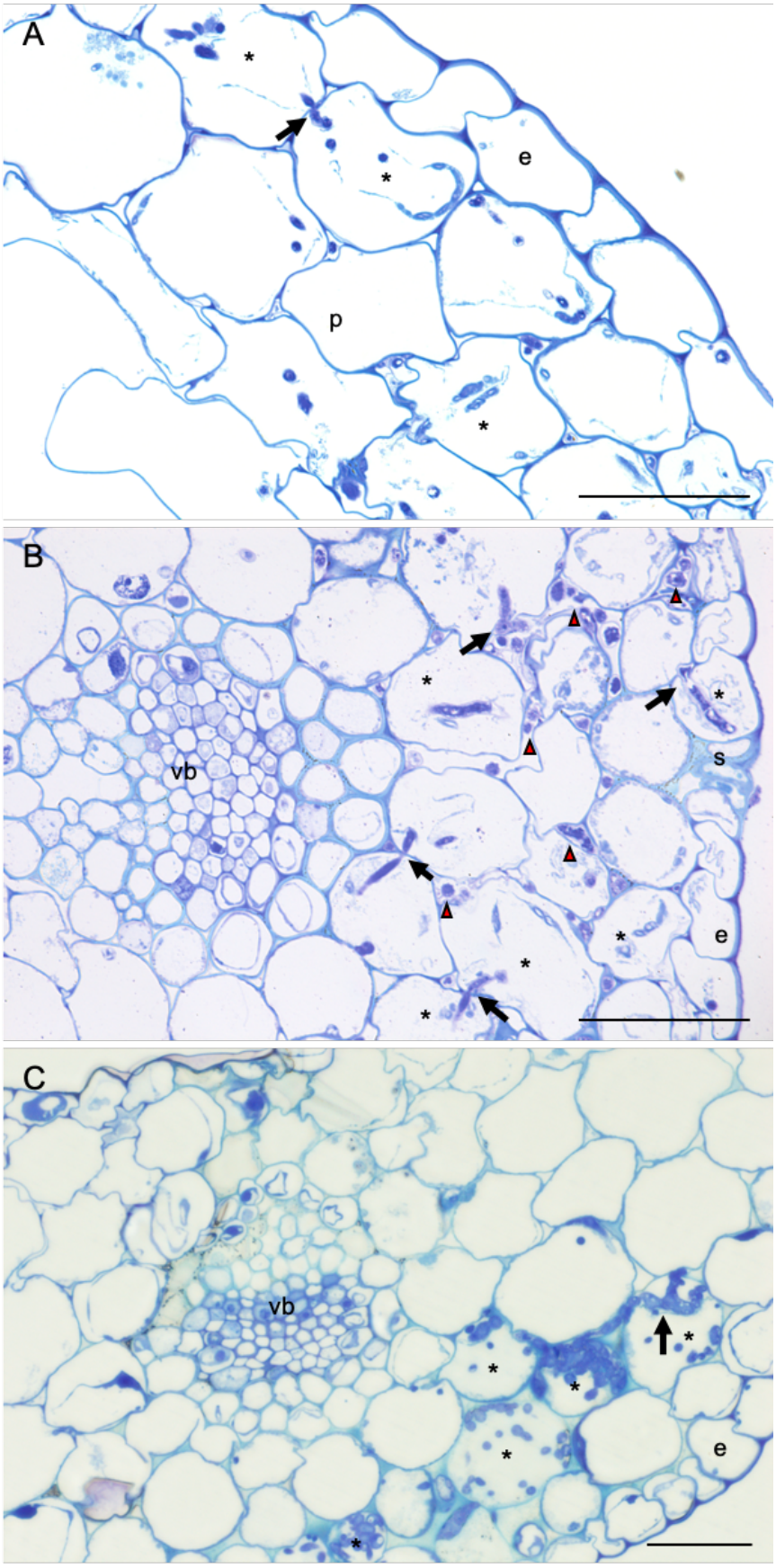
A
e
p
B
vb
s
e
C
vb
e

Figure 4.19 – *Fusarium graminearum*, PH-1, intracellular colonisation via pit-fields in the wheat coleoptile. All sections fixed in LR white resin, 1 µm thick and stained with 0.1% toluidine blue O, pH 9. (A) Hyphae travelling cell-to-cell via a pit-field. (B) and (C) Hyphae travelling across a cell before using a pit-field to pass to the next. All sections shown are transverse. ab = abaxial, ad = adaxial, e = epidermis, p = parenchyma, vb = vascular bundle, * = cells colonised intracellularly with hyphae. Black arrows = intracellular hyphae pit-field crossing points, red arrowheads = intercellular hyphae (only those that are confirmed are labelled). Bars = 50 µm.

As the hyphae undulate within the tissue it was difficult to visualise the entirety of the hyphal structure via sectioning, as well as the *F. graminearum* hyphal interaction. Preliminary tests were therefore done to identify ways in which the inoculated coleoptile could be imaged with greater depth and detail; as these were only proof of concept experiments, testing the efficiency of staining methods, these investigations were not repeated. One approach was to stain *F. graminearum* using the WGA-Alexa Fluor 488 conjugate *in planta*. The staining protocol was successfully adapted for use in the coleoptile – images for this can be seen in Fig. 4.20. WGA is a lectin that binds to chitin and displays green fluorescence (excitation/emission maxima ~495/519 nm) (https://www.thermofisher.com/order/catalog/product/W11261#/W11261). The three controls, untreated, water control no stain, and water control + WGA-Alexa Fluor 488, displayed no fluorescence due to the lack of fungi, however the inoculated samples did display strong fluorescence, clearly outlining the abundance of *F. graminearum* structure either on or within the wheat coleoptile tissue. From Fig. 4.20 the coleoptile tissues appear more abundant in hyphae

than what was seen in the PH-1 fixed samples (Fig. 4.12). The confocal images in Fig. 4.20 capture one to two cells deep into the tissue, however it is likely some surface hyphae are also in focus making quantification in this system more difficult. It should also be noted that hyphae were generally more abundant near the vasculature in the imaging system, similar to that seen in the fixed tissues.

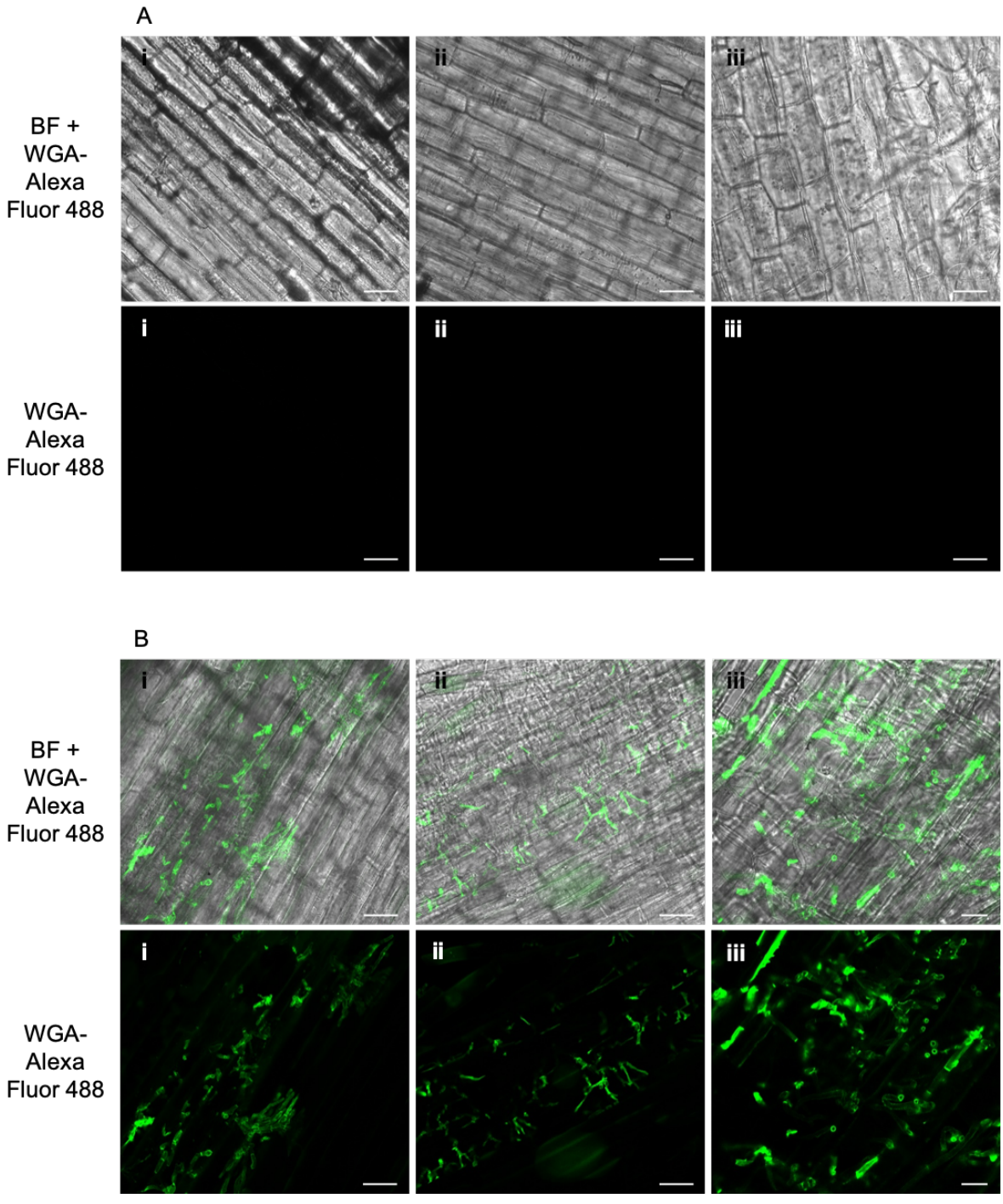

Figure 4.20 – *Fusarium graminearum*, PH-1, wheat germ agglutinin (WGA)-Alexa Fluor 488 staining in the coleoptile. All images taken in wheat coleoptile tissue, 3 days post inoculation. Panel A: (i) Untreated control (ii) Water inoculated coleoptile, no stain (iii) Water inoculated coleoptile + WGA-Alexa Fluor 488. Panel (B) All images show successful staining of the PH-1 *F. graminearum* strain with WGA-Alexa Fluor 488. All images taken using a confocal microscope. Excitation/emission wavelengths ~495/519 nm. BF = brightfield. Bar = panel A; 50 μm, panel B; i,ii = 50 μm, iii = 20 μm.

Many fungal imaging systems rely upon the use of WGA with a cell wall dye to analyse hyphal trajectory. A second preliminary experiment was carried out using PI, a red fluorescent protein (excitation/emission wavelengths of 493/636 nm) which binds to DNA. However, PI is unable to permeate live cells, at which point plant cell walls become stained instead. This stain can therefore also be used as an indicator of cell viability. Even though staining of *F. graminearum* with WGA was successful, an *F. graminearum* PH-1:GFP strain (Fig. 4.21) was available. Stains can become toxic to cells over time, therefore for the purpose of analysing infection in real-time in future experiments, a combination of the *F. graminearum* GFP reporter strain and PI should be used to visualise the interaction. These results can be seen in Fig 4.22. The untreated and water inoculated, unstained controls displayed no autofluorescence that would otherwise interfere with the imaging process. Stained untreated and stained water control samples both displayed PI fluorescence at the cell wall, this also demonstrated the water inoculation process did not induce a response. The PI stained, PH-1:GFP inoculated sample displayed successful infection and hyphal progression could

be more easily visualised. Hyphae could clearly be seen colonising cells intracellularly, with some possible evidence of crossing at PFs, however this is not clear. This methodology would be well suited to studying this interaction in future projects.

Callose staining was also attempted on resin-embedded samples. However, this was unsuccessful, with the aniline blue protocol needing refining. This had not been attempted previously at Rothamsted Research, with aniline blue staining primarily being used on fresh plant samples.

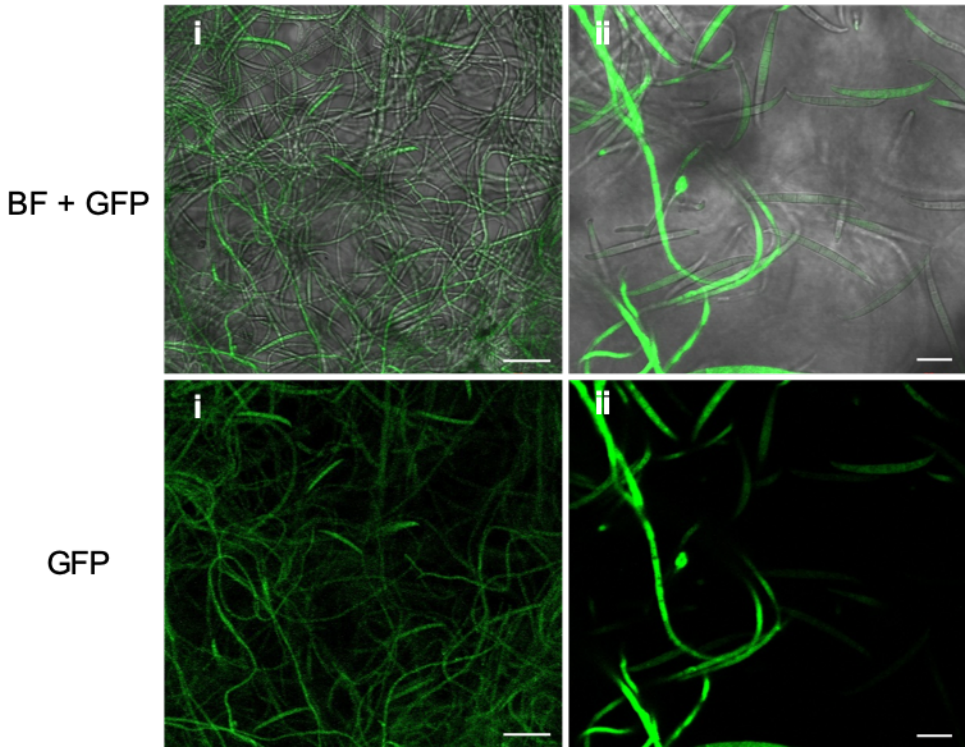

Figure 4.21 – *Fusarium graminearum*, PH-1:GFP strain *in vitro*. (i) BF + GFP and (ii) GFP only. Grown on synthetic nutrient poor agar (SNA) as described in Chapter 2. Images taken using confocal laser scanning microscopy. Excitation/emission maxima~488/509 nm. BF = brightfield. Bar: i = 50 μm, ii = 20 μm.

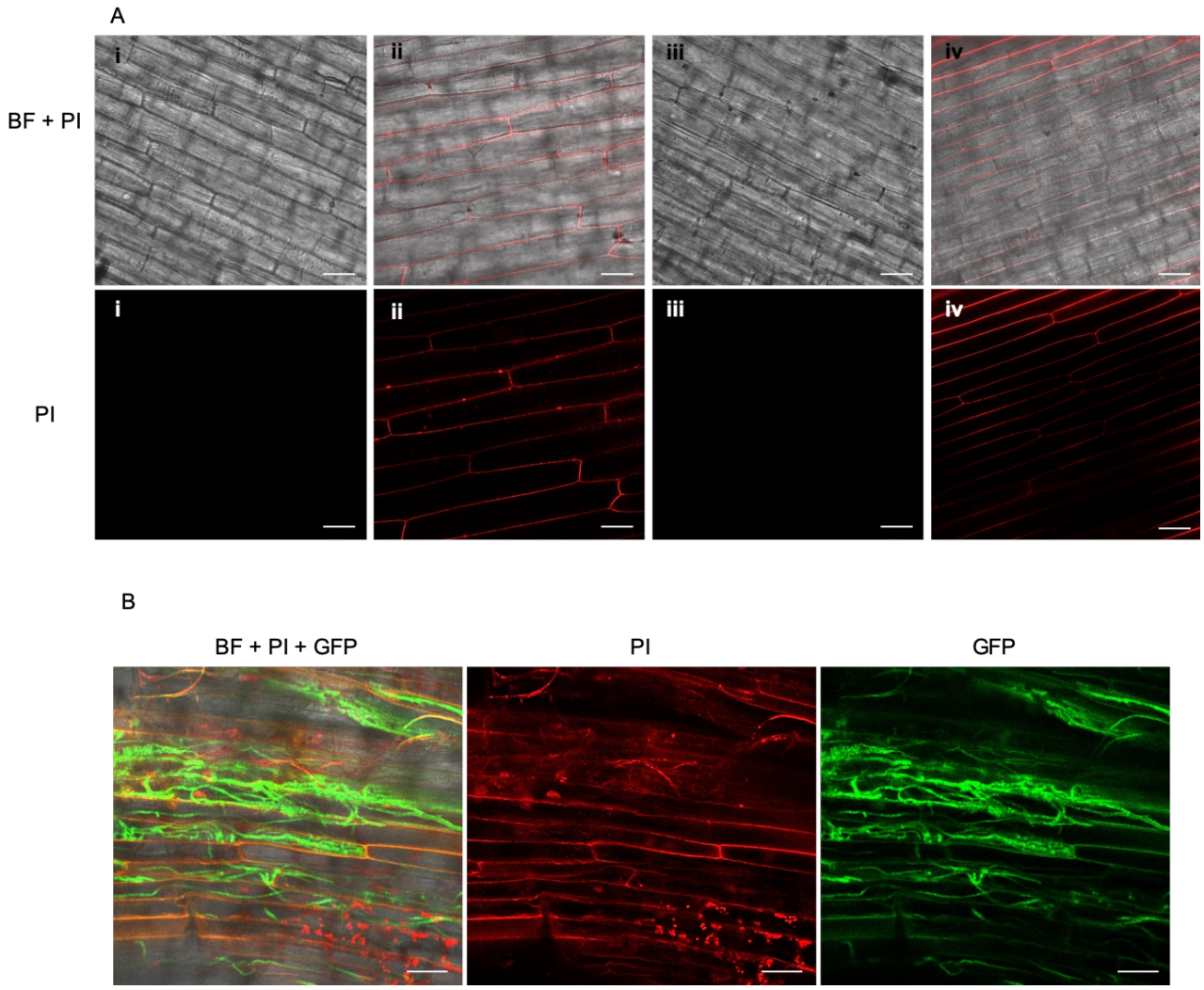

Figure 4.22 – *Fusarium graminearum*, PH-1:GFP strain with propidium iodide (PI) in the wheat coleoptile (3 days post inoculation). All images taken in wheat coleoptile tissue, 3 days post inoculation. Panel A: Controls. (i) Untreated, unstained (ii) Untreated + PI (iii) Water inoculated, unstained (iv) Water inoculated + PI. Panel B: PH-1:GFP inoculated coleoptile tissue. All images taken using confocal microscopy. Excitation/emission maxima for PI~493/636 nm, excitation/emission maxima for GFP~488/509 nm. BF = brightfield. Bar = 50 μm.

4.4 Discussion

As the third most highly produced crop, wheat is a critical staple food source worldwide. Despite there being a wide range of wheat research being done, from pathology studies to genetics, publicly available comprehensive wheat floral morphological data combined with cell biology datasets rarely exist (https://www.cerealsdb.uk.net/cerealgenomics/WheatBP/Documents/DOC_WheatBP.php). With the aim to study the *F. graminearum*-wheat interaction and to identify the role of PD in intracellular hyphal growth, uninoculated wheat floral tissues were studied microscopically, focusing on morphological and cellular characteristics. Additionally, the development of the high throughput wheat coleoptile assay provides a new system in which to study the *F. graminearum*-wheat interaction at the cellular level[303].

Resin-embedded samples were shown to clearly depict floral wheat tissue and coleoptile morphology. Previous evidence demonstrates *F. graminearum* can enter wheat floral tissue via stomata located on the glumes, resulting in FHB[162]. Images presented here suggest the glumes may not be the only stomatal entry point within the floral tissues. The palea, lemma and rachis also possess stomata, indicating a possible hyphal entry point (Fig 4.5); this has been shown to be the case for the lemma in *F. graminearum* infection of barley[367]. Similarly, the coleoptile tissue also contains stomata, which has been shown here and in a recent study to be a hyphal entry point into the host (Fig. 4.12)[355]. Phenotypic characteristics, such as the 'interlocking' cells of the lemma parenchymal layer, will aid research in plant development; any effect of these cells and their development on *F. graminearum* infection has yet to be determined. The longitudinal and transverse rachis sections show small gaps in the cell walls,

which are possibly PFs. However, these are typically hard to identify using light microscopy.

The wheat floral infection assay takes two to three months to complete, from sowing the seed to scoring FHB symptoms. The wheat coleoptile assay was therefore considered a high-throughput approach that may also be suitable for studying the *F. graminearum*-PD interaction. Previous to this project, the wheat floral tissue PFs had already been identified as a means for *F. graminearum* hyphae to grow between cells[113]. A recent study also identified PFs/PD in the wheat coleoptile, however this study only used the epidermis, and not the whole wheat coleoptile, for infection[355]. This approach made imaging easier, however, to obtain a clearer picture of how *F. graminearum* interacts with tissue *in planta*, this approach was not taken forward here. From this study *F. graminearum* was shown to penetrate the coleoptile cell walls using penetration pegs[355]. Toxisomes were formed during infection, callose deposition occurred at cell walls and complete cell-to-cell invasion via PFs was achieved[355]. The cellular characteristics of the wheat coleoptile tissue had not been characterised in any detail. In the present study the coleoptile was fixed, providing a unique view of how *F. graminearum* hyphae traverse wheat coleoptile tissue. We now know that the coleoptile assay can be used as a high-throughput assay for studying the *F. graminearum*-PD interaction, as shown in Fig. 4.12, and can clearly be imaged using fixed samples, infiltrated with LR white resin.

Coleoptile growth with and without *F. graminearum* infection was statistically analysed. A study from 1961 explored how wheat coleoptiles grew – identifying 90% of the cells as undergoing cell division – the outer epidermis did not – for up to 60h, and cell expansion occurring alongside cell division up to 96h[368]. In the

present study, there was found to be no significant differences between the growth of untreated coleoptiles, water-inoculated coleoptiles and PH-1 inoculated coleoptiles[368]. Most extension growth was seen between days 3 and day 4, whereas the inoculations occurred on day 3 – Fig. 4.8. From day 5 onwards, considerable infection and macroscopic lesion development had occurred. The results shown in Table 4.2 indicate the coleoptiles did not have a statistically significant reduced growth rate prior to or after infection. Overall, the data suggests *F. graminearum* infection has a negligible effect on overall coleoptile growth and is unlikely to affect the growth process at a cellular or molecular level.

Some of the experiments reported here will need to be repeated in the future, time-restrictions have meant this was not possible here. Both the untreated (Fig. 4.7) and water inoculated controls (Fig. 4.9) showed no signs of infection as did the two *F. graminearum* mutant strains, ΔFgGT2 and ΔFgMAP1 (Fig 4.13 and Fig. 4.14 respectively). Plasmolysed cells were frequent in both the control and PH-1 inoculated coleoptiles (Fig. 4.12) suggesting this may be an artefact of the fixing process. This had not been quantitatively analysed however and may be something to investigate further in future projects, to rule out the formal possibility that this cellular response is a result of a host reaction or a molecular attack on host secretion/overall host cell physiology by the fungus. Plasmolysis per se as a plant response to pathogen attack has previously not been identified in other plant-pathogen interactions. It should also be noted here that a coleoptile transcriptome study determined no DON was produced in the *F. graminearum*-coleoptile interaction, in the hexaploid wheat cultivar, Zhongyuan 98-68[303]. However, this has not been measured in Bobwhite and therefore DON production still needs to be quantified here.

The wild-type PH-1 inoculated coleoptiles displayed nuclei with strand like projections. There are four main explanations as to what these could be: a plasmolysed membrane surrounding the nucleus, actin filaments, transvacuolar strands (threads of cytoplasm surrounded by the vacuole, connecting one cytoplasmic area to the next) or Hechtian strands (strands connecting the PM to the cell wall in plasmolysed cells)[369-372]. In a couple of these scenarios staining of the PM could determine if the cells have undergone plasmolysis and consequently if there is Hechtian strand formation. FM4-64 is a dye that is able to stain the PM (as well as endomembrane compartments) in plant tissue[297]. Alternatively, a PM reporter line could be used, but one does not currently exist in wheat (Chapter 5). To determine if these strands are actin filaments, the stain rhodamine-phalloidin can be used in fixed tissues[373]. Transvacuolar strands may be determined by the tonoplast stain MDY-64[374]. Once again there is currently no published vacuole fluorescent marker line available. However, a wheat actin fluorescent marker line has been produced, this is currently unpublished (Michael Deeks, University of Exeter – personal communication).

With the aim of producing an *F. graminearum* infection model, both 3D and mathematical, in the future, I quantified hyphae in PH-1 infected coleoptile tissue. The number of intracellular and intercellular hyphae were quantified as well as the number of times hyphae crossed possible PFs. These hyphae were counted per field of view, focusing on the vasculature where most if not all hyphae were concentrated. Ideally the number of hyphae per cell would be explored, but to do this in a non-biased way, as only a small number of cells within the coleoptile contain hyphae, is a small project by itself – this methodology would also discount

any intercellular colonisation. As well as the sample size being quite small for the analysis done here, the number of hyphae on the lesion half of the section, in comparison to the non-lesion side, was very high, creating a dataset with two extremes. A GLMM could therefore not be fitted to this data without extensive data manipulation[366]. Increasing the number of samples analysed in similar studies as well investigating alternative parameters, for example hyphal density per cell, the number of plasmolysed cells and hyphal size would help improve this analysis – an automated system would be recommended for this. A larger transect through the sample is also recommended to monitor any hyphal changes from one cell to the next.

In the rachis, hyphae are shown to first grow intercellularly before transitioning to intracellular growth and traversing PFs[113]. Even though no quantitative data is available for *F. graminearum* rachis infection, hyphae growing through PFs seems to be a rarer event in the coleoptile upon initial observation, however there is currently no data to support this (Table 4.3). The cut edge of the coleoptile allows hyphae to immediately enter cells and colonise intracellularly. The statistical analysis displayed in this chapter (Fig. 4.16-Fig. 4.18) suggests there are fewer intercellular hyphae than intracellular hyphae in the coleoptile, this difference is unlikely to be so prominent in the rachis. Variations in rachis and coleoptile tissue structure may also account for some differences in hyphal growth. Another feature of coleoptile infection to note is that hyphae did not invade the vasculature as seen in the rachis, potentially suggesting *F. graminearum* does not express the same repertoire of enzymes and secondary metabolites in the coleoptile tissue as the floral tissue, which would allow the fungus to successfully complete this additional colonisation route [303]. 'Ghost'

hyphae, hyphae devoid of content, were also not visualised in the coleoptile as seen in the rachis – there was no cellular indications the hyphae were undergoing autophagy in the coleoptile, this was still true at 5 dpi (Fig. 4.23)[165]. It is possible *F. graminearum* hyphae remain alive for longer in the coleoptile as a result of no DON induction; application of DON in early root colonisation can inhibit infection[375].

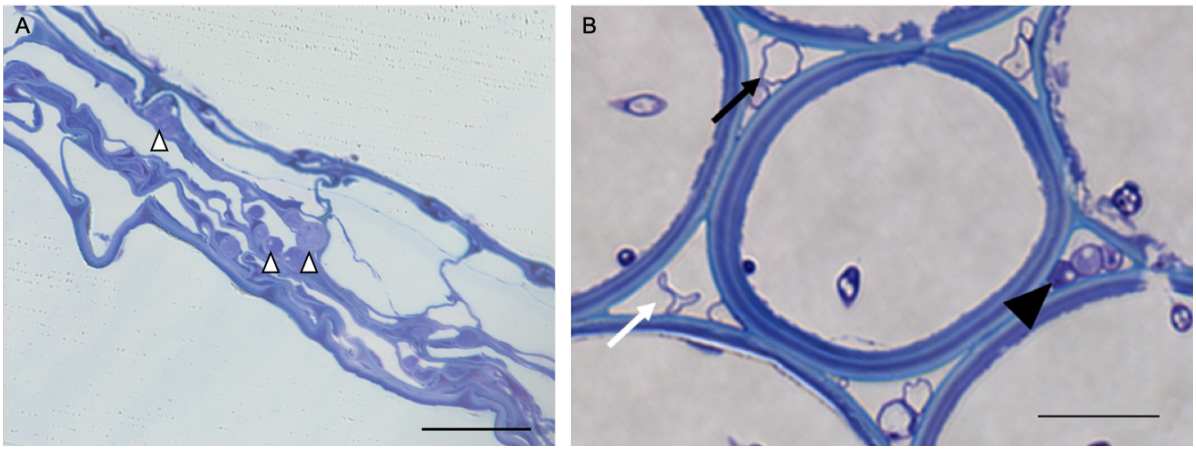

Figure 4.23 – Absence of *Fusarium graminearum* 'ghost' hyphae in wheat coleoptile tissue. (A) Coleoptile tissue 5 days post-inoculation, no 'ghost' hyphae can be identified. (B) Rachis tissue 12 days post inoculation with ghost hyphae. White arrowheads = healthy hyphae, black arrowheads = intercellular hyphae, black arrow = hyphae devoid of content (ghost hyphae), white arrow = collapsed hyphae. Bar: A = 25μm; B = 15μm. Image B is taken from Brown *et al.* 2011.

To investigate how the wheat coleoptile-*F. graminearum* interaction may be viewed in greater detail by live-cell imaging, WGA and PI (Fig. 4.20 and Fig. 4.22 respectively) were shown to help efficiently visualise *F. graminearum* hyphae *in planta*. These images demonstrated a live-cell imaging system can be efficiently

used for study of the *F. graminearum*-coleoptile interaction. To be able to compare cellular characteristics of the coleoptile infection to that in the rachis, fixed samples needed to be used, as this was the format of the rachis data that already existed[113]. The abundance of hyphae observed colonising the coleoptile can in part be attributed to surface hyphae that are washed off when preparing fixed samples. These figures also suggest hyphae should be seen in LS sections, which was not the case here – it may be a case of sectioning in exactly the right plane. The thorough wiping of the surface of a sample post initial imaging should help to reveal the abundance of hyphae on the coleoptile surfaces. A separate scanning electron microscopy image analysis would also help to clarify this point.

Callose staining was unsuccessful when attempted as part of this project. However, once the correct protocol has been identified this test is likely to be informative. It is likely that the ΔFgGT2 and ΔFgMAP1 mutants are prevented from colonising other cells by a callose boundary being formed around the initially infected cell as a host response[376,377]. In conjunction with this reporter lines could help circumvent the use of stains, most of which damage the tissue over time. There is already a GFP *F. graminearum* strain which has been used here (Fig. 4.21 and Fig. 4.22) but wheat reporter lines may also prove useful to achieving this goal. Here I have characterised the wheat floral and coleoptile tissue for future cellular and molecular study of the *F. graminearum*-PD interaction and provided future directions for this.

CHAPTER 5: Generation of wheat plasma membrane (PM) reporter lines to study fungal infection *in planta*

Note this chapter is taken from the following:

SWBio DTP rotation project 2 – Characterisation of wheat autofluorescence and the generation of plasma membrane reporter lines to further understand fungal infection mechanisms (2017)

5.1 Introduction

Owing to recent advances in PD research, and the understanding that these structures play a role in pathogen progression, investigations into the previously rarely studied PD-fungal pathogen interface are now possible[242,378,379]. As the PM is continuous within the PD, connecting adjacent cells, generating a wheat PM reporter line would not only be useful to this project but to other members of the wheat pathogen and wheat biology communities, allowing for live-cell imaging *in planta*.

The proteins chosen to label the wheat PM were *At*LTI6b (previously RCI2b) from *A. thaliana* – a 54 amino acid low temperature and salt responsive protein (At3g05890, UniProtID: Q0DKW8) – and *Zm*ROP7 from *Zea mays* – a 212 amino acid GTPase (UniProtID: Q9LEC6) [290,380-382]. The main reason for selecting these was because both genes had previously been shown in the literature to work successfully as PM markers in their respective species (Fig. 5.1). By constructing a series of PM labelled reporter lines, potentially with different expression levels, I therefore aimed to help identify some of the cellular and molecular mechanisms needed for the transition from intercellular to intracellular hyphal growth during

the wheat-*F. graminearum* interaction. In this chapter, with specialist help from others, I have focused on achieving the following:

- Production of expression cassettes in vectors suitable for high efficiency stable wheat transformation.
- Production of expression cassettes in vectors suitable for high efficiency particle bombardment for use in epidermal cell-fungal interactions.
- Production of new stable wheat PM reporter lines via particle bombardment.
- Characterisation of $T_0T_1T_2$ generations of the wheat PM reporter lines.
- Use of the two most successful and representative wheat PM reporter lines (harbouring different constructs) to explore the *F. graminearum*-PD interaction.

In this chapter, I specifically wanted to test the hypothesis that stable wheat PM reporter lines are effective tools in characterising the *F. graminearum*-PD interaction at the cellular level.

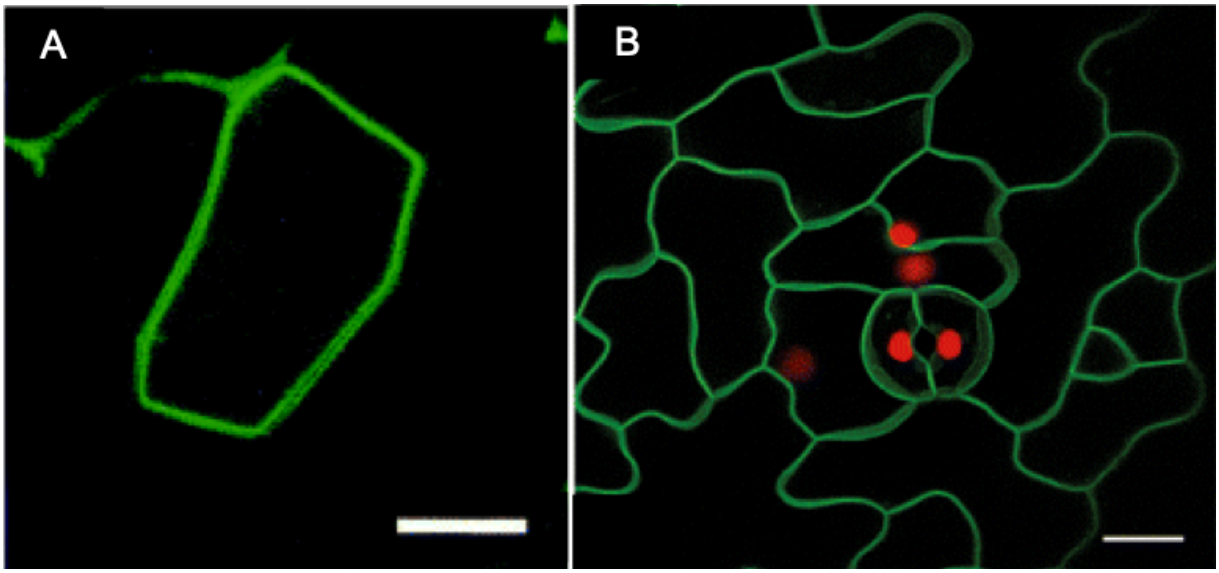

Figure 5.1 – GFP-ROP7 and EGFP-LTI6B PM localisation. (A) GFP-ROP7: single optical section showing localisation to the periphery of the cell. A small nuclear signal can also be seen. Immature maize cells transiently transformed via particle bombardment, bar = 10 µm. Image taken from Ivanchenko *et al.* 2001. (B) EGFP-LTI6B: localisation to the plasma membrane (nuclei are highlighted in red using the H2B-YFP marker). Taken from Kurup *et al.* 2005. These lines were originally produced by randomly fusing GFP with cDNA sequences before transforming *A. thaliana* with a modified *Agrobacteria* mediated transformation method (Cutler *et al.* 2000). Bar = 10 µm.

5.2 Experimental procedures

Due to the nature of these experiments no technical replicates were performed.

5.2.1 Protein secondary structure predictions

The freely available online software Phyre^{2} was used to determine protein structure and functional domains for the proteins of interest, *At*LTI6b and *Zm*ROP7^{383}. This analysis provided information on the secondary protein structure, transmembrane (TM) domain predictions and a predicted protein model.

5.2.2 Vector construct design and cloning for particle bombardment

Prior to synthesis by GenScript®, the nucleotide sequence of *At*LTI6b was codon-optimised for expression in wheat; in *Zm*ROP7 interfering restriction sites were removed. These sequence modifications were done manually using the Geneious© software with the help of Alison Huttly, Rothamsted Research. Overexpression vectors containing a tagRFP reporter gene, pRRes208.355 (PM-localising gene inserted at the N-terminus of tagRFP) and pRRes208.454 (PM-

localising gene inserted at the C-terminus of tagRFP), were provided by Alison Huttly, Rothamsted Research. At the time of writing these had not been published. Restriction digests were done for all vectors: pUC57:ROP7 (*NcoI/HpaI*), pUC57:LTI6b (*NcoI/HpaI*), pRRes208.355 (*NcoI/EcI136II*) and pRRes208.454 (*BspHI/HpaI*) – using enzymes purchased from NEB® and Promega®. Fragments were separated via gel electrophoresis before being processed using the Qiagen QIAquick® Gel Extraction Kit. Ligations to produce four constructs: pRRes208.355:ROP7-RFP, pRRes208.454:RFP-ROP7, pRRes208:355:LTI6b-RFP and pRRes208.454:RFP-LTI6b (Appendix 15 and Appendix 16) were carried out using T4 DNA ligase (Promega®). Transformations were done using JM109 competent *Escherichia coli* and the suppliers' protocol (Promega®). Plasmid extraction was completed using the Qiagen QIAprep® SPIN Miniprep Kit before sequencing (Eurofins®).

5.2.3 Stable/transient wheat transformation

Embryo isolation, preparation of materials for particle bombardment, and operation of the PDS-1000/Helium particle gun, have all been described previously[384]. All experiments were carried out with assistance from the Rothamsted Research Specialist Cereal Transformations team using the spring wheat cultivar (*cv.*) Bobwhite, which is fully susceptible to *F. graminearum* infections (Chapter 2). A plasmid containing the selective gene marker *bar,* conferring resistance to the herbicide Basta was co-bombarded. This was repeated for transient leaf tissue bombardments; small leaf segments were used for this. Transient transformation experiments were repeated three times in wheat embryos and once in leaf tissue. For transient transformation bombardments, per construct 16 wheat embryos and more than 3 leaf tissue samples were used (these have not been classified as biological replicates due to the design of the

experiment. This this was only a preliminary test to assess if the constructs would function *in planta*). For the stable transformation bombardments more than 10 embryos (>10 biological replicates) were bombarded with each construct. The stable transformation bombardments were not repeated.

5.2.4 Plant material and growth

Putative transformants were initially cultured by the Cereal Transformations team from callus. Once individual plants could be identified (any sister transformants taken from the same callus line were carefully labelled, once tested via PCR one of each pair could be discarded) these were then potted using Rothamsted prescription soil mix and grown under controlled glasshouse conditions: 16h day – 20°C and 8h night – 16°C cycles. Leaf samples from the T_0 generation were taken by the Cereal transformations team for PCR analysis – confirming the presence of the PM target gene and selection marker. Selection marker PCR conditions and primers are listed in Alotaibi *et al.* 2018[385]. T_0 leaf samples were taken from the second flag leaf, and frozen immediately in liquid nitrogen before being stored at -80°C. Once dried, ears were harvested and threshed by the Rothamsted Research glasshouse team. T_1 plants were subsequently grown in the same glasshouse conditions and samples taken for copy number and genotype analysis as described below.

Seeds were stored in the designated seed storage unit at Rothamsted Research, in two containers (one enclosed within the other). The number of seeds per line was recorded and seeds were aliquoted 10 at a time – the new number was then noted.

5.2.5 Microscopic analysis of transient and stable transformants

For the transient transformants, the Leica M205 FA stereomicroscope was used

to visualise tagRFP expression in the embryos and leaf tissue at 24, 48 and 72h post bombardment. At 48h, the Zeiss LSM780 confocal microscope was used to assess LTI6b and ROP7 protein localisation. For the stable T_0 wheat transformants, once maturity had been reached, leaf samples (biological replicates) were taken from the second flag leaf and imaged for PM reporter gene expression (one sample was taken per plant). The Leica M205 FA stereomicroscope was used to visualise tagRFP expression strength in the leaf tissue, to allow for comparisons between lines. The Zeiss LSM780 confocal microscope was subsequently used to assess LTI6b and ROP7 protein localisation within the leaf. All microscope settings were configured to the fluorescent protein DsRed (excitation maximum: 558 nm, emission maximum: 583 nm).

5.2.6 Wheat PM reporter line T_1 root assay

Petri dishes were lined with filter paper (Whatman™ grade 1) and split into quarters. Two seeds (due to low seed counts only two biological replicates were used) from each individual wheat transgenic lines (T_1 generation) were placed in each quarter of the filter paper, before being soaked with water. Each petri-dish was then sealed with parafilm. Plates were then left at room temperature (approximately 20°C) for 3-4 days to permit seed germination. Once the wheat seedlings were large enough to handle each root was analysed by two phases of microscopy. The Leica M205 FA stereomicroscope was used to visualise tagRFP expression in the roots. To allow for comparisons in fluorescence between samples – the root was not manipulated for this experiment. The Zeiss LSM780 confocal microscope was subsequently used to assess LTI6b and ROP7 protein localisation within the root. Single roots were selected with good root hair growth, dissected from the seedling and placed upon a glass slide, mounted using a

single drop of water, before being carefully flattened and imaged immediately. All microscope settings were configured to the fluorescent protein DsRed (excitation maximum: 558 nm, emission maximum: 583 nm).

5.2.7 Genotype and copy number analysis of the T_1 generation

Ten seeds per line were sown with 20 being sown for the most promising PM reporter lines. Five plants (five biological replicates) from each line were then sampled, selected randomly for copy number and zygosity determination (using g-Count™technology) by IDna Genetics, Norwich Research Park, UK. For the most promising reporter lines, an additional five plants were sampled. IDna Genetics developed tagRFP-specific primers to detect the ROP7 and LTI6b constructs within the T_1 generation following segregation. For primer design, 9 primer pairs were produced and tested on T_1 samples (in total 32 biological replicates: 16 for LTI6b and 16 for ROP7, completely randomized and unlabelled to prevent bias when testing for the experiment itself) by IDna, to ensure the primers did not bind to plant DNA or plasmid DNA that was not part of the tag-RFP gene. The data produced consisted of the estimated number of copies, the probable number of copies assuming Mendelian segregation, and the most likely genotype class. Where seeds had failed to germinate, these lines were not sampled and therefore not all lines have 5 or 10 independent plant samples to their name. The remaining plants whose samples were not sent for analysis had leaf samples taken and stored at -80°C. Please note: No statistical analysis section has been included in this chapter as no statistical analysis has been performed by me. The determination of copy number, the probable number of copies assuming Mendelian segregation and genotype class, were calculated by IDna Genetics as part of their in-house analysis.

5.2.8 Coleoptile analysis of the T_2 generation

The coleoptile assay was used as a high-throughput screen for the wheat PM reporter line T_2 generation. For each homozygous plant (as well as the control lines), five seeds (five biological replicates) were sown to account for any ongoing segregation. A small section of each coleoptile was excised after 6 days of growth, mounted onto a slide using water and scanned and imaged for tagRFP expression (excitation maxima = 558nm, emission maxima = 584nm) using the Zeiss LSM780 confocal microscope. Each sample was imaged using 20x and 40x objectives. An allocated time of 5 minutes was given per sample to look for PM fluorescence – if none was found an image was taken anyway. Any samples that looked as though they may be expressing tagRFP were plasmolysed – 0.8M mannitol, drawn across the sample using filter paper for 30-40 min. These samples were imaged using the same microscope conditions as discussed above.

5.2.9 Image acquisition and image archiving for wheat PM reporter line samples

All images were taken using the Zeiss LSM780 confocal microscope and Leica M205 FA stereomicroscope provided by the Rothamsted Research bioimaging department. Following analysis of each sample, each image was exported. Editing of images was done in CorelDraw X7. It should be noted these were only slight changes and were applied equally to all images in terms of brightness etc. This approach ensured the matching of the image seen in the bioimaging department – there is some discrepancy due to the differences in technology quality between bioimaging and computers/software outside of this facility. All images have been processed where necessary and logged in an Excel

spreadsheet detailing the image, tissue, date, conditions, microscope, magnification and anything of scientific interest noted. All raw files are saved on the bioimaging drive, images have been exported and saved on a shared work drive, with backups on my OneDrive and personal hard drive.

5.3 Results

5.3.1 Secondary protein structure characterisation of ROP7 and LTI6b

Before transient bombardment of the PM reporter constructs, the secondary protein structure of *At*ROP7 and *At*LTI6b was investigated – these can be seen in Fig 5.2 and Fig. 5.3 respectively. The modified ROP7 and LTI6b proteins were also analysed and were shown to be extremely similar – the analysis for these can therefore be found in Appendix 17 and 18.

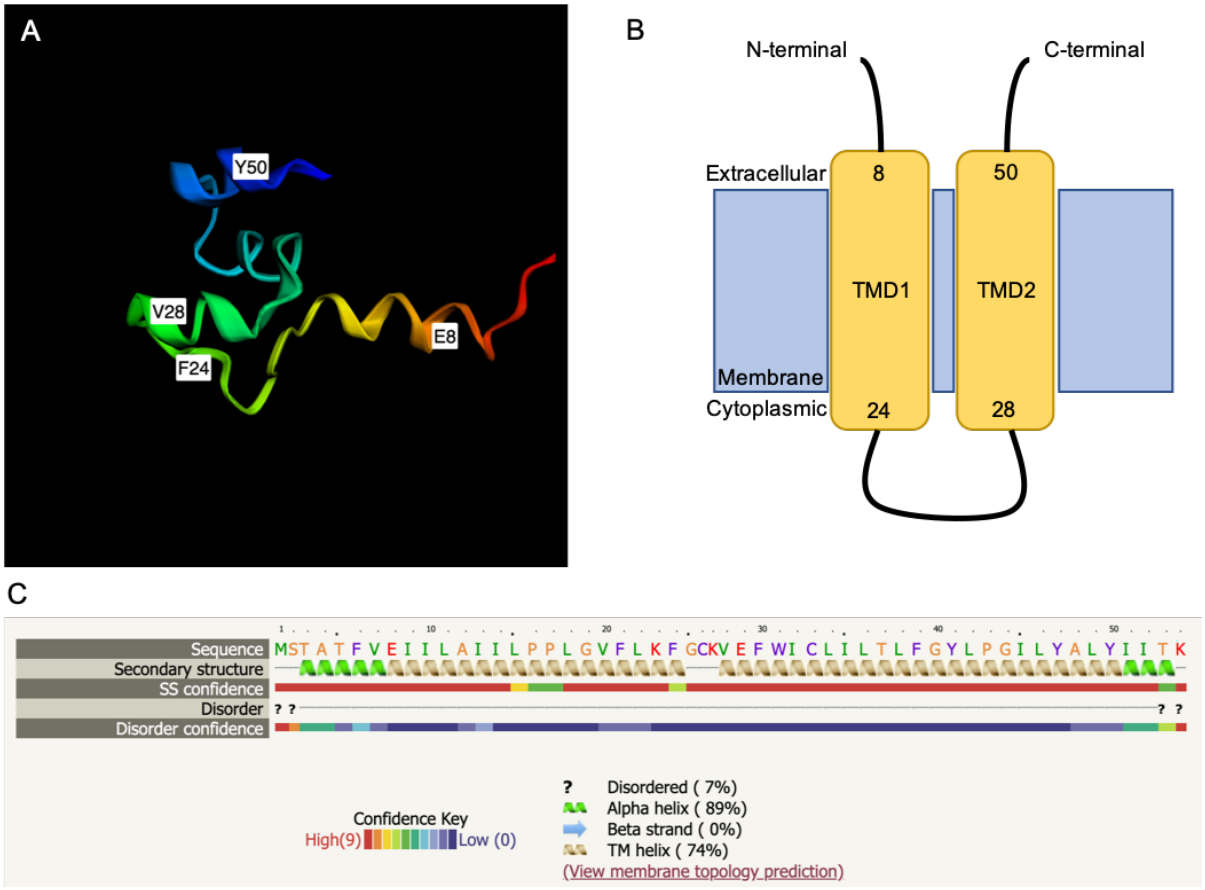

Figure 5.2 – Structural analysis of *At*LTI6b. All analysis has been conducted using Phyre[2]. (A) Finalised structural model of *At*LTI6b. Labelled amino acids indicate the two transmembrane domains (TMD) seen in part (B). Coloured red to blue, corresponding to the N- and C-termini. (B) TMD of the *At*LTI6b protein. (C) *At*LTI6b secondary protein structure. Structural analysis for the modified LTI6b protein can be found in Appendix 17.

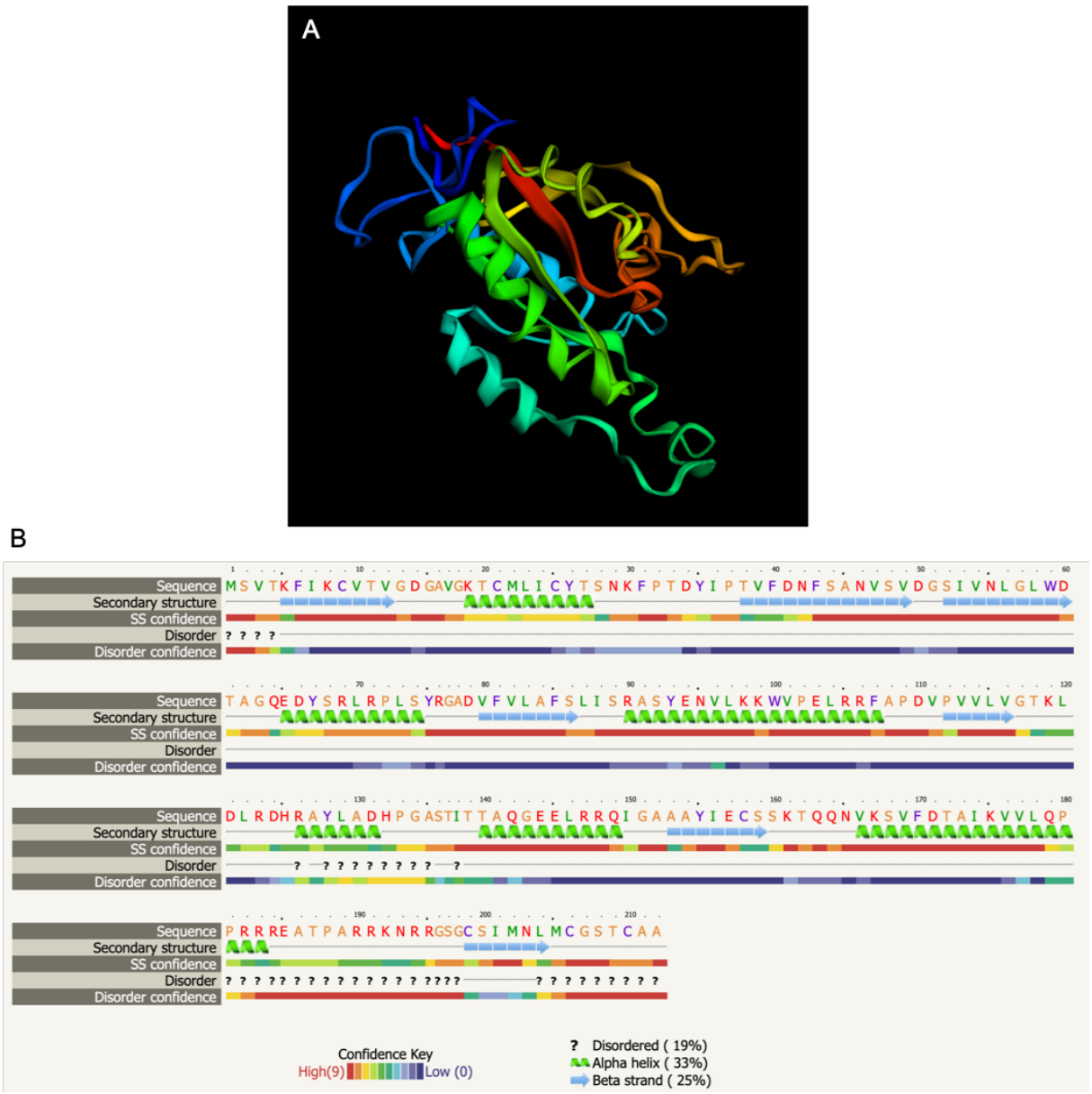

Figure 5.3 – Structural analysis of *Zm*ROP7. All analysis has been conducted using Phyre[2]. (A) Finalised structural model of *Zm*ROP7. Coloured red to blue, corresponding to the N- and C-termini. (B) *Zm*ROP7 secondary protein structure. Structural analysis for the modified ROP7 protein can be found in Appendix 18.

LTI6b is 54 amino acids in length and primarily contains helical structures, with two TMDs. Its initial discovery and characterisation demonstrated that within the protein there were similarities with other N-terminal peptides which shared consensus features with signal peptides from other transmembrane proteins[380].

Furthermore LTI6b lacked any organelle signal peptide; this first eluded to its localisation at the PM[380]. On the other hand, ROP7 is 212 amino acids and has no TMDs. ROP7 resides below the PM, functioning in signal transduction pathways, and consists of both helical and sheet structures [386]. ROP7 lacks a specific signal peptide but, contains an internal CaaX domain in the hypervariable region (HVR) that is required for PM association (Fig. 5.4). Collectively, these predictions suggest differences in structure, function and how the two proteins locate to the PM (Fig. 5.2, Fig. 5.3 and Fig. 5.4).

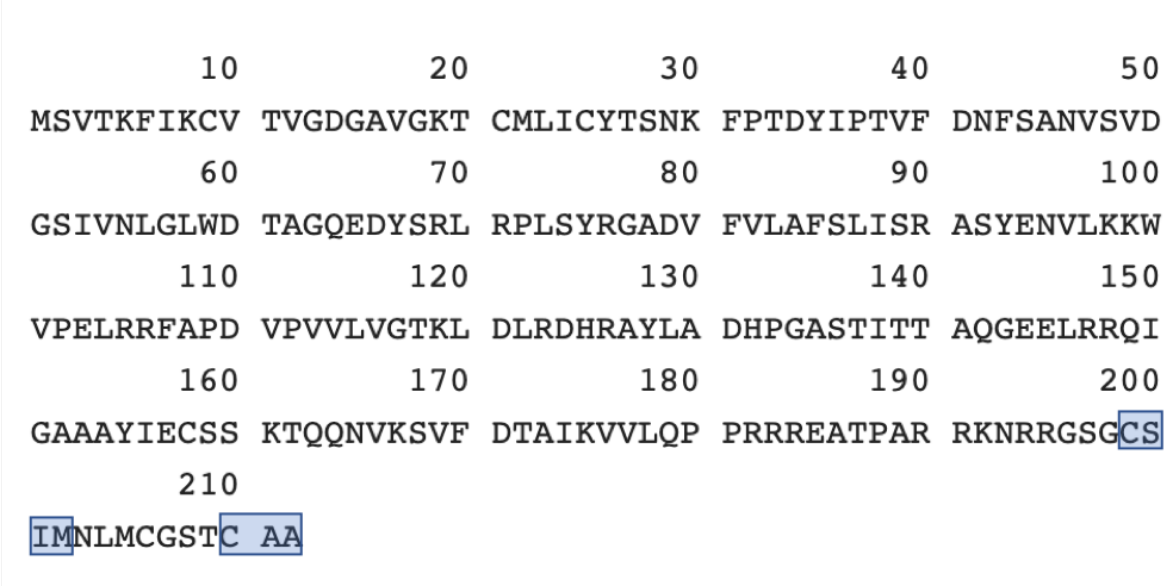

Figure 5.4 – Plasma membrane targeting CaaX domains in *Zm*ROP7. Two CaaX domains have been highlighted in blue. The one at the C-terminal lacks the final amino acid, with the cysteine residue not needed for targeting to the PM. The internal CaaX motif (CSIM) is needed for proper PM targeting, with the cysteine residue being essential for this. Sequence was retrieved from UniProt.

5.3.2 Transient bombardment of PM reporter constructs demonstrates differences in the localisation of ROP7 and LTI6b fusion proteins

Overall, four constructs were produced, with each PM-localised gene being present at both the C and N terminus of tagRFP, utilising the two overexpression

vectors, pRRes208.454 and pRRes208.355 (Alison Huttly, Rothamsted Research) (Fig. 5.5 and Appendix 15). For each construct the wheat actin promoter was chosen to drive the marker gene, being both constitutive and ubiquitous[387]. Before stable transgenic lines were produced, transient tests on both wheat embryos (Fig. 5.6) and leaf tissue were carried out to investigate the localisation of the constructs. Leaf tissue results can be found in Appendix 19. The embryo results are generally representative of the leaf tissue results; however, the Cereal Transformations Team at Rothamsted Research were more experienced in using embryos for testing transient constructs. Therefore, embryonic tissue was used for these preliminary transient transformations to check for construct expression patterns. The 48h post- bombardment time point was chosen for microscopic analysis, as tagRFP expression levels were at their highest during this period. Variation in localisation was observed between all four constructs with all rounds of particle bombardment being successful (Fig. 5.7). Both ROP7 constructs demonstrated PM localisation. Low-level background fluorescence could be seen in all samples, with fluorescence being greatest at the PM, suggesting tagRFP localisation. On the other hand, both LTI6b constructs showed localisation in punctate structures throughout the cell, with the exception of the vacuole, suggesting these tagged proteins may accumulate within endomembrane compartments. This localisation pattern can be seen in Fig. 5.6 and Fig. 5.7.

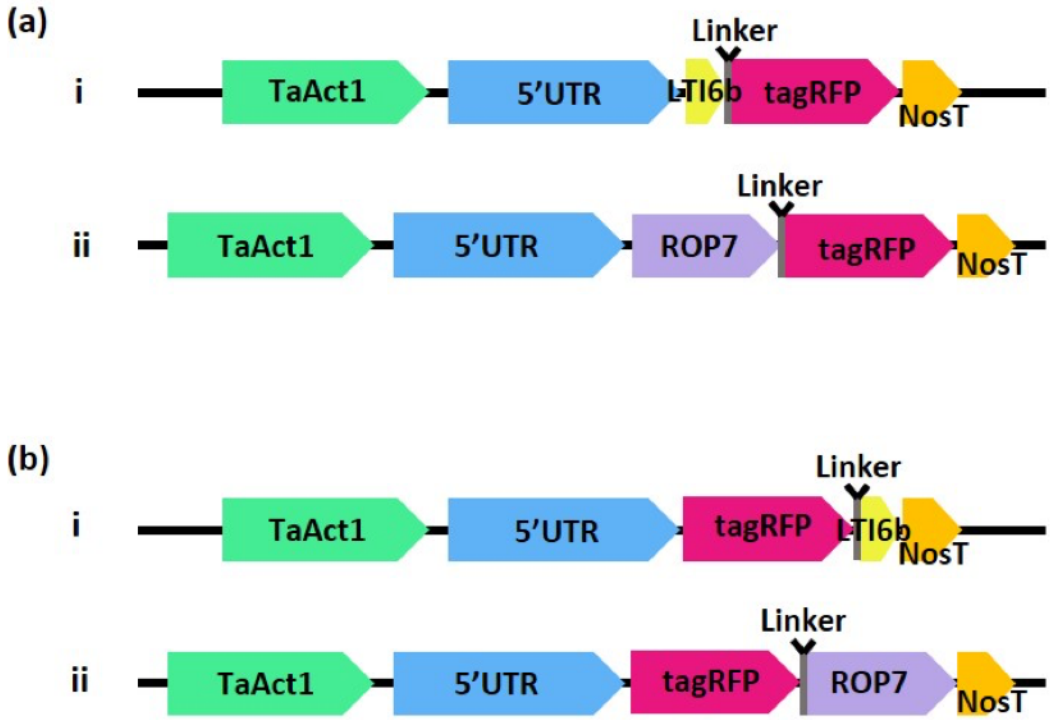

Figure 5.5 – Wheat plasma membrane reporter constructs. The wheat Act1 promoter (green), 5'UTR (blue), linker (grey), tagRFP fluorescent gene (pink) and Nos terminator (orange) form the PM reporter constructs. Each gene has been inserted at both the N terminus, (a) pRRes208.355, and the C terminus, (b) pRRes208.454 of the tagRFP gene – i. LTI6b, ii. ROP7. Not drawn to scale, component sizes are relative.

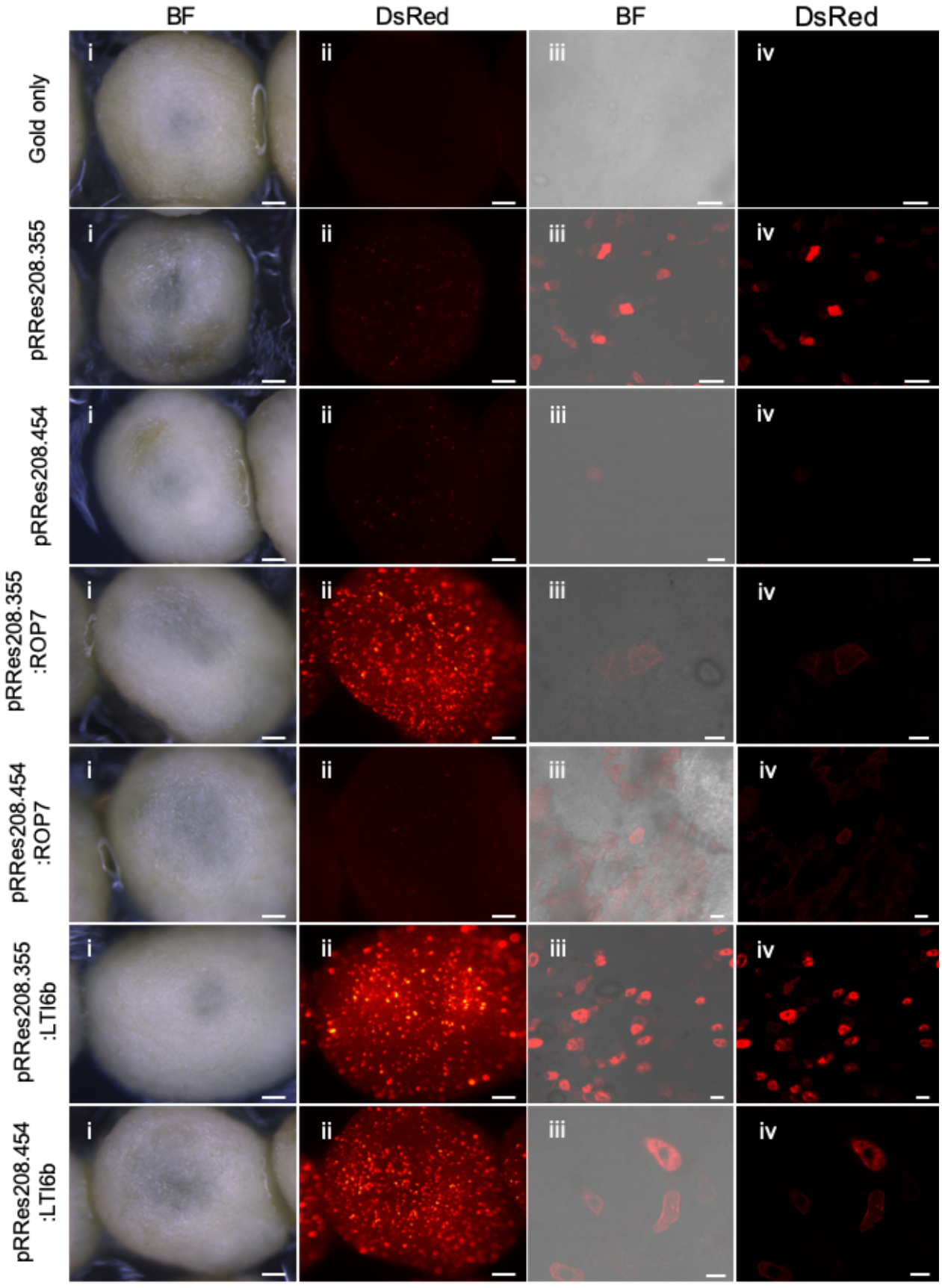
BF
DsRed
BF
DsRed
Gold only
pRRes208.355
pRRes208.454
pRRes208.355 :ROP7
pRRes208.454 :ROP7
pRRes208.355 :LTI6b
pRRes208.454 :LTI6b
i
ii
iii
iv

Figure 5.6 –Transient transformation of plasma membrane constructs into wheat embryos. All images were taken 48 h following bombardment of wheat *cv.* Bobwhite embryos. (i) and (ii) display stereomicroscope images of bombarded embryos under Bright Field (BF) light or UV light (DsRed). Bar = 250 µm. (iii) and (iv) represent confocal images displaying protein localisation. Bars: gold only, pRRes208.355 = 50 µm, pRRes208.454 = 10 µm, pRRes208.355:ROP7, pRRes208.454:ROP7, pRRes208.355:LTI6b, pRRes208.454:LTI6b = 20 µm. For all images red fluorescence indicates successful particle bombardment and tagRFP expression.

Of the four constructs tested, two would be taken forward for stable transformation, one ROP7 and one LTI6b construct, to give the best chance of success (Fig. 5.7). The construct pRRes208.355:ROP7-RFP (hereafter referred to as ROP7-RFP) was chosen due to less background fluorescence, than its counterpart pRRes208.454:RFP-ROP7 (hereafter referred to as RFP-ROP7). Whereas the construct pRRes208.454:RFP-LTI6b (hereafter referred to as RFP-LTI6b) was selected over pRRes208.355:LTI6b-RFP (hereafter referred to as LTI6b-RFP), because even though this tagged protein accumulated in the secretory pathway, the tagged protein still demonstrated some reporter gene expression at the PM as well as less background fluorescence. Refer to Table 5.1 for construct names and abbreviations.

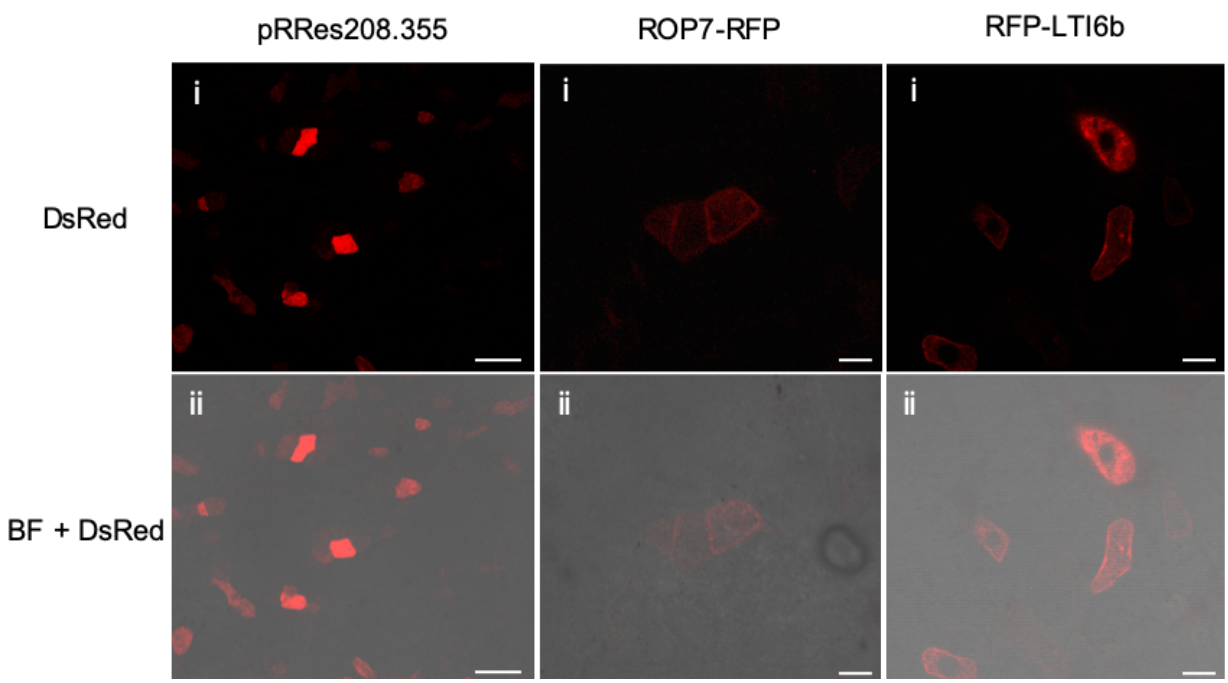

Figure 5.7 – Selected constructs for stable wheat transformation. Images are a close-up of those displayed in Figure 5.6. (i) DsRed only. (ii) BF and DsRed. Images taken using a confocal microscope to show the localisation of tagRFP expression in bombarded wheat embryos. pRRes208.355 was chosen as a control to contrast against the localisation signatures from the other two constructs (the other controls in Fig. 5.6 were not suitable for this). Bars: pRRes208.355 = 50 µm; ROP7-RFP and RFP-LTI6b = 20µm. BF = brightfield.

Table 5.1 Construct names and abbreviations

Vector	Vector and construct	In-text abbreviation	Particle bombardment number (B)	Transformant line name example (B: bombardment, R: experimental round/repeat, P: plant number)
pRRes208.355 (construct inserted at the N-terminus of *tagRFP*)	pRRes208.355: LTI6b-RFP	LTI6b-RFP	-	-
	pRRes208.355: ROP7-RFP	**ROP7-RFP**	3731 and 3733	B3731 R5P6 B3733 R3P4
pRRes208.454 (construct inserted at the C-terminus of *tagRFP*	pRRes208.454: RFP-LTI6b	**RFP-LTI6b**	3741	B3741 R3P12c
	pRRes208.454: RFP-ROP7	RFP-ROP7	-	-

Please note, names highlighted in bold represent the two constructs taken forward for stable transformations.

5.3.3 Assessment of stable T_0 PM reporter lines by microscopy of mature leaf tissue did not create an effective initial screen

The T_0 generation was screened (Fig. 5.8) to determine whether successful PM reporter lines could be selected early in the transformation process; typically screening for fluorescence would be carried out in the T_1 generation. As previously mentioned, *F. graminearum* primarily infects the floral tissue of the host; however, in this case the floral tissue was needed to ensure a good seed yield from each independent wheat line. Therefore, leaf samples were taken for confocal and UV fluorescence microscopic analysis (Fig. 5.9). From these samples I could not determine if there was any PM fluorescence. The emissions that could be detected were predominantly a result of chloroplast autofluorescence. Nevertheless, as shown in Fig. 5.9, there was a high quantity of variation between samples, some of which could be interpreted as PM

fluorescence or natural variation between the plants themselves. I therefore concluded that screening of the T_0 generation should not be performed in future experiments and no further information could be extracted from screening at this stage.

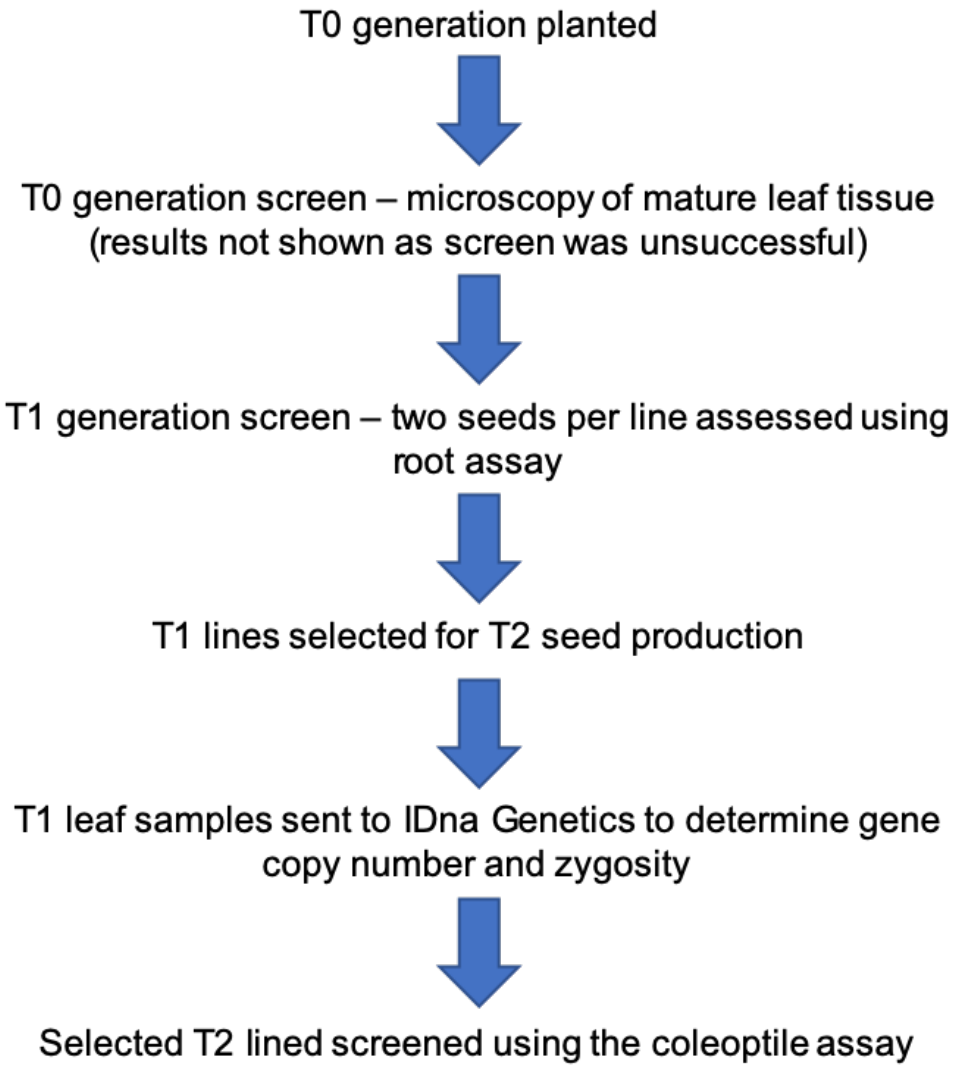

Figure 5.8 – Stable wheat plasma membrane reporter line transformant screening summary.

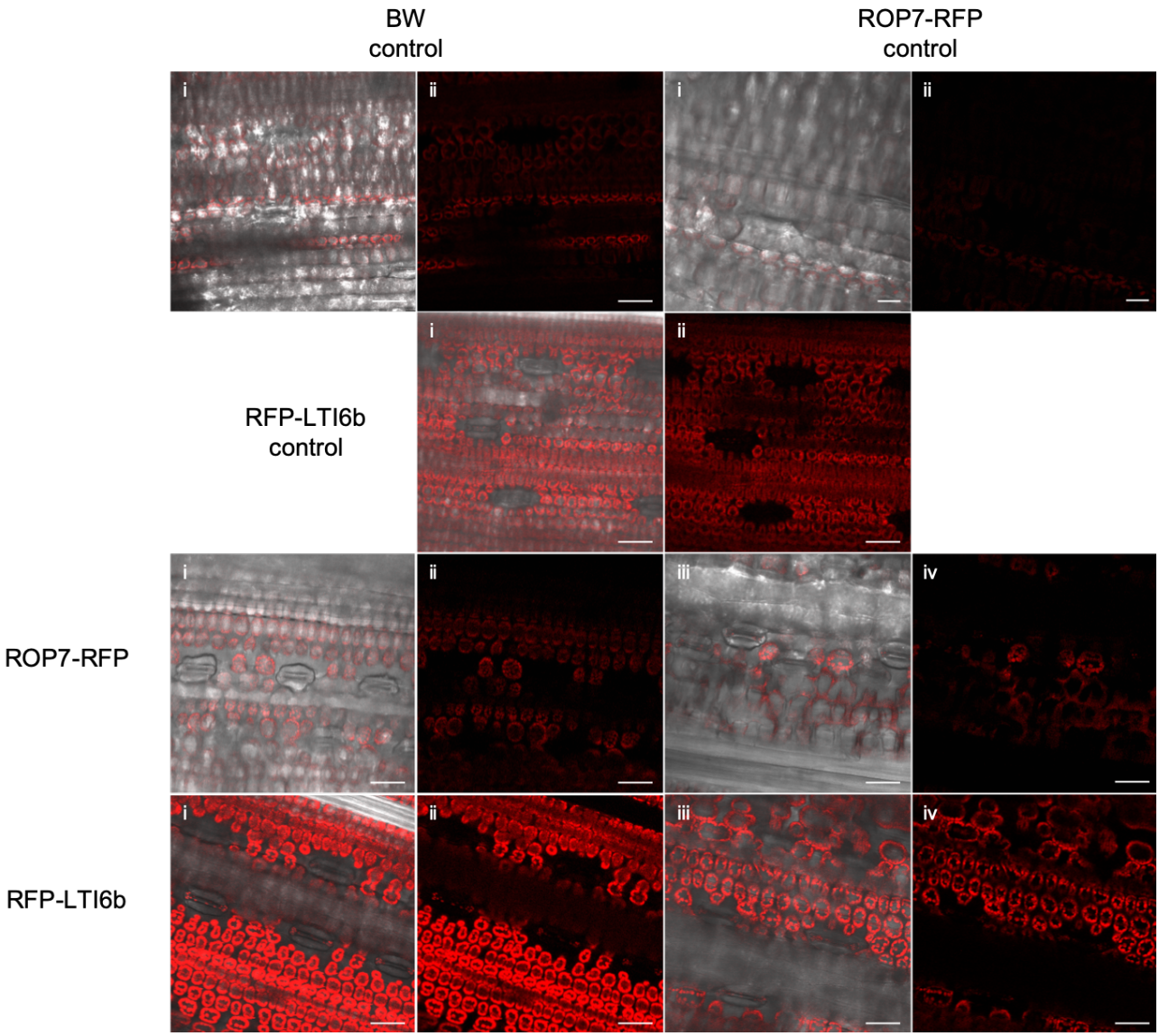

Figure 5.9 – Screening of T_0 stable transformants in wheat leaf tissue. Confocal images of mature wheat tissue. Images representative of all lines transformed with the same construct. Controls – BW control: plant without particle bombardment, ROP7-RFP and RFP-LTI6b controls: lines transformed with selection plasmid only, no fluorescent marker – i) BF and DsRed ii) DsRed only. ROP7-RFP and RFP-LTI6b: i) BF and DsRed ii) DsRed only – chloroplast autofluorescence, iii) BF and DsRed iv) DsRed only – possible PM fluorescence. Bars = 50 µm with the exception of ROP7-RFP control where bar = 20 µm.

5.3.4 Screening the T_1 generation using a root assay

Screening the T_1 generation for expression of the gene of interest is the most reliable way of determining successful lines, as it is at this stage that genetic segregation occurs. If the T_0 plant harbours a single integration locus, for every fourth plant in the next generation, one would expect to obtain one line harbouring the PM reporter construct in a homozygous state, two heterozygous plants and one that lacked the construct. In situations where DNA integration has occurred at multiple loci in the genome, more complex genetic segregation ratios would be anticipated. The amount of T_1 seed produced from the T_0 generation was relatively low, in comparison to other transgenic lines produced by the Cereal Transformations team – most likely a result of the warmer than average temperature during the summer of 2018 as well as the *cv*. BW being used instead of the usual cultivars Cadenza or Fielder. Most lines yielded less than 100 seeds with a few lines producing as few as 7 (Appendix 20).

Table 5.2 – Wheat transformant lines taken forward for T_2 seed production.

Transformant	No. of lines to screen in T_0 generation	No. of lines selected for T_2 seed production
ROP7-RFP	42	12
RFP-LTI6b (set 1)	15	5
RFP-LTI6b (set 2)*	27	-

Footnotes:

Lines were selected following root assay screening of the T_1 generation. Controls not included.

Note: The LTI6b-RFP transformants were generated in two sets as a result of particle gun malfunction during the first particle bombardment experiment. At the time of writing this second set is currently at the stage T_1 seed harvest and is therefore a generation behind the first set (approximately 6 months) – see Appendix 21.

To determine if any of the lines, for both constructs, displayed any PM fluorescence, a high-throughput root assay was designed to assess and select which T_1 lines to take forward to the T_2 generation (Fig. 5.10). Roots were detached for analysis on the confocal microscope, but only immediately before imaging to reduce any induced plant defence responses. Control roots (*cv*. Bobwhite), shown in Fig. 5.10, demonstrated that there is no/very little autofluorescence.

Of the 42 independent primary transformants for ROP7-RFP, 12 lines were selected for the T_1 generation, from eight different repeats (Table 5.2 and Appendix 20). From those selected to represent the ROP7-RFP line, plant B3731

R5P6, displayed the clearest PM fluorescence (Fig. 5.10). However, like the results shown in the transient transformation tests (Fig. 5.6 and Fig. 5.7) the construct was lowly expressed. Of the 15 independent primary transformants generated for construct RFP-LTI6b, three lines were selected for the T_1 generation, from three different repeats. From those selected lines, B3741 R3P12c gave the clearest PM expression (Fig. 5.10), however the sub-cellular localisation, although at the edge of the cell, was diffuse and could have been a result of autofluorescence either at the membrane or in the cytoplasm if cytoplasmic space was limited by the vacuole.

There are considerably less RFP-LTI6b primary transformants, due to a previous problem with the particle gun. However, a second round of RFP-LTI6b transformants were produced at a later date by the Cereal Transformation team. These 27-independent primary transformants (excluding the controls) have yet to be screened at the T_1 generation stage via the root assay for PM fluorescence (Appendix 21).

The initial transient transformant experiments done using bombarded embryos had revealed accumulation of the ROP7-RFP tagged protein faintly at the PM whereas the more easily detectable LTI6b tagged protein was present in endomembrane compartments as well as at the PM (Fig. 5.6 and Fig. 5.7). In comparison to the T_1 root assay results for ROP7-RFP, the image for RFP-LTI6b line 3741 R3P12c shows in some regions a more diffuse expression pattern, indicating a possible difference in protein localisation/accumulation, however it is likely this is tissue autofluoresence. In this case the T_1 screen was inconclusive.

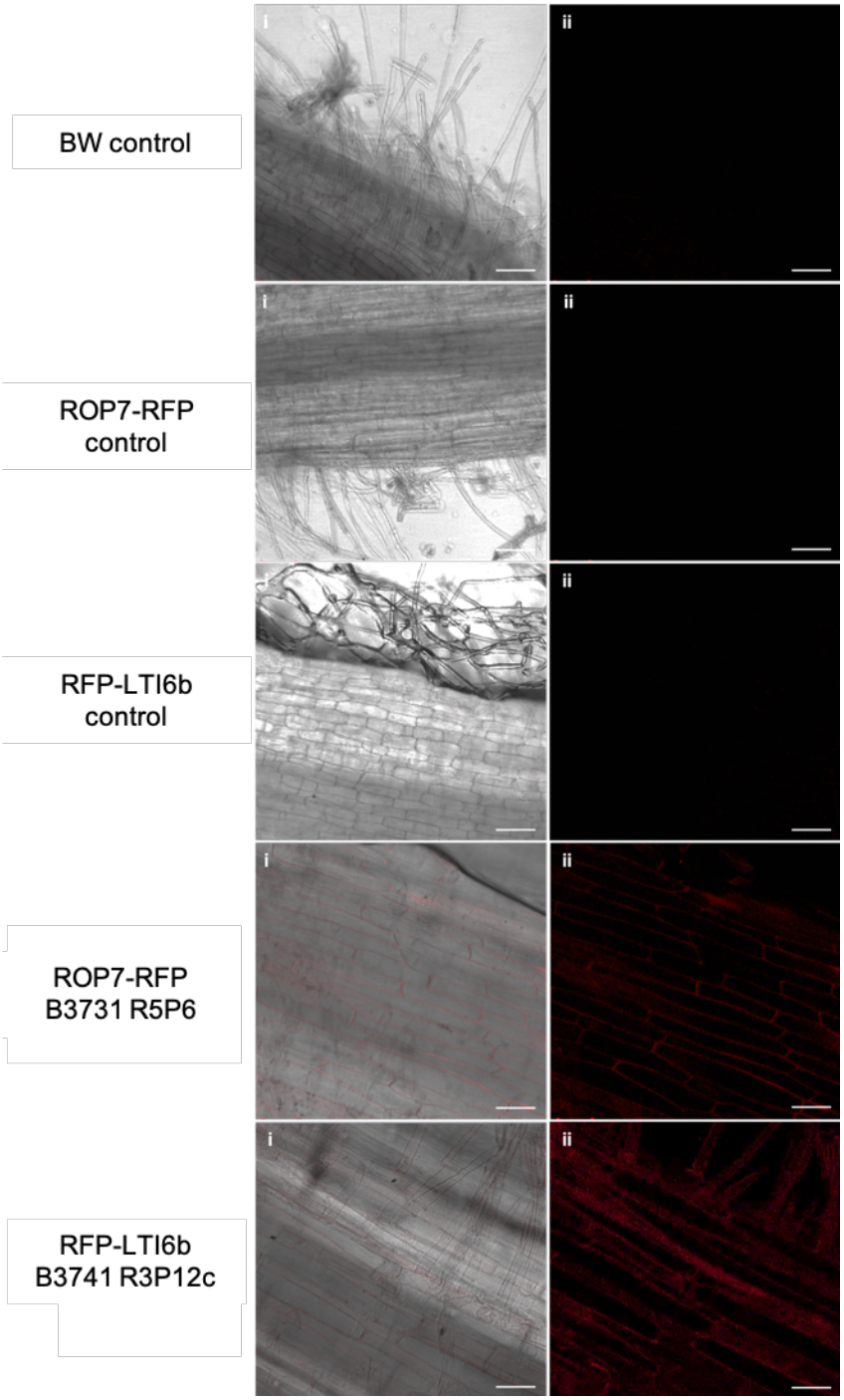

Figure 5.10 – Wheat T_1 transformant root assay screen. Confocal images of root cell PM gene expression. i) BF and DsRed ii) DsRed only. Controls: bars = 100 µm. ROP7 and LTI6b lines: bars = 50 µm.

5.3.5 Determining copy number and genotype of T_1 PM reporter lines

Following preliminary analysis of the T_1 lines, the selected twelve ROP7-RFP and four RFP-LTI6b lines were grown to maturity. These lines were then sampled according to the protocol listed in section 5.2.7 of Experimental Procedures. Ten seeds per line were sown with 20 being sown for the most promising lines, B3731 R5P6 and B3741 R3P12c. Five plants from each line were then sampled with an additional five for B3731 R5P6 and B3741 R3P12c to determine copy number and zygosity.

For B3731 ROP7-RFP, six transformation lines (not including the controls) were selected for copy number, zygosity testing and for use in the T_2 generation. Four out of six lines were confirmed to have hemizygous samples, with two of these lines, B3731 R4P5 and B3731 R6P2 possessing one and three homozygous samples respectively. Copy number for the homozygous B3731 R4P5 plant was 12 but was much lower in the three homozygous B3731 R6P2 plants, which all had copy numbers of four. No homozygous or confirmed hemizygous plant samples were present for B3731 R5P6. Line B3731 R5P2 had no zygosity indicated suggesting the PM constructs were not present in any of these samples.

For the ROP7-RFP B3733 six lines were sent for analysis (not including the control sample). All lines, except B3731 R2P6, had hemizygous lines present. B3733 R2P5 and B3733 R4P5 had one homozygous sample each, and copy numbers of 6 and 7 respectively, with B3733 R3P4 and 3733 R4P4 having two, however here the homozygous samples had high copy numbers, in comparison to the B3731 samples, at 70 and 80 respectively for the 2 lines.

In terms of the LTI6b B3741 lines no homozygous samples were identified with only one hemizygous sample for B3741 R3P6, although this also exhibited a high copy number of 56. For line B3741 R3P14, the genotype class was listed as multi for all samples suggesting these lines are segregating for more than one insertion event. To recover these samples, it would be easiest to self individuals with the lowest copy numbers in order to pick homozygous plants in the next generation. For both of the most promising lines, B3731 R5P6 and B3741 R3P12c, no homozygous or confirmed heterozygous samples were identified. The raw data can be found in Appendix 22, this information is summarised in Fig. 5.11.

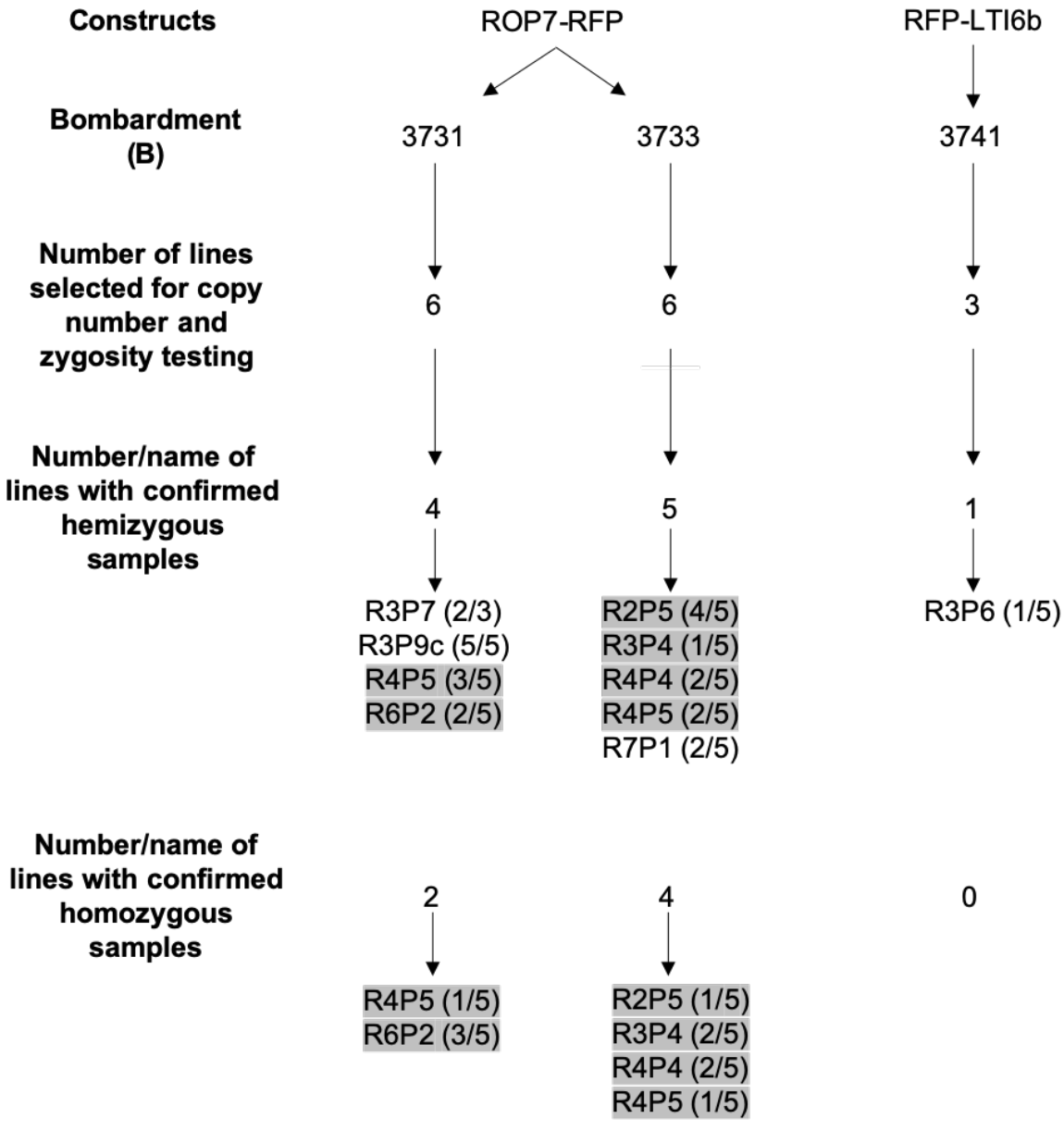

Figure 5.11 – Summary of copy number and zygosity analysis of T_1 plasma membrane reporter line transformants. Values in brackets represent the number of samples with specified zygosity/number of total samples. Highlighted lines indicate those with both hemizygous and homozygous samples.

5.3.6 T_2 PM reporter lines coleoptile assay

Limited time availability (as a result of Covid-19 restrictions), in conjunction with the evidence shown above, confirming a lack of PM reporter fluorescence, resulted in the high-throughput coleoptile assay being used to screen the T_2 homozygous lines for PM fluorescence. For RFP-LTI6b, no homozygous lines were identified, the single hemizygous line was therefore included in this experiment. These lines can be identified using Fig. 5.11. ROP7-RFP line B3731 R5P6 and RFP-LTI6b line B3741 R3P12c were shown to have produced no homozygous or hemizygous plants (a few samples were 'possibly hemizygous' for B3731 R5P6 but this was not confirmed), to rule out any chance of the results being mixed up, two T_2 seeds from four individual plants from both the B3731 R5P6 and B3741 R3P12c lines had their coleoptiles analysed in the same format as for the homozygotes. The probability of therefore not analysing a homozygous line, if these results had been labelled incorrectly, was low. Plasmolysis was carried out on samples where there was a possibility of PM fluorescence, however any areas of a sample that may have shown tagRFP expression could not be identified following this, suggesting they were artefacts of the sampling process (control images for this plasmolysis can be seen in the Appendix 23). Any fluorescence seen was a result of chlorophyll autofluorescence being present and could not be identified as tagRFP fluorescence – this could be

viewed differently depending upon the layer within the sample that was being imaged. These results can be seen in Appendix 24. Therefore, no successful wheat PM reporter lines were produced in this instance.

5.4 Discussion

Some pathogens have been shown to successfully colonise host tissue and cause cell death by utilising plant specific channels called PD, which in normal conditions regulate cell-to-cell communication and respond to external stimuli by altering their SEL. More recently research has demonstrated that some pathogens can manipulate and grow through PD, one of which is *F. graminearum*. Unlike other cereal crop-fungal pathogen interactions, such as that seen between rice and *M. oryzae*, the tools to image the wheat-fungal interactions at the PD in real time are not readily available. Therefore, this part of the project aims to produce transgenic wheat PM reporter lines that would help visualise the interaction between the host and the pathogen, *F. graminearum,* at the infection front, as the infection proceeds from the asymptomatic to the symptomatic phase and coincidentally from intercellular to intracellular hyphal growth and wheat cell death.

As PD are PM lined, the approach taken was to produce transgenic wheat PM reporter lines, a tool that would have many other uses both inside and outside the field of plant pathology. Due to the previously reported success of two genes, LTI6b and ROP7 as PM markers in their native hosts (*Arabidopsis* and maize, respectively), these were chosen for stable transformation into hexaploid wheat[290,381,382]. With most fungal reporter strains and organelle markers being GFP-tagged, tagRFP was the preferred fluorescent protein for the wheat PM reporter lines; taking into consideration the use of already available GFP *F.*

graminearum strains in conjunction with the new wheat PM reporter lines in future studies[163,388]. Before synthesis these genes were codon optimised for protein translation in wheat. Homologues of both selected genes were shown to be present in hexaploid wheat but due to the complex hexaploid nature of the wheat genome and uncertainty as to whether these genes would retain the same or similar function, bombardment of non-native optimised genes was the preferred experimental approach. The genes were inserted at both the N terminus (pRRes208.355) and C terminus (pRRes208.454) of the reporter gene to determine if tag position made any difference in their expression levels and/or localisation patterns. Production and investigation of all four constructs increased the likelihood of a successful wheat PM reporter line being produced.

Variation was seen in tagRFP gene expression and localisation, following transient transformation in wheat embryo and leaf-sheath tissue; this was due to a variety of factors. All four constructs were expressed but localisation between the ROP7 and LTI6b constructs was vastly different. ROP7-RFP and RFP-ROP7 possibly displayed some low-level localisation at the PM, whereas LTI6b-RFP and RFP-LTI6b did not display PM fluorescence, but instead accumulated in the endomembrane compartments of the cell in punctate structures (Fig. 5.6 and Appendix 19); no fluorescence could be seen in the vacuole. However, in the case of the C-terminal construct, even though there was localisation in the endomembrane compartments, the outline of the cells was also more fluorescent, indicating the tagRFP reporter protein would be targeted to the PM in addition to accumulating elsewhere. Once again, no fluorescence was seen in the vacuole. This difference between the localisation in the LTI6b and ROP7 construct could be accounted for by the variations in their secondary structures as discussed in section 5.3.1 (Fig. 5.2 and Fig. 5.3).

Of the two LTI6b constructs available, the RFP-LTI6b construct was taken forward for stable wheat transformation. Even though RFP-LTI6b did not efficiently localise to the PM this construct was deemed to still be useful in host-pathogen analyses as a marker of secretory pathways and potentially punctate membrane structures in the cell. Accumulation of a protein in the secretory pathway can be a result of protein overexpression, resulting in altered localisation patterns, particularly if these pathways are saturable[382,389,390]. For example, GFP dimer production and misfolding, when targeted to membrane microdomains, can result in aggregate formation[390]. In the present study it was therefore possible similar problems could occur during tagRFP overexpression as a result of the constitutively expressed wheat actin promoter. Furthermore, LTI6b possesses a small TMD, with only two amino acid residues predicted to be in the apoplastic cavity, making LTI6b a relatively mobile PM protein capable of altering its location within a cell[391]. In comparison, both RFP-ROP7 and ROP7-RFP were lowly expressed but displayed some PM localisation in the transient transformations. However, diffuse low-level tagRFP expression made any possible PM localisation unclear. Previously, maize studies have successfully demonstrated ROP7's PM localisation – see Fig. 5.1 in the introduction to this chapter[382,386,392].

Transient transformations have a limited expression lifespan, with tagRFP fluorescence peaking at about 48 h after transformation with little expression after 72 h; there is therefore a limited time to perform plasmolysis and therefore this experiment was not performed in the transients. Of the two ROP7 constructs ROP7-RFP was chosen for stable transformation due to this construct being marginally more highly expressed than RFP-ROP7.

In total 42 independent ROP7 lines and 15 independent LTI6b lines were screened in the T_0 generation (Figure 5. 9 and Table 5.2). For this, mature wheat leaf tissue was used for imaging on both the stereomicroscope and confocal microscope – however no differences could be seen between samples because of tissue age and autofluorescence. The excitation and emission spectra of tagRFP is similar to that of chlorophyll. As chloroplasts are abundant in leaf tissue any additional fluorescence seen could not be distinguished from that of chloroplast autofluorescence and could not be confirmed as gene expression at the PM. Regarding this, T_0 line's will not be analysed in the future. Following this a high throughput root screening assay was developed for the assessment of the T_1 lines. Low levels of expression could be viewed for both constructs at the PM in the T_1 roots. Low gene expression levels here prevented the use of plasmolysis to confirm protein localisation. This was attempted for the analysis of the T_2 generation.

Mature T_1 leaf tissue samples from multiple plants per line, selected for strong expression levels (relative to all the lines analysed), were sampled to test for zygosity and copy number. Few homozygous lines were detected, with none of the most fluorescently intense samples in the T_1 root assay – B3731 R5P6 and B3741 R3P12c – possessing any homozygous genotypes. This therefore demonstrates the possibility of autofluorescent root samples, possibly caused by damage upon sample dissection. For those showing both homozygous, hemizygous and null samples, for example B3731 R4P5 and B3733 R4P5, these ratios suggest the samples follow Mendelian segregation. However, only five samples per line were sent for analysis, it is therefore likely that those lines for B3731 and B3733 that did not follow Mendelian ratios were an artefact of chance, and that sending more samples per line for analysis would solve this issue. In the

case of B3741 (RFP-LTI6b) these lines seem to be skewed towards null samples, PCR tests did confirm the presence of the *LTI6b* gene, it is therefore possible the gene has been lost, or rearranged and is no longer detectable in the progeny. The PM reporter specific probes based around the tagRFP sequence had been shown to work by IDna Genetics and the presence of the construct in some plants demonstrates there is not a problem with the test or probe. The selected lines from the T_2 generation have been propagated for future experiments with GFP expressing strains of *F. graminearum,* to investigate the *F. graminearum*-PD interaction. The plants considered to be homozygous, were selected for T_2 transformant generation coleoptile tests, but no PM fluorescence was seen.

The PD-PM is formed of its own microdomains containing complexes that do not exist elsewhere. A recent study has shown that a receptor complex within the host forms in response to chitin perception, with individual components being able to change their locations and interactions in response to chitin treatment[242]. In turn this then produces a signalling cascade resulting in callose deposition at the PD and consequently PD closure[242]. This study was able to demonstrate individual components of a receptor complex were present in both the PM and PD-PM, and were able to integrate an immune response[242]. The wheat PM reporter lines produced here were primarily generated to help determine the interaction between *F. graminearum* and the PD at the cellular and molecular levels. The PD PM has been shown to consist of a different proteinaceous make-up in comparison to the main PM body surrounding the plant cell. Both LTI6b and ROP7 have been shown to localise to the PM, but does this still hold true for the PD PM and if so, do they still retain the same function? This will not be determined until the wheat PM reporter lines are used in practice and images of the PD PM are obtained.

Why the production of a successful PM reporter line has not been achieved in the project will be discussed in the general discussion. However, some of the possible explanations have been discussed below:

- Gene silencing may occur as a result of transgene expression.
- Copy number, position effect (where the inserted gene is placed) and DNA methylation can all affect transgene expression.
- The copy number analysis demonstrated that none of the lines that were homozygous were single copy lines. Post-transcriptional gene silencing means multiple copy lines may exhibit a greater tendency to show lower expression levels, increased methylation of the integrated gene in each plant generation is also possible. This is possibly why in this case neither construct resulted in the generation of wheat lines with any significant expression by the T_2 stage.
- The constructs could be lethal to the host, selecting against the transformants that would otherwise be successful.
- The linker between the FP tag and the sequence for the PM localised protein or another small part of the construct may be preventing expression. It may be that the linker was the wrong size or composition[393-395]. However, the vectors used were upgraded versions of those previously used for transformations. The pRRes208.355 vector had been used for multiple successful transient transformations (this could not be confirmed for pRRes208.454), as well as other vectors in the dataset i.e. pRRes208.380 a nuclear targeted plasmid control (personal communication – Alison Huttly, Rothamsted Research). Successful transient transformations therefore give some confidence the linker is not completely inhibiting expression of the fusion protein. They had not been

tested in stable transformations.

As previously mentioned, for a single integration locus following normal Mendelian segregation it would be expected that the segregation ratio of homozygous: hemizygous: no target gene integration at the T_1 stage would be 1:2:1. At first glance the copy number analysis suggests this is the case for some of the lines presented here. However, due to only 5 plants being analysed per line this cannot be confirmed. It is therefore recommended that future experiments are scaled up – a minimum of 15 plants per transformant line is recommended. The more plants sent for analysis the more accurately characterised the segregation ratio will be. In the interest of expense this was not done here. However, to the best of my knowledge at the time of writing there is no literature stating the number of transformants needed for successful copy number analysis in stable transformants and this can therefore not be compared. It should also be noted that nearly all transformations were initially successful, the selective marker and genes of interest were present within the plants. Therefore, scaling up the number of embryos initially transformed will unlikely benefit the final number of successful transformants.

The wheat PM reporter lines tested here were assessed in both leaf, root and coleoptile tissues, with all obtaining similar negative results. The constitutive, ubiquitous, wheat actin promoter should have ensured fluorescence in all tissues. Fluorescent PM reporter lines already exist in *A. thaliana* (EGFP-LTI6b), maize (GFP-ROP7) and rice (LTI6b-GFP)[290,386,396]. These lines were not used for the experiments here as the main aim of this study was to characterise FHB in wheat. Even though *A. thaliana* has been used as a model for this infection process, it is a dicot and is therefore not always representative of the *F. graminearum*-wheat

interaction[77,397]. Additionally, a GFP *F. graminearum* reporter strain has previously been produced and therefore the fluorescent marker used needed to contrast with this i.e. RFP[163,388]. Attempts were made to get hold of the maize and rice reporter lines, which were not already at Rothamsted Research, however this was not possible.

Transgenic wheat PM reporter lines would not only benefit the cereal pathology community but would also be beneficial to the study of other pathosystems as well as other cellular studies in wheat. Wheat PM reporter lines have not previously been reported. Even if only lowly expressed tagRFP-PM lines are produced, if the tagged PM contrasts well with the GFP *F. graminearum* strains available, this will allow for detailed analysis of wheat-pathogen interactions. For example, to explore the PD-*F. graminearum* interface at both the cellular and molecular level in real-time and thereby significantly advance our understanding of *Fusarium* infections and the FHB disease formation process.

Both constructs were shown to provide a good level of PM fluorescence +/- endomembrane fluorescence in transient assays (Fig. 5.6 and Fig. 5.7). Therefore, these constructs could be successfully used in transient bombardment assays to explore the powdery mildew-cereal interactions in greater detail. Even though the fungus is epidermal specific and never colonises intracellularly from cell-to-cell, transient assays, using these two new constructs, could be used to explore how the PM and possibly the PD connections change at sites of initial infection. Colony expansion during compatible interactions and the various spatial and temporal events at the PM could also be compared to other known responses, occurring during different incompatible interactions.

CHAPTER 6: Bioinformatic analysis of plasmodesmata-associated proteins in the *F. graminearum* wheat host

6.1 Introduction

Characterising the wheat-*F. graminearum* interaction at the cellular level (Chapter 4), demonstrates PD involvement during successful infection but does not elucidate the role PD play at the molecular level. To gain a greater understanding of PD regulation during infection and how *F. graminearum* can manipulate these channels, I have taken an approach to identify PD-associated wheat genes responsible for altering PD permeability. In future work these genes will be knocked down using virus induced gene silencing (VIGS) to assess their effect on *F. graminearum* infection progression. A summary of VIGS can be seen in Fig. 6.1 and Appendix 25, however this will not be discussed in detail as the focus of this chapter is the bioinformatics analysis. Unfortunately, due to Covid-19 restrictions the VIGS experiment could not be carried out here and will be performed in a follow-up project.

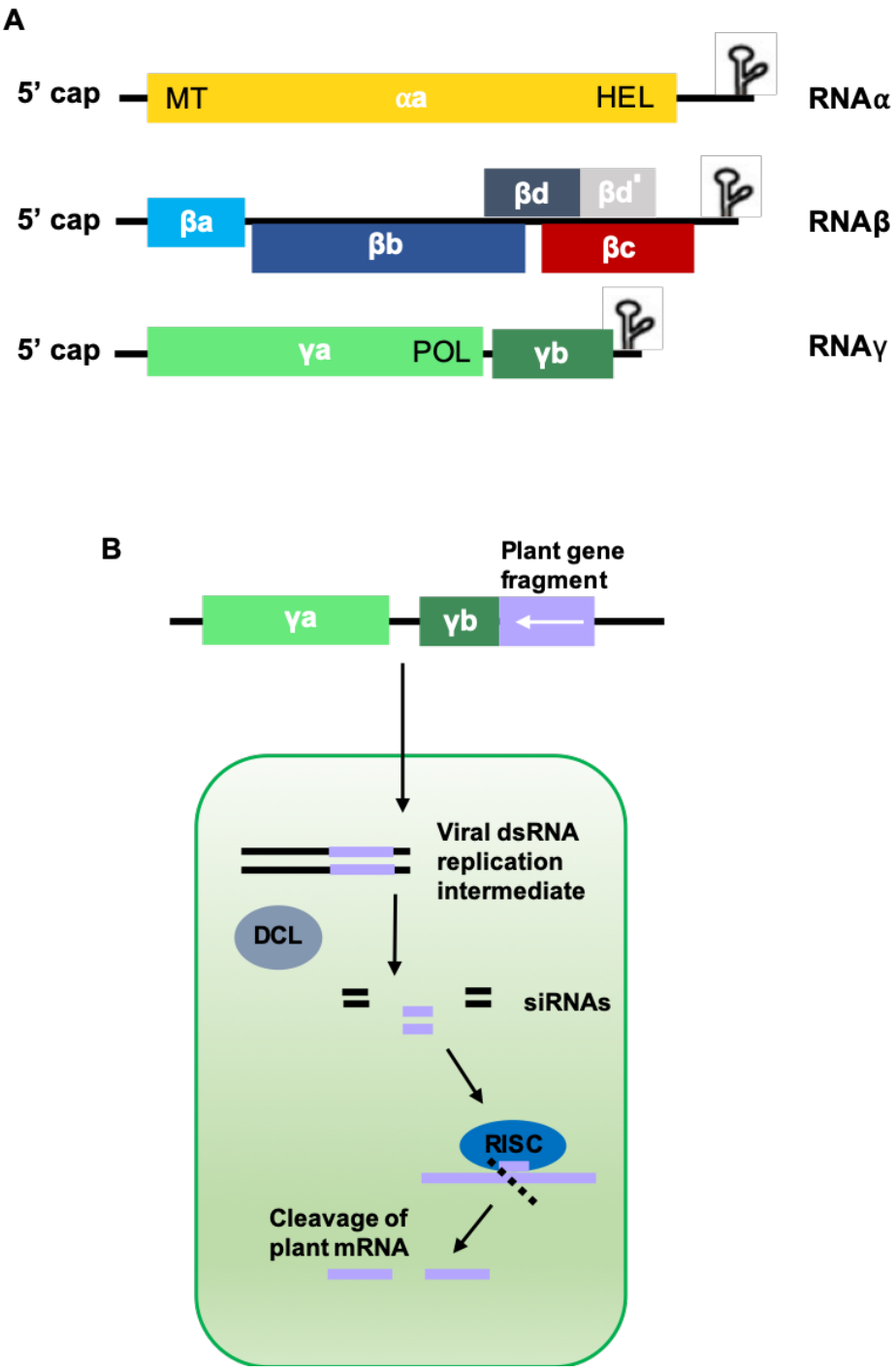
A
5' cap
MT
αa
HEL
RNAα
5' cap
βa
βb
βd
βd'
βc
RNAβ
5' cap
γa
POL
γb
RNAγ
B
Plant gene fragment
γa
γb
Viral dsRNA replication intermediate
DCL
siRNAs
RISC
Cleavage of plant mRNA

Figure 6.1 – The barley stripe mosaic virus (BSMV) virus-induced gene silencing (VIGS) mechanism. (A) The BSMV genome – the genome contains three RNAs that are capped at the 5' end and have a tRNA-like hairpin secondary structure at the 3' end. RNAα encodes an αa replicase and possesses a methyl transferase (MT) and helicase (HEL) domain. RNAβ encodes coat (βa) and movement proteins (βb, βc and βd), (βd' is a small protein expressed via the translational readthrough of βd) and RNAγ encodes a polymerase (POL) (γa) and is involved in viral pathogenicity (γb). (B) VIGS mechanism – a fragment from the gene of interest is cloned downstream of the γb open reading frame in the BSMV RNAγ. The plant is then inoculated with a mixture of the three RNAs, RNAα, RNAβ and RNAγ (with the inserted gene fragment), this is not shown in the diagram. Upon cell entry, dsRNA formed during viral replication is recognised and cleaved by dicer-like enzymes (DCLs). These siRNAs are 21-22 nucleotides in length, one strand is incorporated into the RNA-induced silencing complex (RISC). These complexes then initiate cleavage of complementary single-stranded RNAs to the incorporated one, inducing gene silencing. This figure has been adapted from Lee *et al.* (2012).

6.1.1 Chapter aims and hypotheses

In this chapter I therefore propose to use bioinformatic approaches to identify wheat PD-associated genes to help answer the hypothesis: *F. graminearum* utilises the PD for intracellular hyphal growth, aiding successful colonisation of wheat floral and non-floral tissues.

To identify possible protein candidates two different protein groups were focused on: a) proteins involved in callose deposition and degradation and b) proteins known to be specifically associated with the PD, both of which control PD permeability and alter their behaviour in response to pathogenic infection. There are currently no studies on wheat PD-associated or wheat callose degradation proteins. A study into wheat callose deposition has been conducted, however this explored gene expression and not the function of callose deposition in terms of biotic stimuli i.e. a pathogenic fungus[398]. Consequently, genes of interest have first been identified in *A. thaliana* – these are discussed extensively in the results section below.

6.2 Experimental procedures

6.2.1 Bioinformatics

All bioinformatics analyses were carried out using the programmes listed in Table 6.1. Please refer to this for all bioinformatic procedures relating to the identification of gene candidates suitable for the VIGS experiments.

Another bioinformatics study was carried out beside this one to allow for a comparative approach to be taken when attempting to identify VIGS candidates (Kostya Kanyuka, leader of wheat functional genomic experimentation within the wheat pathogenomics team at Rothamsted Research). Any differences in software used will be addressed in the results/discussion. VIGS fragments were designed using the si-Fi21 software (Version 1.2.3-0008) for RNAi target design. Primers were developed using Geneious Prime© (Version 2020.2).

Table 6.1 Bioinformatics software to determine virus induced gene silencing gene candidates.

Database/software (Version used)	Function	URL	Reference(s)
Clustal Omega (1.2.4)	Multiple sequence alignment tool.	https://www.ebi.ac.uk/Tools/msa/clustalo/	Sievers *et al.* (2011)
EnsemblPlants (release 47)	A genome centric resource for plant species of interest. Provides information on gene sequences, gene models, annotations and loci.	https://plants.ensembl.org/index.html	Howe *et al.* (2019)
Interpro (80.0)	Prediction of protein families, domains and important sites.	https://www.ebi.ac.uk/interpro/	Mitchell *et al.* (2019)
NCBI BLAST* (+2.10.1)	Finds regions of similarity between biological sequences and calculates the statistical significance.	https://blast.ncbi.nlm.nih.gov/Blast.cgi	Altschul *et al.* (1990)
PANTHER~ (15.0)	Protein classification system built to enable high-throughput analyses.	http://www.pantherdb.org/	Huaiyu *et al.* (2019)
Pfam (33.1)	Identification of protein domains.	https://pfam.xfam.org/	El-Gebali *et al.* (2019)

Phyre2^ (2.0)	Prediction of protein structure/function.	http://www.sbg.bio.ic.ac.uk/~phyre2/html/page.cgi?id=index	Kelley *et al.* (2015)
Prosite (2020_03)	Database of domains, families and functional sites.	https://prosite.expasy.org/	Sigrist *et al.* (2012)
TAIR** (TAIR10)	A database for the model plant species, Arabidopsis, of genetic and molecular data.	https://www.arabidopsis.org/index.jsp	Huala *et al.* (2001)
Wheat Gene Expression Browser (RefSeq1.1)	RNA-seq data analysis and visualisation programme.	http://www.wheat-expression.com/	Borrill *et al.* (2016) Ramirez-Gonzalez *et al.* (2018)
WoLF PSORT (release 2005)	Uses a proteins amino acid sequence to predict subcellular localisation.	https://wolfpsort.hgc.jp/	Horton *et al.* (2007)

*National Center for Biotechnology Information Basic Local Alignment Search Tool

** The Arabidopsis Information Resource

^Protein Homology/analogy recognition engine

~ Protein Analysis Through Evolutionary Relationships

6.3 Results

6.3.1 Identifying genes of interest in *Arabidopsis*

To determine candidate genes involved in PD function and callose deposition, knowledge of the *A. thaliana* genome and transcriptome was used to identify gene families of interest. Silencing of PD-associated genes had not been performed previously, therefore it was important that a range of different candidate gene families were researched extensively to expand the possibility of success. In total four *A. thaliana* candidates were chosen. This pipeline can be seen in Fig. 6.2. **From personal communication with Christine Faulkner, John Innes Centre, a PD researcher, it was determined that the following gene families and selected genes would be ideal candidates for bioinformatic analyses and VIGS. These genes were relatively well characterised in the literature and known to interact with the PD compared with other possible candidates.**

Callose deposition and degradation are controlled by two separate enzyme groups – the glucan synthase-like (GSL) enzymes, previously referred to as the callose synthases (CalS), and the ß-1,3-glucanases, respectively. Callose regulation is not only fundamental in controlling PD permeability but also processes including: sieve pore regulation, pollen development, vascular differentiation, cell plate formation, biotic and abiotic stress responses – it was therefore speculated that by silencing a gene involved with PD permeability, other processes may also be compromised as a result of each GSL or ß-1,3-glucanase being multi-functional[261,378]. Both of these gene families do not have specific genetic markers or molecular features that indicate localisation to the PD.

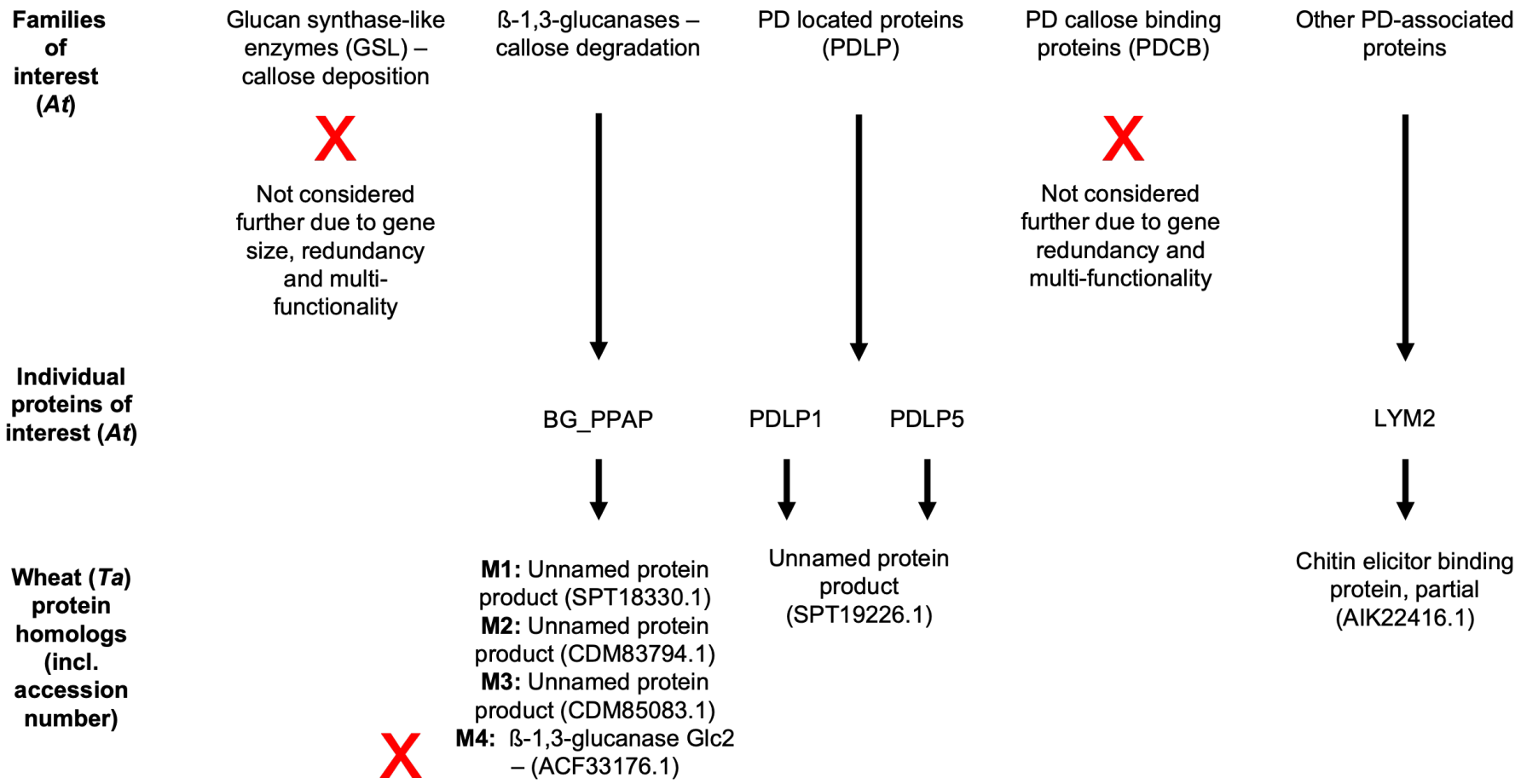
Families of interest (At)
Glucan synthase-like enzymes (GSL) – callose deposition
ß-1,3-glucanases – callose degradation
PD located proteins (PDLP)
PD callose binding proteins (PDCB)
Other PD-associated proteins
X
Not considered further due to gene size, redundancy and multi-functionality
X
Not considered further due to gene redundancy and multi-functionality
Individual proteins of interest (At)
BG_PPAP
PDLP1
PDLP5
LYM2
Wheat (Ta) protein homologs (incl. accession number)
M1: Unnamed protein product (SPT18330.1)
M2: Unnamed protein product (CDM83794.1)
M3: Unnamed protein product (CDM85083.1)
M4: ß-1,3-glucanase Glc2 – (ACF33176.1)
X
Unnamed protein product (SPT19226.1)
Chitin elicitor binding protein, partial (AIK22416.1)

Figure 6.2 – Flowchart of virus-induced gene silencing candidate selection. Red crosses indicate a discarded gene/protein candidate that was no longer considered. For M4 this reason is a low identity match to *At*BG-PPAP.

In total there are 12 *A. thaliana GSL* genes (10 in rice and 12 in maize), with GSL3, GSL9 and GSL11 having unknown functions – Table 6.2 and Fig. 6.3[265,399]. Most of these genes have multiple functions, with these purposes differing between species. For example, in *A. thaliana,* GSL8 functions in microspore development, callose deposition at cell plates during cytokinesis, as well as callose deposition at PDs during the phototropic response; the ortholog in rice, CRR1, is involved in vascular differentiation and ovary expansion as well as auxin induction[260,400-402]. Most GSL's have 40-50 exons and are 2000 aa in length, larger than most plant genes, with the exceptions of *GSL1* and *GSL5* which have two and three exons respectively[261,403]. GSL5 is involved in pathogen-induced callose deposition (as well as pollen development and fertility, salicylic acid-, wound- and iron-induced callose deposition)[260,376,404,405]. GSL5 has been reported to increase callose formation in response to wounding or pathogenic attack, with *GSL5* knockout mutants being unable to produce papillae[404]. However, this callose depletion rendered the plants more resistant and not more susceptible to pathogenic attack, possibly as a result of defence machinery hinderance[404]. Due to the large gene size as well as uncertainty in gene functions and redundancies, and many GSL's having multiple functionalities, this gene family was not explored any further.

The ß-1,3-glucanases, involved in callose degradation, were subsequently investigated. The *A. thaliana* β-1,3-glucanase family consists of 50 genes, 44 of which have been grouped into 13 expression clusters – established by their distinct developmental programmes (Fig. 6.4)[406]. Only four have been studied in any detail and are shown in Table 6.3. All classes have N-terminal secretion signals, a core glycosyl hydrolase 17 family domain (GH-17) and several are GPI-anchored[406]. Genes in group M are expressed constitutively and show minimal changes in expression in response to stress (including biotic stressors)[406]. It is likely many of these have multiple functions, however *At*BG_PPAP (*A. thaliana* ß-1,3-glucanase_putative Pd-associated protein) (AT5G42100) is highlighted as functioning in the degradation of PD-associated callose, being identified in PD-enriched fractions from *Arabidopsis,* as well as *At*BG_PPAP:GFP localising with aniline-blue stained callose at PD[407]. In summary this enzyme is 45kDa and 425aa in length (residing on chromosome 5), also targets the ER and is most highly expressed in flowers and siliques[407]. The KO mutant shows increased levels of callose and a hypothesised decreased susceptibility to viral infection[407]. *At*BG_PPAP was taken forward for investigation as a possible VIGS candidate.

Table 6.2 Glucan synthase-like callose deposition enzyme genes in *Arabidopsis thaliana* and their protein functions.

Gene name	Gene ID	Function
GSL1 (CalS11)	AT4G04970	Separation of microspores
GSL2 (CalS5)	AT2G13680	Male gametophyte development
GSL3 (CalS2)	AT2G31960	Unknown
GSL4 (CalS8)	AT3G14570	Basal PD callose and H_2O_2-induced PD callose
GSL5 (CalS12)	AT4G03550	Pollen development and fertility Response to SA-, wound-, iron- and pathogen induced callose deposition
GSL6 (CalS1)	AT1G05570	Callose synthesis at the cell plate SA-dependent callose synthesis
GSL7 (CalS7)	AT1G06490	Phloem sieve elements
GSL8 (CalS10)	AT2G36850	Microspore development Cell plates during cytokinesis PD during the phototropic response
GSL9 (CalS4)	AT5G36870	Unknown
GSL10 (CalS9)	AT3G07160	Microspore development and plant growth
GSL11 (CalS6)	AT3G59100	Unknown
GSL12 (CalS3)	AT5G13000	PDs in the stele, roots and phloem

Previous gene nomenclature shown in brackets.

Adapted from Wu *et al.* 2018.

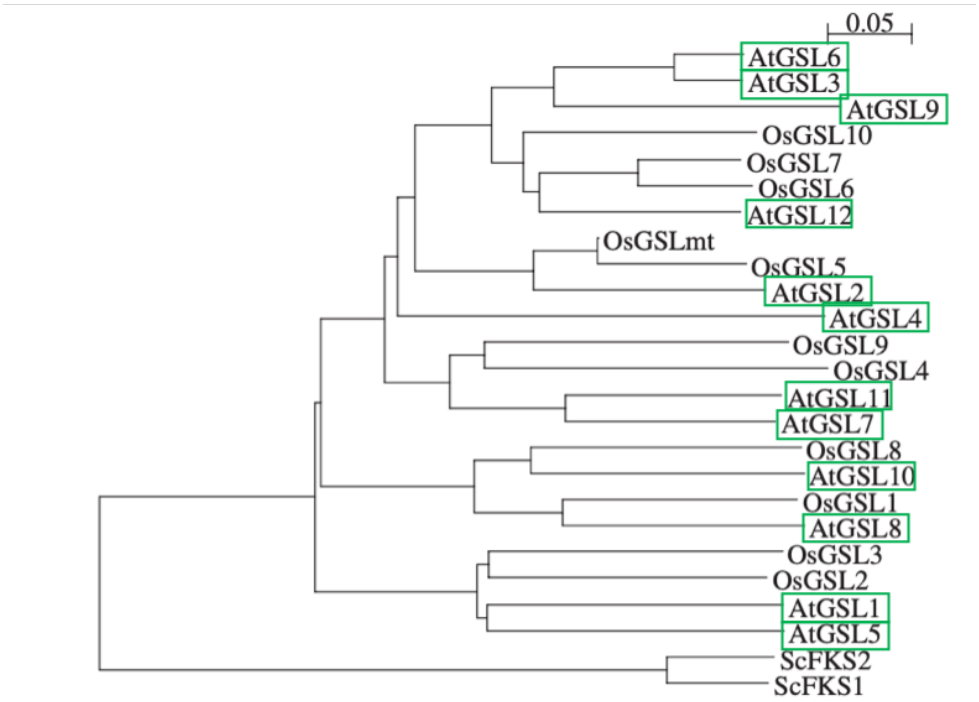

Figure 6.3 – Phylogenetic tree of Glucan synthase-like enzymes. Protein sequences aligned in ClustalW 1.83. Tree constructed using the NJ (Neighbor-Joining) algorithm and drawn using NJplot. *A. thaliana* proteins highlighted by green boxes. Adapted from Yamaguchi *et al.* 2005.

Table 6.3 ß-1,3-glucanase genes in *Arabidopsis thaliana* and their protein functions.

Gene name	Gene ID	Function (degradation)
AtBG_ppap	At5g42100	PD-associated callose
PdBG1	At3g13560	LRP[1] during lateral root development
PdBG2	At2g01630	LRP[1] during lateral root development
BG6	At4g16260	Copper-induced PD callose degradation

Only listed those of known function. Adapted from Wu *et al.* 2018.

[1] LRP, lateral root primordia

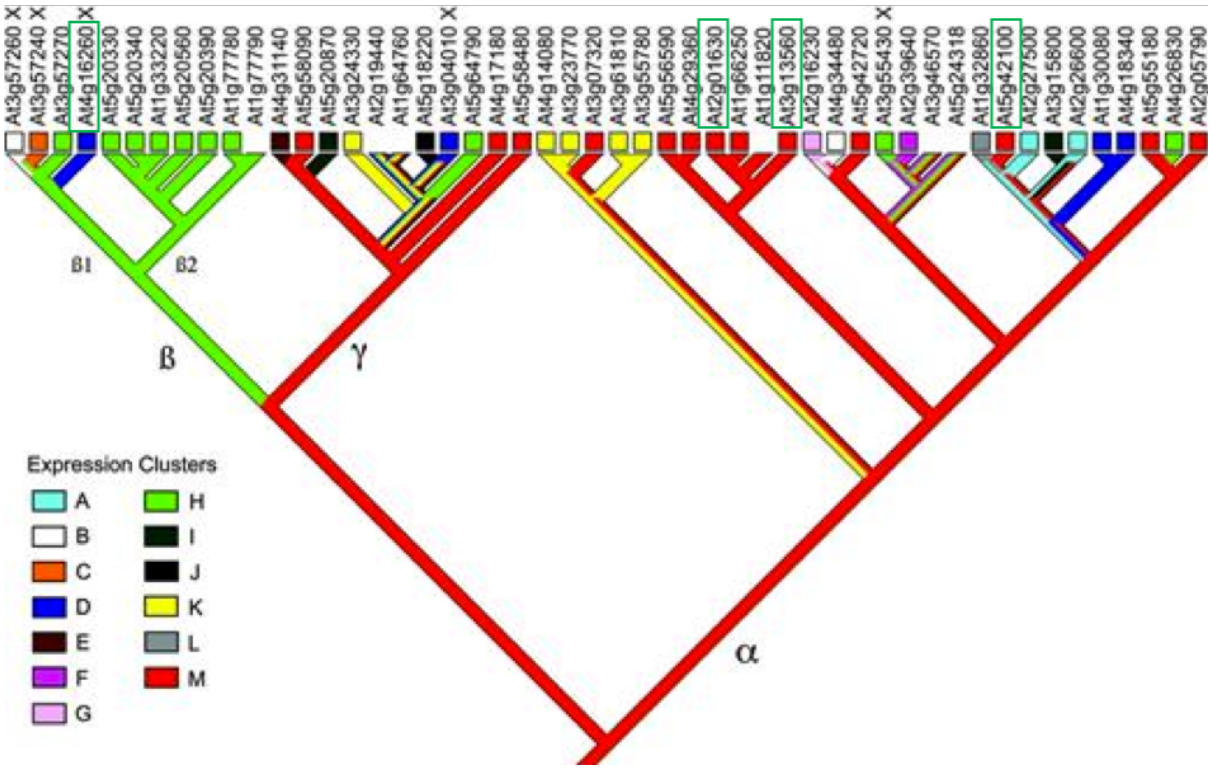

Figure 6.4 – Phylogenetic tree of ß-1,3-glucanases. Coloured boxes indicate expression profile clustering, those with no box are considered to have null states. These colours and their corresponding expression clusters are shown in the legend. Where a branch is depicted with multiple colours this shows the branches association with multiple possible states. X marks pathogenesis-related glucanases identified through fungal stress response experiments. Gene ID names circled with green boxes correspond to those shown in table 6.2. Taken from Doxey *et al*. 2007.

Having identified a candidate involved in callose degradation, candidates involved in PD function were considered – primarily the PD-located proteins (PDLP's). The *A. thaliana* proteome contains 8 PDLPs (PDLP1-PDLP8 – Table 6.4 and Fig. 6.5) which show PD targeting, are PD-specific (unlike the GSL's and ß-1,3-glucanases) and are approximately 30.2-35.3kDa[264]. PDLPs contain two extracellular domains of unknown function 26 (DUF26) domains[264]. The PDLP's are type I transmembrane (TM) proteins with the TM domain containing the PD localisation sequence, negatively regulating PD-mediated macromolecular diffusion[264]. PDLPs have been shown to be trafficked along the secretory pathway to reach the PD and more specifically the PM lining the PD interior[264]. All PDLP's have diverse expression patterns, but the specific biological function of each PDLP member has not yet been established. PDLP1 and PDLP5 are the two most widely explored within the literature.

PDLP1 has previously been shown to locate to punctate spots on the cell wall, which remain in place following plasmolysis, co-localising with callose, characteristic of PD group organisation in PFs[264]. Overexpression of *PDLP1* leads to impaired GFP trafficking. Whereas a *PDLP1* KO mutant does not have the opposite effect, whereby GFP diffusion was no different from that seen in WT *A. thaliana* leaves, this is most likely a result of genetic redundancy and tissue expression overlap[264]. Similarly, PDLP5 is known to regulate PD permeability, correlated with enhanced callose deposition and has a role in innate immunity[408]. All PDLP proteins, including PDLP5, were identified as a result of sequence homology with PDLP1[264]. PDLP5 localises to the median cavity of the PD, similar to viral MPs, with some viral proteins having the capacity to interfere with PDLP5 activity[408]. A main advantage of using PDLP5 as a VIGS candidate, in

comparison to PDLP1, is that PDLP5 shows no functional redundancy[408]. *PDLP5* overexpression decreases PD permeability and initiates cell death, leading to chlorosis and lesion formation, this is linked to salicylic acid production[408]. It is also probable that genes involved in callose deposition/degradation and PD function share signalling pathways, this is the case for *PDLP5* and *GSL6*[260]. Both PDLP1 and PDLP5 were taken forward as possible candidates.

Table 6.4 Plasmodesmata-located protein (PDLPs) genes in *Arabidopsis thaliana* and their protein functions.

Gene name	Gene ID	Function
PDLP1	AT5G43980	Intercellular movement of molecules through the PD. Varying patterns of tissue expression and consequently variations in how they control molecular movement.
PDLP2	AT1G04520	
PDLP3	AT2G33330	
PDLP4	AT3G04370	
PDLP5	AT1G70690	
PDLP6	AT2G01660	
PDLP7	AT5G37660	
PDLP8	AT3G60720	

All PDLPs are involved in intercellular movement but the specific functions for most are unknown.

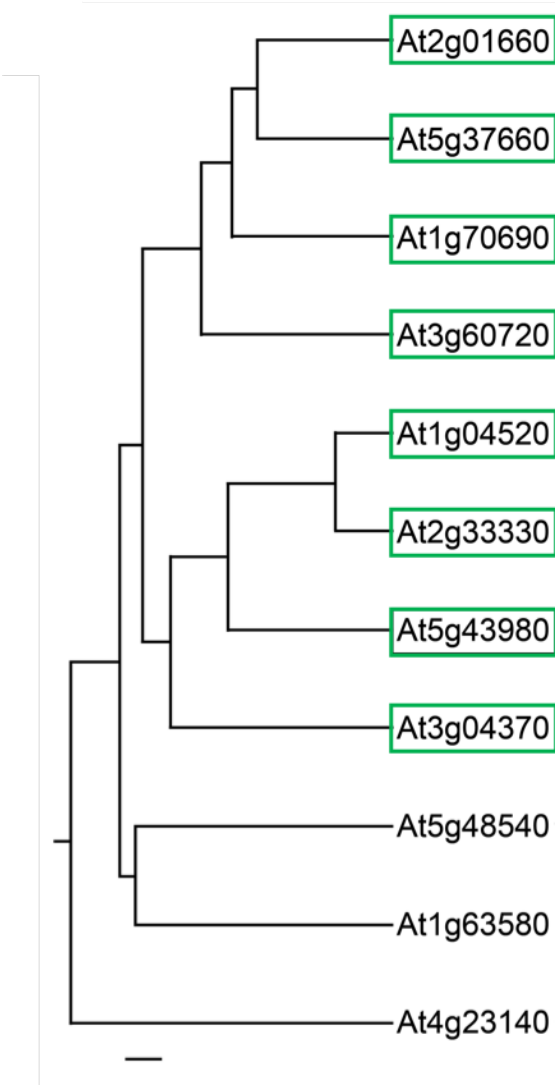

Figure 6.5 – Phylogenetic tree of *Arabidopsis thaliana* plasmodesmata-located proteins (PDLPs). Green boxes highlight PDLP1-PDLP8 as shown in table 6.4. PDLP2-PDLP8 were all identified as a result of their homology with PDLP1 (At5g43980). This analysis revealed the presence of two clades within the PDLP family. Bar size is not listed in the paper. Adapted from Thomas *et al.* 2008 – no value is given for the scale bar.

The callose-binding proteins (PDCBs) were also considered as VIGS candidates. PDCBs are PD-localised proteins with callose binding activity[409]. Structurally they consist of an N-terminal signal peptide, an X8 domain, an unstructured middle region and a GPI anchor motif at the C-terminus[409]. There are 11 PDCB-like

proteins in *A. thaliana* which localise to the neck region of PD[409] (Table 6.5 and Fig. 6.6). KO mutants of *PDCB2* and *PDCB3*, both single and double mutants, show no phenotype, demonstrating their functional redundancy[409]. It is thought these proteins may participate in the stabilisation of PD callose or specific microdomains; evidence also suggests they may have roles as developmental regulators[409]. PDCB1, a 21kDa protein, with N- and C-terminal signal sequences that direct the protein to the external face of the PM, has the potential to provide a structural anchor between the PM component of PDs and the cell wall[409]. PDCB1 overexpression lines exhibit increased callose deposition and arrest intercellular trafficking through PD[409]. PDCB2 overexpression lines failed, suggesting the importance of these proteins in plant development[260]. Evidence of functional redundancy and multifunctionality resulted in the PDCBs being disregarded as possible VIGS targets.

Table 6.5 Callose-binding protein (PDCBs) genes in *Arabidopsis thaliana* and their protein functions.

Gene name	Gene ID	Function
PDCB1	At5g61130	All involved in callose regulation, more specific functions have not been characterised in detail.
PDCB2	At5g08000	
PDCB3	At1g18650	
PDCB4	At1g69295	
PDCB5	At3g58100	

Only five PDCBs are listed here as they have all been shown to localise to the PD – corresponding with Fig. 6.6.

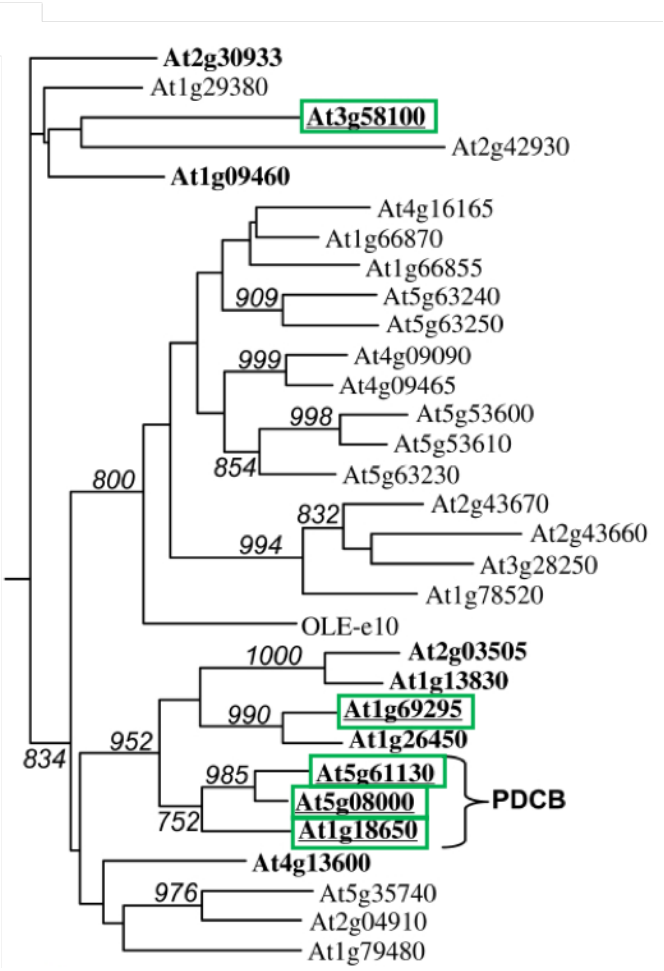

Figure 6.6 – Phylogenetic tree of callose-binding proteins (PDCBs) X8 domains. Green boxes highlight PDCB1-PDCB5 (as shown in Table 6.5) which have all been shown to localise to plasmodesmata (PD). The PDCB subfamily PDCB1-PDCB3 is indicated. Bootstrap values above 70% are shown. Adapted from Simpson *et al.* 2009.

The final VIGS gene candidate selected was *LYM2*. *AtLYM2* is a gene primarily involved in chitin perception, producing the protein LysM domain-containing GPI-anchored protein 2, located at the PD-PM, is 350 aa in length and brings about a reduction in the molecular flux through the PD[262,410]. It was first identified in *A. thaliana* as a result of being a homolog of the chitin elicitor binding protein in rice (CEBiP)[411]. There are three family members in *A. thaliana* and five in rice (Table 6.6 and Fig. 6.7), meaning the LYM/CEBiP families are relatively small, lessening the degree of functional redundancy and increasing the chances of silencing multiple genes in the same family[411]. VIGS constructs for the *LYM2* wheat ortholog, *TaCEBiP*, had already been produced for an experiment with *Z. tritici*[412].

Table 6.6 *LYM* genes in *Arabidopsis thaliana* and their protein functions.

Gene name	Gene ID	Function
LYM1	At1g21880	Detection of peptidoglycans
LYM2	At2g17120	Chitin perception
LYM3	At1g77630	Detection of peptidoglycans

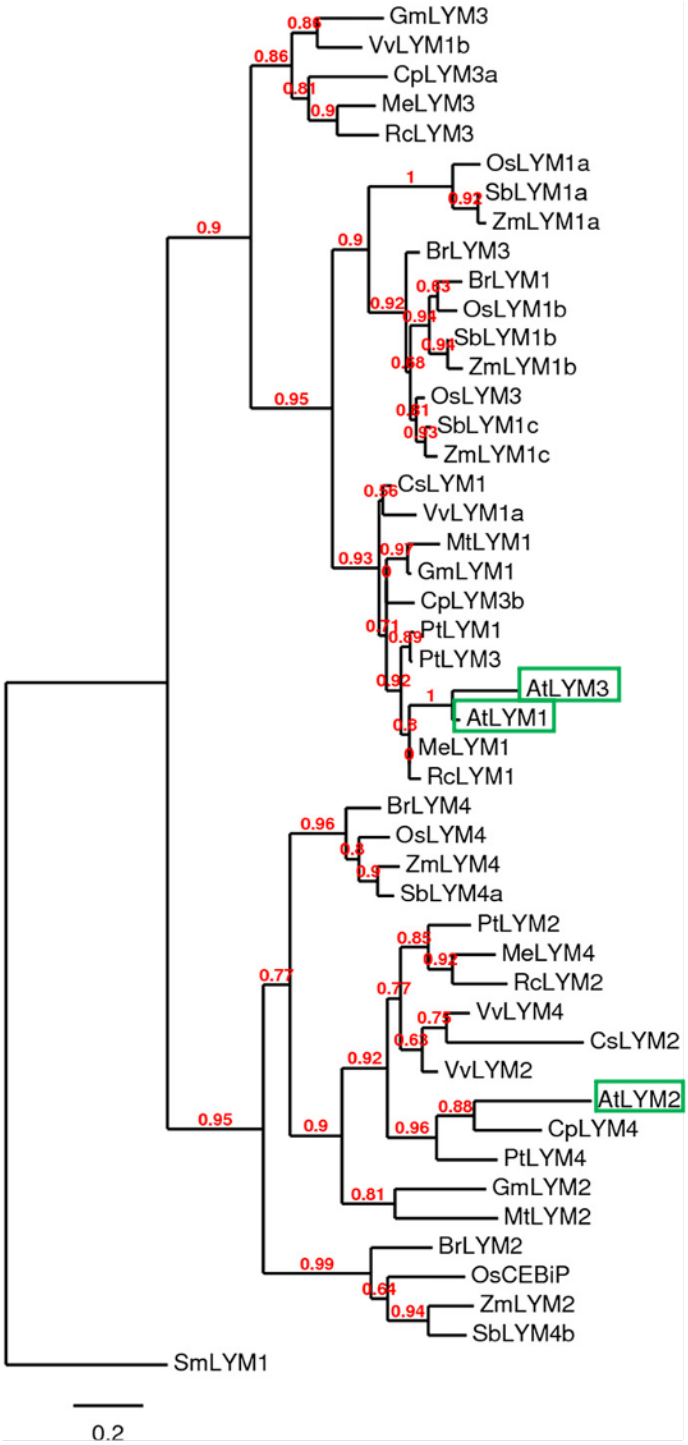

Figure 6.7 – Phylogenetic tree of LYM proteins. Green boxes highlight the *Arabidopsis thaliana* LYM proteins. The tree was rooted with LYM1 from *Selaginella moellendorfii* (SmLYM1) with red labels representing respective bootstrap values. Adapted from Fliegmann *et al.* 2011.

6.3.2 Bioinformatic screening of *A. thaliana* VIGS candidates reveals homologous unnamed wheat protein products (Analysis 1)

Following the identification of *AtBG_PPAP, AtPDLP1, AtPDLP5 and AtLYM2* as possible VIGS target, a series of bioinformatics software (listed in Table 6.1) was used as a screen to characterise their suitability as VIGS candidates and identify wheat orthologs. A summary of this workflow can be seen in Fig. 6.8.

6.3.2.1 *At*BG_PPAP

To allow for comparisons to be made between *A. thaliana* and wheat orthologs and to ensure critical domains are maintained between the two, structural analyses was carried out. This determined *At*BG_PPAP contained a glycoside hydrolase family 17 (GH-17) domain, and a single transmembrane domain (TMD) as shown in Fig. 6.9**.** Protein localisation predictions were not conclusive (Appendix 26).

Subsequent analysis focused on the identification of any *At*BG_PPAP wheat orthologs. The *At*BG_PPAP protein sequence was aligned and compared to the *T. aestivum* (hexaploid wheat) proteome. Detailed NCBI BLAST analysis can be seen in table of Appendix 27. The top four matches, three unnamed protein products and an annotated β-1,3-glucanase, were selected for further analysis as a result of their significantly higher identity percentage scores. The fourth contender, a β-1,3-glucanase, was identified as Glc2 (Accession: ACF33176.1).

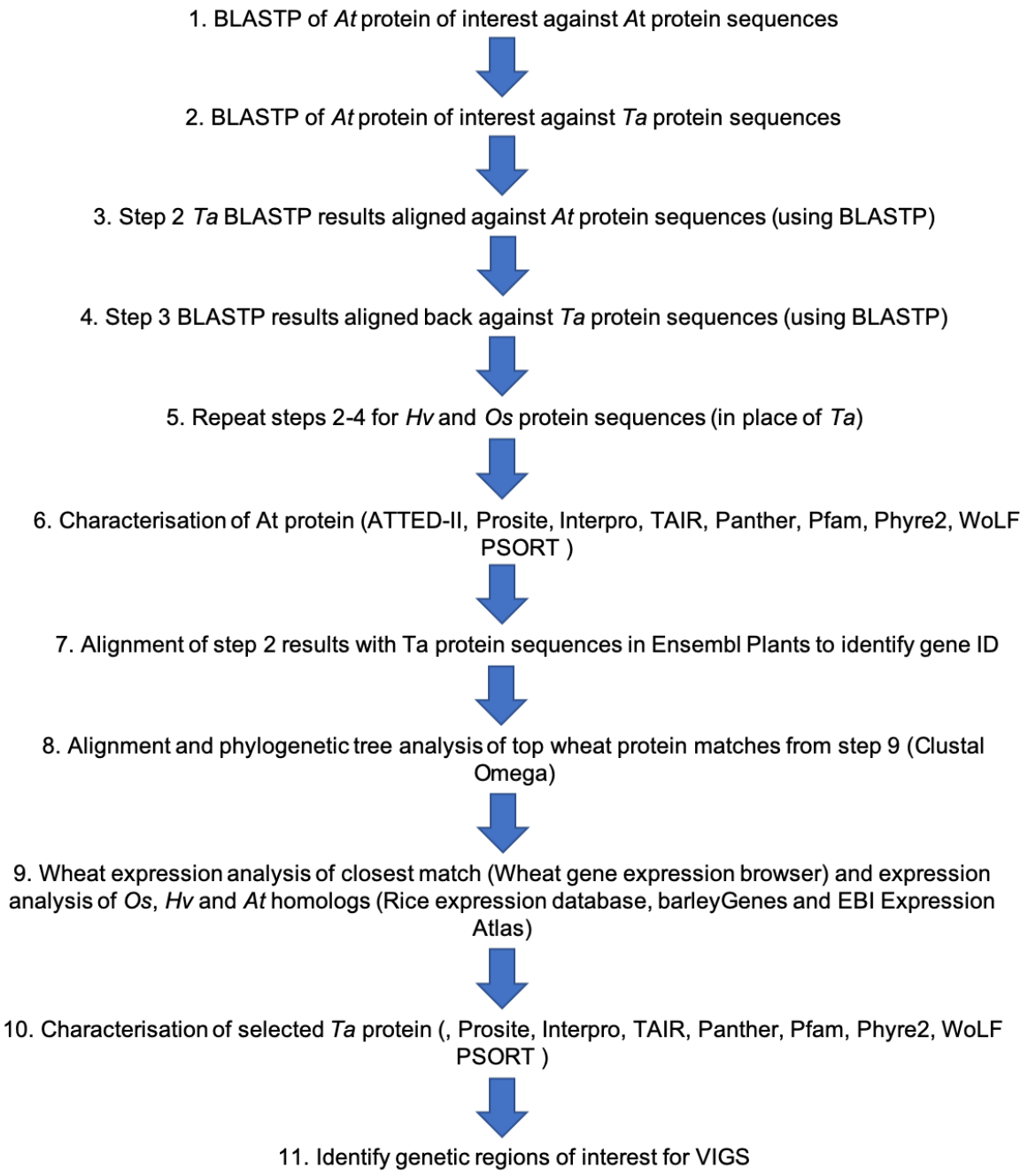

Figure 6.8 – Workflow for the identification of wheat candidate genes for virus induced silencing (VIGS). Software used for each step is included in brackets. Table 6.1 can also be referred to for more information.

Consequently, these top four AtBG_PPAP wheat matches were aligned back against the *A. thaliana* proteome in a reciprocal BLAST search to check their reliability as possible homologs. Please note from this point onwards these four matches will be referred to as M1-M4 in order of the alignment results: M1 (accession: SPT18330.1), M2 (accession: CDM83794.1), M3 (accession: CDM85083.1) and M4 (Glc2; accession: ACF33176.1). M1-M3 aligned to glycosyl hydrolase superfamily proteins in the *A. thaliana* proteome as the top match, with matches to *At*BG_PPAP being further down in the alignment. Even though *At*BG_PPAP was not the top match in the alignment, M1-M3 were still carried forwards as this alignment analysis still displayed M1-M3 shared identity with *At*BG_PPAP as well as other members of the glycosyl hydrolase family. M4 matched to the *At*BG_PPAP with a much lower identity score (Appendix 27). For this reason, M4 was discarded as a possible VIGS candidate. Refer to Table 6.7 for *At*BG_PPAP wheat orthologs and their abbreviated names.

To confirm M1-M3 were the best wheat VIGS candidates, rice and barley orthologs were also investigated. The rice ortholog, Os10g0160100, was identified from a list of plant homologs (TAIR, Fig. 6.1). Alignment of this sequence to the *A. thaliana* proteome demonstrated its conservation with *At*BG_PPAP; once aligned to the *T. aestivum* proteome, M1-M3 were in the top three protein matches. A barley ortholog was identified by aligning AtBG_PPAP against the *Hordeum vulgare* genome, accession: KAE8777097.1, a putative β-1,3-glucanase. When aligned back to the *A. thaliana* proteome this ortholog matched to *At*BG_PPAP; when aligned to the *T. aestivum* proteome the barley ortholog matched most closely with a hypothetical wheat protein. Investigating

the barley ortholog here did therefore not produce any conclusive results. These results are summarised in Appendix 27.

*At*BG_PPAP, M1-M3, and the rice and barley orthologs, were aligned against each other, to investigate areas of sequence conservation – Fig. 6.10 (and Appendix 28 for the phylogenetic tree). Thirteen regions of 5 or more bases, showed regions of high similarity.

Table 6.7 *At*BG_PPAP wheat orthologs and their abbreviations used in the main text.

Abbreviated name	Accession number	Wheat gene name
M1	SPT18330.1	*TraesCS2D02G292500.1* *TraesCS2B02G311200.1* *TraesCS2A02G294700.1*
M2	CDM83794.1	*TraesCS3B02G278400.1* *TraesCS3D02G249500.1* *TraesCS3D02G249500.2*
M3	CDM85083.1	*TraesCS3B02G406200.1* *TraesCS3A02G374000.1* *TraesCS3D02G366700.2*

M1 is 390 aa in length and a member of the glycosyl hydrolase family 1. An alignment analysis was conducted of the most closely related wheat genes to look for large similarities or differences between the sequences (Fig. 6.11 and Appendix 29 for the phylogenetic tree). Seventeen regions of high similarity (5 or more base matches) were identified with high regions of dissimilarity at both the C and N terminus (important areas for the signalling and localisation of the protein). For the following results, *TraesCS2D02G292500.1* was considered the

closest wheat gene match to the M1 wheat sequence and was therefore used to produce the following results. This gene is located on chromosome 2 of the D genome. Gene structure can be seen in Appendix 30.

Wheat gene expression analysis was carried out, specifying the hexaploid wheat cultivar Chinese Spring (used most commonly in experiments) and 'other' (including Bobwhite, a cultivar susceptible to *F. graminearum*). The expression heatmap for *TraesCS2D02G292500.1*, displayed the gene was most highly expressed in the leaf and shoot, although this was still low. Little to no expression was seen in response to pathogens. These trends were also shown by the gene's homoeologues, listed on the wheat gene expression atlas as *TraesCS2B02G311200.1* and *TraesCS2A02G294700.1* (situated on chromosome 2 of the B and A genomes respectively) – how these are determined can be found in Ramírez-González *et al.* 2018 paper[413]. These results can be seen in Fig. 6.12.

	3D model	Transmembrane domain
*At*BG_PPAP		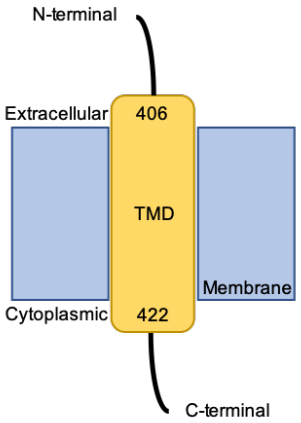
TraesCS2D02G292500.1	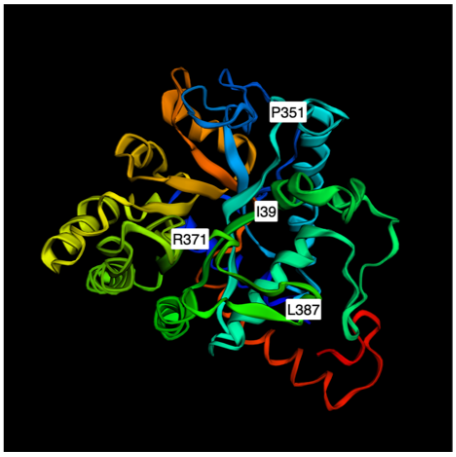	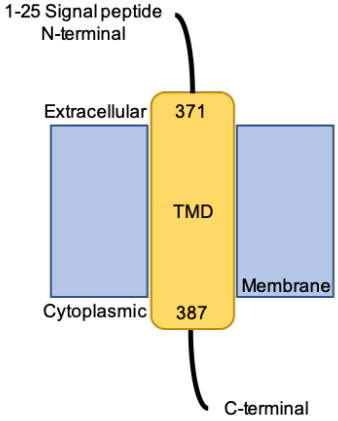
TraesCS3B02G278400.1	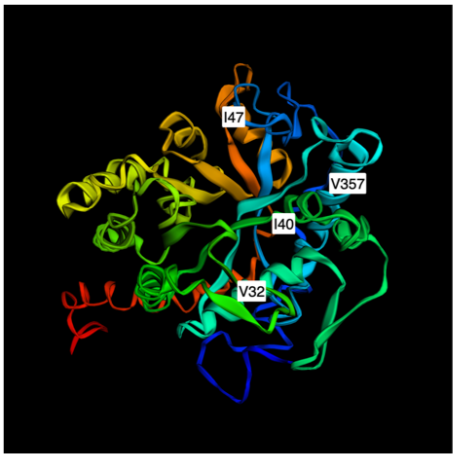	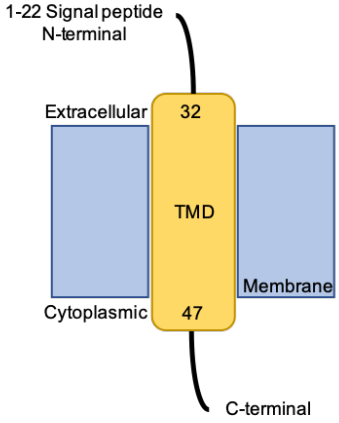
TraesCS3B02G406200.1	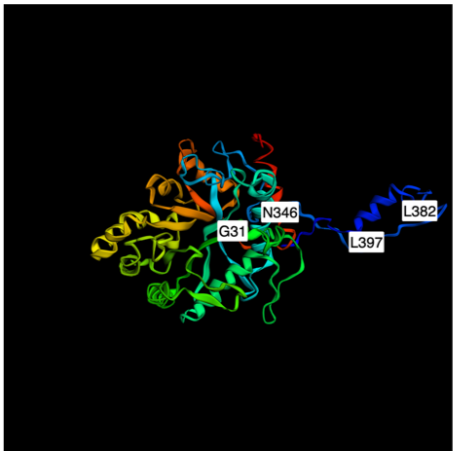	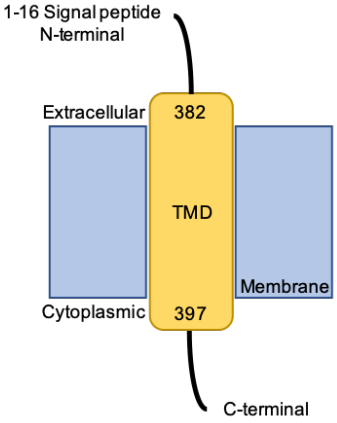

Figure 6.9 – Predicted protein structure for *At*BG_PPAP and wheat orthologs. Transmembrane domain (TMD) nucleotide positions can be seen on the 3D model (left) and correspond to the TMD diagram (right), the other values referenced on the 3D model correspond with the position of the GH-17 domain. Proteins were modelled using Phyre[2] (Table 6.1). 3D model colours from red to blue (rainbow) indicate the structure from the N (red) to C-terminus (blue).

Like *At*BG_PPAP, the structure of TraesCS2D02G292500.1 contained a GH-17 domain and had a predicted active site at 133-276 bp; the protein is predicted to have one TMD with nucleotides 1-25 representing a signal peptide, this can be seen in Fig. 6.9. Protein localisation prediction was not conclusive (Appendix 31).

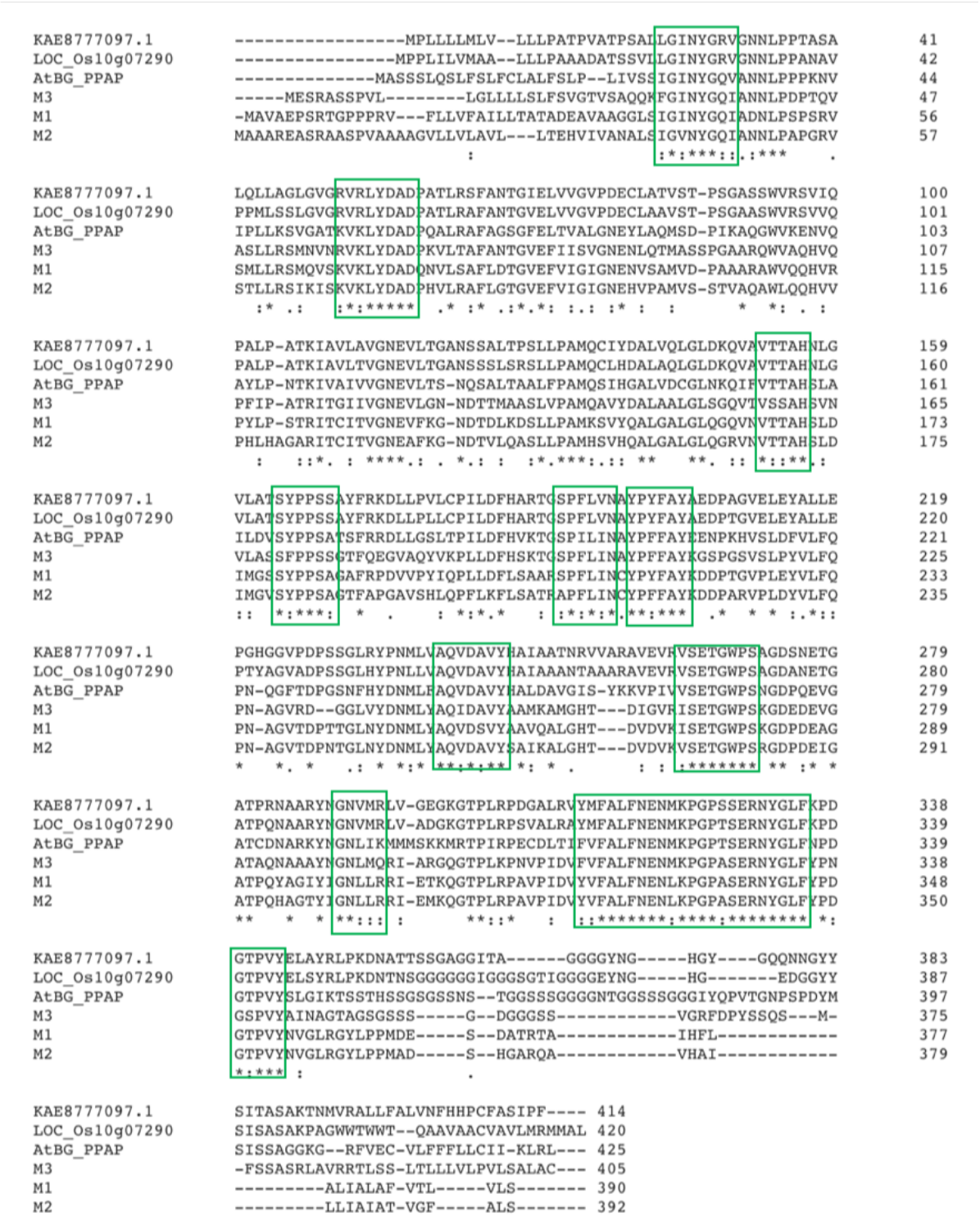

Figure 6.10 – Alignment of *At*BG_PPAP, wheat, rice and barley orthologs. Barley ortholog = KAE8777097.1, rice = LOC_Os10g07290, wheat = M1, M2 and M3. Green boxes indicate areas of similarity, five amino acids or more. '*' a single conserved residue, ':' conservation between groups with strongly similar properties, '.' Conservation between groups of weakly similar properties. Alignment was carried out using the Clustal Omega software (Table 6.1).

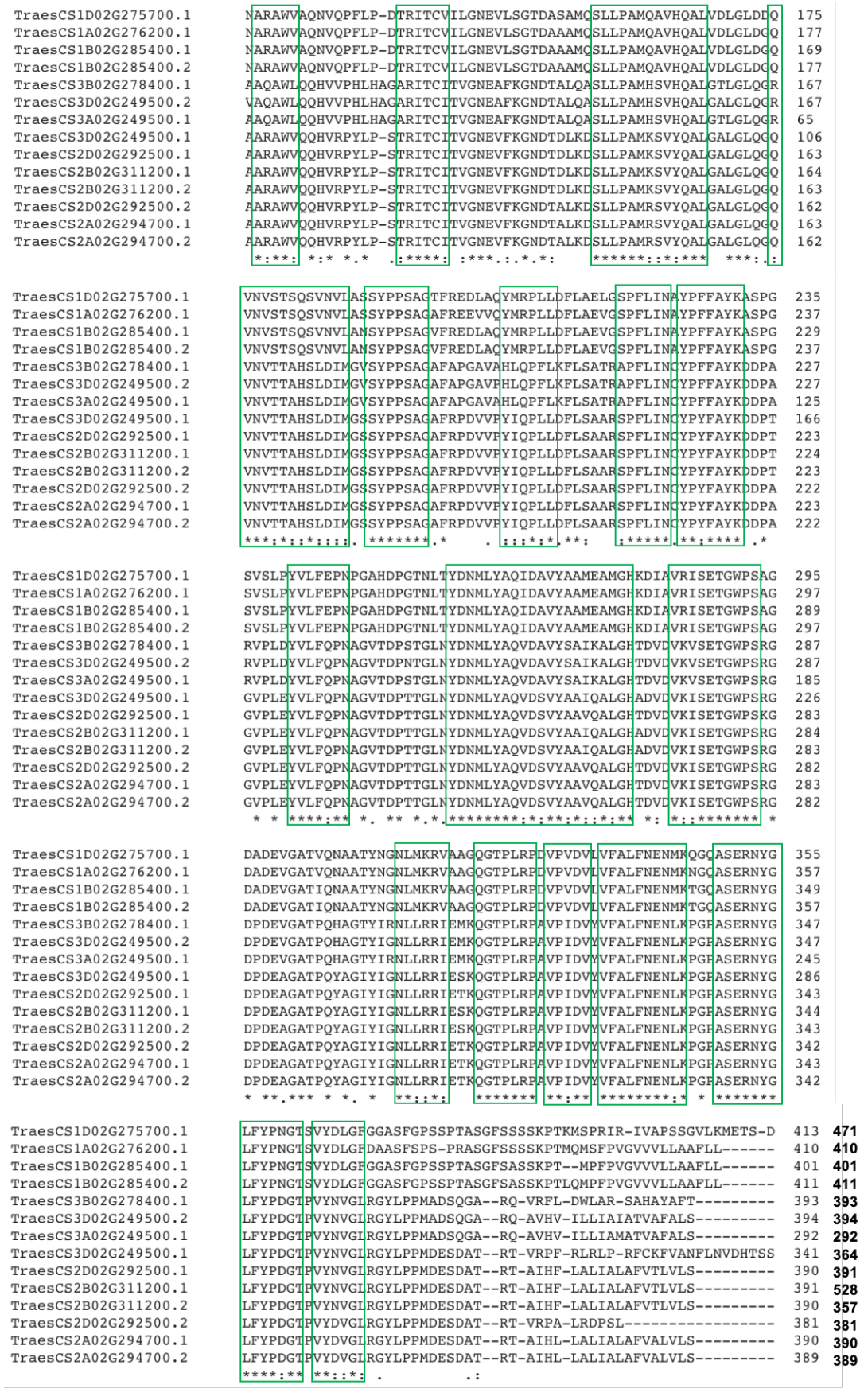
TraesCS1D02G275700.1 NARAWVAQNVQPFLP-DTRITCVILGNEVLSGTDASAMQSLLPAMQAVHQALVDLGLDDQ 175
TraesCS1A02G276200.1 NARAWVAQNVQPFLP-DTRITCVILGNEVLSGTDAAAMQSLLPAMQAVHQALVDLGLDGQ 177
TraesCS1B02G285400.1 NARAWVAQNVQPFLP-DTRITCVILGNEVLSGTDAAAMQSLLPAMQAVHQALVDLGLDGQ 169
TraesCS1B02G285400.2 NARAWVAQNVQPFLP-DTRITCVILGNEVLSGTDAAAMQSLLPAMQAVHQALVDLGLDGQ 177
TraesCS3B02G278400.1 AAQAWLQQHVVPHLHAGARITCITVGNEAFKGNDTALQASLLPAMHSVHQALGTLGLQGR 167
TraesCS3D02G249500.2 VAQAWLQQHVVPHLHAGARITCITVGNEAFKGNDTALQASLLPAMHSVHQALGALGLQGR 167
TraesCS3A02G249500.1 AAQAWLQQHVVPHLHAGARITCITVGNEAFKGNDTALQASLLPAMHSVHQALGTLGLQGR 65
TraesCS3D02G249500.1 AARAWVQQHVRPYLP-STRITCITVGNEVFKGNDTDLKDSLLPAMKSVYQALGALGLQGQ 106
TraesCS2D02G292500.1 AARAWVQQHVRPYLP-STRITCITVGNEVFKGNDTDLKDSLLPAMKSVYQALGALGLQGQ 163
TraesCS2B02G311200.1 AARAWVQQHVRPYLP-STRITCITVGNEVFKGNDTDLKDSLLPAMKSVYQALGALGLQGQ 164
TraesCS2B02G311200.2 AARAWVQQHVRPYLP-STRITCITVGNEVFKGNDTDLKDSLLPAMKSVYQALGALGLQGQ 163
TraesCS2D02G292500.2 AARAWVQQHVRPYLP-STRITCITVGNEVFKGNDTALKDSLLPAMRSVYQALGALGLQGQ 162
TraesCS2A02G294700.1 AARAWVQQHVRPYLP-STRITCITVGNEVFKGNDTALKDSLLPAMRSVYQALGALGLQGQ 163
TraesCS2A02G294700.2 AARAWVQQHVRPYLP-STRITCITVGNEVFKGNDTALKDSLLPAMRSVYQALGALGLQGQ 162
TraesCS1D02G275700.1 VNVSTSQSVNVLASSYPPSAGTFREDLAQYMRPLLDFLAELGSPFLINAYPFFAYKASPG 235
TraesCS1A02G276200.1 VNVSTSQSVNVLASSYPPSAGAFREEVVQYMRPLLDFLAEVGSPFLINAYPFFAYKASPG 237
TraesCS1B02G285400.1 VNVSTSQSVNVLANSYPPSAGVFREDLAQYMRPLLDFLAEVGSPFLINAYPFFAYKASPG 229
TraesCS1B02G285400.2 VNVSTSQSVNVLANSYPPSAGVFREDLAQYMRPLLDFLAEVGSPFLINAYPFFAYKASPG 237
TraesCS3B02G278400.1 VNVTTAHSLDIMGVSYPPSAGAFAPGAVAHLQPFLKFLSATRAPFLINCYPFFAYKDDPA 227
TraesCS3D02G249500.2 VNVTTAHSLDIMGVSYPPSAGAFAPGAVFHLQPFLKFLSATRAPFLINCYPFFAYKDDPA 227
TraesCS3A02G249500.1 VNVTTAHSLDIMGVSYPPSAGAFAPGAVAHLQPFLKFLSATRAPFLINCYPFFAYKDDPA 125
TraesCS3D02G249500.1 VNVTTAHSLDIMGSSYPPSAGAFRPDVVFYIQPLLDFLSAARSPFLINCYPYFAYKDDPT 166
TraesCS2D02G292500.1 VNVTTAHSLDIMGSSYPPSAGAFRPDVVFYIQPLLDFLSAARSPFLINCYPYFAYKDDPT 223
TraesCS2B02G311200.1 VNVTTAHSLDIMGSSYPPSAGAFRPDVVFYIQPLLDFLSAARSPFLINCYPYFAYKDDPT 224
TraesCS2B02G311200.2 VNVTTAHSLDIMGSSYPPSAGAFRPDVVFYIQPLLDFLSAARSPFLINCYPYFAYKDDPT 223
TraesCS2D02G292500.2 VNVTTAHSLDIMGSSYPPSAGAFRPDVVFYIQPLLDFLSAARSPFLINCYPYFAYKDDPA 222
TraesCS2A02G294700.1 VNVTTAHSLDIMGSSYPPSAGAFRPDVVFYIQPLLDFLSAARSPFLINCYPYFAYKDDPA 223
TraesCS2A02G294700.2 VNVTTAHSLDIMGSSYPPSAGAFRPDVVFYIQPLLDFLSAARSPFLINCYPYFAYKDDPA 222
TraesCS1D02G275700.1 SVSLPYVLFEPNPGAHDPGTNLTYDNMLYAQIDAVYAAMEAMGHKDIAVRISETGWPSAG 295
TraesCS1A02G276200.1 SVSLPYVLFEPNPGAHDPGTNLTYDNMLYAQIDAVYAAMEAMGHKDIAVRISETGWPSAG 297
TraesCS1B02G285400.1 SVSLPYVLFEPNPGAHDPGTNLTYDNMLYAQIDAVYAAMEAMGHKDIAVRISETGWPSAG 289
TraesCS1B02G285400.2 SVSLPYVLFEPNPGAHDPGTNLTYDNMLYAQIDAVYAAMEAMGHKDIAVRISETGWPSAG 297
TraesCS3B02G278400.1 RVPLDYVLFQPNAGVTDPSTGLNYDNMLYAQVDAVYSAIKALGHTDVDVKVSETGWPSRG 287
TraesCS3D02G249500.2 RVPLDYVLFQPNAGVTDPNTGLNYDNMLYAQVDAVYSAIKALGHTDVDVKVSETGWPSRG 287
TraesCS3A02G249500.1 RVPLDYVLFQPNAGVTDPSTGLNYDNMLYAQVDAVYSAIKALGHTDVDVKVSETGWPSRG 185
TraesCS3D02G249500.1 GVPLEYVLFQPNAGVTDPTTGLNYDNMLYAQVDSVYAAIQALGHADVDVKISETGWPSRG 226
TraesCS2D02G292500.1 GVPLEYVLFQPNAGVTDPTTGLNYDNMLYAQVDSVYAAVQALGHTDVDVKISETGWPSKG 283
TraesCS2B02G311200.1 GVPLEYVLFQPNAGVTDPTTGLNYDNMLYAQVDSVYAAIQALGHADVDVKISETGWPSRG 284
TraesCS2B02G311200.2 GVPLEYVLFQPNAGVTDPTTGLNYDNMLYAQVDSVYAAIQALGHADVDVKISETGWPSRG 283
TraesCS2D02G292500.2 GVPLEYVLFQPNAGVTDPTTGLNYDNMLYAQVDSVYAAVQALGHTDVDVKISETGWPSRG 282
TraesCS2A02G294700.1 GVPLEYVLFQPNAGVTDPTTGLNYDNMLYAQVDSVYAAVQALGHTDVDVKISETGWPSRG 283
TraesCS2A02G294700.2 GVPLEYVLFQPNAGVTDPTTGLNYDNMLYAQVDSVYAAVQALGHTDVDVKISETGWPSRG 282
TraesCS1D02G275700.1 DADEVGATVQNAATYNGNLMKRVAAGQGTPLRPDVPVDVLVFALFNENMKQGQASERNYG 355
TraesCS1A02G276200.1 DADEVGATVQNAATYNGNLMKRVAAGQGTPLRPDVPVDVLVFALFNENMKNGQASERNYG 357
TraesCS1B02G285400.1 DADEVGATIQNAATYNGNLMKRVAAGQGTPLRPDVPVDVLVFALFNENMKTGQASERNYG 349
TraesCS1B02G285400.2 DADEVGATIQNAATYNGNLMKRVAAGQGTPLRPDVPVDVLVFALFNENMKTGQASERNYG 357
TraesCS3B02G278400.1 DPDEVGATPQHAGTYIRNLLRRIEMKQGTPLRPAVPIDVYVFALFNENLKPGFASERNYG 347
TraesCS3D02G249500.2 DPDEVGATPQHAGTYIGNLLRRIEMKQGTPLRPAVPIDVYVFALFNENLKPGFASERNYG 347
TraesCS3A02G249500.1 DPDEVGATPQHAGTYIRNLLRRIEMKQGTPLRPAVPIDVYVFALFNENLKPGFASERNYG 245
TraesCS3D02G249500.1 DPDEAGATPQYAGIYIGNLLRRIESKQGTPLRPAVPIDVYVFALFNENLKPGFASERNYG 286
TraesCS2D02G292500.1 DPDEAGATPQYAGIYIGNLLRRIETKQGTPLRPAVPIDVYVFALFNENLKPGFASERNYG 343
TraesCS2B02G311200.1 DPDEAGATPQYAGIYIGNLLRRIESKQGTPLRPAVPIDVYVFALFNENLKPGFASERNYG 344
TraesCS2B02G311200.2 DPDEAGATPQYAGIYIGNLLRRIESKQGTPLRPAVPIDVYVFALFNENLKPGFASERNYG 343
TraesCS2D02G292500.2 DPDEAGATPQYAGIYIGNLLRRIETKQGTPLRPAVPIDVYVFALFNENLKPGFASERNYG 342
TraesCS2A02G294700.1 DPDEAGATPQYAGIYIGNLLRRIETKQGTPLRPAVPIDVYVFALFNENLKPGFASERNYG 343
TraesCS2A02G294700.2 DPDEAGATPQYAGIYIGNLLRRIETKQGTPLRPAVPIDVYVFALFNENLKPGFASERNYG 342
TraesCS1D02G275700.1 LFYPNGTSVYDLGFGGASFGPSSPTASGFSSSSKPTKMSPRIR-IVAPSSGVLKMETS-D 413 471
TraesCS1A02G276200.1 LFYPNGTSVYDLGFDAASFSPS-PRASGFSSSSKPTMQMSFPVGVVVLLAAFLL------ 410 410
TraesCS1B02G285400.1 LFYPNGTSVYDLGFGGASFGPSSPTASGFSASSKPT--MPFPVGVVVLLAAFLL------ 401 401
TraesCS1B02G285400.2 LFYPNGTSVYDLGFGGASFGPSSPTASGFSASSKPTLQMPFPVGVVVLLAAFLL------ 411 411
TraesCS3B02G278400.1 LFYPDGTFVYNVGLRGYLPPMADSQGA--RQ-VRFL-DWLAR-SAHAYAFT--------- 393 393
TraesCS3D02G249500.2 LFYPDGTFVYNVGLRGYLPPMADSQGA--RQ-AVHV-ILLIAIATVAFALS--------- 394 394
TraesCS3A02G249500.1 LFYPDGTFVYNVGLRGYLPPMADSQGA--RQ-AVHV-ILLIAMATVAFALS--------- 292 292
TraesCS3D02G249500.1 LFYPDGTFVYNVGLRGYLPPMDESDAT--RT-VRPF-RLRLP-RFCKFVANFLNVDHTSS 341 364
TraesCS2D02G292500.1 LFYPDGTFVYNVGLRGYLPPMDESDAT--RT-AIHF-LALIALAFVTLVLS--------- 390 391
TraesCS2B02G311200.1 LFYPDGTFVYNVGLRGYLPPMDESDAT--RT-AIHF-LALIALAFVTLVLS--------- 391 528
TraesCS2B02G311200.2 LFYPDGTFVYNVGLRGYLPPMDESDAT--RT-AIHF-LALIALAFVTLVLS--------- 390 357
TraesCS2D02G292500.2 LFYPDGTFVYDVGLRGYLPPMDESDAT--RT-VRPA-LRDPSL---------------- 381 381
TraesCS2A02G294700.1 LFYPDGTFVYDVGLRGYLPPMDESDAT--RT-AIHL-LALIALAFVALVLS--------- 390 390
TraesCS2A02G294700.2 LFYPDGTFVYDVGLRGYLPPMDESDAT--RT-AIHL-LALIALAFVALVLS--------- 389 389

Figure 6.11 – Alignment of M1/M2 wheat protein orthologs. Green boxes indicate areas of similarity, five amino acids or more. '*' a single conserved residue, ':' conservation between groups with strongly similar properties, '.' Conservation between groups of weakly similar properties. Regions at the beginning and end of the alignment are not shown as there are few to no matches – bold numbers represent the total length of each gene. Alignment was carried out using the Clustal Omega software (Table 6.1).

M2 was determined to be 392aa in length and similarly to M1 is part of the glycosyl hydrolase family I. M2 was aligned to wheat gene, *TraesCS3B02G278400.1,* on chromosome three in the B genome (gene structure can be found in the Appendix 30). The alignment analysis for M2 was equal to that for M1 and can be viewed in Fig. 6.11 and Appendix 29 (phylogenetic tree). The wheat gene expression atlas demonstrated *TraesCS3B02G278400.1* has two homoeologues which are splice variants of one another, *TraesCS3D02G249500.1* and *TraesCS3D02G249500.2,* both of which are situated in the D genome. Unlike *TraesCS2D02G292500.1* (M1), which displayed highest expression in the leaf and shoot, *TraesCS3B02G278400.1*, exhibited highest expression in the roots, as did the homoeologues *TraesCS3D02G249500.2*; *TraesCS3D02G249500.1,* showing low to no expression across all treatments. These results can be seen in Fig. 6.12.

Structural characterisation of TraesCS3B02G278400.1 was similar to that of *At*BG_PPAP and TraesCS2D02G292500.1, possessing a GH-17 domain, a signal peptide from nucleotides 1-22 and a single TMD – Fig. 6.9. However, the TMD was shown to occur at the beginning of the protein sequence in this case. Protein localisation prediction was not conclusive (Appendix 31).

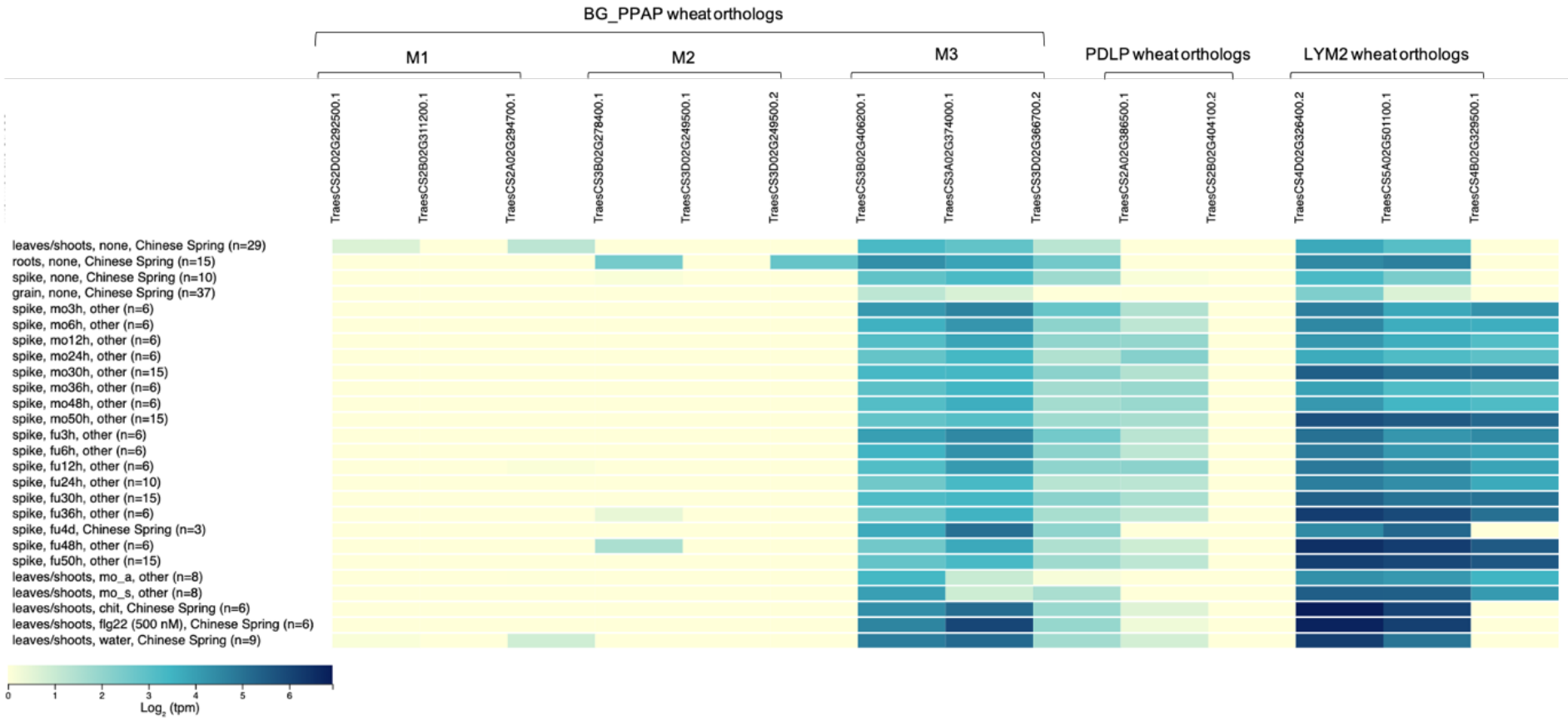
BG_PPAP wheat orthologs
M1
M2
M3
PDLP wheat orthologs
LYM2 wheat orthologs
TraesCS2D02G292500.1
TraesCS2B02G311200.1
TraesCS2A02G294700.1
TraesCS3B02G278400.1
TraesCS3D02G249500.1
TraesCS3D02G249500.2
TraesCS3B02G406200.1
TraesCS3A02G374000.1
TraesCS3D02G366700.2
TraesCS2A02G386500.1
TraesCS2B02G404100.2
TraesCS4D02G326400.2
TraesCS5A02G501100.1
TraesCS4B02G329500.1
leaves/shoots, none, Chinese Spring (n=29)
roots, none, Chinese Spring (n=15)
spike, none, Chinese Spring (n=10)
grain, none, Chinese Spring (n=37)
spike, mo3h, other (n=6)
spike, mo6h, other (n=6)
spike, mo12h, other (n=6)
spike, mo24h, other (n=6)
spike, mo30h, other (n=15)
spike, mo36h, other (n=6)
spike, mo48h, other (n=6)
spike, mo50h, other (n=15)
spike, fu3h, other (n=6)
spike, fu6h, other (n=6)
spike, fu12h, other (n=6)
spike, fu24h, other (n=10)
spike, fu30h, other (n=15)
spike, fu36h, other (n=6)
spike, fu4d, Chinese Spring (n=3)
spike, fu48h, other (n=6)
spike, fu50h, other (n=15)
leaves/shoots, mo_a, other (n=8)
leaves/shoots, mo_s, other (n=8)
leaves/shoots, chit, Chinese Spring (n=6)
leaves/shoots, flg22 (500 nM), Chinese Spring (n=6)
leaves/shoots, water, Chinese Spring (n=9)
0
1
2
3
4
5
6
Log2 (tpm)

Figure 6.12 – Wheat gene expression heatmap for *AtBG_PPAP, AtPDLP and AtLYM2*, wheat orthologs. Data is shown for *AtBG_PPAP* (M1, M2 and M3), *AtPDLP* and *AtLYM2* wheat orthologs and their homoeologues. The left column details experimental conditions from which the expression data was taken, from left to right: high tissue level, stress-disease, high-level variety and sample size. The cultivars selected include: Chinese spring (CS) and Other (this includes Bobwhite, however most disease experiments were carried out in a range of cultivars). Important abbreviations/acronyms:, mo (when followed by a timestamp) = mock inoculation; fu = *Fusarium graminearum*; mo_a = *Magnaporthe oryzae* asymptomatic; mo_s = *Magnaporthe oryzae* symptomatic; chit = chitin; h = hour; d = day. This heatmap was created using the wheat gene expression atlas as detailed in Table 6.1.

The final β-1,3-glucanase wheat ortholog candidate M3, was a 405 aa unnamed protein product from the glycosyl hydrolase family 1. The wheat gene which most closely matched M3 was *TraesCS3B02G406200.1* on chromosome three (gene structure can be found in the Appendix 30). An alignment of the most closely matched sequences revealed 10 regions, of five bases or more, with high levels of sequence similarity (Fig. 6.13 and Appendix 32). *TraesCS3A02G374000.1* and *TraesCS3D02G366700.2* were identified as homoeologues to *TraesCS3B02G406200.1*, both of which reside on chromosome three in the A and D genomes respectively, with *TraesCS3B02G406200.1* being on the B genome. The expression for *TraesCS3B02G406200.1* is much greater than for the other two orthologs and is seen to be highest in the leaves and shoots with

some expression in the spike. The homoeologue, *TraesCS3D02G366700.2*, shows lower levels of expression. Gene expression levels do not seem to change significantly in response to pathogen invasion. However, *TraesCS3A02G374000.1* is more highly expressed in response to flg22 and chitin than tissue without infection, suggesting a possible response to pathogenic invasion (as seen in Fig. 6.12). The gene expression pattern seen here is substantially different from the ones seen for *TraesCS2D02G292500.1* (M1) and *TraesCS3B02G278400.*1 (M2).

As seen for *At*BG_PPAP, TraesCS2D02G292500.1 and TraesCS3B02G278400.1, TraesCS3B02G406200.1 contained a GH-17 domain, a single TMD and a signal peptide spanning from nucleotides 1-16 (Fig. 6.9). Protein localisation prediction was inconclusive (Appendix 31).

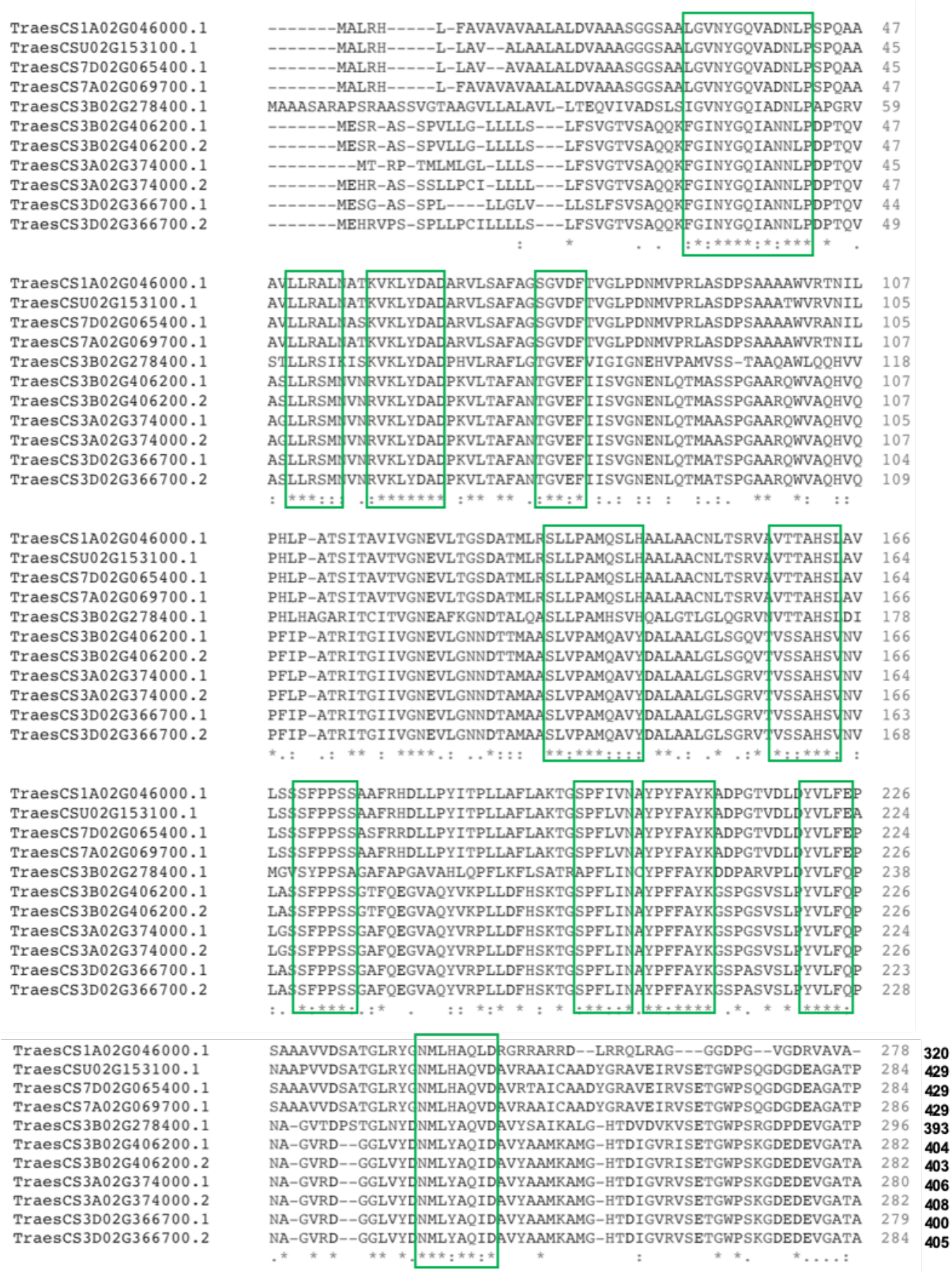
TraesCS1A02G046000.1 -------MALRH-----L-FAVAVAVAALALDVAAASGGSAALGVNYGQVADNLPSPQAA 47
TraesCSU02G153100.1 -------MALRH-----L-LAV--ALAALALDVAAAGGGSAALGVNYGQVADNLPSPQAA 45
TraesCS7D02G065400.1 -------MALRH-----L-LAV--AVAALALDVAAASGGSAALGVNYGQVADNLPSPQAA 45
TraesCS7A02G069700.1 -------MALRH-----L-FAVAVAVAALALDVAAASGGSAALGVNYGQVADNLPSPQAA 47
TraesCS3B02G278400.1 MAAASARAPSRAASSVGTAAGVLLALAVL-LTEQVIVADSLSIGVNYGQIADNLPAPGRV 59
TraesCS3B02G406200.1 -------MESR-AS-SPVLLG-LLLLS---LFSVGTVSAQQKFGINYGQIANNLPDPTQV 47
TraesCS3B02G406200.2 -------MESR-AS-SPVLLG-LLLLS---LFSVGTVSAQQKFGINYGQIANNLPDPTQV 47
TraesCS3A02G374000.1 ---------MT-RP-TMLMLGL-LLLS---LFSVGTVSAQQKFGINYGQIANNLPDPTQV 45
TraesCS3A02G374000.2 -------MEHR-AS-SSLLPCI-LLLL---LFSVGTVSAQQKFGINYGQIANNLPDPTQV 47
TraesCS3D02G366700.1 -------MESG-AS-SPL----LLGLV---LLSLFSVSAQQKFGINYGQIANNLPDPTQV 44
TraesCS3D02G366700.2 -------MEHRVPS-SPLLPCILLLLS---LFSVGTVSAQQKFGINYGQIANNLPDPTQV 49
TraesCS1A02G046000.1 AVLLRALNATKVKLYDADARVLSAFAGSGVDFTVGLPDNMVPRLASDPSAAAAWVRTNIL 107
TraesCSU02G153100.1 AVLLRALNATKVKLYDADARVLSAFAGSGVDFTVGLPDNMVPRLASDPSAAATWVRVNIL 105
TraesCS7D02G065400.1 AVLLRALNASKVKLYDADARVLSAFAGSGVDFTVGLPDNMVPRLASDPSAAAAWVRANIL 105
TraesCS7A02G069700.1 AVLLRALNATKVKLYDADARVLSAFAGSGVDFTVGLPDNMVPRLASDPSAAAAWVRTNIL 107
TraesCS3B02G278400.1 STLLRSIKISKVKLYDADPHVLRAFLGTGVEFVIGIGNEHVPAMVSS-TAAQAWLQQHVV 118
TraesCS3B02G406200.1 ASLLRSMNVNRVKLYDADPKVLTAFANTGVEFIISVGNENLQTMASSPGAARQWVAQHVQ 107
TraesCS3B02G406200.2 ASLLRSMNVNRVKLYDADPKVLTAFANTGVEFIISVGNENLQTMASSPGAARQWVAQHVQ 107
TraesCS3A02G374000.1 AGLLRSMNVNRVKLYDADPKVLTAFANTGVEFIISVGNENLQTMAASPGAARQWVAQHVQ 105
TraesCS3A02G374000.2 AGLLRSMNVNRVKLYDADPKVLTAFANTGVEFIISVGNENLQTMAASPGAARQWVAQHVQ 107
TraesCS3D02G366700.1 ASLLRSMNVNRVKLYDADPKVLTAFANTGVEFIISVGNENLQTMATSPGAARQWVAQHVQ 104
TraesCS3D02G366700.2 ASLLRSMNVNRVKLYDADPKVLTAFANTGVEFIISVGNENLQTMATSPGAARQWVAQHVQ 109
TraesCS1A02G046000.1 PHLP-ATSITAVIVGNEVLTGSDATMLRSLLPAMQSLHAALAACNLTSRVAVTTAHSLAV 166
TraesCSU02G153100.1 PHLP-ATSITAVTVGNEVLTGSDATMLRSLLPAMQSLHAALAACNLTSRVAVTTAHSLAV 164
TraesCS7D02G065400.1 PHLP-ATSITAVTVGNEVLTGSDATMLRSLLPAMQSLHAALAACNLTSRVAVTTAHSLAV 164
TraesCS7A02G069700.1 PHLP-ATSITAVTVGNEVLTGSDATMLRSLLPAMQSLHAALAACNLTSRVAVTTAHSLAV 166
TraesCS3B02G278400.1 PHLHAGARITCITVGNEAFKGNDTALQASLLPAMHSVHQALGTLGLQGRVNVTTAHSLDI 178
TraesCS3B02G406200.1 PFIP-ATRITGIIVGNEVLGNNDTTMAASLVPAMQAVYDALAALGLSGQVTVSSAHSVNV 166
TraesCS3B02G406200.2 PFIP-ATRITGIIVGNEVLGNNDTTMAASLVPAMQAVYDALAALGLSGQVTVSSAHSVNV 166
TraesCS3A02G374000.1 PFLP-ATRITGIIVGNEVLGNNDTAMAASLVPAMQAVYDALAALGLSGRVTVSSAHSVNV 164
TraesCS3A02G374000.2 PFLP-ATRITGIIVGNEVLGNNDTAMAASLVPAMQAVYDALAALGLSGRVTVSSAHSVNV 166
TraesCS3D02G366700.1 PFIP-ATRITGIIVGNEVLGNNDTAMAASLVPAMQAVYDALAALGLSGRVTVSSAHSVNV 163
TraesCS3D02G366700.2 PFIP-ATRITGIIVGNEVLGNNDTAMAASLVPAMQAVYDALAALGLSGRVTVSSAHSVNV 168
TraesCS1A02G046000.1 LSSSFPPSSAAFRHDLLPYITPLLAFLAKTGSPFIVNAYPYFAYKADPGTVDLDYVLFEP 226
TraesCSU02G153100.1 LSSSFPPSSAAFRHDLLPYITPLLAFLAKTGSPFLVNAYPYFAYKADPGTVDLDYVLFEA 224
TraesCS7D02G065400.1 LSSSFPPSSASFRRDLLPYITPLLAFLAKTGSPFLVNAYPYFAYKADPGTVDLDYVLFEP 224
TraesCS7A02G069700.1 LSSSFPPSSAAFRHDLLPYITPLLAFLAKTGSPFLVNAYPYFAYKADPGTVDLDYVLFEP 226
TraesCS3B02G278400.1 MGVSYPPSAGAFAPGAVAHLQPFLKFLSATRAPFLINCYPFFAYKDDPARVPLDYVLFQP 238
TraesCS3B02G406200.1 LASSFPPSSGTFQEGVAQYVKPLLDFHSKTGSPFLINAYPFFAYKGSPGSVSLPYVLFQP 226
TraesCS3B02G406200.2 LASSFPPSSGTFQEGVAQYVKPLLDFHSKTGSPFLINAYPFFAYKGSPGSVSLPYVLFQP 226
TraesCS3A02G374000.1 LGSSFPPSSGAFQEGVAQYVRPLLDFHSKTGSPFLINAYPFFAYKGSPGSVSLPYVLFQP 224
TraesCS3A02G374000.2 LGSSFPPSSGAFQEGVAQYVRPLLDFHSKTGSPFLINAYPFFAYKGSPGSVSLPYVLFQP 226
TraesCS3D02G366700.1 LASSFPPSSGAFQEGVAQYVRPLLDFHSKTGSPFLINAYPFFAYKGSPASVSLPYVLFQP 223
TraesCS3D02G366700.2 LASSFPPSSGAFQEGVAQYVRPLLDFHSKTGSPFLINAYPFFAYKGSPASVSLPYVLFQP 228
TraesCS1A02G046000.1 SAAAVVDSATGLRYGNMLHAQLDRGRRARRD--LRRQLRAG---GGDPG--VGDRVAVA- 278 320
TraesCSU02G153100.1 NAAPVVDSATGLRYGNMLHAQVDAVRAAICAADYGRAVEIRVSETGWPSQGDGDEAGATP 284 429
TraesCS7D02G065400.1 SAAAVVDSATGLRYGNMLHAQVDAVRTAICAADYGRAVEIRVSETGWPSQGDGDEAGATP 284 429
TraesCS7A02G069700.1 SAAAVVDSATGLRYGNMLHAQVDAVRAAICAADYGRAVEIRVSETGWPSQGDGDEAGATP 286 429
TraesCS3B02G278400.1 NA-GVTDPSTGLNYDNMLYAQVDAVYSAIKALG-HTDVDVKVSETGWPSRGDPDEVGATP 296 393
TraesCS3B02G406200.1 NA-GVRD--GGLVYDNMLYAQIDAVYAAMKAMG-HTDIGVRISETGWPSKGDEDEVGATA 282 404
TraesCS3B02G406200.2 NA-GVRD--GGLVYDNMLYAQIDAVYAAMKAMG-HTDIGVRISETGWPSKGDEDEVGATA 282 403
TraesCS3A02G374000.1 NA-GVRD--GGLVYDNMLYAQIDAVYAAMKAMG-HTDIGVRVSETGWPSKGDEDEVGATA 280 406
TraesCS3A02G374000.2 NA-GVRD--GGLVYDNMLYAQIDAVYAAMKAMG-HTDIGVRVSETGWPSKGDEDEVGATA 282 408
TraesCS3D02G366700.1 NA-GVRD--GGLVYDNMLYAQIDAVYAAMKAMG-HTDIGVRVSETGWPSKGDEDEVGATA 279 400
TraesCS3D02G366700.2 NA-GVRD--GGLVYDNMLYAQIDAVYAAMKAMG-HTDIGVRVSETGWPSKGDEDEVGATA 284 405

Figure 6.13 – Alignment of the M3 wheat protein orthologs. Green boxes indicate areas of similarity, five amino acids or more. '*' a single conserved residue, ':' conservation between groups with strongly similar properties, '.' Conservation between groups of weakly similar properties. Regions at the end of the alignment are not shown as there are few to no matches – bold numbers represent the total length of each gene. Alignment was carried out using the Clustal Omega software (Table 6.1).

6.3.2.2 AtPDLP1 and AtPDLP5

Firstly, an alignment of PDLP1-8 was performed – results shown in Fig. 6.14 (the phylogenetic tree for this can be seen in Appendix 33). Across all 8 proteins there were few regions of similarity, those that did occur were only a few amino acids long.

```
PDLP8      -----MRRLFL---FSLLFLFFYS--SSSSRSSSESHIFIYGGCSPEKYT---------- 40
PDLP5      --------MIKTKTTSLLCFLLTAVILMNPSSSSPTDNYIYAVCSPAKFS---------- 42
PDLP6      --------MFAT--KTVLFIAVVSLL--GTFSSAAVDTFIYGGCSQEKYF---------- 38
PDLP7      MPMAKLRNIIKT--LSIFFFLIAATAPSLSSATSATDTFVFGGCSQQKFS---------- 48
PDLP4      ---MVVHLISLL--TQTLALIILSLPSIINTSQLDYDTLVFKQCDPLDANILQKATTKSP 55
PDLP1      ---------MKL--TYQFFIFWFFLPFFAISGDDDYKNLIFKGCANQKSP---------- 39
PDLP2      MGLSI--SFLSI--IMMMCLLFPDLNVVVKSATTEYTTLIYKGCARQQFS---------- 46
PDLP3      MGFYSLKQLLLL--YIIIMALFSDLK-LAKSSSPEYTNLIYKGCARQRLS---------- 47
                        :            .       ::  *

PDLP8      -----PNTPFESNRDTFLSSVVTSSSDASFNSFAVGNDSSSSSSSSAVFGLYQCRDDLRS 95
PDLP5      -----PSSGYETNLNSLLSSFVTSTAQTRYANFTVPTGK--PEPTVTVYGIYQCRGDLDP 95
PDLP6      -----PGSPYESNVNSLLTSFVSSASLYTYNNFTTN-GI--SGDSSSVYGLYQCRGDLSS 90
PDLP7      -----PASAYESNLNSLLTSLVNSATYSSYNNFTIM-GS--SS-SDTARGLFQCRGDLSM 99
PDLP4      NYSNQNLFLRAQALSSFLRKLESESSRSKFLKTLVGNE------KHAVSGWFQCREDYPS 109
PDLP1      ----DPTGVFSQNLKNLFTSLVSQSSQSSFASVTSGTDN-----TTAVIGVFQCRGDLQN 90
PDLP2      ----DPSGLYSQALSAMFGSLVSQSTKTRFYKTTTGTS------TTTITGLFQCRGDLSN 96
PDLP3      ----DPSGLYSQALSAMYGLLVTQSTKTRFYKTTTGTTS-----QTSVTGLFQCRGDLSN 98
                      . :   . ..::   : .             :  * :*** *

PDLP8      --SDCSKCIQTSVDQITLICPY------SYGASLQLEGCFLRYETNDFLGK--------- 138
PDLP5      --TACSTCVSSAVAQVGALCSN------SYSGFLQMENCLIRYDNKSFLGV--------- 138
PDLP6      GSGDCARCVARAVSRLGSLCAM------ASGGALQLEGCFVKYDNTTFLGV--------- 135
PDLP7      --PDCATCVARAVSQVGPLCPF------TCGGALQLAGCYIKYDNISFLGQ--------- 142
PDLP4      --EICHKCVGDLREISSRSCGN------ATSARIHLRGCHLIYKFERIDTPGAQVNNHHK 161
PDLP1      --AQCYDCVSKIPKLVSKLCGGGRDDGNVVAARVHLAGCYIRYESSGFRQT--------- 139
PDLP2      --HDCYNCVSRLPVLSDKLCGK------TIASRVQLSGCYLLYEVSGFSQI--------- 139
PDLP3      --NDCYNCVSRLPVLSGKLCGK------TIAARVQLSGCYLLYEISGFAQI--------- 141
               *  *:          *          .. ::: .* : *.   :
```

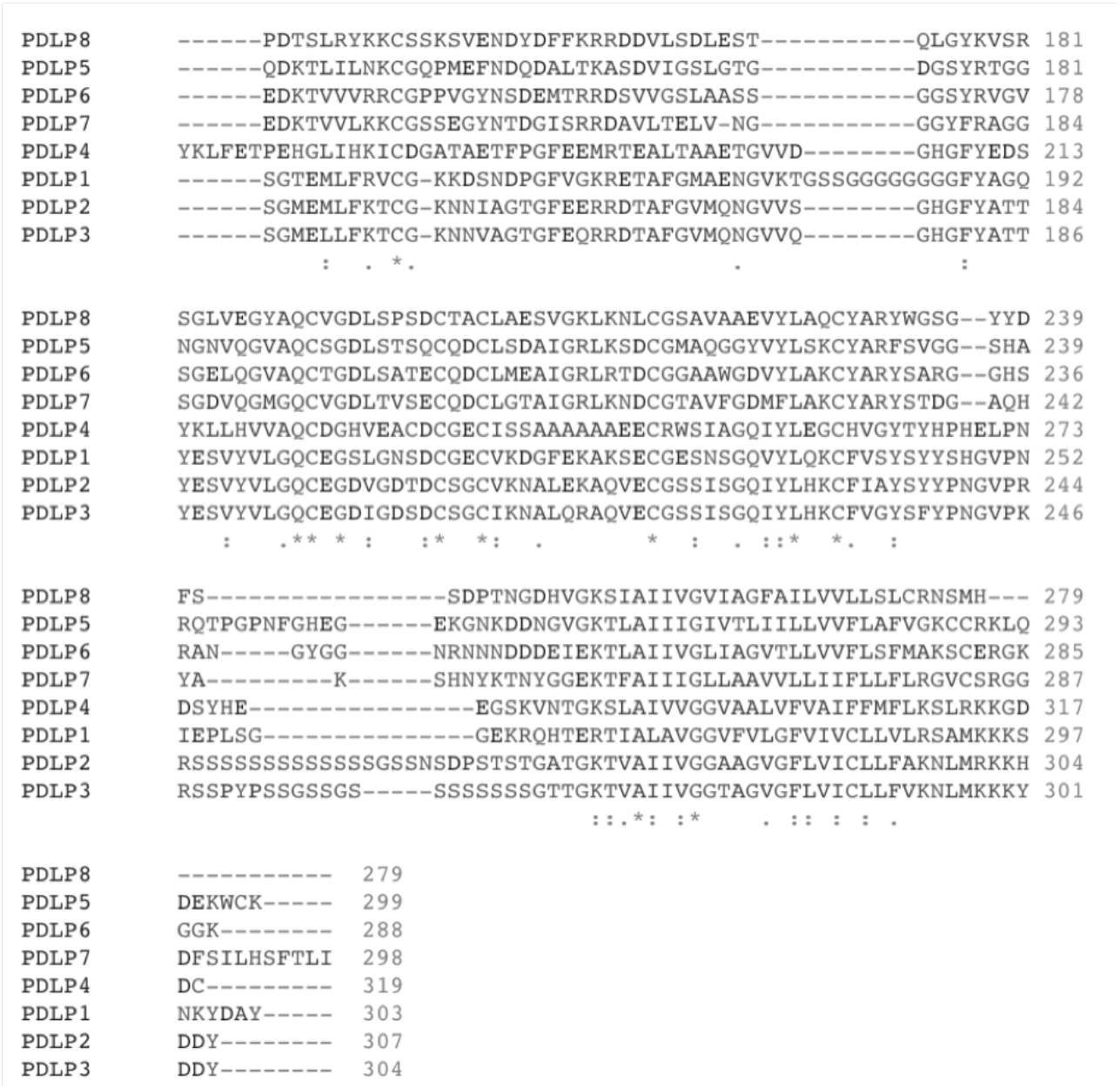

Figure 6.14 – Alignment of the *At*PDLP proteins. '*' a single conserved residue, ':' conservation between groups with strongly similar properties, '.' Conservation between groups of weakly similar properties. Alignment was carried out using the Clustal Omega software (Table 6.1).

Both *At*PDLP1 and *At*PDLP5 are structurally and functionally similar. Both tertiary protein structures contain two salt stress/antifungal GNK2 (Ginkbilobin 2) domains, one TMD, and a predicted signal peptide – Fig. 6.15**.** Protein localisation prediction was inconclusive (Appendix 26).

*At*PDLP1 and *At*PDLP5 were aligned with the *T. aestivum* proteome to identify wheat orthologs (Appendix 34). For both searches the top match was the same (with a higher identity match to *At*PDLP5) – accession number SPT19226.1 – and was identified as an unnamed protein product, this was the only protein investigated further. When SPT19226.1 was aligned back against the *A. thaliana* genome, the top protein match that came back was PDLP8. This was not completely unexpected as these genes are all structurally similar. PDLP1 and PDLP5 were pursued as they are the only PDLP's to have been investigated in the literature.

In addition to investigating the PDLP1 and PDLP5 wheat orthologs as VIGS candidates, rice and barley orthologs were also explored to confirm the alignment results above. For PDLP1 one rice ortholog – Os03g0149500 – was identified. Alignment of *At*PDLP1 sequence against all rice cultivar proteomes, also identified this rice ortholog. When Os03g0149500 was compared to the *A. thaliana* proteome it was most similar to *At*PDLP3. Finally, when Os03g0149500 was aligned against *T. aestivum*, the top result was for SPT19226.1 as seen previously for *A. thaliana* and *T. aestivum*. A barley, cysteine-rich repeat secretory protein 3-like protein (KAE8766664.1) was found to be the most likely ortholog. When aligned to the *A. thaliana* proteome, the highest match was PDLP2. In turn the barley ortholog was aligned against the wheat proteome,

where the most similar sequence was to that of a hypothetical protein – the barley ortholog was therefore not conclusive. All results can be found in Appendix 27.

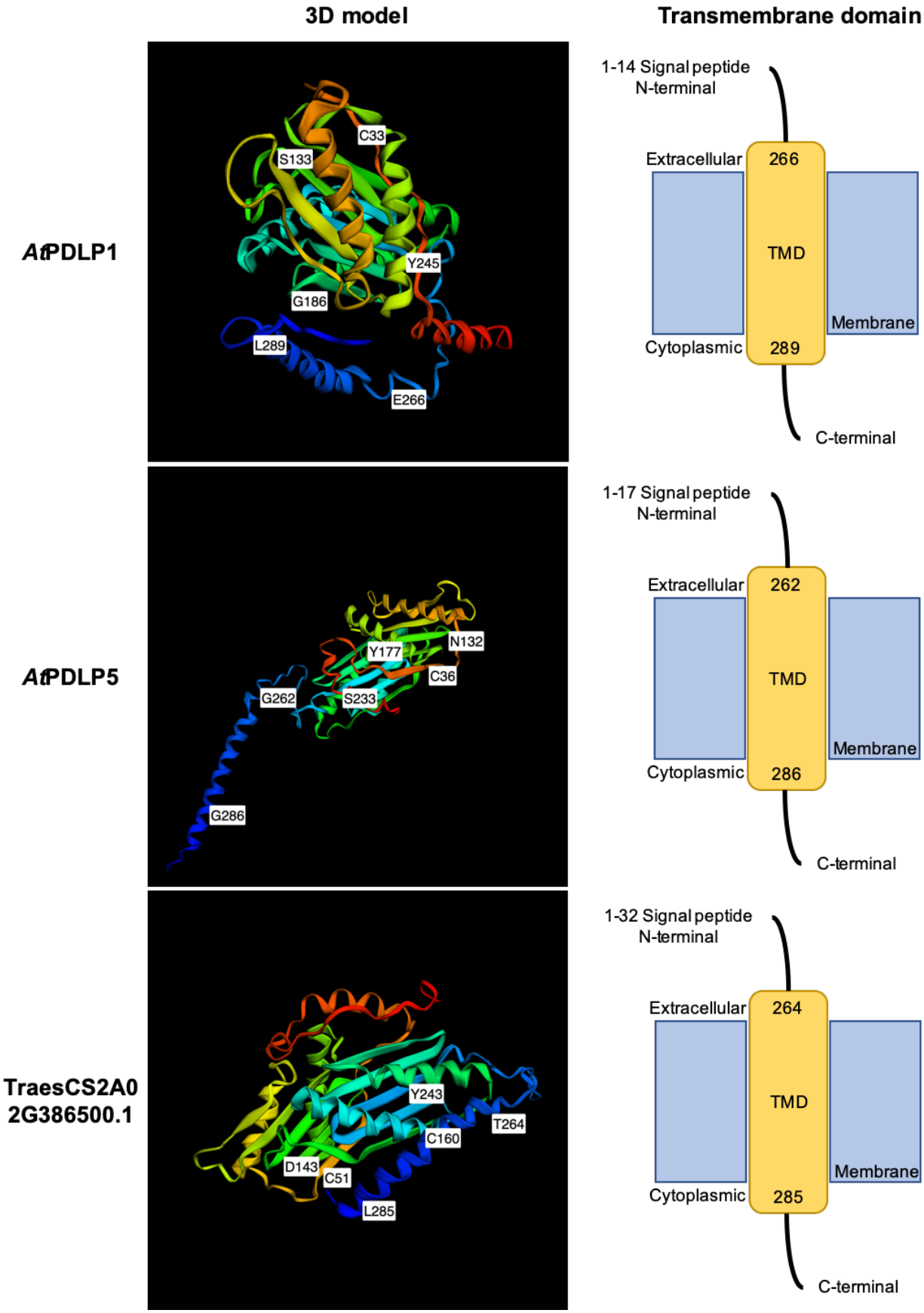

Figure 6.15 – Predicted protein structure for *At*PDLP1, *At*PDLP5 and predicted wheat ortholog. Transmembrane domain (TMD) nucleotide positions can be seen on the 3D model (left) and correspond to the TMD diagram (right), the other values referenced on the 3D model correspond with the position of the two salt stress/antifungal GNK2 domains. Proteins were modelled using Phyre[2] (Table 6.1). 3D model colours from red to blue (rainbow) indicate the structure from the N (red) to C-terminus (blue).

This same process was then used for PDLP5. Two rice proteins were identified as potential orthologs – Os02g0734800 and Os06g0253600. Comparative alignments demonstrated Os02g0734800 and Os06g0253600 were very similar and matched closely with the PDLP5 protein sequence. When aligned against *A. thaliana,* Os02g0734800 and Os06g0253600 matched PDLP7 and PDLP6 most closely, respectively. In wheat these rice orthologs both matched to SPT19226.1, as seen for *A. thaliana,* and *T. aestivum*. In barley, the closest possible ortholog was determined to be a cysteine-rich repeat secretory protein 15-like protein (KAE8794631.1). When aligned against the *A. thaliana* proteome the closest match was PDLP8. As seen for PDLP1, when the barley ortholog was aligned against the *T. aestivum* genome, the most similar sequence was to that of a hypothetical protein. An alignment of the *At*PDLP1 and *At*PDLP5 proteins with the rice and barley orthologs can be seen in Fig. 6.16 and Fig. 6.17 respectively (phylogenetic trees for this analysis can be found in Appendices 36 and 37). As for the *At*PDLP alignment there are few areas of sequence similarity (Fig. 6.14).

Figure 6.16 – Alignment of the *At*PDLP1, wheat, rice and barley orthologs. Barley ortholog = KAE8766664.1, rice = Os03g0140500, wheat = SPT19226.1. Green boxes indicate areas of similarity, five amino acids or more. '*' a single conserved residue, ':' conservation between groups with strongly similar properties, '.' Conservation between groups of weakly similar properties. Alignment was carried out using the Clustal Omega software (Table 6.1).

Figure 6.17 – Alignment of the *At*PDLP5, wheat, rice and barley orthologs. Barley ortholog = KAE8794631.1, rice = Os02g0734800 and Os06g0253600, wheat = SPT19226.1. Green boxes indicate areas of similarity, five amino acids or more. '*' a single conserved residue, ':' conservation between groups with strongly similar properties, '.' Conservation between groups of weakly similar properties. Alignment was carried out using the Clustal Omega software (Table 6.1).

The *AtP*DLP wheat gene ortholog, SPT19226.1, is an unnamed protein product and is 292 aa in length. The closest wheat gene corresponding to this protein was identified as *TraesCS2A02G386500.1*, on chromosome two (gene structure can be seen in Appendix 35). An alignment of the top BLASTP matches was then carried out and areas of conservation were identified– these are detailed in Fig. 6.18 (the phylogenetic tree for this analysis can be found in Appendix 38).

Analysing wheat gene expression demonstrated the homoeologue of *TraesCS2A02G386500.1* to be *TraesCS2B02G404100.2*, another candidate from chromosome 2 (B genome). However, in comparison to *TraesCS2A02G386500.1*, this homoeologue was lowly expressed, if at all, in all tissues/conditions. Overall, *TraesCS2A02G386500.1* was expressed at similar levels in response to disease, little or no expression could be seen in the tissues without infection. These results can be seen in Fig. 6.12.

Like PDLP1 and PDLP5, TraesCS2A02G386500.1 is shown to have two salt stress/antifungal GNK2 domains, a single TMD and a signal peptide (Fig. 6.15). Protein localisation prediction was inconclusive (Appendix 31).


traesCS6B02G286000.1 -------MPCYCLGHCLTQSPMPQLRALVAITLLLHLHAAPTAVAQAATGAFIYAGCSPS 53
traesCS6D02G220800.1 ----------MPQLRALVAITLLLHLHAAPTAVAQAATGAFIYAGCSPS 39
traesCS6D02G220800.2 ----------MPQLRALVAITLLLHLHAAPTAVAQAATGAFIYAGCSPS 39
traesCS6D02G220800.3 ----------MPQLRALVAITLLLHLHAAPTAVAQAATGAFIYAGCSPS 39
traesCS2A02G386500.1 MCTFVSPSSAMHLRSQLRRGRVA----AAAAAAILLVIGLGAGFTGADTDTFIYAGCSPS 56
traesCS2B02G404100.1 MCKFVSSSSAMHLGNQLRRGRAA----DAAVAVALLVIGLAAGFTGADTDTFIYAGCSPS 56
traesCS2B02G404100.2 ----------MHLGNQLRRGRAA----DAAVAVALLVIGLAAGFTGADTDTFIYAGCSPS 46
traesCS2B02G404100.3 ----------MHLGNQLRRGRAA----DAAVAVALLVIGLAAGFTGADTDTFIYAGCSPS 46
traesCS6B02G286000.1 KYERDTAFQSNLASLLASIASTASSGATYNSFTAGGGVGQAEAVRTAAYGLYQCRGDLSR 113
traesCS6D02G220800.1 KYERDTAFQSNLDSLLASIASTASSGATYNSFTAGGGVGQAEAARTAAYGLYQCRGDLSR 99
traesCS6D02G220800.2 KYERDTAFQSNLDSLLASIASTASSGATYNSFTAGGGVGQAEAARTAAYGLYQCRGDLSR 99
traesCS6D02G220800.3 KYERDTAFQSNLDSLLASIASTASSGATYNSFTAGGGVGQAEAARTAAYGLYQCRGDLSR 99
traesCS2A02G386500.1 KYQPGTPYEGNLKSLLASITDAAP-NAAYSSFANGTGDG------AAAYGLYQCRGDLGN 109
traesCS2B02G404100.1 KYQPGTPYEGNLKSLLASITNTAP-NAAYSSFANGTGDGG-----AAAYGLYQCRGDLGN 110
traesCS2B02G404100.2 KYQPGTPYEGNLKSLLASITNTAP-NAAYSSFANGTGDGG-----AAAYGLYQCRGDLGN 100
traesCS2B02G404100.3 KYQPGTPYEGNLKSLLASITNTAP-NAAYSSFANGTGDGG-----AAAYGLYQCRGDLGN 100
traesCS6B02G286000.1 GECVACVRETVARLGAVCANSYAASLQVDGCYVRYDASDFVGRADNTVAYRKCSSSSSED 173
traesCS6D02G220800.1 GECVSCVRETVARLGAVCANSYAASLQVDGCYVRYDASDFVGRADNTVAYRKCSSGSSED 159
traesCS6D02G220800.2 GECVSCVRETVARLGAVCANSYAASLQVDGCYVRYDASDFVGRADNTVAYRKCSSGSSED 159
traesCS6D02G220800.3 GECVSCVRETVARLGAVCANSYAASLQVDGCYVRYDASDFVGRADNTVAYRKCSSGSSED 159
traesCS2A02G386500.1 AECAACVRDALAQLGQVCPGAYAASLQLEGCYVRYDGTNFVGRPDTAMVYRKCSASTSAD 169
traesCS2B02G404100.1 GECAACVRDALAQLGQVCPGAYAASLQLEGCYVRYDGTNFVGRPDTAMVYRKCSASTSAD 170
traesCS2B02G404100.2 GECAACVRDALAQLGQVCPGAYAASLQLEGCYVRYDGTNFVGRPDTAMVYRKCSASTSAD 160
traesCS2B02G404100.3 GECAACVRDALAQLGQVCPGAYAASLQLEGCYVRYDGTNFVGRPDTAMVYRKCSASTSAD 160
traesCS6B02G286000.1 AGFLKSRDAVLRELQAQAATGYKLTASGTVQGVAQCLGDIAAPDCAACLAQAVVQLKGTC 233
traesCS6D02G220800.1 AGFLKSRDAVLRELQARAATGYKLTGSGTVQGVAQCLGDIAAPDCTACLAQAVVQLKGTC 219
traesCS6D02G220800.2 AGFLKSRDAVLRELQARAATGYKLTGSGTVQGVAQCLGDIAAPDCTACLAQAVVQLKGTC 219
traesCS6D02G220800.3 AGFLKSRDAVLRELQARAATGYKLTGSGTVQGVAQCLGDIAAPDCTACLAQAVVQLKGTC 219
traesCS2A02G386500.1 AGFLRDRDAVLGALQAAAADGYRVGSSGSVQGVSQCLGDLAAADCTGCLAQAVGQLKGAC 229
traesCS2B02G404100.1 AGFLRDRDAVLGALQA-AADGYRVGSSGSVQGVSQCLGDLAAADCTACLAQAVGQLTGAC 229
traesCS2B02G404100.2 AGFLRDRDAVLGALQA-AADGYRVGSSGSVQGVSQCLGDLAAADCTACLAQAVGQLTGAC 219
traesCS2B02G404100.3 AGFLRDRDAVLGALQA-AADGYRVGSSGSVQGVSQCLGDLAAADCTACLAQAVGQLTGAC 219
traesCS6B02G286000.1 GSALAADVYLEQCYVKYWQNGHDFRSSQ-DYSGDEFGRTVAIIIGILAGLALLVVFISFL 292
traesCS6D02G220800.1 GSALAADVYLEQCYVKYWQNGHDFRSSQ-DYSGDEFGRTVAIIIGILAGLALLVVFISFL 278
traesCS6D02G220800.2 GSALAADVYLEQCYVKYWQNGHDFRSSQ-DYSGDEFGRTVAIIIGILAGLALLVVFISFL 278
traesCS6D02G220800.3 GSALAADVYLEQCYVKYWQNGHDFRSSQ-DYSGDEFGRTVAIIIGILAGLALLVVFISFL 278
traesCS2A02G386500.1 GTALAADVHLAQCYVRYWASGYYFRPSQ-DYSQDDVGRTLAIIIGILAGLALIVVFISFL 288
traesCS2B02G404100.1 GTALAADVHLAQCYVRYWASGYYFRPSQ-DYSQDDVGRTLAIIIGILAGLALIVVFISFL 288
traesCS2B02G404100.2 GTALAADVHLAQCYVRYWASGYYFRPSQEDYSQDDVGRTLAIIIGILAGLALIVVFISFL 279
traesCS2B02G404100.3 GTALAADVHLAQCYVRYWASGYYFRPSQEDYSQDDVGRTLAIIIGILAGLALIVVFISFL 279
traesCS6B02G286000.1 TKAC---------- 296
traesCS6D02G220800.1 AKAC---------- 282
traesCS6D02G220800.2 AKA----------- 281
traesCS6D02G220800.3 AKACKSSKLCRGMQLLGFSQPSQEMRKTINQCSNAMQARNGSFCPYGPGYPQVAAH 334
traesCS2A02G386500.1 KKSC---------- 292
traesCS2B02G404100.1 KKSC---------- 292
traesCS2B02G404100.2 KKSCKGS------- 286
traesCS2B02G404100.3 KKSC---------- 283

Figure 6.18 – Alignment of the PDLP1/PDLP5 wheat protein orthologs. Green boxes indicate areas of similarity, five amino acids or more. '*' a single conserved residue, ':' conservation between groups with strongly similar properties, '.' Conservation between groups of weakly similar properties. Alignment was carried out using the Clustal Omega software (Table 6.1).

6.3.2.3 *At*LYM2

Structural analysis of *A*tLYM2 demonstrated this protein contains two LYSM domains, one TMD and a signal peptide, as seen in Fig. 6.19. Protein localisation prediction analysis was inconclusive (Appendix 26). *At*LYM2 was aligned against *At*LYM1 and *At*LYM3; only a few small areas of similarity could be identified – Fig. 6.20 (phylogenetic analysis can be found in Appendix 39).

Alignment of *At*LYM2 against the *T. aestivum* proteome identified the chitin elicitor binding protein, AIK22416.1, a partial sequence of 186 aa. However, when aligned back against the *A. thaliana* proteome the second match listed was the lysm domain GPI-anchored protein 2 precursor i.e. LYM2. This was therefore considered to be an accurate match and was determined to be the wheat CEBiP. (Results can be found in Appendix 40).

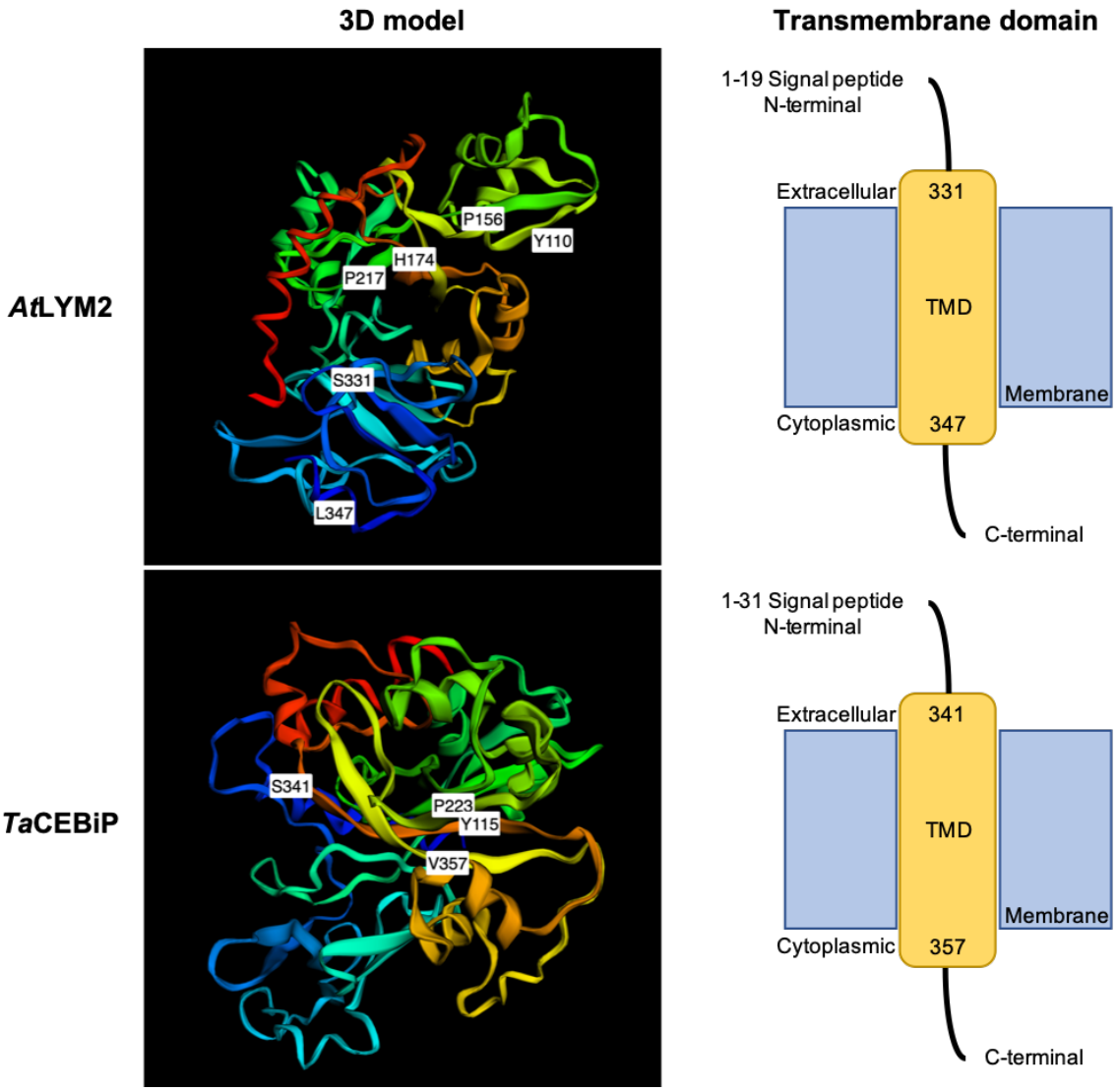

Figure 6.19 – Predicted protein structure for *At*LYM2 and predicted wheat ortholog. Transmembrane domain (TMD) nucleotide positions can be seen on the 3D model (left) and correspond to the TMD diagram (right), the other values referenced on the 3D model correspond with the position of the LYSM domain. Proteins were modelled using Phyre[2] (Table 6.1). 3D model colours from red to blue (rainbow) indicate the structure from the N (red) to C-terminus (blue).

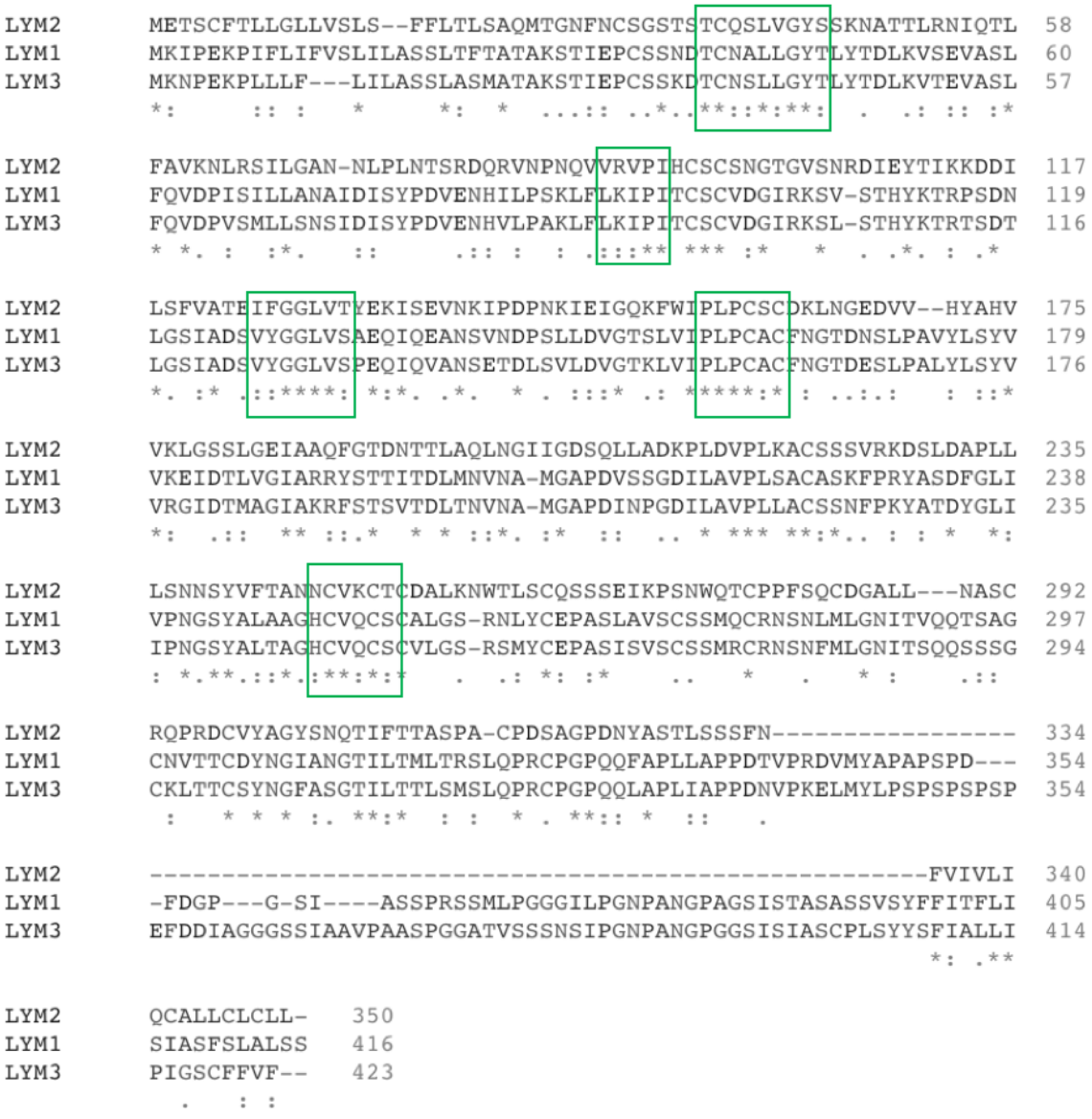

Figure 6.20 – Alignment of the *At*LYM protein family. Green boxes indicate areas of similarity, five amino acids or more. '*' a single conserved residue, ':' conservation between groups with strongly similar properties, '.' Conservation between groups of weakly similar properties. Alignment was carried out using the

To confirm the partial protein, AIK22416.1 is a possible wheat ortholog, homologs in rice and barley were also explored. Three rice homologs were identified: Os03g0133400, Os11g0548600 and Os09g0548200; for this analysis Os03g0133400 was used as it was previously determined to be the chitin elicitor binding protein (CEBiP). When aligned to the *A. thaliana* proteome, CEBiP identified with *At*LYM2 (LYM1 and LYM3 also shared some similarity). Finally, when aligned against the wheat genome the rice CEBiP protein matched most closely with the partial protein previously identified, AIK22416.1. Investigating barley *At*LYM2 homologs yielded similar results. The barley genome, when searched using the *At*LYM2 protein sequence, was shown to contain its own chitin elicitor binding protein, KAE8808384.1. An alignment between the *A. thaliana* genome and KAE8808384.1 revealed a match with *At*LYM2. Therefore, this partial protein was considered the best sequence to move forward with as a likely wheat ortholog. This alignment can be seen in Fig. 6.21 (with phylogenetic analysis in Appendix 41).

A *Ta*CEBiP protein had previously been identified in the literature, however as a result of expired databases and it not having been recorded in any new online databases that were open access, it was important this partial protein (AIK22416.1) was matched correctly to a gene in the *T. aestivum* genome. Aligning this protein fragment against the *T. aestivum* proteome identified 8 peptidoglycan-binding lysin subgroup domain containing proteins (projected from Os03g0133400), these first 8 matches were therefore aligned against one another. In the central regions of the alignment all sequences had high areas of similarity with variation at the N- and C-terminus as expected (Fig. 6.22 and Appendix 42).

Figure 6.21 – Alignment of the *At*LYM2, wheat, rice and barley orthologs. Barley ortholog = KAE8808384.1, rice = Os03g0133400, wheat = traesCS4D02G326400.2. Green boxes indicate areas of similarity, five amino acids or more. '*' a single conserved residue, ':' conservation between groups with strongly similar properties, '.' Conservation between groups of weakly similar properties. Alignment was carried out using the Clustal Omega software (Table 6.1).

Figure 6.22 – Alignment of LYM2 wheat protein orthologs. '*' a single conserved residue, ':' conservation between groups with strongly similar properties, '.' Conservation between groups of weakly similar properties. Regions at the beginning and end of the alignment are not shown as there are few to no matches – bold numbers represent the total length of each gene. Alignment was carried out using the Clustal Omega software (Table 6.1).

Using the phylogenetic tree (Appendix 42) produced alongside the alignment, AIK22416.1 is suggested to be closely related to *TraesCS4D02G326400.2*. To validate, AIK22416.1 was aligned to *TraesCS4D02G326400.2*, producing a 99.46% identity score. The *TraesCS4D02G326400.2* sequence has therefore been selected for further investigations and will now be referred to in this chapter as the *Ta*CEBiP. This gene is situated on chromosome 4 of the D genome (gene structure can be found in the Appendix 43).

Selecting data primarily from the hexaploid wheat cultivars Chinese Spring and Bobwhite the expression of the *Ta*CEBiP was investigated. Homoeologues were listed as *TraesCS5A02G501100.1* – chromosome 5, genome A – and *TraesCS4B02G329500.1* – chromosome 5, genome B. In general, *Ta*CEBiP was highly expressed, much more so than seen for the wheat BG_PPAP and PDLP orthologs, both with and without infection; with the exception of *TraesCS4B02G329500.1,* which was only expressed in infected tissues. Results are shown in Fig. 6.12.

As seen for *At*LYM2, *Ta*CEBiP also contained two LYSM domains, one TMD and a signal peptide, as shown in Fig. 6.19. Protein localisation prediction was inconclusive (Appendix 31).

6.3.3 A comparative bioinformatics study reveals alternative gene candidates (Analysis 2)

A review, published after the above analysis began, detailed how to integrate wheat genetic resources in order to capitalise on discoveries made in *A. thaliana* (this also corresponds to the wheat-training.com resource provided as part of the Designing Future Wheat project)[414]. Access to some software was limited as a result of Covid-19 restrictions. Therefore, to allow for a comparison using the approaches detailed in these databases, Kostya Kanyuka, Rothamsted Research, who had access, provided this analysis. It should also be noted, that the *Ta*CEBiP had already been identified and used for VIGS experiments. A paper published following the bioinformatics analysis conducted above revealed

the *TaCEBiP* is silenced as a result of *F. graminearum* infection. Therefore, this candidate was not explored any further as part of this project[412].

First, *A. thaliana* proteins were aligned against the hexaploid wheat cultivar, Chinese Spring's proteome, including all high and low confidence proteins, using the program Geneious. The full-length sequences of all wheat proteins displaying the highest BLAST bit_scores identified were then aligned (once again using Geneious) using MAFFT, a multiple alignment program for amino acid or nucleotide sequences, against the corresponding *A. thaliana protein*; % protein identity was computed. These numbers can be found in Appendices 44 and 45. Each top wheat gene candidate was then aligned back against the entirety of the *A. thaliana* proteome, recording the score of the corresponding *A. thaliana* protein (this was also applicable for other proteins where there was not a direct match). Using this approach, it is likely that for AtBG_PPAP the most likely orthologues are: *TraesCS4A02G067900.1/ TraesCS4B02G225100.1/ TraesCS4D02G225700.1* with the next closely related gene being *TraesCS1A02G049800.1/TraesCS1B02G072500.1/TraesCS1D02G056500.1*. These results are completely different from those suggested above. Using this same approach for AtPDLP1 and AtPDLP5, it was determined that wheat is likely missing orthologs of these two genes, but likely contains potential orthologs for others such as PDLP2/PDLP3 – *TraesCS5A02G511600.1/TraesCS4B02G342500.1/ TraesCS4D02G338100.1* – and PDLP8 – *TraesCS2A02G386500.1/ TraesCS2B02G404100.2/ TraesCS2D02G491400LC.1*. These results were picked up in the reciprocal BLASTs in *A. thaliana* in my previous analysis, confirming these results. These results can be seen in Appendices 44 and 45.

6.3.3.1 VIGS fragment/primer design

VIGS fragments were designed using the aforementioned genes by Kostya Kanukya, Rothamsted Research, UK (si-Fi21 software (Version 1.2.3-0008)). For the top *At*BG_PPAP candidate (*TraesCS4A02G067900.1/ TraesCS4B02G225100.1/ TraesCS4D02G225700.1)* as well as the potential PDLP orthologs, PDLP2/3 and PDLP8, VIGS fragments could all successfully be identified. However, for the second *At*BG_PPAP candidate, *TraesCS1A02G049800.1/ TraesCS1B02G072500.1/ TraesCS1D02G056500.1*, a VIGS fragment could not be designed for specific silencing without creating a substantial off-target effect onto several sequence related genes, this was due to the ortholog being related to many homologous genes. The full-length primer sequences with their corresponding adaptors can be seen listed in Table 6.8.

Table 6.8 – Primer sequences for virus-induced gene silencing (VIGS) candidate genes.

Wheat ortholog/primer name	Sequence (adaptor in bold)
*Ta*BG_PPAP_R1	**AAGGAAGTTTAA**GCAAACCTCGACAAGCAGATC
*Ta*BG_PPAP_F1	**AACCACCACCACCGT**CACGAGGAGGTTGGGATAGTG
*Ta*PDLP2/3_R1	**AAGGAAGTTTAA**GACCTCTCCAACGTCGACTG
*Ta*PDLP2/3_F1	**AACCACCACCACCGT**CCTTCTTCTTGACCAGGCTTC
*Ta*PDLP8_R1	**AAGGAAGTTTAA**GTACAGGGTGGGCAGCTC
*Ta*PDLP8_F1	**AACCACCACCACCGT**GAAGGAGATGAAGACCACGATGA

6.3.4 Assays to be used to evaluate the VIGS plants in the presence and absence of *F. graminearum* infections

Even though the VIGS experiments could not be performed as part of this project, one of the main aims of this project is to identify how PD-associated proteins affect *F. graminearum* infection progression. Scoring FHB symptoms will be conducted every 3 days; however, this may not be fine-tuned enough to reveal what is happening at a smaller scale. Therefore, other assays need to be used to evaluate *F. graminearum* infection. VIGS plants both with and without infection will be assessed as well as WT controls.

In the absence of *F. graminearum* infection any phenotypic changes as a result of the VIGS construct can be assessed. The silencing of genes involved in PD regulation could have a detrimental effect on the plant host. Application of the virus containing the genes of interest during wheat ear formation, could affect floral tissue development. To assess this, the wheat spike and spikelet number will be measured and compared to the WT controls. In cases where silencing of a gene, in this case the wheat *BG_PPAP* ortholog, results in a callose increase it may be possible that reductions in PD permeability may prevent or slow down the movement of the BSMV virus. It has already been hypothesised that the *AtBG_PPAP* KO mutant will have decreased susceptibility to viral infection[407]. BSMV movement will therefore need to be assessed, with and without the gene of interest – this can be done using virus specific antibodies. The wheat BG_PPAP and PDLP orthologs affect callose degradation or deposition, respectively. Comparing the quantity of callose deposited before infection using aniline blue, in both live and fixed samples, can be investigated via CLSM. This

will determine if the gene of interest has had its desired effect on callose at the PD and will also help predict what will happen under infection conditions.

For VIGS plants both with the absence and presence of *F. graminearum* infection, microscopic screening will be the best approach to determine the effects of the silenced gene at the cellular level. Plasmolysis of cells can be investigated in fixed samples – *F. graminearum* infected wheat lines will most likely exhibit this phenotype. The development of wheat PM reporter lines would be of particular use in this instance (Chapter 5). Using specific stains (discussed in Chapter 4) nuclear strand-like projections strand formation can be assessed. Hyphal colonisation of floral tissues can be quantified using fixed samples (Chapter 4). Fungal biomass can also be determined within the spikelet – RT-qPCR or quantitative assays using WGA *in planta* can be adapted for this purpose[364,415].

The predicted outcome for these assays can be seen in Table 6.9 below.

Table 6.9 – Predicted outcomes for virus-induced gene silencing (VIGS) plasmodesmata assays in the presence and absence of *Fusarium graminearum*.

	Virus +/- constructs only				With *F. graminearum* infection			
Assay	**No virus**	**BSMV-MCS**	**BG_PPAP VIGS plants**	**PDLP VIGS plants**	**No virus**	**BSMV-MCS**	**BG_PPAP VIGS plants**	**PDLP VIGS plants**
Wheat spike growth	x	x	?	?	x	x	?	?
BSMV movement	x	x	**✓ (Decrease viral movement)**	x	x	x	**✓ (Decrease viral movement)**	x
Callose quantification	x	?[2]	**✓ (Increase in callose)**	**✓ (Decrease in callose)**	✓ (Increase in callose) [2]	?[2]	**✓ (Increase in callose as a result of infection and VIGS)**	**✓ (Small or no increase in callose due to infection and activation of other callose depositing proteins)**
Plasmolysis	x	x	x	x	✓ [3]	✓ [3]	✓ [3]	✓ [3]
Strand formation	x	x	x	x	? [4]	? [4]	? [4]	? [4]
Hyphal quantification	x	x	x	x	✓ [3]	✓ [3]	**✓ (Decrease in infection as greater callose deposition)**	**✓ (Increase in infection as less callose deposition)**
Fungal biomass	x	x	x	x	✓ [3]	✓ [3]	**✓ (Decrease in infection as greater callose deposition)**	**✓ (Increase in infection as less callose deposition)**

Key:
X = no predicted effect on the assay results
✓ = predicted effect on the assay results (these are stated in brackets
? = unknown
Bold lettering = different predicted affect than seen in the wild type (WT)
1 Changes in plasmodesmata permeability may affect spikelet growth but this has not been investigated.
2 Callose could be degraded by BSMV in order to aid its own infection. This had not been studied in the literature.
3 As a result of *F. graminearum* infection only.
4 Nuclear strand-like projections have only been recorded in wheat coleoptile tissue (Chapter 4).

6.4 Discussion

Manipulation of PD-associated proteins has previously been carried out in an attempt to learn gene function, this has been done via the production of stable mutants. For BG_PPAP a T-DNA insertion mutant that did not transcribe the gene was produced in *A. thaliana*, elucidating that this protein was located at the PD-PM, controlled callose degradation and functioned in gating the PD[407]. For PDLP1 a KO mutant in *A. thaliana*, demonstrated the PD localisation of a protein that affected cell-to-cell communication[264]. A knock-down mutant of PDLP5 in *A. thaliana*, led to the discovery that PDLP5 is able to modulate the PD and interact with the innate immune system[408]. Finally, a KO LYM2 *A. thaliana* mutant demonstrated the protein's ability to help detect chitin and therefore control PD molecular flux[262,410]. It is likely that even if there are no phenotypic symptoms following the loss of these genes other biological systems within the plant will be significantly affected. PDLP1 has been shown to regulate callose deposition during downy mildew infection; however how PD proteins affect the *F. graminearum* infection process (as well as for many other pathogens) has not been studied in detail[416]. Taking these factors into consideration the best approach to study the effect of PD functioning proteins on the progress of *F. graminearum* infection was considered to be VIGS, silencing the genes of interest and assessing how wheat floral infection progresses when the PD permeability is altered.

Table 6.10 – Summary of predicted wheat orthologs.

Analysis	*Arabidopsis thaliana* gene	Wheat orthologs identified
1	BG_PPAP	*(M1)* *TraesCS2D02G292500.1* *TraesCS2B02G311200.1* *TraesCS2A02G294700.1* (M2) *TraesCS3B02G278400.1* *TraesCS3D02G249500.1* *TraesCS3D02G249500.2* (M3) *TraesCS3B02G406200.1* *TraesCS3A02G374000.1* *TraesCS3D02G366700.2*
	PDLP1/5	*TraesCS2A02G386500.1* *TraesCS2B02G404100.2*, *TraesCS2A02G386500.1*
	LYM2	*TraesCS4D02G326400.2* *TraesCS5A02G501100.1* *TraesCS4B02G329500.1*
2	BG_PPAP	TraesCS4A02G067900.1 TraesCS4B02G225100.1 TraesCS4D02G225700.1 TraesCS1A02G049800.1 TraesCS1B02G072500.1 TraesCS1D02G056500.1
	PDLP2/3	TraesCS5A02G511600.1 TraesCS4B02G342500.1 TraesCS4D02G338100.1
	PDLP8	TraesCS2A02G386500.1 TraesCS2B02G404100.2 TraesCS2D02G491400LC.1

In this study, four potential VIGS candidate were chosen: BG_PPAP, PDLP1, PDLP5 and LYM2. Wheat orthologs were identified and characterised for future wheat VIGS experiments. A range of proteins were selected to alter different PD permeability mechanisms and pathogen-PD interactions. A recently published review was able to effectively summarise wheat genetic and bioinformatic resources and how they could be used to identify wheat orthologs quickly and efficiently when extrapolating from *A. thaliana* data[414]. Here this approach (Analysis 2), using non-open access software, and an analysis using free online software and characterising each protein (Analysis 1), were used to compare the results gained and assess the advantages and disadvantages of each approach. It is important to note that the bioinformatics predictions made here arise from the Chinese Spring genome, and that new genomic data from the 10+ wheat genome project (10wheatgenomes.com) should be explored to confirm or refute these findings. A recap of all genes identified in both analyses can be found in Table 6.10.

This comparative wheat ortholog analysis revealed very different results depending upon the approach taken. For BG_PPAP, analysis 1 highlighted three unnamed protein products (M1-M3) as the closest wheat gene orthologs, all were shown to possess the GH-17 domains characteristic of the β-1,3-glucanase family. Even though this was the case, analysis 2 revealed very different results, identifying completely different wheat orthologs; *TraesCS4A02G067900.1* was also shown to possess a GH-17 domain. As this approach followed a recently published established software pipeline, it is likely that the results from analysis 2 are more reliable. However, the identity percentage scores for the reciprocal BLAST analyses of the analysis 2 wheat ortholog against the *A. thaliana*

proteome are very similar – for M1, M2 and M3 these are, 53.7%, 53.85% and 52.24%, respectively; for *TraesCS4A02G067900.1* it is 54.44%. Currently, there is no evidence to suggest the size of the wheat β-1,3-glucanase family and even though M1-M3 may be less likely to be BG_PPAP wheat orthologs than TraesCS4A02G067900.1, it does not mean they are not β-1,3-glucanases possessing similar functions. In either analysis silencing an alternative β-1,3-glucanase may have detrimental effects for the plant due to their involvement in a series of different developmental processes.

Importantly before beginning this analysis, and for those that will carry on this project, it should be taken into consideration that any change to PD behaviour would most likely have an adverse effect on plant health, due to the multifunctional role of many of these proteins in development. PD are essential for cell-to-cell communication and silencing genes that would otherwise alter PD permeability will affect molecular flux throughout the plant. Previously, PDLP mutant *A. thaliana* lines were shown to have a dwarf phenotype when PDLP1, PDLP2 and PDLP3 were knocked out[264]. However, when only one of these genes is removed the plant has no visible phenotype, this genetic redundancy could alleviate some of the effects of gene silencing[264]. More recently an inducible PDLP overexpression vector (unpublished, Christine Faulkner, John Innes Centre) has been produced in *A. thaliana,* which may therefore relieve some of the stress the plant may face from restricted molecular movement. Whether the aforementioned possible side-effects will be a problem for this experiment cannot be concluded until the experiment has taken place. As the VIGS experiment will take part once the floral wheat tissue has already developed, any side-effects

that do occur may be small, however how this will affect *F. graminearum* infection is unknown.

Using analysis 1, PDLP1 and PDLP5, as well as the wheat orthologs, were all shown to have two salt stress/antifungal domains (GNK2), suggesting these sequences may be part of the same family. However, during the alignment analyses PDLP2, PDLP3 and PDLP8 were shown to be closer to the wheat ortholog identified, but for the sake of this analysis the top unnamed protein product was taken forward. In analysis 2 these claims were supported further, identifying no PDLP1 or PDLP5 orthologs in wheat but possible wheat orthologs to PDLP2, PDLP3 and PDLP8, respectively. As the potential orthologs from analysis 1 were shown to have similar functionalities to the *At*PDLP proteins, it is possible there are wheat proteins that work with similar functions but have not yet been annotated. All *At*PDLPs have been shown to locate to the PD and therefore silencing PDLP2/3/8 may also work as successful VIGS candidates. However, there is very little information on these in the literature in comparison to PDLP1/5.

Durable disease resistance to filamentous fungi such as *F. graminearum* is hard to accomplish, with most practices only achieving partial resistance – this is discussed more extensively in Chapter 1. The motivation for using VIGS in order to investigate PD-associated genes/proteins is that by understanding how these proteins affect *F. graminearum* infection, cultivars will be able to be produced with altered PD permeability (assuming the plant remains healthy). The β-1,3-glucanase family consists of pathogenesis related (PR) proteins which can be induced with the application of stresses including pathogen infection[417]. However, as previously discussed not all β-1,3-glucanases locate to the PD and those that

do can have multiple functions. Commonly β-1,3-glucanases have been shown to hydrolase fungal cell walls during infection, usually in conjunction with chitinase isozymes [417]. Producing transgenic wheat lines with engineered resistant traits is one way to introduce resistant genes that are not from the same species and therefore cannot be introduced by conventional breeding. The wheat cultivar Bobwhite has been transformed with barley β-1,3-glucanase transgenes, as well as a barley thaumatin-like protein 1 (tlp-1) and a wheat α-1-purothionin, before being inoculated with *F. graminearum*[418]. These transgenic wheat plants were contaminated with lower DON concentrations with decreased FHB severity, displaying enhanced FHB resistance[418]. It is therefore likely that the coexpression of β-1,3-glucanases with other anti-fungal proteins could be used as a tool to slow-down the progression of FHB in wheat. It may be possible that the silencing or overexpression of the VIGS candidates here could have a similar effect. PD specific β-1,3-glucanases have not been greatly researched within the last decade.

From the analysis in this chapter, it has been predicted that it is unlikely wheat has a PDLP1/5 ortholog, however it may be the case this family is smaller in wheat or that there are similar proteins that carry out the same functions. All PDLPs regulate cell-to-cell movement, however, this interaction has recently become more complex. PDLP5 has been shown to self-interact, with computational modelling predicting the PDLP5 TMD have a propensity to dimerise[419]. This very specific form of dimerization is predicted to be essential for the activation of PDLP5 activity via Ax_3G, a functionally essential motif[419]. Due to conservation between family members, it is hypothesised that other PDLPs may share similar behaviour. There are various reasons why PDLPs may do this: A)

to switch between an active and inactive state, B) to form a signalling complex and C) to attract other membrane proteins to the PD[419]. Due to the number of molecular interactions PDLPs may have within and between cells, how would this affect the plant if a PDLP was silenced or overexpressed? As some groups of PDLPs show some genetic redundancy, whereas others don't, are there some that dimerize and others that remain as single molecules?

The PDLP proteins can be identified by their DUF26 domains, which are also found in cysteine-rich receptor-like protein kinases. PDLP ectodomains have been shown to have some similarity to fungal lectins, and therefore may interact with carbohydrate monomers[420]. This behaviour is similar to that seen in LysM-domain-containing carbohydrate receptors[421]. As discussed for the PDLPs, it is likely the VIGS candidates selected here form complexes between themselves as well as with other molecules. If silencing these genes has detrimental effects for the plant, other proteins within the complex may be considered if wheat orthologs can be found; the overall aim of the experiment would therefore remain the same but may avoid problems such as redundancy and multi-functionality.

LYM2 is fundamental in detecting chitin upon infection and a wheat CEBiP has previously been identified[412]. Even though it has been chosen as a possible VIGS candidate here, it is likely silencing the wheat CEBiP will have little effect on *F. graminearum* infection but may instead result in decreased plant health before infection. Following the start of this bioinformatics analysis, evidence revealed that upon infection *F. graminearum* secretes a small RNA, Fg-sRNA1[422]. This has been shown, both in *in vivo* experiments, in *Nicotiana benthamiana* and in wheat, to effectively silence the wheat CEBiP upon infection[422]. In this case it may be a

best to overexpress the LYM2 protein as this may be able to saturate the *F. graminearum* response and help in the detection of chitin and PD permeability regulation.

Silencing the wheat BG_PPAP and PDLP potential orthologs may elucidate plant defence mechanisms that can be used to obtain durable wheat resistance. Not all *A. thaliana* genes have wheat orthologs and it is therefore likely similar genes and mechanisms are yet to be identified and annotated. The difference between bioinformatic approaches can greatly affect the end results and this should be taken into account when trying to extrapolate from one species to another. In conclusion, the wheat BG_PPAP ortholog identified on analysis 2 is the best VIGS candidate for the first experimental silencing experiment in wheat, to explore PD function in the presence and absence of *F. graminearum* infections.

CHAPTER 7: General discussion

This project has explored and developed new tools, methodologies and datasets, to aid in the understanding of how fungal pathogens communicate with plant cells and cause disease, which is helping to define the cellular and molecular mechanisms underpinning wheat-fungal interactions. A *Z. tritici* metabolic biosensor has been designed and produced to assess the fungal-stomata interaction for compatible and incompatible interactions. Although not successful here, solutions have been discussed and this biosensor is likely to be an effective tool in the future. Datasets have been produced, exploring wheat coleoptile tissue at the cellular level, both with and without *F. graminearum* infection – indicating differences between infection in the floral rachis and the young coleoptile, specifically in terms of intracellular growth and the PD interface. The coleoptile is an understudied wheat tissue and these comparative datasets reveal *F. graminearum* to be a highly flexible pathogenic species. Wheat PM reporter lines have been established, and although currently unsuccessful have the potential to change future research. Three of the four PM reporter constructs generated were shown to work well in transient assays and therefore may be useful to explore epidermal specific fungal-wheat interactions. Finally, wheat PD-associated protein ortholog VIGS candidates – BG_PPAP, PDLPs, LYM2 – were identified by using cross species genome and transcriptome bioinformatics analysis. These candidate gene sequences will be assayed in follow-up projects. At the beginning of this project these wheat orthologs had not been formally recognised and were therefore unavailable to both the plant pathology community and wheat research groups. A combination of comparative floral and coleoptile data, wheat PM reporter lines and VIGS candidates, can all be used to study

fungal-PD interactions, this has previously not been explored extensively in *F. graminearum* research.

7.1 Summary of key findings, developments and new resources

The three original project hypotheses have been repeated here as a reference to the key findings further discussed below:

1. *Z. tritici* metabolic biosensors can identify key changes at the cellular and molecular levels during compatible and incompatible interactions.
2. Stable wheat PM reporter lines are effective tools in identifying the *F. graminearum*-PD interaction at the cellular level.
3. *F. graminearum* utilises the PD for intracellular hyphal growth, aiding successful colonisation of wheat floral and non-floral tissues.

- **Development of a *Z. tritici* metabolic biosensor**

The production of a ratiometric metabolic biosensor, mitroGFP2-Orp1 (Chapter 3), to assess the stress of *Z. tritici* during compatible and incompatible interactions in wheat, was not entirely successful[331,335]. A second biosensor Perceval had previously been shown to be effective but could not be cloned successfully for use in this study[319]. However, this study and the findings so far gained have laid the foundations for the production of an improved biosensor. Low expression of the mitroGFP2-Orp1 construct in transformed *Z. tritici* can be improved upon, producing transformants with high expression. This can be achieved using three main approaches: western blot analysis to confirm *in planta* expression, using the endogenous *Orp* promoter, and codon optimisation of the *GFP* gene[293]. Answering the original hypothesis: *Z. tritici* metabolic biosensors

can identify key changes at the cellular and molecular levels during compatible and incompatible interactions, will allow researchers to identify key changes at the stomatal aperture during compatible and incompatible interactions. In 2016, the mitochondrial mt-roGFP2 biosensor was used to assess the oxidative state of epidermal mitochondria in the host during barley powdery mildew infection, demonstrating mitochondria nearer the infection site are under greater oxidative stress and cluster at the fungal penetration site[423,424]. In industry, genetically-encoded biosensors are being produced and adapted to monitor the production of chemicals, pharmaceuticals and fuel, in yeast (*Saccharomyces cerevisiae*) – it may be possible to use similar methodologies to produce metabolic biosensors in *Z. tritici* in the future[425]. This study was done during rotation project 1 at the University of Exeter before I moved to the laboratories at Rothamsted Research to analyse the *F. graminearum*- wheat interaction.

- **Optimisation of wheat tissue imaging**

There is currently no pre-existing database that contains open-access images of wheat floral tissue. On the other hand, infected wheat floral tissue images do exist in several published papers, for example to study spikelet to spikelet infection in the wheat ear (palea, lemma and rachis), and even in the analysis of infection cushions on the wheat palea, to help perform transcriptomic analyses on the virulence factors produced [113,426]. Characterisation of wheat floral tissue (Chapter 4) revealed the structure of the rachis, palea and lemma prior to infection. A series of different sectioning and imaging techniques were tested, but sectioning following tissue fixation and infiltration in LR white resin was deemed the most successful and also permitted direct comparative analyses with floral datasets previously published by Rothamsted scientists. The data generated in this study

will be added to a suitable wheat tissue database, most likely the DFW resources portal (https://designingfuturewheat.org.uk/resources/) and/or WheatBP (http://www.cerealsdb.uk.net/cerealgenomics/WheatBP/Documents/DOC_WheatBP.php). This information will be important as a foundation for comparing tissue before and after infection by different floral wheat pathogens, for example in spikelets infected with yellow rust or wheat blast. This part of the project provided a robust method alongside new knowledge, that could then be used to test the three original hypotheses proposed.

- **Cellular biology traits in the *F. graminearum* infected coleoptile**

Prior to investigating the cellular biology of wheat infection, coleoptile growth, with and without infection, was investigated. Statistical analysis showed there was no significant difference in growth between control and inoculated samples. However, a small difference was seen on the growth curves produced, whereby PH-1 coleoptiles finished slightly behind the controls in terms of length. To investigate whether this is an effect of the fungus or a result of chance variation, more samples will need to be measured.

The coleoptile assay had previously been developed as a high throughput methodology to compare different strains during *F. graminearum* infection of coleoptile and floral spikelets but, had not been studied extensively at the cellular level[303]. A recent study had characterised some spatiotemporal features of coleoptile infection, using confocal microscopy, including intracellular hyphal growth[355]. However, in this earlier study, the removal and analysis of the top epidermal cell layer failed to provide sufficient detail on the infection process that could be used to answer the project's hypotheses[355]. Fixation of the tissue in LR

white resin prior to sectioning was deemed to be the best approach (Chapter 4). Four characteristics typical of *F. graminearum* PH-1 infection of floral tissue that have been reported in several previous FHB disease development studies were not observed in the Fusarium-coleoptile pathosystem[113,162,168]. Firstly, there was a lack of plant parenchyma cells densely packed with hyphae near the vasculature. Secondly, in the colonised coleoptile cells nuclear strand-like projections were observed. Thirdly, no enlarged 'ghost' hyphae devoid of cellular contents were observed anywhere in the interaction tissue, whereas these become prevalent once visible symptoms appear in rachis tissue[165]. Fourthly, hyphal entry via stomata was rarely observed, whereas in floral tissue although infrequent this process has been documented well in the literature as a main entry point for *F. graminearum*[155,162]. Possibly the coleoptiles possess fewer stomata which may account for this difference. Tissue sections taken at some distance from the visible WT PH-1 lesions and / or obtained from the non-inoculated side of the coleoptile revealed very little evidence of *F. graminearum* infection being nearby, with the tissue containing only a few, if any, hyphae – this was the case for all explored samples. Therefore, these samples provided an excellent within-sample control. Interestingly, there was evidence in the wheat coleoptile of intracellular hyphal growth via the PD, indicating its usefulness in high-throughput PD analysis experiments. This study, therefore confirms PD colonisation in coleoptile tissues, which was first reported by Qiu et al. 2019[355]. Collectively, these new studies on the *Fusarium* infection process in the coleoptile tissue lays the groundwork for answering the third hypothesis: *F. graminearum* utilises the PD for intracellular hyphal growth.

The genes, *GT2* – encoding for the glucosyltransferase 2 enzyme – and *MAP1* – encoding for a MAPK homologous to PMK1 in *M. oryzae* – are both essential for *F. graminearum* pathogenicity in wheat spikelets[302,357,358]. The ∆FgGT2 mutant is non-pathogenic in wheat ears and severely impaired in hyphal growth, similarly ∆FgMAP1 is unable to penetrate and spread in the spikelet (excluding the anther tissues)[357]. In the coleoptile both mutants did not colonise the tissue, no hyphal growth could be observed in the fixed sections, suggesting infection was halted upon hyphal entry. Even though the ∆FgGT2 inoculated coleoptiles displayed some macroscopic symptoms of infection, possibly a defensive reaction, hyphae could not be identified in the microscopic field.

- **Quantification of *F. graminearum* infection**

PH-1 coleoptile infection was quantified in terms of the number of intracellular hyphae, intercellular hyphae and PD penetration events (Chapter 4). Most of the observations and quantitative assessments were taken near the vascular tissue, using water inoculated samples and the vascular bundle away from the lesion in the infected sample as controls. Due to the structure of the data only simple analyses could be carried out – a mathematical model could not be fitted. However, variation in infection stage at 3 dpi between samples, a higher ratio of intracellular hyphae to intercellular hyphae, and few PF penetration events in the coleoptile, was still determined. Interestingly, in the Qiu 2019 paper, when *F. graminearum* colonised the wheat coleoptile epidermis only, PF penetration events occurred frequently – the difference between infection in the epidermis and intact coleoptile needs to be investigated further[355].

How hyphal quantification can be improved will be discussed in more detail below. This dataset will be very useful when exploring and comparing other *F. graminearum* single and higher order gene deletion strains, and may also be compared against floral tissue data to assess the overall reliability of the coleoptile assay at the cellular level as a surrogate for the floral pathosystem[303,355,427]. Once again, this data contributes to answering the third hypothesis: *F. graminearum* utilises the PD for intracellular growth.

- **Wheat PM reporter line development and testing using root and coleoptile assays**

Stable wheat transformants were produced via particle bombardment using the designed ROP7-RFP and RFP-LTI6b constructs (Chapter 5). Presence of the constructs was detected in each plant generation and as expected some homozygous lines were identified in the T_1 generation, following genetic segregation analyses. However, no RFP fluorescence specifically at the PM was identified in any of the stably transformed plants. The contrast of RFP against that of the GFP *F. graminearum* reporter strains already available from previous studies, would have permitted improved visualisation of the PD-hyphal interaction at the cellular level and dynamic live imaging studies[143,163,388]. There are various reasons as to why these stably transformed wheat reporter lines did not express RFP specific fluorescence at the PM. Several explanations were proposed and discussed in Chapter 5 as well as in section 7.2 below. In the future, if such PM tagged wheat lines could be produced their availability would benefit not only the wheat pathogen community but also those interested in other aspects of wheat biology, for example cell wall morphology.

- **Potential orthologues of established PD localised proteins as the targets for VIGS in wheat**

Very few PD associated proteins are fully characterised, and almost all of these have been identified and investigated in dicotyledonous species e.g. the PDLPs in *Arabidopsis*[264,419]. The proteins of interest that were used to identify wheat orthologs were all from *A. thaliana*: BG_PPAP, PDLP1, PDLP5 and LYM2. A comparison of two analyses, one whereby open access software was utilised and another where licenced paid for software was used, identified alternative wheat orthologs[414]. This has highlighted a gap in wheat proteome/genome analysis and in inter-cereal species analyses, whereby programmes need to be made more accessible. The wheat BG_PPAP ortholog was determined to be the best candidate for VIGS, alongside PDLP2/3/8 (Chapter 6). Both analyses suggested the wheat proteome did not contain orthologs for the well-studied PDLP1 and PDLP5 proteins. Evidence published following this bioinformatics analysis suggested silencing the wheat CEBiP (ortholog of AtLYM2) would have little effect on *F. graminearum* infection progression due to the fungus silencing the gene upon infection[422]. However, the function of this gene still needs to be formally tested via VIGS. Wheat genes identified as possible VIGS candidate are presented in Table 7.1 below.

Table 7.1 – Summary of predicted wheat orthologs (Chapter 6).

Analysis	*Arabidopsis thaliana* gene	Wheat orthologs identified
1	BG_PPAP	*(M1)* *TraesCS2D02G292500.1* *TraesCS2B02G311200.1* *TraesCS2A02G294700.1* (M2) *TraesCS3B02G278400.1* *TraesCS3D02G249500.1* *TraesCS3D02G249500.2* (M3) *TraesCS3B02G406200.1* *TraesCS3A02G374000.1* *TraesCS3D02G366700.2*
	PDLP1/5	*TraesCS2A02G386500.1* *TraesCS2B02G404100.2*, *TraesCS2A02G386500.1*
	LYM2	*TraesCS4D02G326400.2* *TraesCS5A02G501100.1* *TraesCS4B02G329500.1*
2	BG_PPAP	TraesCS4A02G067900.1 TraesCS4B02G225100.1 TraesCS4D02G225700.1 TraesCS1A02G049800.1 TraesCS1B02G072500.1 TraesCS1D02G056500.1
	PDLP2/3	TraesCS5A02G511600.1 TraesCS4B02G342500.1 TraesCS4D02G338100.1
	PDLP8	TraesCS2A02G386500.1 TraesCS2B02G404100.2 TraesCS2D02G491400LC.1

Due to time and training limitations, the wet biology – VIGS experiment segment of this study could not be done but, its completion should help to answer hypothesis three, by analysing the *F. graminearum*-PD interaction at the molecular level. The best approach here would be to silence genes from both analyses – it is possible to silence two genes at once – making this experiment more time and cost-effective. VIGS in FHB research is an extremely useful tool and helps to identify molecular interactions between *F. graminearum* and wheat during floral infection. In recent studies focus has been given to investigating genes involved in FHB resistance. In one study a receptor-like kinase, *Ta*LRRK-6D, was identified as being upregulated in early *F. graminearum* infection[428]. Silencing of the gene via VIGS indicated *Ta*LRRK-6D's has a role in the salicylic acid pathway, and that expression of this receptor is needed to allow for successful signalling of this hormonal pathway in plant defence[428].

7.2 Experimental limitations, solutions and short-term follow-up activities

This project provided the foundations for successful development of the new tools and methods that will not only answer the original hypotheses postulated but will aid the detailed cellular and molecular investigations of other plant-pathogen interactions. However, during the development of this study various challenges were faced along the way.

Several different avenues of investigation were attempted to characterise the wheat floral and coleoptile tissues, but due to the extent of the task many of these will be pursued further in future projects. Please note that to use the coleoptile assay to such an extent was not in the original plan, this chapter was adapted as a result of Covid-19 restrictions; characterising and quantifying infection of both

PH-1 and mutant *F. graminearum* strains in the floral tissues had been the original goal of Chapter 4.

As a result of selecting the coleoptile as the main study tissue, the following questions are still unanswered:

- What are the strand-like projections surrounding the nuclei? Plasmolysed PM? Actin filaments? Transvacuolar strands? Hechtian strands? Or are these a result of how the samples were prepared and stained? These strand-like projections were only seen in PH-1 coleoptiles and not in the controls.
- Is the hyphal density in the coleoptile lower than that observed in the rachis? Is hyphal density highest just below the coleoptile surface?
- In the literature no DON is produced during coleoptile infection, I did not attempt to confirm this previously reported finding[303]. What would happen to the infection process if a small quantity of DON is applied to coleoptile tissues prior to or during the infection process? For *F. graminearum* wheat root infection, root hyphal colonisation was seen to be much higher when inoculated with a strain producing low to no DON (PH-1Δ*tri5)* than a high DON producing strain (10100004)[375]. Will the addition of DON therefore inhibit coleoptile colonisation by *F. graminearum*? Would the Δ*tri5* mutant successfully colonise the wheat coleoptile?
- The coleoptile goes through a period of intense growth, primarily cell elongation. Do the hyphae undergo intercalary growth as the coleoptile cells expand – *Epichlöe* endophytic hyphae have been shown to attach to expanding host cells allowing them to grow with the tissue apoplast[429]. Do hyphae rip apart in the process, or do hyphae exit the coleoptile to the

surface through stomata and escape the elongation process and subsequently re-enter plant tissue once coleoptile extension ceases? Do the hyphae during coleoptile colonisation compensate and have less branching as a result of this extreme plant growth rate?

- Are the ratios of the various wall polymers in the coleoptile wall different to those in mature wheat floral tissue, especially the rachis?
- Is the pattern of hyphal growth in the coleoptile similar to that of the rachis?
- *F. graminearum* clearly uses the PD to progress intracellularly in the coleoptile but not as frequently as that seen in the rachis. Is the mode of colonisation in the wheat floral tissues different to that in the coleoptile? Do the *Fusarium* hyphae always head for the path of least resistance to grow successfully through different plant tissues?

To fully image the coleoptile tissue during infection, as well as the wheat floral spike, both transverse (TS) and longitudinal (LS) samples/sections need to be taken and explored in detail. Without this an accurate depiction of each cell and tissue region cannot be gained. Hyphae are most clearly seen in the TS sections. By comparison, observations of plant cell nuclei in colonised, soon to be colonised and control tissues, are more clearly observed and quantified in LS sections.

At the beginning of this project, an additional aim had been to create a 3D model of the *F. graminearum* infection process in wheat tissue. However, the quantitative data that was needed for this task was not available at the start of this project, and I have been unable to generate sufficient data to be at the point to attempt modelling of the interaction. There is currently no literature for

producing a cellular infection model of filamentous fungi in any plant species. Recently, a tool for quantifying filamentous fungi growth and morphology has been produced, the fungal feature tracker (FFT), measuring spore number and morphology, mycelium area, hyphal tip number and hyphal length[430]. A similar approach for the *F. graminearum* infection would improve overall data analysis efficiency, relieving problems with the subjectivity of measurements, but would need to be adapted for infection *in planta*. The analysis carried out here, quantifying infection within the coleoptile will provide a starting point for the data needed to produce an *F. graminearum* infection model for both the wheat floral tissues and coleoptile. Ideally, more samples would have been fixed, sectioned and assessed in detail but due to time-constraints in the laboratory this was not possible. It should also be noted that with more data a comparison can be made as to how infection of the coleoptile tissue is comparable to that of the wheat spike, and whether or not this high-throughput assay can replicate similar results to those previously reported in the wheat floral tissues. Hyphal density, hyphal length and hyphal distribution within the tissue should all be quantified in future studies, when a suitable automated system is available. As discussed in Chapter 4, live-cell imaging will likely help in the advancement of characterising the cellular mechanisms of the coleoptile-*F. graminearum* interaction through the use of different strains, stains and microscopy techniques. The size of this investigation has meant this proposed modelling activity could not be completed as part of this project.

The main problem faced with the ROP7-RFP and RFP-LTI6b wheat PM reporter lines generated and characterised, was that even though the construct was present in the tissue samples and homologous lines were identified, either none, or exceptionally low, tagRFP reporter protein expression was detected. As a

result of time restrictions gene expression levels in the T_1 samples were not determined by qPCR. Unsuccessful stable transformations are usually not discussed in the literature, even though it is not unusual for this to happen. There are multiple possible reasons for this negative outcome (these have been taken from Chapter 5):

- Gene silencing may occur as a result of transgene expression.
- Copy number, position effect (where the inserted gene is placed) and DNA methylation can all affect transgene expression.
- The copy number analysis demonstrated that none of the lines that were homozygous were single copy lines. Post-transcriptional gene silencing means multiple copy lines may exhibit a greater tendency to show lower expression levels, increased methylation of the integrated gene in each plant generation is also possible. This is possibly why in this case neither construct resulted in the generation of wheat lines with any significant expression by the T_2 stage.
- The constructs could be lethal to the host, selecting against the transformants that would otherwise be successful.
- The linker between the FP tag and the sequence for the PM localised protein or another small part of the construct may be preventing expression. It may be that the linker was the wrong size or composition[393-395]. However, the vectors used were upgraded versions of those previously used for transformations. The pRRes208.355 vector had been used for multiple successful transient transformations (this could not be confirmed for pRRes208.454), as well as other vectors in the dataset i.e. pRRes208.380 a nuclear targeted plasmid control (personal communication – Alison Huttly, Rothamsted Research). Successful

transient transformations therefore give some confidence the linker is not completely breaking the fusion protein. The linker had not previously been tested in stable wheat transformations.

Both the wheat transformation and subsequent transgene copy number analyses are extremely expensive and therefore only five plants for each line were sent for copy number and zygosity analysis. Sending 15 per line would give a better chance of identifying lines, both homozygous and heterozygous, that had higher levels of gene expression. The fluorescent marker tagRFP was chosen to contrast with the GFP-*F. graminearum* strain, high expression of the PM reporter constructs would alleviate any problems with chlorophyll autofluorescence.

Finally, one of the main limitations experienced with identifying VIGS gene candidates (Chapter 6) for investigating PD molecular mechanisms, was access to software as a result of Covid-19 restrictions. The VIGS experiment itself could also not be carried out because the lengthy training could not be done under the local Covid-19 restrictions imposed in Jan 2021. This work will therefore be carried out as part of a follow-up PhD project. As identified in Chapter 6, the wheat CEBiP is silenced by *F. graminearum* during infection and it is therefore not a good VIGS candidate[422]. That this is the only PD-associated gene that is silenced by *F. graminearum* is unlikely. VOX experiments should therefore be performed as an alternative approach. Until these experiments are done there will be no indications as to how the host will be affected.

7.3 Improved infection model for the *F. graminearum* wheat interaction

An enhanced spatiotemporal infection schematic based on a detailed transcriptome study was published in 2017, depicting some of the cellular and

molecular changes between asymptomatic and symptomatic infection during wheat floral infection by *F. graminearum* (Fig. 1.6)[431]. Here, this model has now been expanded, using the information originally displayed in Fig. 1.6, to compare *F. graminearum* infection between the wheat rachis and wheat coleoptile tissues, with one of the main similarities being the 'hourglass' hyphal structure typical of hyphal constriction to pass through areas of the cell wall, possibly PFs, to grow through and colonise one cell to the next. This new comparative model is shown in Fig. 7.1.

7.3.1 *F. graminearum* infection in the wheat rachis versus the wheat coleoptile

The new model displayed here, represents the similarities and differences between the wheat coleoptile and rachis *F. graminearum* interactions, utilising some of the datasets that have been collected in the project. Relative to the wheat spikes, far less is known about the specifics of the coleoptile interaction, transcriptomic studies have been conducted allowing researchers to partition the coleoptile infection process into three main phases: 16 hours after infection (hai) – covert hyphal penetration, 40 hai – rapid fungal proliferation and 64 hai – overt tissue destruction[355]. Whereas the rachis has distinct asymptomatic and symptomatic phases that are maintained over 20 days until floral infection is completed[113]. Some proteins such as, cell wall degrading enzymes (CWDEs) play significant roles in both rachis and coleoptile interactions. In the rachis, cellulases have been shown to interact with two unpublished effectors, FgSSP6/7 and are therefore included in Fig. 7.1. Cellulose had been shown to have been degraded as soon as 3 days after infection[155]. In the coleoptile CWDE accumulation can be split into two distinct phases; degrading the mains chains of

cell wall components, followed by the side chains[303]. This is represented by an increase in CWDE expression at 16 hai and 64 hai, with a reduction at 40 hai[303].

The rachis part of the model however has been updated here to include information on known effectors, which were either previously unknown or not included in the 2017 model. Fgl1 is a secreted lipase, known to be present in the symptomatic stage of infection[159]. Another secreted protein called Osp24, is a cytoplasmic effector that has recently been shown to be important for successful *F. graminearum* infection in the rachis and coleoptile [427]. Osp24 is host-specific, with the deletion mutant displaying significant reductions in virulence in wheat tissue, important for hyphal spread within the wheat rachis, and suppressing cell death. The effectors FgSSP6/7 (as mentioned above) and FgSSP32/33 are also included in the new rachis model – these are currently unpublished; the role of these effectors in the coleoptile are currently unknown.

In the coleoptile, neither DON nor ZEA are induced, whereas in the rachis both are produced[303]. The secondary metabolite gene cluster (SMC) *Fg3_54* is induced 64 hai in coleoptile tissue, along with many other SMCs which do not influence *F. graminearum* virulence; this includes aurofusarin which is also upregulated in the rachis in runner hyphae (it has not been depicted in the rachis in Fig. 7.1 for this reason)[303]. Fusaoctaxin A has been shown to facilitate cell-to-cell invasion and has now been identified as the product of *Fg3_54*, which is expressed both in floral tissue infection cushions and infected coleoptile tissue[267].

Entry of the fungus into the plant tissues varies – in the wheat floral tissues, this tends to happen as a result of the cracked anther during anthesis, via stomata or

using infection cushions. For the coleoptile assay done here, entry has been shown to be possible via the stomata, as well as the cut edge providing an easy site of hyphal entry[303]. However, recent studies have shown the production of an appressorium-like structure on the coleoptile tissue to allow the fungus entry into the cell, when the options mentioned above are not available[355]. In this study, the focus was not to explore plant cell surface events in depth and this information has not been included in Fig. 7.1.

During *F. graminearum* rachis and coleoptile tissue colonisation, both intercellular and intracellular hyphal growth occurs. In both tissues, penetration pegs are used to gain entry into a cell, before growing intracellularly and passing to adjacent cells[113,355]. In the rachis *F. graminearum* has been shown to do this by utilising PFs, most likely choosing the pathway of least resistance, constricting hyphal diameter to pass through, forming an hourglass shape[113]. This also occurs in the coleoptile – and is demonstrated in Chapter 4 and in the literature – however the areas of the cell wall where this occurs have not been confirmed to be PFs[355]. Fig. 7.2 has been produced to identify the gaps between what is known about the rachis-PD interaction and the coleoptile-PD interaction; the coleoptile part of this figure only displays information that has been found during this project. In the rachis, hyphae have been shown to be able to pass through thick cell walls, travel from one PF to the next and grow both vertically and laterally[113]. In comparison to the coleoptile this is a relatively uncommon interaction. In the coleoptile tissue, hyphae pass through PFs less frequently. In this project this could only be imaged in TS sections and hyphae could only be seen passing through single rather than multiple PFs consecutively. A study in 2019, inoculated the coleoptile epidermis only, imaging using CSLM[355]. This infection system displayed hyphae passing

through multiple PFs in the longitudinal plane, however in the longitudinal sections taken in this project hyphae could not be imaged[355]. Due to differences in methodologies this study has not been used to produce Fig. 7.2. Outstanding questions concerning the comparisons in *F. graminearum* PF/PD interactions in the rachis and coleoptile can be seen in Fig. 7.2.

A feature of *F. graminearum* infection in the rachis that is not seen in the coleoptile is the fungus' ability to colonise the vasculature. *Fusarium oxysporum*, a member of the same genus, is mainly a soil pathogen that infects a variety of hosts, including cereals. In seedlings *F. oxysporum* infections are able to spread from the roots to the seedling[432-435]. Once in the seedling, *F. oxysporum* exclusively invades the vasculature, travelling intracellularly[433-436]. Interestingly, the taxonomically closely related species *Epichloë,* a genus of endophytic ascomycetes, which only infects grass species, remains exclusively extracellular throughout most of its *in planta* colonisation phase; little is known about their interactions with PD when the hyphae finally invade the immature floral tissues [437]. Comparing the interactions between wheat rachis/coleoptile infection, *F. oxysporum* and *Epichlöe* in monocots may allude to some of the mechanisms needed to colonise the vasculature. Additionally, the *F. graminearum* GIV2 GPCR gene mutant is unable to colonise intracellularly suggesting this signalling pathway is fully/partially responsible for entry into the wheat cell[438].

As well as highlighting new developments in research, since the 2017 model was published, the new model produced here highlights areas which are critical for possible intervention strategies when tackling FHB disease. Examples are, infection cushion development, DON production, fungal secretion and nutrient

distribution within the fungus itself. Working infection models such as the ones proposed and discussed here are important if we are to visualise and fully understand an interaction – more complex ones will be needed as research in these areas progresses and interaction modelling projects are devised.

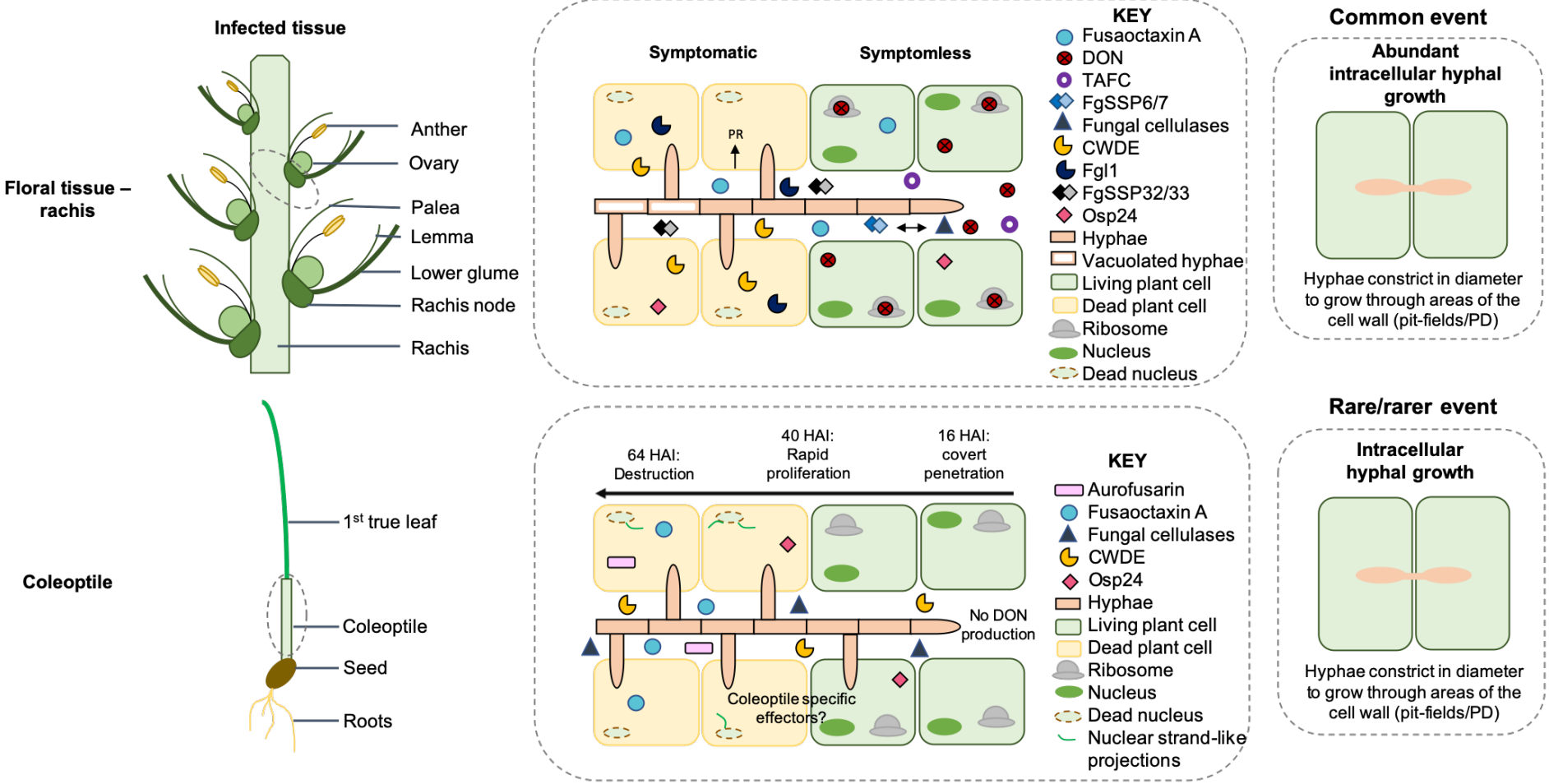
Infected tissue
Floral tissue – rachis
Anther
Ovary
Palea
Lemma
Lower glume
Rachis node
Rachis
Coleoptile
1st true leaf
Coleoptile
Seed
Roots
Symptomatic
Symptomless
PR
KEY
Fusaoctaxin A
DON
TAFC
FgSSP6/7
Fungal cellulases
CWDE
Fgl1
FgSSP32/33
Osp24
Hyphae
Vacuolated hyphae
Living plant cell
Dead plant cell
Ribosome
Nucleus
Dead nucleus
64 HAI: Destruction
40 HAI: Rapid proliferation
16 HAI: covert penetration
No DON production
Coleoptile specific effectors?
KEY
Aurofusarin
Fusaoctaxin A
Fungal cellulases
CWDE
Osp24
Hyphae
Living plant cell
Dead plant cell
Ribosome
Nucleus
Dead nucleus
Nuclear strand-like projections
Common event
Abundant intracellular hyphal growth
Hyphae constrict in diameter to grow through areas of the cell wall (pit-fields/PD)
Rare/rarer event
Intracellular hyphal growth
Hyphae constrict in diameter to grow through areas of the cell wall (pit-fields/PD)

Figure 7.1 – A *Fusarium graminearum*-wheat working model for the rachis and coleoptile tissues. This model depicts *F. graminearum* infection progression in the wheat rachis and coleoptile tissues. For the rachis it compares the symptomless and symptomatic stages of infection, and for the coleoptile the three main infection time points – 16, 40 and 64 hours after inoculation (hai). Both tissues show a transition, in a compatible interaction, from intercellular to intracellular hyphal growth as infection progresses. In the rachis this is confirmed to be via pit-fields, allowing hyphae to travel from one cell to the next. During infection in the rachis and coleoptile, a range of secreted molecules are produced in the different phases of infection – less is known about these in the coleoptile. Abbreviations: CWDE, cell wall degrading enzyme; DON, deoxynivalenol; Fgl1, an effector lipase; FgSSP, *F. graminearum* small secreted protein; Osp24, orphan secreted protein 24 effector; PR, plant response; TAFC, triacetyl fusarinine C. Parts of this figure were adapted from a model produced in the book chapter: Cereal-Fusarium interactions: Improved fundamental insights into Fusarium pathogenomics and cereal host resistance reveal new ways to achieve durable disease control from the currently unpublished book: Achieving durable disease resistance in cereals (expected publishing date: Summer 2021). This model was produced by me and Catherine Walker, John Innes Centre, Norwich, UK.

Rachis

- Hyphae crossing a pit-field is a common event.
- Hyphae can cross through more than one pit-field, consecutively.
- Hyphal growth observed through thick cell walls via pit-fields.
- Hyphae can grow both vertically and laterally.

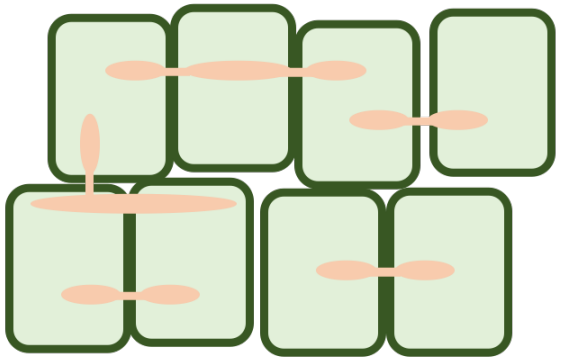

Coleoptile

- Hyphae crossing a pit-field is a rare/rarer event.
- Only evidence of hyphae crossing single pit-fields in this study.
- No evidence hyphae use pit-fields to pass across thick cell walls.
- Hyphae can grow both vertically and laterally (rare).

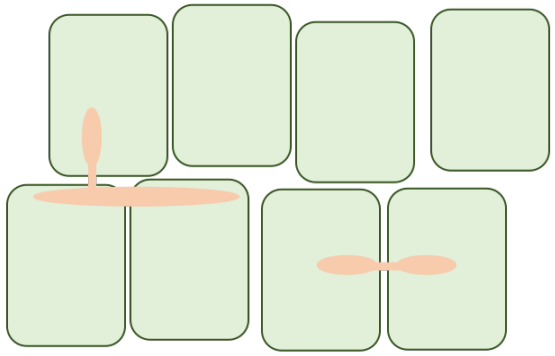

Questions:

1. What is the density of PD in the coleoptile compared to the rachis?
2. At what time point does cell death occur? Before, during or after hyphal entry/exit?
3. Is the composition of the rachis/coleoptile cell walls and plasma membranes different, allowing for these differences in intracellular hyphae behaviour?

Note – intercellular hyphae have been omitted from both images.

KEY:

- Plant cell
- *F. graminearum* hyphae
- Cell wall

Figure 7.2 – Intracellular hyphal growth through pit-fields/plasmodesmata (PD) in *Fusarium graminearum* wheat rachis and coleoptile infection. This model compares *F. graminearum* hyphal growth through the pit-fields/PD in the wheat rachis and coleoptile tissues. What we know about this interaction in each tissue is listed – for the coleoptile this displays information gained from this project. Outstanding questions for both tissues are also listed. Note, the cell wall in the rachis is noticeably thicker.

7.4 Major advances in biological methodologies, genomics and microscopy techniques

7.4.1 Advances in wheat genomics

Advances in next generation sequencing (NGS) has increased the number of plant genomes that can be sequenced and has also allowed for transcriptomic profiling and the development of protein networks. The wheat genome is large and highly complex, and although exceptionally well-studied through many detailed genetic and cytogenetic analyses, up until the early 2010s it has proven difficult to sequence and assemble, preventing wheat researchers from gaining a detailed understanding of genomic organisation and inter-*Triticum* species similarities and differences[439,440].

The International Wheat Genome Sequencing Consortium (IWGSC) was established in 2005, with the main aim of producing a high-quality sequenced genome for bread wheat. Throughout the duration of this project a series of technical advancements were made. The sequence for the largest wheat chromosome 3B was the first to be generated in 2008[441]. A first draft wheat

genome was published in 2014[442]. Over a decade since the wheat chromosome 3B was generated a second version of the ordered and annotated bread wheat (cultivar: Chinese Spring) genome, was made available, IWGSC RefSeq v.2.0 (https://urgi.versailles.inra.fr/). This will continue to be improved upon over time. In this study, the updated bioinformatics analysis for identifying PD VIGS candidates (Chapter 6) has already benefitted from this new resource. A broader general understanding of the hexaploid wheat genome will also allow researchers to understand wheat-pathogen interactions in more detail as well as how methods such as transformations work at the epigenetic level (PM reporter lines; Chapter 5). It should also be noted that the Chinese Spring genome is considerably different to those used commercially. To this end, the 10+ Genome Project (10wheatgenomes.com) whereby the wheat pangenome has been assembled, helping to capture genetic variation between wheat species, has recently been completed. This new database will eventually allow users to compare multiple wheat genomes, branching the gap between wheat species/cultivars used in research and those used commercially.

Clustered regularly interspaced short palindromic repeats (CRISPR)-CRISPR associated systems (Cas) is a recently developed technology which allows for targeted genetic mutations within a host. In hexaploid wheat, for known gene sequences, gene knock-out (KO), deletion or more subtle sequence modifications would rely upon CRISPR-Cas constructs being targeted to the A, B and D genomes. The development of this technology in polyploid species such as wheat has been prevalent over the last few years; validating guide RNA (gRNA) targeting efficiency, producing a tool for gRNA design in wheat, and plans to reduce gluten content for those suffering from coeliac disease[443-445]. This

emerging technology could therefore be used as a targeted approach to investigate PD associated proteins in future experiments, allowing them to be deleted/modified within the genome, serving as an alternative to the VIGS experiment discussed in Chapter 6. However, for wheat it is unlikely this would be an inducible system/only occurring in the mature plant and may therefore target PD protein function to affect general plant growth, development and/or fertility. This technology could also be considered for producing the wheat PM reporter lines (Chapter 5), permitting targeted insertion, allowing for the control of copy number and avoiding regions of the wheat genome where silencing is likely to occur, for example nearby the centromeres or heterochromatic regions, or regions rich in transposable element or small repeats.

An important discussion point highlighted by this project is how gene ortholog expression can be compared between species. The Wheat Expression Browser was published in 2016, at the beginning of this project. Comparatively, those available for rice, barley and *Arabidopsis* produce different outputs making it difficult for inexperienced users to compare between them[413,446]. Where orthologs need to be linked between species, it would be useful to have a collective database for this data/analysis. An open access bioinformatics database combining multiple plant genomes would greatly benefit projects such as that shown in Chapter 6.

7.4.2 Advances in microscopy techniques

This project has primarily focused on stereomicroscopy and confocal laser scanning microscopy (CLSM) to identify the cellular and molecular relationships between fungal pathogens and their hosts. To test a hypothesis accurately, the most suitable bioimaging/sample preparation methodology needs to be used –

targeting a specific plant/fungal tissue that is being analysed or focusing on a particular question.

Optical microscopes, although an extremely important and constantly developing scientific toolset, are limited by their resolution of a few hundred nanometres, much larger than most biological molecules[447]. One of the main problems faced when studying the PD, as discussed in Chapter 4, is imaging. PD are small structures, only 10-50nm in size. Until recently the best way to visualise these channels was to use electron microscopy. However, the evolution of new high-resolution techniques will now make this activity much more accessible and easier to carry out, thereby making imaging approaches more cost effective. In Chapter 4, the *F. graminearum* hyphae were shown to pass through the wheat cell wall growing from one cell to the next. I will now explore and discuss the pros and cons of various microscopy techniques which may help determine if mode of growth was via PFs and consequently PD. I am also interested to find out if the PD are destroyed during this process, and if they have a specific interaction with the fungal pathogen.

Expansion microscopy is a methodology that results in the physical expansion of the specimen to be imaged, avoiding the purchase of any expensive new equipment[448,449]. Although this technology was devised before this PhD project began, it has been extensively refined over the last few years. Biomolecules are typically equipped with anchors which bind them to an *in situ* swellable polymer (or hydrogel) that is synthesised throughout the specimen[447,450]. The specimen is then immersed in a monomer solution, forming crosslinks producing a polyelectrolyte gel[447]. These samples undergo homogenisation before being

added to a solvent resulting in swelling. Molecules are therefore separated in space at greater distances than before, 4.5x in linear dimension and 100x in terms of volume. As a consequence of these procedures, molecules can be seen using optical microscopy, without the need to buy new equipment[447,450]. Since the development of expansion microscopy in 2016, adjusted protocols have been published for use in protein retention, human pathology, nanoscale imaging of RNA and iterative expansion microscopy (whereby the image is expanded a second time)[447,449]. The expansion of plant specimens is relatively under-researched with little known about how plant structures will be affected. A recent study was able to use expansion microscopy to expand barley nuclei and assess chromatin ultrastructure[451]. Wide-field microscopy could help visualise the nuclei, nucleoli and chromatin domains, which were previously invisible, whereas structured illumination microscopy (SIM) (higher resolution), demonstrated the process did not preserve the chromatin ultrastructure[451]. Additionally, this technique has been applied to fungi. In this case CWDEs were first applied to the sample[452]. Utilising SIM and CSLM, images of *F. oxysporum* and *Aspergillus fumigatus* hyphae expressing the fluorescent labels: histone H1-mCherry with Lifeact-sGFP or RFP, as well as *U. maydis* sporidia expressing fluorescent rhodopsins, were gained at a high resolution (4.5x expanded)[452]. It has not yet been determined if expansion microscopy could help visualise PFs/PD using light microscopy. If achieved this could enable the *F. graminearum*-PD interaction to be studied in greater detail.

The first report of detecting single fluorescent molecules was in 1990[453]. Direct stochastic optical reconstruction microscopy (dSTORM) allows imaging up to a resolution of approximately 20 nm. Stochastically activated fluorophores are

recorded over time producing a stack of images[454]. Estimations are made as to the fluorescence emission pattern of single molecules and the location of individual fluorophores[454]. From this data an artificial model can be built, leading to high resolution images, helping to determine cellular structures as well as providing information on single molecules[454]. Plant-tissue limitations, including those with tissue-level imaging and the lack of a single-cell model in plant biology have recently been overcome. Optimisation of photo-switching dyes has adapted dSTORM for plant tissue use; premature cell wall ultrastructure; cellulose, mannans and callose were identified[455]. dSTORM uses an oxygen-scavenging buffer system to produce fluorescence, another variant of this imaging system is Nikon-STORM (N-STORM) which uses an activator/reporter pairing system to emit a signal. A combination of both of these STORM technologies was used just under a decade ago to reveal some of the intricacies of the callose defence mechanism, demonstrating the deposition of a callose layer upon the cell wall nearest the pathogen upon invasion[456]. New developments in this technology for optimisation will hopefully provide more information on callose deposition and other molecular changes in response to plant pathogen invasion in the future. Labelling the wheat PM (Chapter 5) may help build a model of the PD using a STORM technology. Furthermore, using a variety of markers and fluorescent dyes as our knowledge of the PD grows, alongside tools such as wheat PM reporters may help build a model of the *F. graminearum*-PD interaction. At a single-molecule level, this technology, could help determine the location of PD-associated proteins (Chapter 6), to make sure that those targeted for gene silencing/overexpression experiments in respect to PD have minimal off-target effects.

A technology that is now being adapted for the detection of diseased plants is multispectral/hyperspectral imaging[457,458]. Multispectral imaging allows for the separation of different emission wavelengths, letting each signal be visualised, and quantified, individually i.e. if using multiple fluorophores. One such system has been developed to detect at the presymptomatic stage, oilseed rape (*Brassica napus*) infection by *Pyrenopeziza brassicae,* demonstrating its uses in plant breeding and the selection of resistant cultivars[459]. Other examples of similar disease detection models can be seen for Esca, a grapevine trunk disease caused by a variety of pathogenic fungi, and in gray mold leaf infections (*Botrytis cinearea*), among others[460,461]. Established multispectral imaging systems for *Z. tritici* and *F. graminearum* infection already exist for wheat infections and have been shown to be successful in the field[220,315,462]. Using a similar methodology at a cellular scale would allow for separation of wheat autofluorescence when imaging (Chapter 3,4 and 5), this would be especially helpful in terms of imaging lowly expressed wheat PM reporter lines to be used with fungal reporter strains.

7.4.3 Technological advances made in *Z. tritici* and *F. graminearum* research focussing on early pathogen detection

Technological advances in *Z. tritici* and *F. graminearum* research will help develop and answer new hypotheses in the future, following on from this project. Detection of *Z. tritici* in infected wheat crops using qualitative PCR assays has previously been attempted, however even though this work has been published it was later found that these tests produced incorrect results, possibly as a result of variable experimental conditions and / or the genetic diversity of the organism[463-468]. By adjusting PCR assays to coincide with updated genetic databases at regular intervals, and using easily available reagents, these problems have now been alleviated and a new primer set has been developed to

achieve a diagnostic test for *Z. tritici* in leaf samples[463]. Another approach to advancing fungal research is through the development, discovery and characterisation of new fungal mutants. Fungal models exist to study conidiation in ascomycetes i.e. *Aspergillus nidulans*. Deletion of homologous genes in *Z. tritici*, has demonstrated that although not all gene homolog deletions affected pathogenicity or asexual sporulation, meaning the *A. nidulans* model is only partially applicable, two mutants were produced, i.e. *ZtFlbC* and *ZtBrlA2*, which displayed reduced pycnidiospores production in comparison to the IPO323 strain[469]. The discovery of new mutants such as these will help determine new mechanisms in the interaction between the plant host and *Z. tritici* (Chapter 3).

The *Z. tritici* pangenome was published in 2018, revealing that a single reference genome for this pathogenic fungus underestimated the genetics of a highly polymorphic species[470]. In total 9149 genes were identified as a core set. An additional 6600 genes were identified from a small isolate subset and are thought to encode for a large number of effector genes essential for pathogenicity[470]. Similarly, in 2018 the first *F. graminearum* pangenome was established, one group produced the pangenome of all North American strains (60 genomes and the PH-1 reference genome), whilst another focused on 15 from Brazil and five others that were publicly available (plus the PH-1 reference genome), 1681 and 1111 genes were considered as accessory genes, respectively[471,472]. In the latter study, 600 of these were predicted to be new gene calls, identifying 10 new secondary metabolite clusters. New gene clusters were also identified in the N. American study[471,472]. In relation to this project, in *Z. tritici* this data could help determine what genes are needed for a compatible interaction over an incompatible one (Chapter 3), and in *F. graminearum*, this data will help in

identifying transcriptional and virulence gene requirement differences, between wheat rachis and coleoptile infection as well as PD-associated genes (Chapter 4 and Chapter 6).

Similar to *the Z. tritici* qPCR screening assay discussed above, detection assays for *F. graminearum* have been developed over the last few years, feeding into the overall goal of this work, aiming to control *F. graminearum* infection progression. A pre-existing loop-mediated isothermal amplification (LAMP) methodology has been optimised for this purpose and is able to detect the presence of *F. graminearum* in inflorescences as well as in the seed, during the latent infection phase, providing a specific, sensitive, high-throughput test for detection[473].

All the technological advancements listed above in wheat, microscopy and fungal protocols, have implications for studying *F. graminearum* infection biology and will be taken into consideration for the planning of future follow-up projects.

7.5 Role of plasmodesmata in infection

The overall aim of this project was to understand the role of the PD in aiding *F. graminearum* infection progression. There is currently no evidence to suggest *Z. tritici* ever grows intracellularly. Upon the transition from intercellular hyphal growth to intracellular hyphal growth *F. graminearum* has been shown to pass through PFs travelling from one cell to the next[113]. To do this the hyphae must constrict its diameter before expanding back to the original size in the adjacent cell[113]. How *F. graminearum* hyphae grows through these small structures, and why hyphae choose this pathway is still unknown. Since these original

investigations into the cellular interactions between *F. graminearum* and the wheat floral tissue, there have been no further in depth cellular or molecular investigations to understand the interaction between *F. graminearum* and the PD. This has been explored further in Chapters 4, 5 and 6.

7.5.1 Other pathogen-plasmodesmata interactions

As discussed in Chapter 1, the interactions between viruses and the PD, have been studied to a greater extent than for filamentous fungi. Whereas bacteria PD interactions remain relatively underexplored. The fungal ascomycete, *Magnaporthe oryzae*-rice leaf sheath pathosystem, has one of the most thoroughly investigated PD interactions as described in Chapter 1. *M. oryzae* intracellular growth is via PFs and occurs from the 1st epidermal rice cell penetrated[236,396]. From here hyphae grow from the epidermis to the mesophyll before travelling from one leaf mesophyll cell to the next[236,396]. Even though the *M. oryzae*-PD interaction can be used to form hypotheses about the *F. graminearum*-PD interface, it should be noted that the study tissues for *F. graminearum* infection in wheat are the floral tissues, specifically the rachis, which are very different morphologically to leaf tissue. Second the PD colonisation in the rachis by *F. graminearum* does not occur immediately after initial penetration, occurring mid-infection.

For this project, VIGS constructs were designed to investigate some of the molecular mechanisms associated with PD permeability and the SEL (Chapter 6), assessing how these proteins may affect pathogen progression. However, the pathogenic fungus in question must also secrete molecules to manipulate the PD to be able to pass through the PFs and grow from one cell to the next. Upon *M. oryzae* infection the cells remain alive until the hyphae have nearly exited the cell,

with the PD remaining intact. The fungal mitogen-activated protein kinase (MAPK), Pmk1, was recently characterised in *M. oryzae* and is important for the pathogenicity of the fungus (the homolog of this in *F. graminearum* is Map1 which is also known to be required for pathogenicity (Chapter 4))[358]. Using a chemical genetic approach *Pmk1* can be conditionally inactivated, allowing for initial infection to take place successfully, something that cannot be achieved in the *Pmk1* KO mutant[358]. This study concluded that Pmk1 was needed for hyphal constriction, allowing *M. oryzae* to grow intracellularly[358]. Additionally, Pmk1 can control an array of effectors to suppress plant immunity, ensuring the PD remain open[358]. With the Map1 KO mutant (ΔFgMAP1) being available in *F. graminearum* it could be hypothesised that similar control of the fungal-PD interaction would be seen in this system. The chemical needed to deactivate the MAPK of interest *in planta,* 1-naphthyl-PP1 (1NA-PP1), is no longer available, currently making this experiment inaccessible. In the future, other compounds may be produced which will facilitate this experimental approach. Another assay reported in this *M. oryzae* study was the use of a single-mCherry protein (28.8 kDa) and a double-mCherry fusion protein (57.6 kDa) to test PD permeability during infection. Healthy tissue allowed the single-mCherry protein to pass from one cell to the next due to its small size, whereas the double protein was prevented from passing through[358]. By comparison, in early infection the double-mCherry protein was able to diffuse to adjacent cells, displaying an altered PD permeability. Later in infection an increase in callose deposition at the PD is likely to prevent this diffusion[358]. This experiment could easily be performed in the *F. graminearum*-wheat system and would only require access to the relevant vectors, helping identify some of the cellular mechanisms, building upon the information shown in Chapter 4.

Recent findings have started to reveal the various roles effectors play in regulating PD processes, targeting different PD regulators. *Fusarium oxysporum* f. sp. *lycopersici*, is a root-infecting fungus of tomato. During infection the effectors Avr2 and Six5 are secreted, both of which are required for I-2-mediated disease resistance in tomato[474,475]. Using a similar principle to the fluorescent protein diffusion assay used to investigate Pmk1 above, it was shown that Avr2-GFP as well as a double RFP protein could not pass to the adjacent cell without the presence of Six5; individually Six5 cannot alter the fusion of the double RFP protein, demonstrating an important interaction between the two effectors, both of which are therefore needed for successful protein transport through the PD[476]. In susceptible plants this interaction assists successful infection[476]. *Phytophthora brassicae*, an oomycete which infects members of the Brassicaceae family, secretes the RxLR3 effector[477]. This effector has been shown to target the callose synthases, specifically CalS1/2/3, colocalising with PDLP5 (Chapter 6) and corresponding callose deposits[477]. As a result of binding to the CalS, callose deposition is decreased, allowing for molecular flux through the PD to continue[477]. At the time of writing there are no reports in the literature of *M. oryzae* or *F. graminearum* effectors that have been shown to localise to the PD. However, due to the hyphae of both *M. oryzae* and *F. graminearum* passing through PFs it is likely PD specific effectors play a part in this interaction. The use of wheat PM reporter lines (Chapter 4) and the identification of the PD-associated proteins (Chapter 6) will help identify PD specific effectors produced by *F. graminearum.*

Basidiomycetes, such as the smut fungus *Ustilago maydis*, a pathogen of maize, have not been shown to grow from one cell to the next via the PD. In the case of

U. maydis, most hyphae remain intercellular, those that are intracellular, such as those that initially penetrate a cell for entry into the plant, are fully encased in the PM[478,479]. Similarly, *M. oryzae* invasive hyphae are encased in an interfacial membrane, namely the extra-invasive hyphal membrane (EIHM), upon entry to the host during the initial stages of infection, this membrane is eventually disrupted[236]. Whether a similar sort of membrane is formed very early during *F. graminearum* infection in wheat has not so far been reported even though this infection phase has been extensively studied. There is certainly no evidence of PM encasement of *F. graminearum* hyphae during rachis tissue colonisation[113]. Even though *U. maydis* does not directly use PD, secreted effectors i.e. Cmu1, are thought to use these channels to disperse throughout the host in advance of the hyphal infection, thereby manipulating host metabolism to benefit the fungus[480].

As mentioned above bacteria-PD interactions are relatively underexplored. However recently in *Pseudomonas syringae,* the effector HopO1-1 has been identified and been shown to regulate PD in *A. thaliana*[481]. The HopO1-1 effector physically associates with PDLP7 and PDLP5 (Chapter 6), which are involved in bacterial immunity, affecting their stability[481]. This interaction therefore positively affects *P. syringae* infection, maximising its progression by affecting the communication channels of the host[481].

Most PD-associated proteins do not act alone, but instead work as part of a complex system. In response to pathogen attack, it can be hypothesised that multiple components within a complex molecular system need to be manipulated by the pathogen to alter a specific PD mechanism. The cell walls of fungi contain

chitin, a molecule that triggers plant defence responses – effectors therefore aim to suppress defence responses. In *A. thaliana*, LYM2 (a wheat CEBiP has also been identified) mediates chitin-triggered PD closure and is located at the PD-PM[262]. It has recently been shown that LYM2 requires association with two LysM-receptor kinases (RKs), LYK4 and LYK5[242]. LYK4 and LYK5 are initially associated at the PM, upon detection of chitin LYK4 associates with LYM2 at the PD initiating a signalling cascade, triggering chitin-related PD responses[242]. The signalling at the PD-PM is extremely specific and independent of the PM, producing a localised response, independent of both other PM signalling cascades and other immune outputs[242]. These PD PM microdomains may therefore be able to be specifically targeted, away from the general PM, when trying to prevent *F. graminearum* progression. Whether a similar PD control mechanism exists in wheat is not yet known. However, PD specific markers could be produced once more is known about these microdomains (Chapter 5) and new VIGS targets could be identified (Chapter 6).

7.5.2 Project contributions to understanding PD

One of the main aims of this project was to understand how PD permeability alters *F. graminearum* hyphal progression. The tools and datasets produced here work towards this goal. The *F. graminearum*-PD has not previously been investigated extensively at either the cellular or molecular levels.

The PM is continuous with adjacent cells, lining the PD. For this reason, Chapter 5 focused on the development of wheat PM reporter lines. Even though not successful here, this tool would allow live-cell imaging of the wheat-*F. graminearum* interaction, something that cannot be done with high-resolution. A

similar approach has been tested with the rice-*M. oryzae* interaction whereby LTI6b-GFP rice reporter lines allow the user to clearly visualise the hyphae-plant interaction at the cellular level[396]. The production of a successful wheat PM reporter line would also allow the PD-hyphal interaction of other filamentous wheat fungi to be studied in greater detail. Furthermore, from a molecular point of view, the VIGS bioinformatics analysis from Chapter 6 will aid in identifying molecular aspects of the PD role during *F. graminearum* infection. An alternative approach that could be taken to achieve wheat PM tagging is either BSMV-VOX or foxtail mosaic virus (FoMV)-VOX[482,483]. Overexpression of the ROP7 and LTI6b gene used in Chapter 5 to produce wheat PM reporter lines, by VOX should allow for successful visualisation of the *F. graminearum*-PD interaction in the floral tissues. However, this approach would be time-consuming and would not allow visualisation of other wheat tissues, i.e. coleoptile tissue, throughout plant development.

7.5.3 Difficulties that need to be overcome to forward PD research

The main difficulty of imaging PD has been thoroughly discussed above. One other area of difficulty that has not yet been discussed is how PD permeability is investigated. When investigating a novel gene or protein thought to be associated with PD function, it is likely this gene product will only function in a certain tissue, at a certain stage in development, in response to specific stimuli[379]. PD permeability and changes to the SEL is a highly dynamic, continuous process. It is therefore likely that multiple approaches will be needed to assess what molecules are responsible for PD changes i.e. the combination of callose stains and the movement of fluorescent proteins could both be used to assess this (Chapters 4,5 and 6)[379]. PD permeability investigations in both floral tissue and the coleoptile would be needed to identify any differences in PD behaviour

between the two tissues. It may also be advantageous to test new methods/method combinations on wheat coleoptile tissue first (as this is a high-throughput assay) to check the protocol is reliable for use in the floral tissue.

7.6 The impact of this research

The tools and datasets produced in this project to gain a greater understanding of how fungal pathogens communicate with plant cells and cause disease will make an impact in future research. Research of many fungal-plant systems require the development of new tools and methodologies to be developed if they are to be understood at the cellular and molecular level. As discussed in this chapter, issues still remain in finding affordable and efficient solutions to answer questions about small cellular structures such as the PD, but advancements in relevant techniques along with the ideas and methodologies explored here, will hopefully impact a research field that was previously hindered by a lack of readily available resources.

7.6.1 The availability of tools and data to other research groups

This project has further developed and brought together a series of tools that will not only benefit the plant pathology research community but also other scientific fields. Information from Chapters 3-6 will all impact the relevant research fields. However, of particular note are the characterised wheat floral and coleoptile tissues (Chapter 4) and the possible availability of wheat PM reporter lines (Chapter 5). The morphology of healthy wheat floral tissue has previously not been published and is not accessible on any open access agricultural websites. Currently available are photos and microscopic images of wheat grain development, these are available on the WheatBP website

(http://www.cerealsdb.uk.net/cerealgenomics/WheatBP/Documents/DOC_WheatBP.php). The general anatomy of this tissue would have been a significant advantage if it had been available at the start of the project. To be able to identify the cellular organisation of different plant tissues before pathogen infection is crucial if the changes that happen during infection are to be fully understood. Once the data produced in Chapter 4 has been collated properly and all gaps in this dataset are complete, I hope to make these images publicly available via WheatBP. This resource will not only be applicable to the *F. graminearum*-wheat pathosystem but for other key wheat microbe interactions, for example yellow rust. These images will also provide a starting point for researchers wanting to identify any new phenotypic characteristics in wheat TILLING mutant, EMS mutant populations or transgenic lines, with expressing specific reporter constructs produced in the future. In this project, healthy coleoptile (as well as *F. graminearum* inoculated) tissue has been imaged and will be made open access for the same reasons as described for the floral tissue.

The wheat PM reporter lines (Chapter 5) were produced as part of the Designing Future Wheat (DFW) initiative (https://designingfuturewheat.org.uk/resources/), to produce a resource that has been missing from the wheat genetics/functional genomics toolset. Even though producing wheat PM reporter lines has so far been unsuccessful here, the problems and limitations with producing these tools via transformation have been highlighted and will hopefully help generate successful PM reporter lines for wheat in the future. This resource once generated would be made available to the entire wheat biology community.

7.6.2 A transgenic approach to disease control

In Chapter 1, the limitations associated with the current approaches to control FHB disease using improved crop genetics were discussed. Fungicides, although evaluated through rigorous safety testing still have unwanted off-target effects on the ecosystem, as well as being expensive and time consuming to apply. In addition, applying these agrochemicals before FHB develops in the host is difficult; as a result of the asymptomatic phase, farmers cannot determine when the crop becomes infected. Due to this, fungicides will be applied inappropriately, increasing the chances of pathogen resistance to these chemicals. Screening technologies, such as the use of multispectral imaging to detect early presymptomatic disease, is still a long way off from being deployed on a global scale and therefore other control approaches need to be considered and developed as part of an integrated control strategy.

Genetic improvement of crops through conventional breeding, has been used for decades as a way to introduce new disease resistant genes into the host crop. However, a continuously expanding global population now means we need to achieve the same results more quickly – this can be accomplished using genetic modification (GM) and gene editing technologies. Current legislation has led to GM crop restrictions within the EU, with intensive authorisation processes in place (more information concerning this can be seen on the ec.europa.eu website), with several EU countries banning them altogether. In the UK GM crops are not grown commercially but are imported. On the other hand, gene editing is a relatively new technology, with legislation for gene editing crops still being discussed. In 2018, gene editing for crop precision breeding, was voted by the European Court of Justice to follow the same regulations as that for GM organisms[484]. At the time of writing legislation for gene editing in crops is still

being debated in the UK (https://consult.defra.gov.uk/agri-food-chain-directorate/the-regulation-of-genetic-technologies/). If climate change is to be combatted, and both pre-and post-harvest food and feed wastage reduced, sustainable and resilient agriculture needs to be achieved. These regulations surrounding GM and gene editing therefore need to be continuously reviewed.

The new tools and procedures designed and produced here are purely meant for performing in depth fungal pathology research that was previously not possible. However, using the VIGS bioinformatics and consequent experimental results (Chapter 6), there may be reason for this work to impact the use of transgenics in FHB disease control. One approach is by altering PD permeability. Altering these small channels within the host, to slow down or prevent pathogen progression, will need to be fine-tuned, for example triggered by sensing DON production, so as not be detrimental to the host. Therefore, in this case a combination of transgenic and conventional approaches may be the best solution, minimising any off-target effects in the host.

7.7 Future directions for *F. graminearum*-wheat research

An understanding of both the cellular and molecular mechanisms alongside reliable genetic and transcriptomic datasets is essential to understand a pathosystem and develop a means to combat pathogen infection and proliferation. Some of the short-term solutions to problems faced in this project have been discussed above, here the future of long-term *F. graminearum* research in correspondence with the results found here will be discussed.

Imaging *Z. tritici* and *F. graminearum in planta* is not an easy task, stable transgenic plant lines (Chapter 5) are needed to save time and achieve a reliable experimental system that can be replicated, but this is expensive and difficult. The more that is learnt about PD through the use of high-resolution microscopes and molecular studies (Chapter 4 and 6), the more specific PD protein identification will be, allowing researchers to visualise the PD-PM specifically, rather than the PM as a whole. Wheat transformation (Chapter 5) technologies, leading to the over-expression of a gene product(s), can result in unwanted growth developmental phenotypes – recent developments have now shown an inducible transgene system can be initiated but advancements in the understanding of the wheat genome and a need for improved wheat genome annotations are needed[485].

With the discovery of PD-PM complexes, and evidence that effectors in other plant pathosystems localise to the PD, research into how all these components interact would be an interesting path to pursue. Effectors can be characterised by their genetic make-up but do some possess PD signals? At the time of writing no *F. graminearum* effectors that localise to wheat PD have been identified. This is the next step in understanding the PD-*F. graminearum* interaction at the molecular level. Even though some filamentous fungi can be observed to use PD to grow intracellularly, are changes in PD permeability observed when a fungus such as *Z. tritici* invades the tissue but does not cross into the cell, and if so, how does this compare to intracellular colonising fungi?

Hyphal heterogeneity in both *Z. tritici* and *F. graminearum* is something that has yet to be explored at a wholescale level in detail. Heterogeneity does not just

exist at the cellular level in hyphae but also at the molecular level as the hyphae grow within the host. In *Aspergillus oryzae*, septal plugs help maintain hyphal heterogeneity at the molecular level, regulating what passes from one fungal cell to the next; this is controlled by Woronin bodies (an organelle derived from peroxisomes)[486]. In *Z. tritici*, fluorescent tagging of Woronin bodies as well as the fungal plasma membrane revealed that Woronin bodies were recruited to septal pores when cells were wounded[487]. This study also demonstrated that some Woronin bodies moved via an active process traveling from the injured or dead cell to the septal pore[487]. Further exploration of this topic in *F. graminearum* and *Z. tritici* by bioimaging could reveal where proteins are expressed within the fungus and how this affects the surrounding tissues. Identifying where key components i.e. DON synthesising enzymes are located in live tissue, could explain why certain cellular changes occur during infection. Furthermore, in the coleoptile tissue, *F. graminearum* does not produce DON, why is this therefore needed as a virulence factor in mature tissue – this once again highlights the differences in the wheat coleoptile and wheat floral tissue that need to be explored further (Chapter 4)[303].

Finally, the question of whether other *Fusarium* species use the PD to grow intracellularly needs to be addressed. Intercomparisons of different *Fusarium* species' genomes and transcriptomic datasets may allude to single genes or gene clusters that are responsible for passage through the PD. Silencing or overexpression of PD proteins and their effect on pathogen progression may also contribute to answering this question (Chapter 6).

7.8 Concluding remarks

How fungal pathogens communicate with plant cells and cause disease requires a detailed understanding of the host and fungal pathogen individually as well as together. This project has attempted to produce and develop new methodologies, assays, tools and datasets which were not previously available, to answer questions which previously could not be answered. The unsuccessful *Z. tritici* biosensor (Chapter 3) and wheat PM reporter lines (Chapter 5) highlight many of the problems faced when designing new resources, however solutions for these are available and therefore will be accessible to the wheat community in the future. Very detailed infected and non-infected wheat floral tissue and coleoptile cellular datasets have been produced (Chapter 4), identifying characteristics of previously unknown cellular interactions. These will benefit the wider, as well as the plant pathology, wheat research community. Finally, wheat PD orthologs have potentially been identified (Chapter 6). When their molecular functions are deduced in future VIGS studies, it will be possible to assess how each predicted PD localised protein may affect the *F. graminearum*-wheat floral interaction outcome. This work lays the foundations for future *Fusarium* projects as well as determining how PD can play a role in disease resistance to other pathogens in the future.

Appendix 1 – Gateway® PCR primers

Primer name	Sequence 5' -> 3'
MitroGFP2orp1GW F	GGGGACAAGTTTGTACAAAAAAGCAGGCTACCATGTTGTCACTACGTCAATCTATAAG
MitroGFP2orp1GW R	GGGGACCACTTTGTACAAGAAAGCTGGGTCTATTCCACCTCTTTCAAAAGTTCTTC
MitoPerceval2GW F	GGGGACAAAGTTTGTACAAAAAAGCAGGCTACCATGTTGTGTCAACAAATGATCAGAACC
MitoPerceval2GW F	GGGGACCACTTTGTACAAGAAAGCTGGGTTTATAGTGCTTCCTTGCCTTCCTCC

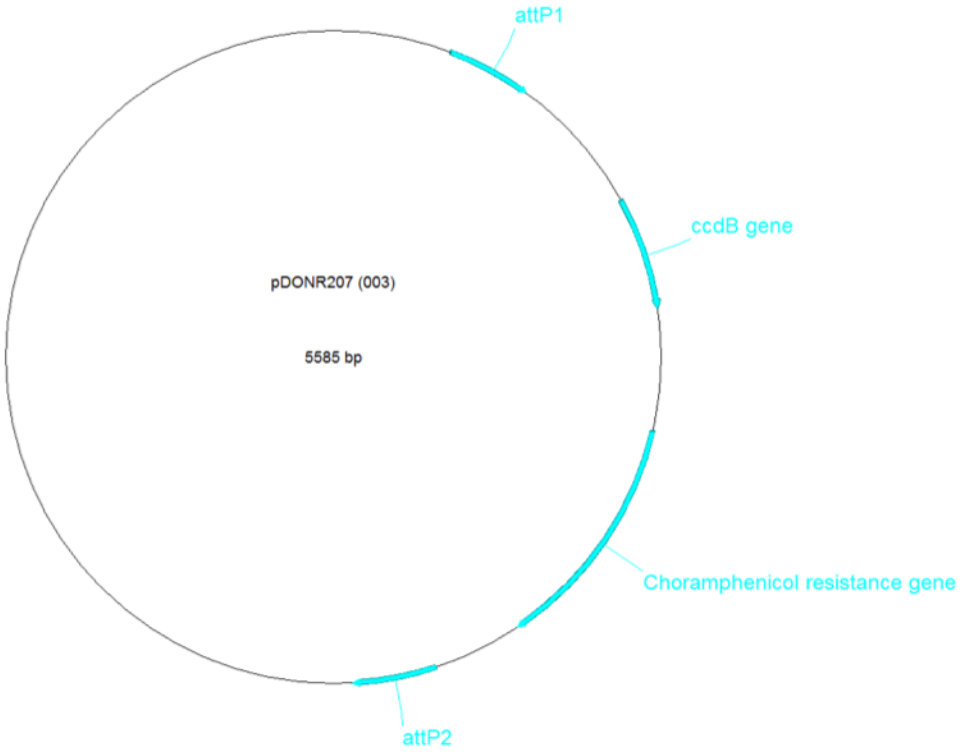

Appendix 2 – pDONR207 vector map

Appendix 3 – mitroGFP-Orp1 sequencing primers

Primer name	Sequence 5' -> 3'
MitroGFP2Orp1seq F1	GACCACATGAAGCAGCACGAC
MitroGFP2Orp1seq F2	CAACGAGAAGCGCGATCACA
MitroGFP2Orp1seq F3	CCTGGCTCTGATGAAGAAATTGCCCA
MitroGFP2Orp1seq R1	CGGGTCTTGTAGTTGCCGTCGTC

A

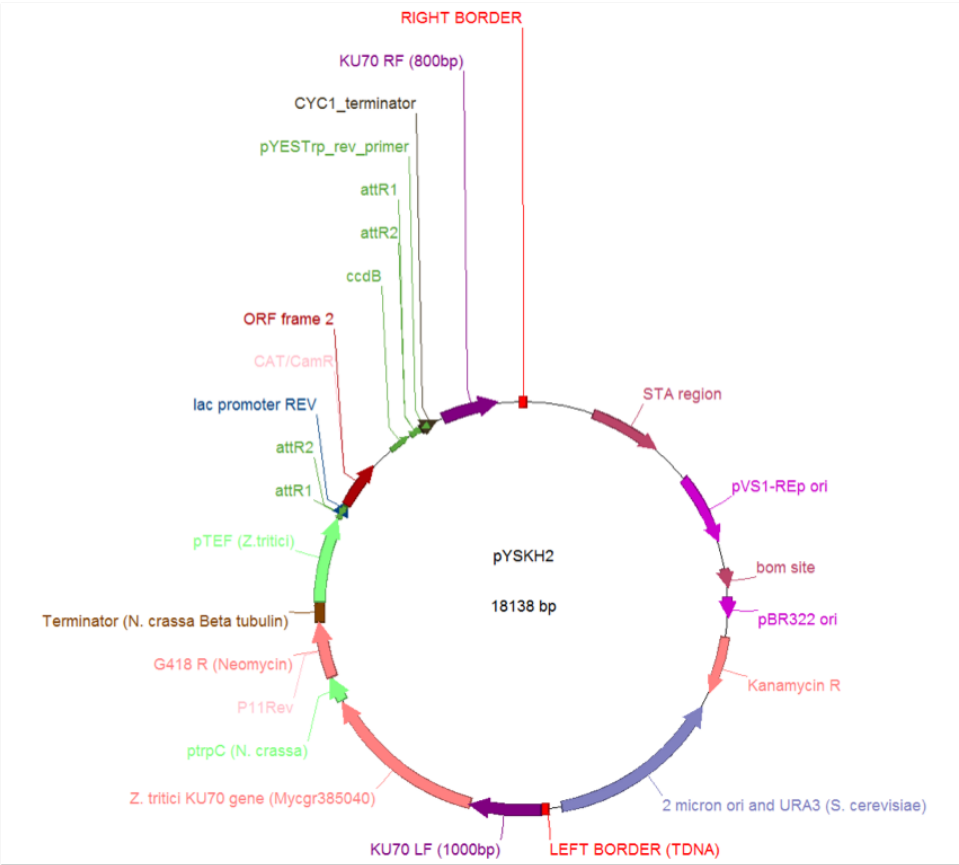

B

Appendix 4 – pYSKH2 (A) and pYSKH3 (B) vector map

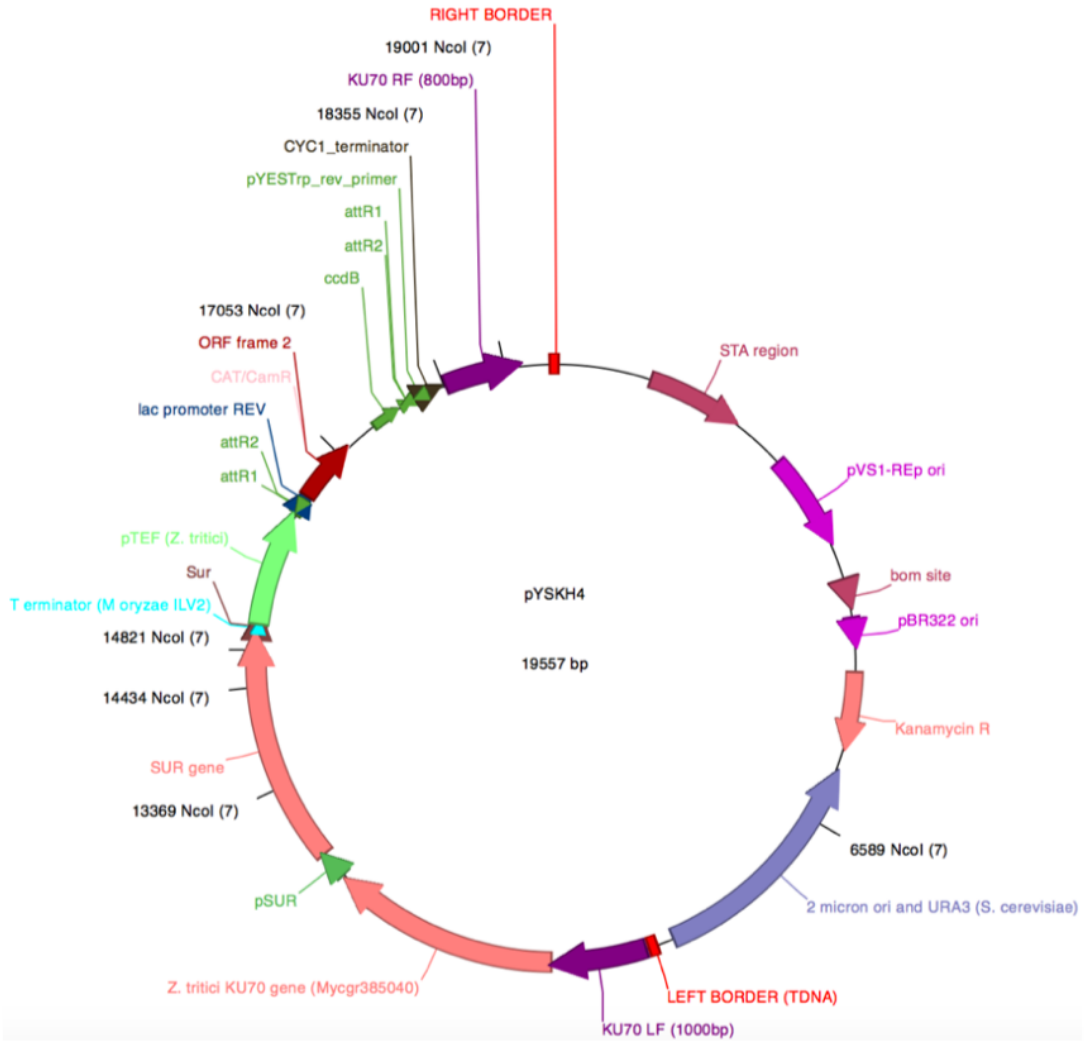

Appendix 5 – pYSKH4 vector map

Appendix 6 – Zymoseptoria tritici overexpression vector selective marker

Primer name	Sequence 5' -> 3'
MARKER-F	CGCGCCGAATTCGAGCTCGGTACCCAA
MARKER-R	TCCCCAACTGGTTCCCGGTCGGCATCTACT

Appendix 7 – GFP spectral analysis data

Excitation wavelength (nm)	Average Signal Intensity (arbitrary units)	Standard error
491	76	15.5
505	75.1	16.2
519	42.7	9.4
532	25.3	5.2
546	14.5	3.3
560	6.1	1.2
573	3.4	0.8
587	2.2	0.5
601	1.4	0.3
614	1	0.3
628	0.9	0.3

Appendix 8 – Raw data and calculation of the standard error of the mean for water inoculated coleoptile growth data.

Replicate 1

		Seedling Pair										Seedling Pair											
		1		2		3		4		5		6		7		8		9		10		Mean	
		Control	Inoculated	Control	Inoculated	Control	Inoculated	Control	Inoculated	Control	Inoculated	Control	Inoculated	Control	Inoculated	Control	Inoculated	Control	Inoculated	Control	Inoculated	Control	Inoculated
Day	1	0	0	0	0	0	0	0	0	0	0	0	0.5	0	0	0	0.5	0	0	0	0	0	0.1
	2	0	3.5	0	0	0	2	1.5	2.5	0	4.5	0	0.5	5	5.5	4.5	3	3	6.5	4.5	5	1.85	3.3
	3	3	12	4	5	3	11	8.5	11.5	4	18.5	4	6	13	13.5	15	9	17	11	15.5	14.5	8.7	11.2
	4	8	21	14.5	13.5	12	19.5	22	19.5	11	26	11	16	19.5	19	19.5	19	21.5	20.5	21	21	16	19.5
	5	22	23	21.5	21	18.5	19.5	23.5	21	16	26	20.5	22	19.5	20	23	23.5	21.5	22	21	25	20.7	22.3
	6	22	23	21.5	21	20.5	21	24	22	16	26	21.5	22	19.5	20	23	23.5	21.5	23	23	25	21.25	22.65
	7	22	23	21.5	21	21.5	21	24	22	16	26	21.5	22	19.5	20	23	23.5	21.5	23	23	25	21.35	22.65
	8	22	23	21.5	21	21.5	21	24	22	16	26	21.5	22	19.5	20	23	23.5	21.5	23	23	25	21.35	22.65
	9	22	23	21.5	21	21.5	21	24	22	16	26	21.5	22	19.5	20	23	23.5	21.5	23	23	25	21.35	22.65
	10	22	23	21.5	21	21.5	21	24	22	16	26	21.5	22	19.5	20	23	23.5	21.5	23	23	25	21.35	22.65

Replicate 2

		Seedling Pair										Seedling Pair											
		1		2		3		4		5		6		7		8		9		10		Mean	
		Control	Inoculated	Control	Inoculated	Control	Inoculated	Control	Inoculated	Control	Inoculated	Control	Inoculated	Control	Inoculated	Control	Inoculated	Control	Inoculated	Control	Inoculated	Control	Inoculated
Day	1	0	0	0	0	0	0	0	0	0	0.5	0	0	0	0	0	0	0	0	0	0	0.1	0.05
	2	4.5	5	3	5.5	5.5	5	5	0	6	4.5	0	0	5	4.5	0	3	0	0.5	3.5	6	5.2	2.65
	3	18	12	10	13	13.5	15	14	5.5	16	15.5	2	14.5	14	12	0	15	0	4	11	16	14.4	13.3
	4	23	18.5	22.5	23	18	17.5	17	21	25.5	22	11	17	19	20.5	9	21	0	6	20.5	18	22.75	19.45
	5	23	21.5	22.5	23.5	21	19	19.5	22	25.5	22	17	22	19	21	12.5	21	0	6	22	20	23.85	21
	6	23	22	22.5	23.5	21	22	23	22	25.5	22	18.5	22	19	21	20	21	15	6	22	20.5	23.95	21.35
	7	23	22	22.5	23.5	21	22	23	22	25.5	22	18.5	22	19	21	20	22	22.5	6	22	20.5	23.95	21.45
	8	23	22	22.5	23.5	21	22	23	22	25.5	22	18.5	22	19	21	20	22	22.5	6	22	20.5	23.95	21.45
	9	23	22	22.5	23.5	21	22	23	22	25.5	22	18.5	22	19	21	20	22	22.5	6	22	20.5	23.95	21.45
	10	23	22	22.5	23.5	21	22	23	22	25.5	22	18.5	22	19	21	20	22	22.5	6	22	20.5	23.95	21.45

Replicate 3

		Seedling Pair										Seedling Pair											
		1		2		3		4		5		6		7		8		9		10		Mean	
		Control	Inoculated	Control	Inoculated	Control	Inoculated	Control	Inoculated	Control	Inoculated	Control	Inoculated	Control	Inoculated	Control	Inoculated	Control	Inoculated	Control	Inoculated	Control	Inoculated
Day	1	0	0	0	0	0.5	0.5	0	0	0	0	0	0	0	0.5	0.5	0	0	0	0.5	0.5	0.1	0.05
	2	3.5	0.5	3	3	3.5	3.5	5.5	5	2.5	3	0	0	3.5	6	7	4.5	0.5	3.5	5.5	6.5	5.2	2.65
	3	12.5	11.5	12	13.5	13.5	13	12	15	10	12.5	1	6	12.5	15	14	13.5	4.5	11	15.5	14.5	14.4	13.3
	4	23	16.5	24	22.5	24.5	22.5	22	21	22	19	4	17.5	26	24	17	23.5	12	22.5	17.5	18	22.75	19.45
	5	24	21.5	24	27	24.5	23	22	21	23.5	20	5	23.5	26	24	21.5	23.5	19	23	17.5	19	23.85	21
	6	24	21.5	24	27	25	23	22	23	23.5	20	5	23.5	28	24	21.5	23.5	21	23	17.5	19	23.95	21.35
	7	24	21.5	24	27	25	23	22	23	23.5	20	5	23.5	28	24	21.5	23.5	21	23	17.5	19	23.95	21.45
	8	24	21.5	24	27	25	23	22	23	23.5	20	5	23.5	28	24	21.5	23.5	21	23	17.5	19	23.95	21.45
	9	24	21.5	24	27	25	23	22	23	23.5	20	5	23.5	28	24	21.5	23.5	21	23	17.5	19	23.95	21.45
	10	24	21.5	24	27	25	23	22	23	23.5	20	5	23.5	28	24	21.5	23.5	21	23	17.5	19	23.95	21.45

Standard error of the mean

Day	Mean (mm)		Standard deviation (mm)		Standard error of the mean (mm)	
	Control	Inoculated	Control	Inoculated	Control	Inoculated
0	0	0	0	0	0	0
1	0.05357143	0.10344828	0.16012815	0.20892772	0.03026138	0.03948363
2	3.05357143	3.37931034	2.2617216	2.12342379	0.42742521	0.40128938
3	10.4285714	11.7758621	5.21899336	3.14860135	0.98629704	0.59502973
4	18.3392857	19.3275862	5.38404047	2.51049385	1.01748801	0.47443874
5	21.1071429	21.3965517	3.0770032	1.84259924	0.58149895	0.34821853
6	21.9107143	21.7241379	2.53662629	1.64670587	0.47937731	0.31119816
7	21.9464286	21.7586207	2.52311254	1.62853198	0.47682345	0.30776362
8	21.9464286	21.7586207	2.52311254	1.62853198	0.47682345	0.30776362
9	21.9464286	21.7586207	2.52311254	1.62853198	0.47682345	0.30776362
10	21.9464286	21.7586207	2.52311254	1.62853198	0.47682345	0.30776362

NB: Grey columns indicate values which were removed from analysis.

Appendix 9 – Raw data and calculation of the standard error of the mean for PH-1 inoculated coleoptile growth data.

Replicate 1

		Seedling Pair										Seedling Pair										Mean	
		1		2		3		4		5		6		7		8		9		10			
		Control	Inoculated	Control	Inoculated	Control	Inoculated	Control	Inoculated	Control	Inoculated	Control	Inoculated	Control	Inoculated	Control	Inoculated	Control	Inoculated	Control	Inoculated	Control	Inoculated
Day	1	0.5	0	0	0	0	0	0	0	0	0	0	0	0	0	0.5	0	0	0.5	0	0	0.1	0.05
	2	6	0.5	3	5	3.5	2.5	5	0.5	6	0.5	6.5	1.5	6.5	0.5	7	4	5	6.5	3.5	5	5.2	2.65
	3	13	10	16	22	11	15.5	19.5	15	11.5	8.5	15.5	5.5	12	9	16.5	16	16	15.5	13	16	14.4	13.3
	4	26	20.5	24.5	23	22	19.5	20	22	22.5	11	21	9.5	21.5	22	25.5	22.5	22	21.5	22.5	23	22.75	19.45
	5	26	21.5	24.5	23.5	24	21.5	24.5	22	22.5	11	21	19.5	21.5	22	25.5	22.5	23	23.5	26	23	23.85	21
	6	26	21.5	24.5	23.5	24	22	24.5	22	22.5	11	21	20.5	21.5	22	25.5	22.5	24	25.5	26	23	23.95	21.35
	7	26	21.5	24.5	23.5	24	23	24.5	22	22.5	11	21	20.5	21.5	22	25.5	22.5	24	25.5	26	23	23.95	21.45
	8	26	21.5	24.5	23.5	24	23	24.5	22	22.5	11	21	20.5	21.5	22	25.5	22.5	24	25.5	26	23	23.95	21.45
	9	26	21.5	24.5	23.5	24	23	24.5	22	22.5	11	21	20.5	21.5	22	25.5	22.5	24	25.5	26	23	23.95	21.45
	10	26	21.5	24.5	23.5	24	23	24.5	22	22.5	11	21	20.5	21.5	22	25.5	22.5	24	25.5	26	23	23.95	21.45

Replicate 2

		Seedling Pair										Seedling Pair										Mean	
		1		2		3		4		5		6		7		8		9		10			
		Control	Inoculated	Control	Inoculated	Control	Inoculated	Control	Inoculated	Control	Inoculated	Control	Inoculated	Control	Inoculated	Control	Inoculated	Control	Inoculated	Control	Inoculated	Control	Inoculated
Day	1	0	0	0.5	0	0	0	0.5	0	0	0	0	0	0	0	0	0	0	0	0.5	0	0.15	0
	2	0	4.5	4	0.5	6.5	5	4.5	0.5	0	5	2.5	2.5	3	4	4.5	5	3.5	0	4	2.5	3.25	2.95
	3	0	15	4	11.5	13.5	12	14.5	7	7.5	15	16	16.5	14	15	13.5	15	16	9	13	11	11.2	12.7
	4	4	20	5.5	22	25	17	23	18	19	21.5	22	22.5	20.5	23	24	22	20.5	18	21.5	19	18.5	20.3
	5	16	21.5	6	22	25	18.5	27	18.5	22	21.5	22	23	22	24	24	24.5	20.5	18	23	21.5	20.75	21.3
	6	16.5	22.5	6	22	25	18.5	27	18.5	22	21.5	22	25	22	24	24	24.5	20.5	18	23	21.5	20.8	21.6
	7	16.5	22.5	6	22	25	18.5	27	18.5	22	21.5	22	25	22	24	24	24.5	20.5	18	23	21.5	20.8	21.6
	8	16.5	22.5	6	22	25	18.5	27	18.5	22	21.5	22	25	22	24	24	24.5	20.5	18	23	21.5	20.8	21.6
	9	16.5	22.5	6	22	25	18.5	27	18.5	22	21.5	22	25	22	24	24	24.5	20.5	18	23	21.5	20.8	21.6
	10	16.5	22.5	6	22	25	18.5	27	18.5	22	21.5	22	25	22	24	24	24.5	20.5	18	23	21.5	20.8	21.6

Replicate 3

		Seedling Pair										Seedling Pair									
		1		2		3		4		5		6		7		8		9		10	
		Control	Inoculated	Control	Inoculated	Control	Inoculated	Control	Inoculated	Control	Inoculated	Control	Inoculated	Control	Inoculated	Control	Inoculated	Control	Inoculated	Control	Inoculated
Day	1	0	0	0	0	0.5	0	0	0	0.5	0	0	0	0	0	0	0	0	0	0	0
	2	5	5	2.5	0.5	6.5	6.5	0	4.5	4	0.5	3.5	4	3.5	3	3	2	3.5	2.5	2	4
	3	14.5	14.5	15.5	7	12	9	6	10	11.5	8.5	11	12	13.5	13	17	13.5	16	15.5	10.5	14.5
	4	23	22	16	21	23.5	18	13	25	21.5	23.5	25	22.5	20.5	21.5	23.5	22.5	22	24	22.5	22.5
	5	23.5	22	19.5	21.5	24	23	20	25	21.5	24	27	22.5	21	22.5	26	24.5	22.5	26.5	23	25
	6	23.5	22	19.5	21.5	24	23	21	25	21.5	24	27	22.5	21	22.5	26	24.5	25	26.5	23	25
	7	23.5	22	19.5	21.5	24	23	21	25	21.5	24	27	22.5	21	22.5	26	24.5	25	26.5	23	25
	8	23.5	22	19.5	21.5	24	23	21	25	21.5	24	27	22.5	21	22.5	26	24.5	25	26.5	23	25
	9	23.5	22	19.5	21.5	24	23	21	25	21.5	24	27	22.5	21	22.5	26	24.5	25	26.5	23	25
	10	23.5	22	19.5	21.5	24	23	21	25	21.5	24	27	22.5	21	22.5	26	24.5	25	26.5	23	25

Standard error of the mean

Day	Mean (mm)		Standard Deviation (mm)		Standard error of the mean (mm)	
	Control	Inoculated	Control	Inoculated	Control	Inoculated
0	0	0	0	0	0	0
1	0.10344828	0.01724138	0.20612541	0.09284767	0.03827653	0.01724138
2	3.93103448	3.03448276	1.94901137	2.01747294	0.36192233	0.37463532
3	13.0862069	12.7241379	3.79395423	3.66105519	0.70451961	0.67984088
4	21.2931034	21	4.27517176	2.94594152	0.79387947	0.54704761
5	23.0344828	22.362069	2.46015038	1.99506781	0.45683846	0.37047479
6	23.2068966	22.5862069	2.39984092	2.06185148	0.44563927	0.38287621
7	23.2068966	22.6206897	2.39984092	2.06005883	0.44563927	0.38254332
8	23.2068966	22.6206897	2.39984092	2.06005883	0.44563927	0.38254332
9	23.2068966	22.6206897	2.39984092	2.06005883	0.44563927	0.38254332
10	23.2068966	22.6206897	2.39984092	2.06005883	0.44563927	0.38254332

NB: Grey columns indicate values which were removed from analysis.

Analysis of variance
==========

Variate: Day2

Source of variation	d.f.(m.v.)	s.s.	m.s.	v.r.	F pr.
Occasion stratum	2	17.535	8.768	1.99	
Occasion.Seedling_Pair stratum					
Treatment	1	2.826	2.826	0.64	0.427
Residual	55(1)	242.501	4.409	1.07	
Occasion.Seedling_Pair.Seedling stratum					
Inoculation	1	14.742	14.742	3.58	0.064
Treatment.Inoculation	1	0.029	0.029	0.01	0.933
Residual	53(5)	218.376	4.120		
Total	113(6)	475.465			

Analysis of variance
==========

Variate: Day2
Probabilities determined from 999 random permutations

Source of variation	d.f.	m.v.	s.s.	m.s.	v.r.	prob.
Occasion stratum	2	0	17.535	8.768	1.99	
Occasion.Seedling_Pair stratum						
Treatment	1	0	2.826	2.826	0.64	0.433
Residual	55	1	242.501	4.409	1.07	
Occasion.Seedling_Pair.Seedling stratum						
Inoculation	1	0	14.742	14.742	3.58	0.078
Treatment.Inoculation	1	0	0.029	0.029	0.01	0.927
Residual	53	5	218.376	4.120		
Total	113	6	475.465			

Analysis of variance
==========

Variate: Day3

Source of variation	d.f.(m.v.)	s.s.	m.s.	v.r.	F pr.
Occasion stratum	2	95.37	47.69	3.12	
Occasion.Seedling_Pair stratum					
Treatment	1	1.26	1.26	0.08	0.775
Residual	55(1)	839.31	15.26	1.07	
Occasion.Seedling_Pair.Seedling stratum					
Inoculation	1	2.32	2.32	0.16	0.688
Treatment.Inoculation	1	12.80	12.80	0.90	0.348
Residual	53(5)	755.85	14.26		
Total	113(6)	1641.75			

Analysis of variance
==========

Variate: Day3
Probabilities determined from 999 random permutations

Source of variation	d.f.	m.v.	s.s.	m.s.	v.r.	prob.
Occasion stratum	2	0	95.37	47.69	3.12	
Occasion.Seedling_Pair stratum						
Treatment	1	0	1.26	1.26	0.08	0.771
Residual	55	1	839.31	15.26	1.07	
Occasion.Seedling_Pair.Seedling stratum						
Inoculation	1	0	2.32	2.32	0.16	0.702
Treatment.Inoculation	1	0	12.80	12.80	0.90	0.376
Residual	53	5	755.85	14.26		
Total	113	6	1641.75			

Analysis of variance
==========

Variate: Day4

Source of variation	d.f.(m.v.)	s.s.	m.s.	v.r.	F pr.

```
Occasion stratum                 2           83.92      41.96
3.04

Occasion.Seedling_Pair stratum
Treatment                        1           14.93      14.93
1.08  0.303
Residual                        55(1)       759.08      13.80
1.04

Occasion.Seedling_Pair.Seedling stratum
Inoculation                      1            2.27       2.27
0.17  0.681
Treatment.Inoculation            1            0.00       0.00
0.00  0.987
Residual                        53(5)       704.46      13.29

Total                          113(6)      1544.56


Analysis of variance
====================

Variate: Day4
Probabilities determined from 999 random permutations

Source of variation                     d.f. m.v.       s.s.
m.s.    v.r.  prob.
Occasion stratum                           2    0      83.92
41.96    3.04
Occasion.Seedling_Pair stratum
Treatment                                  1    0      14.93
14.93    1.08  0.306
Residual                                  55    1     759.08
13.80    1.04
Occasion.Seedling_Pair.Seedling stratum
Inoculation                                1    0       2.27
2.27    0.17  0.708
Treatment.Inoculation                      1    0       0.00
0.00    0.00  0.983
Residual                                  53    5     704.46
13.29
Total                                    113    6    1544.56
```

Analysis of variance
==========

Variate: Day5

Source of variation	d.f.(m.v.)	s.s.	m.s.	v.r.	F pr.
Occasion stratum	2	68.690	34.345	6.22	
Occasion.Seedling_Pair stratum					
Treatment	1	9.578	9.578	1.73	0.193
Residual	55(1)	303.617	5.520	1.12	
Occasion.Seedling_Pair.Seedling stratum					
Inoculation	1	6.636	6.636	1.34	0.252
Treatment.Inoculation	1	1.301	1.301	0.26	0.610
Residual	53(5)	262.150	4.946		
Total	113(6)	645.958			

Analysis of variance
==========

Variate: Day5
Probabilities determined from 999 random permutations

Source of variation	d.f.	m.v.	s.s.	m.s.	v.r.	prob.
Occasion stratum	2	0	68.690	34.345	6.22	
Occasion.Seedling_Pair stratum						
Treatment	1	0	9.578	9.578	1.73	0.209
Residual	55	1	303.617	5.520	1.12	
Occasion.Seedling_Pair.Seedling stratum						
Inoculation	1	0	6.636	6.636	1.34	0.289
Treatment.Inoculation	1	0	1.301	1.301	0.26	0.621
Residual	53	5	262.150	4.946		
Total	113	6	645.958			

Analysis of variance
==========

Variate: Day6

Source of variation	d.f.(m.v.)	s.s.	m.s.	v.r.	F pr.
Occasion stratum	2	45.729	22.865	4.73	
Occasion.Seedling_Pair stratum					
Treatment	1	2.282	2.282	0.47	0.495
Residual	55(1)	265.673	4.830	1.24	
Occasion.Seedling_Pair.Seedling stratum					
Inoculation	1	10.834	10.834	2.79	0.101
Treatment.Inoculation	1	0.017	0.017	0.00	0.947
Residual	53(5)	206.086	3.888		
Total	113(6)	525.116			

Source of variation	d.f.	m.v.	s.s.	m.s.	v.r.	prob.
Occasion stratum	2	0	45.729	22.865	4.73	
Occasion.Seedling_Pair stratum						
Treatment	1	0	2.282	2.282	0.47	0.519
Residual	55	1	265.673	4.830	1.24	
Occasion.Seedling_Pair.Seedling stratum						
Inoculation	1	0	10.834	10.834	2.79	0.111
Treatment.Inoculation	1	0	0.017	0.017	0.00	0.956
Residual	53	5	206.086	3.888		
Total	113	6	525.116			

Appendix 10 – Analysis of Variance (ANOVA) Genstat output for coleoptile growth between days 2 and 6. Performed by Suzanne Clark, Rothamsted Research.

Analysis of variance
==========

Variate: B

Source of variation	d.f.(m.v.)	s.s.	m.s.	v.r.	F pr.
Occasion stratum	2	1.246	0.623	0.31	
Occasion.Seedling_Pair stratum					
Treatment	1	3.940	3.940	1.98	0.165
Residual	55(1)	109.448	1.990	0.97	
Occasion.Seedling_Pair.Seedling stratum					
Inoculation	1	7.110	7.110	3.46	0.069
Treatment.Inoculation	1	3.001	3.001	1.46	0.232
Residual	53(5)	108.980	2.056		
Total	113(6)	220.533			

Analysis of variance
==========

Variate: B
Probabilities determined from 999 random permutations

Source of variation	d.f.	m.v.	s.s.	m.s.	v.r.	prob.
Occasion stratum	2	0	1.246	0.623	0.31	
Occasion.Seedling_Pair stratum						
Treatment	1	0	3.940	3.940	1.98	0.168
Residual	55	1	109.448	1.990	0.97	
Occasion.Seedling_Pair.Seedling stratum						
Inoculation	1	0	7.110	7.110	3.46	0.081
Treatment.Inoculation	1	0	3.001	3.001	1.46	0.237
Residual	53	5	108.980	2.056		
Total	113	6	220.533			

Analysis of variance
==========

Variate: M

```
Source of variation           d.f.(m.v.)      s.s.       m.s.
v.r.  F pr.

Occasion stratum                 2          0.4336     0.2168
1.60

Occasion.Seedling_Pair stratum
Treatment                        1          0.0120     0.0120
0.09  0.767
Residual                        55(1)       7.4666     0.1358
0.84

Occasion.Seedling_Pair.Seedling stratum
Inoculation                      1          0.0035     0.0035
0.02  0.885
Treatment.Inoculation            1          0.1138     0.1138
0.70  0.406
Residual                        53(5)       8.6039     0.1623

Total                          113(6)      15.9723


Analysis of variance
====================

Variate: M
Probabilities determined from 999 random permutations

Source of variation                    d.f. m.v.       s.s.
m.s.    v.r.  prob.
Occasion stratum                          2    0       0.434
0.217    1.60
Occasion.Seedling_Pair stratum
Treatment                                 1    0       0.012
0.012    0.09  0.783
Residual                                 55    1       7.467
0.136    0.84
Occasion.Seedling_Pair.Seedling stratum
Inoculation                               1    0       0.003
0.003    0.02  0.888
Treatment.Inoculation                     1    0       0.114
0.114    0.70  0.422
Residual                                 53    5       8.604
0.162
Total                                   113    6      15.972


Analysis of variance
====================

Variate: C

Source of variation           d.f.(m.v.)      s.s.       m.s.
v.r.  F pr.

Occasion stratum                 2          49.650     24.825
5.13

Occasion.Seedling_Pair stratum
```

```
Treatment                          1           1.811      1.811
0.37  0.543
Residual                        55(1)        266.385      4.843
1.19

Occasion.Seedling_Pair.Seedling stratum
Inoculation                        1          11.977     11.977
2.93  0.093
Treatment.Inoculation              1           0.007      0.007
0.00  0.967
Residual                        53(5)        216.604      4.087

Total                          113(6)        541.222


Analysis of variance
====================

Variate: C
Probabilities determined from 999 random permutations

Source of variation                      d.f. m.v.       s.s.
m.s.    v.r.  prob.
Occasion stratum                            2    0     49.650
24.825    5.13
Occasion.Seedling_Pair stratum
Treatment                                   1    0      1.811
1.811    0.37  0.566
Residual                                   55    1    266.385
4.843    1.19
Occasion.Seedling_Pair.Seedling stratum
Inoculation                                 1    0     11.977
11.977    2.93  0.103
Treatment.Inoculation                       1    0      0.007
0.007    0.00  0.962
Residual                                   53    5    216.604
4.087
Total                                     113    6    541.222
```

Appendix 11 – Analysis of Variance (ANOVA) Genstat output for Gompertz model parameters for coleoptile growth assay. Performed by Suzanne Clark, Rothamsted Research.

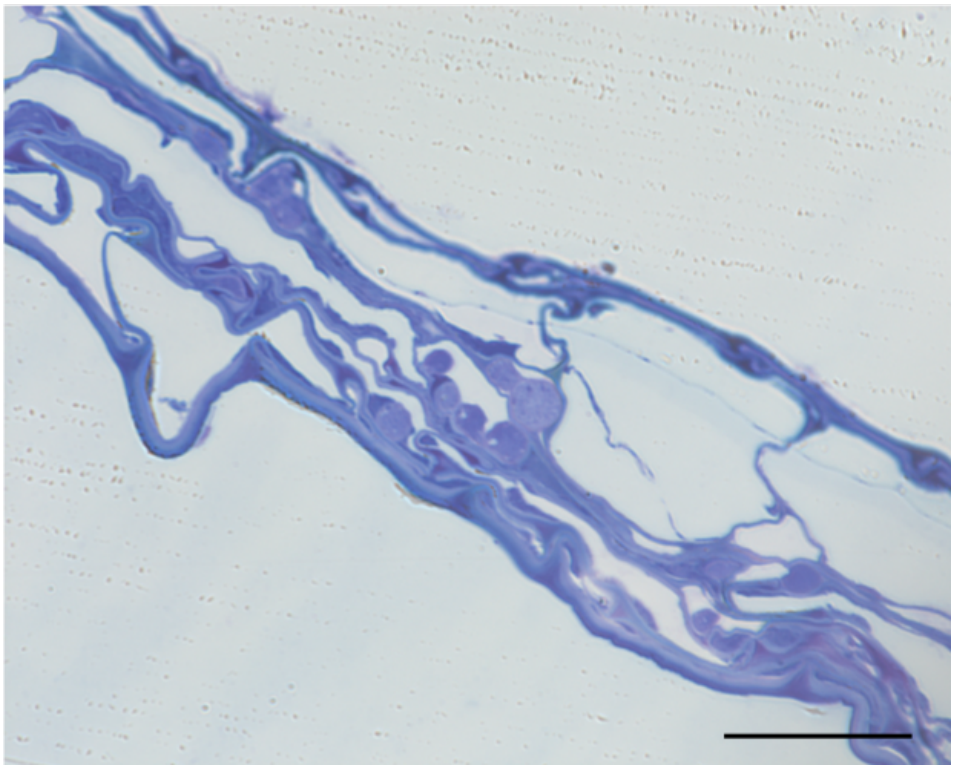

Appendix 12 – PH-1 inoculated wheat coleoptile 5 days post inoculation. Tissue has collapsed and therefore could not be used for determining *F. graminearum* infection characteristics. Bar = 25μm.

Appendix 13 – Hyphal quantification raw data.

Water-inoculated control

	Sample 1							Sample 2							Sample 3						
Distance (µm)	1	5	10	15	20	25	30	1	5	10	15	20	25	30	1	5	10	15	20	25	30
No. of intracellular hyphae	0	0	0	0	0	0	0	0	0	0	0	0	0	0	0	0	0	0	0	0	0
No. of intercellular hyphae	0	0	0	0	0	0	0	0	0	0	0	0	0	0	0	0	0	0	0	0	0
Total no. of hyphae	0	0	0	0	0	0	0	0	0	0	0	0	0	0	0	0	0	0	0	0	0
No. of hyphae crossing pit-fields	0	0	0	0	0	0	0	0	0	0	0	0	0	0	0	0	0	0	0	0	0

PH-1 control – opposite infection

	Sample 1							Sample 2							Sample 3						
Distance (µm)	1	5	10	15	20	25	30	1	5	10	15	20	25	30	1	5	10	15	20	25	30
No. of intracellular hyphae	0	1	2	5	4	1	1	0	2	4	4	3	1	1	2	2	0	1	4	2	1
No. of intercellular hyphae	0	1	2	4	5	4	2	0	0	0	0	0	0	0	3	0	0	0	0	0	0
Total no. of hyphae	0	2	4	9	9	5	3	0	2	4	4	3	1	1	5	2	0	1	4	2	1
No. of hyphae crossing pit-fields	0	0	0	0	0	0	0	0	0	0	0	0	0	0	0	0	0	0	0	0	0

PH-1 inoculated – lesion

	Sample 1							Sample 2							Sample 3						
Distance (µm)	1	5	10	15	20	25	30	1	5	10	15	20	25	30	1	5	10	15	20	25	30
No. of intracellular hyphae	59	40	34	61	106	126	79	15	30	23	37	33	28	31	110	119	90	97	98	86	84
No. of intercellular hyphae	12	16	15	15	28	26	32	3	23	19	25	30	25	24	32	59	44	42	54	43	40
Total no. of hyphae	71	56	49	76	134	152	111	18	53	42	62	63	53	55	142	178	134	139	152	129	124
No. of hyphae crossing pit-fields	0	0	0	0	1	1	0	0	0	0	0	0	0	0	0	2	2	1	1	0	1

NB: In total this experiment took approximately 4 hours to image and 2 to quantify without the use of an automated system.

Analysis of variance
==========

Variate: log_Total_no_of_hyphae

Source of variation	d.f.	s.s.	m.s.	v.r.	F pr.
Sample stratum	2	0.52062	0.26031		
Sample.Half stratum					
Treatment	1	21.00910	21.00910	84.45	0.012
Residual	2	0.49753	0.24877	6.20	
Sample.Section stratum					
Distance	6	0.56472	0.09412	1.42	0.283
Residual	12	0.79305	0.06609	1.65	
Sample.Half.Section stratum					
Treatment.Distance	6	0.11844	0.01974	0.49	0.803
Residual	12	0.48160	0.04013		
Total	41	23.98506			

Tables of means
==========

Variate: log_Total_no_of_hyphae

Grand mean 1.215

Treatment	PH-1 sample (lesion)	PH-1 sample CONTROL
	1.923	0.508

Distance	1	5	10	15	20	25	30
	1.012	1.195	1.143	1.305	1.404	1.265	1.183

Treatment	Distance	1	5	10	15	20
PH-1 sample (lesion)		1.764	1.914	1.821	1.944	2.040
PH-1 sample CONTROL		0.259	0.477	0.466	0.667	0.767

Treatment	Distance	25	30
PH-1 sample (lesion)		2.010	1.965
PH-1 sample CONTROL		0.519	0.401

Standard errors of differences of means

Table	Treatment	Distance	Treatment Distance
rep.	21	6	3
s.e.d.	0.1539	0.1484	0.2351
d.f.	2	12	9.30

Except when comparing means with the same level(s) of
Treatment 0.1882
d.f. 22.65
Distance 0.2159
d.f. 6.70

Back-transformed means

	(10**Means)-1
Treatment	
PH-1 sample (lesion)	82.67
PH-1 sample CONTROL	2.22

REML variance components analysis
==========

Covariance structures defined for random model

Covariance structures defined within terms:

Term	Factor	Model	Order	No. rows
Sample.Half.Section	Sample	Identity	1	3
	Half	Identity	0	2
	Section	Power - city block distance	1	7

Estimated variance components

Random term	component	s.e.
Sample	0.0539	0.0613
Sample.Half	-0.1508	0.3044
Sample.Section	-0.0077	0.0049

Residual variance model

Term	Factor	Model(order)	Parameter	Estimate	s.e.
Sample.Half.Section			Sigma2	0.241	0.3291
	Sample	Identity	-	-	-
	Half	Identity	-	-	-

```
                Section       Power(1)      phi_1
0.9682    0.0472
```

```
Tests for fixed effects
-----------------------
```

```
Sequentially adding terms to fixed model

Fixed term                 Wald statistic  n.d.f.   F statistic
d.d.f.    F pr
Treatment                          250.43       1        250.43
1.9   0.005
Distance                            20.52       6          3.02
8.8   0.068
Treatment.Distance                   1.44       6          0.23
13.8   0.958

Dropping individual terms from full fixed model

Fixed term                 Wald statistic  n.d.f.   F statistic
d.d.f.    F pr
Treatment.Distance                   1.44       6          0.23
13.8   0.958
```

```
Predictions from REML analysis
------------------------------

Response variate: log_Total_no_of_hyphae

Predictions

           Treatment
PH-1 sample (lesion)    1.923
 PH-1 sample CONTROL    0.508

Standard errors

           Treatment
PH-1 sample (lesion)   0.1586
 PH-1 sample CONTROL   0.1586

Approximate average standard error of difference: 0.1229
(calculated on variance
scale)

back-transformed Treatment means

           Treatment
PH-1 sample (lesion)       82.67
 PH-1 sample CONTROL        2.22
```

```
Predictions from REML analysis
------------------------------


Response variate: log_Total_no_of_hyphae

Predictions

Distance        1        5       10       15       20       25
30
           1.012    1.195    1.143    1.305    1.404    1.265
1.183


Standard errors

Distance        1        5       10       15       20       25
30
          0.1744   0.1744   0.1744   0.1744   0.1744   0.1744
0.1744


Approximate average standard error of difference: 0.1453
(calculated on variance
scale)



back-transformed Distance means


     Distance
            1        9.27
            5       14.68
           10       12.91
           15       19.20
           20       24.33
           25       17.39
           30       14.24


* MESSAGE: caution - t-values using d.d.f. from contributing terms
differ by
52.75%; LSD's will be calculated using the maximum value.

            Deviance        9.71
 d.f. of fixed model          14
d.f. of random model           5

Note: omits constant, -log(det(X'X)), that depends only on the
fixed model.


                         Current      Change
            Deviance       18.18       -8.47
 d.f. of fixed model          14           0
d.f. of random model           4          -1

Note: omits constant, -log(det(X'X)), that depends only on the
fixed mode
```

Appendix 14 – Analysis for hyphal quantification data. Performed by Suzanne Clark, Rothamsted Research using Genstat.

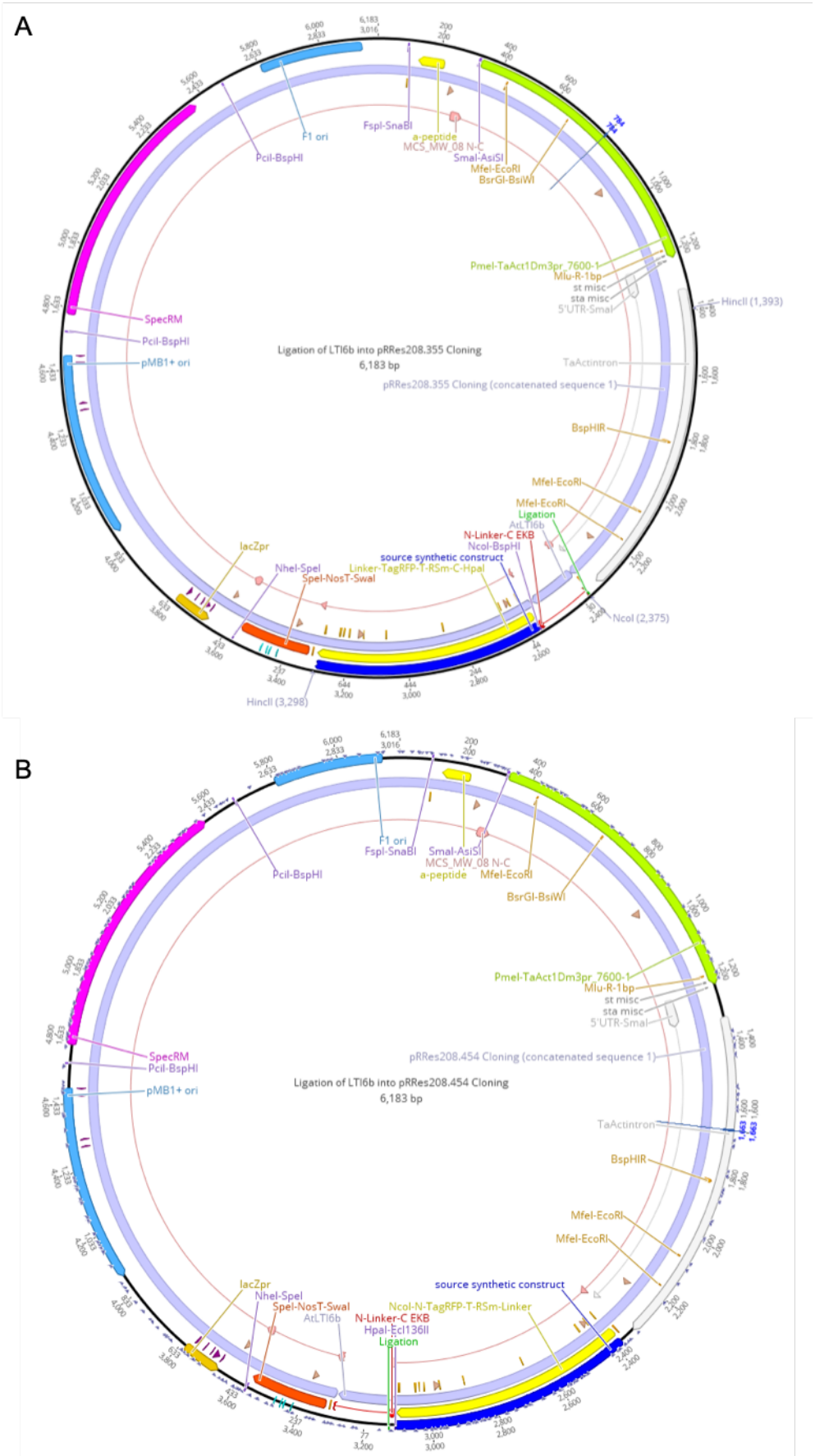
A
Ligation of LTI6b into pRRes208.355 Cloning
6,183 bp
pRRes208.355 Cloning (concatenated sequence 1)
F1 ori
FspI-SnaBI
a-peptide
MCS_MW_08 N-C
SmaI-AsiSI
MfeI-EcoRI
BsrGI-BsiWI
PciI-BspHI
Pmel-TaAct1Dm3pr_7600-1
Mlu-R-1bp
st misc
sta misc
5'UTR-SmaI
HincII (1,393)
SpecRM
PciI-BspHI
pMB1+ ori
TaActintron
BspHIR
MfeI-EcoRI
MfeI-EcoRI
Ligation
AtLTI6b
N-Linker-C EKB
NcoI-BspHI
source synthetic construct
lacZpr
NheI-SpeI
SpeI-NosT-SwaI
Linker-TagRFP-T-RSm-C-HpaI
NcoI (2,375)
HincII (3,298)
B
Ligation of LTI6b into pRRes208.454 Cloning
6,183 bp
pRRes208.454 Cloning (concatenated sequence 1)
F1 ori
FspI-SnaBI
SmaI-AsiSI
MCS_MW_08 N-C
a-peptide
MfeI-EcoRI
BsrGI-BsiWI
PciI-BspHI
Pmel-TaAct1Dm3pr_7600-1
Mlu-R-1bp
st misc
sta misc
5'UTR-SmaI
SpecRM
PciI-BspHI
pMB1+ ori
TaActintron
BspHIR
MfeI-EcoRI
MfeI-EcoRI
source synthetic construct
lacZpr
NheI-SpeI
SpeI-NosT-SwaI
AtLTI6b
N-Linker-C EKB
HpaI-Ecl136II
Ligation
NcoI-N-TagRFP-T-RSm-Linker

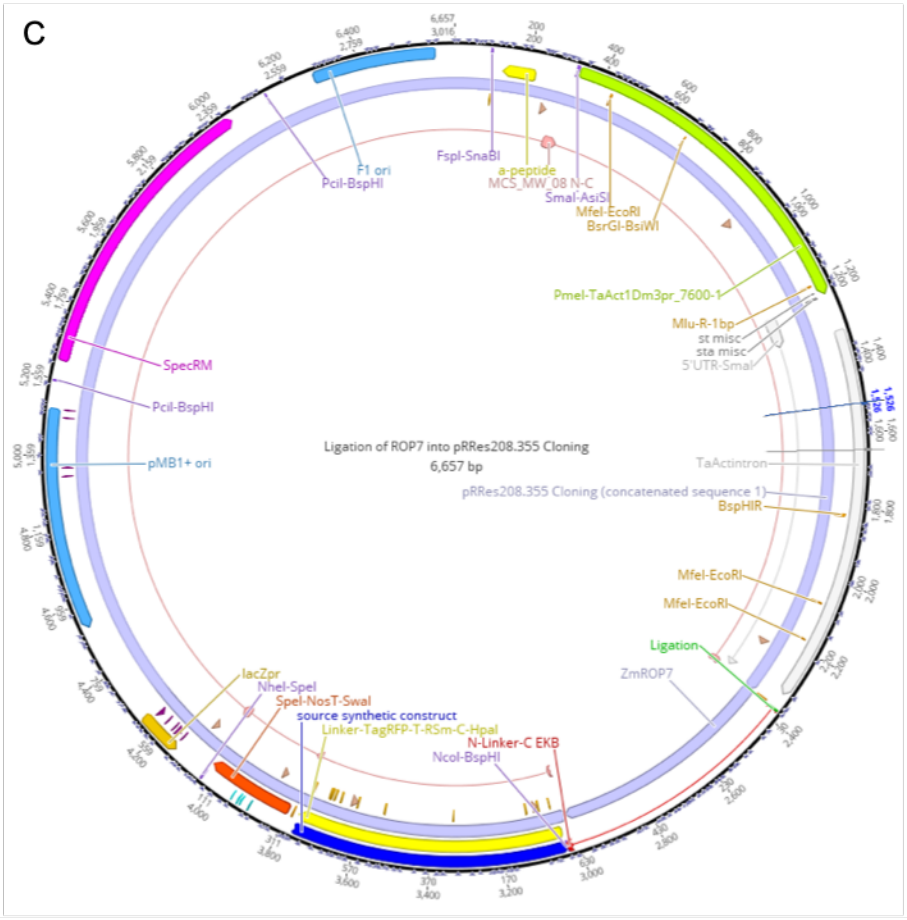
C
Ligation of ROP7 into pRRes208.355 Cloning
6,657 bp
F1 ori
PciI-BspHI
FspI-SnaBI
a-peptide
MCS_MW_08 N-C
SmaI-AsiSI
MfeI-EcoRI
BsrGI-BsiWI
Pmel-TaAct1Dm3pr_7600-1
MluI-R-1bp
st misc
sta misc
5'UTR-SmaI
SpecRM
PciI-BspHI
pMB1+ ori
TaActintron
pRRes208.355 Cloning (concatenated sequence 1)
BspHIR
MfeI-EcoRI
MfeI-EcoRI
Ligation
ZmROP7
lacZpr
NheI-SpeI
SpeI-NosT-SwaI
source synthetic construct
Linker-TagRFP-T-RSm-C-HpaI
N-Linker-C EKB
NcoI-BspHI

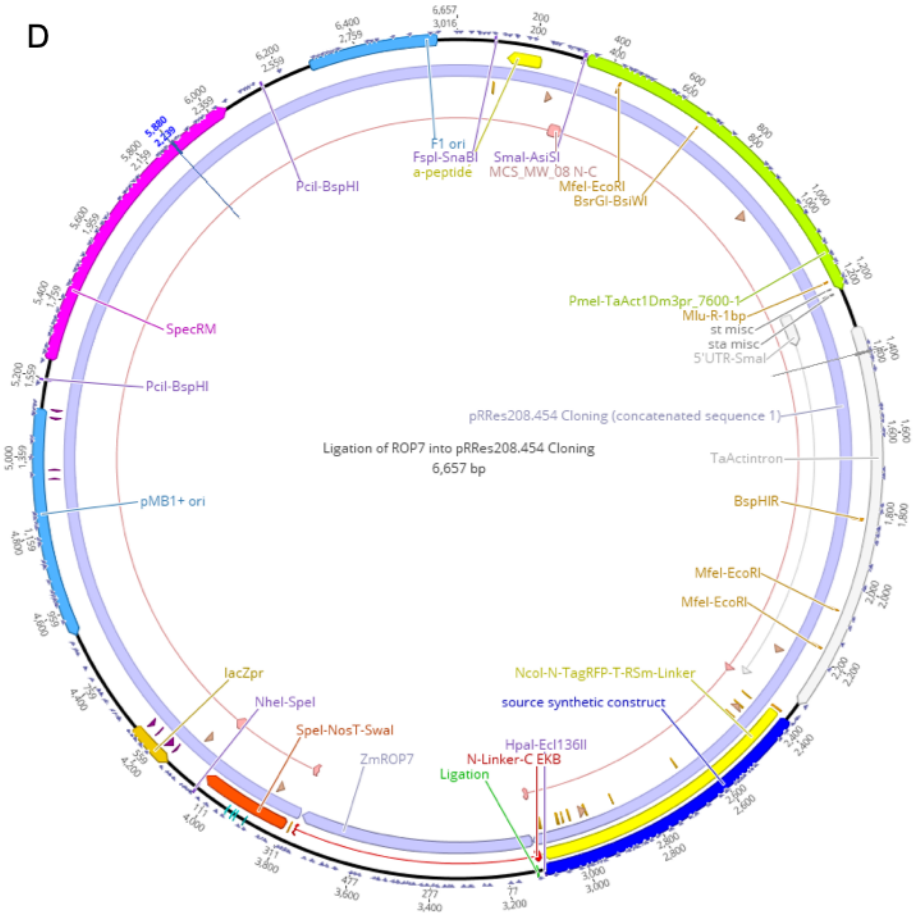
D
Ligation of ROP7 into pRRes208.454 Cloning
6,657 bp
F1 ori
FspI-SnaBI
a-peptide
SmaI-AsiSI
MCS_MW_08 N-C
MfeI-EcoRI
BsrGI-BsiWI
PciI-BspHI
Pmel-TaAct1Dm3pr_7600-1
MluI-R-1bp
st misc
sta misc
5'UTR-SmaI
SpecRM
PciI-BspHI
pRRes208.454 Cloning (concatenated sequence 1)
TaActintron
pMB1+ ori
BspHIR
MfeI-EcoRI
MfeI-EcoRI
lacZpr
NheI-SpeI
SpeI-NosT-SwaI
ZmROP7
NcoI-N-TagRFP-T-RSm-Linker
source synthetic construct
HpaI-EcI136II
N-Linker-C EKB
Ligation

Appendix 15 – Plasma membrane reporter constructs/plasmids for stable wheat transformation. (a) pRRes208.355:LTI6b (b) pRRes208.454:LTI6b (c) pRRes208.355:ROP7 (d) pRRes208.454:ROP7.

Appendix 16 –Primers for verification of wheat plasma membrane reporter constructs.

Primer name	Sequence (5'-3')
p355_F1	CACTCTGAACCGCTGATACC
p355_R1	GTTCACGGTGCCCTCCATGTA
p454_F1	CTGGAAGGCAGAACCGACATGG
p454_R1	GCTCACTCATTAGGCACCC
LTI6b_F1	CGTGTTCCTCAAGTTCGGCTG
ROP7_F1	GCCTACCTTGCTGACCATCC

Labelled as p335 or p454 corresponding to vectors pRRes208.355 and pRRes208.454 respectively.

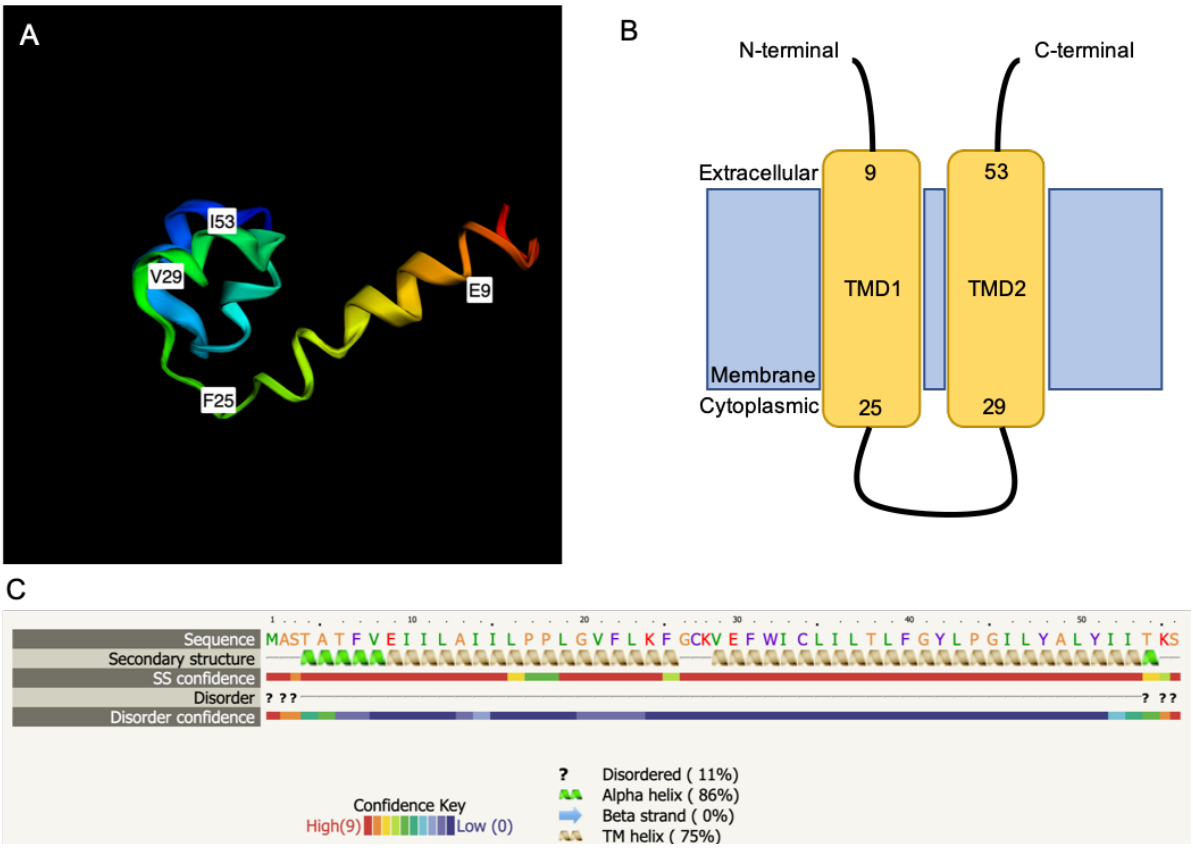

Appendix 17 – Structural analysis of modified *At*LTI6b. All analysis has been conducted using Phyre[2]. (A) Finalised structural model of modified *At*LTI6b. Labelled amino acids indicate the two transmembrane domains (TMD) seen in part (B). Coloured red to blue, corresponding to the N- and C-termini. (B) TMD of the modified *At*LTI6b protein. (C) *At*LTI6b secondary protein structure.

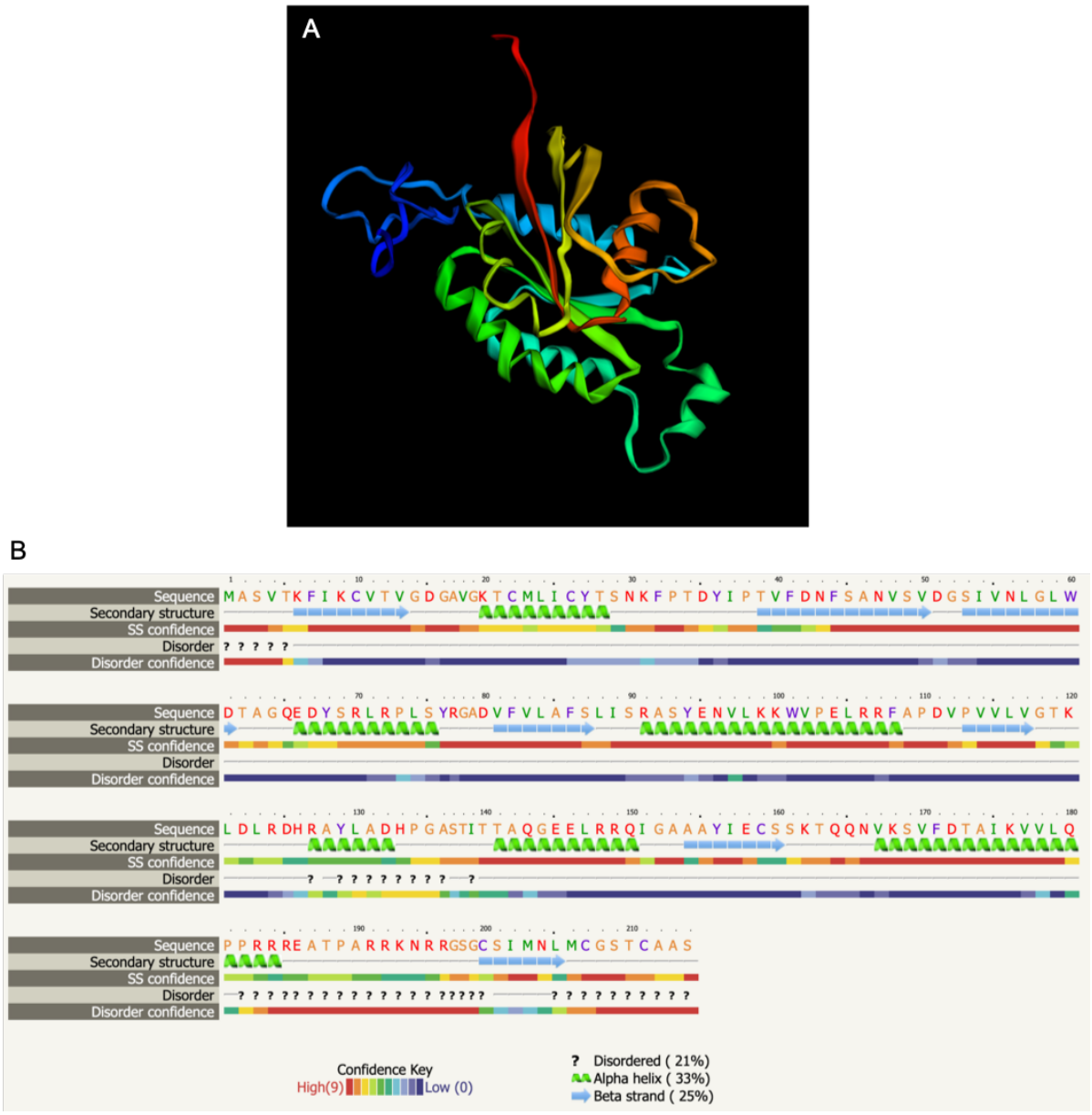

Appendix 18 – Structural analysis of modified *Zm*ROP7. All analysis has been conducted using Phyre[2]. (A) Finalised structural model of modified *Zm*ROP7. Coloured red to blue, corresponding to the N- and C-termini. (B) Modified *Zm*ROP7 secondary protein structure.

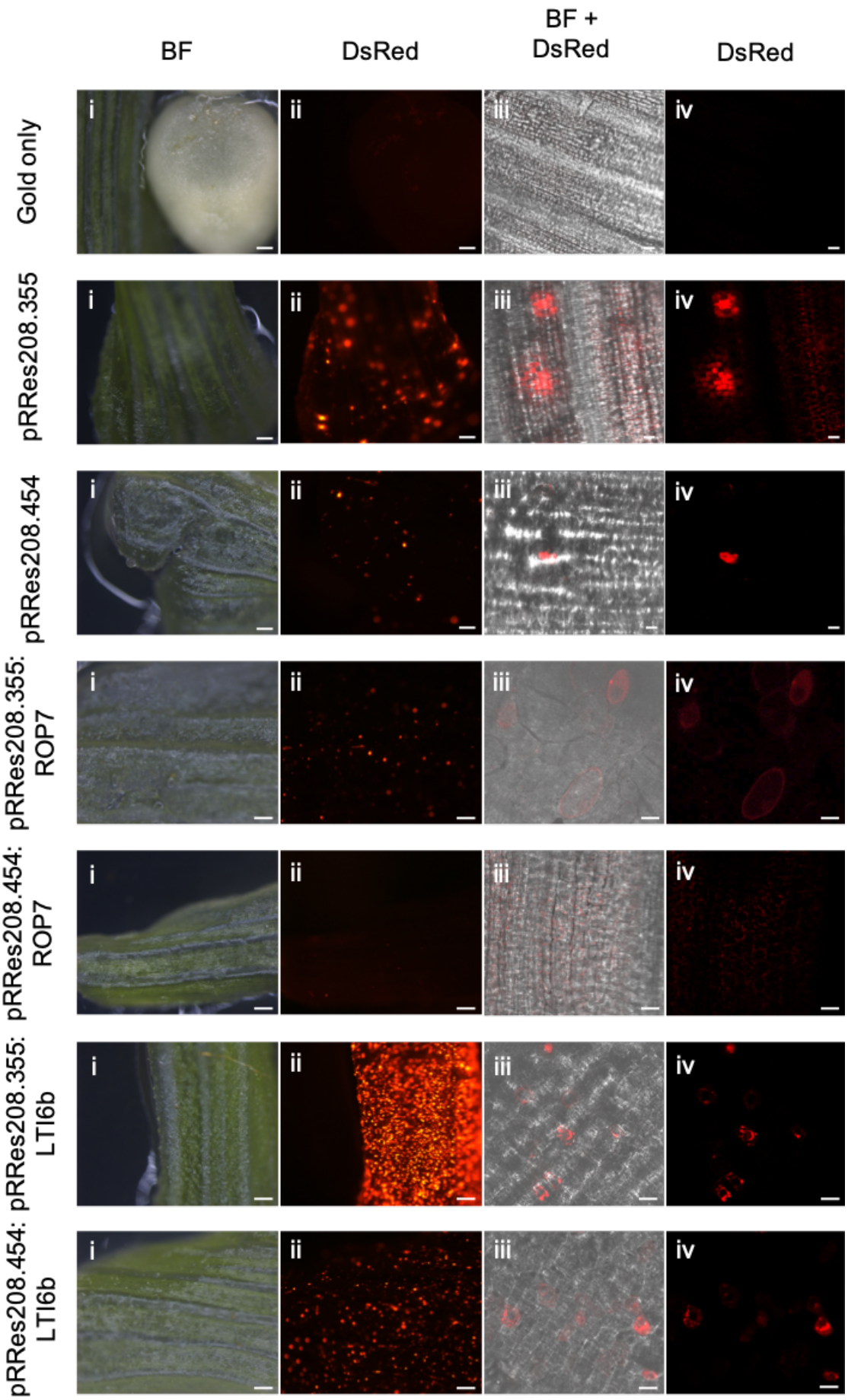
BF
DsRed
BF + DsRed
DsRed
Gold only
pRRes208.355
pRRes208.454
pRRes208.355: ROP7
pRRes208.454: ROP7
pRRes208.355: LTI6b
pRRes208.454: LTI6b
i
ii
iii
iv

Appendix 19 – Transient transformation of plasma membrane constructs in wheat leaf-sheath tissue. All images taken 48 h after bombardment of wheat *cv.* Bobwhite leaf tissue. (i) and (ii) show stereomicroscope images. Bar = 250 µm. Red fluorescence indicates successful particle bombardment and gene/tagRFP expression. Expression can be seen for all constructs with the exception of the negative control (gold only). (iii) and (iv) represent confocal images using a higher magnification displaying protein localisation. Bars (iii and iv): gold only= 50 µm, pRRes208.355, pRRes208.454, pRRes208.355:ROP7, pRRes208.454:ROP7, pRRes208.355:LTI6b, pRRes208.454:LTI6b = 20 µm.

Appendix 20 – Independent wheat plasma membrane line transformant information. Those highlighted and in bold have been selected for T_1 plant and T_2 seed production.

ROP7-RFP

Bombardment	Repeat	Plant	T_1 seed (few seed = less than 100)	Taken forward for T_1 plants based on root assay	No. of seeds planted
3731	**1**	**1**	**Few seed**	**Y**	**10**
3731	2	2	Few seed		
3731	2	6a	Few seed		
3731	3	1a	Few seed		
3731	3	3b	Few seed		
3731	3	4b	Few seed		
3731	3	6	Few seed		
3731	**3**	**7**	**17 seeds only**	**Y**	**3**
3731	3	8	7 seeds only		
3731	**3**	**9c**	**Few seed**	**Y**	**10**
3731	3	11	Few seed		
3731	4	1	Few seed		
3731	4	4a	Few seed		
3731	**4**	**5**	**Few seed**	**Y**	**10**
3731	4	6	Few seed		
3731	4	8	Few seed		
3731	4	9	Few seed		
3731	4	10	Few seed		
3731	4	12	Few seed		
3731	4	13	Few seed		
3731	4	15	Few seed		
3731	4	16	Few seed		
3731	5	1	Few seed		
3731	**5**	**2**	**Few seed**	**Y**	**10**
3731	5	3	Few seed		
3731	5	5	Few seed		
3731	**5**	**6**	**Few seed**	**Y**	**20**
3731	5	8	Few seed		
3731	5	9	Few seed		
3731	5	11	Few seed		
3731	**6**	**2**	**Few seed**	**Y**	**10**
3733	**1**	**1**	**Few seed**	**Y**	**10**
3733	2	3	Few seed		
3733	**2**	**5**	**Few seed**	**Y**	**10**
3733	**2**	**6a**	**Few seed**	**Y**	**10**
3733	3	2	Few seed		
3733	**3**	**4**	**Few seed**	**Y**	**10**
3733	4	3a	Few seed		
3733	**4**	**4**	**Few seed**	**Y**	**10**
3733	**4**	**5**	**Few seed**	**Y**	**10**
3733	4	6	Few seed		
3733	6	2	Few seed		
3733	6	3	Few seed		
3733	**7**	**1**	**Few seed**	**Y**	**10**

RFP-LTI6b

Bombardment	Repeat	Plant	T_1 seed (few seed = less than 100)	Taken forward for T_1 plants based on root assay	No. of seeds planted
3741	**1**	**1**	**Few seed**	**Y**	**10**
3741	3	2	Few seed		
3741	3	3a	Few seed		
3741	3	4a	Few seed		
3741	3	5	Few seed		
3741	**3**	**6**	**Few seed**	**Y**	**10**
3741	3	8b	15 seeds only		
3741	**3**	**12c**	**Few seed**	**Y**	**20**
3741	**3**	**14**	**Few seed**	**Y**	**10**
3741	3	15	Few seed		
3741	3	16	Few seed		
3741	3	17	Few seed		
3741	3	19	Few seed		
3741	**5**	**2**	**Few seed**	**Y**	**10**
3741	7	2a	Few seed		
3741	**7**	**3**	**Few seed**	**Y**	**10**

Appendix 21 – Remaining LTI6b-RFP lines to be processed.

Bombardment	Construct	Repeat /plant	PCR results	Number of seed
B3806	None	R1P1	Control. Lti6B- bar-	Y (few seed)
B3806	pRRes208.454LTI6B	R2P1	Lti6B+ bar+	Y (few seed)
B3806	pRRes208.454LTI6B	R2P2	Lti6B+ bar+	Y (few seed)
B3806	pRRes208.454LTI6B	R2P3	Lti6B+ bar+	Y (few seed)
B3806	pRRes208.454LTI6B	R2P4	Lti6B+ bar+	Y (approx 70 seeds)
B3806	pRRes208.454LTI6B	R2P5	Lti6B+ bar+	Y (few seed)
B3806	pRRes208.454LTI6B	R2P6	Lti6B+ bar+	Y (50 seeds)
B3806	pRRes208.454LTI6B	R2P8	Lti6B+ bar+	Y (24 seeds)
B3806	pRRes208.454LTI6B	R2P9	Lti6B+ bar+	Y (few seed)
B3806	pRRes208.454LTI6B	R3P6	Lti6B- bar+	Bar only. Y (approx 60 seeds)
B3806	pRRes208.454LTI6B	R4P1	Lti6B+(2 bands) bar+	Y (30 seeds)
B3806	pRRes208.454LTI6B	R4P6	Lti6B+ bar+	Y (50 seeds)
B3806	pRRes208.454LTI6B	R5P1	Lti6B+ bar+	Y (few seed)
B3806	pRRes208.454LTI6B	R5P2	Lti6B+ bar+	Y (few seed)
B3806	pRRes208.454LTI6B	R5P4	Lti6B+ bar+	Y (50 seeds)
B3806	pRRes208.454LTI6B	R5P5	Lti6B+ bar+	Y (6 seeds only)
B3806	pRRes208.454LTI6B	R5P7	Lti6B+ bar+	Y (few seed)
B3806	pRRes208.454LTI6B	R7P1	Lti6B+ bar+	Y (few seed)
B3806	pRRes208.454LTI6B	R7P2	Lti6B+ bar+	Y (25 seeds only)
B3806	pRRes208.454LTI6B	R8P7	Lti6B+ bar+	Y (10 seeds only)
B3806	pRRes208.454LTI6B	R8P8	Lti6B+ bar+	Y (1 seed only)
B3806	pRRes208.454LTI6B	R9P1	Lti6B+ bar+	No seed
B3806	pRRes208.454LTI6B	R10P1	Lti6B+ bar+	Y (approx 50 seeds)
B3806	pRRes208.454LTI6B	R11P5	Lti6B+ bar+	Y (few seed)
B3809	None	R1P1	Control. Lti6B- bar-	Y
B3809	pRRes208.454LTI6B	R2P3	Lti6B+ bar+	Y (50 seeds)
B3809	pRRes208.454LTI6B	R4P1	Lti6B+ bar+	Y (40 seeds)
B3809	pRRes208.454LTI6B	R4P5	Lti6B+ bar+	Y (few seed)
B3809	pRRes208.454LTI6B	R5P1	Lti6B- bar+	Bar only. Y (40 seeds)

Appendix 22 – Copy number and zygosity analysis of T_1 wheat PM reporter lines. (IDna genetics, Norwich)

ROP7-RFP

Sample	CompoundName	Copies_RothTag	Prob.Copies	Prob.Class
1	3731 R1P1_2	0	0	Null
2	3731 R1P1_9	0	0	Null
3	3731 R1P1_7	0	0	Null
4	3731 R1P1_10	0	0	Null
5	3731 R1P1_4	0	0	Null
Sample	CompoundName	Copies_RothTag	Prob.Copies	Prob.Class
6	3731 R3P9c_7	3	3	Hemi
7	3731 R3P9c_2	3	3	Hemi
8	3731 R3P9c_8	3	3	Hemi
9	3731 R3P9c_6	3	3	Hemi
10	3731 R3P9c_3	3	3	Hemi
Sample	CompoundName	Copies_RothTag	Prob.Copies	Prob.Class
15	3731 R4P5_4	12	12	Hom
14	3731 R4P5_3	6	6	Hemi
13	3731 R4P5_7	6	6	Hemi
11	3731 R4P5_9	6	6	Hemi
12	3731 R4P5_6	0	0	Null
Sample	CompoundName	Copies_RothTag	Prob.Copies	Prob.Class
16	3731 R5P2_10	0	0	Null
17	3731 R5P2_5	0	0	Null
18	3731 R5P2_1	0	0	Null
19	3731 R5P2_2	0	0	Null
20	3731 R5P2_9	0	0	Null
Sample	CompoundName	Copies_RothTag	Prob.Copies	Prob.Class
28	3731 R5P6_14	18	18	Uncertain
25	3731 R5P6_12	13	13	Hemi?
26	3731 R5P6_5	13	13	Hemi?
22	3731 R5P6_13	13	13	Hemi?
27	3731 R5P6_20	0	0	Null
21	3731 R5P6_4	0	0	Null
23	3731 R5P6_11	0	0	Null
24	3731 R5P6_10	0	0	Null
29	3731 R5P6_3	0	0	Null
Sample	CompoundName	Copies_RothTag	Prob.Copies	Prob.Class
30	3731 R6P2_5	4	4	Hom
33	3731 R6P2_4	4	4	Hom
34	3731 R6P2_1	4	4	Hom
32	3731 R6P2_3	2	2	Hemi
31	3731 R6P2_9	2	2	Hemi
Sample	CompoundName	Copies_RothTag	Prob.Copies	Prob.Class
37	3731 R3P7_2	4	4	Hemi
36	3731 R3P7_1	4	4	Hemi
35	3731 R3P7_3	0	0	Null
Sample	CompoundName	Copies_RothTag	Prob.Copies	Prob.Class
38	3733 R1P1_5	0	0	Null
39	3733 R1P1_9	0	0	Null
40	3733 R1P1_4	0	0	Null
41	3733 R1P1_2	0	0	Null
42	3733 R1P1_7	0	0	Null

ROP7-RFP

Sample	CompoundName	Copies_RothTag	Prob.Copies	Prob.Class
44	3733 R2P5_10	6	6	Hom
46	3733 R2P5_1	3	3	Hemi
45	3733 R2P5_3	3	3	Hemi
47	3733 R2P5_2	3	3	Hemi
43	3733 R2P5_5	3	3	Hemi
Sample	CompoundName	Copies_RothTag	Prob.Copies	Prob.Class
48	3733 R2P6_6	0	0	Null
49	3733 R2P6_9	0	0	Null
51	3733 R2P6_4	0	0	Null
52	3733 R2P6_1	0	0	Null
50	3733 R2P6_2	No_amplification	No_amplification	No_amplification
Sample	CompoundName	Copies_RothTag	Prob.Copies	Prob.Class
55	3733 R3P4_9	70	70	Hom
56	3733 R3P4_2	66	70	Hom
57	3733 R3P4_10	38	35	Hemi
53	3733 R3P4_1	0	0	Null
54	3733 R3P4_3	0	0	Null
Sample	CompoundName	Copies_RothTag	Prob.Copies	Prob.Class
62	3733 R4P4_2	81	80	Hom
61	3733 R4P4_5	77	80	Hom
60	3733 R4P4_10	40	40	Hemi
59	3733 R4P4_3	39	40	Hemi
58	3733 R4P4_6	No_amplification	No_amplification	No_amplification
Sample	CompoundName	Copies_RothTag	Prob.Copies	Prob.Class
66	3733 R4P5_7	7	8	Hom
64	3733 R4P5_6	4	4	Hemi
63	3733 R4P5_5	4	4	Hemi
65	3733 R4P5_3	0	0	Null
67	3733 R4P5_8	0	0	Null
Sample	CompoundName	Copies_RothTag	Prob.Copies	Prob.Class
70	3733 R7P1_9	12	12	Hemi
69	3733 R7P1_10	12	12	Hemi
72	3733 R7P1_5	0	0	Null
68	3733 R7P1_7	0	0	Null
71	3733 R7P1_6	0	0	Null

RFP-LTI6b

Sample	CompoundName	Copies_RothTag	Prob.Copies	Prob.Class
73	3741 R1P1_6	0	0	Null
74	3741 R1P1_3	0	0	Null
75	3741 R1P1_10	0	0	Null
76	3741 R1P1_8	0	0	Null
77	3741 R1P1_1	0	0	Null
Sample	CompoundName	Copies_RothTag	Prob.Copies	Prob.Class
82	3741 R3P6_9	56	56	Hemi
80	3741 R3P6_3	0	0	Null
81	3741 R3P6_4	0	0	Null
78	3741 R3P6_8	0	0	Null
79	3741 R3P6_10	0	0	Null
Sample	CompoundName	Copies_RothTag	Prob.Copies	Prob.Class
83	3741 R3P12c_13	0	0	Null
84	3741 R3P12c_3	0	0	Null
91	3741 R3P12c_4	0	0	Null
85	3741 R3P12c_12	0	0	Null
86	3741 R3P12c_5	0	0	Null
88	3741 R3P12c_9	0	0	Null
89	3741 R3P12c_6	0	0	Null
90	3741 R3P12c_7	0	0	Null
87	3741 R3P12c_17	No_amplification	No_amplification	No_amplification
Sample	CompoundName	Copies_RothTag	Prob.Copies	Prob.Class
96	3741 R3P14_4	6	6	Multi
92	3741 R3P14_1	5	5	Multi
95	3741 R3P14_6	4	4	Multi
93	3741 R3P14_5	4	4	Multi
94	3741 R3P14_7	3	3	Multi

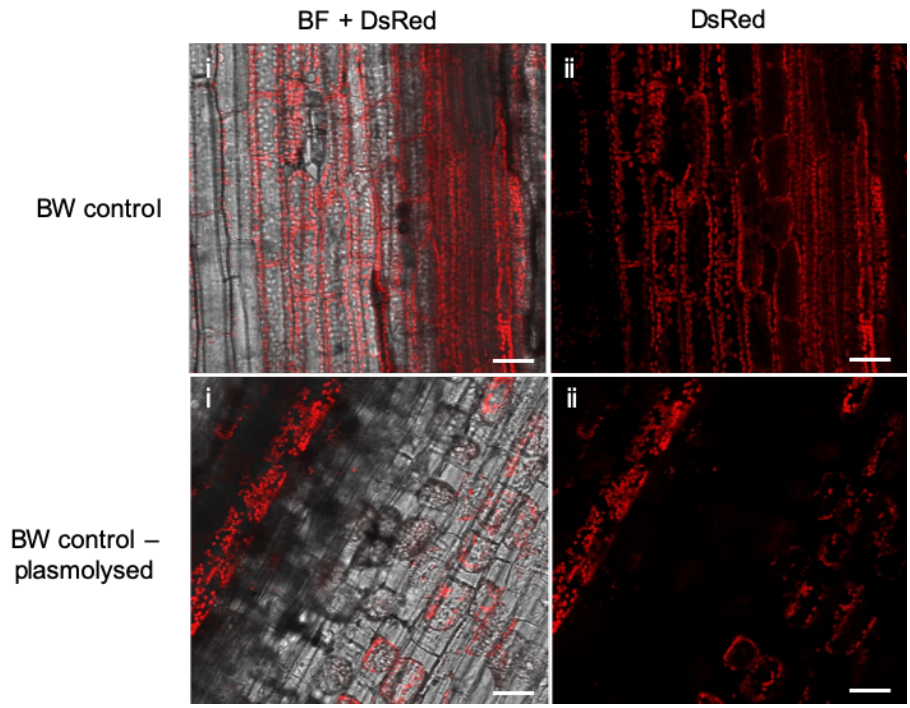

Appendix 23 – Wheat coleoptile plasmolysis. (i) BF + DsRed. (ii) DsRed only. 0.8M mannitol was used to plasmolysed cells. Bar = 50μm.

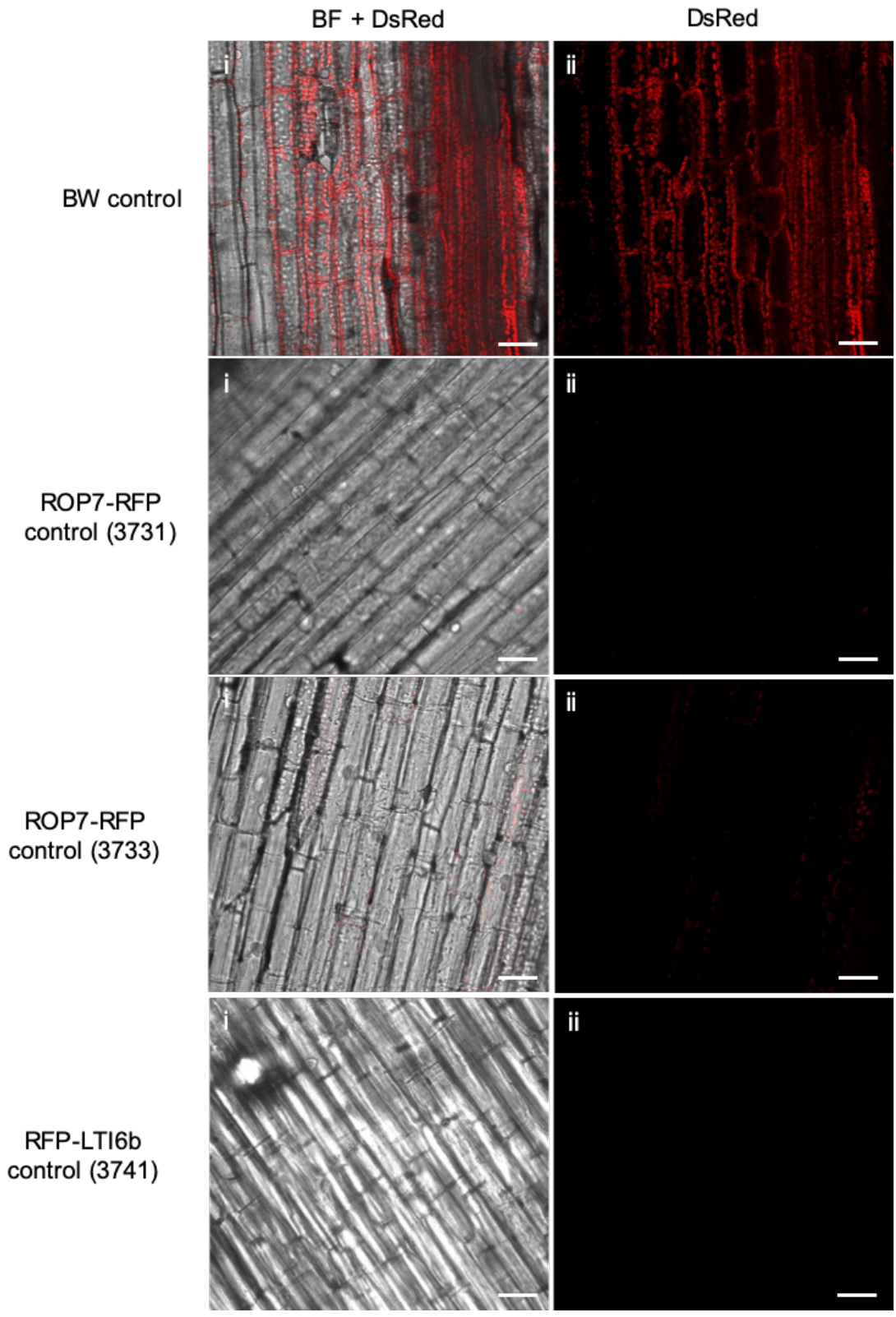
BF + DsRed
DsRed
BW control
ROP7-RFP control (3731)
ROP7-RFP control (3733)
RFP-LTI6b control (3741)
i
ii

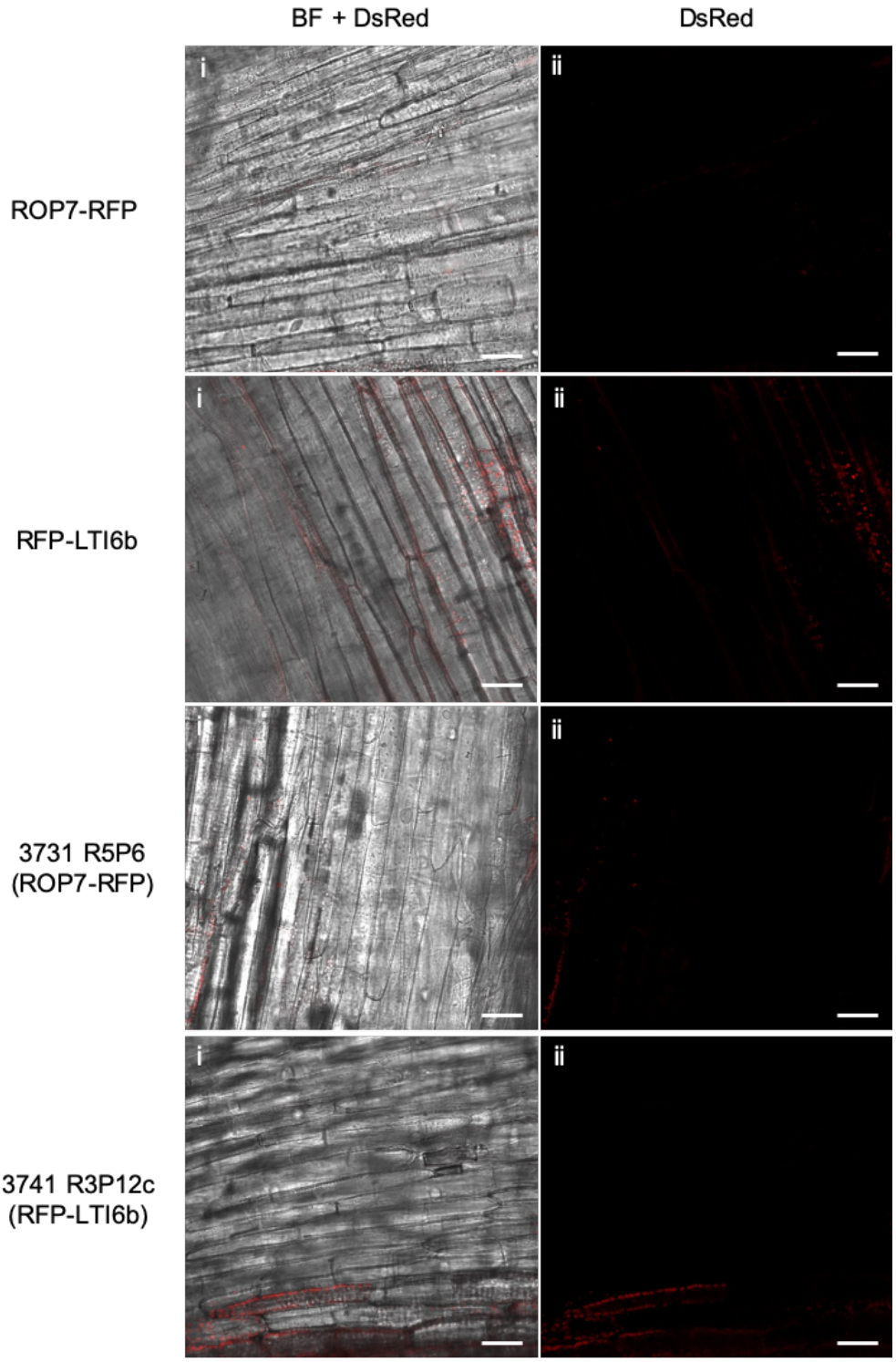

Appendix 24 – T_2 wheat plasma membrane screening in coleoptile tissue. (i) BF + DsRed. (ii) DsRed only. The Bobwhite (BW) control is taken in an area with high fluorescence here shown by the chloroplasts for comparison. The ROP7-RFP and RFP-LTI6b lines, including the two most promising lines which are also included are representative of all other lines/plants tested. Bar = 50μm.

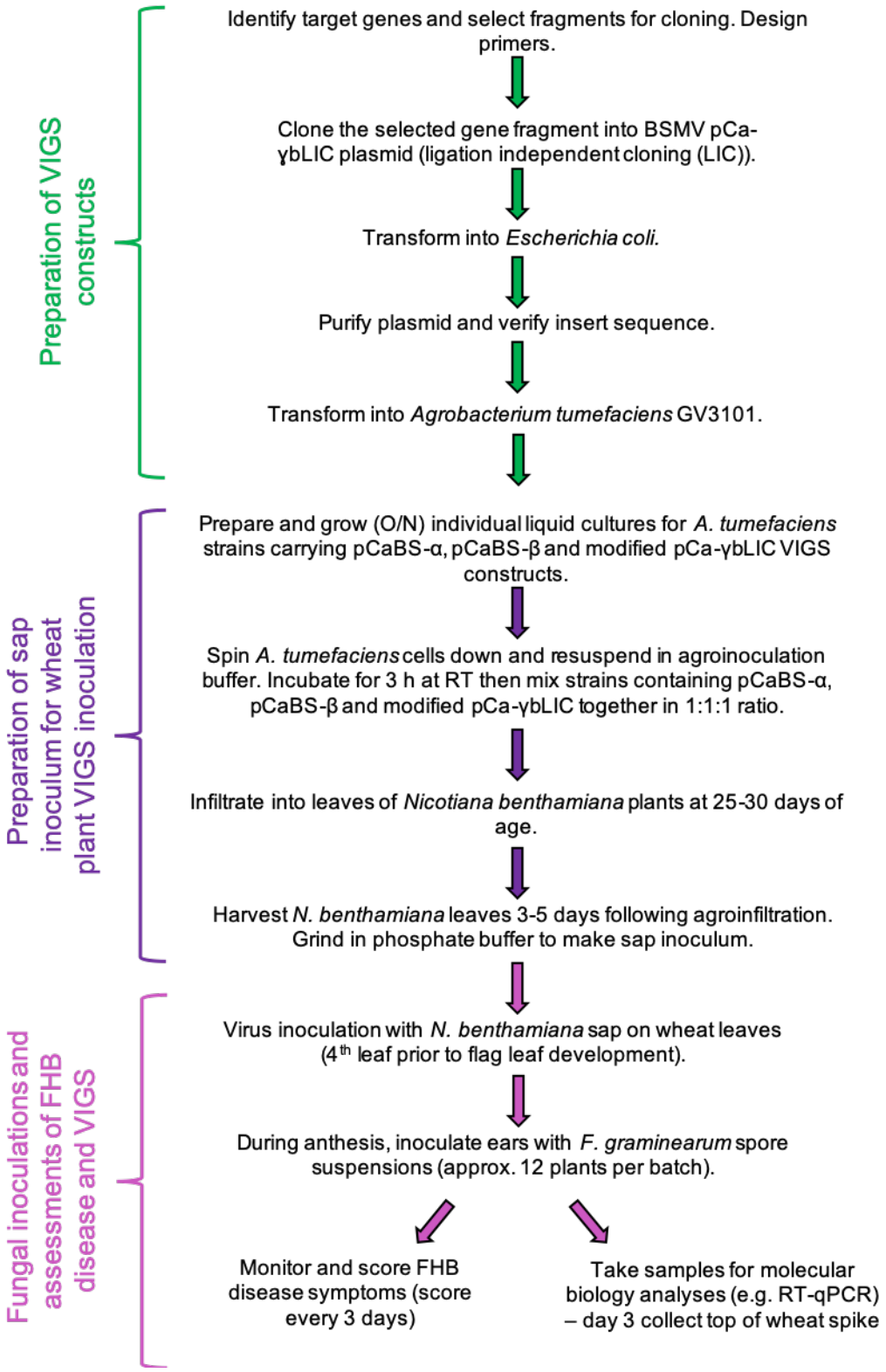

Appendix 25 – Virus-induced gene silencing (VIGS) workflow. Adapted from Ana Machado, Rothamsted Research, unpublished.

Appendix 26 – Protein localisation predictions for *Arabidopsis thaliana* virus-induced gene silencing (VIGS) candidates.

	Protein localisation WoLFPSORT prediction score				
Cellular compartment		BG_PPAP (At5g42100)	PDLP1 (At5g43980)	PDLP5 (At1g70690)	LYM2 (At2g17120)
	Chloroplast	1	-	7	11
	Endoplasmic reticulum	1	-	-	-
	Extracellular	4	6	4	1
	Golgi	2	2	-	-
	Mitochondria	2	-	-	-
	Plasma membrane	1	1	-	1
	Vacuole	3	5	3	1

Appendix 27 – BLAST analysis results for AtBG_PPAP and cereal orthologs.

Query protein (species)	Organism database searched	Protein match (Accession)	E-value	Percentage identification (%)
BG_PPAP (At)	Ta	Unnamed protein product (SPT18330.1)*	1e-121	53.70
	Ta	Unnamed protein product (CDM83794.1)	8e-121	53.85
	Ta	Unnamed protein product (CDM85083.1)	2e-120	53.23
	Ta	ß-1,3-glucanase (ACF33176.1)	5e-87	44.62
SPT18330.1 (Ta)	At	Glycosyl hydrolase superfamily protein (NP_973548.1)*	5e-164	62.29
	At	BG_PPAP (OAO91127.1)	9e-121	53.70
	At	BG_PPAP (OAO91126.1)	1e-120	53.70
CDM85083.1 (Ta)	At	Glycosyl hydrolase superfamily protein (NP_565652.1)*	7e-161	61.30
	At	BG_PPAP (OAO91127.1)	2e-120	53.85
	At	BG_PPAP (OAO91126.1)	3e-120	53.85
CDM85083.1 (Ta)	At	Glycosyl hydrolase superfamily protein (NP_973548.1)*	5e-155	63.50
	At	BG_PPAP (OAO91127.1)	1e-120	52.24
	At	BG_PPAP (OAO91126.1)	2e-120	52.24
ACF33176.1 (Ta)	At	Unnamed protein product (VYS53595.1)*	1e-158	60.06
	At	BG_PPAP (OAO91127.1)	2e-90	44.62
	At	BG_PPAP (OAO91126.1)	2e-90	44.62

Q33AWJ (Os)	At	CDS (AAF31288.1)*	7e-128	53.05
	At	BG_PPAP (OAO91127.1)	5e-127	56.44
	At	BG_PPAP (OAO91126.1)	7e-127	56.44
	Ta	Unnamed protein product (SPT18330.1)*	4e-125	52.71
	Ta	Unnamed protein product (CDM83794.1)	3e-111	51.84
	Ta	Unnamed protein product (CDM85083.1)	1e-119	54.94
	Ta	ß-1,3-glucanase (ACF33176.1)	6e-89	42.46
KAE8777097.1 (Hv)	At	ß-1,3-glucanase (NP_974868.1)*	1e-125	56.13
	At	BG_PPAP (OAO91127.1)	4e-125	55.83
	At	BG_PPAP (OAO91126.1)	7e-125	55.83
	Ta	Hypothetical protein CFC21_010231 (KAF6993319.1)*	0.0	90.05
	Ta	Unnamed protein product (CDM85083.1)	5e-117	53.56
	Ta	Unnamed protein product (CDM83794.1)	3e-105	49.69
	Ta	ß-1,3-glucanase (ACF33176.1)	3e-82	42.59

* Top alignment match in the analysis

At = *Arabidopsis thaliana*

Ta = *Triticum aestivum*

Os = *Oryza sativa*

Hv = *Hordeum vulgare*

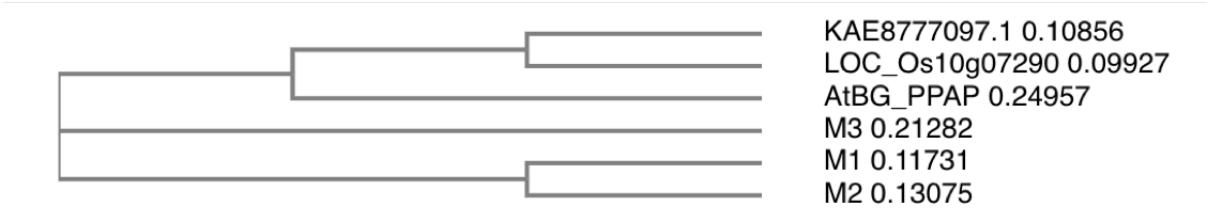

Appendix 28 – Phylogenetic tree of BG_PPAP orthologs. AtBG_PPAP = *Arabidopsis thaliana* ortholog, KAE8777097.1 = barley ortholog, LOC_Os10g07290 = rice ortholog. M1-M3 = wheat orthologs. Values represent a sequence distance measure.

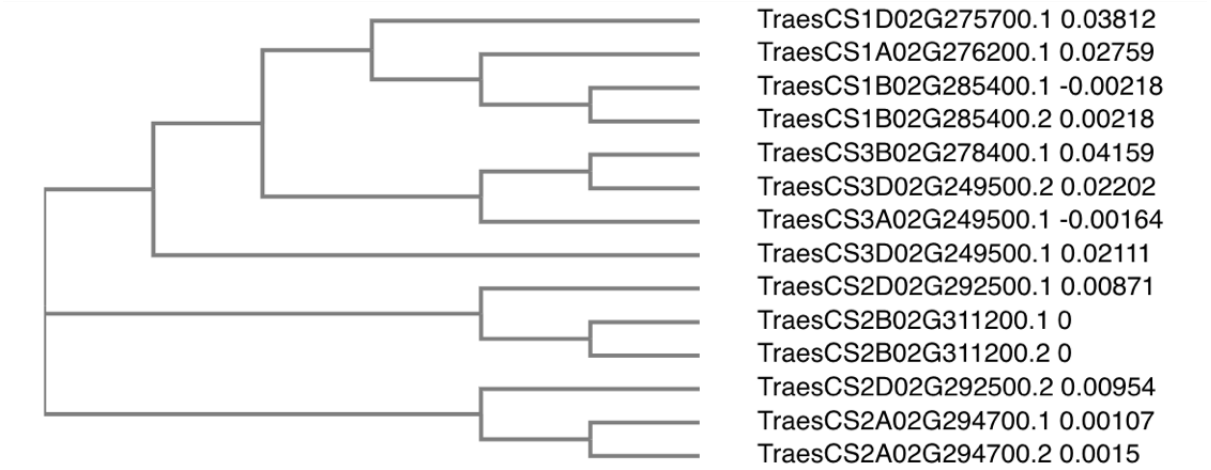

Appendix 29 – Phylogenetic tree/alignment of *At*BG_PPAP wheat orthologs M1/M2. Values represent a sequence distance measure.

AtBG_PPAP

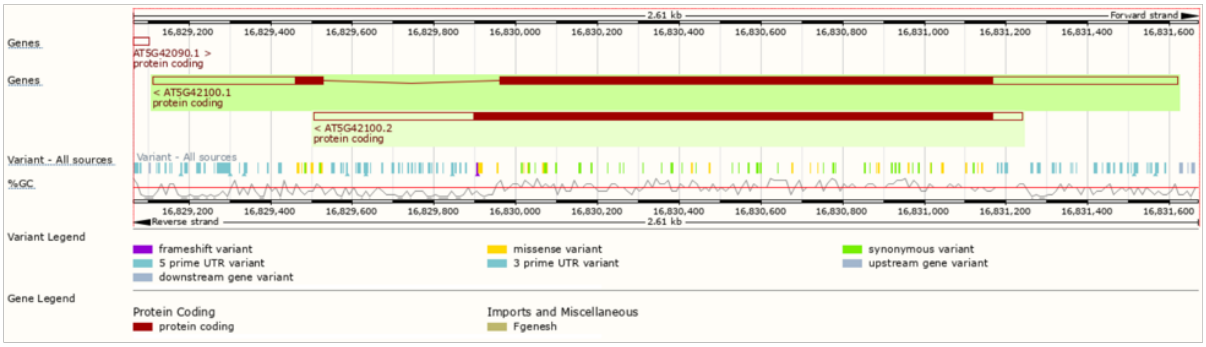

TraesCS2D02G292500.1

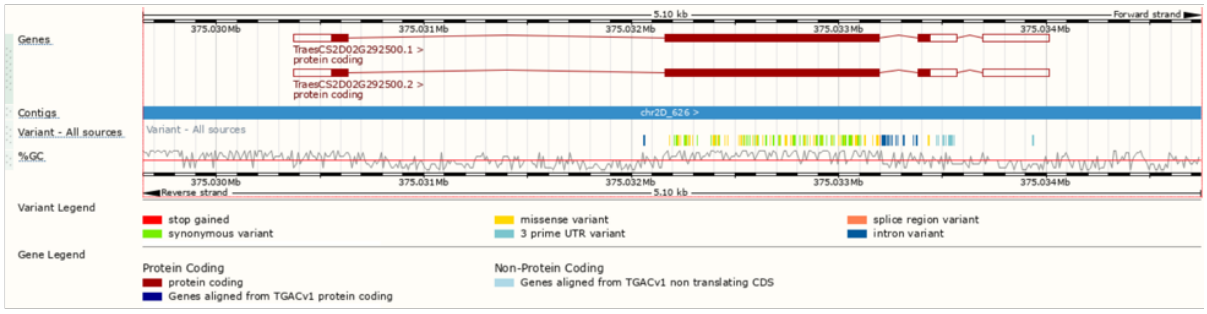

TraesCS3B02G278400.1

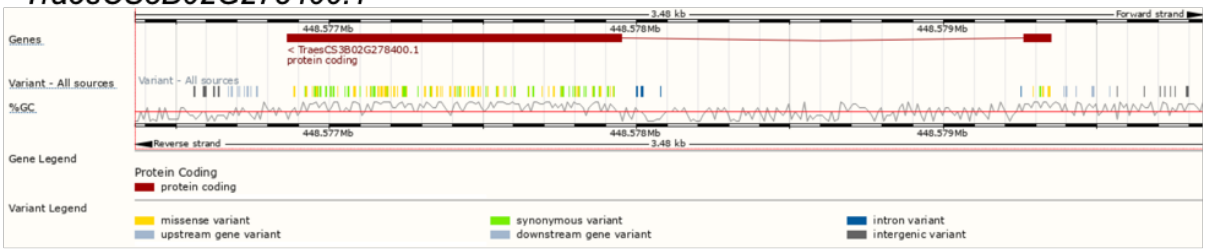

TraesCS3B02G406200.1

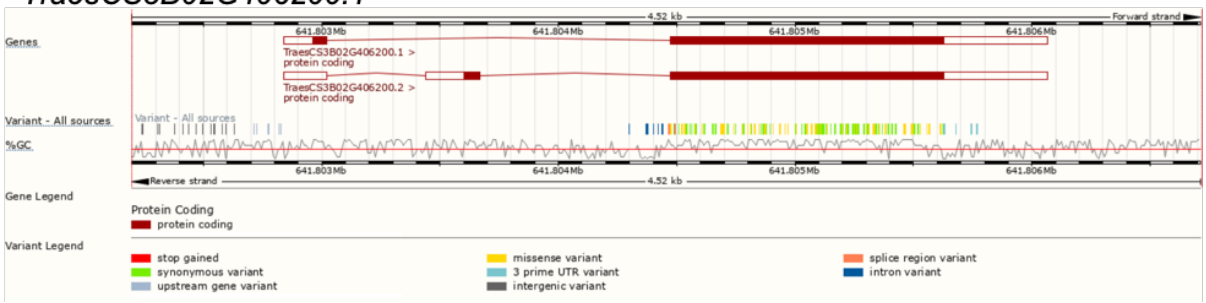

Appendix 30 – Gene structure of *At*BG_PPAP and wheat orthologs. From top to bottom the three wheat orthologs are M1-M3 respectively. As the scale is small, dark red represents protein coding regions of the gene and any splice variants.

Appendix 31 – Protein localisation predictions for virus-induced gene silencing (VIGS) candidate wheat orthologs.

	Protein localisation WoLFPSORT prediction score					
Cellular compartment		BG_PPAP M1	BG_PPAP M2	BG_PPAP M3	PDLP	LYM2
	Chloroplast	-	2	6	5	2
	Cytosol_plasma membrane	4.5	-	-	-	-
	Endoplasmic reticulum	4	-	-	3	2
	Extracellular	1	4	3	3	-
	Golgi	-	1	-	-	3.5
	Golgi_plasma membrane	-	-	-	-	4.5
	Mitochondria	1	1	1	1	-
	Nucleus	-	1	1	-	-
	Peroxisome	-	-	1	-	-
	Plasma membrane	7.5	-	-	2	4.5
	Vacuole	-	5	2	-	2

Appendix 32 – Phylogenetic tree/alignment of *At*BG_PPAP wheat ortholog M3.

Values represent a sequence distance measure.

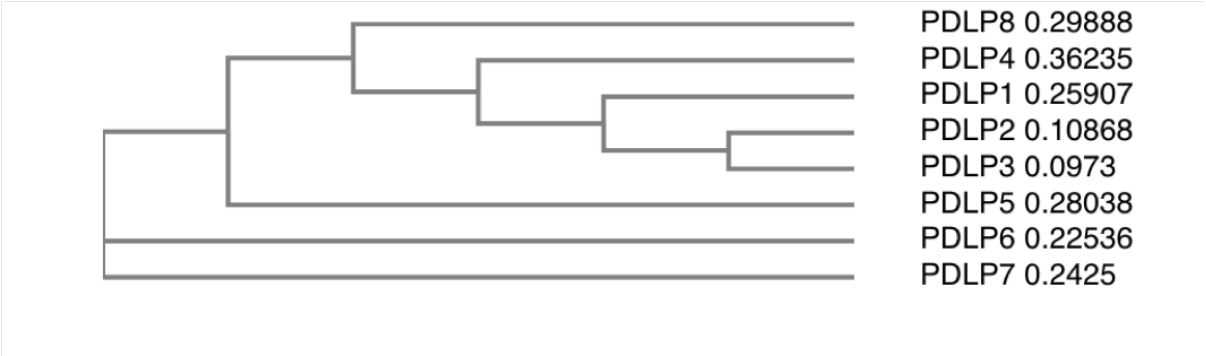

Appendix 33 – Phylogenetic tree/alignment of *At*PDLPs. Values represent a sequence distance measure.

Appendix 34 – BLAST analysis results for AtPDLP1/5 and cereal orthologs.

Query protein (species)	Organism database searched	Protein match (Accession)	E-value	Percentage identification (%)
PDLP1 (At)	Ta	Unnamed protein product (SPT19226.1)*	2e-33	29.93
PDLP5 (At)	Ta	Unnamed protein product (SPT19226.1)*	6e-62	39.78
SPT19226.1 (Ta)	At	PDLP8 (NP_001326962.1)*	6e-85	46.46
	At	PDLP1 (OAO92834.1)	2e-27	28.41
Q0DVA3 (Os)	At	PDLP3 (NP_565764.1)*	1e-85	45.07
	At	PDLP1 (OAO92834.1)	5e-63	42.96
	Ta	Unnamed protein product (SPT19226.1)*	3e-34	29.25
Os02g0734800 (Os)	At	Unnamed protein product (BAB08312.1)*	4e-58	46.38
	At	PDLP1 (OAO92834.1)	8e-24	29.00
	Ta	Unnamed protein product (SPT19226.1)	3e-55	44.76

Os06g0253600 (Os)	At	Unknown (AAM63232.1)*	7e-57	37.79
	At	PDLP1 (OAO92834.1)	2e-23	30.67
	Ta	Unnamed protein product (SPT19226.1)	1e-60	38.14
KAE8766664.1 (Hv)	At	PDLP2 (NP_171946.2)*	5e-80	43.13
	At	PDLP1 (OAO92834.1)	5e-60	41.79
	Ta	Hypothetical protein CFC21 068937 (KAF7062325.1)*	2e-150	89.86
	Ta	Unnamed protein product (SPT19226.1)	1e-26	29.84
KAE8794631.1 (Hv)	At	PDLP8 (NP_191631.2)*	5e-85	46.64
	Ta	Hypothetical protein CFC21 018217 (KAF7002782.1)*	0.0	89.62
	Ta	Unnamed protein product (SPT19226.1)	4e-180	89.73

* Top alignment match in the analysis

At = *Arabidopsis thaliana*

Ta = *Triticum aestivum*

Os = *Oryza sativa*

Hv = *Hordeum vulgare*

AtPDLP1

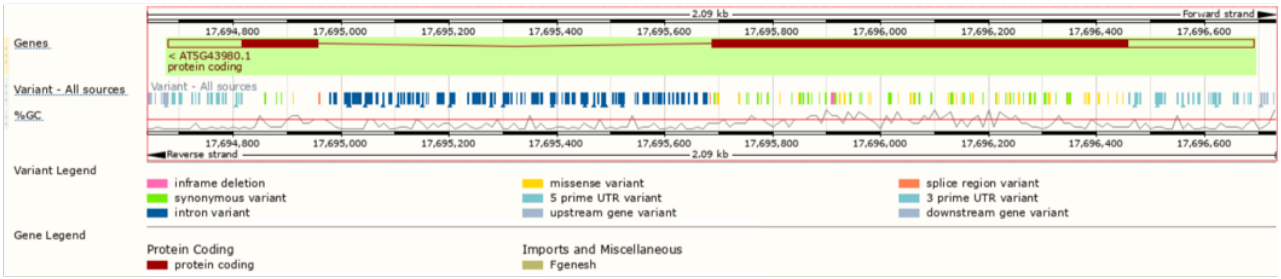

AtPDLP5

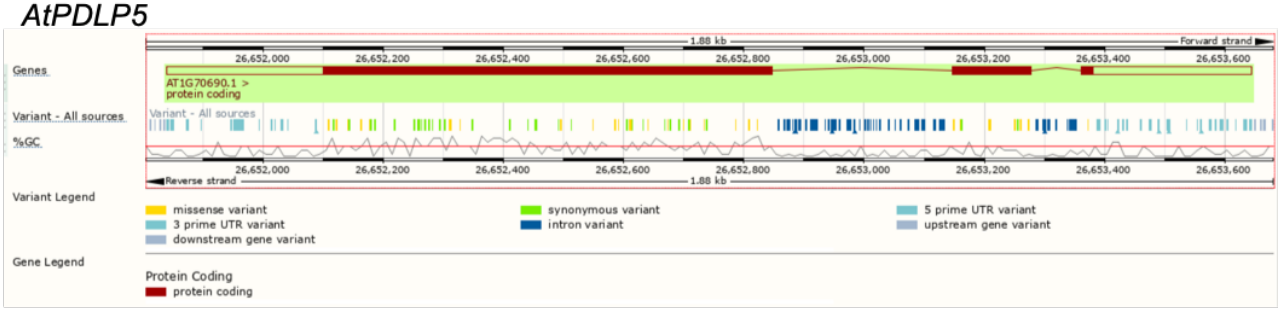

TraesCS2A02G386500.1

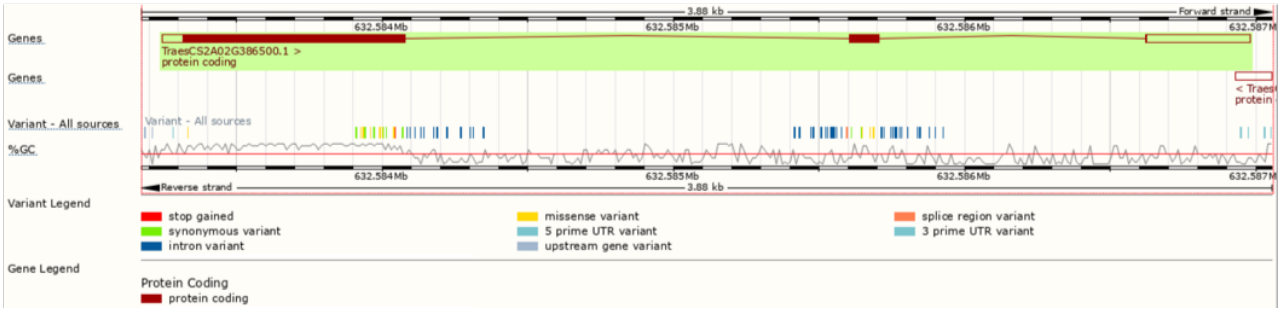

Appendix 35 – Gene structure of *At*PDLP1/5 and wheat ortholog. As the scale is small, dark red represents protein coding regions of the gene and any splice variants.

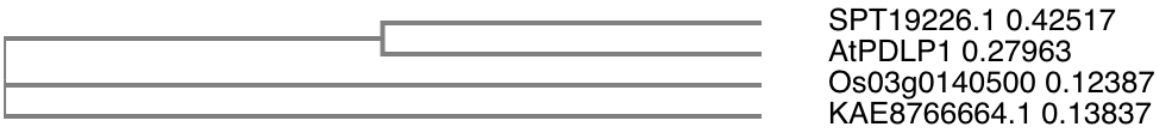

Appendix 36 – Phylogenetic tree of PDLP1 orthologs. AtPDLP1= *Arabidopsis thaliana* ortholog, KAE8766664.1 = barley ortholog, Os03g0140500 = rice ortholog. SPT19226.1 = wheat ortholog. Values represent a sequence distance measure.

Appendix 37 – Phylogenetic tree of PDLP5 orthologs. AtPDLP1= *Arabidopsis thaliana* ortholog, KAE8794631.1 = barley ortholog, Os02g0734800 and Os06g0253600 = rice ortholog. SPT19226.1 = wheat ortholog. Values represent a sequence distance measure.

Appendix 38 – Phylogenetic tree/alignment of *At*PDLP1/5 wheat orthologs. Values represent a sequence distance measure.

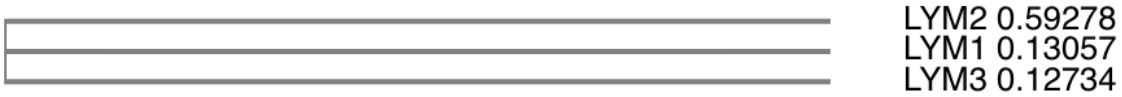

Appendix 39 – Phylogenetic tree/alignment of *At*LYMs. Values represent a sequence distance measure.

Appendix 40 – BLAST analysis results for AtLYM2 and cereal orthologs.

Query protein (species)	Organism database searched	Protein match (Accession)	E-value	Percentage identification (%)
LYM2 (At)	Ta	Chitin elicitor binding protein (AIK22416.1)*	3e-14	36.13
	Ta	Unnamed protein product (CDM82405.1)	9.1	33.33
AIK22416.1 (Ta)	At	Unknown (AAM65912.1)*	2e-17	33.16
	At	lysm domain GPI-anchored protein 2 precursor (NP_565406.1)	9e-17	32.98
Os03g0133400 (Os)	At	lysm domain GPI-anchored protein 2 precursor (NP_565406.1) *	5e-59	36.14
	Ta	Chitin elicitor binding protein (AIK22416.1)*	4e-71	65.24
KAE8808384.1 (Hv)	At	Unnamed protein product (CAD5318708.1)*	2e-61	40.46
	At	lysm domain GPI-anchored protein 2 precursor (NP_565406.1)	2e-61	40.46
	Ta	Hypothetical protein CFC21 063289 (KAF7055809.1)*	0	88.07
	Ta	Chitin elicitor binding protein (AIK22416.1)	4e-103	86.34

* Top alignment match in the analysis

At = *Arabidopsis thaliana*

Ta = *Triticum aestivum*

Os = *Oryza sativa*

Hv = *Hordeum vulgare*

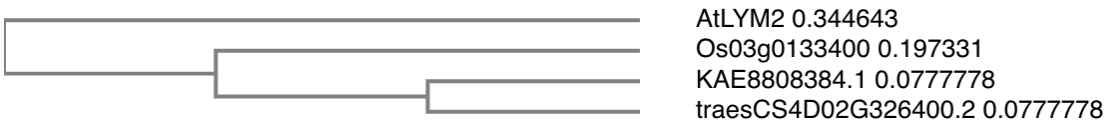

Appendix 41 – Phylogenetic tree of LYM2 orthologs. AtLYM2= *Arabidopsis thaliana* ortholog, KAE8808384.1 = barley ortholog, Os03g0133400 = rice ortholog. traesCS4D02G326400.1 = wheat ortholog. Values represent a sequence distance measure.

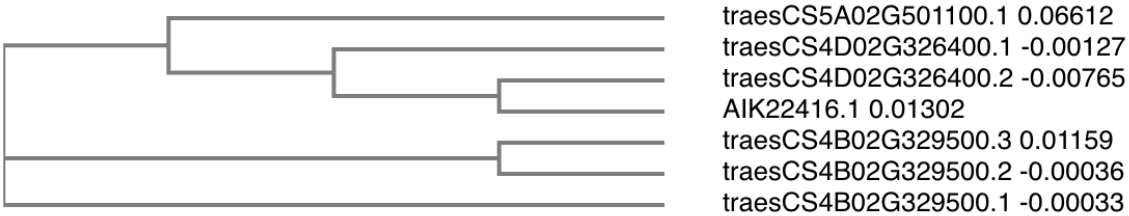

Appendix 42 – Phylogenetic tree/alignment of *At*LYM2 wheat orthologs. Values represent a sequence distance measure.

AtLYM2

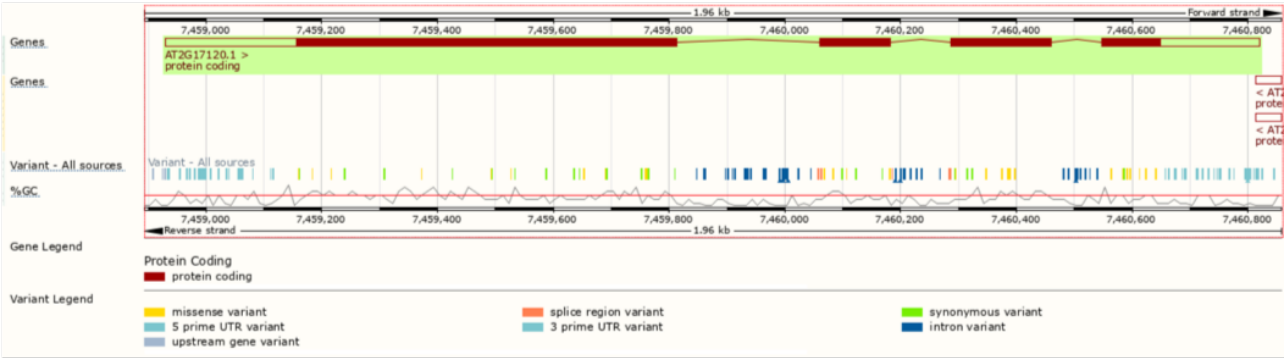

TraesCS4D02G326400.2

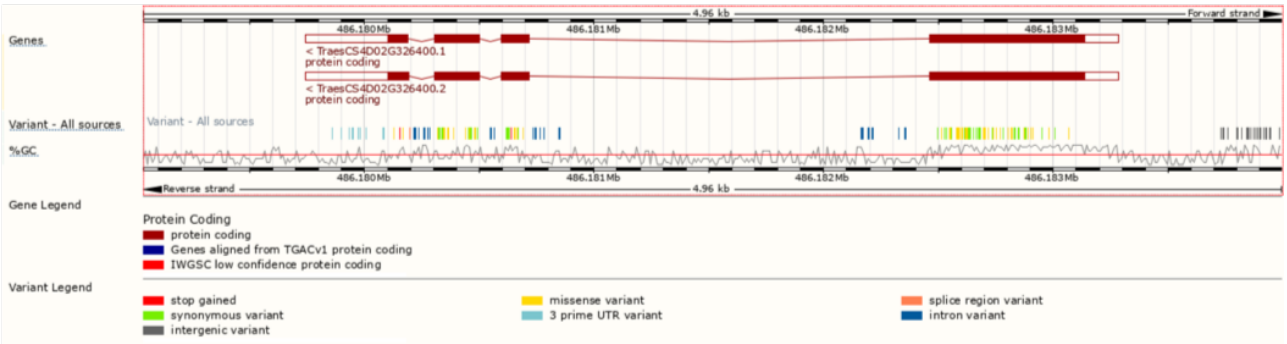

Appendix 43 – Gene structure of *At*LYM2 and wheat ortholog. As the scale is small, dark red represents protein coding regions of the gene and any splice variants.

Appendix 44 – Identification of AtBG_PPAP wheat orthologs using Analysis 2.

Gene	Bit-Score BLAST vs wheat proteome	% identity FL proteins alignment	BLAST score vs AtBG_PPAP	Top BLAST score vs At proteome
TraesCS4A02G067900.1	375.9	45.0	377	AtBG_PPAP (At5g42100)
TraesCS4B02G225100.1	377.1	45.0		
TraesCS4D02G225700.1	377.1	45.0		
TraesCS1A02G049800.1	359.8	46.6	369	372 (At1g32860)
TraesCS1B02G072500.1	358.2	46.8		
TraesCS1D02G056500.1	373.6	47.8		
TraesCS1A02G276200.1	365.9	43.7	363	403 (At2g27500)
TraesCS1B02G285400.1	364.8	45.2		
TraesCS1D02G275700.1	366.7	44.3		
TraesCS3A02G249500.1	355.5	44.6	358	450 (At2g27500)
TraesCS3B02G278400.1	355.9	43.9		
TraesCS3D02G249500.2	358.2	44.9		
TraesCS3A02G374000.2	355.1	46.0	355	444 (At2g27500)
TraesCS3B02G406200.2	357.5	46.0		
TraesCS3D02G366700.2	353.2	45.1		
TraesCS2A02G294700.1	362.8	42.4	358	465 (At2g27500)
TraesCS2B02G311200.2	360.1	43.3		
TraesCS2D02G292500.2	358.6	42.9		

Appendix 45 – Identification of AtPDLP wheat orthologs using Analysis 2.

Gene	Bit-Score BLAST vs wheat proteome	% identity FL proteins alignment	BLAST score vs AtPDLP1	Top BLAST score vs At proteome
TraesCS5A02G511600.1	171.4	38.1	190	242 (AtPDLP2&3; At2g33330 & At1g04520)
TraesCS4B02G342500.1	176.8	38.4	196	240 (AtPDLP2&3; At2g33330 & At1g04520)
TraesCS4D02G338100.1	168.3	36.8	191	243 (AtPDLP2&3; At2g33330 & At1g04520)
TraesCS2A02G386500.1	124.0	27.8	107	259 (AtPDLP8; At3g60720)
TraesCS2B02G404100.2	122.5	26.6	106	260 (AtPDLP8; At3g60720)
TraesCS2D02G491400LC.1	126.3	27.2	112	258 (AtPDLP8; At3g60720)

Gene	Bit-Score BLAST vs wheat proteome	% identity FL proteins alignment	BLAST score vs AtPDLP5	Top BLAST score vs At proteome
TraesCS2A02G386500.1	196.8	36.2	180	259 (AtPDLP8; At3g60720)
TraesCS2B02G404100.2	199.5	36.6	182	260 (AtPDLP8; At3g60720)
TraesCS2D02G491400LC.1	199.1	32.9	182	258 (AtPDLP8; At3g60720)
TraesCS6A02G238400.1	164.5	34.5	147	226 (AtPDLP8; At3g60720)
TraesCS6B02G286000.1	171.0	34.1	154	240 (AtPDLP8; At3g60720)
TraesCS6D02G220800.1	175.3	34.5	159	244 (AtPDLP8; At3g60720)

REFERENCES

1 UN. New Cooperation for Global Food Security. *Panel discussion* (2009).

2 Organization, W. H. *Obesity and overweight*, <https://www.who.int/news-room/fact-sheets/detail/obesity-and-overweight> (2018).

3 FAO. The State of Food and Agriculture, 2013: Food Systems for Better Nutrition. (Food and Agriculture Organization of the United Nations, Rome, 2013).

4 Lejon, E. & Frankelius, P. Sweden innovation power. (Elmia, Jönköping, Sweden, 2015).

5 Rose, D. C. & Chilvers, J. Agriculture 4.0: Broadening Responsible Innovation in an Era of Smart Farming. *Frontiers in Sustainable Food Systems* **2**, 7, doi:10.3389/fsufs.2018.00087 (2018).

6 Wolfert, S., Ge, L., Verdouw, C. & Bogaardt, M. J. Big Data in Smart Farming - A review. *Agricultural Systems* **153**, 69-80, doi:10.1016/j.agsy.2017.01.023 (2017).

7 Shi, X. J. *et al.* State-of-the-Art Internet of Things in Protected Agriculture. *Sensors* **19**, 24, doi:10.3390/s19081833 (2019).

8 Fones, H. N. *et al.* Threats to global food security from emerging fungal and oomycete crop pathogens. *Nature Food* **1**, 332-342, doi:10.1038/s43016-020-0075-0 (2020).

9 Carolan, M. Publicising Food: Big Data, Precision Agriculture, and Co-Experimental Techniques of Addition. *Sociologia Ruralis* **57**, 135-154, doi:10.1111/soru.12120 (2017).

10 Driessen, C. & Heutinck, L. F. M. Cows desiring to be milked? Milking robots and the co-evolution of ethics and technology on Dutch dairy

farms. *Agriculture and Human Values* **32**, 3-20, doi:10.1007/s10460-014-9515-5 (2015).

11 FAO & ITU. E-Agriculture in Action: Drones for Agriculture. (2018).

12 IWMI. *Rainfed agriculture*, <iwmi.cgiar.org/issues/rainfed-agriculture/summary/> (

13 www.fao.org/news/story/en/item/1106977/icode/. (2018).

14 Sarwar, M. H., Sarwar, M. F., Sarwar, M., Qadri, N. A. & Moghal, S. The importance of cereals (Poaceae: Gramineae) nutrition in human health: A review. *Journal of Cereals and Oilseeds* **4**, 32-35, doi:10.5897/JCO12.023 (2013).

15 Perniola, M., Lovelli, S., Arcieri, M. & Amato, M. in *The Sustainability of Agro-Food and Natural Resource Systems in the Mediterranean Basin* (ed A. Vastola) 15-27 (Springer, Cham, 2015).

16 *World food situation - FAO cereal supply and demand brief*, 2021).

17 FAO. *Cereal yield (kg per hectare)*, <data.worldbank.org/indicator/AG.YLD.CREL.KG> (

18 *World food situation - FAO cereal supply and demand brief*, 2019).

19 FAO. Save and Grow in practice: maize, rice, wheat. A guide to sustainable cereal production., (2016).

20 Cassman, K. G., Dobermann, A., Walters, D. T. & Yang, H. Meeting cereal demand while protecting natural resources and improving environmental quality. *Annual Review of Environment and Resources* **28**, 315-358, doi:10.1146/annurev.energy.28.040202.122858 (2003).

21 Conway, G. R. & Barbier, E. B. *After the Green Revolution: Sustainable agriculture for development*. (Earthscan, 1990).

22 Bebber, D. P., Ramotowski, M. A. T. & Gurr, S. J. Crop pests and pathogens move polewards in a warming world. *Nature Climate Change* **3**, 985-988, doi:10.1038/nclimate1990 (2013).

23 Bebber, D. P. in *Annual Review of Phytopathology, Vol 53* Vol. 53 *Annual Review of Phytopathology* (ed N. K. VanAlfen) 335-356 (Annual Reviews, 2015).

24 Oostendorp, M., Kunz, W., Dietrich, B. & Staub, T. Induced disease resistance in plants by chemicals. *European Journal of Plant Pathology* **107**, 19-28, doi:10.1023/a:1008760518772 (2001).

25 Juroszek, P. & von Tiedemann, A. Potential strategies and future requirements for plant disease management under a changing climate. *Plant Pathology* **60**, 100-112, doi:10.1111/j.1365-3059.2010.02410.x (2011).

26 Oerke, E. C. Crop losses to pests. *Journal of Agricultural Science* **144**, 31-43, doi:10.1017/s0021859605005708 (2006).

27 Savary, S. *et al.* The global burden of pathogens and pests on major food crops. *Nature Ecology & Evolution* **3**, 430-+, doi:10.1038/s41559-018-0793-y (2019).

28 McDonald, B. A. & Stukenbrock, E. H. Rapid emergence of pathogens in agro-ecosystems: global threats to agricultural sustainability and food security. *Philosophical Transactions of the Royal Society B-Biological Sciences* **371**, 9, doi:10.1098/rstb.2016.0026 (2016).

29 Sauquet, H. *et al.* The ancestral flower of angiosperms and its early diversification. *Nature Communications* **8**, doi:10.1038/ncomms16047 (2017).

30 Doyle, J. A. in *Annual Review of Earth and Planetary Sciences, Vol 40* Vol. 40 *Annual Review of Earth and Planetary Sciences* (ed R. Jeanloz) 301-326 (Annual Reviews, 2012).

31 Magallon, S., Hilu, K. W. & Quandt, D. Land plant evolutionary timeline: gene effects are secondary to fossil constraints in relaxed clock estimation of age and substitution rates. *American Journal of Botany* **100**, 556-573, doi:10.3732/ajb.1200416 (2013).

32 Magallon, S., Gomez-Acevedo, S., Sanchez-Reyes, L. L. & Hernandez-Hernandez, T. A metacalibrated time-tree documents the early rise of flowering plant phylogenetic diversity. *New Phytologist* **207**, 437-453, doi:10.1111/nph.13264 (2015).

33 Beaulieu, J. M., O'Meara, B. C., Crane, P. & Donoghue, M. J. Heterogeneous Rates of Molecular Evolution and Diversification Could Explain the Triassic Age Estimate for Angiosperms. *Systematic Biology* **64**, 869-878, doi:10.1093/sysbio/syv027 (2015).

34 Foster, C. S. P. *et al.* Evaluating the Impact of Genomic Data and Priors on Bayesian Estimates of the Angiosperm Evolutionary Timescale. *Systematic Biology* **66**, 338-351, doi:10.1093/sysbio/syw086 (2017).

35 Rebolleda-Gomez, M. *et al.* Gazing into the anthosphere: considering how microbes influence floral evolution. *New Phytologist* **224**, 1012-1020, doi:10.1111/nph.16137 (2019).

36 Junker, R. R., Romeike, T., Keller, A. & Langen, D. Density-dependent negative responses by bumblebees to bacteria isolated from flowers. *Apidologie* **45**, 467-477, doi:10.1007/s13592-013-0262-1 (2014).

37 Wei, N. & Ashman, T. L. The effects of host species and sexual dimorphism differ among root, leaf and flower microbiomes of wild

strawberries in situ. *Sci Rep* **8**, 12, doi:10.1038/s41598-018-23518-9 (2018).

38 Aleklett, K., Hart, M. & Shade, A. The microbial ecology of flowers: an emerging frontier in phyllosphereresearch. *Botany* **92**, 14, doi:10.1139/cjb-2013-0166 (2014).

39 Govind, S. R., Jogaiah, S., Abdelrahman, M., Shetty, H. S. & Tran, L. S. P. Exogenous Trehalose Treatment Enhances the Activities of Defense-Related Enzymes and Triggers Resistance against Downy Mildew Disease of Pearl Millet. *Frontiers in Plant Science* **7**, 12, doi:10.3389/fpls.2016.01593 (2016).

40 Shetty, H. S. *et al.* Bioimaging structural signatures of the oomycete pathogen Sclerospora graminicola in pearl millet using different microscopic techniques. *Scientific Reports* **9**, 11, doi:10.1038/s41598-019-51477-2 (2019).

41 Ngugi, H. K. & Scherm, H. in *Annual Review of Phytopathology* Vol. 44 *Annual Review of Phytopathology* 261-282 (Annual Reviews, 2006).

42 Martinez-Espinoza, A. D., Garcia-Pedrajas, M. D. & Gold, S. E. The Ustilaginales as plant pests and model systems. *Fungal Genetics and Biology* **35**, 1-20, doi:10.1006/fgbi.2001.1301 (2002).

43 Norelli, J. L., Jones, A. L. & Aldwinckle, H. S. Fire blight management in the twenty-first century - Using new technologies that enhance host resistance in apple. *Plant Disease* **87**, 756-765, doi:10.1094/pdis.2003.87.7.756 (2003).

44 Islam, M. T. *et al.* Emergence of wheat blast in Bangladesh was caused by a South American lineage of Magnaporthe oryzae. *Bmc Biology* **14**, 11, doi:10.1186/s12915-016-0309-7 (2016).

45 Wenneker, M., Pham, K. T. K., Woudenberg, J. H. C. & Thomma, B. Identification of Alternaria spp. as causal agent of dead flower buds disease of pear (Pyrus communis) in the Netherlands and methods for disease control. *European Journal of Plant Pathology* **155**, 967-981, doi:10.1007/s10658-019-01827-7 (2019).

46 Fonseca, W. L. *et al.* Morphological, molecular phylogenetic and pathogenic analyses of Erysiphe spp. causing powdery mildew on cashew plants in Brazil. *Plant Pathology* **68**, 1157-1164, doi:10.1111/ppa.13032 (2019).

47 Boedi, S. *et al.* Comparison of Fusarium graminearum Transcriptiomes on living or Dead Wheat Differentitates Substrate-Responsive and Defense-Responsive Genes. *Frontiers in Microbiology* **7**, 24, doi:10.3389/fmicb.2016.01113 (2016).

48 Hu, M. J., Dowling, M. E. & Schnabel, G. Genotypic and Phenotypic Variations in Botrytis spp. Isolates from Single Strawberry Flowers. *Plant Disease* **102**, 179-184, doi:10.1094/pdis-06-17-0891-re (2018).

49 Jaiswal, S. *et al.* Transcriptomic signature reveals mechanism of flower bud distortion in witches'-broom disease of soybean (Glycine max). *Bmc Plant Biology* **19**, 12, doi:10.1186/s12870-018-1601-1 (2019).

50 Tomkins, M., Kliot, A., Maree, A. F. M. & Hogenhout, S. A. A multi-layered mechanistic modelling approach to understand how effector genes extend beyond phytoplasma to modulate plant hosts, insect vectors and the environment. *Current Opinion in Plant Biology* **44**, 39-48, doi:10.1016/j.pbi.2018.02.002 (2018).

51 Orlovskis, Z. & Hogenhout, S. A. A Bacterial Parasite Effector Mediates Insect Vector Attraction in Host Plants Independently of Developmental

Changes. *Frontiers in Plant Science* **7**, 9, doi:10.3389/fpls.2016.00885 (2016).

52 Rotenberg, D. & Whitfield, A. E. Molecular interactions between tospoviruses and thrips vectors. *Current Opinion in Virology* **33**, 191-197, doi:10.1016/j.coviro.2018.11.007 (2018).

53 Schachterle, J. K., Zeng, Q. & Sundin, G. W. Three Hfq-dependent small RNAs regulate flagellar motility in the fire blight pathogen Erwinia amylovora. *Molecular Microbiology* **111**, 1476-1492, doi:10.1111/mmi.14232 (2019).

54 Adkar-Purushothama, C. R., Sano, T. & Perreault, J. P. Viroid-derived small RNA induces early flowering in tomato plants by RNA silencing. *Molecular Plant Pathology* **19**, 2446-2458, doi:10.1111/mpp.12721 (2018).

55 Oeser, B. *et al.* Cross-talk of the biotrophic pathogen Claviceps purpurea and its host Secale cereale. *Bmc Genomics* **18**, 19, doi:10.1186/s12864-017-3619-4 (2017).

56 Song, J. H. *et al.* Rice false smut fungus hijacks the rice nutrients supply by blocking and mimicking the fertilization of rice ovary. *Environmental Microbiology* **18**, 3840-3849, doi:10.1111/1462-2920.13343 (2016).

57 Groen, S. C. *et al.* Virus Infection of Plants Alters Pollinator Preference: A Payback for Susceptible Hosts? *Plos Pathogens* **12**, 28, doi:10.1371/journal.ppat.1005790 (2016).

58 McArt, S. H. *et al.* Floral Scent Mimicry and Vector-Pathogen Associations in a Pseudoflower-Inducing Plant Pathogen System. *Plos One* **11**, 19, doi:10.1371/journal.pone.0165761 (2016).

59 Kazan, K. & Lyons, R. The link between flowering time and stress tolerance. *Journal of Experimental Botany* **67**, 47-60, doi:10.1093/jxb/erv441 (2016).

60 Das, A., Lee, S. H., Hyun, T. K., Kim, S. W. & Kim, J. Y. Plant volatiles as method of communication. *Plant Biotechnology Reports* **7**, 9-26, doi:10.1007/s11816-012-0236-1 (2013).

61 Huang, M. *et al.* The major volatile organic compound emitted from Arabidopsis thaliana flowers, the sesquiterpene (E)-beta-caryophyllene, is a defense against a bacterial pathogen. *New Phytologist* **193**, 997-1008, doi:10.1111/j.1469-8137.2011.04001.x (2012).

62 Burdon, R. C. F., Junker, R. R., Scofield, D. G. & Parachnowitsch, A. L. Bacteria colonising Penstemon digitalis show volatile and tissue-specific responses to a natural concentration range of the floral volatile linalool. *Chemoecology* **28**, 11-19, doi:10.1007/s00049-018-0252-x (2018).

63 Junker, R. R. *et al.* Composition of epiphytic bacterial communities differs on petals and leaves. *Plant Biology* **13**, 918-924, doi:10.1111/j.1438-8677.2011.00454.x (2011).

64 Cao, X. Q. *et al.* A detached petal disc assay and virus-induced gene silencing facilitate the study of Botrytis cinerea resistance in rose flowers. *Horticulture Research* **6**, 11, doi:10.1038/s41438-019-0219-2 (2019).

65 Liu, X. T. *et al.* Comparative RNA-Seq analysis reveals a critical role for brassinosteroids in rose (Rosa hybrida) petal defense against Botrytis cinerea infection. *Bmc Genetics* **19**, 10, doi:10.1186/s12863-018-0668-x (2018).

66 Ederli, L. *et al.* Arabidopsis flower specific defense gene expression patterns affect resistance to pathogens. *Frontiers in Plant Science* **6**, 13, doi:10.3389/fpls.2015.00079 (2015).

67 Wu, X. J. *et al.* The Orthotospovirus nonstructural protein NSs suppresses plant MYC-regulated jasmonate signaling leading to enhanced vector attraction and performance. *Plos Pathogens* **15**, 21, doi:10.1371/journal.ppat.1007897 (2019).

68 Gordon, A. *et al.* Genetic and transcriptional dissection of resistance to Claviceps purpurea in the durum wheat cultivar Greenshank. *Theoretical and Applied Genetics* **133**, 1873-1886, doi:10.1007/s00122-020-03561-9 (2020).

69 Cui, Z. H. *et al.* Linkage mapping combined with association analysis reveals QTL and candidate genes for three husk traits in maize. *Theoretical and Applied Genetics* **131**, 2131-2144, doi:10.1007/s00122-018-3142-2 (2018).

70 Peil, A. *et al.* Mapping of fire blight resistance in Malus xrobusta 5 flowers following artificial inoculation. *Bmc Plant Biology* **19**, 12, doi:10.1186/s12870-019-2154-7 (2019).

71 Iannone, L. J. *et al.* Seed-transmitted Epichloe sp endophyte alleviates the negative effects of head smut of grasses (Ustilago bullata) on Bromus auleticus. *Fungal Ecology* **29**, 45-51, doi:10.1016/j.funeco.2017.06.001 (2017).

72 Morris, M. M., Frixione, N. J., Burkert, A. C., Dinsdale, E. A. & Vannette, R. L. Microbial abundance, composition, and function in nectar are shaped by flower visitor identity. *Fems Microbiology Ecology* **96**, 14, doi:10.1093/femsec/fiaa003 (2020).

73 Slack, S. M., Outwater, C. A., Grieshop, M. J. & Sundin, G. W. Evaluation of a contact sterilant as a niche-clearing method to enhance the colonization of apple flowers and efficacy of Aureobasidium pullulans in the biological control of fire blight. *Biological Control* **139**, 9, doi:10.1016/j.biocontrol.2019.104073 (2019).

74 Purahong, W. *et al.* Plant Microbiome and Its Link to Plant Health: Host Species, Organs and Pseudomonas syringae pv. actinidiae Infection Shaping Bacterial Phyllosphere Communities of Kiwifruit Plants. *Frontiers in Plant Science* **9**, 16, doi:10.3389/fpls.2018.01563 (2018).

75 Hettiarachchige, I. K. *et al.* Generation of Epichloe Strains Expressing Fluorescent Proteins Suitable for Studying Host-Endophyte Interactions and Characterisation of a T-DNA Integration Event. *Microorganisms* **8**, 19, doi:10.3390/microorganisms8010054 (2020).

76 Clough, S. J. & Bent, A. F. Floral dip: a simplified method for Agrobacterium-mediated transformation of Arabidopsis thaliana. *Plant Journal* **16**, 735-743, doi:10.1046/j.1365-313x.1998.00343.x (1998).

77 Urban, M., Daniels, S., Mott, E. & Hammond-Kosack, K. Arabidopsis is susceptible to the cereal ear blight fungal pathogens Fusarium graminearum and Fusarium culmorum. *Plant Journal* **32**, 961-973, doi:10.1046/j.1365-313X.2002.01480.x (2002).

78 Chen, X. W., Steed, A., Harden, C. & Nicholson, P. Characterization of Arabidopsis thaliana-Fusarium graminearum interactions and identification of variation in resistance among ecotypes. *Molecular Plant Pathology* **7**, 391-403, doi:10.1111/j.1364-3703.2006.00349.x (2006).

79 Cuzick, A., Urban, M. & Hammond-Kosack, K. Fusarium graminearum gene deletion mutants map1 and tri5 reveal similarities and differences in

the pathogenicity requirements to cause disease on Arabidopsis and wheat floral tissue. *New Phytologist* **177**, 990-1000, doi:10.1111/j.1469-8137.2007.02333.x (2008).

80 Scholthof, K. B. G. *et al.* Top 10 plant viruses in molecular plant pathology. *Molecular Plant Pathology* **12**, 938-954, doi:10.1111/j.1364-3703.2011.00752.x (2011).

81 Decroocq, V. *et al.* Multiple resistance traits control Plum pox virus infection in Arabidopsis thaliana. *Molecular Plant-Microbe Interactions* **19**, 541-549, doi:10.1094/mpmi-19-0541 (2006).

82 Andargie, M. & Li, J. X. Arabidopsis thaliana: A Model Host Plant to Study Plant-Pathogen Interaction Using Rice False Smut Isolates of Ustilaginoidea virens. *Frontiers in Plant Science* **7**, 10, doi:10.3389/fpls.2016.00192 (2016).

83 Fan, J. *et al.* Current understanding on Villosiclava virens, a unique flower-infecting fungus causing rice false smut disease. *Mol. Plant Pathol.* **17**, 1321-1330, doi:10.1111/mpp.12362 (2016).

84 Fujita, N. *et al.* Development of the VIGS System in the Dioecious Plant Silene latifolia. *International Journal of Molecular Sciences* **20**, 12, doi:10.3390/ijms20051031 (2019).

85 Li, C. J., Yamagishi, N., Kasajima, I. & Yoshikawa, N. Virus-induced gene silencing and virus-induced flowering in strawberry (Fragaria x ananassa) using apple latent spherical virus vectors. *Horticulture Research* **6**, 10, doi:10.1038/s41438-018-0106-2 (2019).

86 Goulin, E. H., dos Santos, P. J. C., Dalio, R. D. & Machado, M. A. In vitro symptom induction of Colletotrichum abscissum infection in detached

sweet orange flowers. *Journal of Plant Pathology* **101**, 695-699, doi:10.1007/s42161-018-00220-3 (2019).

87 Jafari, M., Minaei, S. & Safaie, N. Detection of pre-symptomatic rose powdery-mildew and gray-mold diseases based on thermal vision. *Infrared Physics & Technology* **85**, 170-183, doi:10.1016/j.infrared.2017.04.023 (2017).

88 Hayashi, K., Yoshida, T. & Hayano-Saito, Y. Detection of white head symptoms of panicle blast caused by Pyricularia oryzae using cut-flower dye. *Plant Methods* **15**, 9, doi:10.1186/s13007-019-0548-z (2019).

89 Vilanova, L., Usall, J., Teixido, N. & Torres, R. Assessment of viable conidia of Monilinia fructicola in flower and stone fruit combining propidium monoazide (PMA) and qPCR. *Plant Pathology* **66**, 1276-1287, doi:10.1111/ppa.12676 (2017).

90 Garcia-Benitez, C. *et al.* Proficiency of real-time PCR detection of latent Monilinia spp. infection in nectarine flowers and fruit. *Phytopathologia Mediterranea* **56**, 242-250, doi:10.14601/Phytopathol_Mediterr-20486 (2017).

91 Yamagishi, N., Li, C. J. & Yoshikawa, N. Promotion of Flowering by Apple Latent Spherical Virus Vector and Virus Elimination at High Temperature Allow Accelerated Breeding of Apple and Pear. *Frontiers in Plant Science* **7**, 10, doi:10.3389/fpls.2016.00171 (2016).

92 Joshi, N. K., Ngugi, H. K. & Biddinger, D. J. Bee Vectoring: Development of the Japanese Orchard Bee as a Targeted Delivery System of Biological Control Agents for Fire Blight Management. *Pathogens* **9**, 11, doi:10.3390/pathogens9010041 (2020).

93 Klee, S. M. *et al.* Erwinia amylovora Auxotrophic Mutant Exometabolomics and Virulence on Apples. *Applied and Environmental Microbiology* **85**, 19, doi:10.1128/aem.00935-19 (2019).

94 Weir, E., Lawlor, A., Whelan, A. & Regan, F. The use of nanoparticles in anti-microbial materials and their characterization. *Analyst* **133**, 835-845, doi:10.1039/b715532h (2008).

95 Nokkrut, B. O., Pisuttipiched, S., Khantayanuwong, S. & Puangsin, B. Silver Nanoparticle-Based Paper Packaging to Combat Black Anther Disease in Orchid Flowers. *Coatings* **9**, 10, doi:10.3390/coatings9010040 (2019).

96 Hao, Y. *et al.* Potential Applications and Antifungal Activities of Engineered Nanomaterials against Gray Mold Disease Agent Botrytis cinerea on Rose Petals. *Frontiers in Plant Science* **8**, 9, doi:10.3389/fpls.2017.01332 (2017).

97 Roberts, J. M. K., Ireland, K. B., Tay, W. T. & Paini, D. Honey bee-assisted surveillance for early plant virus detection. *Annals of Applied Biology* **173**, 285-293, doi:10.1111/aab.12461 (2018).

98 Burnham, A. J. Scientific Advances in Controlling Nosema ceranae (Microsporidia) Infections in Honey Bees (Apis mellifera). *Frontiers in Veterinary Science* **6**, 8, doi:10.3389/fvets.2019.00079 (2019).

99 Purkiss, T. & Lach, L. Pathogen spillover from Apis mellifera to a stingless bee. *Proceedings of the Royal Society B-Biological Sciences* **286**, 9, doi:10.1098/rspb.2019.1071 (2019).

100 Giacomini, J. J. *et al.* Medicinal value of sunflower pollen against bee pathogens. *Scientific Reports* **8**, 10, doi:10.1038/s41598-018-32681-y (2018).

101 Hien, D. *et al.* Plant-Mediated Effects on Mosquito Capacity to Transmit Human Malaria. *Plos Pathogens* **12**, 17, doi:10.1371/journal.ppat.1005773 (2016).

102 Kenney, A. *et al.* The potential for flower nectar to allow mosquito to mosquito transmission of Francisella tularensis. *Plos One* **12**, 12, doi:10.1371/journal.pone.0175157 (2017).

103 Summerell, B. A. in *Annual Review of Phytopathology, Vol 57, 2019* Vol. 57 *Annual Review of Phytopathology* (eds J. E. Leach & S. E. Lindow) 323-339 (Annual Reviews, 2019).

104 Dean, R. *et al.* The Top 10 fungal pathogens in molecular plant pathology. *Molecular Plant Pathology* **13**, 414-430, doi:10.1111/j.1364-3703.2011.00783.x (2012).

105 O'Donnell, K. *et al.* Phylogenetic analyses of RPB1 and RPB2 support a middle Cretaceous origin for a clade comprising all agriculturally and medically important fusaria. *Fungal Genetics and Biology* **52**, 20-31, doi:10.1016/j.fgb.2012.12.004 (2013).

106 Kimura, M., Tokai, T., Takahashi-Ando, N., Ohsato, S. & Fujimura, M. Molecular and genetic studies of Fusarium trichothecene biosynthesis: Pathways, genes, and evolution. *Biosci. Biotechnol. Biochem.* **71**, 2105-2123, doi:10.1271/bbb.70183 (2007).

107 McMullen, M., Jones, R. & Gallenberg, D. Scab of wheat and barley: A re-emerging disease of devastating impact. *Plant Dis.* **81**, 1340-1348, doi:10.1094/pdis.1997.81.12.1340 (1997).

108 Goswami, R. S. & Kistler, H. C. Heading for disaster: Fusarium graminearum on cereal crops. *Molecular Plant Pathology* **5**, 515-525, doi:10.1111/j.1364-3703.2004.00252.x (2004).

109 King, R., Brown, N. A., Urban, M. & Hammond-Kosack, K. E. Inter-genome comparison of the Quorn fungus Fusarium venenatum and the closely related plant infecting pathogen Fusarium graminearum. *Bmc Genomics* **19**, 19, doi:10.1186/s12864-018-4612-2 (2018).

110 Fisher, M. C., Hawkins, N. J., Sanglard, D. & Gurr, S. J. Worldwide emergence of resistance to antifungal drugs challenges human health and food security. *Science* **360**, 739-742, doi:10.1126/science.aap7999 (2018).

111 Nganje, W. E., Kaitibie, S., Wilson, W. W., Leistritz, L. F. & Bangsund, D. A. Economic impacts of Fusarium head blight in wheat and barley: 1993-2001. 53 (North Dakota State University, AgEcon, 2004).

112 *www.fao.org/faostat*.

113 Brown, N. A., Urban, M., Van De Meene, A. M. L. & Hammond-Kosack, K. E. The infection biology of Fusarium graminearum: Defining the pathways of spikelet to spikelet colonisation in wheat ears. *Fungal Biology* **114**, 555-571, doi:10.1016/j.funbio.2010.04.006 (2010).

114 Valverde-Bogantes, E. *et al.* Recent population changes of Fusarium head blight pathogens: drivers and implications. *Canadian Journal of Plant Pathology*, 15, doi:10.1080/07060661.2019.1680442.

115 Aoki, T., Ward, T. J., Kistler, H. C. & O'Donnel, K. Systemics, phylogeny and trichothecene mycotoxin potential of Fusarium head blight cereal pathogens. *JSM Mycotoxins* **62**, 91-102 (2012).

116 van der Lee, T., Zhang, H., van Diepeningen, A. & Waalwijk, C. Biogeography of Fusarium graminearum species complex and chemotypes: a review. *Food Additives and Contaminants Part a-*

Chemistry Analysis Control Exposure & Risk Assessment **32**, 453-460, doi:10.1080/19440049.2014.984244 (2015).

117 Xu, X. M. *et al.* Predominance and association of pathogenic fungi causing Fusarium ear blightin wheat in four European countries. *European Journal of Plant Pathology* **112**, 143-154, doi:10.1007/s10658-005-2446-7 (2005).

118 Nielsen, L. K. *et al.* Fusarium Head Blight of Cereals in Denmark: Species Complex and Related Mycotoxins. *Phytopathology* **101**, 960-969, doi:10.1094/phyto-07-10-0188 (2011).

119 Jennings, P., Coates, M. E., Walsh, K., Turner, J. A. & Nicholson, P. Determination of deoxynivalenol- and nivalenol-producing chemotypes of Fusarium graminearum isolated from wheat crops in England and Wales. *Plant Pathology* **53**, 643-652, doi:10.1111/j.0032-0862.2004.01061.x (2004).

120 Backhouse, D. Global distribution of Fusarium graminearum, F-asiaticum and F-boothii from wheat in relation to climate. *European Journal of Plant Pathology* **139**, 161-173, doi:10.1007/s10658-013-0374-5 (2014).

121 Logrieco, A., Bottalico, A., Mule, G., Moretti, A. & Perrone, G. Epidemiology of toxigenic fungi and their associated mycotoxins for some Mediterranean crops. *European Journal of Plant Pathology* **109**, 645-667, doi:10.1023/a:1026033021542 (2003).

122 Proctor, R., Hohn, T. & McCormick, S. Reduced virulence of *Gibberella zeae* caused by disruption of a trichothecene toxin synthetic gene. *Molecular Plant-Microbe Interactions* **8**, 593-601 (1995).

123 Proctor, R., Hohn, T., McCormick, S. & Desjardins, A. *TRI6* encodes an unusual zinc-finger protein involved in regulation of trichothecene

biosynthesis in *Fusarium sporotrichioides*. *Applied and Environmental Microbiology* **61**, 1923-1930 (1995).

124 Mielniczuk, E. & Skwaryło-Bednarz, B. Fusarium Head Blight, Mycotoxins and Strategies for Their Reduction. *Agronomy* **10**, doi:10.3390/agronomy10040509 (2020).

125 Hussein, H. S. & Brasel, J. M. Toxicity, metabolism, and impact of mycotoxins on humans and animals. *Toxicology* **167**, 101-134, doi:10.1016/s0300-483x(01)00471-1 (2001).

126 Bennett, J. W. & Klich, M. Mycotoxins. *Clinical Microbiology Reviews* **16**, 497-+, doi:10.1128/cmr.16.3.497-516.2003 (2003).

127 Medema, M. H., Cimermancic, P., Sali, A., Takano, E. & Fischbach, M. A. A Systematic Computational Analysis of Biosynthetic Gene Cluster Evolution: Lessons for Engineering Biosynthesis. *Plos Computational Biology* **10**, 12, doi:10.1371/journal.pcbi.1004016 (2014).

128 Villafana, R. T., Ramdass, A. C. & Rampersad, S. N. Selection of Fusarium Trichothecene Toxin Genes for Molecular Detection Depends on TRI Gene Cluster Organization and Gene Function. *Toxins* **11**, 25, doi:10.3390/toxins11010036 (2019).

129 Lazarus, C. M., Williams, K. & Bailey, A. M. Reconstructing fungal natural product biosynthetic pathways. *Natural Product Reports* **31**, 1339-1347, doi:10.1039/c4np00084f (2014).

130 Desjardins, A. E. & Plattner, R. D. Fumonisin B-1-nonproducing strains of Fusarium verticillioides cause maize (Zea mays) ear infection and ear rot. *Journal of Agricultural and Food Chemistry* **48**, 5773-5780, doi:10.1021/jf000619k (2000).

131 Marasas, W. F. O. Fumonisins: History, world-wide occurrence and impact. *Fumonisins in Food* **392**, 1-17 (1996).

132 WHO. *Fumonisins*, <who.int/foodsafety/Food_Safety_Digest_Fumonisins_EN.pdf> (2018).

133 Mwalwayo, D. S. & Thole, B. Prevalence of aflatoxin and fumonisins (B-1. *Toxicology Reports* **3**, 173-179, doi:10.1016/j.toxrep.2016.01.010 (2016).

134 Sweeney, M. J. & Dobson, A. D. W. Molecular biology of mycotoxin biosynthesis. *Fems Microbiology Letters* **175**, 149-163, doi:10.1016/s0378-1097(99)00103-2 (1999).

135 Yazar, S. & Omurtag, G. Z. Fumonisins, Trichothecenes and Zearalenone in Cereals. *International Journal of Molecular Sciences* **9**, 2062-2090, doi:10.3390/ijms9112062 (2008).

136 Zhang, G. L., Feng, Y. L., Song, J. L. & Zhou, X. S. Zearalenone: A Mycotoxin With Different Toxic Effect in Domestic and Laboratory Animals' Granulosa Cells. *Frontiers in Genetics* **9**, 8, doi:10.3389/fgene.2018.00667 (2018).

137 D'Mello, J. P. F., Placinta, C. M. & Macdonald, A. M. C. Fusarium mycotoxins: a review of global implications for animal health, welfare and productivity. *Animal Feed Science and Technology* **80**, 183-205, doi:10.1016/s0377-8401(99)00059-0 (1999).

138 Poor, M. *et al.* Interactions of zearalenone with native and chemically modified cyclodextrins and their potential utilization. *Journal of Photochemistry and Photobiology B-Biology* **151**, 63-68, doi:10.1016/j.jphotobiol.2015.07.009 (2015).

139 Shifrin, V. I. & Anderson, P. Trichothecene mycotoxins trigger a ribotoxic stress response that activates c-Jun N-terminal kinase and p38 mitogen-activated protein kinase and induces apoptosis. *Journal of Biological Chemistry* **274**, 13985-13992, doi:10.1074/jbc.274.20.13985 (1999).

140 Moon, Y. & Pestka, J. J. Deoxynivalenol-induced mitogen-activated protein kinase phosphorylation and IL-6 expression in mice suppressed by fish oil. *Journal of Nutritional Biochemistry* **14**, 717-726, doi:10.1016/j.jnutbio.2003.08.009 (2003).

141 Sobrova, P. *et al.* Deoxynivalenol and its toxicity. *Interdiscip Toxicol.* **3**, 94-99, doi:10.2478/v10102-010-0019-x (2010).

142 Ward, T. J. *et al.* An adaptive evolutionary shift in Fusarium head blight pathogen populations is driving the rapid spread of more toxigenic Fusarium graminearum in North America. *Fungal Genetics and Biology* **45**, 473-484, doi:10.1016/j.fgb.2007.10.003 (2008).

143 Jansen, C. *et al.* Infection patterns in barley and wheat spikes inoculated with wild-type and trichodiene synthase gene disrupted Fusarium graminearum. *Proceedings of the National Academy of Sciences of the United States of America* **102**, 16892-16897, doi:10.1073/pnas.0508467102 (2005).

144 Proctor, R. H., McCormick, S. P., Alexander, N. J. & Desjardins, A. E. Evidence that a secondary metabolic biosynthetic gene cluster has grown by gene relocation during evolution of the filamentous fungus Fusarium. *Molecular Microbiology* **74**, 1128-1142, doi:10.1111/j.1365-2958.2009.06927.x (2009).

145 Gardiner, D. M., Kazan, K. & Manners, J. M. Nutrient profiling reveals potent inducers of trichothecene biosynthesis in Fusarium graminearum.

Fungal Genetics and Biology **46**, 604-613, doi:10.1016/j.fgb.2009.04.004 (2009).

146 Kistler, H. C. & Broz, K. Cellular compartmentalization of secondary metabolism. *Frontiers in Microbiology* **6**, 11, doi:10.3389/fmicb.2015.00068 (2015).

147 Boenisch, M. J. *et al.* Structural reorganization of the fungal endoplasmic reticulum upon induction of mycotoxin biosynthesis. *Scientific Reports* **7**, 13, doi:10.1038/srep44296 (2017).

148 Menke, J., Weber, J., Broz, K. & Kistler, H. C. Cellular Development Associated with Induced Mycotoxin Synthesis in the Filamentous Fungus Fusarium graminearum. *Plos One* **8**, 12, doi:10.1371/journal.pone.0063077 (2013).

149 Tang, G. F., Chen, Y., Xu, J. R., Kistler, H. C. & Ma, Z. H. The fungal myosin I is essential for Fusarium toxisome formation. *Plos Pathogens* **14**, 23, doi:10.1371/journal.ppat.1006827 (2018).

150 AHDB. *Risk assessment for fusarium mycotoxins in wheat*, <ahdb.org.uk/knowledge-library/risk-assessment-for-fusarium-mycotoxins-in-wheat> (

151 *Food Standards Agency. Mycotoxins*, <food.gov.uk/business-guidance/mycotoxins> (2018).

152 *Food Standards Agency. The UK Code of Good Agricultural Practice to Reduce Fusarium Mycotoxins in Cereals*, <food.gov.uk/sites/default/files/media/document/fusariumcop.pdf> (2007).

153 Sutton, J. C. Epidemiology of wheat head blight and maize ear rot caused by *Fusarium graminearum*. *Can. J. Plant Pathol.* **4**, 195-209 (1982).

154 Parry, D. W., Jenkinson, P. & McLeod, L. Fusarium ear blight (scab) in small-grain cereals - a review. *Plant Pathol.* **44**, 207-238, doi:10.1111/j.1365-3059.1995.tb02773.x (1995).

155 Wanjiru, W. M., Kang, Z. S. & Buchenauer, H. Importance of cell wall degrading enzymes produced by Fusarium graminearum during infection of wheat heads. *European Journal of Plant Pathology* **108**, 803-810 (2002).

156 Boenisch, M. J. & Schafer, W. Fusarium graminearum forms mycotoxin producing infection structures on wheat. *Bmc Plant Biology* **11**, 13, doi:10.1186/1471-2229-11-110 (2011).

157 Bormann, J., Boenisch, M. J., Bruckner, E., Firat, D. & Schafer, W. The Adenylyl Cyclase Plays a Regulatory Role in the Morphogenetic Switch from Vegetative to Pathogenic Lifestyle of Fusarium graminearum on Wheat. *Plos One* **9**, 13, doi:10.1371/journal.pone.0091135 (2014).

158 Kang, Z. S. & Buchenauer, H. Cytology and ultrastructure of the infection of wheat spikes by Fusarium culmorum. *Mycological Research* **104**, 1083-1093, doi:10.1017/s0953756200002495 (2000).

159 Voigt, C. A., Schafer, W. & Salomon, S. A secreted lipase of Fusarium graminearum is a virulence factor required for infection of cereals. *Plant Journal* **42**, 364-375, doi:10.1111/j.1365-313X.2005.02377.x (2005).

160 Cuomo, C. A. *et al.* The Fusarium graminearum genome reveals a link between localized polymorphism and pathogen specialization. *Science* **317**, 1400-1402, doi:10.1126/science.1143708 (2007).

161 Walter, S., Nicholson, P. & Doohan, F. M. Action and reaction of host and pathogen during Fusarium head blight disease. *New Phytologist* **185**, 54-66, doi:10.1111/j.1469-8137.2009.03041.x (2010).

162 Pritsch, C., Muehlbauer, G. J., Bushnell, W. R., Somers, D. A. & Vance, C. P. Fungal development and induction of defense response genes during early infection of wheat spikes by Fusarium graminearum. *Molecular Plant-Microbe Interactions* **13**, 159-169, doi:10.1094/mpmi.2000.13.2.159 (2000).

163 Miller, S. S., Chabot, D. M. P., Ouellet, T., Harris, L. J. & Fedak, G. Use of a Fusarium graminearum strain transformed with green fluorescent protein to study infection in wheat (Triticum aestivum). *Canadian Journal of Plant Pathology-Revue Canadienne De Phytopathologie* **26**, 453-463, doi:10.1080/07060660409507165 (2004).

164 Trail, F. For Blighted Waves of Grain: Fusarium graminearum in the Postgenomics Era. *Plant Physiol.* **149**, 103-110, doi:10.1104/pp.108.129684 (2009).

165 Brown, N. A. *et al.* Characterisation of the *Fusarium graminearum*-wheat floral interaction. *J. Pathog.*, doi:10.4061/2011/626345 (2011).

166 Guenther, J. C. & Trail, F. The development and differentiation of Gibberella zeae (anamorph : Fusarium graminearum) during colonization of wheat. *Mycologia* **97**, 229-237, doi:10.3852/mycologia.97.1.229 (2005).

167 Ribichich, K. F., Lopez, S. E. & Vegetti, A. C. Histopathological spikelet changes produced by Fusarium graminearum in susceptible and resistant wheat cultivars. *Plant Disease* **84**, 794-802, doi:10.1094/pdis.2000.84.7.794 (2000).

168 Brown, N. A., Evans, J., Mead, A. & Hammond-Kosack, K. E. A spatial temporal analysis of the Fusarium graminearum transcriptome during symptomless and symptomatic wheat infection. *Molecular Plant Pathology* **18**, 1295-1312, doi:10.1111/mpp.12564 (2017).

169 King, R., Urban, M., Hammond-Kosack, M. C. U., Hassani-Pak, K. & Hammond-Kosack, K. E. The completed genome sequence of the pathogenic ascomycete fungus Fusarium graminearum. *Bmc Genomics* **16**, 21, doi:10.1186/s12864-015-1756-1 (2015).

170 King, R., Urban, M. & Hammond-Kosack, K. E. Annotation of Fusarium graminearum (PH-1) Version 5.0. *Microbiology Resource Announcements* **5**, 2, doi:10.1128/genomeA.01479-16 (2017).

171 Brown, N. A., Antoniw, J. & Hammond-Kosack, K. E. The Predicted Secretome of the Plant Pathogenic Fungus Fusarium graminearum: A Refined Comparative Analysis. *Plos One* **7**, 14, doi:10.1371/journal.pone.0033731 (2012).

172 Hao, G. X., McCormick, S., Usgaard, T., Tiley, H. & Vaughan, M. M. Characterization of Three Fusarium graminearum Effectors and Their Roles During Fusarium Head Blight. *Frontiers in Plant Science* **11**, 13, doi:10.3389/fpls.2020.579553 (2020).

173 Dill-Macky, R. & Jones, R. K. The effect of previous crop residues and tillage on Fusarium head blight of wheat. *Plant Disease* **84**, 71-76, doi:10.1094/pdis.2000.84.1.71 (2000).

174 Wegulo, S. N., Baenziger, P. S., Nopsa, J. H., Bockus, W. W. & Hallen-Adams, H. Management of Fusarium head blight of wheat and barley. *Crop Protection* **73**, 100-107, doi:10.1016/j.cropro.2015.02.025 (2015).

175 Bai, G. H., Su, Z. Q. & Cai, J. Wheat resistance to Fusarium head blight. *Canadian Journal of Plant Pathology* **40**, 336-346, doi:10.1080/07060661.2018.1476411 (2018).

176 Bai, G. H. & Shaner, G. Management and resistance in wheat and barley to Fusarium head blight. *Annual Review of Phytopathology* **42**, 135-161, doi:10.1146/annurev.phyto.42.040803.140340 (2004).

177 Rudd, J. C., Horsley, R. D., McKendry, A. L. & Elias, E. M. Host plant resistance genes for fusarium head blight: Sources, mechanisms, and utility in conventional breeding systems. *Crop Science* **41**, 620-627, doi:10.2135/cropsci2001.413620x (2001).

178 Liu, S. X. *et al.* Toward positional cloning of Fhb1, a major QTL for Fusarium head blight resistance in wheat. *Cereal Research Communications* **36**, 195-201, doi:10.1556/CRC.36.2008.Suppl.B.15 (2008).

179 Zhuang, Y. B., Gala, A. & Yen, Y. Identification of Functional Genic Components of Major Fusarium Head Blight Resistance Quantitative Trait Loci in Wheat Cultivar Sumai 3. *Molecular Plant-Microbe Interactions* **26**, 442-450, doi:10.1094/mpmi-10-12-0235-r (2013).

180 Basnet, B. R., Glover, K. D., Ibrahim, A. M. H., Yen, Y. & Chao, S. M. A QTL on chromosome 2DS of 'Sumai 3' increases susceptibility to Fusarium head blight in wheat. *Euphytica* **186**, 91-101, doi:10.1007/s10681-011-0495-x (2012).

181 Li, G. L. & Yen, Y. Jasmonate and ethylene signaling pathway may mediate Fusarium head blight resistance in wheat. *Crop Science* **48**, 1888-1896, doi:10.2135/cropsci2008.02.0097 (2008).

182 Paudel, B. *et al.* WFhb1-1 plays an important role in resistance against Fusarium head blight in wheat. *Scientific Reports* **10**, 15, doi:10.1038/s41598-020-64777-9 (2020).

183 Hao, Y. F., Rasheed, A., Zhu, Z. W., Wulff, B. B. H. & He, Z. H. Harnessing Wheat Fhb1 for Fusarium Resistance. *Trends in Plant Science* **25**, 1-3, doi:10.1016/j.tplants.2019.10.006 (2020).

184 McMullen, M. *et al.* A Unified Effort to Fight an Enemy of Wheat and Barley: Fusarium Head Blight. *Plant Disease* **96**, 1712-1728, doi:10.1094/pdis-03-12-0291-fe (2012).

185 Yoshida, M. *et al.* Effect of the Timing of Fungicide Application on Fusarium Head Blight and Mycotoxin Contamination in Wheat. *Plant Disease* **96**, 845-851, doi:10.1094/pdis-10-11-0819 (2012).

186 Paul, P. A. *et al.* Efficacy of triazole-based fungicides for Fusarium head blight and deoxynivalenol control in wheat: A multivariate meta-analysis. *Phytopathology* **98**, 999-1011, doi:10.1094/phyto-98-9-0999 (2008).

187 Spolti, P., Del Ponte, E. M., Dong, Y. H., Cummings, J. A. & Bergstrom, G. C. Sensitivity in a Contemporary Population of Fusarium graminearum from New York Wheat and Competitiveness of a Tebuconazole-Resistant Isolate. *Plant Disease* **98**, 607-613, doi:10.1094/pdis-10-13-1051-re (2014).

188 Chen, Y. & Zhou, M. G. Characterization of Fusarium graminearum Isolates Resistant to Both Carbendazim and a New Fungicide JS399-19. *Phytopathology* **99**, 441-446, doi:10.1094/phyto-99-4-0441 (2009).

189 Baffoni, L. *et al.* Microbial inoculants for the biocontrol of Fusarium spp. in durum wheat. *Bmc Microbiology* **15**, 10, doi:10.1186/s12866-015-0573-7 (2015).

190 Matarese, F., Sarrocco, S., Gruber, S., Seidl-Seiboth, V. & Vannacci, G. Biocontrol of Fusarium head blight: interactions between Trichoderma and mycotoxigenic Fusarium. *Microbiology-Sgm* **158**, 98-106, doi:10.1099/mic.0.052639-0 (2012).

191 McMullen, M. *et al.* Integrated strategies for Fusarium head blight management in the United States. *Cereal Research Communications* **36**, 563-568, doi:10.1556/CRC.36.2008.Suppl.B.45 (2008).

192 Saunders, D. G. O., Pretorius, Z. A. & Hovmoller, M. S. Tackling the re-emergence of wheat stem rust in Western Europe. *Communications Biology* **2**, 3, doi:10.1038/s42003-019-0294-9 (2019).

193 Singh, R. P. *et al.* in *Annual Review of Phytopathology, Vol 49* Vol. 49 *Annual Review of Phytopathology* (eds N. K. VanAlfen, G. Bruening, & J. E. Leach) 465-481 (Annual Reviews, 2011).

194 Xu, Q. *et al.* An effector protein of the wheat stripe rust fungus targets chloroplasts and suppresses chloroplast function. *Nature Communications* **10**, 13, doi:10.1038/s41467-019-13487-6 (2019).

195 Liu. The stripe rust fungal effector PEC6 suppresses pattern-triggered immunity in a host species-independent manner and interacts with adenosine kinases (2016). *New Phytologist* **213**, 1556-1556, doi:10.1111/nph.14362 (2017).

196 Narang, D. *et al.* Discovery and characterisation of a new leaf rust resistance gene introgressed in wheat from wild wheat Aegilops peregrina. *Scientific Reports* **10**, 9, doi:10.1038/s41598-020-64166-2 (2020).

197 McIntosh, R. A. *et al. 2007 Supplement* (KOMUGI Integrated Wheat Science Database, 2007).

198 Bolton, M. D., Kolmer, J. A. & Garvin, D. F. Wheat leaf rust caused by Puccinia triticina. *Molecular Plant Pathology* **9**, 563-575, doi:10.1111/j.1364-3703.2008.00487.x (2008).

199 Troch, V. *et al.* Formae speciales of cereal powdery mildew: close or distant relatives? *Molecular Plant Pathology* **15**, 304-314, doi:10.1111/mpp.12093 (2014).

200 Jorgensen, J. H. Genetics of powdery mildew resistance in barley. *Critical Reviews in Plant Sciences* **13**, 97-119, doi:10.1080/07352689409701910 (1994).

201 Weibull, J. *et al.* in *Diversity in barley (Hordeum vulgare)* 143-178 (Elsevier Science B.V., 2003).

202 AHDB. *Powdery mildew in cereals*, <ahdb.org.uk/powderymildew> (

203 Both, M. & Spanu, P. D. in *Plant-Pathogen Interactions (Annual Plant Reviews)* Vol. 11 (ed N.J. Talbot) (Blackwell Publishing and CRC Press, 2009).

204 Menardo, F., Praz, C. R., Wicker, T. & Keller, B. Rapid turnover of effectors in grass powdery mildew (Blumeria graminis). *Bmc Evolutionary Biology* **17**, 14, doi:10.1186/s12862-017-1064-2 (2017).

205 Nowara, D. *et al.* HIGS: Host-Induced Gene Silencing in the Obligate Biotrophic Fungal Pathogen Blumeria graminis. *Plant Cell* **22**, 3130-3141, doi:10.1105/tpc.110.077040 (2010).

206 Whigham, E. *et al.* Broadly Conserved Fungal Effector BEC1019 Suppresses Host Cell Death and Enhances Pathogen Virulence in Powdery Mildew of Barley (Hordeum vulgare L.). *Molecular Plant-Microbe Interactions* **28**, 968-983, doi:10.1094/mpmi-02-15-0027-fi (2015).

207 Zhang, Y. *et al.* The Highly Conserved Barley Powdery Mildew Effector BEC1019 Confers Susceptibility to Biotrophic and Necrotrophic Pathogens in Wheat. *International Journal of Molecular Sciences* **20**, 16, doi:10.3390/ijms20184376 (2019).

208 Suffert, F., Sache, I. & Lannou, C. Assessment of quantitative traits of aggressiveness in Mycosphaerella graminicola on adult wheat plants. *Plant Pathol.* **62**, 1330-1341, doi:10.1111/ppa.12050 (2013).

209 Jorgensen, L. N. *et al.* IPM Strategies and Their Dilemmas Including an Introduction to www.eurowheat.org. *J. Integr. Agric.* **13**, 265-281, doi:10.1016/s2095-3119(13)60646-2 (2014).

210 Polley, R. W. & Thomas, M. R. SURVEYS OF DISEASES OF WINTER-WHEAT IN ENGLAND AND WALES, 1976 1988. *Ann. Appl. Biol.* **119**, 1-20, doi:10.1111/j.1744-7348.1991.tb04839.x (1991).

211 O'Driscoll, A., Kildea, S., Doohan, F., Spink, J. & Mullins, E. The wheat-Septoria conflict: a new front opening up? *Trends Plant Sci.* **19**, 602-610, doi:10.1016/j.tplants.2014.04.011 (2014).

212 Fones, H. & Gurr, S. The impact of Septoria tritici Blotch disease on wheat: An EU perspective. *Fungal Genet. Biol.* **79**, 3-7, doi:10.1016/j.fgb.2015.04.004 (2015).

213 McDonald, M. C. *et al.* Rapid Parallel Evolution of Azole Fungicide Resistance in Australian Populations of the Wheat Pathogen Zymoseptoria tritici. *Applied and Environmental Microbiology* **85**, 14, doi:10.1128/aem.01908-18 (2019).

214 Brown, J. K. M., Chartrain, L., Lasserre-Zuber, P. & Saintenac, C. Genetics of resistance to Zymoseptoria tritici and applications to wheat

breeding. *Fungal Genet. Biol.* **79**, 33-41, doi:10.1016/j.fgb.2015.04.017 (2015).

215 Goodwin, S. B. Back to basics and beyond: increasing the level of resistance to Septoria tritici blotch in wheat. *Austral. Plant Pathol.* **36**, 532-538, doi:10.1071/ap07068 (2007).

216 Lynch, K. M. *et al.* Control of Zymoseptoria tritici cause of septoria tritici blotch of wheat using antifungal Lactobacillus strains. *J. Appl. Microbiol.* **121**, 485-494, doi:10.1111/jam.13171 (2016).

217 Kildea, S. *et al.* Bacillus megaterium shows potential for the biocontrol of septoria tritici blotch of wheat. *Biol. Control* **47**, 37-45, doi:10.1016/j.biocontrol.2008.07.001 (2008).

218 Kettles, G. J. & Kanyuka, K. Dissecting the Molecular Interactions between Wheat and the Fungal Pathogen Zymoseptoria tritici. *Front. Plant Sci.* **7**, 7, doi:10.3389/fpls.2016.00508 (2016).

219 Brading, P. A., Verstappen, E. C. P., Kema, G. H. J. & Brown, J. K. M. A gene-for-gene relationship between wheat and Mycosphaerella graminicola, the Septoria tritici blotch pathogen. *Phytopathology* **92**, 439-445, doi:10.1094/phyto.2002.92.4.439 (2002).

220 Wang, Y. X., Zia-Khan, S., Owusu-Adu, S., Miedaner, T. & Muller, J. Early Detection of Zymoseptoria tritici in Winter Wheat by Infrared Thermography. *Agriculture-Basel* **9**, 11, doi:10.3390/agriculture9070139 (2019).

221 Bearchell, S. J., Fraaije, B. A., Shaw, M. W. & Fitt, B. D. L. Wheat archive links long-term fungal pathogen population dynamics to air pollution. *Proc. Natl. Acad. Sci. U. S. A.* **102**, 5438-5442, doi:10.1073/pnas.0501596102 (2005).

222 Gouache, D. *et al.* Modelling climate change impact on Septoria tritici blotch (STB) in France: Accounting for climate model and disease model uncertainty. *Agric. For. Meteorol.* **170**, 242-252, doi:10.1016/j.agrformet.2012.04.019 (2013).

223 McDonald, M. C., McDonald, B. A. & Solomon, P. S. Recent advances in the Zymoseptoria tritici-wheat interaction: insights from pathogenomics. *Frontiers in Plant Science* **6**, 5, doi:10.3389/fpls.2015.00102 (2015).

224 Shipton, W. A., Boyd, S. R. J., Rosielle, A. A. & Shearer, B. I. Common Septoria disease of wheat. *Botanical Review* **37**, 231-+, doi:10.1007/bf02858957 (1971).

225 Palma-Guerrero, J. *et al.* Comparative transcriptomic analyses of Zymoseptoria tritici strains show complex lifestyle transitions and intraspecific variability in transcription profiles. *Molecular Plant Pathology* **17**, 845-859, doi:10.1111/mpp.12333 (2016).

226 Marshall, R. *et al.* Analysis of Two in Planta Expressed LysM Effector Homologs from the Fungus Mycosphaerella graminicola Reveals Novel Functional Properties and Varying Contributions to Virulence on Wheat. *Plant Physiology* **156**, 756-769, doi:10.1104/pp.111.176347 (2011).

227 Kettles, G. J., Bayon, C., Canning, G., Rudd, J. J. & Kanyuka, K. Apoplastic recognition of multiple candidate effectors from the wheat pathogen Zymoseptoria tritici in the nonhost plant Nicotiana benthamiana. *New Phytologist* **213**, 338-350, doi:10.1111/nph.14215 (2017).

228 Cruz, C. D. & Valent, B. Wheat blast disease: danger on the move. *Tropical Plant Pathology* **42**, 210-222, doi:10.1007/s40858-017-0159-z (2017).

229 O'Leary, M. *What is wheat blast?*, <cimmyt.org/news/what-is-wheat-blast> (2019).

230 Gomes, D. P., Rocha, V. S., Pereira, O. L. & de Souza, M. A. Damage of wheat blast on the productivity and quality of seeds as a function of the initial inoculum in the field. *Journal of Seed Science* **39**, 66-74, doi:10.1590/2317-1545v39n1172688 (2017).

231 Islam, M. T. *et al.* Wheat blast: a new threat to food security. *Phytopathol Res* **2**, doi:10.1186/s42483-020-00067-6 (2020).

232 Goddard, R. *et al.* Dissecting the genetic basis of wheat blast resistance in the Brazilian wheat cultivar BR 18-Terena. *Bmc Plant Biology* **20**, 15, doi:10.1186/s12870-020-02592-0 (2020).

233 Anh, V. L. *et al.* Rmg8, a New Gene for Resistance to Triticum Isolates of Pyricularia oryzae in Hexaploid Wheat. *Phytopathology* **105**, 1568-1572, doi:10.1094/phyto-02-15-0034-r (2015).

234 Anh, V. L. *et al.* Rmg8 and Rmg7, wheat genes for resistance to the wheat blast fungus, recognize the same avirulence gene AVR-Rmg8. *Molecular Plant Pathology* **19**, 1252-1256, doi:10.1111/mpp.12609 (2018).

235 Ceresini, P. C. *et al.* Wheat Blast: Past, Present, and Future. *Annual Review of Phytopathology, Vol 56* **56**, 427-456, doi:10.1146/annurev-phyto-080417-050036 (2018).

236 Kankanala, P., Czymmek, K. & Valent, B. Roles for rice membrane dynamics and plasmodesmata during biotrophic invasion by the blast fungus. *Plant Cell* **19**, 706-724, doi:10.1105/tpc.106.046300 (2007).

237 Tufan, H. A. *et al.* Wheat blast: histopathology and transcriptome reprogramming in response to adapted and nonadapted Magnaporthe

isolates. *New Phytologist* **184**, 473-484, doi:10.1111/j.1469-8137.2009.02970.x (2009).

238 Wilson, R. A. & Talbot, N. J. Under pressure: investigating the biology of plant infection by Magnaporthe oryzae. *Nature Reviews Microbiology* **7**, 185-195, doi:10.1038/nrmicro2032 (2009).

239 Robards, A. W. Ultrastructure of plasmodesmata. *Protoplasma* **72**, 315-&, doi:10.1007/bf01279056 (1971).

240 Burch-Smith, T. M. & Zambryski, P. C. in *Annual Review of Plant Biology, Vol 63* Vol. 63 *Annual Review of Plant Biology* (ed S. S. Merchant) 239-260 (Annual Reviews, 2012).

241 Tilney, L. G., Cooke, T. J., Connelly, P. S. & Tilney, M. S. The structure of plasmodesmata as revealed by plasmolysis, detergent extraction and protease digestion. *J. Cell Biol.* **112**, 739-747, doi:10.1083/jcb.112.4.739 (1991).

242 Cheval, C. *et al.* Chitin perception in plasmodesmata characterizes submembrane immune-signaling specificity in plants. *Proceedings of the National Academy of Sciences of the United States of America* **117**, 9621-9629, doi:10.1073/pnas.1907799117 (2020).

243 Ehlers, K. & Kollmann, R. Primary and secondary plasmodesmata: structure, origin, and functioning. *Protoplasma* **216**, 1-30, doi:10.1007/BF02680127 (2001).

244 Hepler, P. K. Endoplasmic-reticulum in the formation of the cell plate and plasmodesmata. *Protoplasma* **111**, 121-133, doi:10.1007/bf01282070 (1982).

245 Staehlin, L. A. & Hepler, P. K. Cytokinesis in higher plants. *Cell* **84**, 821-824, doi:10.1016/s0092-8674(00)81060-0 (1996).

246 Burch-Smith, T. M., Stonebloom, S., Xu, M. & Zambryski, P. C. Plasmodesmata during development: re-examination of the importance of primary, secondary, and branched plasmodesmata structure versus function. *Protoplasma* **248**, 61-74, doi:10.1007/s00709-010-0252-3 (2011).

247 Ehlers, K. & van Bel, A. J. E. Dynamics of plasmodesmal connectivity in successive interfaces of the cambial zone. *Planta* **231**, 371-385, doi:10.1007/s00425-009-1046-8 (2010).

248 Faulkner, C., Akman, O. E., Bell, K., Jeffree, C. & Oparka, K. Peeking into pit fields: A multiple twinning model of secondary plasmodesmata formation in tobacco. *Plant Cell* **20**, 1504-1518, doi:10.1105/tpc.107.056903 (2008).

249 Oparka, K. J. *et al.* Simple, but not branched, plasmodesmata allow the nonspecific trafficking of proteins in developing tobacco leaves. *Cell* **97**, 743-754, doi:10.1016/s0092-8674(00)80786-2 (1999).

250 Kim, I., Kobayashi, K., Cho, E. & Zambryski, P. C. Subdomains for transport via plasmodesmata corresponding to the apical-basal axis are established during Arabidopsis embryogenesis. *Proc. Natl. Acad. Sci. U. S. A.* **102**, 11945-11950, doi:10.1073/pnas.0505622102 (2005).

251 Schulz, A. Plasmodesmal widening accompanies the short-term increase in symplasmic phloem unloading in pea root-tips under osmotic-stress. *Protoplasma* **188**, 22-37, doi:10.1007/bf01276793 (1995).

252 Sivaguru, M. *et al.* Aluminum-induced 1 -> 3-beta-D-glucan inhibits cell-to-cell trafficking of molecules through plasmodesmata. A new mechanism of aluminum toxicity in plants. *Plant Physiol.* **124**, 991-1005, doi:10.1104/pp.124.3.991 (2000).

253 Cui, W. & Lee, J. Y. Arabidopsis callose synthases CalS1/8 regulate plasmodesmal permeability during stress. *Nat. Plants* **2**, 9, doi:10.1038/nplants.2016.34 (2016).

254 Tucker, E. B. Translocation in the staminal hairs of *Setcreasea purpurea* .1. A study of cell ultrastructure and cell-to-cell passage of molecular probes. *Protoplasma* **113**, 193-201, doi:10.1007/bf01280907 (1982).

255 Goodwin, P. B. Molecular-size limit for movement in the symplast of the *Elodea* leaf. *Planta* **157**, 124-130, doi:10.1007/bf00393645 (1983).

256 Erwee, M. G. & Goodwin, P. B. Symplast domains in extrastellar tissues of *Egeria densa* Plaanch. *Planta* **163**, 9-19, doi:10.1007/bf00395891 (1985).

257 Terry, B. R. & Robards, A. W. Hydrodynamic radius alone governs the mobility of molecules through plasmodesmata. *Planta* **171**, 145-157, doi:10.1007/bf00391090 (1987).

258 Burnell, J. N. An enzymic method for measuring the molecular-weight exclusion limit of plasmodesmata of bundle sheath-cells of C-4 plants. *Journal of Experimental Botany* **39**, 1575-1580, doi:10.1093/jxb/39.11.1575 (1988).

259 Xu, M., Cho, E. N., Burch-Smith, T. M. & Zambryski, P. C. Plasmodesmata formation and cell-to-cell transport are reduced in decreased size exclusion limit 1 during embryogenesis in Arabidopsis. *Proc. Natl. Acad. Sci. U. S. A.* **109**, 5098-5103, doi:10.1073/pnas.1202919109 (2012).

260 Wu, S. W., Kumar, R., Iswanto, A. B. B. & Kim, J. Y. Callose balancing at plasmodesmata. *Journal of Experimental Botany* **69**, 5325-5339, doi:10.1093/jxb/ery317 (2018).

261 Chen, X.-Y. & Kim, J.-Y. Callose synthesis in higher plants. *Plant Signalling and Behaviour* **4**, 489-492, doi:10.4161/psb.4.6.8359 (2009).

262 Faulkner, C. *et al.* LYM2-dependent chitin perception limits molecular flux via plasmodesmata. *Proceedings of the National Academy of Sciences of the United States of America* **110**, 9166-9170, doi:10.1073/pnas.1203458110 (2013).

263 Lim, G. H. *et al.* Plasmodesmata Localizing Proteins Regulate Transport and Signaling during Systemic Acquired Immunity in Plants. *Cell Host Microbe* **19**, 541-549, doi:10.1016/j.chom.2016.03.006 (2016).

264 Thomas, C. L., Bayer, E. M., Ritzenthaler, C., Fernandez-Calvino, L. & Maule, A. J. Specific targeting of a plasmodesmal protein affecting cell-to-cell communication. *Plos Biology* **6**, 180-190, doi:10.1371/journal.pbio.0060007 (2008).

265 Ellinger, D., Sode, B., Falter, C. & Voigt, C. A. Resistance of callose synthase activity to free fatty acid inhibition as an indicator of Fusarium head blight resistance in wheat. *Plant Signalling and Behaviour* **9**, doi:10.4161/psb.28982 (2014).

266 Blumke, A. *et al.* Secreted Fungal Effector Lipase Releases Free Fatty Acids to Inhibit Innate Immunity-Related Callose Formation during Wheat Head Infection. *Plant Physiol.* **165**, 346-358, doi:10.1104/pp.114.236737 (2014).

267 Jia, L. J. *et al.* A linear nonribosomal octapeptide from Fusarium graminearum facilitates cell-to-cell invasion of wheat. *Nat. Commun.* **10**, 20, doi:10.1038/s41467-019-08726-9 (2019).

268 Boller, T. & Felix, G. in *Annual Review of Plant Biology* Vol. 60 *Annual Review of Plant Biology* 379-406 (Annual Reviews, 2009).

269 Leborgne-Castel, N. & Bouhidel, K. Plasma membrane protein trafficking in plant-microbe interactions: a plant cell point of view. *Front. Plant Sci.* **5**, doi:10.3389/fpls.2014.00735 (2014).

270 Win, J. *et al.* Effector Biology of Plant-Associated Organisms: Concepts and Perspectives. *Cold Spring Harb Symp Quant Biol* **77**, 235-247 (2012).

271 Green, E. R. & Mecsas, J. Bacterial Secretion Systems: An Overview. *Microbiol. Spectr.* **4**, 19, doi:10.1128/microbiolspec.VMBF-0012-2015 (2016).

272 Alexander, T., Toth, R., Meier, R. & Weber, H. C. Dynamics of arbuscule development and degeneration in onion, bean, and tomato with reference to vesicular-arbuscular mycorrhizae in grasses. *Canadian Journal of Botany-Revue Canadienne De Botanique* **67**, 2505-2513, doi:10.1139/b89-320 (1989).

273 Bonfante, P. & Genre, A. Mechanisms underlying beneficial plant-fungus interactions in mycorrhizal symbiosis. *Nat. Commun.* **1**, 11, doi:10.1038/ncomms1046 (2010).

274 Cheval, C. & Faulkner, C. Plasmodesmal regulation during plant-pathogen interactions. *New Phytologist*, 62-67 (2018).

275 Lee, J. Y. & Lu, H. Plasmodesmata: the battleground against intruders. *Trends Plant Sci.* **16**, 201-210, doi:10.1016/j.tplants.2011.01.004 (2011).

276 Lee, J. Y., Yoo, B. C. & Lucas, W. J. Parallels between nuclear-pore and plasmodesmal trafficking of information molecules. *Planta* **210**, 177-187, doi:10.1007/pl00008124 (2000).

277 Brandner, K. *et al.* Tobacco mosaic virus movement protein interacts with green fluorescent protein-tagged microtubule end-binding protein 1. *Plant Physiol.* **147**, 611-623, doi:10.1104/pp.108.117481 (2008).

278 Harries, P. A. *et al.* Differing requirements for actin and myosin by plant viruses for sustained intercellular movement. *Proc. Natl. Acad. Sci. U. S. A.* **106**, 17594-17599, doi:10.1073/pnas.0909239106 (2009).

279 Optimax. *Stereo Microscope Basics*, <optimaxonline.com/newsdetails.php?newsld=1> (

280 Berkeley, U. o. C. *The Stereo Microscope*, <microscopy.berkeley.edu/courses/tlm/stereo/index/html> (

281 Jonkman, J. & Brown, C. M. Any way you slice it - A comparison of confocal microscopy techniques. *J Biomol Tech* **26**, 54-65, doi:10.7171/jbt.15-2602-003 (2015).

282 Prasher, D. C., Eckenrode, V. K., Ward, W. W., Prendergast, F. G. & Cormier, M. J. Primary structure of *Aequorea victoria* green-fluorescent protein. *Gene* **111**, 229-233, doi:10.1016/0378-1119(92)90691-h (1992).

283 Shimomura, O., Johnson, F. H. & Saiga, Y. Extraction, purification and properties of Aequorin, a bioluminescent protein from luminous hydromedusan, *Aequorea*. *Journal of Cellular and Comparative Physiology* **59**, 223-&, doi:10.1002/jcp.1030590302 (1962).

284 Berg, R. H. & Beauty, R. N. Fluorescent protein applications in plants. *Methods in Cell Biology* **85**, 153-157, doi:dos.org/10.1016/S0091-679X(08)85008-X (2008).

285 Birnbaum, K. *et al.* A gene expression map of the Arabidopsis root. *Science* **302**, 1956-1960, doi:10.1126/science.1090022 (2003).

286 Birnbaum, K. *et al.* Cell type-specific expression profiting in plants via cell sorting of protoplasts from fluorescent reporter lines. *Nat. Methods* **2**, 615-619, doi:10.1038/nmeth0805-615 (2005).

287 DeBlasio, S. L., Sylvester, A. W. & Jackson, D. Illuminating plant biology: using fluorescent proteins for high-throughput analysis of protein localization and function in plants. *Brief. Funct. Genomics* **9**, 129-138, doi:10.1093/bfgp/elp060 (2010).

288 Ausubel, F. M. Arabidopsis Genome. A Milestone in Plant Biology. *Plant Physiol.* **124**, doi:10.1104/pp.124.4.1451 (2000).

289 Martienssen, R. A. Weeding out the genes: the Arabidopsis genome project. *Funct Integr Genomics* **1**, 2-11, doi:10.1007/s101420000006 (2000).

290 Cutler, S. R., Ehrhardt, D. W., Griffitts, J. S. & Somerville, C. R. Random GFP :: cDNA fusions enable visualization of subcellular structures in cells of Arabidopsis at a high frequency. *Proc. Natl. Acad. Sci. U. S. A.* **97**, 3718-3723, doi:10.1073/pnas.97.7.3718 (2000).

291 Corcel, M., Devaux, M. F., Guillon, F. & Barron, C. Comparison of UV and visible autofluorescence of wheat grain tissues in macroscopic images of cross-sections and particles. *Comput. Electron. Agric.* **127**, 281-288, doi:10.1016/j.compag.2016.06.016 (2016).

292 Lee, H. Y., Lee, S. E., Woo, J., Choi, D. & Park, E. Split Green Fluorescent Protein System to Visualise Effectors Delivered from Bacteria During Infection. *Journal of Visualised Experiments*, doi:10.3791/57719 (2018).

293 Kilaru, S. *et al.* A codon-optimized green fluorescent protein for live cell imaging in Zymoseptoria tritici. *Fungal Genetics and Biology* **79**, 125-131, doi:10.1016/j.fgb.2015.03.022 (2015).

294 Kilaru, S., Schuster, M., Ma, W. & Steinberg, G. Fluorescent markers of various organelles in the wheat pathogen *Zymoseptoria tritici*. *Fungal Genetics and Biology* **105**, 16-27 (2017).

295 Mochizuki, S., Minami, E. & Nishizawa, Y. Live-cell imaging of rice cytological changes reveals the importance of host vacuole maintenance for biographic invasion by blast fungus, *Magnaporthe oryzae*. *Microbiologyopen* **4**, 952-966, doi:10.1002/mbo3.304 (2015).

296 Jones, K., Kim, D. W., Park, J. S. & Khang, C. H. Live-cell fluorescence imaging to investigate the dynamics of plant cell death during infection by the rice blast fungus Magnaporthe oryzae. *BMC Plant Biol.* **16**, 8, doi:10.1186/s12870-016-0756-x (2016).

297 Rigal, A., Doyle, S. M. & Robert, S. Live-cell imaging of FM4-64, a tool for tracing the endocytic pathways in Arabidopsis root cells. *Methods Mol. Biol.*, 93-103, doi:10.1007/978-1-4939-1902-4_9 (2015).

298 Bell, K. & Oparka, K. Imaging plasmodesmata. *Protoplasma* **248**, 9-25, doi:10.1007/s00709-010-0233-6 (2011).

299 Epel, B. L., Padgett, H. S., Heinlein, M. & Beachy, R. N. Plant virus movement protein dynamics probed with a GFP-protein fusion. *Gene* **173**, 75-79, doi:10.1016/0378-1119(95)00678-8 (1996).

300 Oparka, K. J. & Read, N. D. *The use of fluorescent probes for studies of living plant cells*. 27-50 (IRL Oxford, 1994).

301 Guenoune-Gelbart, D., Elbaum, M., Sagi, G., Levy, A. & Epel, B. L. Tobacco mosaic virus (TMV) replicase and movement protein function

synergistically in facilitating TMV spread by lateral diffusion in the plasmodesmal desmotubule of Nicotiana benthamiana. *Mol. Plant-Microbe Interact.* **21**, 335-345, doi:10.1094/mpmi-21-3-0335 (2008).

302 Urban, M., Mott, E., Farley, T. & Hammond-Kosack, K. The Fusarium graminearum MAP1 gene is essential for pathogenicity and development of perithecia. *Molecular Plant Pathology* **4**, 347-359, doi:10.1046/j.1364-3703.2003.00183.x (2003).

303 Zhang, X. W. *et al.* In Planta Stage-Specific Fungal Gene Profiling Elucidates the Molecular Strategies of Fusarium graminearum Growing inside Wheat Coleoptiles. *Plant Cell* **24**, 5159-5176, doi:10.1105/tpc.112.105957 (2012).

304 Francisco, C. S., Ma, X., Zwyssig, M. M., McDonald, B. A. & Palma-Guerrero, J. Morphological changes in response to environmental stresses in the fungal plant pathogen Zymoseptoria tritici. *Sci Rep* **9**, 18, doi:10.1038/s41598-019-45994-3 (2019).

305 Sanchez-Vallet, A., McDonald, M. C., Solomon, P. S. & McDonald, B. A. Is Zymoseptoria tritici a hemibiotroph? *Fungal Genetics and Biology* **79**, 29-32, doi:10.1016/j.fgb.2015.04.001 (2015).

306 Kema, G. H. J., Yu, D. Z., Rijkenberg, F. H. J., Shaw, M. W. & Baayen, R. P. Histology of the pathogenesis of Mycosphaerella graminicola in wheat. *Phytopathology* **86**, 777-786, doi:10.1094/Phyto-86-777 (1996).

307 Hilu, H. M. & Bever, W. M. Inoculation, oversummering, and suscept-pathogen relationship of *Septoria-tritici* on Triticum species. *Phytopathology* **47**, 474-480 (1957).

308 Shetty, N. P. *et al.* Association of hydrogen peroxide with restriction of Septoria tritici in resistant wheat. *Physiological and Molecular Plant Pathology* **62**, 333-346, doi:10.1016/s0885-5765(03)00079-1 (2003).

309 Duncan, K. E. & Howard, R. J. Cytological analysis of wheat infection by the leaf blotch pathogen Mycosphaerella graminicola. *Mycological Research* **104**, 1074-1082, doi:10.1017/s0953756299002294 (2000).

310 Shetty, N. P. *et al.* Role of hydrogen peroxide during the interaction between the hemibiotrophic fungal pathogen Septoria tritici and wheat. *New Phytologist* **174**, 637-647, doi:10.1111/j.1469-8137.2007.02026.x (2007).

311 Keon, J. *et al.* Transcriptional adaptation of Mycosphaerella graminicola to programmed cell death (PCD) of its susceptible wheat host. *Molecular Plant-Microbe Interactions* **20**, 178-193, doi:10.1094/mpmi-20-2-0178 (2007).

312 Habig, M., Bahena-Garrido, S. M., Barkmann, F., Haueisen, J. & Stukenbrock, E. H. The transcription factor Zt107320 affects the dimorphic switch, growth and virulence of the fungal wheat pathogen Zymoseptoria tritici. *Molecular Plant Pathology* **21**, 124-138, doi:10.1111/mpp.12886 (2020).

313 Kellner, R. *et al.* Expression Profiling of the Wheat Pathogen Zymoseptoria tritici Reveals Genomic Patterns of Transcription and Host-Specific Regulatory Programs. *Genome Biology and Evolution* **6**, 1353-1365, doi:10.1093/gbe/evu101 (2014).

314 Seybold, H. *et al.* A fungal pathogen induces systemic susceptibility and systemic shifts in wheat metabolome and microbiome composition.

Nature Communications **11**, 12, doi:10.1038/s41467-020-15633-x (2020).

315 Anderegg, J., Hund, A., Karisto, P. & Mikaberidze, A. In-Field Detection and Quantification of Septoria Tritici Blotch in Diverse Wheat Germplasm Using Spectral-Temporal Features. *Frontiers in Plant Science* **10**, 19, doi:10.3389/fpls.2019.01355 (2019).

316 Kuzdralinski, A. *et al.* Novel Primer Sets for Rapid Detection of Zymoseptoria tritici in Wheat. *Plant Disease* **105**, 251-254, doi:10.1094/pdis-02-20-0318-sc (2021).

317 Schuster, M. *et al.* Red fluorescent proteins for imaging Zymoseptoria tritici during invasion of wheat. *Fungal Genetics and Biology* **79**, 132-140, doi:10.1016/j.fgb.2015.03.025 (2015).

318 Liu, Y. & Wang, M. Design, Optimization and Application of Small Molecule Biosensor in Metabolic Engineering. *Frontiers in Microbiology* **8**, 10, doi:10.3389/fmicb.2017.02012 (2017).

319 Berg, J., Hung, Y. P. & Yellen, G. A genetically encoded fluorescent reporter of ATP:ADP ratio. *Nat. Methods* **6**, 161-166, doi:10.1038/nmeth.1288 (2009).

320 Kennedy, H. J. *et al.* Glucose generates sub-plasma membrane ATP microdomains in single islet beta-cells - Potential role for strategically located mitochondria. *J. Biol. Chem.* **274**, 13281-13291, doi:10.1074/jbc.274.19.13281 (1999).

321 Bell, C. J., Manfredi, G., Griffiths, E. J. & Rutter, G. A. in *Mitochondria, 2nd Edition* Vol. 80 *Methods in Cell Biology* (eds L. A. Pon & E. A. Schon) 341-352 (Elsevier Academic Press Inc, 2007).

322 Bell, C. J., Manfredi, G., Griffiths, E. J. & Rutter, G. A. *Mitochondria*. 2 edn, Vol. 80 341-352 (Elsevier Academic Press Inc., 2007).

323 Yildiz, O., Kalthoff, C., Raunser, S. & Kuhlbrandt, W. Structure of GlnK1 with bound effectors indicates regulatory mechanism for ammonia uptake. *Embo Journal* **26**, 589-599, doi:10.1038/sj.emboj.7601492 (2007).

324 Ninfa, A. J. & Jiang, P. PII signal transduction proteins: sensors of alpha-ketoglutarate that regulate nitrogen metabolism. *Current Opinion in Microbiology* **8**, 168-173, doi:10.1016/j.mib.2005.02.011 (2005).

325 Durand, A. & Merrick, M. In vitro analysis of the Escherichia coli AmtB-GlnK complex reveals a stoichiometric interaction and sensitivity to ATP and 2-oxoglutarate. *Journal of Biological Chemistry* **281**, 29558-29567, doi:10.1074/jbc.M602477200 (2006).

326 Baird, G. S., Zacharias, D. A. & Tsien, R. Y. Circular permutation and receptor insertion within green fluorescent proteins. *Proceedings of the National Academy of Sciences of the United States of America* **96**, 11241-11246, doi:10.1073/pnas.96.20.11241 (1999).

327 Walia, A., Waadt, R. & Jones, A. M. in *Annual Review of Plant Biology, Vol 69* Vol. 69 *Annual Review of Plant Biology* (ed S. S. Merchant) 497-524 (Annual Reviews, 2018).

328 Nakano, M., Imamura, H., Nagai, T. & Noji, H. Ca2+ Regulation of Mitochondrial ATP Synthesis Visualized at the Single Cell Level. *Acs Chemical Biology* **6**, 709-715, doi:10.1021/cb100313n (2011).

329 Vevea, J. D., Wolken, D. M. A., Swayne, T. C., White, A. B. & Pon, L. A. Ratiometric Biosensors that Measure Mitochondrial Redox State and

ATP in Living Yeast Cells. *Jove-Journal of Visualized Experiments*, 12, doi:10.3791/50633 (2013).

330 Li, W. Y. *et al.* Tissue-specific accumulation of pH-sensing phosphatidic acid determines plant stress tolerance. *Nature Plants* **5**, 1012-1021, doi:10.1038/s41477-019-0497-6 (2019).

331 Gutsche, M. *et al.* Proximity-based Protein Thiol Oxidation by H2O2-scavenging Peroxidases. *Journal of Biological Chemistry* **284**, 31532-31540, doi:10.1074/jbc.M109.059246 (2009).

332 Slesak, I., Libik, M., Karpinska, B., Karpinski, S. & Miszalski, Z. The role of hydrogen peroxide in regulation of plant metabolism and cellular signalling in response to environmental stresses. *Acta Biochimica Polonica* **54**, 39-50, doi:10.18388/abp.2007_3267 (2007).

333 Delaunay, A., Pflieger, D., Barrault, M. B., Vinh, J. & Toledano, M. B. A thiol peroxidase is an H2O2 receptor and redox-transducer in gene activation. *Cell* **111**, 471-481, doi:10.1016/s0092-8674(02)01048-6 (2002).

334 Rodrigues-Pousada, C. *et al.* Yeast AP-1 like transcription factors (Yap) and stress response: a current overview. *Microbial Cell* **6**, 267-285, doi:10.15698/mic2019.06.679 (2019).

335 Nietzel, T. *et al.* The fluorescent protein sensor roGFP2-Orp1 monitors in vivo H2O2 and thiol redox integration and elucidates intracellular H2O2 dynamics during elicitor-induced oxidative burst in Arabidopsis. *New Phytologist* **221**, 1649-1664, doi:10.1111/nph.15550 (2019).

336 Kema, G. H. J., Verstappen, E. C. P. & Waalwijk, C. Avirulence in the wheat septoria tritici leaf blotch fungus Mycosphaerella graminicola is

controlled by a single locus. *Molecular Plant-Microbe Interactions* **13**, 1375-1379, doi:10.1094/mpmi.2000.13.12.1375 (2000).

337 Steinberg, G. Cell biology of Zymoseptoria tritici: Pathogen cell organization and wheat infection. *Fungal Genetics and Biology* **79**, 17-23, doi:10.1016/j.fgb.2015.04.002 (2015).

338 Sidhu, Y. S. *et al.* A suite of Gateway (R) compatible ternary expression vectors for functional analysis in Zymoseptoria tritici. *Fungal Genetics and Biology* **79**, 180-185, doi:10.1016/j.fgb.2015.03.021 (2015).

339 Flowers, J. L. & Vaillancourt, L. J. Parameters affecting the efficiency of Agrobacterium tumefaciens-mediated transformation of Colletotrichum graminicola. *Current Genetics* **48**, 380-388, doi:10.1007/s00294-005-0034-1 (2005).

340 Sidhu, Y. S. *et al.* Exploitation of sulfonylurea resistance marker and non-homologous end joining mutants for functional analysis in Zymoseptoria tritici. *Fungal Genetics and Biology* **79**, 102-109, doi:10.1016/j.fgb.2015.04.015 (2015).

341 Zwiers, L. H. & De Waard, M. A. Efficient Agrobacterium tumefaciens-mediated gene disruption in the phytopathogen Mycosphaerella graminicola. *Current Genetics* **39**, 388-393, doi:10.1007/s002940100216 (2001).

342 Motteram, J. *et al.* Molecular Characterization and Functional Analysis of MgNLP, the Sole NPP1 Domain-Containing Protein, from the Fungal Wheat Leaf Pathogen Mycosphaerella graminicola. *Molecular Plant-Microbe Interactions* **22**, 790-799, doi:10.1094/mpmi-22-7-0790 (2009).

343 Yang, F. & Naqvi, N. I. Sulfonylurea resistance reconstitution as a novel strategy for ILV2-specific integration in Magnaporthe oryzae. *Fungal Genetics and Biology* **68**, 71-76, doi:10.1016/j.fgb.2014.04.005 (2014).

344 Bielska, E. *et al.* Long-distance endosome trafficking drives fungal effector production during plant infection. *Nature Communications* **5**, 14, doi:10.1038/ncomms6097 (2014).

345 Liu, D., Evans, T. & Zhang, F. Z. Applications and advances of metabolite biosensors for metabolic engineering. *Metabolic Engineering* **31**, 35-43, doi:10.1016/j.ymben.2015.06.008 (2015).

346 Engler, C., Kandzia, R. & Marillonnet, S. A One Pot, One Step, Precision Cloning Method with High Throughput Capability. *Plos One* **3**, 7, doi:10.1371/journal.pone.0003647 (2008).

347 Prelich, G. Gene Overexpression: Uses, Mechanisms, and Interpretation. *Genetics* **190**, 841-854, doi:10.1534/genetics.111.136911 (2012).

348 Cohen, B. A., Amsellem, Z., Maor, R., Sharon, A. & Gressel, J. Transgenically enhanced expression of indole-3-acetic acid confers hypervirulence to plant pathogens. *Phytopathology* **92**, 590-596, doi:10.1094/phyto.2002.92.6.590 (2002).

349 Heller, J., Meyer, A. J. & Tudzynski, P. Redox-sensitive GFP2: use of the genetically encoded biosensor of the redox status in the filamentous fungus Botrytis cinerea. *Molecular Plant Pathology* **13**, 935-947, doi:10.1111/j.1364-3703.2012.00802.x (2012).

350 Pendergrass, W., Wolf, N. & Poot, M. Efficacy of MitoTracker Green (TM) and CMXRosamine to measure changes in mitochondrial membrane potentials in living cells and tissues. *Cytometry Part A* **61A**, 162-169, doi:10.1002/cyto.a.20033 (2004).

351 Samalova, M., Meyer, A. J., Gurr, S. J. & Fricker, M. D. Robust anti-oxidant defences in the rice blast fungus Magnaporthe oryzae confer tolerance to the host oxidative burst. *New Phytologist* **201**, 556-573, doi:10.1111/nph.12530 (2014).

352 Kilaru, S. *et al.* A gene locus for targeted ectopic gene integration in Zymoseptoria tritici. *Fungal Genetics and Biology* **79**, 118-124, doi:10.1016/j.fgb.2015.03.018 (2015).

353 Zhong, Z. M. *et al.* A small secreted protein in Zymoseptoria tritici is responsible for avirulence on wheat cultivars carrying the Stb6 resistance gene. *New Phytologist* **214**, 619-631, doi:10.1111/nph.14434 (2017).

354 Haueisen, J. *et al.* Highly flexible infection programs in a specialized wheat pathogen. *Ecology and Evolution* **9**, 275-294, doi:10.1002/ece3.4724 (2019).

355 Qiu, H. *et al.* Spatiotemporal nature of *Fusarium graminearum*-wheat coleoptile interactions. *Phytopathol Res* **1**, doi:10.1186/s42483-019-0033-7 (2019).

356 O'Brien, T. P. & Thimann, K. V. Histological studies on the coleoptile. I. Tissue and cell types in the coleoptile tip. *American Journal of Botany* **52**, 910-918 (1965).

357 King, R. *et al.* A conserved fungal glycosyltransferase facilitates pathogenesis of plants by enabling hyphal growth on solid surfaces. *Plos Pathogens* **13**, 26, doi:10.1371/journal.ppat.1006672 (2017).

358 Sakulkoo, W. *et al.* A single fungal MAP kinase controls plant cell-to-cell invasion by the rice blast fungus. *Science* **359**, 1399-+, doi:10.1126/science.aaq0892 (2018).

359 Ruzin, S. *Plant Microtechniques and Microscopy*. (Oxford University Press, 1999).

360 Winsor, C. P. The Gompertz curve as a growth curve. *PNAS* **1** (1932).

361 Paine, C. E. T. *et al.* How to fit nonlinear plant growth models and calculate growth rates: an update for ecologists. *Methods in Ecology and Evolution* **3**, 245-256, doi:10.1111/j.2041-210X.2011.00155.x (2012).

362 Patterson, H. D. & Thompson, R. Recovery of inter-block information when block sizes are unequal. *Biometrika* **58**, 545-554, doi:10.1093/biomet.58.3.454 (1971).

363 Benitez-Alfonso, Y., Faulkner, C., Ritzenthaler, C. & Maule, A. J. Plasmodesmata: Gateways to Local and Systemic Virus Infection. *Molecular Plant-Microbe Interactions* **23**, 1403-1412, doi:10.1094/mpmi-05-10-0116 (2010).

364 Ayliffe, M. *et al.* A Simple Method for Comparing Fungal Biomass in Infected Plant Tissues. *Molecular Plant-Microbe Interactions* **26**, 658-667, doi:10.1094/mpmi-12-12-0291-r (2013).

365 Jensen, K. H. & Zwieniecki, M. A. Physical Limits to Leaf Size in Tall Trees. *Physical Review Letters* **110**, 5, doi:10.1103/PhysRevLett.110.018104 (2013).

366 Mcculloch, C. E. & Neuhaus, J. M. Generalized linear mixed models. *Wiley StatsRef*, doi:10.1002/9781118445112.stat07540 (2014).

367 Boddu, J., Cho, S., Kruger, W. M. & Muehlbauer, G. J. Transcriptome analysis of the barley-Fusarium graminearum interaction. *Molecular Plant-Microbe Interactions* **19**, 407-417, doi:10.1094/mpmi-19-0407 (2006).

368 Wright, S. T. C. Growth and cellular differentiation in the wheat coleoptile (*Triticum vulgare* L.):I. Estimation of cell number, cell volume and certain nitrogenous constituents. *Journal of Experimental Botany*, 303-318, doi:10.1093/jxb/12.2.303 (1961).

369 Yoneda, A., Ohtani, M., Katagiri, D., Hosokawa, Y. & Demura, T. Hechtian Strands Transmit Cell Wall Integrity Signals in Plant Cells. *Plants-Basel* **9**, 8, doi:10.3390/plants9050604 (2020).

370 Underwood, W. The plant cell wall: a dynamic barrier against pathogen invasion. *Frontiers in Plant Science* **3**, 6, doi:10.3389/fpls.2012.00085 (2012).

371 Mellersh, D. G. & Heath, M. C. Plasma membrane-cell wall adhesion is required for expression of plant defense responses during fungal penetration. *Plant Cell* **13**, 413-424, doi:10.1105/tpc.13.2.413 (2001).

372 Madina, M. H., Rahman, M. S., Zheng, H. Q. & Germain, H. Vacuolar membrane structures and their roles in plant-pathogen interactions. *Plant Molecular Biology* **101**, 343-354, doi:10.1007/s11103-019-00921-y (2019).

373 Gonzalez-Gutierrez, A. G., Verdin, J. & Rodriguez-Garay, B. Simple Whole-Mount Staining Protocol of F-Actin for Studies of the Female Gametophyte in Agavoideae and Other Crassinucellate Ovules. *Frontiers in Plant Science* **11**, 11, doi:10.3389/fpls.2020.00384 (2020).

374 Scheuring, D., Schöller, M., Kleine-Wehn, J. & Löfke, C. in *Plant Cell Expansion* Vol. 1242 *Methods in Molecular Biology* (ed J. Estevez) 83-92 (Humana Press, 2014).

375 Winter, M., Samuels, P. L., Dong, Y. & Dill-Macky, R. Trichothecene production is detrimental to early root colonization by Fusarium

culmorum and F-graminearum in fusarium crown and root rot of wheat. *Plant Pathology* **68**, 185-195, doi:10.1111/ppa.12929 (2019).

376 Nishimura, M. T. *et al.* Loss of a callose synthase results in salicylic acid-dependent disease resistance. *Science* **301**, 969-972, doi:10.1126/science.1086716 (2003).

377 Ellinger, D. & Voigt, C. A. Callose biosynthesis in arabidopsis with a focus on pathogen response: what we have learned within the last decade. *Annals of Botany* **114**, 1349-1358, doi:10.1093/aob/mcu120 (2014).

378 Amsbury, S., Kirk, P. & Benitez-Alfonso, Y. Emerging models on the regulation of intercellular transport by plasmodesmata-associated callose. *Journal of Experimental Botany* **69**, 105-115, doi:10.1093/jxb/erx337 (2018).

379 Sager, R. E. & Lee, J. Y. Plasmodesmata at a glance. *Journal of Cell Science* **131**, 7, doi:10.1242/jcs.209346 (2018).

380 Capel, J., Jarillo, J. A., Salinas, J. & MartinezZapater, J. M. Two homologous low-temperature-inducible genes from Arabidopsis encode highly hydrophobic proteins. *Plant Physiology* **115**, 569-576, doi:10.1104/pp.115.2.569 (1997).

381 Kurup, S. *et al.* Marking cell lineages in living tissues. *Plant J.* **42**, 444-453, doi:10.1111/j.1365-313X.2005.02386.x (2005).

382 Kirienko, D. R., Luo, A. D. & Sylvester, A. W. Reliable Transient Transformation of Intact Maize Leaf Cells for Functional Genomics and Experimental Study. *Plant Physiol.* **159**, 1309-1318, doi:10.1104/pp.112.199737 (2012).

383 Kelley, L. A., Mezulis, S., Yates, C. M., Wass, M. N. & Sternberg, M. J. E. The Phyre2 web portal for protein modeling, prediction and analysis. *Nature Protocols* **10**, 845-858, doi:10.1038/nprot.2015.053 (2015).

384 Sparks, C. A. & Jones, H. D. in *Cereal Genomics: Methods and Protocols* Vol. 1099 (eds Robert J. Henry & Agnelo Furtado) Ch. 17, 201-218 (Springer Science+Business New York, 2014).

385 Alotaibi, S. S., Sparks, C. A., Parry, M. A. J., Simkin, A. J. & Raines, C. A. Identification of Leaf Promoters for Use in Transgenic Wheat. *Plants-Basel* **7**, 19, doi:10.3390/plants7020027 (2018).

386 Ivanchenko, M., Vejlupkova, Z., Quatrano, R. S. & Fowler, J. E. Maize ROP7 GTPase contains a unique, CaaX box-independent plasma membrane targeting signal. *Plant J.* **24**, 79-90, doi:10.1046/j.1365-313x.2000.00855.x (2000).

387 Hill-Ambroz, K. L., Weeks, J. T., Baenziger, P. S. & Graybosch, R. A. Constitutive promoter expression of transgenes in wheat (Triticum aestivum). *Cereal Research Communications* **29**, 9-16 (2001).

388 Skadsen, R. W. & Hohn, T. A. Use of Fusarium graminearum transformed with gfp to follow infection patterns in barley and Arabidopsis. *Physiological and Molecular Plant Pathology* **64**, 45-53, doi:10.1016/j.pmpp.2004.04.003 (2004).

389 Brandizzi, F. *et al.* ER quality control can lead to retrograde transport from the ER lumen to the cytosol and the nucleoplasm in plants. *Plant J.* **34**, 269-281, doi:10.1046/j.1365-313X.2003.01728.x (2003).

390 Lisenbee, C. S., Karnik, S. K. & Trelease, R. N. Overexpression and mislocalization of a tail-anchored GFP redefines the identity of

peroxisomal ER. *Traffic* **4**, 491-501, doi:10.1034/j.1600-0854.2003.00107.x (2003).

391 Martiniere, A. *et al.* Cell wall constrains lateral diffusion of plant plasma-membrane proteins. *Proc. Natl. Acad. Sci. U. S. A.* **109**, 12805-12810, doi:10.1073/pnas.1202040109 (2012).

392 Nibau, C., Wu, H. M. & Cheung, A. Y. RAC/ROP GTPases: 'hubs' for signal integration and diversification in plants. *Trends Plant Sci.* **11**, 309-315, doi:10.1016/j.tplants.2006.04.003 (2006).

393 Xue, F., Gu, Z. & Feng, J. A. LINKER: a web server to generate peptide sequences with extended conformation. *Nucleic Acids Research* **32**, W562-W565, doi:10.1093/nar/gkh422 (2004).

394 Arai, R., Ueda, H., Kitayama, A., Kamiya, N. & Nagamune, T. Design of the linkers which effectively separate domains of a bifunctional fusion protein. *Protein Engineering* **14**, 529-532, doi:10.1093/protein/14.8.529 (2001).

395 Chichili, V. P. R., Kumar, V. & Sivaraman, J. Linkers in the structural biology of protein-protein interactions. *Protein Science* **22**, 153-167, doi:10.1002/pro.2206 (2013).

396 Giraldo, M. C. *et al.* Two distinct secretion systems facilitate tissue invasion by the rice blast fungus Magnaporthe oryzae. *Nature Communications* **4**, 12, doi:10.1038/ncomms2996 (2013).

397 Brewer, H. C. & Hammond-Kosack, K. E. Host to a Stranger: Arabidopsis and Fusarium Ear Blight. *Trends in Plant Science* **20**, 651-663, doi:10.1016/j.tplants.2015.06.011 (2015).

398 Voigt, C. A., Schafer, W. & Salomon, S. A comprehensive view on organ-specific callose synthesis in wheat (Triticum aestivum L.): glucan

synthase-like gene expression, callose synthase activity, callose quantification and deposition. *Plant Physiology and Biochemistry* **44**, 242-247, doi:10.1016/j.plaphy.2006.05.001 (2006).

399 Richmond, T. A. & Somerville, C. R. The cellulose synthase superfamily. *Plant Physiology* **124**, 495-498, doi:10.1104/pp.124.2.495 (2000).

400 Guseman, J. M. *et al.* Dysregulation of cell-to-cell connectivity and stomatal patterning by loss-of-function mutation in Arabidopsis CHORUS (GLUCAN SYNTHASE-LIKE 8). *Development* **137**, 1731-1741, doi:10.1242/dev.049197 (2010).

401 Han, X. *et al.* Auxin-Callose-Mediated Plasmodesmal Gating Is Essential for Tropic Auxin Gradient Formation and Signaling. *Developmental Cell* **28**, 132-146, doi:10.1016/j.devcel.2013.12.008 (2014).

402 Song, L. Z., Wang, R. C., Zhang, L., Wang, Y. M. & Yao, S. G. CRR1 encoding callose synthase functions in ovary expansion by affecting vascular cell patterning in rice. *Plant Journal* **88**, 620-632, doi:10.1111/tpj.13287 (2016).

403 Verma, D. P. S. & Hong, Z. L. Plant callose synthase complexes. *Plant Molecular Biology* **47**, 693-701, doi:10.1023/a:1013679111111 (2001).

404 Jacobs, A. K. *et al.* An Arabidopsis callose synthase, GSL5, is required for wound and papillary callose formation. *Plant Cell* **15**, 2503-2513, doi:10.1105/tpc.016097 (2003).

405 Ellinger, D. *et al.* Elevated Early Callose Deposition Results in Complete Penetration Resistance to Powdery Mildew in Arabidopsis. *Plant Physiology* **161**, 1433-1444, doi:10.1104/pp.112.211011 (2013).

406 Doxey, A. C., Yaish, M. W. F., Moffatt, B. A., Griffith, M. & McConkey, B. J. Functional divergence in the Arabidopsis beta-1,3-glucanase gene

family inferred by phylogenetic reconstruction of expression states. *Molecular Biology and Evolution* **24**, 1045-1055, doi:10.1093/molbev/msm024 (2007).

407 Levy, A., Erlanger, M., Rosenthal, M. & Epel, B. L. A plasmodesmata-associated beta-1,3-glucanase in Arabidopsis. *Plant Journal* **49**, 669-682, doi:10.1111/j.1365-313X.2006.02986.x (2007).

408 Lee, J. Y. *et al.* A Plasmodesmata-Localized Protein Mediates Crosstalk between Cell-to-Cell Communication and Innate Immunity in Arabidopsis. *Plant Cell* **23**, 3353-3373, doi:10.1105/tpc.111.087742 (2011).

409 Simpson, C., Thomas, C., Findlay, K., Bayer, E. & Maule, A. J. An Arabidopsis GPI-Anchor Plasmodesmal Neck Protein with Callose Binding Activity and Potential to Regulate Cell-to-Cell Trafficking. *Plant Cell* **21**, 581-594, doi:10.1105/tpc.108.060145 (2009).

410 Shinya, T. *et al.* Functional Characterization of CEBiP and CERK1 Homologs in Arabidopsis and Rice Reveals the Presence of Different Chitin Receptor Systems in Plants. *Plant and Cell Physiology* **53**, 1696-1706, doi:10.1093/pcp/pcs113 (2012).

411 Fliegmann, J. *et al.* Biochemical and phylogenetic analysis of CEBiP-like LysM domain-containing extracellular proteins in higher plants. *Plant Physiology and Biochemistry* **49**, 709-720, doi:10.1016/j.plaphy.2011.04.004 (2011).

412 Lee, W. S., Rudd, J. J., Hammond-Kosack, K. E. & Kanyuka, K. Mycosphaerella graminicola LysM Effector-Mediated Stealth Pathogenesis Subverts Recognition Through Both CERK1 and CEBiP Homologues in Wheat. *Molecular Plant-Microbe Interactions* **27**, 236-243, doi:10.1094/mpmi-07-13-0201-r (2014).

413 Ramirez-Gonzalez, R. H. *et al.* The transcriptional landscape of polyploid wheat. *Science* **361**, 662-+, doi:10.1126/science.aar6089 (2018).

414 Adamski, N. M. *et al.* A roadmap for gene functional characterisation in crops with large genomes: Lessons from polyploid wheat. *Elife* **9**, 30, doi:10.7554/elife.55646 (2020).

415 Horevaj, P., Milus, E. A. & Bluhm, B. H. A real-time qPCR assay to quantify Fusarium graminearum biomass in wheat kernels. *Journal of Applied Microbiology* **111**, 396-406, doi:10.1111/j.1365-2672.2011.05049.x (2011).

416 Caillaud, M. C. *et al.* The Plasmodesmal Protein PDLP1 Localises to Haustoria-Associated Membranes during Downy Mildew Infection and Regulates Callose Deposition. *Plos Pathogens* **10**, 13, doi:10.1371/journal.ppat.1004496 (2014).

417 Balasubramanian, V., Vashisht, D., Cletus, J. & Sakthivel, N. Plant beta-1,3-glucanases: their biological functions and transgenic expression against phytopathogenic fungi. *Biotechnology Letters* **34**, 1983-1990, doi:10.1007/s10529-012-1012-6 (2012).

418 Mackintosh, C. A. *et al.* Overexpression of defense response genes in transgenic wheat enhances resistance to Fusarium head blight. *Plant Cell Reports* **26**, 479-488, doi:10.1007/s00299-006-0265-8 (2007).

419 Wang, X., Luna, G. R., Arighi, C. N. & Lee, J. Y. An evolutionarily conserved motif is required for Plasmodesmata-located protein 5 to regulate cell-to-cell movement. *Communications Biology* **3**, 12, doi:10.1038/s42003-020-1007-0 (2020).

420 Vaattovaara, A. *et al.* Mechanistic insights into the evolution of DUF26-containing proteins in land plants. *Communications Biology* **2**, 18, doi:10.1038/s42003-019-0306-9 (2019).

421 Hohmann, U., Lau, K. & Hothorn, M. in *Annual Review of Plant Biology, Vol 68* Vol. 68 *Annual Review of Plant Biology* (ed S. S. Merchant) 109-137 (Annual Reviews, 2017).

422 Jian, J. & Liang, X. One Small RNA of Fusarium graminearum Targets and Silences CEBiP Gene in Common Wheat. *Microorganisms* **7**, 12, doi:10.3390/microorganisms7100425 (2019).

423 Albrecht, S. C. *et al.* Redesign of Genetically Encoded Biosensors for Monitoring Mitochondrial Redox Status in a Broad Range of Model Eukaryotes. *Journal of Biomolecular Screening* **19**, 379-386, doi:10.1177/1087057113499634 (2014).

424 Fuchs, R. *et al.* Immobilized Subpopulations of Leaf Epidermal Mitochondria Mediate PENETRATION2-Dependent Pathogen Entry Control in Arabidopsis. *Plant Cell* **28**, 130-145, doi:10.1105/tpc.15.00887 (2016).

425 Qiu, C. X., Zhai, H. T. & Hou, J. Biosensors design in yeast and applications in metabolic engineering. *Fems Yeast Research* **19**, 12, doi:10.1093/femsyr/foz082 (2019).

426 Mentges, M. *et al.* Infection cushions of Fusarium graminearum are fungal arsenals for wheat infection. *Molecular Plant Pathology* **21**, 1070-1087, doi:10.1111/mpp.12960 (2020).

427 Jiang, C. *et al.* An orphan protein of Fusarium graminearum modulates host immunity by mediating proteasomal degradation of TaSnRK1 alpha.

Nature Communications **11**, 13, doi:10.1038/s41467-020-18240-y (2020).

428 Thapa, G. *et al.* A Pathogen-Responsive Leucine Rich Receptor Like Kinase Contributes to Fusarium Resistance in Cereals. *Frontiers in Plant Science* **9**, 15, doi:10.3389/fpls.2018.00867 (2018).

429 Christensen, M. J. *et al.* Epichloe endophytes grow by intercalary hyphal extension in elongating grass leaves. *Fungal Genetics and Biology* **45**, 84-93, doi:10.1016/j.fgb.2007.07.013 (2008).

430 de Ulzurrun, G. V. D., Huang, T. Y., Chang, C. W., Lin, H. C. & Hsueh, Y. P. Fungal feature tracker (FFT): A tool for quantitatively characterizing the morphology and growth of filamentous fungi. *Plos Computational Biology* **15**, 20, doi:10.1371/journal.pcbi.1007428 (2019).

431 Brown, N. A., Evans, J., Mead, A. & Hammond-Kosack, K. E. A spatial temporal analysis of the *Fusarium graminearum* transcriptome during symptomless and symptomatic wheat infection. *Molecular Plant Pathology* (2017).

432 Banerjee, A. & Mittra, B. Morphological modification in wheat seedlings infected by Fusarium oxysporum. *European Journal of Plant Pathology* **152**, 521-524, doi:10.1007/s10658-018-1470-3 (2018).

433 Di Pietro, A., Madrid, M. P., Caracuel, Z., Delgado-Jarana, J. & Roncero, M. I. G. Fusarium oxysporum: exploring the molecular arsenal of a vascular wilt fungus. *Molecular Plant Pathology* **4**, 315-325, doi:10.1046/j.1364-3703.2003.00180.x (2003).

434 Bishop, C. D. & Cooper, R. M. An ultrastructural-study of root invasion in 3 vascular wilt diseases. *Physiological Plant Pathology* **22**, 15-& (1983).

435 Bishop, C. D. & Cooper, R. M. An ultrastructural-study of vascular colonization in 3 vascular wilt diseases .1. Colonisation of susceptible cultivars. *Physiological Plant Pathology* **23**, 323-343, doi:10.1016/0048-4059(83)90018-8 (1983).

436 Agrios, G. N. *Plant Pathology*. 5th edn, 922 (Elsevier Academic Press, 2005).

437 Zhang, W. *et al.* Defining the pathways of symbiotic Epichloe colonization in grass embryos with confocal microscopy. *Mycologia* **109**, 153-161, doi:10.1080/00275514.2016.1277469 (2017).

438 Jiang, C. *et al.* An expanded subfamily of G-protein-coupled receptor genes in Fusarium graminearum required for wheat infection. *Nature Microbiology* **4**, 1582-1591, doi:10.1038/s41564-019-0468-8 (2019).

439 Brenchley, R. *et al.* Analysis of the breadwheat genome using whole-genome shotgun sequencing. *Nature* **491**, 705-710, doi:10.1038/nature11650 (2012).

440 Appels, R. *et al.* Shifting the limits in wheat research and breeding using a fully annotated reference genome. *Science* **361**, 661-+, doi:10.1126/science.aar7191 (2018).

441 Paux, E. *et al.* A physical map of the 1-gigabase bread wheat chromosome 3B. *Science* **322**, 101-104, doi:10.1126/science.1161847 (2008).

442 Mayer, K. F. X. *et al.* A chromosome-based draft sequence of the hexaploid bread wheat (Triticum aestivum) genome. *Science* **345**, 11, doi:10.1126/science.1251788 (2014).

443 Arndell, T. *et al.* gRNA validation for wheat genome editing with the CRISPR-Cas9 system. *Bmc Biotechnology* **19**, 12, doi:10.1186/s12896-019-0565-z (2019).

444 Cram, D. *et al.* WheatCRISPR: a web-based guide RNA design tool for CRISPR/Cas9-mediated genome editing in wheat. *Bmc Plant Biology* **19**, 8, doi:10.1186/s12870-019-2097-z (2019).

445 Jouanin, A. *et al.* CRISPR/Cas9 Gene Editing of Gluten in Wheat to Reduce Gluten Content and Exposure-Reviewing Methods to Screen for Coeliac Safety. *Frontiers in Nutrition* **7**, 15, doi:10.3389/fnut.2020.00051 (2020).

446 Borrill, P., Ramirez-Gonzalez, R. & Uauy, C. expVIP: a Customizable RNA-seq Data Analysis and Visualization Platform. *Plant Physiology* **170**, 2172-2186, doi:10.1104/pp.15.01667 (2016).

447 Wassie, A. T., Zhao, Y. X. & Boyden, E. S. Expansion microscopy: principles and uses in biological research. *Nature Methods* **16**, 33-41, doi:10.1038/s41592-018-0219-4 (2019).

448 Chen, F., Tillberg, P. W. & Boyden, E. S. Expansion microscopy. *Science* **347**, 543-548, doi:10.1126/science.1260088 (2015).

449 Chang, J. B. *et al.* Iterative expansion microscopy. *Nature Methods* **14**, 593-+, doi:10.1038/nmeth.4261 (2017).

450 Gao, R., Asano, S. M. & Boyden, E. S. Q&A: Expansion microscopy. *Bmc Biology* **15**, 9, doi:10.1186/s12915-017-0393-3 (2017).

451 Kubalova, I. *et al.* Prospects and limitations of expansion microscopy in chromatin ultrastructure determination. *Chromosome Research* **28**, 355-368, doi:10.1007/s10577-020-09637-y (2020).

452 Gotz, R. *et al.* Expansion Microscopy for Cell Biology Analysis in Fungi. *Frontiers in Microbiology* **11**, 10, doi:10.3389/fmicb.2020.00574 (2020).

453 Shera, E. B., Seitzinger, N. K., Davis, L. M., Keller, R. A. & Soper, S. A. Detection of single fluorescent molecules. *Chemical Physics Letters* **174**, 553-557, doi:10.1016/0009-2614(90)85485-u (1990).

454 Endesfelder, U. & Heilemann, M. in *Advanced Fluorescence Microscopy* Vol. 1251 (ed P. Verveer) 263-276 (Humana Press, New York, NY, 2015).

455 Peaucelle, A., Wightman, R. & Haas, K. T. Multicolor 3D-dSTORM Reveals Native-State Ultrastructure of Polysaccharides' Network during Plant Cell Wall Assembly. *Iscience* **23**, 36, doi:10.1016/j.isci.2020.101862 (2020).

456 Eggert, D., Naumann, M., Reimer, R. & Voigt, C. A. Nanoscale glucan polymer network causes pathogen resistance. *Scientific Reports* **4**, 6, doi:10.1038/srep04159 (2014).

457 Mishra, P., Lohumi, S., Khan, H. A. & Nordon, A. Close-range hyperspectral imaging of whole plants for digital phenotyping: Recent applications and illumination correction approaches. *Computers and Electronics in Agriculture* **178**, 11, doi:10.1016/j.compag.2020.105780 (2020).

458 Pandey, P., Ge, Y. F., Stoerger, V. & Schnable, J. C. High Throughput In vivo Analysis of Plant Leaf Chemical Properties Using Hyperspectral Imaging. *Frontiers in Plant Science* **8**, 12, doi:10.3389/fpls.2017.01348 (2017).

459 Veys, C. *et al.* Multispectral imaging for presymptomatic analysis of light leaf spot in oilseed rape. *Plant Methods* **15**, 12, doi:10.1186/s13007-019-0389-9 (2019).

460 Bendel, N. *et al.* Evaluating the suitability of hyper- and multispectral imaging to detect foliar symptoms of the grapevine trunk disease Esca in vineyards. *Plant Methods* **16**, 18, doi:10.1186/s13007-020-00685-3 (2020).

461 Fahrentrapp, J., Ria, F., Geilhausen, M. & Panassiti, B. Detection of Gray Mold Leaf Infections Prior to Visual Symptom Appearance Using a Five-Band Multispectral Sensor. *Frontiers in Plant Science* **10**, 14, doi:10.3389/fpls.2019.00628 (2019).

462 Dammer, K. H., Moller, B., Rodemann, B. & Heppner, D. Detection of head blight (Fusarium ssp.) in winter wheat by color and multispectral image analyses. *Crop Protection* **30**, 420-428, doi:10.1016/j.cropro.2010.12.015 (2011).

463 Kuzdraliński, A. *et al.* Novel primer sets for rapid detection of *Zymoseptoria tritici* in wheat. *Plant Disease*, doi:10.1094/PDIS-02-20-0318-sc (2020).

464 Beck, J. J. & Ligon, J. M. Polymerase chain-reaction assays for the detection of *Stagonospora nodorum* and *Septoria tritici* in wheat. *Phytopathology* **85**, 319-324, doi:10.1094/Phyto-85-319 (1995).

465 Consolo, V. F., Albani, C. M., Beron, C. M., Salerno, G. L. & Cordo, C. A. A conventional PCR technique to detect Septoria tritici in wheat seeds. *Australasian Plant Pathology* **38**, 222-227, doi:10.1071/ap08099 (2009).

466 Fraaije, B. A., Lovell, D. J., Rohel, E. A. & Hollomon, D. W. Rapid detection and diagnosis of Septoria tritici epidemics in wheat using a

polymerase chain reaction PicoGreen assay. *Journal of Applied Microbiology* **86**, 701-708, doi:10.1046/j.1365-2672.1999.00716.x (1999).

467 Fraaije, B. A., Lovell, D. J., Coelho, J. M., Baldwin, S. & Hollomon, D. W. PCR-based assays to assess wheat varietal resistance to blotch (Septoria tritici and Stagonospora nodorum) and rust (Puccinia striiformis and Puccinia recondita) diseases. *European Journal of Plant Pathology* **107**, 905-917, doi:10.1023/a:1013119206261 (2001).

468 Guo, J. R., Schnieder, F. & Verreet, J. A. Presymptomatic and quantitative detection of Mycosphaerella graminicola development in wheat using a real-time PCR assay. *Fems Microbiology Letters* **262**, 223-229, doi:10.1111/j.1574-6968.2006.00393.x (2006).

469 Tiley, A. M. M., Foster, G. D. & Bailey, A. M. Exploring the Genetic Regulation of Asexual Sporulation in Zymoseptoria tritici. *Frontiers in Microbiology* **9**, 14, doi:10.3389/fmicb.2018.01859 (2018).

470 Plissonneau, C., Hartmann, F. E. & Croll, D. Pangenome analyses of the wheat pathogen Zymoseptoria tritici reveal the structural basis of a highly plastic eukaryotic genome. *Bmc Biology* **16**, 16, doi:10.1186/s12915-017-0457-4 (2018).

471 Kelly, A. C. & Ward, T. J. Population genomics of Fusarium graminearum reveals signatures of divergent evolution within a major cereal pathogen. *Plos One* **13**, 32, doi:10.1371/journal.pone.0194616 (2018).

472 Machado, A. K. *et al.* Analysis of Fusarium graminearum pangenome. *Phytopathology* **108**, 110-110 (2018).

473 Gupta, S. *et al.* Molecular detection of Fusarium graminearum causing head blight of wheat by loop mediated isothermal amplification (LAMP)

assay. *Indian Phytopathology* **73**, 667-672, doi:10.1007/s42360-020-00261-8 (2020).

474 Schmidt, S. M. *et al.* MITEs in the promoters of effector genes allow prediction of novel virulence genes in Fusarium oxysporum. *Bmc Genomics* **14**, 21, doi:10.1186/1471-2164-14-119 (2013).

475 Houterman, P. M. *et al.* The effector protein Avr2 of the xylem-colonizing fungus Fusarium oxysporum activates the tomato resistance protein I-2 intracellularly. *Plant Journal* **58**, 970-978, doi:10.1111/j.1365-313X.2009.03838.x (2009).

476 Cao, L. X., Blekemolen, M. C., Tintor, N., Cornelissen, B. J. C. & Takken, F. L. W. The Fusarium oxysporum Avr2-Six5 Effector Pair Alters Plasmodesmatal Exclusion Selectivity to Facilitate Cell-to-Cell Movement of Avr2. *Molecular Plant* **11**, 691-705, doi:10.1016/j.molp.2018.02.011 (2018).

477 Tomczynska, I., Stumpe, M., Doan, T. G. & Mauch, F. A Phytophthora effector protein promotes symplastic cell-to-cell trafficking by physical interaction with plasmodesmata-localised callose synthases. *New Phytologist* **227**, 1467-1478, doi:10.1111/nph.16653 (2020).

478 Doehlemann, G. *et al.* Establishment of compatibility in the Ustilago maydis/maize pathosystem. *Journal of Plant Physiology* **165**, 29-40, doi:10.1016/j.jplph.2007.05.016 (2008).

479 Doehlemann, G. *et al.* Pep1, a Secreted Effector Protein of Ustilago maydis, Is Required for Successful Invasion of Plant Cells. *Plos Pathogens* **5**, 16, doi:10.1371/journal.ppat.1000290 (2009).

480 Djamei, A. *et al.* Metabolic priming by a secreted fungal effector. *Nature* **478**, 395-+, doi:10.1038/nature10454 (2011).

481 Aung, K. *et al.* Pathogenic Bacteria Target Plant Plasmodesmata to Colonize and Invade Surrounding Tissues(CC-BY). *Plant Cell* **32**, 595-611, doi:10.1105/tpc.19.00707 (2020).

482 Lee, W. S., Hammond-Kosack, K. E. & Kanyuka, K. Barley Stripe Mosaic Virus-Mediated Tools for Investigating Gene Function in Cereal Plants and Their Pathogens: Virus-Induced Gene Silencing, Host-Mediated Gene Silencing, and Virus-Mediated Overexpression of Heterologous Protein. *Plant Physiology* **160**, 582-590, doi:10.1104/pp.112.203489 (2012).

483 Bouton, C. *et al.* Foxtail mosaic virus: A Viral Vector for Protein Expression in Cereals. *Plant Physiology* **177**, 1352-1367, doi:10.1104/pp.17.01679 (2018).

484 Callaway, E. CRISPR plants now subject to tough laws in European Union. *Nature* **560**, doi:10.1038/d41586-018-05814-06 (2018).

485 Harrington, S. A. *et al.* A heat-shock inducible system for flexible gene expression in cereals. *Plant Methods* **16**, 16, doi:10.1186/s13007-020-00677-3 (2020).

486 Bleichrodt, R. J. *et al.* Hyphal heterogeneity in Aspergillus oryzae is the result of dynamic closure of septa by Woronin bodies. *Molecular Microbiology* **86**, 1334-1344, doi:10.1111/mmi.12077 (2012).

487 Steinberg, G., Schuster, M., Hacker, C., Kilaru, S. & Correia, A. ATP prevents Woronin bodies from sealing septal pores in unwounded cells of the fungus Zymoseptoria tritici. *Cellular Microbiology* **19**, 10, doi:10.1111/cmi.12764 (2017).